Ophiolites: Mantle Sources, Melt Evolution and Emplacement Mechanisms

Preface

YILDIRIM DILEK
Miami University, Department of Geology and Environmental Earth Science, USA.
E-mail: dileky@miamioh.edu

DOI: 10.18814/epiiugs/2015/v38i4/82417

Ophiolites have played a significant role in investigating and better understanding the structural and geochemical makeup of ancient oceanic lithosphere, fluid–rock interactions and biochemical cycles in its crustal and mantle evolution, and the nature and distribution of former plate boundaries (Dilek and Newcomb, 2003, and the papers therein; Dilek, 2003; Flower and Dilek, 2003). The ophiolite concept has undergone a major transformation since the original Penrose definition of ophiolites in 1972 through systematic and interdisciplinary studies of many ophiolites around the world, as well as through the synenergistic interactions among the scientific communities studying ophiolites and in-situ oceanic lithosphere at active spreading environments in modern ocean basins. One of the most important results of ophiolite studies over the years has been the uncovering of a large diversity in the internal structure and geochemical compositions of ophiolites and in their emplacement mechanisms. Dilek and Furnes (2011) introduced a new ophiolite classification to explain this diversity within the framework of different tectonic settings of magmatic construction of oceanic lithosphere. More recent studies have also shown that the mineralogy and geochemical compositions of crustal and mantle sequences in most ophiolites do not represent a simple melt–residua relationship, and that many ophiolites display compositional and geochemical heterogeneities at different scales that are not consistent with steady-state magmatic accretion at a spreading center (Dilek and Furnes, 2014, and references therein).

The papers in this special issue highlight some of these recent findings and new interpretations on the mantle sources, melt evolution and emplacement mechanisms of various ophiolites. In the first paper, Saccani and co-authors (Saccani et al., 2015, this issue) describe the geological and geochemical characteristics of Neotethyan mafic-ultramafic rock sequences in fossil ocean – continent transition zones (OCTZ) and discuss their melt evolution. Oceanic lithosphere developed in ancient OCTs constitutes a continental margin ophiolite (CMO). The authors argue that the igneous stratigraphy and geochemical signatures of CMOs within the Neotethyan realm reflect the extent of geochemical heterogeneity, partial melting degrees, and melt evolution patterns in the continental lithospheric mantle prior to the onset of seafloor spreading in rifted margins. Presenting the relevant geochemical data and discrimination diagrams, they show that magmas of the extrusive sequences in the studied Neotethyan ophiolites were derived from compositionally distinct mantle sources, which were pre-conditioned by previous subduction and plume events in the geological history of the region (Dilek, 2003). These OCT-generated continental margin ophiolites precede mid-ocean ridge and subduction-related ophiolites in the history of the magmatic construction of oceanic lithosphere during the Wilson cycle evolution of ocean basins.

In the second paper, Yang and Dilek (Yang and Dilek, 2015, this issue) document the geological occurrence and the geochemical features of the Jurassic-early Cretaceous ocean island basalt-type and alkaline mafic rocks within the Yarlung-Zangbo suture zone (YZSZ) in Southern Tibet. These alkaline rock sequences are tectonically interleaved with the ophiolite massifs and also occur in mélange formations along the YZSZ. Composed mainly of lavas, massive diabase and gabbroic rocks, these alkaline rock associations exhibit uniform chondrite-

normalized REE patterns with light rare earth element (LREE) enrichment and heavy rare earth element (HREE) depletion, and primitive mantle normalized trace element patterns with significant large-ion lithophile element (LILE) enrichment, similar to those of modern OIB and the Hawaiian alkaline basalts. The authors interpret these assemblages as OIB- and Plume-type (P-type) oceanic crustal rocks (Dilek, 2003), derived from magmas, which were produced by partial melting of plume–metasomatized asthenospheric mantle source during the early stages of the opening of a Neotethyan seaway between Proto-India and India. The interpretations in this paper are consistent and in agreement with the data and models provided by Saccani and his co-authors (Saccani et al., 2015, this issue) from the western domains of the Neotethyan realm.

In the following paper, Balestro and his co-authors (Balestro et al., 2015, this study) document the internal structure and tectonic fabric of the Jurassic Monviso ophiolite in the Western Alps (Italy), and show that this ophiolite represents an on-land exposure of an oceanic core complex. Their model depicts simple-shear seafloor spreading kinematics during the opening of the Ligurian–Piedmont ocean basin within the Alpine Tethys that led to the development of the Monviso oceanic core complex. One of the most important aspects of this paper is the recognition of a shear zone (Baracun Shear Zone), marking the detachment fault system of the oceanic core complex, despite the strong high-pressure metamorphic overprint that all ophiolitic rocks experienced during the Alpine orogeny. This fossil detachment fault system includes ductilely to cataclastically deformed blocks and clasts of Fe-Ti and Mg-Al metagabbros in a matrix composed of mylonitic serpentinite and talc-chlorite schist with high Ni–Cr concentrations and high Cl contents. The authors interpret the Monviso ophiolite and the Baracun Shear Zone as a peridotite-localized oceanic core complex, and argue that this extensional deformation fabric was not associated with any stage of the subsequent subduction zone tectonics of the Western Alps.

Shin and his co-authors present the late Miocene – early Pliocene Taitao ophiolite in the Chilean Patagonia as a case study of the emplacement mechanism and magmatic evolution of a ridge-trench intersection (RTI) ophiolite (Shin et al., 2015, this issue). The Taitao ophiolite has a complete, Penrose-type ophiolite sequence, and represents an uplifted, on-land segment of the modern Chile Rise oceanic lithosphere. Its geochemical makeup reflects a complex magmatic history involving interactions between the subducting ridge, the overlying continental crust, and the lithospheric mantle. The authors posit that the MORB-like lavas erupted along the Chile Rise near the subduction zone might have been contaminated by partial melts derived from a lower crustal material. They also argue that alteration of upper mantle peridotites by seawater along fracture zones may have played an important role in affecting the magma chemistry in this ridge-trench intersection environment. Granitic plutons that are slightly younger than the igneous age of the Taitao ophiolite intrude the ophiolitic subunits and the Andean crust and provide further constraints on magma formation processes at RTI settings. Shin and his co-authors envision that magmas of these granitic intrusions may have formed as a result of partial melting of hot oceanic crust near the subducting mid-ocean ridge segment. Subsequent contamination of these magmas by lower crustal material and/or the metasomatized subarc mantle was probably important in further modifying the granitic magmas. Ridge-trench intersections and associated plate boundary interactions were likely to be common along the active margins of continental masses in the past, and hence we should be able to identify older examples of RTI ophiolites in the geological record.

A different type of ophiolite emplacement mechanism is presented in the next paper by Fareeduddin and Dilek (2015, this issue) from an exhumed Neotethyan accretionary wedge complex near the Indo-Burma plate boundary in NE India. The Nagaland Hill – Manipur ophiolite belt in this area represents the southern extension of the Neotethyan Yarlung-Zhangbo suture zone in Southern Tibet, connecting this on-land exposure of the late Mesozoic collision front in the north with a modern arc-trench system in the Andaman Sea region in the south. The authors argue that the ophiolitic occurrences in the Nagaland Hill – Manipur area represent a typical subduction channel mélange, which evolved during the fast subduction of the Neotethyan oceanic lithosphere beneath Asia – Sundaland. The existence of eclogitic and blueschist mineral and rock assemblages spatially associated with the ophiolitic subunits in the melange and the ductile, cataclastic and brittle deformation fabrics in them strongly support the subduction channel origin of the melange. The authors postulate that the exhumation of this mélange was facilitated by return flow within a subduction channel at the plate interface between the downgoing Indian continental margin and the Triassic – early Cretaceous accretionary prism of the overlying Burma plate. The shallow dip angle of the subducting Indian plate that was acquired following the initial India – Asia collision in the early Eocene was a primary cause for the upper plate deformation and exhumation in the accretionary prism. The ophiolitic material in the Nagaland Hill – Manipur melange was derived mainly from the downgoing plate, similar to the RTI Taitao ophiolite (Shin et al., 2015, this issue), but unlike the suprasubduction zone ophiolites (Dilek and Furnes, 2014).

The overview of the Paleozoic ophiolites along the Variscan Galicia suture zone in the NW Iberian Peninsula in the following paper by Arenas and Sanchez (2015, this issue) demonstrates the diversity of these ophiolites in their internal structure and

geochemical makeup. The authors present a compelling case of a possible RTI ophiolite (Cambrian in age), among other suprasubduction zone types along the Variscan suture zone in NW Iberia. The rift-drift, seafloor spreading and subduction zone tectonics of the Variscan ophiolites took place during the Wilson cycle evolution of the Rheic Ocean and the assembly of the supercontinent Pangea (Dilek and Robinson, 2003).

The last two papers in the special issue involve the occurrence of chromitites in ophiolitic peridotites and their petrogenetic evolution. Castro and her co-authors (Castro et al., 2015, this issue) present a detailed study of Cr-rich and Al-rich chromitites in the Havana-Matanzas ophiolites in Western Cuba. Using the chromian spinel compositions in these rocks and the platinum group mineral occurrences in the Cr-rich chromitites, the authors postulate that melts from which the ophiolitic crustal rocks evolved had island-arc tholeiite – boninite and back-arc basin basalt (BABB) affinities (Dilek and Furnes, 2014), and that these melts were in equilibrium with Cr-rich and Al-rich chromitites. The bimodal compositions of the chromitite deposits in the Western Cuban ophiolites were likely controlled by the degree of melt – rock interaction during percolation of subduction-driven melts through variably depleted peridotites in a mantle wedge.

The last paper by Yang et al. (2015, this issue) documents the geological occurrence and geochemical characteristics of diamonds and other ultrahigh-pressure (UHP) minerals in ophiolitic mantle peridotites and podiform chromitites from four different orogenic belts in the world. This study is a follow-up to the papers previously published by the same authors (Yang et al., 2014, 2015), and provides a much more extensive dataset on ophiolite-hosted diamonds and the related ophiolites. The authors demonstrate that diamonds and UHP minerals occur in both high-Cr and high-Al chromitites, regardless of the compositions of their host chromites. The existence of a wide range of highly reduced minerals, such as Ni-Mn-Co alloys, Fe-Si and Fe-C phases, and moissanite (SiC) as accompanying mineral separates or inclusions in diamonds indicates super-reducing conditions of their environment of formation. These observations and data suggest chromite crystallization depths around >380 km, near the mantle transition zone. The findings of this study are likely to modify the existing views on the shallow mantle origin of oceanic peridotites and the petrogenesis of mantle sequences in ophiolite complexes.

Acknowledgements

I thank the authors of the papers for their valuable contributions in this special issue and to the evolving ophiolite concept in general. I am particularly indebted to Dr. Fareeduddin, the Editor of Episodes, for his enthusiastic support throughout the preparation of this special issue. On behalf of all the authors, I would like to extend our collective appreciation to Dr. Brian Marker, Chair of the IUGS Publications Committee, for his editorial oversight and help.

References

Arenas, R. and Martínez, S.S., 2015, Variscan ophiolites in NW Iberia: Tracking Lost Paleozoic Oceans and the Assembly of Pangea. Episodes, v. 38, No. 4, pp. 315-333, doi: 10.18814/epiiugs/2015/v38i4/82427.

Balestro, G., Festa, A., Dilek, Y. and Tartarotti, P., 2015, Pre-Alpine Extensional Tectonics of a Peridotite-Localized Oceanic Core Complex in the Late Jurassic, High-Pressure Monviso ophiolite (Western Alps). Episodes, v. 38, No. 4, pp. 266-282, doi: 10.18814/epiiugs/2015/v38i4/82421.

Castro, A.I.L., Proenza, J.A., Zaccarini, F., Garuti, G., and Sarlabous, M.S.C.B., 2015, Al-and Cr-rich chromitites from the Eastern Havana-Matanzas ophiolites (Western Cuba). Episodes, v. 38, No. 4, pp. 334-343, doi: 10.18814/epiiugs/2015/v38i4/82429.

Dilek, Y., 2003, Ophiolite pulses, mantle plumes and orogeny. Geological Society of London, Special Publications, v. 218, p. 9-19.

Dilek, Y. and Newcomb, S., 2003, Ophiolite concept and the evolution of geological thought. Geological Society of America Special Papers, v. 373, The Geological Society of America, Boulder, CO 80301, ISBN 0-8137-2373-6.

Dilek, Y. and Furnes, H., 2011, Ophiolite genesis and global tectonics: Geochemical and tectonic fingerprinting of ancient oceanic lithosphere. Geological Society of America Bulletin, v. 123, pp. 387–411.

Dilek, Y. and Furnes, H., 2014, Ophiolites and Their Origins. Elements, v. 10, pp. 93–100.

Fareeduddin and Dilek, Y., 2015, Structure and Petrology of the Nagaland-Manipur Hill Ophiolite Melange Zone, NE India: A Fossil Tethyan Subduction Channel at the India – Burma Plate Boundary. Episodes, v. 38, No. 4, pp. 298-314, doi: 10.18814/epiiugs/2015/v38i4/82426.

Flower, M.F.J. and Dilek, Y., 2003, Arc-trench rollback and forearc accretion: 1. A collision-induced mantle flow model for Tethyan ophiolites: In, Geological Society of London Special Publications, v. 218, p. 21-42.

Saccani, E., Dilek, Y., Marroni, M., and Pandolfi, L., 2015, Continental Margin Ophiolites of Neotethys: Remnants of Ancient Ocean–Continent Transition Zone (OCTZ) Lithosphere and Their Geochemistry, Mantle Sources and Melt Evolution Patterns. Episodes, v. 38, No. 4, pp. 230-249, doi: 10.18814/epiiugs/2015/v38i4/82418.

Shin, K.-C., Anma, R., Nakano, T., Orihashi, Y., and Ike, S.-I., 2015, The Taitao ophiolite-granite complex, Chile: Emplacement of ridge-trench intersection oceanic lithosphere on land and origin of calc-alkaline I-type granites. Episodes, v. 38, No. 4, pp. 283-297, doi: 10.18814/epiiugs/2015/v38i4/82424.

Yang, G.X. and Dilek, Y., 2015, OIB- and P-Type Ophiolites Along the Yarlung-Zangbo Suture Zone (YZSZ), Southern Tibet: Poly-Phase Melt History and Mantle Sources of the Neotethyan Oceanic Lithosphere. Episodes, v. 38, No. 4, pp. 250-265, doi: 10.18814/epiiugs/2015/v38i4/82420.

Yang, J.S., Robinson, P.T., and Dilek, Y., 2014, Diamonds in Ophiolites. Elements, v. 10, p. 127–130.

Yang, J.S., Meng, F.C., Xu, X.Z., Robinson, P.T., Dilek, Y., Makeyev, A.B., Wirth, R., Wiedenbeck, M., Cliff, J., 2015a, Diamonds, native elements and metal alloys from chromitites of the Ray-Iz ophiolite of the Polar Urals. Gondwana Research, v. 27, pp. 459–485.

Yang, J.S., Robinson, P.T., and Dilek, Y., 2015, Diamond-bearing Ophiolites and Their Geological Occurrence. Episodes, v. 38, No. 4, pp. 344-364, doi: 10.18814/epiiugs/2015/v38i4/82430.

by Emilio Saccani [1], Yildirim Dilek [2], Michele Marroni [3], Luca Pandolfi [3]

Continental margin ophiolites of Neotethys: Remnants of Ancient Ocean–Continent Transition Zone (OCTZ) lithosphere and their geochemistry, mantle sources and melt evolution patterns

[1] Dip. di Fisica e Scienze della Terra, Univ. di Ferrara, Via Saragat 1, 44123 Ferrara, Italy. *Corresponding author E-mail: sac@unife.it*
[2] Dept. of Geology & Environmental Earth Science, Miami University, Oxford, OH 45056, USA
[3] Dip. di Scienze della Terra, Univ. di Pisa, Via S. Maria 53, 56126 Pisa, Italy

DOI: 10.18814/epiiugs/2015/v38i4/82418

We present an overview of the geology, geochemistry and petrogenesis of continental margin ophiolites (CMO), which represent the lithospheric remnants of rift-generated paleo ocean – continent transition zones (OCTZ) in orogenic belts. The igneous stratigraphy and geochemical signatures of Neotethyan CMOs reflect the extent of geochemical heterogeneity, partial melting degrees, and melt evolution patterns in the continental lithospheric mantle prior to the onset of seafloor spreading in rifted margins. Basaltic rocks of the Jurassic CMOs in the External Ligurian units of the Northern Apennines have N-MORB and G-MORB affinities with strong HREE/MREE depletion, and represent the products of partial melting of a heterogeneous sub-continental lithospheric mantle containing small volumes of garnet pyroxenite layers. These extrusive rocks were erupted directly on the exhumed fertile spinel lherzolites of Adria during its OCTZ evolution. Volcanic rocks of the Triassic CMOs in the Albanide-Hellenide orogenic belt are represented by calc-alkaline suites; alkaline basalts and subordinate trachybasalts, trachyandesites, and trachytes; transitional to sub-alkaline plume-type P-MORB basalts; sub-alkaline enriched, E-MORB basalts; and, sub-alkaline N-MORB basalts. Upper mantle peridotites are not exposed. Magmas of these extrusive rock associations were derived from compositionally distinct mantle sources, which were affected by previous subduction and plume events in the geological history of the region. The CMOs in the Zagros orogenic belt include metamorphosed lherzolites with gabbro and mafic dike intrusions, which show N-MORB and G-MORB affinities. Basalts and basaltic andesites making up the majority of the Zagros volcanic sequences have E-MORB and P-MORB affinities, whereas minor alkaline rocks that are composed of basalts, trachybasalts and trachytes display OIB signatures. The mantle sources of the Zagros CMOs were progressively enriched in Th and Nb. The OIB component of the mantle beneath the Zagros OCTZ was derived from previous plume events during the early Carboniferous, when Paleotethys was undergoing its rift-drift tectonics. The observed differences in the igneous stratigraphy and geochemical affinities of these Neotethyan CMOs are a result of extreme mantle heterogeneity caused by previous subduction and plume events during the Wilson Cycle evolution of the older Paleotethys.

Introduction

Ophiolites represent fragments of ancient oceanic lithosphere (Dewey and Bird, 1971; Coleman, 1971) that were incorporated into continental margins during a variety of plate interactions (see Dilek and Furnes, 2011). They are commonly found along suture zones, which mark major boundaries between amalgamated plates or accreted terranes (Dilek, 2003a; Lister and Forster, 2009). Ophiolites record magmatic activities and tectonic processes associated with the construction and consumption of ancient oceanic basins from their rift–drift and sea floor spreading stages to subduction initiation

and final closure phases. Magmatism during each of these phases produces ultramafic to mafic and evolved rock assemblages, which have distinct internal structures, geochemical afûnities, and age ranges, depending on their original tectonic setting of formation. The geological record of the Wilson cycle evolution of ocean basins is, therefore, partially preserved in most ophiolite complexes along suture zones.

The Penrose definition of an ophiolite is a "*distinctive assemblage of ultramafic and mafic rocks*" that includes, from bottom to top, tectonized peridotites, cumulate peridotites, and pyroxenites overlain by layered gabbros, sheeted basaltic dikes, a volcanic sequence, and a sedimentary cover ('Penrose-type igneous sequence'; Anonymous, 1972, p. 24). An ophiolite may be incomplete or tectonically dismembered, and it can also be metamorphosed. Dilek and Furnes (2011, 2014) have recently argued that this original Penrose definition of ophiolites (Anonymous, 1972) is inadequate to explain the significant variations in the internal structures, compositions, geochemical signatures, and emplacement mechanisms of ophiolites. They have introduced a more detailed classification based on the characteristic internal structures, geochemical fingerprints, and regional tectonics of ophiolites. Among the most important parameters controlling the magmatic evolution of different ophiolite types are: (1) the rate, geometry and nature of seafloor spreading, (2) the proximity of a spreading center to a plume or trench, (3) mantle composition, temperature and fertility, and (4) the availability of fluids (Dilek and Furnes, 2014).

In their new classification, Dilek and Furnes (2011, 2014) have defined the Continental Margin (CM) ophiolites as mafic-ultramafic and sedimentary rock assemblages that formed during the continental breakup and embryonic oceanic crust generation at ocean-continent transition zones (OCTZ). These ophiolites do not have the ideal Penrose-type igneous sequence and generally include fertile peridotites of continental lithospheric mantle that are directly overlain by basaltic lavas and hemi-pelagic sedimentary rocks. Basaltic rocks display a normal (N-) MORB geochemistry characterized by marked garnet signatures commonly typified by depletion in heavy rare earth elements (HREE) with respect to middle rare earth elements (MREE). Saccani (2015) used the term G-MORB (garnet-influenced MORB) for identifying this basaltic sub-type, which can easily be distinguished from typical N-MORBs using Ce-Dy-Yb systematics (see Fig. 8 in Saccani, 2015). The petrogenesis of CM ophiolites involves small degrees of partial melting of little depleted lithospheric mantle and slowly uprising asthenosphere in magma-poor, "cold rift" tectonic settings (Dilek et al., 1998). Thus, CM ophiolites constitute an important end-member of the entire ophiolite spectrum (Dilek, 2003a).

Some of the best examples of CM ophiolites include the Jurassic ophiolites in the Ligurian units of the Northern Apennines (e.g., Montanini et al., 2008; Marroni and Pandolfi, 2007), Alpine Corsica (Durand-Delga, 1984; Malavieille et al., 1998; Saccani et al., 2008a), and the Western Alps (Lagabrielle and Cannat, 1990; Desmurs et al., 2002; Rampone et al., 2005; Manatschal and Müntener, 2009; Festa

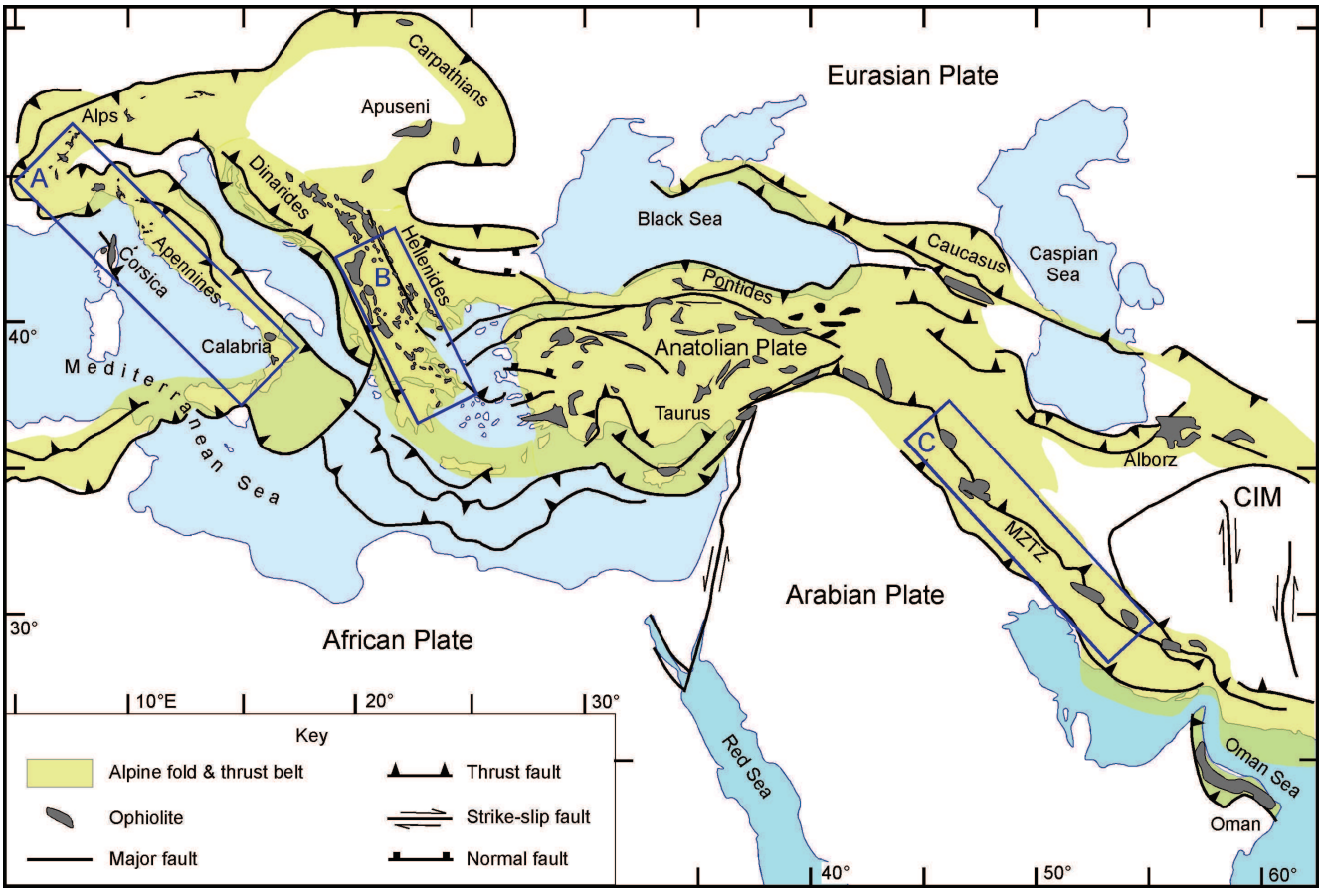

Figure 1. Distribution of major ophiolitic complexes in the Alpine orogenic belts from the central Mediterranean area to the Oman Sea. The major tectonic lineaments are also shown. Boxes indicate the investigated areas. A: Western Tethys ophiolites (Alps-Corsica-Apennine-Calabria); B: Albanide-Hellenide ophiolites; C: Zagros ophiolites. MZTZ: Main Zagros Thrust Zone, CIM: Central Iranian Microcontinent.

et al., 2015; Balestro et al. 2015;), and the early Cretaceous Dongba-Purang ophiolites in southern Tibet (Liu et al., 2015; Yang and Dilek, 2015). However, many more CM ophiolites are yet to be documented in the Phanerozoic and Precambrian orogenic belts through systematic structural field and geochemical studies. Most CM ophiolites are commonly multiply deformed and metamorphosed, undergone subduction-exhumation processes, and/or incorporated into sub-ophiolitic mélanges as blocks or thrust sheets (Dilek, 2003a; Dilek and Robinson, 2003). Thus, recognition of CM ophiolites and associated tectonostratigraphic units in continental collisional zones may be particularly difficult at best.

In this paper we examine the geological and geochemical characteristics of continental margin ophiolites of Neotethyan origin (Fig. 1), and discuss their melt evolution in OCTZs. We first review the geological and magmatic features of rifted continental margins. We then describe the geology and geochemistry of three continental margin ophiolites in different domains of the Neotethyan realm, in the Western Alps–Alpine Corsica–Northern Apennines (i.e., the Western or Alpine Tethys), in the Albanide-Hellenide belt (Pindos-Mirdita ocean basin), and in the Zagros orogenic belt in Iran. We next compare and contrast various petrogenetic models for the formation of these ophiolites, focusing on their mantle sources and melt evolution. We think that this overview of continental margin ophiolites will help us differentiate similar mafic-ultramafic rock associations of ancient OCTZs that have been otherwise unrecognized in collisional orogenic belts.

Rifted Continental Margins

Rifted continental margins and OCTZs have been divided into "non-volcanic" (Iberia-type) and "volcanic" (East Greenland-type) types, based largely on the study of the Central and North Atlantic regions by the deep Ocean Drilling Program (e.g., Whitmarsh et al. 2001). Non-volcanic rifted margins are invariably magma-poor and are considered to have undergone extension that varied vertically and laterally both in space and time. Simple shear (Wernicke, 1981) and detachment (Lister et al., 1991) models have been proposed to interpret this depth-dependent extension (Royden and Keen, 1980; Kusznir and Karner, 2007), and to explain the differences observed in the tectonic architecture of modern magma-poor rifted continental margins. The first step in the evolutionary path in these models (Fig. 2a) is the formation of offset rift basins via distributed deformation (Huismans and Beaumont, 2007; Beaumont and Ings, 2012; Chenin and Beaumont, 2013). The subsequent extensional deformation becomes focused leading to the development of a major basin bounded by listric faults. This rifting process is characterized by a profound asymmetric geometry and formation of transitional zones with variable width where the thickness of the continental crust decreases abruptly. Little surface magmatism occurs during continued rifting. The resulting magma-poor continental margins and the related OCTZs are thus characterized by exhumation of serpentinized continental mantle lithosphere as well as high- grade metamorphic rocks of lower crust (Fig. 2b). The best modern analogue for such magma-poor rifted margins is the Iberia–Newfoundland conjugate margins pair (e.g. Péron-Pinvidic and Manatschal, 2009; Van Avendonk et al., 2009; Sibuet and Tucholke, 2013). A very thin oceanic crust may form in the initial stages of spreading, following the continental breakup.

The majority of rifted continental margins worldwide are

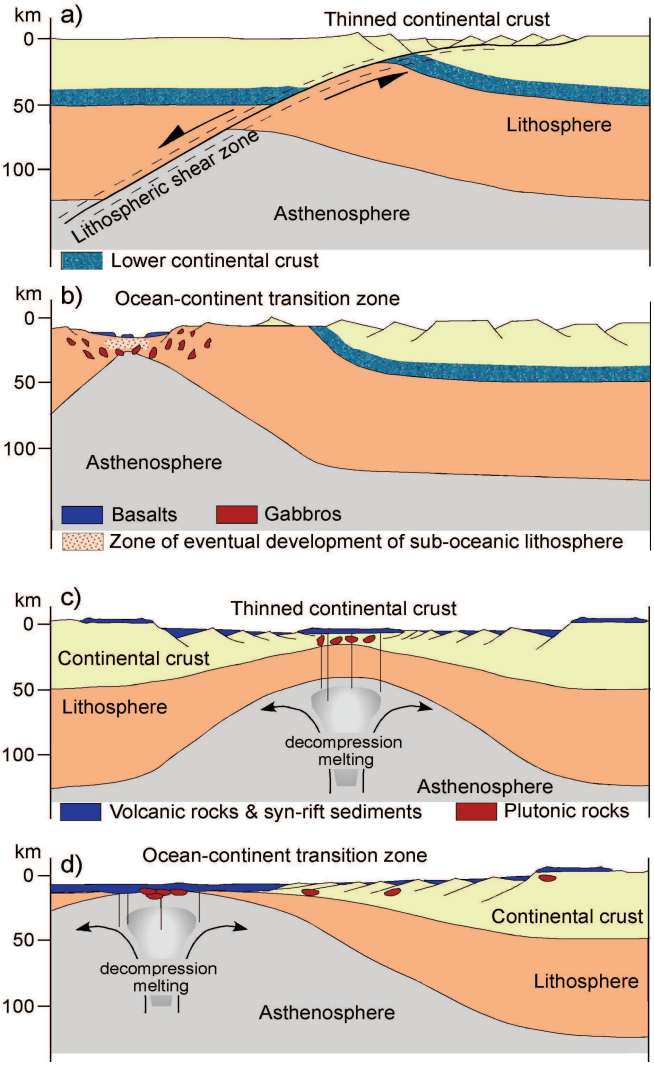

Figure 2. Simplified rift-drift models for magma-poor (a, b) and volcanic (c, d) continental rifted margins.

represented by volcanic types, which are generally characterized by thick wedges (up to 15 km) of volcanic flows (Hinz, 1981; Mutter et al., 1982; Menzies et al., 2002; Skogseid, 2001) that form seaward dipping seismic reflectors. The rifting mechanism produces a crustal architecture that shows an overall symmetry (Fig. 2c). Crustal thinning typically occurs over a comparably short distance in the order of 50 to 100 km. As a consequence, the volcanic rifted continental margins are typically devoid of exposures of subcontinental mantle or high-grade lower crust. The lack of strong passive margin subsidence during and after breakup and the presence at depth of a dense lower crustal body with anomalously high seismic velocities (Vp>7.1 km/s) are also characteristic features of volcanic rifted margins (Planke et al., 1991; Eldholm et al., 2000). Volcanic rifted margins are commonly associated with large igneous provinces (LIPs) onshore (Fig. 2c), and major regional dike swarms and sills (Coffin and Eldholm, 1994; Dilek, 2003b). Examples of LIPs associated with volcanic rifted margins include the North Atlantic Igneous Province (e.g., Kerr, 1994; Storey et al., 2007) and the Kerguelen–India–Antarctica–southwestern Australia area (e.g., Coffin et al., 2002). As the regional extensional stress regime remains active and rifting continues, a seafloor spreading system becomes established following the crustal breakup whereby normal oceanic crust is produced (Fig. 2d).

Continental Margin Ophiolites of Western Tethys

Regional Geology

The ophiolites in the Northern Apennines, Alpine Corsica, and Western Alps (Fig. 1) represent the remnants of the Western Tethys Ocean (also known as Liguria-Piemonte Ocean or Alpine Tethys). This oceanic basin developed in a western seaway of the Tethyan realm between Europe–Corsica and Adria continental domains after the Triassic to middle Jurassic rifting and the middle to late Jurassic seafloor spreading episodes (Manatschal and Müntener, 2009 and quoted references). The Western Tethys oceanic basin has been interpreted as a narrow (<600 km-wide) seaway, developed as a result of ultra slow spreading (e.g., Marroni and Pandolfi, 2007). Major reorganizations in plate motions and plate boundary configurations within the Tethyan system in the late Cretaceous led to oblique convergence between Europe-Corsica and Adria that resulted in the development of an intra-oceanic subduction zone within the Western Tethys oceanic basin (e.g., Marroni et al., 2010 for the Northern Apennines and Compagnoni, 2003 for the Western Alps). Following the terminal closure of the Western Tethys oceanic basin in the early Tertiary, Adria and Europe collided leading to the development of a thick, doubly-verging orogenic wedge in the Alpine-Apennine mountain system. Continental margin ophiolites were thrust eastwards in the Northern Apennines and westward in the Western Alps and Alpine Corsica during this continental collision stage.

The ophiolites in the Western Alps and the Schistes Lustrés of Corsica display eclogite to blueschist facies metamorphic overprint as a record of the subduction events in the Western Tethys oceanic basin. In contrast, the ophiolites in the Internal Ligurian (IL) units of the Northern Apennines, and Alpine Corsica (Pineto, Balagne and Rio Magno) are only weakly metamorphosed but strongly deformed. These features are interpreted to have resulted from shallow level, low-P accretion (Marroni and Pandolfi, 2003; Marroni et al., 2004; Meneghini et al., 2009). The upper mantle peridotites, gabbros and basalts in the External Ligurian (EL) units occur, however, in a different structural position. They occur as blocks embedded in a Santonian-Campanian sedimentary mélange, which also includes fragments of granitoids and mafic granulites of the Hercynian continental crust (e.g. Casanova and Ragola Complexes; Marroni et al., 2001).

Geochemistry

Mantle lherzolites

Studies of the ophiolites in the Western Alps and the Northern Apennines have revealed high degrees of chemical and isotopic heterogeneity in their upper mantle peridotites (Rampone et al., 1995, 1998, 2005, Montanini et al., 2006; Rampone and Hofmann, 2012). These findings led to the recognition of two major types of upper mantle sequences in the Ligurian units of the Northern Apennines: the mantle peridotites of the EL units, and the mantle peridotites of the IL units.

The upper mantle peridotites of the EL units consist mainly of fertile spinel lherzolites, representing the subcontinental lithospheric mantle exhumed during the early stages of continental rifting, which led to the opening of the Jurassic Western Tethys oceanic basin. The isotopic ages of these peridotites range between 2.4 Ga and 780 Ma, and their Sr and Nd isotopic compositions are also similar to those of the subcontinental orogenic spinel lherzolites documented from the western Mediterranean region (Rampone et al., 1995). The fertile nature of these upper mantle peridotites is demonstrated by relatively high REE concentrations coupled with a moderate LREE/HREE depletion (Fig.3a), as well as high Al_2O_3 (Fig.3b) and CaO contents (Rampone et al., 1995). Several meters-thick garnet-bearing clinopyroxenite to websterite layers locally occur within the mantle sequences of the EL units (Montanini et al., 2006).

The upper mantle peridotites of the IL units consist of clinopyroxene-poor spinel lherzolites, which represent a rare example of the depleted mantle lithosphere of the Jurassic Ligurian Tethys (Rampone et al., 1998). These rocks exhibit severe depletion in highly incompatible elements, such as LREE (Fig. 3a), and less pronounced depletion in Al_2O_3 (Fig. 3b), CaO, Sc, and V. These geochemical features are consistent with those of a residual mantle, which

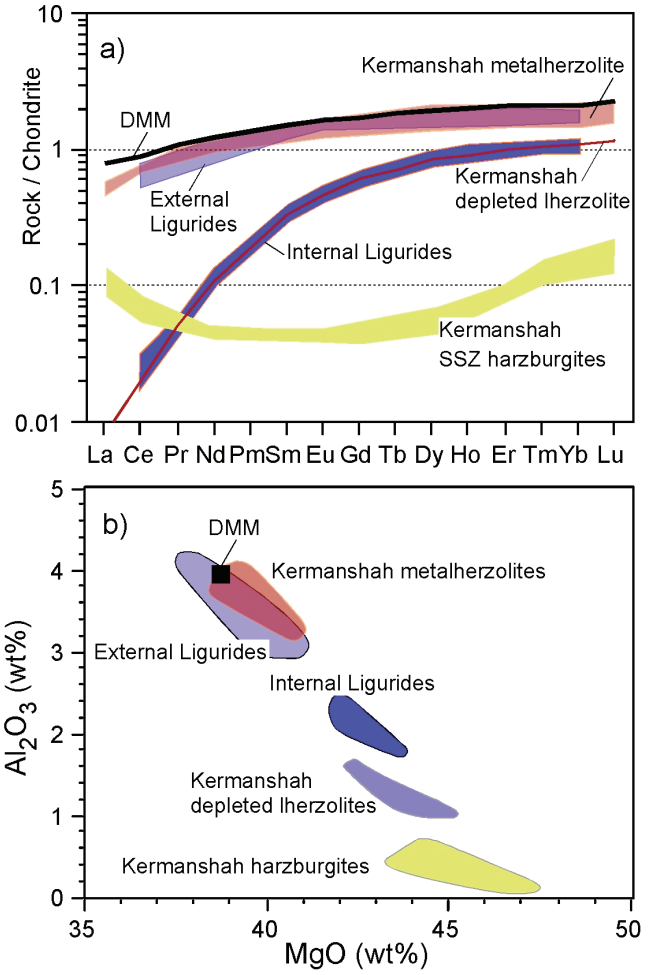

Figure 3. (a) Chondrite–normalized rare earth element (REE) compositional variation, and (b) variation of Al_2O_3 vs. MgO for mantle peridotites from the Western Tethys and Zagros ophiolites. The average composition of the depleted MORB mantle (DMM) is shown for comparison (data from Workmann and Hart, 2005). Normalizing values are from Sun and McDonough (1989). For data source, see Table 1, as well as Allahyari et al. (2010) for Kermanshah depleted lherzolites and harzburgites.

underwent low-degrees (<10%) of repeated episodes of partial melting, initiated in the garnet stability field (Rampone et al., 1998). The available Sr and Nd isotopic compositions of these peridotites indicate an extremely depleted signature, and the Sm/Nd model ages suggest their partial melting experience during the Permian (Rampone et al., 1998). These observations and data suggest that the mantle rocks in the IL units represent the products of upwelling and melting of a MORB-type asthenosphere that formed in response to the onset of regional extensional tectonics, which led to the opening of the Western Tethys Ocean.

Basaltic and metabasaltic rocks

Although limited in volume, basaltic rocks are widespread in the Western Tethyan ophiolites. They mainly occur as blueschists and eclogites in the Western Alps, Alpine Corsica, and Calabria, and as unmetamorphosed basaltic lavas in the IL and EL units, as well as in some units in Alpine Corsica (Balagne, Nebbio, Pineto, Rio Magno). Two varieties of basaltic rocks are identified in the Western Tethyan ophiolites, regardless of their metamorphic grade: (1) basaltic rocks showing the typical geochemical features of N-MORB, and (2) N-MORB lavas displaying marked garnet influence in the melt source; these basaltic rocks have been defined as G-MORB (garnet-influenced MORB) by Saccani (2015).

N-MORB rocks crop out in Alpine Corsica and the EL units of the Northern Apennines, and are represented mainly by basalts and minor basaltic andesites. These rocks show a clear sub-alkaline nature, as evidenced by their very low Nb/Y ratios (0.04-0.09). Their TiO_2 (0.98 – 1.78 wt%), P_2O_5 (0.13 – 0.40 wt%), Zr (53-192 ppm) and Y (20-48 ppm) contents, as well as Ti/V ratios (29-48), are highly similar to those of modern MORBs. The Nb and Th values plot along the MORB-OIB array and cluster towards relatively depleted compositions (Fig. 4a). These rocks show LREE depletion with respect to both MREE (La_N/Sm_N = 0.47-0.67) and HREE (La_N/Yb_N = 0.53-0.91). In the discrimination diagram of Saccani (2015), these basaltic rocks plot in the typical N-MORB field (Fig. 4b).

Basaltic rocks with G-MORB affinities are volumetrically predominant in the Western Tethys ophiolites with respect to N-MORB (Table 1). These rocks generally show a wide range of fractionation degrees (Mg# = 81.7 - 50.5). Basaltic compositions are volumetrically predominant, whereas basaltic andesitic and ferrobasaltic rocks are subordinate. These basaltic rocks have overall chemical compositions that are highly similar to that of N-MORBs, as evidenced by their TiO_2 (1.07 – 2.33 wt%), P_2O_5 (0.10 – 0.44 wt%), Zr (37 - 281 ppm) and Y (15 - 57 ppm) contents, as well as by their Nb/Y (0.04 – 0.20) and Ti/V ratios (28-56). Although G-MORBs largely overlap with N-MORB compositions in Figure 4a, there is a tendency for G-MORBs to plot towards compositions that are less depleted in Th and Nb. Because of their comparatively higher contents in these elements as well as in their LREE/HREE ratios, some authors have interpreted these rocks as transitional-type MORBs (T-MORBs), generated from slightly enriched mantle sources during the onset of oceanic spreading (e.g., Venturelli et al., 1979). In their re-evaluation of this interpretation, Montanini et al. (2008) and Saccani et al. (2008a) have observed that these rocks typically show significant depletion in HREE with respect to MREE, and that their $(Dy/Yb)_N$ ratios (1.15 to 1.59; Fig. 4b) are higher than that of typical N-MORB (Dy_N/Yb_N = 1; Sun and McDonough, 1989). They have suggested, therefore, that the LREE/HREE enrichment was related to depletion in HREE rather than enrichment in LREE. They hence interpreted the HREE/MREE depletion as a clear garnet signature of their mantle sources.

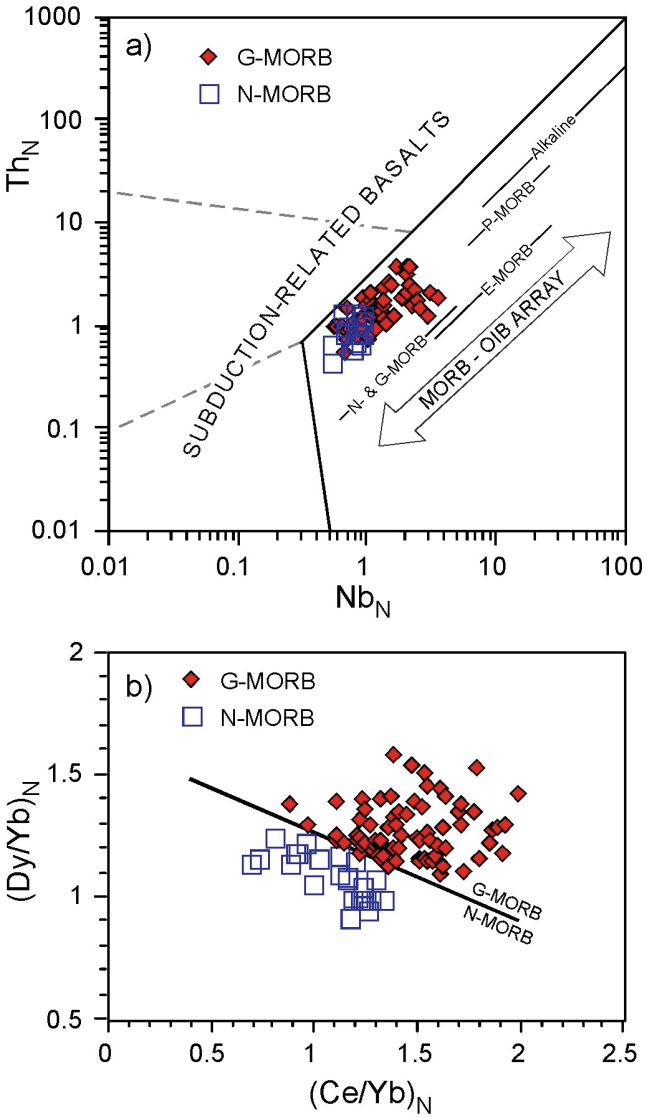

Figure 4. (a) N-MORB-normalized Th_N vs. Nb_N diagram (Saccani, 2015) for basalts and metabasalts from the Western Tethys (Alps, Alpine Corsica, Apennine, and Calabria) ophiolites. Abbreviations, MORB: mid-ocean ridge basalt, N-: normal type, E-: enriched type, P-: plume type, G-: garnet-influenced type. Bars showing the compositional variation of N-, E-, P-MORBs and alkaline basalt from worldwide ophiolites are from Saccani (2015). (b) Chondrite-normalized $(Dy/Yb)_N$ vs. $(Ce/Yb)_N$ diagram (Saccani, 2015) used for discriminating between G-MORB (garnet-influenced MORB) and N-MORB. Compared to N-MORBs, G-MORBs show a marked garnet signatures testified by HREE/MREE depletion (Saccani, 2015). Normalization values in both panels are from Sun and McDonough (1989). For data source, see Table 1.

Mantle sources and petrogenesis of basaltic and metabasaltic rocks of the Western Tethys ophiolites

Compositional variations observed in mafic rock suites commonly reflect the effects of fractional crystallization of olivine, plagioclase, and clinopyroxene in relatively evolved rocks (see Saccani et al.,

Table 1. Age, regional distribution, geochemical type, and related references of Jurassic and Triassic rocks in the key areas examined in this paper. [(1)]: Age constrained on geological bases (see Saccani et al., 2008b for the W Vardar zone ophiolites and Saccani et al., 2013a for the Kermanshah ophiolites)

Region	Unit	Age	Rock-type	References
		Western Tethys ophiolites		
		Mantle lherzolites		
N. Apennine	External Liguride			Rampone et al., 1995
	Internal Liguride			Rampone et al., 1998
		Basalts		
W Alps	Platta	Jurassic	G	Desmurs et al., 2002
Corsica	Pineto, Rio Magno, Balagne	Jurassic	G, N	Saccani et al., 2000; Saccani et al., 2008a
	Schistes Lustres	Jurassic	G, N	Saccani et al., 2008a
N Apennine	External Ligurides	Jurassic	G, N	Marroni et al., 1998; Vannucci et al., 1993
	Internal Ligurides	Jurassic	G	Cortesogno & Gaggero, 1992; Rampone et al., 1998
Calabria	Pollino	Jurassic	G	E. Saccani's unpublished data
		Albanide-Hellenide ophiolites		
		Basalts		
Mirdita	W & E Belt mélanges	L-Triassic	N, E	Bortolotti et al., 2004; Tashko et al., 2007
	Porava (S Mirdita)	M-L-Triassic	N, AB	Bortolotti et al., 2006
Hellenides	Othrys mélange	M-L-Triassic	N, E, P, AB, CAB	Photiades at al., 2003; Bortolotti et al., 2008; Monjoie et al., 2008; Capedri et al., 1997
	Koziakas mélange	M-L-Triassic	N, E, P, AB	Capedri et al., 1997; Saccani et al., 2003a; Chiari et al., 2012
	Argolis mélange	Triassic[(1)]	N, E, P, AB	Capedri et al., 1997; Saccani et al., 2003b; Saccani & Photiades, 2005
	W Vardar zone mélange	Triassic[(1)]	N, E, AB, CAB	Saccani et al., 2008b
	Vardoussia mélange	M-L-Triassic	N, P, CAB	Capedri et al., 1997; Bortolotti et al., 2009
	Avdella mélange (Pindos)	L-Triassic	N, P, AB	Capedri et al., 1997; Jones & Robertson, 1991
	Kerassies	L-Triassic	E, AB	Pe-Piper, 1998
	Evvia & Samos	E-M-Triassic	AB	Pe-Piper & Panagos, 1989; Pe-Piper & Kotopouli, 1991
	Atalanti	Triassic	CAB	Capedri et al., 1997
	Edipsos, Kremasta, Giona	M-Triassic	CAB	Pe-Piper, 1983; Pe-Piper & Panagos, 1989, Pe-Piper & Piper, 1991
	Formation à blocs	L-Triassic	CAB	Pe-Piper, & Mavroniki 1990
	Metalliko-Kilkis	E-Triassic	CAB	Asvesta, 1992
		Zagros ophiolites		
		Metalherzolites		
Zagros	Kermanshah	Pre-Jurassic[(1)]		Saccani et al., 2013a
		Metagabbros and metadykes		
	Kermanshah	Pre-Jurassic[(1)]	G, N	Saccani et al., 2013a
		Basalts		
	Kermanshah	Pre-Jurassic[(1)]	E, P, AB	Ghazi Hassanipak, 1999; Saccani et al., 2013a
	Sarve-Abad	Pre-Jurassic[(1)]	E, P	Saccani et al., 2014

2008a). Most of the rocks examined in this study have Mg# less than 70, that is, lower than the Mg# of > 70 inferred for primary melts of MORB-type lherzolites (Sinton and Detrick, 1992). For this reason, our discussion on the petrogenesis of these rocks is based only on the most primitive samples. The petrogenesis of basalts and metabasalts in the Western Tethys ophiolites and the characteristic features of their mantle sources have been discussed extensively by Montanini et al. (2008) for the EL units, and by Saccani et al. (2008a) for the basalt and metabasalt occurrences in Alpine Corsica. We summarize the salient points and conclusions of these studies here, using the LREE/HREE vs. MREE/HREE ratios (Fig. 5) that are particularly useful for highlighting the garnet influence in mantle melt sources.

The main distinctive feature between N-MORBs and G-MORBs lies in different fractionation trends among LREE, MREE, and HREE that cannot be explained by fractional crystallization alone; however, it can be explained by variable influence of a garnet signature in their mantle sources (Montanini et al., 2008). The garnet signature can be related either to deep initiation of melting in the garnet peridotite stability field, or to the melting of a heterogeneous mantle source characterized by garnet-bearing mafic/ultramafic layers. The diagram in Figure 5 shows that primitive N-MORB compositions are compatible with 10 – 20% partial melting of a depleted MORB-type mantle (DMM) source in the spinel stability field. In contrast, the compositions of primitive G-MORBs are compatible with either partial melting of a DMM source bearing garnet pyroxenites, or partial

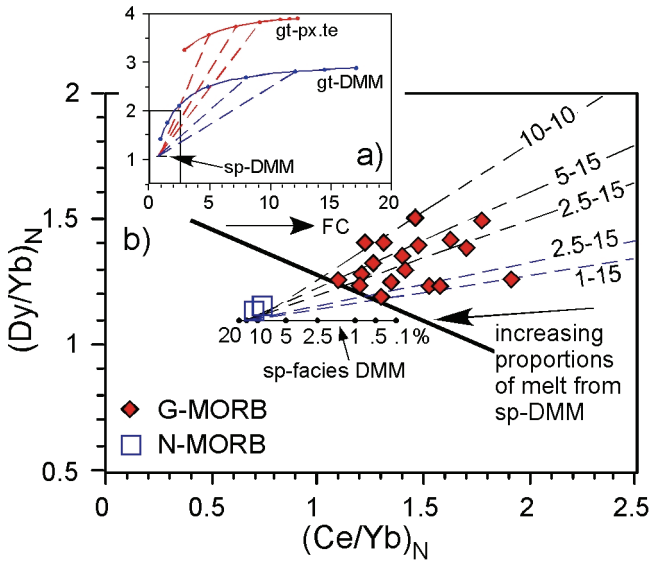

Figure 5. (a) Batch melting curves on $(Dy/Yb)_N$ vs. $(Ce/Yb)_N$ diagram for a garnet pyroxenite (gt-px.te) and a depleted MORB mantle (DMM) source in both garnet (gt) and spinel (sp) stability fields. Dashed lines represent the mixing lines of various melt fractions from different sources. DMM composition is from Workman and Hart (2005) garnet-pyroxenite composition is from Liu et al. (2005); Source modes, melting proportions, and partition coefficient are given in Appendix A. Box indicates the area expanded in panel (b). (b) Plot of the most primitive basalts and metabasalts from Western Tethys ophiolites on the close up of the melting model in panel (a). Red dashed lines represent the mixing lines of various melt fractions between DMM in the spinel stability field + garnet-pyroxenite relics; blue dashed lines represent mixing lines of various melt fractions between DMM in the spinel stability field + DMM in the garnet stability field. The percentages of melt fractions from each source are indicated on the mixing line (e.g., 5-15 indicates 5% partial melt of sp-DMM that mix with 15% partial melt of gt-pyroxenite). Mixing proportions between different partial melts are not shown. However, samples plot in the range from 0.9 – 0.6 melt from sp-DMM + 0.1 – 0.4 melt from other sources. Abbreviations, N-MORB: normal-type mid-ocean ridge basalt; G-MORB: garnet influenced MORB. See text for further explanations.

melting of a DMM source that started to melt in the garnet lherzolite field (~1 – 2.5% melting) and that it continued to higher degrees (~15% melting) in the spinel lherzolite field. All samples from the Western Tethys basalts and metabasalts fall within the mantle array (Fig. 4a), suggesting that a chemical influence of a lower crust component was limited or absent.

Basaltic lavas in the EL units of the Northern Apennines were likely the products of partial melting of a heterogeneous sub-continental lithospheric mantle bearing small volumes of garnet pyroxenite layers (Montanini et al., 2008). There exist several different interpretations for the inferred origin of garnet in the mantle melt source of these lavas. It might have been produced by relict garnet-pyroxenite material left in the depleted mantle source after the delamination and sinking of parts of the deep garnet-pyroxenite-bearing lithospheric mantle (Piccardo, 2008). Alternatively, it might have resulted from partial melting of a depleted MORB-type mantle source that initially started in the garnet-facies mantle and then continued in the spinel-facies mantle (Saccani et al., 2008a).

Continental Margin Ophiolites in the Albanide-Hellenide Segment of the Alpine Orogen

Geology

The NW-SE-trending Albanide-Hellenide mountain belt (Fig. 1) is part of the Alpine orogenic system and stretches from Slovenia and Serbia in the north to the mainland Greece in the south. Its late Mesozoic-Cenozoic tectonics was controlled mainly by the oblique convergence and continental collision between Adria and Europe, whereas its early Mesozoic tectonics was dominated by continental rifting, rift-drift tectonics and opening of an oceanic domain within the Neotethyan realm (e.g., Shallo and Dilek, 2003; Dilek et al., 2007, 2008; Bortolotti et al., 2013 and quoted references). Whether there was one or were two separate basins in this oceanic domain is still a subject of debate in the literature. Regardless of the paleogeography of the inferred ocean basin(s), final continental break-up and initial seafloor spreading in the Albanide-Hellenide segment of the Neotethyan system appear to have occurred in the Carnian–Norian (Bortolotti et al., 2013).

The main rift-drift events that lead to the opening of the Neotethys basin(s) in the region took place in the early–middle Triassic (Robertson et al., 1991). Upper Scythian and lower Anisian sub-marine lavas, locally associated with red limestones and cherts, are overlain by transgressive mid-Triassic limestones in the Tripolitsa, Subpelagonian and Pelagonian tectonic zones (Pe-Piper, 1998). Submarine volcanic rocks that are stratigraphically associated with late Anisian radiolarian cherts occur in the sub-ophiolitic mélanges in the Albanide-Hellenide belt (Jones et al., 1992, Chiari et al., 1996; Ozsvart et al., 2011). Rift-related volcanism appears to have continued into the late Triassic, as documented in numerous localities in the Albanide-Hellenide belt (see Table 1). Similar Triassic rift-related volcanic rocks intercalated with hemipelagic sedimentary rock sequences are widespread elsewhere in the Dolomite Alps of northern Italy (Winterer and Bosellini, 1981), in the Dinarides (Bébien et al., 1978, Pamiç, 1984), and in the Taurides of southern Turkey (Dilek and Rowland, 1993; Dilek et al., 1999).

Geochemistry of Triassic mafic volcanic rocks

Five main types of Triassic mafic to intermediate volcanic rock associations are distinguished in the Albanide-Hellenide belt (see Table 1 for localities and references): (1) calc-alkaline (CAB) and minor shoshonitic basalts, basaltic andesites and andesites; (2) alkaline basalts and subordinate trachybasalts, trachyandesites, and trachytes (e.g., Saccani et al., 2003a); (3) transitional to sub-alkaline basalts showing marked LREE/HREE enrichment, resembling plume-type MORB (P-MORB) compositions; (4) sub-alkaline basalts showing moderate LREE/HREE enrichment, resembling enriched-type MORB (E-MORB) compositions; and (5) sub-alkaline basalts showing N-MORB chemistry. We briefly summarize below the geochemical features of these main types of Triassic basaltic rock associations based on the existing literature (see Table 1 for regional distribution and references). Most of these volcanic rock associations are incorporated into sub-ophiolitic mélange units as discrete tectonic slices or blocks. However, only volcanic rocks that are spatially associated with Triassic sedimentary

rocks (either carbonate rocks or radiolarian cherts) are described below.

Calc-alkaline volcanic rocks

Triassic calc-alkaline volcanic rocks are found in several extrusive units of the Hellenide belt, and rarely in the sub-ophiolitic mélanges of the Othris, Vardoussia, and Almopias ophiolites (Table 1). The calc-alkaline rocks in the Metalliko-Kilkis area are Lower Triassic in age (Asvesta, 1992), whereas all the other rock units are Middle to Upper Triassic in age. The main rock types include basalts, basaltic andesites, andesites, dacites and rhyolites, although basalts and basaltic andesites are more extensive by volume. Basaltic and andesitic rocks have low to moderate TiO_2 (0.7–1.5 wt%), Zr (64 - 218 ppm), and Y (16 – 47 ppm). They are sub-alkaline in nature (Fig. 6a), show significant Th enrichment with respect to Nb (Fig. 6b), and plot in the compositional field for calc-alkaline basaltic rocks. These rocks are characterized by incompatible element patterns with positive anomalies of Th, U, La, Ce and marked negative anomalies of Ta, Nb, Hf, and Ti (e.g., Pe-Piper and Piper, 1991; Capedri et al., 1997; Pe-Piper, 1998; Bortolotti et al., 2009). They show highly variable LREE/HREE enrichments, with La_N/Yb_N ratios ranging from ~2 to ~11.

Alkaline basaltic rocks

Triassic alkaline rocks occur as hundreds of meters-thick successions in the volcanic sequences of the Porava unit in South Albania (Bortolotti et al., 2006), and on the islands of Evvia and Samos in Greece (Pe-Piper and Panagos, 1989; Pe-Piper and Kotopouli, 1991). They are also widespread in sub-ophiolitic mélanges of the Subpelagonian zone, where they are mainly represented by basalts, and subordinately by trachybasalts, trachyandesites, and trachytes (Capedri et al., 1997; Saccani et al., 2003a; Saccani and Photiades, 2005; Bortolotti et al., 2009). In the Vardar zone to the east, however, they are represented by metabasaltic rocks showing intense deformation (Saccani et al., 2008b). The alkaline nature of these rocks is marked by their Nb/Y ratios >1.4 (Fig. 6a). Basaltic rocks have relatively high TiO_2 (1.4 – 3.4 wt%) and P_2O_5 (0.2 – 1 wt%) contents, and display significant enrichment in Th and Nb (Fig. 6b), as well as marked LREE/HREE enrichments (La_N/Yb_N = 3.8-26.0). These elements and many incompatible element ratios (e.g., Th/Yb = 0.8-4.3; Ta/Yb = 0.4-3.2) are highly similar to those observed in typical ocean island basalts (OIB) (Sun and McDonough, 1989), suggesting that magmas of these rocks in the Vardar Zone may have originated from an OIB-like mantle source. Pb and Nd isotope compositions of the Evvia and Samos alkali basalts resemble those of Saint Helena or Afar OIB, although their Pb isotopic compositions are similar to those of the Aegean granitoids suggesting a hint of crustal contamination (Pe-Piper, 1998). However, all transitional to alkaline basalts plot within the MORB - OIB array in Figure 6b, indicating that any possible chemical contamination from the lower crust should have been very limited.

Highly enriched (plume-type) mid-ocean ridge basalts (P-MORBs)

Middle to Late Triassic P-MORBs consisting of pillowed and massive lavas occur as thrust sheets within sub-ophiolitic mélanges beneath the Hellenide ophiolites (Table 1). These rocks are

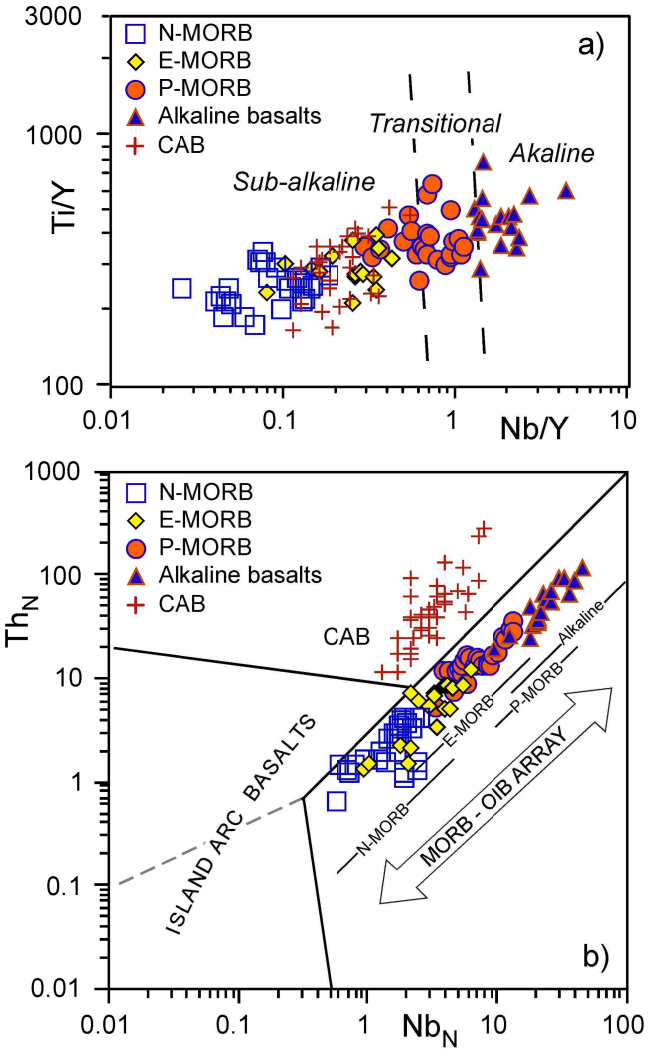

Figure 6. (a) Ti/Y vs. Nb/Y diagram (Pearce, 1982), and (b) N-MORB-normalized Th_N vs. Nb_N diagram (Saccani, 2015) for Triassic basalts from the Albanide-Hellenide ophiolites. Abbreviations, MORB: mid-ocean ridge basalt, N-: normal type, E-: enriched type, P-: plume type, CAB: calc-alkaline basalt. Bars showing the compositional variation of N-, E-, P-MORBs and alkaline basalt from worldwide ophiolites are from Saccani (2015). Normalization values are from Sun and McDonough (1989). See Table 1 for data source.

characterized by rather variable chemical compositions and fractionation degrees (Mg#=80-52). Their compositions range from basalt to ferrobasalt (FeO_t = ~11–14 wt%), indicating that they are sub-alkaline to transitional in nature (Fig. 6a). They have TiO_2 = 0.83-2.28 wt%, P_2O_5 = 0.15-0.43 wt%, Zr = 45-196 ppm, and Y = 13-40 ppm, reminiscent of the geochemical features of plume-type MORBs (e.g., Schilling et al., 1983) generated at plume-proximal mid-ocean ridge settings. These basalts show marked enrichment in Th and Nb (Fig. 6b), as well as in Ta, Hf, and LREE. Their LREE abundance is generally lower than 100 x chondrite (e.g., Saccani and Photiades, 2005) with La_N/Yb_N=2.71-7.82.

Enriched mid-ocean ridge basalts (E-MORBs)

Middle to Upper Triassic E-MORBs are widespread in the sub-

ophiolitic mélanges of both the Mirdita-Subpelagonian and Vardar tectonic zones in the Albanide-Hellenide belt (Table 1). The E-MORB rocks consist of pillowed and massive lavas of basaltic and ferrobasaltic compositions, showing a clear sub-alkaline affinity (Fig. 6a). The E-MORBs examined in this study have rather variable chemical compositions and fractionation degrees (Mg#=75-52). Their TiO_2 (0.61-1.70 wt%) values are generally lower than those in P-MORBs, whereas their P_2O_5 (0.08-0.42 wt%), Zr (30-125 ppm), and Y (14-42 ppm) contents are comparable to those of P-MORBs. The examined E-MORBs are characterized by a moderate Th and Nb (Fig. 6b) enrichment coupled with moderate LREE/HREE (La_N/Yb_N=1.4-3.3) and LREE/MREE (La_N/Sm_N=1.0-1.7) enrichments. The overall geochemistry of these rocks is highly similar to that of modern E-MORBs (Sun and McDonough, 1989).

Normal mid-ocean ridge basalts

Middle to Upper Triassic rocks showing N-MORB chemistry are mainly found in sub-ophiolitic mélanges (Table 1). Nonetheless, they are also common in the Middle to Upper Triassic volcanic successions of the Porava unit (South Albania), where they are associated with alkaline basalts (Bortolotti et al., 2006). N-MORBs are represented by basalts, basaltic andesites, and ferrobasalts in the Mirdita-Subpelagonian zone, as well as by intensely deformed metabasalts in the sub-ophiolitic mélanges of the West Vardar zone (Saccani and Photiades, 2005; Saccani et al., 2008b).

N-MORBs display a clear sub-alkaline affinity (Fig. 6a) and are characterized by variable chemical compositions and fractionation degrees (Mg# = 70.0 - 52.0 in basalts and basaltic andesites and 58.6 - 37.0 in ferrobasalts). However, their overall geochemical features are similar to those of basalts generated at mid-ocean ridges. They have TiO_2 = 0.75 - 2.43 wt%, P_2O_5 = 0.03 - 0.30 wt%, Zr = 45 - 125 ppm, and Y = 21 - 49 ppm, and their FeO_t contents ranges from 7.19 to 11.19 wt%. They display little Th, and Nb depletion or enrichment relative to other incompatible elements (e.g., Pe-Piper, 1998; Saccani and Photiades, 2005; Bortolotti et al., 2006, 2008). In Figure 6b their Th and Nb compositions plot within the typical N-MORB values (Saccani, 2015). Although they show a wide range of compositional variations, most of the samples cluster towards more enriched compositions and partly overlap with E-MORB samples. Basalts show variable depletions in LREE with respect to MREE and HREE, as evidenced by their La_N/Sm_N (0.46 - 0.99) and La_N/Yb_N (0.38 - 1.00) ratios, in line with their N-MORB affinity.

Mantle sources and petrogenesis of basaltic rocks

Calc-alkaline basalts (CAB) display Ta, Nb, and Ti depletion, suggesting that their mantle source was already depleted as a result of previous melt extraction events (Pearce, 1982). The Th/Nb relative enrichment (Fig. 6b) suggests that these mantle sources were significantly influenced by an arc-type geochemical component (Pearce, 1982; Saccani, 2015). CAB magmatism peaked in the middle late Triassic, and was spatially and temporally associated with rift-related igneous activity producing alkaline basalts and highly enriched to depleted MORBs in the absence of an active subduction (Pe-Piper, 1998). Isotopic data suggest that CABs formed under extensional conditions from partial melting of hydrated, melt-depleted peridotites in the sub-continental mantle along the northern margin of Gondwana (Pe-Piper, 1998). Depletion and further hydration of this mantle source probably took place earlier, during a Hercynian subduction event.

Several authors have suggested, based on isotopic and trace element data, that Triassic alkaline basalts of the Albanide-Hellenide ophiolites were derived from partial melting of a plume-type source; variably enriched, subalkaline and transitional MORB rocks were derived, on the other hand, from partial melting of MORB-type mantle sources, which were influenced by different OIB-type chemical contribution (e.g., Pe-Piper, 1998; Saccani and Photiades, 2005). Partial melting that generated enriched basalts may have occurred either in the deep (garnet-facies) or in the shallow (spinel-facies) mantle (Saccani and Photiades, 2005).

To constrain the nature of the mantle source and the depth of melting during the rift-drift phases is fundamental for better reconstructing the nature of geodynamic processes occurring during the initial phases of an oceanic basin evolution. However, a rigorous quantification of the melting processes is not possible because the composition of the mantle sources can only be postulated. Saccani and Photiades (2005) have shown that small variations in the hygromagmatophile element ratios within each rock group can be observed suggesting that magmas of different rocks within each group may have been derived from mantle sources that were slightly different in composition. However, a semi-quantitative modeling of the incompatible elements can place some constraints on the mode and nature of the mantle processes at a regional scale.

We present in Figure 7 a non-modal, batch partial melting model, using Th and Nb/Yb ratio. This diagram has the advantage to combine two types of information in a single plot. The abundance of Th and Nb is used to evaluate the enrichment of the source, whereas the Nb/Yb ratio is sensitive to the presence of residual garnet in the source. In this Figure, four compositionally different mantle sources that undergo partial melting in both garnet- and spinel-facies are considered: (1) DMM source (Workman and Hart, 2005); (2) OIB-type source (Lustrino et al., 2002) with Nb = 1.5 ppm, Th = 0.18 ppm, Yb = 0.353 ppm; (3) a theoretical, slightly enriched DMM source with Nb = 0.63 ppm, Th = 0.08 ppm, Yb = 0.353 ppm; and (4) a theoretical, enriched DMM source with Nb = 0.79 ppm, Th = 0.10 ppm, Yb = 0.353 ppm. The compositions of the sources 3 and 4 were assumed based on modeling, as recently presented by Saccani et al. (2013a, 2014).

Primitive alkaline basalts are compatible with low degree partial melting (0.5 – 1%) of an OIB-type mantle source starting in the garnet-facies mantle and continuing to greater extent (2.5 – 5%) in the spinel-facies (polybaric melting). Alternatively, the chemistry of these basalts can be explained by very low degree of melting (< 0.1%) of enriched DMM sources in the garnet facies (Fig. 7). However, such a very low degree of melting is unreasonable, and therefore this hypothesis is ruled out.

The chemistry of N-MORB rocks generally points to melt generation from a depleted MORB-type mantle at shallow levels. In fact, the Th-Nb-Yb composition of primary N-MORBs can be explained by variable degrees (generally, 8 - 20 %) of partial melting of a DMM source in the spinel facies (Fig. 7).

E-MORBs have Th and Nb compositions, which are slightly enriched compared to those of N-MORBs (Fig. 6b). Therefore, it can be postulated that E-MORBs represent melts derived from more enriched sources compared to N-MORBs. The modeling in Figure 7 shows that E-MORB compositions are compatible with variable degrees (~5 - 20 %) of partial melting of a slightly enriched DMM

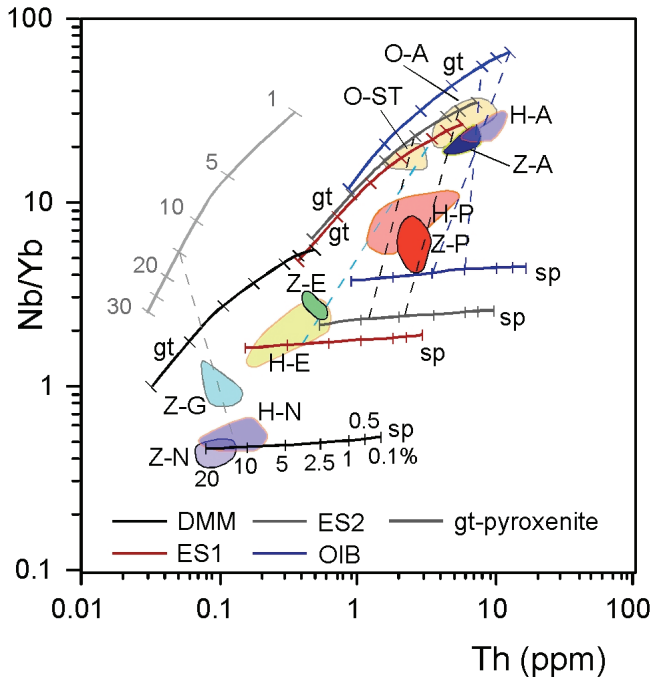

Figure 7. Plot of the Th vs. Nb/Yb compositional variations of the most primitive basalts from the Albanide-Hellenide and Zagros ophiolites, as well as batch melting curves for garnet-pyroxenite, depleted MORB mantle (DMM), and variably enriched theoretical mantle sources (ES1, ES2, OIB) in both garnet (gt) and spinel (sp) stability fields. ES1: slightly enriched source, ES2: moderately enriched source; OIB: ocean island basalt-type enriched source. Dashed lines represent the mixing lines of various melt fractions from different sources. DMM composition is from Workman and Hart (2005). Source modes, melting proportions, and partition coefficient are given in Appendix A. Ticks on the melting curves indicate the same percentages of melt fractions as shown for the sp-DMM. See text for further explanations. Abbreviations, O: Oman; H: Albanide-Hellenide; Z: Zagros; A: alkaline; ST: subalkaline-transitional; P: plume-type mid-ocean ridge (MOR); E: enriched-type MOR; N: normal-type MOR; G: garnet-influenced MOR.

source (ES1) in the spinel facies. Alternatively, E-MORBs may have been derived from polybaric melting of a DMM source, starting in the garnet facies. However, the REE compositions of these rocks (not shown) cannot be explained by this melting process alone.

P-MORBs have Th and Nb contents that plot toward the enriched values within the MORB–OIB array (Fig. 6b). Although definitely enriched in many incompatible elements, the overall chemical composition of these rocks points to a MORB-type composition. Therefore, we can rule out the possibility of their genesis from an OIB-type source. However, it can be postulated that these rocks represent melts derived from more enriched sources compared to N-MORBs and E-MORBs. The diagram in Figure 7 shows that the Th-Nb-Yb composition of primitive P-MORBs is compatible with polybaric melting of the theoretical enriched source (ES2) starting in the garnet-facies (0.5 – 2.5% melt) and continuing into the spinel facies (5 – 10% melt). Alternatively, primitive P-MORBs may have been derived from polybaric melting of a slightly enriched source (ES1). However, this hypothesis would require implausible melting proportions, that is: very low degree of melting in the garnet-facies (<0.5%), followed by a much greater extent of melting in the spinel-facies (e≥20%). In addition, the difference between hygro-magmatophile element ratios of E-MORBs and P-MORBs (not shown) suggests that they were derived from compositionally distinct mantle sources.

Continental margin ophiolites in the Zagros Belt

Regional Geology

The Zagros ophiolites crop out along the Main Zagros Thrust Zone (MZTZ) in western Iran and display a complete record of the rift-drift, seafloor spreading and subduction zone tectonic evolution of the Southern Neotethyan Ocean. The Southern Neotethyan seaway opened in the Iranian–Oman segment during the Early–Middle Triassic (Agard et al., 2005; Robertson, 2007) and evolved between Arabia and the Sanandaj-Sirjan continental block (Berberian and King, 1981; Alavi, 1994; Agard et al., 2005; Mouthereau et al., 2012). The MZTZ ophiolites include, from NW to SE, the Penjween ophiolites in Iraq (Aswad et al., 2011) and the Sarve-Abad, Kermanshah, Neyriz, and Baft ophiolites in Iran (Ghazi and Hassanipak, 1999; Babaie et al., 2006; Allahyari et al., 2010, 2014; Rajabzadeh and Dehkordi, 2013; Shafaii Moghadam et al., 2013; Saccani et al., 2013a, 2014). They are temporally equivalent to the Oman ophiolite in the south (Glennie, 2000).

From the southwest to the northeast and structurally upward, three main tectonic units occur along the MZTZ: (1) the Zagros Fold Belt, (2) the Zagros Crush zone (or High Zagros) with ophiolites, and (3) the Sanandaj-Sirjan zone (SSZ). The Zagros fold belt consists mainly of Triassic to Upper Cretaceous shelf carbonates overlain by a Paleocene to Pliocene sedimentary succession. These shelf deposits have been interpreted to represent the Arabian passive margin (Stöcklin, 1968).

The Sanandaj-Sirjan zone consists of metamorphic and sedimentary sequences (Stöcklin, 1968; Berberian and King, 1981) that are composed of a Precambrian–Paleozoic continental basement, unconformably overlain by Permian-Triassic limestones, Jurassic phyllites with metavolcanic rocks, and Barremian-Aptian limestones (Stöcklin, 1968). The Jurassic sequence is intruded by late Jurassic–late Cretaceous calc-alkaline plutons. From the Middle Jurassic to the Cretaceous, the Sanandaj-Sirjan zone represented an Andean-type margin with robust calc-alkaline magmatism (e.g., Stöcklin, 1968; Berberian and King, 1981; Ghasemi and Talbot, 2006).

The Zagros Crush zone is composed of imbricated tectonic slices including: (1) Upper Triassic–Cretaceous limestones (Bisotun unit) and radiolarites deposited on the subsiding peri-Arabian shelf (see Stöcklin, 1968 for a detailed review); (2) ophiolitic units, (3) Upper Cretaceous sedimentary rocks and calc-alkaline andesitic lavas, and (4) Eocene–Miocene sedimentary deposits and volcanic rocks. Although Sabzehei and others (1968) described the Upper Cretaceous sedimentary-volcanic sequences as part of the Crush zone, it is likely that these units belong to the Andean-type volcanic arc that developed on the southern margin of the Sanandaj-Sirjan continental block (Berberian and King, 1981) because they show a clear calc-alkaline affinity.

Ophiolitic remnants commonly occur in a tectonic mélange (Stöcklin, 1968), which includes ophiolitic subunits as isolated and

dismembered blocks. These ophiolitic subunits are represented by: (1) upper mantle peridotites; (2) ultramafic cumulates, (3) gabbroic sequences; (4) dike rocks; and (4) pillow basalts. Also included in this melange are metamorphosed lherzolites and gabbros that are intruded by numerous basaltic dikes.

Upper mantle peridotites are volumetrically the most abundant ophiolitic subunit, and are represented mainly by harzburgites and subordinate depleted lherzolites, locally intruded by pyroxenite dikes and dunite–chromitite bands (Allahyari et al., 2010; Rajabzadeh and Dehkordi, 2013; Shafaii Moghadam et al., 2013). Ultramafic cumulates have been described from the NW part of the Zagros Belt, namely in the Penjween area (Aswad et al., 2011) and in the Sarve-Abad ophiolites (Allahyari et al., 2014). These upper mantle peridotites and ultramafic cumulates are interpreted as the mantle residua and the cumulate sequence, respectively (Allahyari et al., 2010, 2014; Aswad et al., 2011; Rajabzadeh and Dehkordi, 2013; Shafaii Moghadam et al., 2013). Gabbros crop out in the Sarve-Abad, Kermanshah, Neyriz and Baft ophiolites, and are locally associated with troctolites and/or diorites and plagiogranites, as well as basaltic dikes and pillow lavas (Ghazi and Hassanipak, 1999; Babaie et al., 2006; Allahyari et al., 2010, 2014; Rajabzadeh and Dehkordi, 2013; Saccani et al., 2013a, 2014; Shafaii Moghadam et al., 2013). Gabbros and basalts mainly occur as isolated blocks in the Kermanshah, Neyriz and Baft areas, whereas an incomplete ophiolite sequence of cumulate and isotropic gabbros, microgabbros, a dike complex, a dike/pillow transition zone and pillow lavas exist in the Sarve-Abad area. Gabbroic and volcanic rocks from the MZTZ ophiolites display a wide range of geochemical affinities, ranging from E-MORB to P-MORB, and alkaline basalts and trachytes (Ghazi and Hassanipak, 1999; Babaie et al., 2006; Allahyari et al., 2010, 2014; Rajabzadeh and Dehkordi, 2013; Saccani et al., 2013a, 2014; Shafaii Moghadam et al., 2013).

Metamorphosed ophiolites have so far been described only from the Kermanshah area, where they mainly consist of foliated metagabbros crosscut by numerous metabasaltic dikes. Strongly serpentinized and foliated meta-peridotites occur below these metagabbros and consist of sub-continental meta-lherzolites, analogous to those exposed in the EL units of the Northern Apennines (Saccani et al., 2013a). Metagabbros and the associated mafic dikes have a general N-MORB affinity, but two sub-groups of rocks are also recognized: (1) rocks showing no garnet influence, and (2) rocks showing a marked garnet influence (Saccani et al., 2013a).

The Zagros ophiolites were emplaced onto the Arabian continental margin in the Campanian–Maastrichtian as a result of an arc–continent collision (Desmons and Beccaluva, 1983; Ricou, 1994; Agard et al., 2005; Dilek and Sandvol, 2009; Aswad et al., 2011; Saccani et al., 2013a). Andean-type, active margin magmatism continued along the southern edge of the Sanandaj-Sirjan block between the late Cretaceous and the Eocene, and produced calc-alkaline volcanic and plutonic rocks (Berberian and King, 1981; Agard et al., 2005; Ghasemi and Talbot, 2006). The collision of Arabia with Eurasia in the middle Miocene caused thrusting of the Eocene magmatic rocks over the ophiolite complexes.

Geochemistry

Metalherzolites, metagabbros and metabasaltic dikes

Metalherzolites of the Kermanshah ophiolite can readily be distinguished from the lherzolites representing MORB residual mantle and harzburgites, representing SSZ residual mantle in other MZTZ ophiolites (e.g., Penjween: Aswad et al., 2011; Neyriz: Babaie et al., 2006; Rajabzadeh and Dehkordi, 2013; Baft: Shafaii Moghadam et al., 2013). The Zagros metalherzolites have higher HFSE (high field strength elements) and REE concentrations (Fig. 3a) compared to the other upper mantle peridotites (Saccani et al., 2013a). Their REE values (Fig. 3a) and TiO_2, Al_2O_3 (Fig. 3b), CaO, MgO, Ni, and Cr contents are highly similar to those of the sub-continental lherzolites in the EL units of the Northern Apennines (Saccani et al., 2013a). Hence, we have interpreted these Zagros metalherzolites to represent the sub-continental mantle of the Arabian margin (Saccani et al., 2013a).

Magmatic protoliths of the metagabbros were composed of olivine-gabbros and both cumulate and isotropic gabbros, whereas those of dike intrusions in the metagabbros were made of basalts (Saccani et al., 2013a). Both isotropic metagabbros and metabasaltic dikes have relatively high contents of TiO_2, Zr, Y, and V, and relatively low Al_2O_3. These rocks are subalkaline in nature (Fig. 8a), and plot along the MORB-OIB array towards relatively depleted compositions in the discrimination diagrams (Fig. 8b). They can be subdivided, however, into distinct, N-MORB and G-MORB groups on this discrimination diagram (Fig. 8b).

The Zagros N-MORB rocks include some of the metabasaltic dikes, which display smooth MREE/HREE enrichments (Dy_N/Yb_N = 1.07 to 1.11) and marked LREE/MREE depletion (Ce_N/Dy_N = 0.68 - 0.87). In contrast, G-MORB rocks include metagabbros and some metabasaltic dikes. These G-MORB rocks display flat N-MORB normalized HFSE patterns, and chondrite-normalized REE compositions showing LREE/MREE depletion (Ce_N/Dy_N = 0.77 – 1.22), coupled with marked MREE/HREE enrichment (Dy_N/Yb_N = 1.31 – 1.44) (Saccani et al., 2013a). Such MREE/HREE enrichment is significantly higher than that of typical N-MORB (e.g., Dy_N/Yb_N=0.99, Sun and McDonough, 1989). These values are comparable to those of equivalent basalts from the EL units in the Northern Apennines.

Volcanic rocks

The Zagros E-MORBs are represented by basalts and basaltic andesites showing a sub-alkaline nature (Fig. 8a). These rocks are characterized by slightly enriched LILE/HFSE and LREE/HREE patterns. They also have a generally lower concentration of incompatible elements with respect to those of P-MORBs and alkaline rocks (e.g., Saccani et al., 2013a).

P-MORBs in the Zagros ophiolites are represented by basalts, basaltic andesites and rare andesites that generally have a sub-alkaline to transitional nature (Fig. 8a) These rocks display multi-element patterns significantly enriched in LILE and LREE compared to HFSE and HREE, respectively, with $(La/Yb)_N$ ratios ranging from 2.46 to 4.37 (see Ghazi and Hassanipak, 1999; Saccani et al., 2013a, 2014). These patterns are similar to those of typical P-MORB from modern oceanic settings (e.g., Schilling et al., 1983).

Alkaline rocks in the Zagros are represented mainly by basalts and subordinately by trachybasalts and trachytes, displaying a clear alkaline nature (Fig. 8a). Alkaline basalts show high abundance in HFSE with respect to N-MORB and display LREE/MREE and LREE/HREE enriched patterns (see Ghazi and Hassanipak, 1999; Saccani et al., 2013a, 2014). In the discrimination diagram in Figure 8b, these

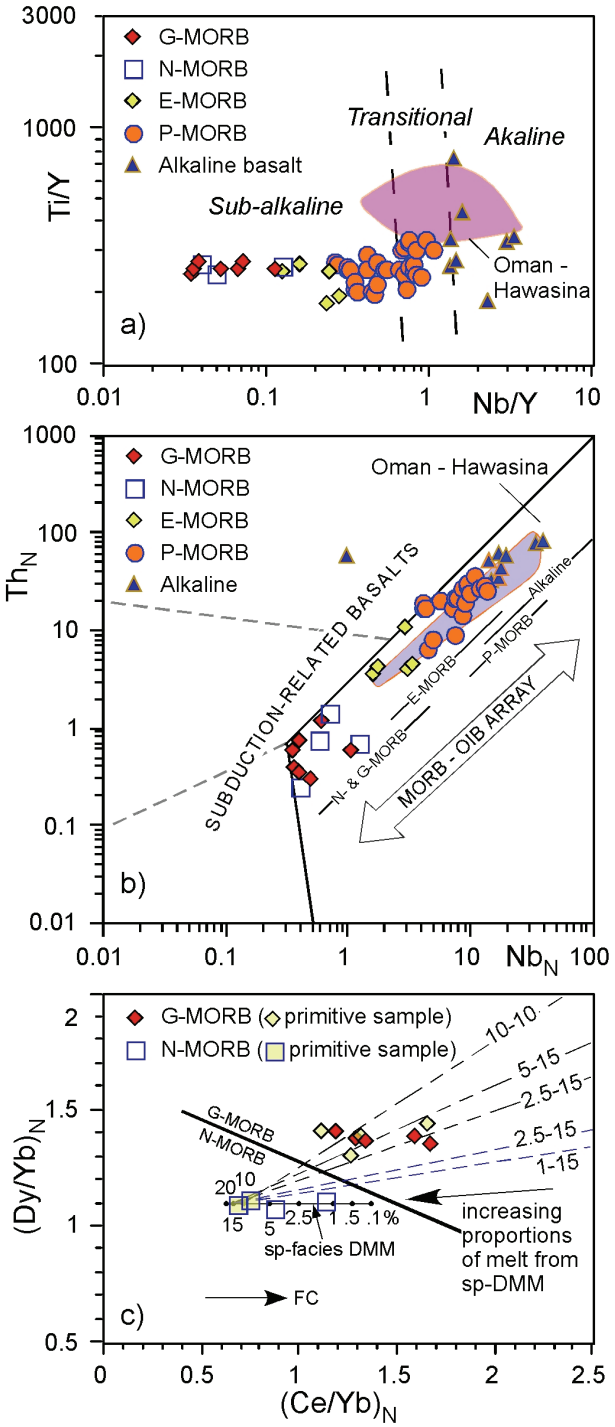

Figure 8. (a) Ti/Y vs. Nb/Y diagram (Pearce, 1982), and (b) N-MORB-normalized Th_N vs. Nb_N diagram (Saccani, 2015) for basalts and metabasalts from the Zagros ophiolites. Abbreviations, MORB: mid-ocean ridge basalt, N-: normal type, E-: enriched type, P-: plume type, G-: garnet-influenced type. Bars showing the compositional variation of N-, G-, E-, P-MORBs and alkaline basalt from worldwide ophiolites are from Saccani (2015). The compositional variation of basalts from the Hawasina Nappe from Oman ophiolites (Chauvet et al., 2011) is shown for comparison. (c) Chondrite-normalized $(Dy/Yb)_N$ vs. $(Ce/Yb)_N$ diagram (Saccani, 2015) used for discriminating between G-MORB and N-MORB. Normalization values in both panels (b) and (c) are from Sun and McDonough (1989). See Table 1 for data source.

volcanic units from the MZTZ ophiolites show a continuous compositional variation from the less enriched to the more enriched rocks. Their overall geochemistry resembles that of alkaline basalts generated in within-plate ocean island settings (OIB-type).

Mantle sources and petrogenesis of basaltic rocks

Our modeling in Figure 7 shows that N-MORB primitive metabasalts may have been derived from ~15–20% non-modal batch partial melting of a DMM source (Workman and Hart, 2005) in the spinel-facies. In contrast, the LREE/HREE (Ce/Yb) and MREE/HREE (Dy/Yb) ratios of G-MORB metagabbros and primitive metabasalts are compatible with ~10–15% partial melting of DMM with garnet-pyroxenite layers in the spinel-facies (Figs. 7 and 8c). Based on these figures we can exclude a possible genesis of G-MORBs from polybaric melting of a DMM source starting in the garnet-facies and then continuing into larger degrees of partial melting in the spinel-facies. Such melting process would result in comparatively lower MREE/HREE ratios. Alternatively, the LREE/HREE and MREE/HREE ratios of G-MORB could theoretically be generated by large degree (10–15%) of partial melting of a DMM source in the garnet-facies, followed by a lower extent of melting in the spinel facies (Fig. 7). However, this scenario is also implausible.

Many geochemical indicators (basically, highly incompatible and hygromagmatophile elements) suggest that the E-MORBs, P-MORBs, and alkaline basalts in the Sarve-Abad and Kermanshah ophiolites were originated from chemically distinct mantle sources, which started melting at different depths (see Saccani et al., 2013a, 2014). Primary E-MORBs are compatible with ~10% partial melting of a DMM source slightly enriched in LREE and incompatible elements (e.g., Th, Nb, and Ta), whereas the primary P-MORB may result from ~8% partial melting of a DMM source, significantly enriched in LREE and incompatible elements (Saccani et al., 2013a, 2014). Both these rock-types were generated from partial melting in the spinel-facies mantle. However, a very limited contribution from the garnet-facies mantle cannot be excluded. In contrast, the REE systematics displayed by the alkaline basalts suggests that primary melts of these rocks were produced by the mixing of small melt fractions (~1%) from garnet-facies with larger melt fractions (~4%) from spinel-facies, derived from partial melting of an OIB-type lherzolite mantle. The results of our modeling, using Th vs. Nb/Yb in Figure 7, are consistent with these conclusions. We can see in this figure that mantle sources that are progressively enriched in Th and Nb are required to explain the compositional variations observed from E-MORBs to P-MORBs and alkaline basalts in the Zagros ophiolites. It is worth noting that the oldest melts in the production of the Middle to Late Triassic basaltic rocks in the conjugate Oman margin show isotopic evidence for lower crustal contamination.

Discussion

Tectono-magmatic model for the rift-drift evolution of the Alpine Tethys

The rifting model proposed for the Western Tethys oceanic basin is mainly based on the reconstruction of the architecture of a deformed and metamorphosed continental margin pair, currently exposed in the Northern Apennines and Alpine Corsica. The first rifting stage started in the Middle Triassic (Fig. 9a) and was preceded by a long-

lived extensional deformation episode in the Permo-Triassic that involved the transition from a gravitational collapse of the Variscan orogenic crust to the inception of a true rift-drift phase. In the Northern Apennines, evidence for this rifting phase can be found at Punta Bianca, where a middle Triassic extensional basin sequence consisting of marine deposits intercalated with alkaline basaltic flows crops out (Stoppa, 1985). Rifting-related middle Triassic faults also occur in the continental domain of Alpine Corsica and in the Western Alps (Durand-Delga; 1984; Froitzheim and Manatschal, 1996). The geometry of these normal faults, which are west-facing in the Southalpine and Austroalpine domains (Bernoulli et al., 1979; Bertotti et al., 1993) and east-facing in the Briançonnais and Dauphinois domains (Lemoine and Trumpy, 1987), suggests that this first rifting phase was dominated by lithospheric-scale stretching by pure shear extension (Fig. 9a).

The second stage of rifting (Fig. 9b) via an asymmetric, simple-shear kinematics developed in the Middle Jurassic (e.g., Marroni et al., 1998). However, the main episode of normal faulting associated with dismemberment of the carbonate platforms took place in the early Jurassic, as documented from the Adria continental margin sequences in the Northern Apennines (Bernoulli et al., 1979), Alpine Corsica (Durand-Delga, 1984) and Western Alps (Bertotti et al., 1993). The asymmetric crustal architecture of these continental margins can be deduced from the structure of the Corsica – Northern Apennine conjugate margin pair.

Reconstruction of the OCTZ at the European margin indicates the existence of upper continental crustal rocks, displaying prominent topographic escarpments produced by high-angle normal faults (Fig. 9b1). Slide blocks in the late Cretaceous sedimentary mélanges (e.g., Casanova Complex; Marroni et al., 1998) of the EL units show, on the other hand, that the Adria rifted margin was characterized by a wide OCTZ with subcontinental lithospheric mantle and lower continental crust exhumed on the seafloor, and tectonically overlain by extensional allochthons (or extensional rafts) (Fig. 9b1). Adria represented the lower plate in this asymmetric extension scenario, whereas Europe marked the upper plate (Marroni and Pandolfi, 2007 and quoted references). The middle to late Jurassic oceanic crust formation was characterized by a magma-poor, slow-spreading mid-ocean ridge system. The more internal oceanic areas experienced limited volcanism, which took place directly on the exhumed, serpentinized mantle peridotites, gabbros, and/or ophiolitic breccias, as deduced from the IL units and the Schistes Lustrés units (Fig. 9b3). The middle to late Jurassic rift-drift stage was associated with upwelling of asthenospheric mantle in response to lithospheric extension and continental rifting. This extensional phase was associated with limited partial melting of heterogeneous mantle

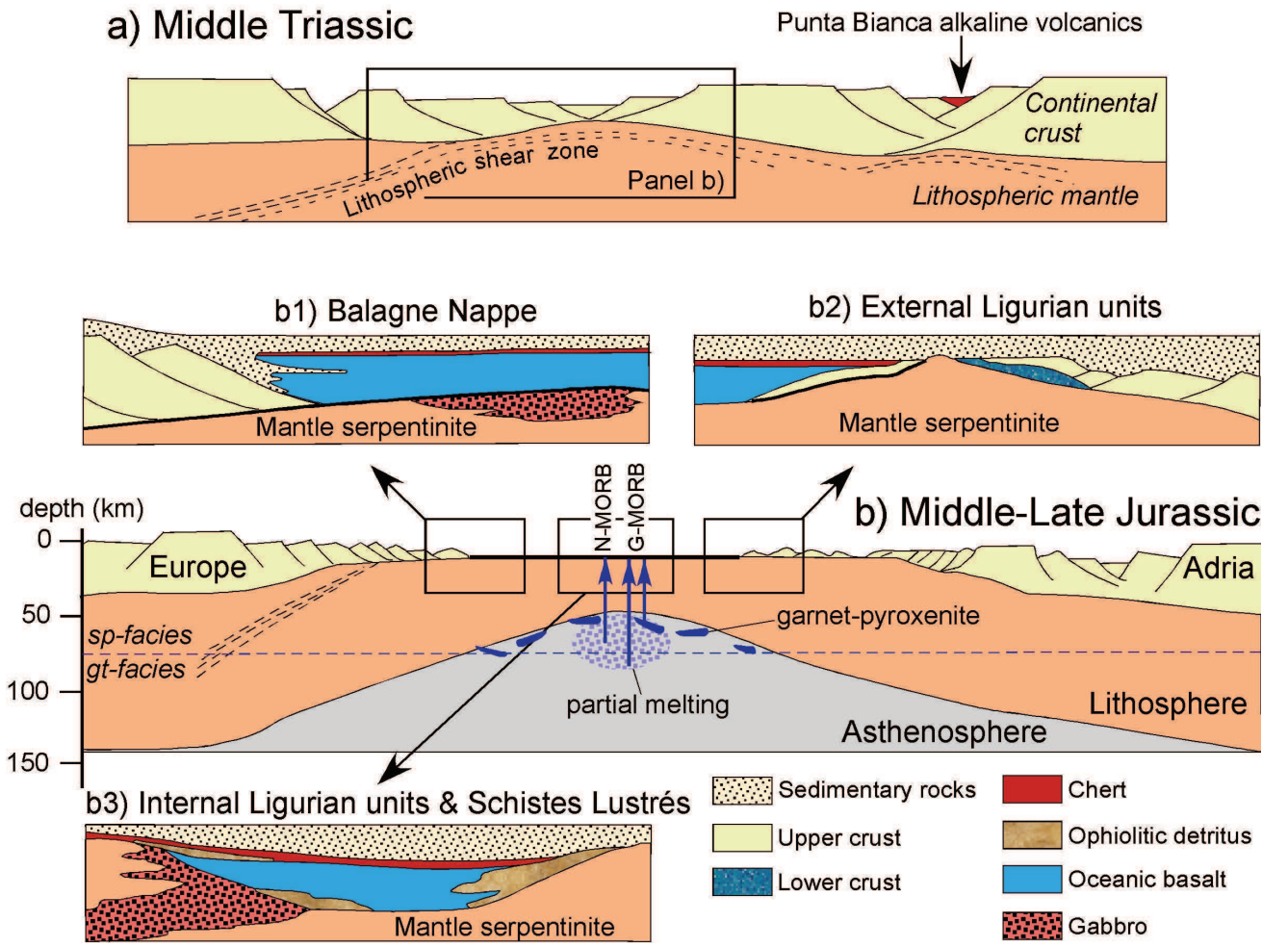

Figure 9. 2-D cartoons showing the rift-drift, tectono-magmatic evolution of the Western Tethys ocean basin (modified from Marroni and Pandolfi, 2007). Generalized stratigraphic and magmatic settings in different sections of the Western Tethys are also shown. (b1) European margin ocean-continent transition zone (OCTZ); (b2) Adria margin OCTZ; (b3) internal oceanic area.

sources, locally bearing garnet-pyroxenite relics (Fig.9b). Piccardo (2008) suggested that garnet-pyroxenite relics were left in the DMM melting source after the delamination and sinking of portions of the deep garnet-pyroxenite-bearing lithospheric mantle. This partial melting process resulted in the formation of G-MORB type rocks now exposed in the Western Tethyan ophiolites. However, a minor amount of G-MORBs may have been generated from polybaric partial melting, which started in the garnet lherzolite field and continued to higher degrees in the spinel lherzolite field. The model in Figure 9b can also explain the occurrence of volumetrically minor basalts with typical N-MORB compositions in several ophiolitic units in Alpine Corsica (Saccani et al., 2008a), as well as in the Ligurian ophiolites (Rampone et al., 2005). N-MORB primary melts could also be produced by partial melting of a pure DMM source, which did not contain garnet-bearing rocks.

Tectono-magmatic model for the rift-drift evolution of the Albanide-Hellenide belt

The Triassic rift-drift phase in the Albanide-Hellenide segment of Neotethys involved the formation of alkaline and variably enriched rocks with plume-like chemical signatures, and with calc-alkaline and shoshonitic rocks displaying SSZ-type chemical features. However, the extant geological evidence suggests that the Triassic extension and the early phase of oceanic crust formation at the OCTZ within the Albanide-Hellenide segment of Neotethys were not associated with a major mantle plume event or a contemporaneous active subduction (Pe-Piper, 1998). There is no physical evidence, such as regional doming, anomalous thermal regime, and basaltic plateaus, supporting the existence of a mantle plume in this area. In contrast, Wooler et al. (1992) have suggested that subsidence rates were small, and that there was hardly any uplift, with the rift shoulders remaining near the sea-level. The lack of magmatic evolution from more depleted to more enriched rocks that is commonly observed in plume-related magmatism, the absence of basaltic plateaus, and a relatively small volume of plume-related volcanic rocks collectively argue against the existence of a well established, long-lasting mantle plume in the region.

Calc-alkaline and shoshonitic rocks were produced, contemporaneously with the formation of alkaline basalts, between the early and late Triassic in both continental (e.g., Kremasta, Evia) and oceanic settings (e.g., Edipsos, Othrys mélange, and west Vardar zone mélange (see Table 1 for references). Magmas of these calc-alkaline rocks may have been produced by partial melting of hydrated, melt-depleted peridotite in the sub-continental mantle. Pe-Piper (1998) has suggested that a previous, Hercynian subduction event that produced an Andean-type arc on the northeastern margin of Gondwana may have played an important role in hydrating the subcontinental lithospheric mantle. Subsequent partial melting of this previously metasomatized lithospheric mantle during the Triassic extension and rifting episode would have then produced calc-alkaline and shoshonitic melts. The occurrence of similar extensional, Triassic calc-alkaline and shoshonitic rocks with similar petrogenesis has also been documented from the Southern Alps (e.g., Bonadiman et al., 1994).

We present in Figure 10 an interpretive model depicting the development of the rift-drift phases of the opening of the Albanide-Hellenide Neotethys. This model implies a heterogeneous sub-continental mantle, in which the hydrated-depleted (SSZ-type) mantle portions left by the earlier Hercynian subduction events occur in the lithospheric mantle. In contrast, the OIB-type metasomatized portions are likely to be prominent in the asthenospheric mantle (Fig. 10a). We infer that convective thinning of the lithosphere might have brought SSZ-type mantle portions of the lithospheric mantle into direct contact with asthenospheric temperatures. These SSZ mantle portions, which had their solidus lowered by the addition of volatiles, underwent partial melting leading to the eruption of calc-alkaline and shoshonitic lavas starting in the early Triassic. Meanwhile, the uprising OIB-type metasomatized asthenospheric mantle underwent polybaric partial melting, which generated alkaline basalts associated in space and time with the calc-alkaline rocks (Fig. 10b). Subsequently, during the middle and late Triassic variably enriched (E-MORB and P-MORB) and depleted (N-MORB) magmas were also generated by partial melting in the spinel-facies mantle (Fig. 10b) and were erupted at the OCTZ. We deduce that N-MORBs were generated from uprising primitive asthenospheric sources, whereas E-MORBs and P-MORBs may have been generated either from variably metasomatized mantle portions, or by complex interactions (e.g., source contamination, magma mixing, etc.) between OIB-type metasomatized mantle and primitive asthenospheric mantle. The abundance of calc-alkaline rocks

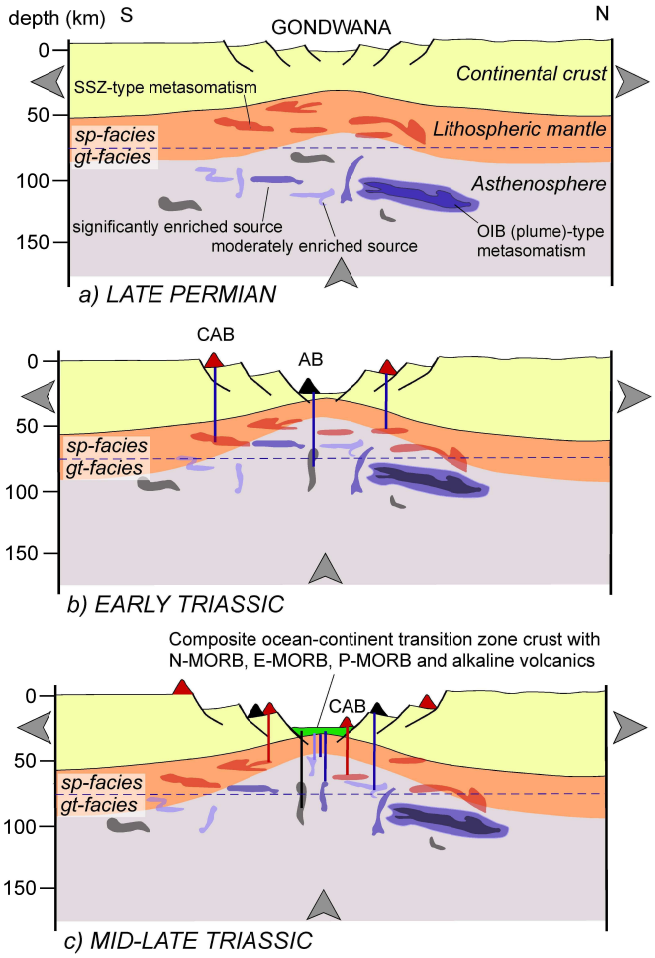

Figure 10. 2-D cartoons depicting the rift-drift, tectono-magmatic evolution of the Neotethyan Ocean in the Albanide-Hellenide sector. Abbreviations, SSZ: supra-subduction zone; OIB: ocean island basalt; CAB: calc-alkaline basalt; AB: alkaline basalt; MORB: mid-ocean ridge basalt; N-: normal-type; E-: enriched-type; P-: plume-type; sp: spinel; gt: garnet.

seems to have decreased from the middle to the late Triassic, and their occurrence appears to be more scattered compared to other rock types. This observation supports the hypothesis that SSZ-type metasomatized mantle portions were likely concentrated in the lithospheric mantle (Fig. 10a). By the end of the Triassic, the rift-drift phase gave way into seafloor spreading, and then the involvement of the sub-continental heterogeneous mantle sources in magmatism ceased. Consequently, the production of CABs, alkaline basalts, E-MORBs and P-MORBs ended in the latest Triassic. From the early Jurassic onwards, the oceanic crust was generated entirely by the eruption of N-MORBs in response to uprising of sub-oceanic primitive mantle.

Tectono-magmatic model for the rift-drift evolution of the Southern Neotethys

Triassic ophiolitic rocks found in the northwestern section of the MZTZ include: (1) metalherzolites and metagabbros, crosscut by metabasaltic dikes. Structurally and compositionally, all these rocks resemble those similar ophiolitic subunits in the Alpine-Apennine system; (2) gabbros, dikes and pillow lavas ranging in composition from E-MORB to P-MORB and alkaline basalts. Similar basalts are also abundant in the Oman – UAE ophiolites south of the Persian Gulf (Chauvet et al., 2011).

A tectono-magmatic model for explaining the tectonic evolution of the Kermanshah and Sarve-Abad ophiolites has been proposed earlier by Saccani et al. (2013a, 2014). Here, we present a refined version of this model and summarize it, with a particular focus on the rift-drift development of the Southern Neotethys (Fig. 11). Prior to the Triassic, this region was part of a coherent Arabian-Iranian continental platform (Fig. 11a). The Sanandaj-Sirjan continental block started rifting away from Arabia in the early Triassic, or perhaps earlier, in the late Permian (Ghasemi and Talbot, 2006; Azizi and Moinevaziri, 2009; Saccani et al., 2013a; Whitechurch et al., 2013). As in the Western Tethys, the Sanandaj-Sirjan block was rifted from the northern margin of Arabia through asymmetrical passive extension (Fig. 11b), as also postulated by Dilek et al. (1991) and Dilek and Thy (1998) for the Kizildag ophiolite in southern Turkey that is interpreted to be the westward continuation of the Zagros ophiolites.

This simple shear extension led to the exhumation of the sub-continental mantle of Afro-Arabia, which is now represented by the Kermanshah metalherzolites. In the meantime, upwelling of the underlying asthenosphere in response to lithospheric extension and continental rifting was associated with limited partial melting of heterogeneous mantle sources, locally bearing garnet-pyroxenite relics (Fig. 11b). Similar to the Western Tethys, this magmatic episode led to the emplacement of volumetrically small quantities of gabbros and dikes with either N-MORB or G-MORB chemistry, originated from partial melting of a pure DMM source or a DMM source bearing garnet-pyroxenite relics, respectively. However, in contrast to the Western Tethys, rift-drift and seafloor spreading stages in the Southern Neotethys were also characterized by the marked influence of OIB-type (plume-type?) components associated with the uprising of asthenospheric mantle (Fig. 11c). The polybaric partial melting of an OIB-type enriched source led to the production of alkaline basalts (Fig. 11d1), whereas the partial melting of a MORB-type mantle, which was heterogeneously modified by OIB-type components, resulted in the production of both P- and E-MORBs (Figs. 11d2, d3).

The MZTZ ophiolites represent a particular case of a Continental Margin-type ophiolite, as introduced by Dilek and Furnes (2011,

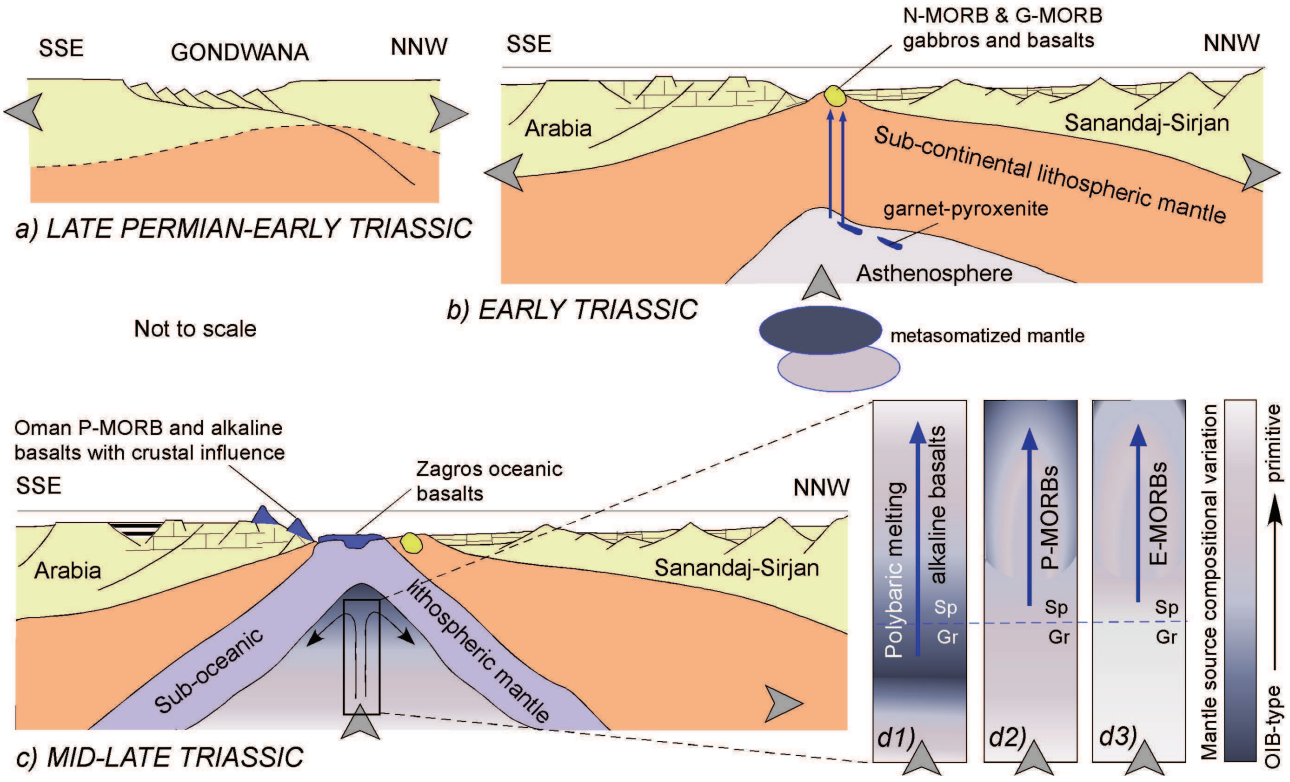

Figure 11. 2-D cartoons (modified from Saccani et al., 2013a) depicting the rift-drift, tectono-magmatic evolution of the Southern Neotethyan Ocean. Abbreviations, OIB: ocean island basalt; MORB: mid-ocean ridge basalt; N-: normal-type; E-: enriched-type; P-: plume-type; G: garnet-influenced type; Sp: spinel-facies mantle; Gt: garnet-facies mantle.

2014). The mineral chemistry, geochemistry and isotopic data (Saccani et al., 2013a, 2014) suggest that these ophiolites may in fact represent the combination of Continental Margin- and Plume-type ophiolites. However, whether chemically enriched rocks represent derivation from OIB-like asthenosphere, or from a metasomatized mantle that was previously enriched by OIB-type components is unknown. In other words, the plume-type geochemical signature displayed by the middle Triassic MZTZ and Oman basalts does not necessarily provide evidence for the concomitant existence of an active mantle plume in the northern Gondwana area. Similar to our observations in the Triassic Neotethys section of the Albanide-Hellenide orogenic belt to the west, no clear evidence has been documented supporting the existence of a mantle plume in the Arabian-Iranian area during this time. Rather, a relatively small volume of plume-related volcanic rocks argues against the existence of a mantle plume. Chauvet et al. (2011) have suggested that the plume-type signature of the conjugate Oman lithospheric mantle was produced by pervasive metasomatism that was caused by the percolation of Permian plume-related melts through it (Lapierre et al., 2004). Mantle plume activities appear to have characterized the opening of Paleotethys during the Devonian-Carboniferous (see Xiao et al., 2008 and references therein; Xu et al., 2015). Therefore, in the lack of any direct evidence, we postulate that the OIB-type geochemical signature of the MZTZ ophiolites and Oman basalts was most likely inherited from previous mantle plume activities that occurred in the same area during the early Carboniferous opening of Paleotethys (Saccani et al., 2013b).

Conclusions

Continental Margin (CM) ophiolites consist of mafic-ultramafic and sedimentary rock assemblages developed during the continental breakup and embryonic oceanic crust generation at ocean-continent transition zones (OCTZ). These ophiolites are commonly highly dismembered and occur as tectonic slices in sub-ophiolitic mélanges. Their petrogenesis generally involves small degrees of partial melting of less depleted, continental lithospheric mantle and slowly upwelling asthenospheric mantle. Compositional heterogeneities in the sub-continental mantle strongly control the igneous stratigraphy and geochemical signatures of CM ophiolites. This heterogeneity is mainly a result of previous subduction events and/or earlier plume melt interactions with host peridotites, creating mantle contingency. This phenomenon is well illustrated by the occurrence of coeval calc-alkaline basalts and shoshonites, N-MORBs, alkaline basalts, E-MORBs, and P-MORBs in the Triassic CM ophiolites in the Albanide-Hellenide belt. The inferred hydrated and depleted (SSZ-type) mantle residues in the Adria continental lithospheric mantle were the products of earlier Hercynian subduction events in the late Paleozoic. PMORBs and E-MORBs in the Zagros Continental Margin ophiolites were produced by partial melting of a MORB-type continental lithospheric mantle, which was heterogeneously modified by previous mantle plume events that took place during the early Carboniferous opening of Paleotethys.

Continental margin ophiolites are also diverse in terms of their internal structure and igneous stratigraphy. Some CM ophiolites are devoid of mantle peridotites, analogous to volcanic rifted margins. The Triassic Albanide-Hellenide ophiolites are a good example of this type, although they have volumetrically limited volcanic products and extensional calc-alkaline rocks, atypical of volcanic rifted margins. The CM ophiolites in the Zagros belt (e.g., Kermanshah ophiolite) contain continental lithospheric mantle lherzolites and gabbros crosscut by basaltic dikes and overlain by basaltic pillow lavas. This igneous stratigraphy is similar to the one displayed by the EL ophiolites (Western Tethys ophiolites) and documented from non-volcanic (or magma-poor) rifted margins. However, upwelling of an asthenospheric mantle with plume-influenced components resulted in the eruption of alkaline basalts and enriched sub-alkaline basalts in the Kermanshah CM ophiolites, a phenomenon that is unlike of magma-poor, rifted margins. These findings from the three cases of CM ophiolites we report in this study indicate that the fossil examples of the OCTZ crustal architecture and magmatic record do not invariably match with those of the two end-members of rifted margins (volcanic vs. non-volcanic). The rates and kinematics of rifting, the existence (or not) of an active plume, upwelling rates of the asthenospheric mantle in response to lithospheric thinning, and the mode and scale of mantle heterogeneity caused by previous subduction and plume events strongly affect the rift architecture and the geochemical character of an OCTZ lithosphere.

Acknowledgements

Special thanks go to V. Bortolotti, G. Principi (University of Florence, Italy), M. Chiari (CNR-IGG, Florence, Italy), A. Festa (University of Torino, Italy), A. Photiades (I.G.M.E., Athens, Greece), I. Prempti, F. Mustafa (GjeoAlba, Tirane, Albania), M. Shallo (Chicago, USA), I. Milushi (Tirana Polytechnic University, Albania), and K. Allahyari (Shahid Beheshti University, Tehran, Iran) for their assistance during fieldwork in various ophiolites and ophiolite belts covered in this study. We would also like to thank H. Furnes and Ö. Elitok for their constructive and insightful reviews of our manuscript.

References

Agard, P., Omrani, L., Jolivet, L. and Mouthereau, F., 2005, Convergence history across Zagros (Iran): constraints from collisional and earlier deformation: International Journal of Earth Science (Geologische Rundschau), v. 94, pp. 401-419.

Alavi, M., 1994. Tectonics of the Zagros orogenic belt of Iran: new data and interpretations: Tectonophysics, v. 229, pp. 211-238.

Allahyari, K., Saccani, E., Pourmoafi, M., Beccaluva, L. and Masoudi, F., 2010, Petrology of mantle peridotites and intrusive mafic rocks from the Kermanshah ophiolitic complex (Zagros belt, Iran): Implications for the geodynamic evolution of the Neo-Tethyan oceanic branch between Arabia and Iran: Ofioliti, v. 35, pp. 71-90.

Allahyari, K., Saccani, E., Rahimzadeh, B. and Zeda, O., 2014, Mineral chemistry and petrology of highly magnesian ultramafic cumulates from the Sarve-Abad (Sawlava) ophiolites (Kurdistan, NW Iran): New evidence for boninitic magmatism in intra-oceanic fore-arc setting in the Neo-Tethys between Arabia and Iran: Journal of Asian Earth Sciences, v. 79: pp. 312-328, doi: 10.1016/j.jseaes.2013.10.005.

Anonymous, 1972, Penrose field conference on Ophiolites: Geotimes, v. 17, pp. 24-25.

Asvesta, A., 1992, Magmatism and associated sedimentation during the first stage of the opening of the Vardar oceanic basin in the Triassic time: Ph.D. Thesis, University of Thessaloniki, 439 p.

Aswad, K.J.A., Aziz, N.R.H. and Koy, H.A., 2011, Cr-spinel compositions in serpentinites and their implications for the petrotectonic history of the Zagros Suture Zone, Kurdistan Region, Iraq: Geological Magazine, v. 148, pp. 802-818, doi:10.1017/S0016756811000422.

Azizi, H. and Moinevaziri, H., 2009, Review of the tectonic setting of Cretaceous to Quaternary volcanism in northwestern Iran: Journal of Geodynamics, v. 47, pp. 167-179.

Babaie, H., Babaei, A., Ghazi, A.M. and Arvin, M., 2006, Geochemical, $^{40}Ar/^{39}Ar$ age, and isotopic data for crustal rocks of the Neyriz ophiolite,

Iran: Canadian Journal of Earth Sciences, v. 43, pp. 57-70, doi:10.1139/e05-111.

Balestro, G., Festa, A., Dilek, Y. and Tartarotti, P., 2015, Pre-Alpine extensional tectonics of a peridotite-localized oceanic core complex in the Late Jurassic, high pressure Monviso ophiolite (Western Alps): Episodes, v. 38, no. 4, pp. 266-282, doi:10.18814/epiiugs/2015/v38i4/82421.

Beaumont, C. and Ings, S.J., 2012, Effect of depleted continental lithosphere counterflow and inherited crustal weakness on rifting of the continental lithosphere: general results: Journal of Geophysical Research, v.117, B08407, http://dx.doi.org/10.1029/2012JB009203.

Bébien, J., Blanchet, R., Cadet, J.-P., Charvet, J., Chorowicz, J., Lapierre, H. and Rampnoux, J.-P., 1978, Le volcanisme Triasique des Dinarides en Yougoslavie: sa place dans l'évolution Géotectonique Peri-Méditerranéenne: Tectonophysics, v. 47, pp. 159-176.

Berberian, M. and King, G.C.P., 1981, Towards a palaeogeography and tectonic evolution of Iran: Canadian Journal of Earth Sciences, v. 18, pp. 210-265.

Bernoulli, D, Kälin, O and Patacca, E., 1979, A sunken continental margin of Tethys: the Northern and central Apennines, in Beaudoin, B. and Purser, B.H., eds, Sédimentation Jurassique W-européen: ASF Publication Spéciale, v. 1, pp. 197-210.

Bertotti, G, Picotti, V, Bernoulli, D and Castellarin, A., 1993, From rifting to drifting: tectonic evolution of the South-Alpine upper crust from the Triassic to the Early Cretaceous: Sedimentary Geology, v. 86, pp. 53-76.

Bonadiman, C., Coltorti, M. and Siena, F., 1994, Petrogenesis and T-fO2 estimates of Mt.Monzoni complex (Central Dolomites, Southern Alps): a Triassic shoshonotic intrusion in a transcurrent geodynamic setting: European Journal of Mineralogy, v. 6, pp. 943-966.

Bortolotti, V., Chiari, M., Kodra, A., Marcucci, M., Mustafa, F., Principi, G. and Saccani, E., 2004, New evidence for Triassic MORB magmatism in the northern Mirdita Zone ophiolites (Albania): Ofioliti, v. 29, pp. 243-246.

Bortolotti, V., Chiari, M., Kodra, A., Martucci, M., Marroni, M., Mustafa, F., Prela, M., Pandolfi, L., Principi, G. and Saccani, E., 2006, Triassic MORB magmatism in the southern Mirdita zone (Albania): Ofioliti, v. 31, pp. 1-9.

Bortolotti, V., Chiari, M., Marcucci, M., Photiades, A., Principi, G. and Saccani, E., 2008, New geochemical and age data on the ophiolites from the Othrys area (Greece): Implication for the Triassic evolution of the Vardar ocean: Ofioliti, v. 33, pp. 135-151.

Bortolotti, V., Carras, N., Chiari, M., Fazzuoli, M., Marcucci, M., Nirta, G., Principi, G. and Saccani, E., 2009, The ophiolite-bearing melange in the Early Tertiary Pindos Flysch of Etolia (central Greece): Ofioliti, v. 34, pp. 83-94.

Bortolotti, V., Chiari, M., Marroni, M., Pandolfi, L., Principi, G. and Saccani, E., 2013, Geodynamic evolution of the ophiolites from Albania and Greece (Dinaric-Hellenic belt): One, two or more oceanic basins?: International Journal of Earth Sciences, v. 102, pp. 783-811, doi:10.1007/s00531-012-0835-7.

Capedri, S., Toscani, L., Grandi, R., Venturelli, G., Papanikolaou, D. and Skarpelis, N.S., 1997, Triassic volcanic rocks of some type-localities from the Hellenides: Chemie der Erde, v. 57, pp. 257-276.

Chauvet F., Lapierre H., Maury R. C., Bosch D., Basile C., Cotten J., Brunet P. and Campillo S., 2011, Triassic alkaline magmatism of the Hawasina Nappes: Post-breakup melting of the Oman lithospheric mantle modified by the Permian Neotethyan Plume: Lithos, v. 122, pp. 122-136.

Chenin, P. and Beaumont, C., 2013, Influence of offset weak zones on the development of rift basins: activation and abandonment during continental extension and breakup: Journal of Geophysical Research, v. 118, pp. 1698-1720, http://dx.doi.org/10.1002/jgrb.50138.

Chiari, M., Marcucci, M., Cortese, G., Ondrejickova, A. and Kodra, A., 1996, Triassic radiolarian assemblages in the Rubik area and Cukali zone, Albania: Ofioliti, v. 21, pp. 77-84.

Chiari, M., Bortolotti, V., Marcucci, M., Photiades, A., Principi, G. and Saccani, E., 2012, Radiolarian biostratigraphy and geochemistry of the Koziakas massif ophiolites (Greece): Bulletin de la Societé géologique de France, v. 183, pp. 287-306.

Coffin, M.F. and Eldholm. O., 1994, Large igneous provinces: Crustal structure, dimensions, and external consequences: Reviews of Geophysics, v. 32, pp. 1-36.

Coffin, M.F., Pringle, M.S., Duncan, R.A., Gladczenko, T.P., Storey, M., Mueller, R.D. and Gahagan L.A., 2002, Kerguelen hotspot magma output since 130 Ma. Journal of Petrology, v. 43, pp. 1121-1139.

Coleman, R.G., 1971, Plate tectonic emplacement of upper mantle peridotites along continental edges: Journal of Geophysical Research, v. 76, pp. 1212-1222, doi: 10.1029/JB076i005p01212.

Compagnoni, R., 2003, HP metamorphic belt of the western Alps: Episodes, v. 26, pp. 200-204.

Cortesogno, L. and Gaggero, L., 1992, The basaltic dikes in the Bracco gabbroic massif: petrology of the earliest phases of basaltic activity in the northern Apennines ophiolites: Ofioliti, v. 17, pp. 183-198.

Desmons, J. and Beccaluva, L., 1983, Mid-ocean ridge and island-arc affinities in ophiolites from Iran: palaeographic implications: Chemical Geology, v. 39, pp. 39-63.

Desmurs, L., Muntener, O. and Manatschal, G., 2002, Onset of magmatic accretion within a magma-poor rifted margin: a case study from the Platta ocean-continent transition, eastern Switzerland: Contribution to Mineralogy and Petrology, v. 144, pp. 365-382, doi 10.1007/s00410-002-0403-4.

Dewey, J.F., and Bird, J.M., 1971, The origin and emplacement of the ophiolite suite: Appalachian ophiolites in Newfoundland: Journal of Geophysical Research, v. 76, pp. 3179-3206, doi: 10.1029/JB076i014p03179.

Dilek, Y., 2003a, Ophiolite concept and its evolution: Geological Society of America Special Paper, v. 373, pp. 1–16.

Dilek, Y., 2003b, Ophiolite pulses, plumes and orogeny: Geological Society, London, Special Publications, v. 218, p. 9-19.

Dilek, Y., Moores, E.M., Delaloye, M. and Karson, J.A., 1991, Amagmatic extension and tectonic denudation in the Kizildag Ophiolite, southern Turkey: Implications for the evolution of Neotethyan oceanic crust: Ministry of Petroleum and Minerals, Sultanate of Oman, pp. 485-500.

Dilek, Y. and Rowland, J.C., 1993, Evolution of a conjugate passive margin pair in Mesozoic southern Turkey: Tectonics, v. 12, pp. 954-970, doi: 10.1029/93TC01060.

Dilek, Y. and Thy, P., 1998, Structure, petrology and seafloor spreading tectonics of the Kizildag ophiolite, Turkey: Geological Society, London, Special Publications, v. 148, p. 43-69.

Dilek, Y., Moores, E.M., and Furnes, H., 1998, Structure of modern oceanic crust and ophiolites and implications for faulting and magmatism at oceanic spreading centers: American Geophysical Union Monograph, v. 106, p. 219-265.

Dilek, Y., Thy, P., Hacker, B., and Grundvig, S., 1999, Structure and petrology of Tauride ophiolites and mafic dike intrusions (Turkey): Implications for the Neotethyan ocean: Geological Society of America Bulletin, v. 111, p. 1192-1216.

Dilek, Y. and Robinson, P.T., 2003. Ophiolites in Earth History: Introduction: Geological Society, London, Special Publication, v. 218, pp. 1-8, doi: 10.1144/gsl.sp.2003.218.01.01.

Dilek, Y., Furnes, H., and Shallo, M., 2007, Suprasubduction zone ophiolite formation along the periphery of Mesozoic Gondwana: Gondwana Research, v. 11, p. 435-475.

Dilek, Y., Furnes, H., and Shallo, M., 2008, Geochemistry of the Jurassic Mirdita Ophiolite (Albania) and the MORB to SSZ evolution of a marginal basin oceanic crust: Lithos, v. 100, pp. 174-209.

Dilek, Y. and Sandvol, E., 2009, Seismic structure, crustal architecture and tectonic evolution of the Anatolian-African Plate Boundary and the Cenozoic Orogenic Belts in the Eastern Mediterranean Region: Geological Society, London, Special Publications, v. 327, p. 127-160.

Dilek, Y. and Furnes, H., 2011, Ophiolite genesis and global tectonics: Geochemical and tectonic fingerprinting of ancient oceanic lithosphere: Geological Society of America Bulletin, v. 123, pp. 387-411, doi: 10.1130/B30446.1.

Dilek, Y. and Furnes, H., 2014, Ophiolites and their origins: Elements, v. 10, pp. 93-100, doi: 10.2113/gselements.10.2.93.

Durand-Delga, M., 1984, Principaux traits de la Corse alpine et corrélations avec les Alpes ligures: Memorie della Società Geologica Italiana, v. 28, pp. 285-329.

Eldholm, O., Gladczenko, T.P., Skogseid, J., and Planke, S., 2000, Atlantic volcanic margins: a comparative study: Geological Society of London Special Publication, v. 167, pp. 411-428.

Festa, A., Balestro, G., Dilek, Y., and Tartarotti, P., 2015, A Jurassic Oceanic Core Complex in the High-P Monviso Ophiolite (Western Alps, NW Italy): Lithosphere, v. 7, No. 6, pp. 646-652.

Froitzheim, N. and Manatschal, G., 1996, Kinematics of Jurassic rifting, mantle exhumation, and passive-margin formation in the Austroalpine and Penninic nappes (eastern Switzerland): Geological Society of America Bulletin, v. 108, pp. 1120-1133.

Ghasemi, A. and Talbot, C.J., 2006, A new tectonic scenario for the Sanandaj–Sirjan Zone (Iran): Journal of Asian Earth Sciences, v. 26, pp. 683-693.

Ghazi, A.M. and Hassanipak, A.A., 1999, Geochemistry of subalkaline and alkaline extrusives from the Kermanshah ophiolite, Zagros Suture Zone, western Iran: implications on Tethyan plate tectonics: Journal of Asian Earth Science, v. 17, pp. 319-332.

Glennie, K.W., 2000, Cretaceous tectonic evolution of Arabia's eastern plate margin: a tale of two oceans: SEPM (Society for Sedimentary Geology) Special Publication, v. 69, pp. 9-20.

Hinz, K., 1981, A hypothesis on terrestrial catastrophes: wedges of very thick oceanward dipping layers beneath passive continental margins - their origin and paleoenvironmental significance: Geologisches Jahrbuch Reihe E, pp. 3-28.

Huismans, R.S. and Beaumont, C., 2007, Roles of lithospheric strain softening and heterogeneity in determining the geometry of rifts and continental margins: Geological Society London Special Publication, v. 282, pp. 111-138.

Jones, G. and Robertson, A.H.F., 1991, Tectono-stratigraphic evolution of the Mesozoic Pindos ophiolite and related units, northwestern Greece: Journal of the Geological Society London, v. 148, pp. 267-288.

Jones, C.H., Wernicke, B.P., Farmer, G.L., Walker, J.D., Coleman, D.S., McKenna, L.W. and Perry, F.V., 1992, Variations across and along a major continental rift: an interdisciplinary study of the Basin and Range province, western USA: Tectonophysics, v. 213, pp. 57-96.

Kerr, A.C., 1994, Lithospheric thinning during the evolution of continental large igneous provinces: A case study from the North Atlantic Tertiary Province. Geology, v. 22, pp. 1027-1030.

Kusznir, N.J. and Karner, G.D., 2007, Continental lithospheric thinning and breakup in response to upwelling divergent mantle flow: application to the Woodlark, Newfoundland and Iberia margins: Geological Society London Special Publication, v. 282, pp. 389-419.

Lagabrielle, Y. and Cannat, M., 1990, Alpine Jurassic ophiolites resemble the modern central Atlantic basement: Geology, v. 18, pp. 319-322.

Lapierre, H., Samper, A., Bosch, D., Maury, R.C., Béchennec, F., Cotten, J., Demant, A., Brunet, P., Keller, F. and Marcoux, J., 2004, The Tethyan plume: geochemical diversity of Middle Permian basalts from the Oman rifted margin: Lithos, v. 74, pp. 167-198.

Lemoine, M. and Trumpy, R., 1987, Pre-oceanic rifting in the Alps: Tectonophysics, v. 133, pp. 305-320.

Lister, G.S., Etheridge, M.A. and Symonds, P.A., 1991, Detachment models for the formation of passive continental margins: Tectonics, v. 10, pp. 1038-1064.

Lister, G., and Forster, M., 2009, Tectonic mode switches and the nature of orogenesis: Lithos, v. 113, pp. 274-291, doi: 10.1016/j.lithos.2008.10.024.

Liu, F., Yang, J.-S., Dilek, Y., Xu, Z.-Q., Xu, X.-Z., Liang, F.-H., Chen, S.-Y., and Lian, D.-Y., 2015, Geochronology and geochemistry of basaltic lavas in the Dongbo and Purang ophiolites of the Yarlung-Zangbo Suture zone: Plume-inûuenced continental margin-type oceanic lithosphere in southern Tibet: Gondwana Research, v. 27, p. 701-718.

Liu, Y., Gao, S., Lee, C.-T.A., Hu, S., Liu, X., and Yuan, H., 2005, Melt–peridotite interactions: Links between garnet pyroxenite and high-Mg# signature of continental crust: Earth and Planetary Science Letters, v. 234, pp. 39-57.

Lustrino, M., Melluso, L. and Morra, V., 2002, The transition from alkaline to tholeiitic magmas: a case study from the Orosei-Dorgali Pliocene volcanic district (NE Sardinia, Italy): Lithos, v. 63, pp. 83-113.

Malavieille, J., Chemenda, A. and Larroque, C., 1998, Evolutionary model for Alpine Corsica: mechanism for ophiolite emplacement and exhumation of high-pressure rocks: Terra Nova, v. 10, pp. 317-322.

Manatschal, G., and Müntener, O., 2009, A type sequence across an ancient magma-poor ocean-continent transition: The example of the western Alpine Tethys ophiolites: Tectonophysics, v. 473, pp. 4-19, doi: 10.1016 j.tecto.2008.07.021.

Marroni, M., Molli, G., Montanini, A. and Tribuzio, R., 1998, The association of continental crust rocks with ophiolites in the Northern Apennines (Italy): implications for the continent-ocean transition in the Western Tethys: Tectonophysics, v. 292, pp. 43-66.

Marroni, M., Molli, G., Ottria, G. and Pandolfi, L., 2001, Tectono-sedimentary evolution of the External Liguride Units (Northern Apennine, Italy): insights in the precollisional history of a fossil ocean-continent transition zone: Geodinamica Acta, v. 14, pp. 307-320.

Marroni, M. and Pandolfi, L., 2003, Deformation history of the ophiolite sequence from Balagne Nappe (Northern Corsica): insights in the tectonic evolution of the alpine Corsica: Geological Journal, v. 38, pp. 67-83.

Marroni, M., Pandolfi. L. and Meneghini F., 2004, From accretion to exhumation in a fossil accretionary wedge: a case history from Gottero Unit (Northern Apennines, Italy): Geodinamica Acta, v. 17, pp. 41-53.

Marroni, M. and Pandolfi, L., 2007, The architecture of the Jurassic Ligure-Piemontese oceanic basin: tentative reconstruction along the Northern Apennine - Alpine Corsica transect: International Journal of Earth Sciences, v. 96, pp. 1059-1078.

Marroni, M., Meneghini, F., and Pandolfi, L., 2010, Anatomy of the Ligure-Piemontese subduction system: evidences from Late Cretaceous-Middle Eocene convergence-related deposits from Northern Apennines (Italy): International Geology Review, v. 10-12, pp. 1160-1192.

Meneghini, F., Marroni, M., Moore, J.C., Pandolfi, L. and Rowe, C.D., 2009, The process of underplating in the geologic record: structural diversity between the Franciscan Complex (California), the Kodiak Complex (Alaska) and the Internal Ligurian Units (Italy): Geological Journal, v. 44, pp. 126-152.

Menzies, M.A., Klemperer, S.L., Ebinger, C.J. and Baker, J., 2002, Characteristics of volcanic rifted margins: Geological Society of America Special Paper, v. 362, pp. 1-14.

Monjoie, P., Lapierre, H., Tashko, A., Mascle, G.H., Dechamp, A., Muceku, B. and Brunet, P., 2008, Nature and origin of the Triassic volcanism in Albania and Othrys: a key to understanding the Neotethys opening? Bulletin de la Societé géologique de France, v. 179, pp. 411-425.

Montanini, A., Tribuzio, R. and Anczkiewicz, R., 2006, Exhumation history of a garnet pyroxenite bearing mantle section from a continent–ocean transition (Northern Apennine ophiolites, Italy): Journal of Petrology, v. 47, pp. 1943-1971, doi:10.1093/petrology/egl032.

Montanini, A., Tribuzio, R. and Vernia, L., 2008. Petrogenesis of basalts and gabbros from an ancient continent–ocean transition (External Liguride ophiolites, Northern Italy): Lithos, v. 101, pp. 453-479, doi: 10.1016/j.lithos.2007.09.007.

Mouthereau, F., Lacombe, O. and Vergés, J., 2012, Building the Zagros collisional orogen: Timing, strain distribution and the dynamics of Arabia/Eurasia plate convergence: Tectonophysics, v. 532–535, pp. 27-60, http://dx.doi.org/10.1016/j.tecto.2012.01.022.

Mutter, J.C., Talwani, M. and Stoffa, P.L., 1982, Origin of seaward-dipping reflectors in oceanic crust off the Norwegian margin by "subaerial sea-floor spreading": Geology, v. 10, pp. 353-357.

Ozsvart, P., Dosztaly, L., Migiros, G., Tselepidis, V. and Kovacs, S., 2011, New radiolarian biostratigraphic age constraints on Middle Triassic basalts and radiolarites from the Inner Hellenides (Northern Pindos and Othris Mountains, Northern Greece) and their implications for the geodynamic evolution of the early Mesozoic Neotethys: International Journal of Earth Science, v. 101, pp. 1487-1501, doi:10.1007/s00531-010-0628-9.

Pamiç, J., 1984, Triassic magmatism of the Dinarides in Yugoslavia: Tectonophysics, v. 109, pp. 273-307.

Pearce, J.A., 1982, Trace element characteristics of lavas from destructive plate boundaries: in Thorpe, R.S., ed, Andesites: New York, J. Wiley and Sons, pp. 525-548.

Pe-Piper, G., 1983, The Triassic volcanic rocks of Tyros, Zarouhla, Kalamae, and Epidavros, Peloponnese, Greece: Schweizerische Mineralogische und Petrographische Mitteilungen, v. 63, pp. 249-266.

Pe-Piper, G., 1998, The nature of Triassic extension-related magmatism in Greece: Evidence from Nd and Pb isotope geochemistry: Geological Magazine, v. 135, pp. 331-348.

Pe-Piper, G. and Panagos, A.G., 1989, Geochemical characteristics of the Triassic volcanic rocks of Evia: Petrogenetic and tectonic Implications: Ofioliti, v. 14, pp. 33-50.

Pe-Piper, G. and Mavroniki, M., 1990, Petrology, geochemistry and regional significance of the Triassic volcanic rocks of the Western Parnassos isopic zone of Greece: Ofioliti, v. 15, pp. 269-285.

Pe-Piper, G. and Piper, D.J.W., 1991, Early Mesozoic oceanic subduction-related volcanic rocks, Pindos basin, Greece: Tectonophysics, v. 192, pp. 273-292.

Pe-Piper, G. and Kotopouli, C.N., 1991, Geochemical characteristics of the Triassic igneous rocks of the Island of Samos, Greece: Neues Jahrbruch fur Mineralogie Abhandlungen, v. 162, pp. 135-150.

Péron-Pinvidic, G. and Manatschal, G., 2009, The final rifting evolution at deep magma-poor passive margins from Iberia-Newfoundland: A new point of view: International Journal Earth Science, v. 98, pp. 1581-97.

Photiades, A., Saccani, E. and Tassinari, R., 2003, Petrogenesis and tectonic setting of volcanic rocks from the Subpelagonian ophiolitic mélange in the Agoriani area (Othrys, Greece): Ofioliti, v. 28, pp. 121-135.

Piccardo, G.B., 2008, The Jurassic Ligurian Tethys, a fossil ultraslow-spreading ocean: the mantle perspective: Geological Society of London Special Publication, v. 293, pp. 11-34.

Planke, S., Skogseid, J., and Eldholm, O., 1991, Crustal structure off Norway, 62° to 70° north: Tectonophysics, v. 189, pp. 91-107.

Rajabzadeh, M.A. and Dehkordi, T.N., 2013, Investigation on mantle peridotites from Neyriz ophiolite, south of Iran: geodynamic signals: Arabian Journal of Geoscience, v. 6, pp. 4445-4461, doi: 10.1007/s12517-012-0687-2.

Rampone, E., Hofmann, A.W., Piccardo, G.B., Vannucci, R., Bottazzi, P. and Ottolini, L., 1995, Petrology, mineral and isotope geochemistry of the External Liguride peridotites (Northern Apennines, Italy): Journal of Petrology, v. 36, pp. 81-105.

Rampone, E., Hofmann, A.W. and Raczek, I., 1998, Isotopic constraints within the Internal Liguride ophiolites (N. Italy): The lack of a genetic mantle-crust link: Earth and Planetary Science Letters, v. 163, pp.175-189.

Rampone, E., Romairone, A., Abouchami, W., Piccardo, G.B., and Hofmann, A.W., 2005, Chronology, petrology, and isotope geochemistry of the Erro-Tobbio peridotites (Ligurian Alps, Italy): Records of late Palaeozoic lithospheric extension: Journal of Petrology, v. 46, pp. 799-827, doi: 10.1093/petrology/egi001.

Rampone, E. and Hofmann, A.W., 2012, A global overview of isotopic heterogeneities in the oceanic mantle: Lithos, v. 148, pp. 247-261, doi:10.1016/j.lithos.2012.06.018.

Ricou, L.E., 1994, Tethys reconstructed - plates, continental fragments and their boundaries since 260-Ma from Central-America to South-eastern Asia: Geodinamica Acta, v. 7, pp. 169-218.

Robertson, A.H.F., 2007, Overview of tectonic settings related to the rifting and opening of Mesozoic ocean basins in the Eastern Tethys: Oman, Himalayas and Eastern Mediterranean regions: Geological Society, London Special Publication, v. 282, pp. 325-389.

Robertson, A.H.F., Clift, P.D.C., Degnan, P.J. and Jones, G., 1991, Palaeogeographic and palaeotectonic evolution of the Eastern Mediterranean Neotethys: Palaeogeography, Palaeoclimatology, Palaeoecology, v. 87, pp. 289-343.

Royden, L. and Keen, C.E., 1980, Rifting processes and thermal evolution of the continental margin of eastern Canada determined from subsidence curves: Earth and Planetary Science Letters, v. 51, pp. 343-361.

Sabzehei, M., Gourabjiri, A. and Eslamdoust, F., 1968, Geological map of Paweh and West Paweh, 1/100.000 scale: Geological Survey of Iran, Tehran.

Saccani, E., 2015, A new method of discriminating different types of post-Archean ophiolitic basalts and their tectonic significance using Th-Nb and Ce-Dy-Yb systematics: Geoscience Frontiers, v.6, pp. 481-501, http://dx.doi.org/10.1016/j.gsf.2014.03.006.

Saccani, E., Padoa, E. and Tassinari, R., 2000, Preliminary data on the Pineto gabbroic massif and Nebbio Basalts: progress toward the geochemical characterization of Alpine Corsica Ophiolites: Ofioliti, v. 25, pp. 75-85.

Saccani, E., Photiades, A. and Padoa, E., 2003a, Geochemistry, petrogenesis and tectono-magmatic significance of volcanic and subvolcanic rocks from the Koziakas Mélange (Western Thessaly, Greece): Ofioliti, v. 28, pp. 43-57.

Saccani, E., Padoa, E. and Photiades, A., 2003b, Triassic mid-ocean ridge basalts from the Argolis Peninsula (Greece): new constraints for the early oceanization phases of the Neo-Tethyan Pindos basin: Geological Society London Special Publications, v. 218, pp. 109-127.

Saccani, E. and Photiades, A., 2005, Petrogenesis and tectono-magmatic significance of volcanic and subvolcanic rocks in the Albanide-Hellenide ophiolitic mélanges: The Island Arc, v. 14, pp. 494-516.

Saccani, E., Principi, G., Garfagnoli, F. and Menna, F., 2008a, Corsica ophiolites: Geochemistry and petrogenesis of basaltic and metabasaltic rocks: Ofioliti, v. 33, pp. 187-207.

Saccani, E., Photiades, A., Santato, A. and Zeda, O., 2008b, New evidence for supra-subduction zone ophiolites in the Vardar zone from the Vermion massif (northern Greece): Implication for the tectono-magmatic evolution of the Vardar oceanic basin: Ofioliti, v. 33, pp. 65-85.

Saccani, E., Allahyari, K., Beccaluva, L. and Bianchini, G., 2013a, Geochemistry and petrology of the Kermanshah ophiolites (Iran): Implication for the interaction between passive rifting, oceanic accretion, and plume-components in the Southern Neo-Tethys Ocean: Gondwana Research, v. 24, pp. 392-411, http://dx.doi.org/10.1016/j.gr.2012.10.009.

Saccani, E., Azimzadeh, Z., Dilek, Y. and Jahangiri, A., 2013b, Geochronology and Petrology of the Early Carboniferous Misho Mafic Complex (NW Iran), and Implications for the Melt Evolution of Paleo-Tethyan Rifting in Western Cimmeria: Lithos, v. 162-163, pp. 264-278.

Saccani, E., Allahyari, K. and Rahimzadeh, B., 2014, Petrology and geochemistry of mafic magmatic rocks from the Sarve-Abad ophiolites (Kurdistan region, Iran): Evidence for interaction between MORB-type asthenosphere and OIB-type components in the southern Neo-Tethys Ocean: Tectonophysics, v. 621, pp. 132-147, doi:10.1016/j.tecto.2014.02.011.

Shafaii Moghadam, H., Stern, R.J., Chiaradia, M. and Rahgoshay, M., 2013, Geochemistry and tectonic evolution of the Late Cretaceous Gogher-Baft ophiolite, central Iran: Lithos, v. 168-169, pp. 33-47, doi: 10.1016/j.lithos.2013.01.013.

Shallo, M. and Dilek, Y., 2003, Development of the ideas on the origin of Albanian ophiolites: Geological Society of America Special Paper, v. 373, pp. 351-364.

Schilling, J.-G., Zajac, M., Evans, R., Johnston, T., White, W., Devine, J.D. and Kingsley, R., 1983, Petrologic and geochemical variations along the Mid-Atlantic Ridge: American Journal of Science, v. 283, pp. 510-586.

Sibuet, J.-C. and Tucholke, B.E., 2013, The geodynamic province of transitional litho-sphere adjacent to magma-poor continental margins: Geological Society of London Special Publication, v. 369, pp. 429-452, http://dx.doi.org/10.1144/SP369.15.

Sinton, J.M. and Detrick, R.S., 1992, Mid-ocean ridge magma chambers: Journal of Geophysical Research, v. 97, pp. 197-216.

Skogseid, J., 2001, Volcanic margins: geodynamic and exploration aspects: Marine and Petroleum Geology, v. 18, pp. 457-461.

Stöcklin, J., 1968, Structural history and tectonics of Iran: A review: Bulletin of the American Association of Petroleum Geologists, v. 52, pp. 1229-1258.

Stoppa, F., 1985, Problematiche petrologiche e geologiche delle prasiniti di Punta Bianca (La Spezia): Memorie della Società Geologia Italiana, v. 30, pp. 127-134.

Storey, M., Duncan, R.A. and Tegner C., 2007, Timing and duration of volcanism in the North Atlantic Igneous Province: implications for geodynamics and links to the Iceland hotspot. Chemical Geology, v. 241, pp. 264-281.

Sun, S.-s. and McDonough, W.F., 1989, Chemical and isotopic-systematics of oceanic basalts: implications for mantle composition and processes: Geological Society of London Special Publications, v. 42, pp. 313-345.

Tashko, A., Mascle, G.H., Muceku, B. and Lapierre, H., 2007, Nd, Pb isotope and trace element signatures of the Triassic volcanism in Albania. The relationship to the NeoTethys opening: Albanian Journal of Natural and Technical Science, v.1, pp. 3-23.

Van Avendonk, H.J.A., Lavier, L.L., Shillington, D.J. and Manatschal, G., 2009: Extension of continental crust at the eastern Grand Banks, Newfoundland: Tectonophysics, v. 468, pp. 131-148. http://dx.doi.org/10.1016/j.tecto.2008.05.030.

Vannucci, R., Rampone, E., Piccardo, G.B., Ottolini, L. and Bottazzi, P., 1993, Ophiolitic magmatism in the Ligurian Tethys: An ion microprobe study of basaltic clinopyroxenes: Contribution to Mineralogy and Petrology, v. 115, pp. 123-137.

Venturelli, G., Capedri, S., Thorpe, R.S. and Potts, P.J., 1979, Rare-earth and other element distribution in some ophiolitic metabasalts of Corsica, Western Mediterranean: Chemical Geology, v. 24, pp. 339-353.

Wernicke, B., 1981, Low-angle normal faults in the Basin and Range province-nappe tectonics in an extending orogeny: Nature, v. 291, pp. 645-648.

Whitechurch, H., Omrani, J., Agard, P., Humbert, F., Montigny, R. and Jolivet L., 2013, Evidence for Paleocene–Eocene evolution of the foot of the Eurasian margin (Kermanshah ophiolite, SW Iran) from back-arc to arc: Implications for regional geodynamics and obduction: Lithos, v. 182–183, pp. 11-32.

Whitemarsh, R.B., Manatschal, G. and Minshull, T.A., 2001, Evolution of

magma-poor continental margins: From final rifting to seafloor spreading: Nature, v. 413, pp. 150-154.

Winterer, E.L. and Bosellini A., 1981, Subsidence and sedimentation on Jurassic passive continental margin, Southern Alps, Italy: American Association of Petroleum Geologists Bulletin, v. 65, pp. 394-421.

Wooler, D.A., Smith, A.G. and White, N., 1992, Measuring lithospheric stretching on Tethyan passive margins: Journal of the Geological Society London, v. 149, pp. 517-532.

Workman, R.K. and Hart, S.R., 2005, Major and trace element composition of the depleted MORB mantle (DMM): Earth and Planetary Science Letters, v. 231, pp. 53-72.

Xiao, L., He, Q., Pirajno, F., Ni, P., Du, J., Wei, Q., 2008, Possible correlation between a mantle plume and the evolution of Paleo-Tethys Jinshajiang Ocean: Evidence from a volcanic rifted margin in the Xiaru-Tuoding area, Yunnan, SW China: Lithos, v. 100, pp. 112-126.

Xu, Z.Q., Dilek, Y., Cao, H., Yang, J.S., Robinson, P., Ma, C.Q., Li, H., Jolivet, M., Roger, F., Chen, X.J., 2015, Paleo-Tethyan Evolution of Tibet as Recorded in the East Cimmerides and West Cathaysides: Journal of Asian Earth Sciences, v. 105, pp. 320-337, doi: 10.1016/j.jseaes.2015.01.021.

Yang, G.X. and Dilek, Y., 2015, OIB and P-Type Ophiolites along the Yarlung-Zangbo Suture Zone (YZSZ), Southern Tibet: Poly-Phase melt history and mantle sources of the Neotethyan Oceanic Lithosphere: Episodes, v. 38, No. 4, pp. 250-265, doi:10.18814/epiiugs/2015/v38i4/82420.

APPENDIX - A

Initial compositions and melting modes of different sources, as well as the partition coefficients (KD) used in the melting models in Figs. 5, 7, 8c.

Source composition

	Depleted MORB mantle	Enriched source 1 (ES1)	Enriched source 2 (ES2)	Ocean island basalt	Garnet pyroxenite
Th (ppm)	0.0068	0.08	0.1	0.18	0.017
Nb (ppm)	0.1277	0.6	0.8	1.5	0.48
Yb (ppm)	0.353	0.353	0.353	0.353	0.84

	ol	opx	cpx	gt	sp
Source Mode					
garnet-facies[a]	0.57	0.21	0.13	0.09	
spinel-facies[b]	0.578	0.27	0.119		0.033
garnet-pyroxenite			0.7	0.3	
Melting Mode					
gt-facies[a]	0.04	-0.19	1.05	0.11	
sp-facies[b]	0.1	0.27	0.5		0.13
garnet-pyroxenite			0.7	0.3	
KD					
garnet-facies					
Yb	0.0015[1]	0.049[1]	0.28[1]	5.73[2]	
Th	0.0001[1]	0.058[3]	0.00026[1]	0.0001[1]	
Nb	0.063[4]	0.01[5]	0.05[1]	0.0003[6]	
spinel-facies					
Yb	0.0015[1]	0.049[1]	0.28[1]		0.01[1]
Th	0.0001[1]	0.058[3]	0.00026[1]		0.0024[7]
Nb	0.063[4]	0.003[5]	0.05[1]		0.001[8]
garnet-pyroxenite					
Yb			0.43[9]	7.86[10]	
Th			0.0083[11]	0.001[10]	
Nb			0.05[1]	0.0008[10]	

Abbreviations, ol: olivine; opx: orthopyroxene; cpx: clinopyroxene; gt: garnet; sp: spinel.

References

a: Kinzler, R.J., 1997: Journal of Geophysical Research, v. 102, pp. 853-874.
b: Thirlwall, M. et al., 1994: Journal of Petrology, v. 35, pp. 839 879.
1: McKenzie, D. and O'Nions, R.K., 1991: Journal of Petrology, v. 32, pp. 1021-1091.
2: Shimizu, H., 1980: Geochemical Journal, v. 14, pp. 185-202.
3: Kennedy, A.K. et al., 1993: Earth and Planetary Science Letters, v. 115, pp. 177-195, doi:10.1016/0012-821X(93)90221-T.
4: Ewart, A. and Griffin, W.L., 1994: Chemical Geology , v. 117, pp. 251-284, doi: 10.1016/0009-2541(94)90131-7.
5: Keleman, P.B. and Dunn, J.T., 1992: EOS, Transactions of the American Geophysical Union, v. 73, pp. 656-657.
6: Green, T. et al., 2000: Lithos, v. 53, pp. 165-187, doi: 10.1016/S0024-4937(00)00023-2.
7: Klemme, S. et al., 2006: Chemical Geology, v. 234, pp. 251-263, doi: 10.1016/j.chemgeo.2006.05.005.
8: Adam, J. and Green, T., 2006: Contributions to Mineralogy and Petrology, v. 152, pp. 1-17.
9: Hart, S.R. and Dunn, T., 1993: Contributions to Mineralogy and Petrology, v. 113, pp. 1-8.
10: Zack, T. et al., 1997: Neues Jahrbuch fur Mineralogie, Abhirchen 172, pp. 23-41.
11: Elkins, L., et al. (2008). Earth and Planetary Science Letters 265, pp. 270-286. doi: 10.1016/j.epsl.2007.10.034.

by Gaoxue Yang[a,b], Yildirim Dilek[c]

OIB- and P-type ophiolites along the Yarlung-Zangbo Suture Zone (YZSZ), Southern Tibet: Poly-Phase melt history and mantle sources of the Neotethyan oceanic lithosphere

[a] School of Earth Science and Resources, Chang'an University, Xi'an 710054, China. *Corresponding author E-mail: mllygx@126.com*
[b] Key Laboratory for the study of Focused Magmatism & Giant Ore Deposits, MLR, Xi'an 710054, China
[c] Department of Geology & Environmental Earth Science, Miami University, Oxford, OH 45056, USA. *E-mail: dileky@miamioh.edu*

DOI:10.18814/epiiugs/2015/v38i4/82420

We present an overview of the internal structure of the ophiolite massifs along the Yarlung Zangbo suture zone (YZSZ) in southern Tibet with a focus on the geochemical character and tectonic evolution of the Ocean Island Basalt (OIB) and mafic alkaline rock assemblages associated with these ophiolites. The Jurassic – early Cretaceous lavas, massive diabase and gabbroic rocks are either tectonically intercalated with the early Cretaceous, subduction-influenced ophiolitic units, or occur as thrust sheets or blocks with an early Cretaceous mélange and in a Jurassic-Cretaceous flysch unit structurally beneath these ophiolites. They display uniform chondrite-normalized REE patterns with light rare earth element (LREE) enrichment and heavy rare earth element (HREE) depletion, no obvious Eu anomalies or negative Nb, Ta and Ti anomalies, and primitive mantle normalized trace element patterns with significant large-ion lithophile element (LILE) enrichment, similar to those of modern OIB and the Hawaiian alkaline basalts. These mafic alkaline rock assemblages represent OIB- and Plume-type (P-type) oceanic crustal rocks (with no subduction influence) that formed from magmas produced by partial melting of plume–metasomatized asthenospheric mantle source during the early stages of the opening of a Neotethyan seaway between Proto-India and Eurasia. Subsequent consumption of this OIB–P-type mid-ocean ridge (MOR) oceanic lithosphere at an intraoceanic subduction zone produced the ~130-120 Ma forearc to backarc, SSZ oceanic crust within the same Neotethys. The evolutionary history of the YZSZ ophiolites thus reflects a poly-phase melt history and different mantle melt sources. The final tectonic juxtaposition of the older OIB- and P-type oceanic crustal rocks with SSZ-type oceanic lithosphere fragments took place as the northern passive continental margin of Proto-India collided with and underplated the intraoceanic subduction-accretion system in the late Cretaceous. The YZSZ displays a complete Wilson cycle record of the rift-drift, seafloor spreading and subduction zone tectonic evolution of the Mesozoic Neotethys.

Introduction

The geochemistry and geochronology of the YZSZ ophiolites have been studied extensively during the last twenty years, producing a vast database on the geochemical affinities of different ophiolites and the timing of oceanic crust formation prior to the India – Asia collision (Aitchison et al., 2000; Wang et al., 2000; Yin and Harrison, 2000; Dilek and Newcomb, 2003; Dupuis et al., 2005; Sun et al., 2005; Zhang et al., 2005; Zhou et al., 2005; Guilmette et al., 2008, 2009; Bédard et al., 2009; Dai et al., 2011a, b, 2012; Hébert et al., 2012; Liu et al., 2013; Chan et al., 2015; Xu et al., 2015a). Yet, the interpretations of the tectonic settings of ophiolite genesis, the igneous – metamorphic ages and emplacement mechanisms of ophiolites, and the subduction zone numbers and polarities involved in the evolution of Neotethys are highly diverse and still poorly constrained. The lack of systematic field-based structural work along the YZSZ and of the documentation of the internal structure and stratigraphy of the ophiolite massifs and mélange units is partly responsible for this problem.

In this paper we overview and document the geological occurrence and the geochemical characteristics of a special group of mafic rocks, which are spatially and temporally associated with the ophiolite units

along the 2500-km-long YZSZ. Largely overlooked in the literature, the early Jurassic-early Cretaceous OIB-type and alkaline mafic rocks are tectonically interleaved with the ophiolite massifs, as well as occurring extensively in the mélange formations within the YZSZ and in the Jurassic-Cretaceous flysch deposits structurally beneath the YSZS. They are hence part of the rift-drift, seafloor spreading and subduction zone tectonic evolution of the Neotethyan oceanic lithosphere, evolved between India and Eurasia during the Mesozoic. In the first part of the paper we summarize the spatial distribution and the internal structure of the discrete ophiolite complexes and the associated OIB-type mafic rocks from west to east along the YZSZ. Using some of the most reliable discriminant diagrams, we discuss, based on the extant data, the geochemistry and geochemical characteristics of these OIB-type mafic rocks. We then present an internally coherent tectonic model, synthesizing the structure, petrology, geochemistry and geochronology of the YZSZ ophiolites and the OIB-type rocks associated with them. This paper is intended to stimulate further research and discussions on the YZSZ ophiolites and on the significance of the existence of mafic OIB-type and alkaline oceanic rocks in suture zones in general.

Regional Geology of the Yarlung-Zangbo Suture Zone

The crust of the Tibetan Plateau is made of a series of oceanic and continental terranes bounded by the A'nemaqin–Kunlun, Jinshajiang (JSZ), Bangong–Nujiang (BNSZ), Shuanghu–Dingqing, and Yarlung-Zangbo (YZSZ) suture zones (Fig. 1; Yin and Harrison, 2000; Zhang and Tang, 2009; Xu et al., 2015b). The Yarlung-Zangbo Suture Zone (YZSZ) in the southernmost part of the Tibetan Plateau is the youngest among these suture zones, and has been widely accepted to represent the India – Asia continental collision front with the remnants of the Neotethyan oceanic lithosphere exposed discontinuously along it (e.g., Allègre et al., 1984; Aitchison et al., 2000; Dupuis et al., 2005; Bédard et al., 2009; Zhang et al., 2010; Hébert et al., 2012). These Neotethyan ophiolites occur along two sub-parallel belts within the suture zone: the northern belt includes ophiolite complexes with upper mantle peridotites, gabbros, dikes-sills, extrusive sequences and pelagic-hemipelagic sedimentary rocks, whereas the southern belt consists mainly of peridotite massifs overlain by volcanic-sedimentary rocks. A discontinuous belt of a mélange unit, containing ophiolitic material, deep marine sedimentary rocks, and high-grade metamorphic rocks structurally underlies the ophiolites within the YSZS (Guilmette et al., 2008; Liu et al., 2015; Xu et al., 2015a).

A Mesozoic flysch unit, containing blocks of Upper Permian limestone, lower Triassic pelagic limestone, late Cretaceous calcschist, turbiditic rocks, serpentinite, gabbros, massive diabase, and pillow – massive lavas structurally underlies the YZSZ in the south (Xu et al., 2015a, and the references therein). High-grade metamorphic rocks with highly deformed granitoid intrusions make up the Tethyan Himalaya Sequence structurally beneath the Mesozoic flysch unit (Fig. 1). This Tethyan Himalaya Sequence consists mainly of Proterozoic to Eocene siliciclastic and carbonate sedimentary rocks, interbedded with Paleozoic and Mesozoic volcanic rocks (Yin, 2006), collectively forming the passive margin units of Greater India.

The northern boundary of the YZSZ is a complex, tectonic zone with ophiolitic and mélange units structurally overlying the Xigaze forearc basin sequence (XG in Figure 1) and/or the Gangdese magmatic terrane (GMT in Figure 1) along N-vergent backthrusts

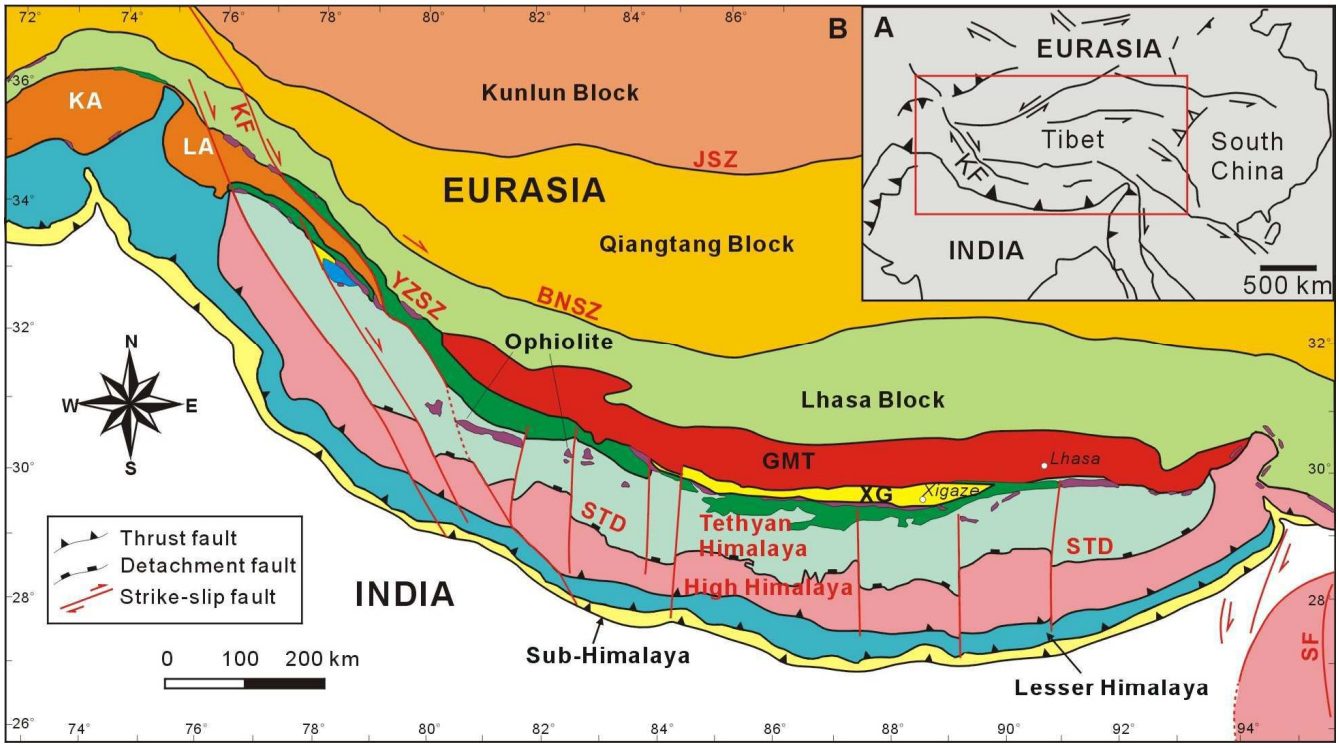

Figure 1. A- Index map of south-central Asia, depicting the major plates and major fault systems in the region. The red box outlines the map area in B. B- Simplified tectonic map of Southern Tibet, showing the major tectonic units, suture zones and fault systems. Key for abbreviations: BNSZ - Bangong Nujiang suture; JSZ - Jinshajing zone; KA – Kohistan arc; LA – Ladakh arc; STD – South Tibet Detachment; XG – Xigaze forearc basin; YZSZ – Yarlung-Zangbo suture zone.

(Xu et al., 2015a, and references therein). The Xigaze forearc basin sequence includes Cretaceous clastic units interbedded with marly carbonate layers (Einsele et al., 1994; Wang et al., 1999, 2012). The Gangdese magmatic terrane consists of late Jurassic to Paleogene calc-alkaline granitoids and andesitic-dacitic-rhyolitic volcanic–volcaniclastic sequences that collectively make up an Andean-type magmatic arc formed above a N-dipping subduction zone beneath the southern margin of Asia (Chung et al., 2005; Chu et al., 2006; Wen et al., 2008a, b; Ji et al., 2009).

YZSZ ophiolites and associated OIB-type rocks

The Yarlung-Zangbo ophiolites crop out along the Yarlung-Zangbo River, and the main massifs include from west to east the Yungbwa, Xiugugabu, Dangqiong, Zhongba, Saga, Sangsang, Jiding, Xigaze, Zedong-Luobusa and the Eastern Himalayan Syntaxis ophiolites (Fig. 2). Recent geochronological and biostratigraphic studies in these ophiolites have revealed crystallization, deposition and metamorphic ages ranging from the middle Jurassic to the early Cretaceous; however, most of the igneous ages of the ophiolites are clustered at 130–120 Ma (Table 1; McDermid et al., 2002; Zhou, 2002; Malpas et al., 2003; Miller et al., 2003; Ziabrev et al., 2003; Wang et al., 2006; Wei et al., 2006a, b; Zhong et al., 2006; Chan et al., 2007; Guilmette et al., 2008, 2009; Li et al., 2008, 2009; Xia et al., 2008b; Dai et al., 2012). Petrological and geochemical studies of various crustal units (lavas, dikes, sills and gabbros) of the YZSZ ophiolites have indicated multi-stage melting episodes in different tectonic settings during their magmatic accretion and evolution, encompassing mid-ocean ridge, and backarc to forearc supra-subduction zone environments (Table 1; McDermid et al., 2002; Hébert et al., 2003; Xia et al., 2003; Dubois-Côté et al., 2005; Zhou et al., 2005; Bédard et al., 2009; Guilmette et al., 2008, 2009; Geng et al., 2010; Dai et al., 2011a, b; Bezard et al., 2011; Liu et al., 2010, 2012; Hébert et al., 2012; Dai et al., 2011b, 2013; Dilek and Furnes, 2014; Liu et al., 2015; Xu et al., 2015a). The Jurassic-Cretaceous mélange unit structurally beneath the YZSZ ophiolites includes coherent blocks of alkaline lavas, gabbros and dikes, and these lithologies are also tectonically interleaved with the ophiolitic units and their volcanic-sedimentary sequences.

In this section we describe the internal structure and stratigraphy of some of the discrete YZSZ ophiolite massifs and the alkaline rock suites spatially associated with them from west to east along the YZSZ. The geographic distribution of the investigated ophiolite massifs is shown in Figure 2. Table 1 summarizes the details of the extant age data from the YZSZ ophiolites and the data sources. The geochemistry of these alkaline rock suites is discussed in the following section.

Dongbo ophiolite

The Neotethyan ophiolites in the westernmost part of the YZSZ occur in two sub-parallel belts (Fig. 2), separated by the Zhongba–Zhada crustal block (Liu et al., 2015; Xu et al., 2015a). The northern sub-belt largely displays a mélange character, whereas the southern sub-belt consists of discontinuous exposures of ophiolites with mafic-ultramafic and volcanic-sedimentary sequences. The Dongbo and

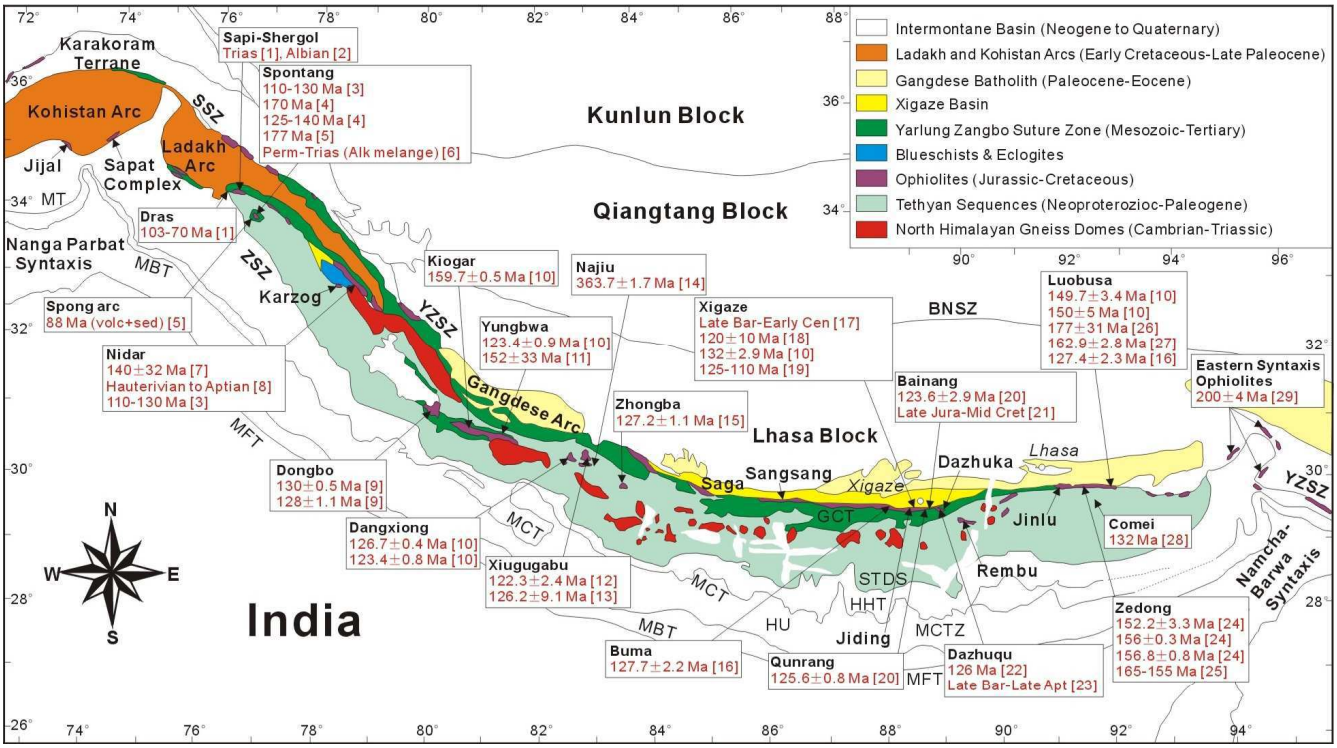

Figure 2. Simplified tectonic map of the Himalaya–Tibet orogenic belt and the Yarlung-Zangbo suture zone, showing the distribution and the ages of the major ophiolite massifs from west to east along the Yarlung-Zangbo suture zone. Data sources are listed in Table 1. Abbreviations: SSZ – Shyok suture zone; ZSZ – Zanskar suture zone; BNSZ – Bangong Nujiang suture; YZSZ – Yarlung-Zangbo Suture Zone. The Himalayan fold-thrust belt is subdivided into structural blocks according to the major discontinuities: GCT – Great Counter thrust; STD – South Tibet detachment; HHT – High Himalaya thrust; MCTZ – Main Central thrust zone; MBT – Main Boundary thrust; MFT – Main Frontal thrust. Data for the map from Yin and Harrison (2000), Goscombe et al. (2006), and Hébert et al. (2012).

Table 1. Summary of the existing geochronological – biostratigraphic data from the Yarlung-Zangbo suture zone ophiolites and OIB-type rocks and key for the references used in Figure 1.

Locality	Dating method	References
Sapi–Shergol mélange	[1 and 2] Rb–Sr on mica and radiolarian cherts	[1] Honneger et al. (1982) [2] Sihna and Mishra (1997)
Dras	[1] $^{87}Sr/^{86}Sr$ in Biotite in granodiorite and U–Pb in zircon in granodiorite	[1] Honneger et al. (1982)
	[3] $^{40}Ar/^{39}Ar$ in amphibole in diorite	[3] Mahéo et al. (2004)
	[4] K–Ar in Hornblende in diorite	[4] Reuber et al. (1989)
Spongtang	[5] U–Pb in zircon in plagiogranite	[5] Pedersen et al. (2001)
	K–Ar in hydrothermal hornblende in calc-alkaline volcanics	[6] Reuber et al. (1987)
Spong arc	[5] U–Pb in zircon in andesite	[5] Pedersen et al. (2001)
Nidar	[3] $^{39}Ar/^{40}Ar$ in amphibole in basaltic andesite	[3] Mahéo et al. (2004)
	[7] $^{147}Sm/^{144}Nd$ in clinopyroxene, plagioclase and whole rock in gabbro	[7] Ahmad et al. (2008)
	[8] Radiolarian fossils	[8] Kojima et al. (2001)
Dongbo	[9] U–Pb in zircon in pyroxenite and gabbro	[9] Xiong et al. (2011)
Kiogar	[10] U–Pb in zircon in cumulate gabbro	[10] Chan et al. (2007)
Yungbwa	[10] U–Pb Zircon in gabbro	[10] Chan et al. (2007)
	[11] $^{40}Ar/^{39}Ar$ in Magnesio Hornblende in basalt	[11] Miller et al. (2003)
Dangxiong	[10] U–Pb Zircon in gabbro	[10] Chan et al. (2007)
Xiugugabu	[12] U–Pb in zircon in micro-gabbro	[12] Wei et al. (2006b)
	[13] Sm–Nd in micro-gabbro	[13] Xu et al. (2008)
Najiu	[14] U–Pb in zircon in gabbro	[14] Dai et al. (2011b)
Zhongba	[15] U–Pb in zircon in diabase	[15] Dai et al. (2012)
Buma	[16] $^{40}Ar/^{39}Ar$ in hornblende in amphibolite	[16] Guilmette et al. (2009)
Xigaze		
Mamidhuorong,	[18] U–Pb in whole rock basalt, diabase and gabbro	[17] Burg and Chen (1984)
Qumei, Baigang, Lhazexian,	[10] U–Pb in zircon in pegmatitic gabbro	[18] Göpel et al. (1984)
Beilie, Xiadamei, Zisong,	[19] Radiolaires	[10] Chan et al. (2007)
(Pazuo, Dayu)		[19] Zyabrev et al. (1999)
Qunrang	[20] $^{40}Ar/^{39}Ar$ in hornblende in amphibolite	[20] Guilmette et al. (2007)
Bainang	[20] $^{40}Ar/^{39}Ar$ in hornblende in amphibolite	[20] Guilmette et al. (2007)
	[21] Radiolarian fossils	[21] Ziabrev et al. (2003)
Dazhuqu	[22] U–Pb in zircon in quartz-diorite	[22] Malpas et al. (2003)
	[23] Radiolarian fossils	[23] Ziabrev et al. (2003)
Zedang	[24] $^{40}Ar/^{39}Ar$ in Hornblende in andesite and U–Pb in zircon and $^{40}Ar/^{39}Ar$ in hornblende in quartz-diorite	[24] McDermid et al. (2002)
	[25] Radiolarian fossils	[25] Hébert et al. (2012)
Luobusa	[16] $^{40}Ar/^{39}Ar$ in hornblende in amphibolite	[16] Guilmette et al. (2009)
	[10] U–Pb in zircon in diabase	[10] Chan et al. (2007)
		[26] Zhou et al. (2002)
		[27] Zhong et al. (2006)
Comei	[28] U–Pb in zircon in basalt and gabbro	[28] Zhu et al. (2009)
Eastern Syntaxis	[29] $^{40}Ar/^{39}Ar$ in clinopyroxene in ultramafic rock	[29] Geng et al. (2006)

Purang ophiolites are situated within the southern sub-belt and are tectonically underlain by a Cretaceous ophiolitic mélange (Liu et al., 2015).

The Dongba ophiolite consists of a volcanic-sedimentary sequence, gabbros, and peridotites with dolerite and pyroxenite dikes. Its volcanic-sedimentary sequence rests directly on the serpentinized peridotites and includes basaltic lavas, volcaniclastic rocks, tuffaceous layers, limestone, red radiolarian chert, and silty shale–sandstone intercalations. Peridotites are composed of harzburgite and dunite with minor lherzolite. Cr-spinels of the Dongbo lherzolite have Cr# [Cr/(Cr+Al)] of 0.2–0.3, whereas Cr# of the harzburgite range from 0.2 to 0.75. U-Pb zircon dating of pyroxenite and gabbro dikes in the harzburgites by LA-ICP-MS has yielded crystallization ages of 130±0.5 Ma and 128±1.1 Ma, respectively, for the Dongbo ophiolite (Fig. 2; Xiong et al., 2011).

Xiugugabu massif

The Xiugugabu ophiolite also occurs in the southern sub-belt in the western YZSZ (Fig. 2) and tectonically overlies the same early Cretaceous mélange to the south as the Dongbo massif. It is composed of harzburgite and clinopyroxene (cpx)-harzburgite intruded by amphibole-bearing micro-gabbro and micro-gabbronorite sills (Bezard et al., 2011). These sill intrusions and their host harzburgites show ductile deformation structures and mylonitic foliation of high-temperature origin. A massive diabase unit stratigraphically overlain by siltstone and hyaloclastic volcanic rocks is faulted against the peridotites in the north. Diabasic rocks have tholeiitic basalt compositions with Mg#s of 0.60-0.63 that are distinctly different from those of the sill intrusions (Mg#s of 0.74-0.86), and show OIB (ocean island basalt) geochemical affinities with a slight crustal contamination fingerprint (Bezard et al., 2011). The Cr#s of the spinel-bearing harzburgites and the cpx-harzburgites vary between 0.20 and 0.80. Bezard et al. (2011) inferred that these upper mantle peridotites might have undergone less than 25% partial melting beneath a mid-ocean ridge spreading center, followed by a refertilization process in a suprasubduction zone setting. Sm-Nd whole-rock and U-Pb zircon dating of micro-gabbro sill rocks in the peridotites has revealed the crystallization ages of 126.2±9.1 Ma and 122.3±2.4 Ma, respectively, for the Xiugugabu massif (Fig. 2; Wei et al., 2006b; Xu et al., 2008).

Zhongba massif

The Zhongba massif occurs west of the 84°E Longitude along the YZSZ (Fig. 2). It makes up a large thrust-sheet within the early Cretaceous mélange, and is tectonically underlain by large blocks of massive diabase and pillow lava rocks. The mélange also includes blocks of chert, limestone and massive basalt.

The Zhongba massif is composed entirely of harzburgites with minor dunite. The Cr-spinels in the harzburgites have Cr# of 0.36–0.56 and Mg#s ranging from 0.57 to 0.72 (Dai et al., 2011b). These highly depleted harzburgites show variable relative enrichment in the most incompatible trace elements, characteristic of subduction-influenced mantle wedge peridotites beneath forearc settings (Parkinson and Pearce, 1998). Diabasic rocks and pillow basalts tectonically below the Zhongba thrust sheet exhibit trace element patterns that are similar to those of the average OIB, Hawaiian alkaline basalts, and OIB-type rocks documented from the other Neotethyan ophiolites along the west-central YZSZ. Zircon U-Pb dating of a diabasic rock sample has yielded a crystallization age of 125.7±0.9 Ma (Dai et al., 2012), which is consistent with the reported igneous ages of crustal rocks from the other YZSZ ophiolites (Table 1).

Saga massif

The Saga massif occurs just east of the 85°E Longitude and forms a ~25-km-long thrust sheet, tectonically overlying the early Cretaceous ophiolitic mélange to the south (Fig. 2). The mélange contains blocks of lherzolitic, dunitic peridotites and garnet- and cpx-bearing amphibolites in a serpentinite matrix (Bédard et al., 2009; Guilmette et al., 2012). Structurally below this mélange in the south is a 2- to 2.5-km-thick unit of meta-gabbro, amphibolite and meta-basaltic rocks that is in turn tectonically underlain by a ~2-km-thick sequence of pillow to massive lavas, diabasic rocks, and Triassic green-red chert.

The upper mantle peridotites in the Saga massif consist of lherzolite and cpx-harzburgite with spinels that have typical Mg#s of 0.70–0.79 and Cr#s of 0.10–0.22 (Bédard et al., 2009). Their trace element patterns resemble those of abyssal peridotites, which experienced low degrees of partial melting (5–12%). Pillow and massive lavas, diabasic rocks, meta-basalts and amphibolites beneath the peridotite massif show incompatible element abundances similar to those of N-MORB, but they also display slight negative Ti and Ta anomalies. The major and trace element geochemistry of the high-grade amphibolite blocks in the mélange suggest mafic protoliths with N-MORB to E-MORB affinities (Guilmette et al., 2012). $^{40}Ar/^{39}Ar$ dating of hornblende separates from these amphibolites has revealed cooling ages of 132–127 Ma (Guilmette et al., 2012).

Sangsang ophiolite

The ~100-km-long Sangsang ophiolite occurs to the east of the Saga massif, between the 86°E and 87°E Longitudes (Fig. 2). Similar to Saga, it tectonically overlies the early Cretaceous ophiolitic mélange to the south, and is separated from the clastic rock sequences of the Cretaceous Xigaze Group to the north by a major fault. The ophiolitic mélange includes blocks of harzburgitic peridotites, alkaline volcanic rocks, sandstone–chert, and is tectonically juxtaposed against the Triassic flysch unit to the south.

The Sangsang massif consists mainly of tectonized peridotites overlain to the north by a thin sliver (< 1km) of gabbro, massive diabase and pillow lavas. The Sangsang peridotites are composed of harzburgite and cpx-harzburgite with spinels having Cr#s of 0.30–0.60, typical of abyssal or forearc mantle peridotites (Bédard et al., 2012). Their trace element characteristics suggest partial melting degrees of 17–30%, higher than those estimated for the peridotites in the Saga massif. Massive diabase and pillow lavas above the peridotites are enriched in incompatible elements, typical of OIB lavas. Alkaline volcanic rocks occurring as blocks in the ophiolitic mélange beneath the Sangsang massif also display OIB affinities (Hébert et al., 2012). The U-Pb SHRIMP dating of zircons from diabasic rocks has revealed a crystallization age of 125.23 Ma (Xia et al., 2008b).

Xigaze ophiolite

The Xigaze ophiolite occurs between the 88°E and 89°30'E Longitudes in the central part of the YZSZ (Fig. 2) and includes the Dazhuqu, Deji, Qunrang, Luqu and Jiding massifs. It is the biggest and most complete ophiolite complex along the entire YZSZ. It tectonically overlies the early Cretaceous ophiolitic mélange to the south along an originally S-vergent thrust fault; however, the late Triassic-early Jurassic flysch sequence south of the YZSZ, the ophiolitic mélange and the Xigaze ophiolite are all imbricated along N-vergent backthrusts, and rest structurally above the late Cretaceous and younger clastic rock sequences of the Xigaze Group in the north (Xu et al., 2015a).

In general, the Xigaze ophiolite consists of upper mantle peridotites, ultramafic cumulates, doleritic and gabbroic dike–sill intrusions in the peridotites, thin (<300 m) gabbro–gabbronorite rocks in some massifs, and an extrusive sequence composed of pillow and massive lavas and tuffaceous volcaniclastic rocks, which are intercalated with radiolarian chert deposits near the top of the extrusive sequence. Siliceous mudstone, chert, radiolarite and fine-grained clastic rocks make up a sedimentary cover of the ophiolite.

The upper mantle units comprise harzburgite, cpx-harzburgite and lherzolite with minor occurrences of dunite and chromitites. The Mg# of these peridotites is in the range of 90.0 – 92.8, and the Cr# of spinels is in the range of 79 to 81 (Bao et al., 2013; Dai et al., 2013). The whole-rock compositions indicate their residual, highly refractory nature, which reflect 15% to 24% partial melting. The U-shaped REE patterns of some of the Xigaze harzburgites suggest their reaction-interaction with boninitic melts in a mantle wedge, as also reported from other Neotethyan ophiolites (Dilek and Thy, 1998, 2009; Dubois-Coté et al., 2005; Dilek et al., 2008; Dilek and Furnes, 2009; Bao et al., 2013; Dai et al., 2013).

The majority of doleritic and gabbro dike–sill intrusions and lavas show LREE depletion similar to N-MORB patterns, and enrichment in LILE and Pb and negative Nb–Ta anomalies, suggesting minor subduction influence in their melt evolution. Some dikes and lavas, on the other hand, display distinctive U-shaped boninitic patterns on N-MORB normalized trace element diagrams. Blocks of mafic lavas and gabbros in the Triassic flysch sequence beneath the ophiolitic mélange of the Xigaze ophiolite have strong OIB geochemical signatures, indicating their origin from within-plate alkaline magmas (Dupuis et al., 2005; Hébert et al., 2012).

U-Pb zircon dating of doleritic dikes in the mantle peridotites of the Dazhuqu and Deji sub-massifs has revealed crystallization ages of 126.1±1.3 Ma and 124.9±1.1 Ma, respectively; a dolerite sill

intrusion in the Deji sub-massif has given a weighted zircon U-Pb mean age of 126.5±4.7 Ma (Table 1). The youngest crystallization age of 123.3±1.5 Ma was obtained from a quartz diorite dike in the Deji peridotite (Dai et al., 2013). The Xigaze ophiolite, thus, displays a narrow age range of 127 Ma to 124 Ma for its late-stage mafic and felsic intrusive rocks. There are no age data available from the alkaline rocks, but their close spatial association with ophiolitic peridotites within the flysch near Renbu suggests that they are not significantly older than the early Cretaceous ages of the YZSZ ophiolites.

Luobusa-Lang County ophiolites

The Luobusa–Lang County ophiolite belt (Fig. 2) is situated in the eastern end of the YZSZ between 92° and 93° of longitudes, and includes the Kangjinla, Luobusa and Baozhigou massifs to the east, the Sangri, Chenbaxiang and Gongbar massifs in the center, and the Zedang massif to the west. This entire ophiolite belt is bounded by two regional, south-dipping, ductile to ductile–brittle thrust faults, the South Luobusa–Zedang thrust (SLZT) and the North Luobusa–Zedang thrust (NLZT) (Liang et al., 2011; Xu et al., 2015b). A highly deformed late Triassic flysch sequence is thrust over the ophiolite belt along the E-W-striking and steeply south-dipping SLZT. The NLZT represents a steeply south-dipping, 200- to 300-m-thick, ductile shear zone, which puts the ophiolitic peridotites on top of the Paleogene Liuqu Conglomerate in the north (Xu et al., 2015a).

In the Kangjinla–Luobusa area, the SLZT consists of mylonitic flysch rocks in its upper and mylonitic peridotites in its lower parts. The late Triassic flysch unit is composed of shale, siltstone-sandstone, and blocks of marble and quartz listwanite. The Luobusa ophiolite in this area constitutes a ~40- to 50-km-long and up to ~ 4-km-wide mafic-ultramafic slab that is thrust northward onto the Gangdese batholith and the Cenozoic terrestrial strata (Yang et al., 2015b). However, an ophiolitic mélange composed of blocks of pillow lavas, volcanic breccia, chert, marble, shale, isotropic gabbro and pyroxenite in a highly sheared serpentinite matrix underlies the ophiolite along its northern margin. Serpentinized peridotites in the mélange are transitional upward into a ~300-m-thick dunite unit, which is overlain by cpx-harzburgites with chromitite bands and pods (Yang et al., 2015b). Structurally upward in the Luobusa ophiolite and overlying the cpx-harzburgites are depleted harzburgites with lenses and pods of chromitite enveloped by dunite (Huang et al., 1981; Zhou et al., 1996, 2002, 2005, 2014; Malpas et al., 2003; Hébert et al., 2003; Robinson et al., 2004; Shi et al., 2007; Yamamoto et al., 2007, 2009; Yang et al., 2007, 2014; Xu et al., 2011, 2014; Xiong et al., 2014).

A detailed account of the petrology and geochemistry of the Luobusa peridotites and crustal units is presented by Yang et al. (2015-this issue). The highly depleted upper harzburgites and the less-depleted cpx-bearing lower harzburgites represent the residues of high-degrees and low-degrees of melting, respectively (Bao et al., 2014). All these peridotites display variously depleted, U-shaped REE patterns, characteristic of those mantle wedge peridotites beneath forearc settings (Parkinson and Pearce, 1998).

The Sangri, Chenbaxiang and Gongbar massifs in the center of the Luobusa–Lang County ophiolite belt are highly dismembered by numerous thrust faults, and occur as blocks in meters to tens of meters in size within an Upper Jurassic to Lower Cretaceous volcanic–sedimentary sequence. The late Triassic flysch unit to the south tectonically rests on this volcanic-sedimentary sequence along the SLZT. Farther west, the Zedang massif occurs as a S-dipping thrust sheet sandwiched between the late Triassic flysch to the south and the late Cretaceous andesitic volcanic rocks of the Gangdese magmatic terrane to the north (Xu et al., 2015a). The ophiolite contains peridotites, podiform chromitites, gabbro, doleritic dikes and volcanic rocks, which are in places tectonically intercalated with middle-late Cretaceous sandstone, phyllite and radiolarite. The Zedang peridotites are composed of cpx-harzburgite, harzburgite with minor lherzolite and dunite (Bao et al., 2014). Volcanic rocks with MORB, island arc tholeiite (IAT) and boninitic geochemical affinities and REE patterns coexist within the Zedang extrusive rock suites (Bao et al., 2014).

The Lang County ophiolite is 70-km-long and constitutes the eastern extension of the Luobusa ophiolite. It includes upper mantle peridotites composed of harzburgite and dunite, and minor occurrences of meta-gabbro, meta-basalts, pillow basalts, dolerite sills and dikes. Basaltic lavas display E-MORB and OIB geochemical affinities.

The Luobusa cpx-harzburgites are crosscut by numerous gabbroic dikes. U/Pb zircon dating of one of these dike rocks has revealed a crystallization age of 148±4.5 Ma (Chan et al., 2007), which is considered as the minimum age of the ophiolite. U–Pb zircon dating of basaltic rocks from the Lang County ophiolite has yielded crystallization ages of 145.7±2.5 Ma and 147.8±3.3 Ma (Zhang et al., 2011). However, gabbroic rocks from the same ophiolite have provided U–Pb zircon ages of 191.4 ± 3.7 Ma (Zhang et al., 2011). These limited age data from the Luobusa-Lang County ophiolites indicate much older magmatic ages from the eastern part of the YZSZ, suggesting that the Neotethyan oceanic lithosphere formation in this part of southern Tibet might have extended further back into the early Jurassic in the east.

Eastern Syntaxis ophiolites (ESO)

These ophiolites are situated at the extreme eastern end of the YZSZ where the Tethyan suture zone makes a sharp hairpin turn to the south between 95° and 96° of longitude and encounters the N-S-oriented, dextral Sagaing Fault (Fig. 1), which separates the Burma microplate in the west from the Sundaland to the east. Ophiolitic lithologies, composed of boninitic dolerite, arc tholeiite, back-arc basalt, amphibolite, and alkaline mafic rocks, occur as dismembered and metamorphosed blocks within a ~N-S-trending mélange zone (Geng et al., 2010; Hébert et al., 2012; Ghose et al., 2014; Fareeduddin and Dilek, 2015). Geochronological data from the Eastern Syntaxis ophiolites in China are nearly non-existent. $^{40}Ar/^{39}Ar$ dating of clinopyroxene separates from an ultramafic rock has revealed a cooling age of 200±4 Ma (Geng et al., 2006). This age is consistent with the U/Pb zircon age of 191.4±3.7 Ma, obtained from the Lang County ophiolite directly to the north. $^{40}Ar/^{39}Ar$ dating of feldspar grains from the earliest subduction-related granites found along the suture zone has provided an age range of 94 to 79 Ma (Geng et al., 2006).

Geochemistry of the OIB-type and alkaline rocks

We have examined the extant geochemical data available in the literature from all alkaline rocks associated with the YZSZ ophiolites as described above, and have screened the major element analyses in order to avoid those samples with high LOI (loss on ignition) values.

We have selected only those samples with <5 wt.% LOI for the least altered samples analyzed, and have then compiled the high-quality data from more than 60 rock samples, including lavas, massive diabase, and gabbros with OIB affinities. A list of the most representative rock samples used in this study and their compositional names together with the ophiolite location and the data sources (references) is given in Table 2. We present the compiled trace element and REE data in Table 3.

The chondrite normalized REE patterns and the primitive mantle normalized trace element spider diagrams are shown in Figures 3 and 4, respectively. The average trends of modern OIB, E-MORB, N-MORB and Hawaiian alkaline basalts are also shown on these plots for comparison (after Sun and McDonough, 1989; Garcia et al., 1995; Hofmann and Jochum, 1996; Xu et al., 2007). All the OIB-like rocks associated with the YZSZ ophiolites display uniform chondrite normalized REE patterns with LREE enrichment and HREE depletion, and with no obvious Eu anomalies. Most of the evaluated samples resemble modern OIB (Sun and McDonough, 1989) and the Hawaiian alkaline basalts, although few show patterns similar to those of E-MORB and N-MORBs (Fig. 3). In the primitive mantle normalized spidergrams (Fig. 4), the examined rocks display trends that are similar to those reported for the Hawaiian alkaline basalts and for the average OIB. There are no obvious negative Nb, Ta, and Ti anomalies.

Rocks produced from subduction-influenced magmas can be easily distinguished from OIB-type alkaline rocks on the V–Ti/1000 discrimination diagram of Shervais (1982). The individual V-Ti diagrams from all examined ophiolites along the YZSZ show that the OIB rock suites plot largely in the alkaline field (Fig. 5), although some rock samples straddle the MORB – Alkaline boundary as well as plotting in the MORB field. On the Th/Yb versus Nb/Yb discrimination diagram (Fig. 6) of Pearce (2008), the majority of the examined rock suites plot closer to the OIB domain within the mantle array, and overlap significantly with the Hawaiian alkaline basalt field shown in the upper right-corner (Key diagram). On the Nb-Zr-Y ternary discrimination diagram, most of the OIB-type rocks from the YZSZ fall in the within-plate alkaline and tholeiitic basalt fields, while few samples plot in the E-MORB field (Fig. 7; Meschede, 1986).

We also applied the binary diagrams of Saccani (2015), which utilize absolute measures of Th and Nb (normalized to the N-MORB composition of Sun and McDonough, 1989), to find out whether the examined rock suites from the YZSZ ophiolites show any subduction zone influence or evidence for crustal contamination, and to better identify their MORB affinities (Fig. 8). Elemental ratios of the examined samples range from E-MORB to P-MORB (plume-type MORBs; Dilek and Furnes, 2011, 2014; Pearce, 2008; Saccani, 2015) and to those in alkaline basalts (Fig. 8A), showing a continuous compositional variation from the less enriched to the more enriched rocks. These rocks exhibit multi-element patterns significantly enriched in LILE compared to HFSE and HREE. The overall geochemistry of the majority of the samples resembles that of alkaline basalts generated in within-plate ocean island settings (Fig. 8A). In terms of their tectonic fingerprint, these alkaline samples from the YZSZ overlap with subduction unrelated rifted margin and ocean–continent transition zone (OCT) rocks (Fig. 8B; Saccani et al., 2015). Only a very few of them may show slight chemical influence of lower crustal contamination in their melt evolution. We hence infer that the YZSZ alkaline rocks were generated from partial melting of a MORB-type asthenospheric source enriched in LREE by an OIB type component (plume-type component).

Table 2. Summary of the extant geochemical data for the OIB-type mafic rocks from the YZSZ.

Sample	Rock type	Location	Reference
11L36-1	Basalt	Dongbo	Liu et al. (2013)
11L36-2	Basalt	Dongbo	Liu et al. (2013)
11L36-4	Basalt	Dongbo	Liu et al. (2013)
11L36-5	Basalt	Dongbo	Liu et al. (2013)
11L37-1	Basalt	Dongbo	Liu et al. (2013)
11L37-4	Basalt	Dongbo	Liu et al. (2013)
11L37-7	Basalt	Dongbo	Liu et al. (2013)
11L37-8	Basalt	Dongbo	Liu et al. (2013)
11L37-9	Basalt	Dongbo	Liu et al. (2013)
09-ZH-56A	Diabase	Xiugugabu	Bezard et al. (2011)
09-ZH-57	Diabase	Xiugugabu	Bezard et al. (2011)
09-ZH-58	Diabase	Xiugugabu	Bezard et al. (2011)
ZEOS-5-01	Pillow basalt	Zhongba	Dai et al. (2012)
ZEOS-5-03	Pillow basalt	Zhongba	Dai et al. (2012)
ZEOS-5-05	Pillow basalt	Zhongba	Dai et al. (2012)
ZEOS-5-08	Pillow basalt	Zhongba	Dai et al. (2012)
ZEOS-6-03	Basalt	Zhongba	Dai et al. (2012)
ZEOS-4-03	Diabase	Zhongba	Dai et al. (2012)
ZEOS-4-04	Diabase	Zhongba	Dai et al. (2012)
ZEOS-4-05	Diabase	Zhongba	Dai et al. (2012)
ZEOS-4-05R	Diabase	Zhongba	Dai et al. (2012)
06-SA-10C	Altered diabase	Saga	Bédard et al. (2009)
06-SA-16	Brecciated basalt	Saga	Bédard et al. (2009)
07-SG-14	Hematized basalt	Sangsang	Bédard et al. (2009)
07-SG-17A	Hematized basalt	Sangsang	Bédard et al. (2009)
07-SG-53	Basalt	Sangsang	Bédard et al. (2009)
07-SG-61	Andesite	Sangsang	Bédard et al. (2009)
07-SG-63A	Gabbro	Sangsang	Bédard et al. (2009)
RB49	Basalt	Rembu	Xia et al. (2008a)
RB50	Basalt	Rembu	Xia et al. (2008a)
RB55	Basalt	Rembu	Xia et al. (2008a)
RB56	Basalt	Rembu	Xia et al. (2008a)
RB58	Basalt	Rembu	Xia et al. (2008a)
RB61	Basalt	Rembu	Xia et al. (2008a)
RB63	Basalt	Rembu	Xia et al. (2008a)
RB70	Basalt	Rembu	Xia et al. (2008a)
RB73	Basalt	Rembu	Xia et al. (2008a)
RB74	Basalt	Rembu	Xia et al. (2008a)
RB141	Basalt	Rembu	Xia et al. (2008a)
RB143	Basalt	Rembu	Xia et al. (2008a)
RB145	Basalt	Rembu	Xia et al. (2008a)
RB146	Basalt	Rembu	Xia et al. (2008a)
RB147	Basalt	Rembu	Xia et al. (2008a)
RB151	Basalt	Rembu	Xia et al. (2008a)
Lz-18	Basalt	Cuolashan	Zhu et al. (2008)
Lz-19	Basalt	Cuolashan	Zhu et al. (2008)
Lz-21	Basalt	Cuolashan	Zhu et al. (2008)
Lz-23	Basalt	Cuolashan	Zhu et al. (2008)
Sg-16	Basalt	Sangdanlin	Zhu et al. (2008)
W-8	Basalt	Sangdanlin	Zhu et al. (2008)
LX03-1	Metabasalt	Lang county	Zhang et al. (2011)
LX03-3	Metabasalt	Lang county	Zhang et al. (2011)
LX03-5	Metabasalt	Lang county	Zhang et al. (2011)
M-68	Metabasalt	Eastern Syntaxis	Geng et al. (2010)
M-114	Metabasalt	Eastern Syntaxis	Geng et al. (2010)
M-124	Metabasalt	Eastern Syntaxis	Geng et al. (2010)
M-125	Metabasalt	Eastern Syntaxis	Geng et al. (2010)
M-149	Metabasalt	Eastern Syntaxis	Geng et al. (2010)
M-153	Metabasalt	Eastern Syntaxis	Geng et al. (2010)
M-18	Metabasalt	Eastern Syntaxis	Geng et al. (2010)
L-21	Metabasalt	Eastern Syntaxis	Geng et al. (2010)

Tectonic evolution of the YZSZ ophiolites and the OIB-type rocks

The YZSZ ophiolites display major variations in their magmatic and metamorphic ages, geochemical affinities and melt evolution patterns. However, almost all the ophiolite massifs and the early

Table 3. Selected trace element contents and ratios for the OIB-type rock assemblages from the YZSZ and typical OIB in the world for comparison. Key to the numbering system for the data: 1-Sun and McDonough (1989); 2-Wilson (1989); 3-Liu et al. (2013); 4-Bezard et al. (2011); 5-Dai et al. (2012); 6-Bédard et al. (2009); 7-Xia et al. (2008a); 8-Zhu et al. (2008); 9-Zhang et al. (2011); 10-Geng et al. (2010).

Element	MORB[1]	OIB[1]	Hawaii[2]	Dongbo[3]	Xiugugabu[4]	Zhongba[5]	Saga[6]	Sangsang[6]	Rembu[7]	Sangdanlin[8]	Lang County[9]	Eastern Syntaxis[10]
Ba (ppm)	6.3-57	350	75-340	341-1537	284-836	40.4-200	37.4-712.3	103-549	109-758	75-140	8.9-25.7	168-678
Rb (ppm)	0.56-5.04	31	4.9-26	39.6-128	60.2-63.3	0.91-11.1	5-12	3-31	1.82-32.2	4.3-10.7	0.37-1.8	12.2-210
Zr (ppm)	73-90	280	115-351	396-545	169.7-314.5	108-281	237-329	135-344	183-394	179-428	137-216	62-191
Nb (ppm)	2.33-8.3	48	8-36	57.7-132	32.2-34.3	15.5-52.1	45.7-70.2	20.7-37.5	40.7-79.9	36.4-87	8.6-11.5	9.8-28
Hf (ppm)	2.03-2.05	7.8	3-8.5	10.7-14.4	5.8-8.98	3.01-6.62	5.04-7.47	3.6-8.7	5-10.5	4.7-9.9	3.6-5.5	1.7-4.8
Th (ppm)	0.12-0.6	4	0.5-2.9	5.7-10.4	7.8-8.9	1.32-6.09	2.65-3.7	1.57-4.49	2.62-6.06	2.2-9.7	2.6-3.6	0.9-8
La (ppm)	2.5-6.3	37	7.58-38	68.7-121.4	37.2-38.6	9.67-39.1	26.1-37.99	17-37.7	33-60.1	27.9-72.3	11.7-17.7	10.1-41.6
Ce (ppm)	7.5-15	35	21-85	150-242	83.6-86.3	23.9-82.7	58.6-80.8	37.5-83.5	66.8-129	58.5-144	27.2-42.9	27.1-98.7
Ce/Nb	1.81-3.22	0.73	2.09-2.7	1.54-3.0	2.52-2.65	1.54-2.04	1.15-1.28	1.72-2.47	1.35-1.77	1.27-2.13	3.16-3.74	1.72-3.53
Th/Nb	0.05-0.07	0.08	0.06-0.08	0.06-0.11	0.24-0.28	0.07-0.13	0.05-0.06	0.08-0.13	0.06-0.1	0.05-0.11	0.3-0.31	0.07-0.29
Hf/Nb	0.24-1.23	0.16	0.19-0.42	0.08-0.22	0.18-0.28	0.13-0.23	0.11-0.12	0.15-0.23	0.09-0.14	0.11-0.24	0.42-0.48	0.07-0.4
Zr/Nb	8.8-31.8	5.83	6.76-14.9	3.32-7.02	5.22-9.77	5.39-9.18	4.7-5.2	6.42-9.17	3.43-5.02	4.37-9.56	15.9-18.9	2.21-12.6
Ba/Nb	2.7-6.9	7.29	8.82-18.75	4.48-11.99	8.29-25.7	1.78-7.34	0.82-10.2	2.93-26.5	1.83-12.13	0.86-3.41	1.03-2.24	11.24-50.9
La/Nb	0.76-1.07	0.77	0.79-1.18	0.69-1.5	1.13-1.19	0.62-0.91	0.54-0.57	0.8-1.06	0.61-0.83	0.61-0.94	1.35-1.58	0.76-1.49
Ba/Th	52.5-95	87.5	117-250	56.8-199.6	31.8-106.7	13.4-102.3	14-193	23.3-350	26.1-189	7.7-63.6	3.47-7.21	83.5-698
Ba/La	2.52-9.05	9.46	8.95-15.96	4.73-16.76	7.4-21.7	1.95-8.6	1.43-18.8	3.1-24.9	2.88-15.1	1.04-4.36	0.76-1.45	12.26-67.13

Cretaceous ophiolitic mélange units within the YZSZ are spatially and temporally associated with OIB-type rock associations, as documented in this study and in some previous studies (Dupuis et al., 2005; Zhang et al., 2005; Xia et al., 2008a; Zhu et al., 2008; Bezard et al., 2011). Geochemical features of these OIB-type extrusive and intrusive rocks are consistent with plume-influenced melt evolution of their magmas.

The YZSZ ophiolitic peridotites appear to have experienced two-stage melt evolution and depletion events. The cpx-rich harzburgites in these peridotites are analogous to the upper mantle peridotites produced after low-degree melt extraction at a mid-ocean ridge setting. The second stage re-melting of these already depleted upper mantle peridotites (residues of the first stage MOR melting) created a higher-degree depleted mantle residue, after they became trapped in a mantle wedge above an intraoceanic subduction zone (Zhou et al., 1996, 2005; Huot et al., 2002; Dilek and Robinson, 2003, and references therein; Chen and Xia, 2008; Liu et al., 2010; Bezard et al., 2011; Dai et al., 2011b; Xu et al., 2015a). This second episode of melting of the already depleted mantle was responsible for the production of island arc tholeiite to boninitic melts enriched in light REE (due to the contribution from the subducting slab) (Dilek and Furnes, 2009; Dilek and Thy, 2009).

On the basis of these petrological – geochemical observations and interpretations, we have developed a tectonic model for the magmatic evolution of the YZSZ ophiolites and the associated OIB-type rock associations, following the model suggested by Xu et al. (2015a). In this refined model the oldest Neotethyan ophiolites (>180 – 140 Ma) that are currently exposed in the easternmost part of the YZSZ are inferred to have formed in a plume-proximal seafloor spreading system (Dilek and Furnes, 2011, 2014) within a Neotethyan seaway, which evolved between Proto-India and Eurasia (Fig. 9A). The oceanic lithosphere that formed during the rift-drift and seafloor spreading stages of the evolution of this Neotethyan seaway contains mafic rock associations produced by E-MORB, P-MORB and OIB-type melts, and fragments of these mafic rock assemblages widely occur within the Triassic through Jurassic-Cretaceous flysch units, the early Cretaceous ophiolitic mélange, and ophiolite complexes along the YZSZ. The role of plume magmatism and plume-metasomatized mantle chemistry in the petrogenetic evolution of rift-drift generated magmatic rocks exposed in suture zones is well documented in the literature (Dilek, 2003; Buiter and Torsvik, 2014).

In addition to the occurrence of P-type and OIB-type ophiolitic lithologies along the entire length of the YZSZ, there is another independent line of evidence for the potential involvement of a regional plume or mantle updraft event in the early history of Neotethys in southern Tibet. The peridotites and chromitite bodies in the Loubusa ophiolite contain in-situ diamonds and other ultrahigh-pressure (UHP) mineral inclusions (Yamamato et al., 2009; Yang et al., 2014, 2015a, 2015b,, and references therein), suggesting that they might have initially originated under very high-temperature and high-pressure conditions. The P-T estimates of the UHP mineral assemblages suggest that the chromitite formation might have initially begun within or near the mantle transition zone (Yang et al., 2015b, and references therein). The early, high-temperature deformation fabrics in the podiform chromitites and peridotites containing UHP inclusions appear to have developed during their ascent from the lower to the upper mantle by a regional-scale, plume-originated updraft (Fig. 9A; Yang et al., 2014). The upwelling OIB melt might have also contained methane fluids originated in the lower mantle, and these

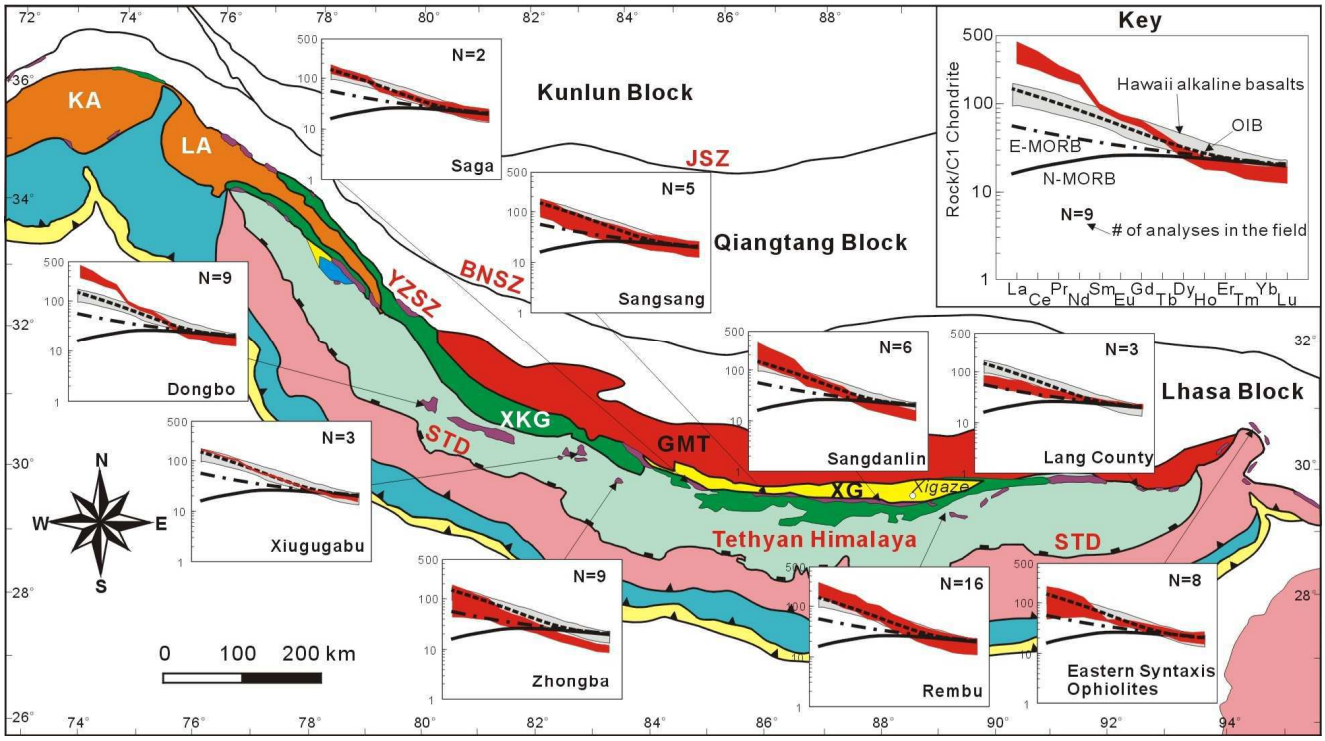

Figure 3. Chondrite-normalized REE diagrams for the OIB-type mafic rocks from the ophiolite massifs investigated in this study. Chondrite normalizing values, and the N-MORB, E-MORB, and OIB trends are from Sun and McDonough (1989). Data for the Hawaii alkaline basalt field are from Garcia et al. (1995), Hofmann and Jochum (1996), and Xu et al. (2007). Map symbols are the same as in Figure 1. Data sources for the chemical compositions of the OIB-type rocks from different ophiolite massifs are listed in Table 2.

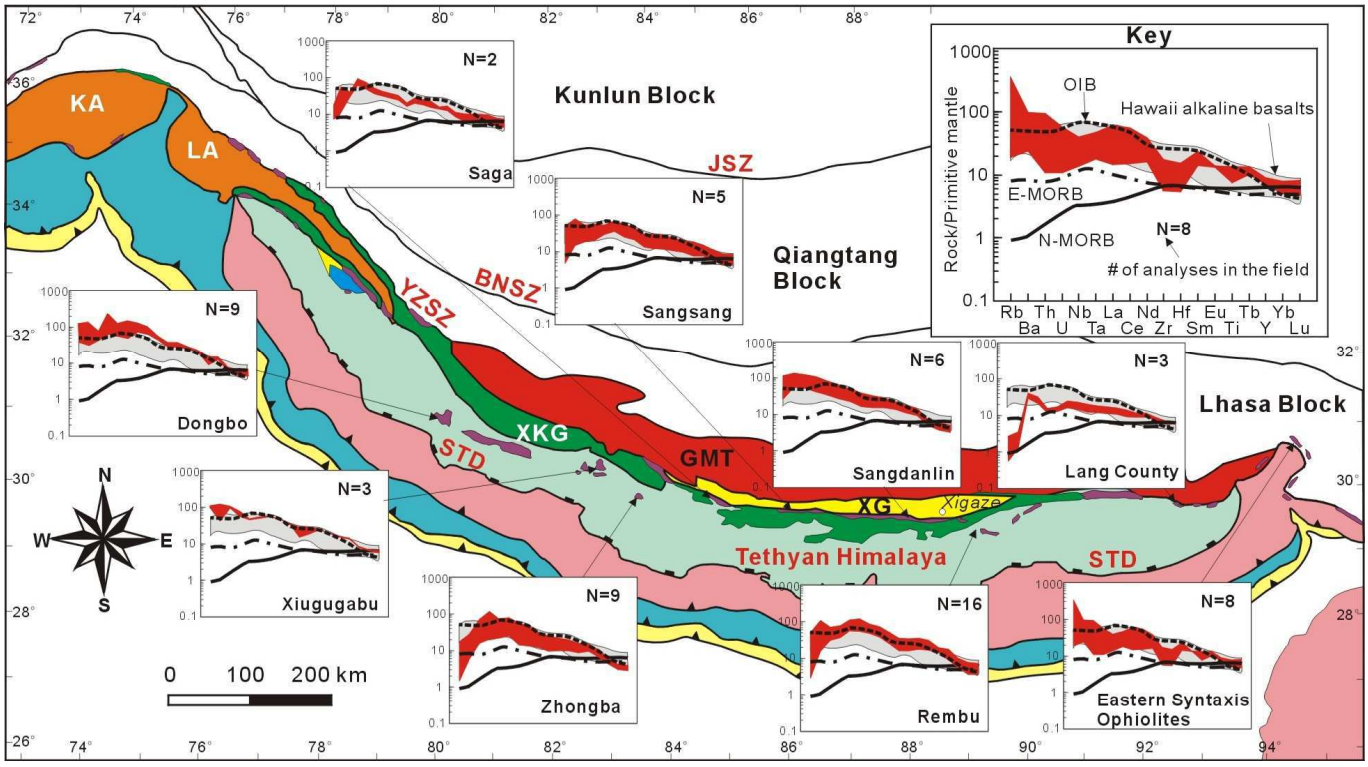

Figure 4. Primitive-mantle-normalized spider diagrams for the OIB-type mafic rocks from the ophiolite massifs investigated in this study. Primitive mantle values, and the N-MORB, E-MORB, and OIB trends are from Sun and McDonough (1989). Data for the Hawaii alkaline basalt field are from Garcia et al. (1995), Hofmann and Jochum (1996), and Xu et al. (2007). Map symbols are the same as in Figure 1. Data sources for the chemical compositions of the OIB-type rocks from different ophiolite massifs are listed in Table 2.

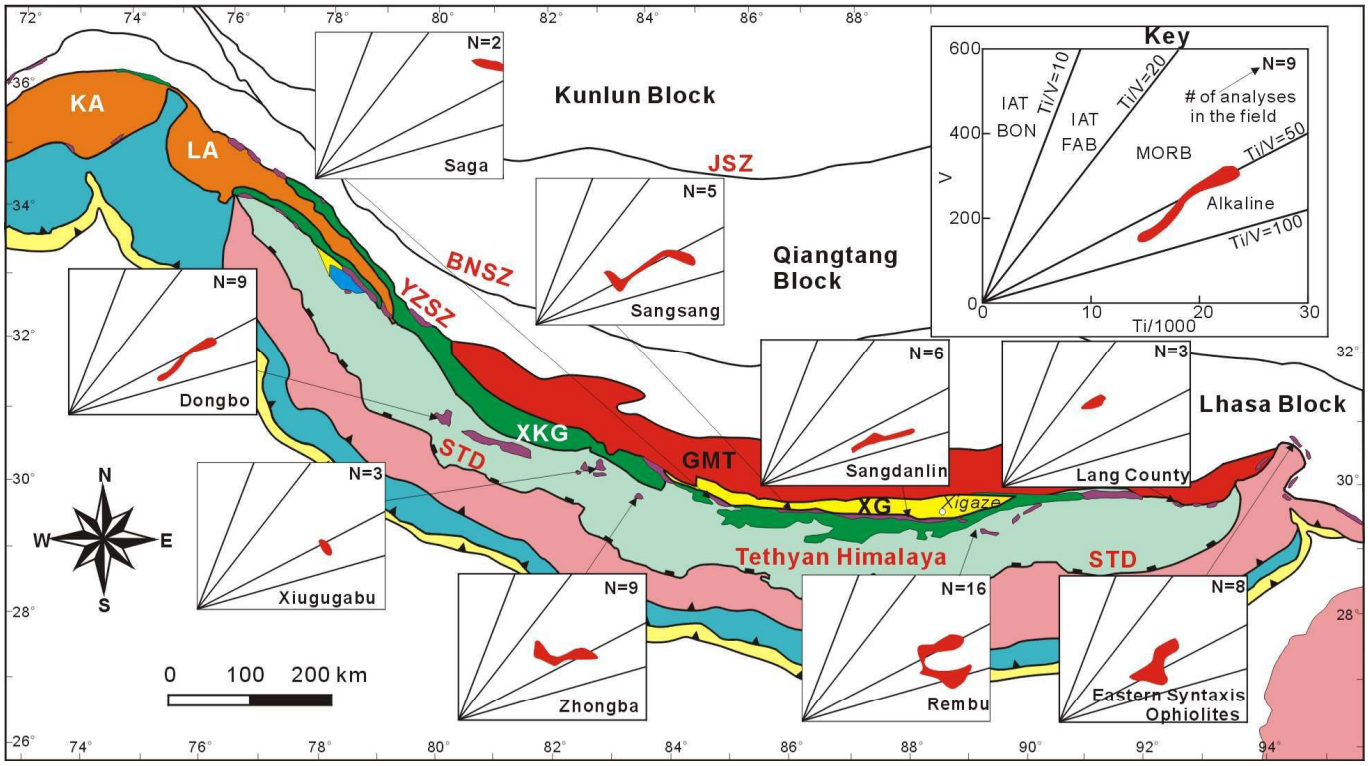

Figure 5. Ti/1000 (ppm) versus V (ppm) diagram (modified after Shervais, 1982) for the OIB-type mafic rocks from the ophiolite massifs investigated in this study. Map symbols are the same as in Figure 1. Data sources for the chemical compositions of the OIB-type rocks from different ophiolite massifs are listed in Table 2.

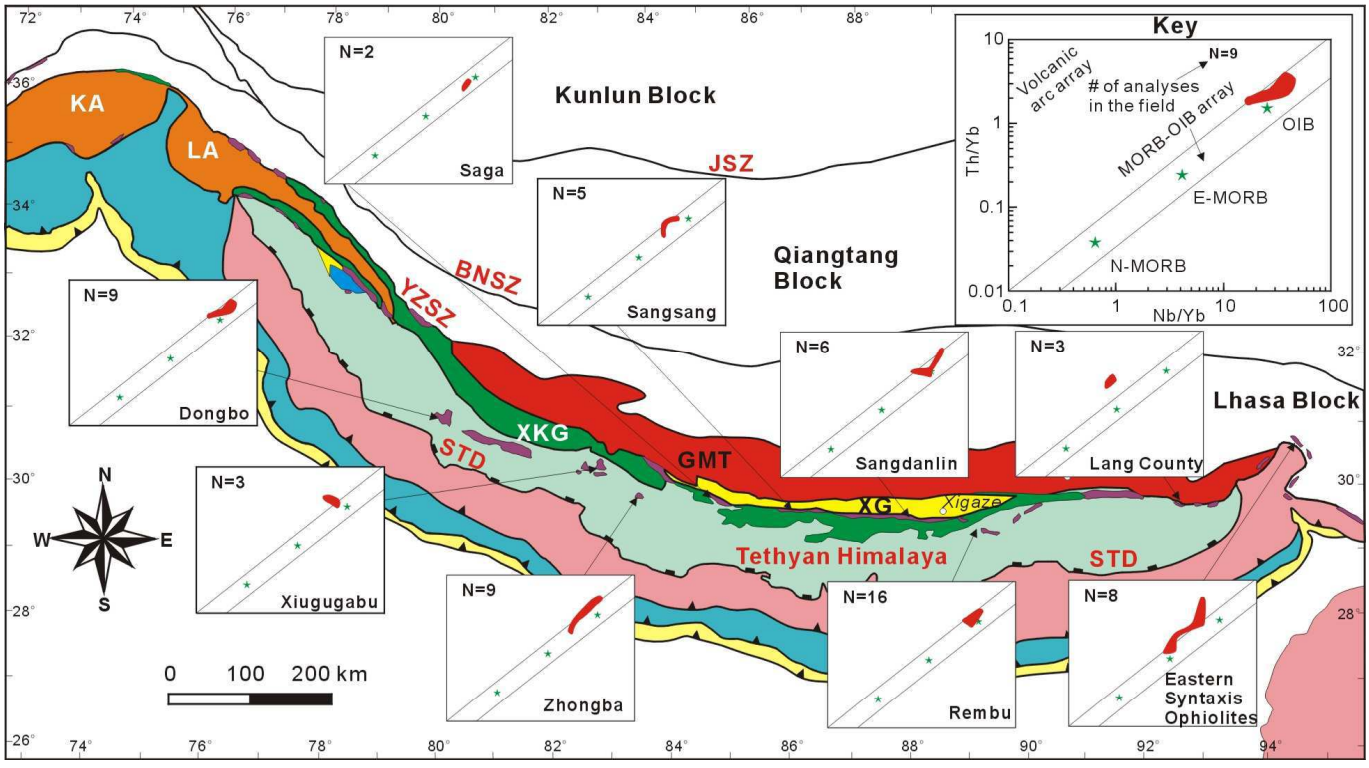

Figure 6. Th/Yb vs Nb/Yb proxy for the OIB-type mafic rocks from the ophiolite massifs investigated in this study. The MORB-OIB array and the volcanic arc array are from Pearce (2008). Map symbols are the same as in Figure 1. Data sources for the chemical compositions of the OIB-type rocks from different ophiolite massifs are listed in Table 2. The data for the Hawaiian alkaline basalt field are from: Chen et al., 1990; Gaffney et al., 2004; Kimura et al., 2006.

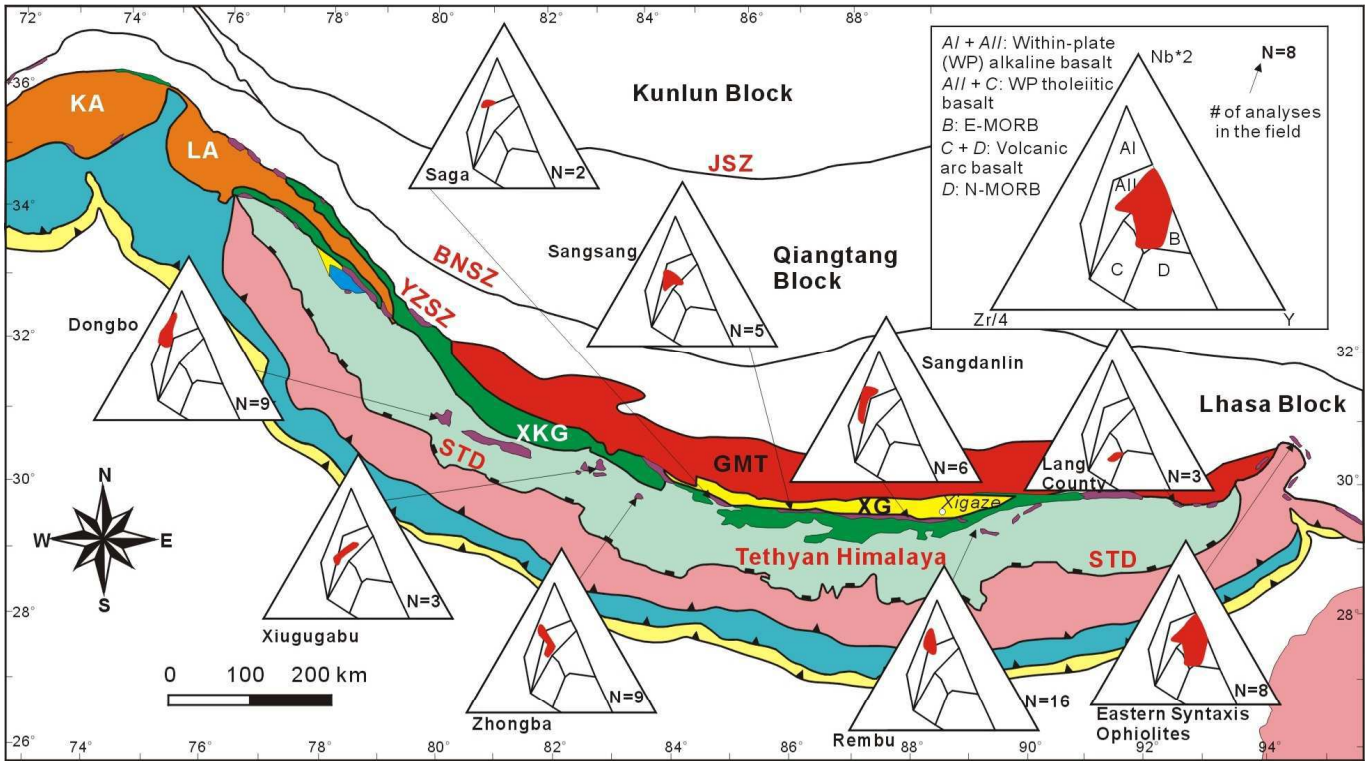

*Figure 7. Nb*2–Zr/4–Y triangular diagram for the OIB-type mafic rocks from the ophiolite massifs investigated in this study. Map symbols are the same as in Figure 1. Data sources for the chemical compositions of the OIB-type rocks from different ophiolite massifs are listed in Table 2.*

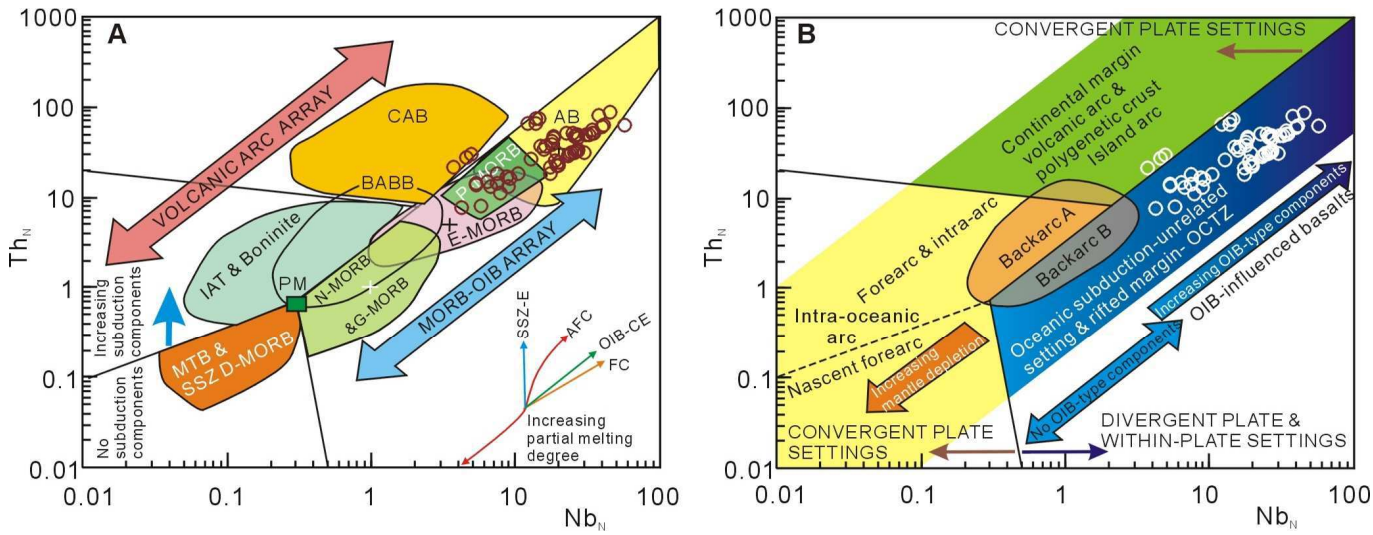

Figure 8: A- N-MORB normalized Th_N vs. Nb_N binary discriminant diagram, showing the compositional variations of different mafic rock-types and their tectonic affinities (after Saccani, 2015) and the distribution of the representative OIB-type rocks from the YZSZ. Vectors mark the trends of compositional variations controlled by the main petrogenetic processes. Abbreviations for vectors: SSZ-E: supra-subduction zone enrichment; AFC: assimilation-fractional crystallization; OIB-CE: ocean island-type (plume-type) component enrichment; FC: fractional crystallization. Crosses represent the compositions of typical N-MORB, E-MORB and OIB (after Sun and McDonough, 1989). Key for other symbols: MORB – mid-ocean ridge basalt; G-MORB – garnet-influenced MORB; N-MORB – normal-type MORB; E-MORB – enriched-type MORB; P-MORB – plume-type MORB; AB – alkaline ocean island basalt; IAT – low-Ti, island arc tholeiite; BON – very low-Ti, boninitic basalt; CAB – calc-alkaline basalt; MTB – medium-Ti basalt; D-MORB – depleted-type MORB; BABB – backarc basin basalt. B- Tectonic interpretation of ophiolitic mafic rock types based on Th_N-Nb_N systematics, and the distribution of the representative OIB-type rocks from the YZSZ. Backarc A – backarc basin basalts (BABB) characterized by input of subduction or crustal components; Backarc B – BABBs with no input of subduction or crustal components (mature intra-oceanic back arcs); OCTZ – ocean-continent transition zone. See text for further discussion.

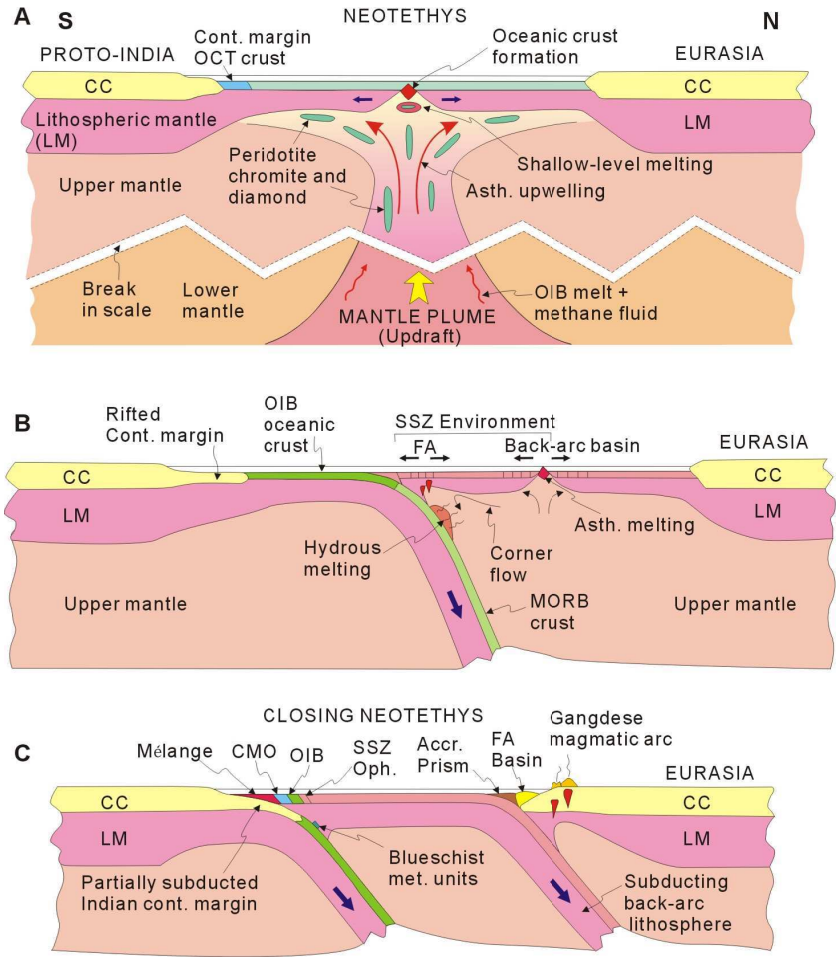

Figure 9: Sequential tectonic model for the evolution of the YZSZ ophiolites and the associated P-type and OIB-type mafic rock assemblages (modified after Xu et al., 2015a). See text for discussion. Key for symbols: CC – Continental crust; CMO – Continental margin ophiolite; FA – Forearc; OCT – Ocean-continent transition; LM – Lithospheric mantle; OIB – Ocean Island Basalt.

fluids might have contributed to the carbon budget in the transition zone and have acted as catalysts for diamond crystallization.

The younger Neotethyan oceanic crust (130–120 Ma) preserved within the YZSZ include mafic-ultramafic rock units that display strong subduction influence in their melt evolution. These subduction-related YZSZ ophiolites formed in forearc to backarc tectonic environments in a suprasubduction zone setting (Hébert et al., 2012; Dai et al., 2013) above a N-dipping, intraoceanic subduction zone during the early Cretaceous (Fig. 9B). The pre-existing oceanic lithosphere that formed via seafloor spreading within the Neotethyan seaway (>170–140 Ma) was consumed at this intraoceanic subduction zone, and the younger SSZ ophiolites (130–120 Ma) were produced through a combination of hydrous melting, corner flow, and slab rollback-driven extensional tectonics in the upper plate. This scenario has been also proposed for the younger (late Cretaceous: 95-92 Ma) Neotethyan ophiolites farther west in the eastern Mediterranean region (Dilek and Flower, 2003; Flower and Dilek, 2003). Tectonic underplating and partial subduction of the northern passive margin of Proto-India beneath the intraoceanic arc system resulted in the telescoping of the SSZ ophiolites and the ophiolitic mélange unit in a stack of S-vergent thrust nappes (Fig. 9C) on top of the continental crust (Tethyan Himalaya) in the lower plate. This arc-continent collision within the Neotethyan realm was instrumental in the initiation of an Andean type convergent margin tectonics along the southern edge of Eurasia that produced the Gangdese magmatic arc and the Xigaze forearc basin in the upper plate, while consuming the backarc generated Neotethyan oceanic lithosphere (Fig. 9C).

Conclusions

A systematic review of the extant geochemical and geochronological data from the YZSZ ophiolites reveals the widespread occurrence of OIB-type and alkaline mafic rock assemblages, which range in age from the earliest Jurassic through early Cretaceous. These rock associations are tectonically intercalated with oceanic rocks both in the ophiolites and ophiolitic mélanges within the YZSZ, or they occur as blocks and thrust sheets within the Jurassic-Cretaceous flysch units structurally below and south of the YZSZ. They display LREE enrichment and HREE depletion, no subduction influence in their trace element patterns, and significant enrichment in LILE in comparison to HFSE and HREE. Compositionally, they resemble modern OIB and the Hawaiian alkaline basalts. Magmas of these OIB-type and alkaline rock associations formed from partial melting of a MORB-type asthenospheric source, enriched by plume component, during the rift-drift and seafloor spreading evolution of the Neotethyan oceanic lithosphere during the Jurassic through Cretaceous. The younger (130-120 Ma) oceanic lithosphere evolved in forearc to backarc SSZ settings above a N-dipping subduction zone, which consumed much of the previously formed Neotethyan oceanic crust. The YZSZ ophiolites hence reflect a poly-phase melt history and different mantle melt sources in their evolutionary history. Tectonic juxtaposition of the geochemically and geochronologically diverse Neotethyan ophiolites took place during their emplacement onto the northern passive margin of Proto-India in the lower plate during the late Cretaceous. The existence within the YZSZ and the suture zones in other Tethyan orogenic belts of OIB-type and alkaline mafic rocks shows that oceanic rocks produced during different stages of the Wilson cycle evolution of ocean basins are commonly well preserved in the crustal architecture of the collision zones (Dilek and Sandvol, 2009).

Acknowledgements

This research was financially supported by the National Nature Science Foundation of China (41303027), and Special Fund for Basic Scientific Research of Central Colleges, Chang'an University (310827153506, 310827153407) to G.-X. Yang. Y. Dilek's research in Tibet and on the Yarlung-Zangbo suture zone ophiolites has been funded by the Chinese Academy of Geological Sciences (Beijing, China). We thank R. Hébert, J.S. Yang, Z.Q. Xu, and F. Liu for insightful discussions on the geology, geochemistry and structure of the Yarlung-Zangbo ophiolites and on various aspects of our study as presented in this paper.

References

Ahmad, T., Tanaka, T., Sachan, H.K., Isalm, R., and Khanna, P.P., 2008, Geochemical and isotopic characteristics of the gabbroic rocks from Nidar ophiolitic complex, Indus Suture Zone, Eastern Ladakh. National Symposium on Milestones in Petrology. Banaras Hindu University and Geological Society of India, Varanasi, pp. 57.

Aitchison, J.C., Davis, A.M., Liu, J., Luo, H., Malpas, J.G., McDermid, I.R.C., Wu, H.Y., Ziabrev, S.V., and Zhou, M.F., 2000, Remnants of a Cretaceous intra-oceanic subduction system within the Yarlung-Zangbo suture (southern Tibet). Earth and Planetary Science Letters, v. 183, pp. 231–244.

Allègre, C.J., Courtillot, V., Tapponnier, P., Hirn, A., Mattauer, M., Coulon, C., Jaeger, J.J., Achache, J., Schärer, U., Marcoux, J., Burg, J.P., Girardeau, J., Armijo, R., Gariépy, C., Göpel, C., Li, T.D., Xiao, X.C., Chang, C.F., Li, G.Q., Lin, B.Y., Teng, J.W., Wang, N.W., Chen, G.M., Han, T.L., Wang, X.B., Den, W.M., Sheng, H.B., Cao, Y.G., Zhou, J., Qiu, H.R., Bao, P.S., Wang, S.C., Wang, B.X., Zhou, Y.X., and Xu, R.H., 1984, Structure and evolution of the Himalaya–Tibet orogenic belt. Nature, v. 307, pp. 17–22.

Bao, P.S., Su, L., Wang, J., and Zhai, Q.G., 2014, Origin of the Zedang and Luobuso ophiolites, Tibet. Acta Geological Sinica, v. 88, p. 669-698.

Bao, P.S., Su, L., Wang, J., and Zhai, Q.G., 2013, Study on the tectonic setting for the ophiolites in Xigaze, Tibet. Acta Geologica Sinica-English Edition, v. 87, pp. 395–425.

Bédard, É., Hébert, R., Guilmette, C., Lesage, G., Wang, C.S., and Dostal, J., 2009, Petrology and geochemistry of the Saga and Sangsang ophiolitic massifs, Yarlung Zangbo Suture Zone, Southern Tibet: Evidence for an arc–back–arc origin. Lithos, v. 113, pp. 48–67.

Bezard, R., Hébert, R., Wang, C.S., Dostal, J., Dai, J.G., and Zhong, H.T., 2011, Petrology and geochemistry of the Xiugugabu ophiolitic massif, western Yarlung Zangbo suture zone, Tibet. Lithos, v. 125, pp. 347–367.

Buiter, S.J.H and Torsvik, T.H., 2014, A review of Wilson Cycle plate margins: A role for mantle plumes in continental break-up along sutures? Gondwana Research, v. 26, p. 627-653.

Burg, J.P., and Chen, G.M., 1984, Tectonic and structural zonation of southern Tibet, China. Nature, v. 311, pp. 219–223.

Chan, G.H.N., Crowley, Q., Searle, M., Aitchison, J.C., and Horstwood, M., 2007, U–Pb zircon ages of the Yarlung Zangbo suture zone ophiolites, south Tibet, 22th Himalaya–Karakorum–Tibet Workshop, Hong Kong, China. Workshop Abstract Volume 12.

Chan, G.H.N., Aitchison, J.C., Crowley, Q., Horstwood, M., Searle, M.P., Parrish, R.R., and Chan, J.S.L., 2015, U–Pb zircon ages for Yarlung Tsangpo suture zone ophiolites, southwestern Tibet and their tectonic implications. Gondwana Research, v. 27, pp. 719–732.

Chen, C., Frey, F., and Garcia, M., 1990, Evolution of alkalic lavas at Haleakala Volcano, east Maui, Hawaii. Contributions to Mineralogy and Petrology, v. 105, pp. 197–218.

Chen, G.W., and Xia, B., 2008. Platinum-group elemental geochemistry of mafic and ultramafic rocks from the Xigaze ophiolite, southern Tibet. Journal of Asian Earth Sciences, v. 32, pp. 406–422.

Chu, M.F., Chung, S.L., Song, B.A., Liu, D.Y., O'Reilly, S.Y., Pearson, N.J., Ji, J.Q., and Wen, D.J., 2006, Zircon U–Pb and Hf isotope constraints on the Mesozoic tectonics and crustal evolution of southern Tibet. Geology, v. 34, pp. 745–748.

Chung, S.L., Chu, M.F., Zhang, Y.Q., Xie, Y.W., Lo, C.H., Lee, T.Y., Lan, C.Y., Li, X.H., Zhang, Q., and Wang, Y.Z., 2005, Tibetan tectonic evolution inferred from spatial and temporal variations in post-collisional magmatism. Earth-Science Reviews, v. 68, pp. 173–196.

Dai, J., Wang, C., Hébert, R., Li, Y., Zhong, H., Guillaume, R., Bezard, R., and Wei, Y., 2011a, Late Devonian OIB alkaline gabbro in the Yarlung Zangbo Suture Zone: Remnants of the Paleo-Tethys? Gondwana Research, v. 19, pp. 232–243.

Dai, J.G., Wang, C.S., Hébert, R., Santosh, M., Li, Y.L., and Xu, J.Y., 2011b, Petrology and geochemistry of peridotites in the Zhongba ophiolite, Yarlung Zangbo Suture Zone: Implications for the early Cretaceous intra-oceanic subduction zone within the Neo-Tethys. Chemical Geology, v. 288, pp. 133–148.

Dai, J., Wang, C., and Li, Y., 2012, Relicts of the Early Cretaceous seamounts in the central-western Yarlung Zangbo Suture Zone, southern Tibet. Journal of Asian Earth Sciences, v. 53, pp. 25–37.

Dai, J., Wang, C., Polat, A., Santosh, M., Li, Y., and Ge, Y., 2013, Rapid forearc spreading between 130–120 Ma: evidence fromgeochronology and geochemistry of the Xigaze ophiolite, southern Tibet. Lithos, v. 172–173, pp. 1–16.

Dilek, Y., 2003, Ophiolite pulses, mantle plumes and orogeny. In, Geological Society, London, Special Publications, v. 218, pp. 9-19.

Dilek, Y., and Flower, M.F.J., 2003, Arc-trench rollback and forearc accretion: 2. Model template for Albania, Cyprus, and Oman In, Geological Society of London Special Publications, v. 218, p. 43-68.

Dilek, Y., and Newcomb, S., 2003, Ophiolite concept and the evolution of geological thought. Geological Society of America Special Papers, v. 373, The Geological Society of America, Boulder, CO 80301, ISBN 0-8137-2373-6.

Dilek, Y. and Robinson, P.T., 2003. Ophiolites in Earth History: Introduction: Geological Society, London, Special Publication, v. 218, pp. 1-8, doi: 10.1144/gsl.sp.2003.218.01.01

Dilek, Y., and Furnes, H., 2009, Structure and geochemistry of Tethyan ophiolites and their petrogenesis in subduction rollback systems. Lithos, v. 113, pp. 1–20.

Dilek, Y., and Furnes, H., 2011, Ophiolite genesis and global tectonics: Geochemical and tectonic fingerprinting of ancient oceanic lithosphere. Geological Society of America Bulletin, v. 123, pp. 387–411.

Dilek, Y., and Furnes, H., 2014, Ophiolites and Their Origins. Elements, v. 10, pp. 93–100.

Dilek, Y., Furnes, H., and Shallo, M., 2008, Geochemistry of the Jurassic Mirdita Ophiolite (Albania) and the MORB to SSZ evolution of a marginal basin oceanic crust. Lithos, v. 100, pp. 174-209.

Dilek, Y., and Thy, P., 1998, Structure, petrology and seafloor spreading tectonics of the Kizildag ophiolite, Turkey. Geological Society, London, Special Publications, v. 148, p. 43-69.

Dilek, Y. and Sandvol, E., 2009, Seismic structure, crustal architecture and tectonic evolution of the Anatolian-African plate boundary and the Cenozoic orogenic belts in the Eastern Mediterranean region. Geological Society, London, Special Publications, v. 329, pp. 127-160, doi: doi:10.1144/SP327.8

Dubois-Côté, V., Hébert, R., Dupuis, C., Wang, C.S., Li, Y.L., and Dostal, J., 2005, Petrological and geochemical evidence for the origin of the Yarlung Zangbo ophiolites, southern Tibet. Chemical Geology, v. 214, pp. 265–286.

Dupuis, C., Hébert, R., Dubois-Côté, V., Wang, C.S., Li, Y.L., and Li, Z.J., 2005, Petrology and geochemistry of mafic rocks from melange and flysch units adjacent to the Yarlung Zangbo Suture Zone, southern Tibet. Chemical Geology, v. 214, pp. 287–308.

Einsele, G., Liu, B., Duerr, S., Frisch, W., Liu, G., Luterbacher, H.P., Ratschbacher, L., Richen, W., Wendt, J., Wetzel, A., Yu, G., Zheng, H., 1994, The Xigaze forearc basin: evolution and facies architecture (Cretaceous, Tibet). Sedimentary Geology, v. 90, pp. 1–32.

Fareeduddin and Dilek, Y., 2015, Structure and Petrology of the Nagaland-Manipur Hill Ophiolite Melange Zone, NE India: A Fossil Tethyan Subduction Channel at the Indo-Myanmar Plate Boundary. Episodes, v. 38, No.4, pp. 298-314, doi: 10.18814/epiiugs/2015/v38i4/82426.

Flower, M.F.J. and Dilek, Y., 2003, Arc-trench rollback and forearc accretion: 1. A collision-induced mantle flow model for Tethyan ophiolites: In, Geological Society of London Special Publications, v. 218, p. 21-42.

Gaffney, A., Nelson, B., and Blichert-Toft, J., 2004, Geochemical constraints on the role of oceanic lithosphere in intra-volcano heterogeneity at West Maui. Hawaii. Journal of Petrology, v. 45, pp. 1663–1687.

Garcia, M.O., Foss, D.J.P., West, H.B., and Mahoney, J.J., 1995, Geochemical

and isotopic evolution of Loihi volcano, Hawaii. Journal of Petrology, v. 36, pp. 1647–1674.

Geng, Q.R., Pan, G.T., Zheng, L.L., Chen, Z.L., Fisher, R.D., Sun, Z.M., Ou, C.S., Dong, H., Wang, X.W., Li, S., Lou, X.Y., and Fu, H., 2006, The eastern Himalayan syntaxis: major tectonic domains, ophiolitic mélanges and geologic evolution. Journal of Asian Earth Sciences, v. 27, pp. 265–285.

Geng, Q.R., Peng, Z.M., and Zhang, Z., 2010, Geochemical study on metamorphosed mafic rocks in ophiolitic zone in the Yarlung Zangbo Great Bend, eastern Tibet, China. Geological Bulletin of China, v. 29, pp. 1781–1794.

Ghose, N.C., Chatterjee, N., and Fareeduddin, 2014, A petrographic atlas of ophiolite: An example from the Eastern India – Asia collision zone. Springer Science, pp. 234.

Göpel, C., Allègre, C.J., and Xu, R.H., 1984, Lead isotopic study of the Xigaze ophiolite (Tibet): the problem of the relationship between magmatites (gabbros, dolerites, lavas) and tectonites (harzburgites). Earth and Planetary Science Letters, v. 69, pp. 301–310.

Goscombe, B., Gray, D., and Hand, M., 2006, Crustal architecture of the Himalayan metamorphic front in eastern Nepal. Gondwana Research, v. 10, pp. 232–255.

Guilmette, C., Hébert, R., Bédard, É., Wang, C.S., Ullrich, T.D., and Dostal, J., 2007, Saga ophiolite, Yarlung Zangbo suture Zone, Tibet: field relationships, discovery of garnet-pyroxene amphibolite and Ar/Ar ages. Workshop Abstract Volume, HKTW 22 Hong Kong, pp. 37.

Guilmette, C., Hébert, R., Dostal, J., Indares, A., Ullrich,T., Bédard, E., and Wang, C.S., 2012, Discovery of a dismembered metamorphic sole in the Saga ophiolitic mélange, South Tibet: Assessing an Early Cretaceous disruption of the Neo-Tethyan supra-subduction zone and consequences on basin closing. Gondwana Research, v. 22, pp. 398–414.

Guilmette, C., Hébert, R., Dupuis, C., Wang, C.S., and Li, Z.J., 2008, Metamorphic history and geodynamic significance of high-grade metabasites from the ophiolitic mélange beneath the Yarlung Zangbo ophiolites, Xigaze area, Tibet. Journal of Asian Earth Sciences, v. 32, pp. 423–437.

Guilmette, C., Hébert, R., Wang, C., and Villeneuve, M., 2009, Geochemistry and geochronology of the metamorphic sole underlying the Xigaze Ophiolite, Yarlung Zangbo Suture Zone, South Tibet. Lithos, v. 112, pp. 149–162.

Hébert, R., Bezard, R., Guilmette, C., Dostal, J., Wang, C.S., and Liu, Z.F., 2012, The Indus-Yarlung Zangbo ophiolites from Nanga Parbat to Namche Barwa syntaxes, southern Tibet: First synthesis of petrology, geochemistry, and geochronology with incidences on geodynamic reconstructions of Neo-Tethys. Gondwana Research, v. 22, pp. 377–397.

Hébert, R., Huot, F., Wang, C.S., and Liu, Z., 2003, Yarlung Zangbo ophiolites, southern Tibet revisited: geodynamic implications from the mineral record. In: Dilek, Y., Robinson, P.T. (Eds.), Ophiolites in Earth History: Special Publication, 218. The Geological Society of London, London, pp. 165–190.

Hofmann, A., and Jochum, K., 1996, Source characteristics derived from very incompatible trace elements in Mauna Loa and Mauna Kea basalts, Hawaii Scientific Drilling Project. Journal of Geophysical Research, v. 101, pp. 831–839.

Honneger, K., Dietrich, V., Frank, W., Gansser, A., Thoni, M., and Trommsdorf, V., 1982, Magmatic and metamorphism in the Ladakh Himalayas (the Indus–Tsangpo suture zone). Earth and Planetary Science Letters, v. 60, pp. 253–292.

Huang, Y.H., Zhon, X.Z., and Wang, X.B., 1981, Pumpellyite from the contact metamorphic zone of ultramafic bodies of Luobusa ophiolite suite, South Tibet. Bulletin de Mineralogie, v. 104, pp. 441–444.

Huot, F., Hébert, R., Varfalvy, V., Beaudoin, G., Wang, C.S., Liu, Z.F., Cotten, J., and Dostal, J., 2002, The Beimarang melange (southern Tibet) brings additional constraints in assessing the origin, metamorphic evolution and obduction processes of the Yarlung Zangbo ophiolite. Journal of Asian Earth Sciences, v. 21, pp. 307–322.

Ji, W.Q., Wu, F.Y., Chung, S.L., Li, J.X., and Liu, C.Z., 2009, Zircon U–Pb geochronology and Hf isotopic constraints on petrogenesis of the Gangdese batholith, southern Tibet. Chemical Geology, v. 262, pp. 229–245.

Kimura, J., Sisson, T., Nakano, N., Coombs, M., and Lipman, P., 2006, Isotope geochemistry of early Kilauea magmas from the submarine Hilina bench: The nature of the Hilina mantle component. Journal of Volcanology and Geothermal Research, v. 151, pp. 51–72.

Kojima, S., Ahmad, T., Tanaka, T., Bagati, T.N., Mishra, M., Kumar, R., Islam, R., and Khanna, P., 2001, Early Cretaceous radiolarians from the Indus suture zone, Ladakh, northern India. News of Osaka Micropaleontologists, v. 12, pp. 257–270.

Li, J.F., Xia, B., Liu, L.W., Xu, L.F., He, G.S., Wang, H., Zhang, Y.Q., and Yang, Z.Q., 2008, SHRIMP U-Pb zircon dating of diabase in the La'nga Co ophiolite, Burang, Tibet, China, and its geological significance. Geological Bulletin of China, v. 27, pp. 1739–1743.

Li, J.F., Xia, B., Liu, L.W., Xu, L.F., He, G.S., Wang, H., Zhang, Y.Q., and Yang, Z.Q., 2009, SHRIMP U-Pb dating for the Gabbro in Qunrang Ophiolite, Tibet: the geochronology constraint for the development of eastern Tetys basin. Geotectonica et Metallogenia, v. 33, pp. 294–298.

Liang, F.H., Xu, Z.Q., Ba, D.Z., Xu, X.Z., Liu, F., Xiong, F.H., and Jia, Y., 2011, Tectonic occurrence and emplacement mechanism of ophiolite from Luobusha–Zedang, Tibet. Acta Petrologica Sinica, v. 27, pp. 3255–3268.

Liu, C.Z., Wu, F.Y., Wilde, S.A., Yu, L.J., and Li, J.L., 2010, Anorthitic plagioclase and pargasitic amphibole in mantle peridotites from the Yungbwa ophiolite (southwestern Tibetan Plateau) formed by hydrous melt metasomatism. Lithos, v. 114, pp. 413–422.

Liu, C.Z., Wu, F.Y., Chu, Z.Y., Ji, W.Q., Yu, L.J., and Li, J.L., 2012, Preservation of ancient Os isotope signatures in the Yungbwa ophiolite (southwestern Tibet) after subduction modification. Journal of Asian Earth Sciences, v. 53, pp. 38–50.

Liu, F., Yang, J.S., Chen, S.Y., Liang, F.H., Niu, X.L., Li, Z.L., and Lian, D.Y., 2013, Ascertainment and environment of the OIB-type basalts from the Dongbo ophiolite in the western part of Yarlung Zangbo Suture Zone. Acta Petrologica Sinica, v. 29, pp. 1909–1932.

Liu, F., Yang, J.S., Dilek, Y., Xu, Z.Q., Xu, X.Z., Liang, F.H., Chen, S.Y., and Lian, D.Y., 2015, Geochronology and geochemistry of basaltic lavas in the Dongbo and Purang ophiolites of the Yarlung-Zangbo Suture zone: Plume-influenced continental margin-type oceanic lithosphere in southern Tibet. Gondwana Research, v. 27, pp. 701–718.

Mahéo, G., Bertrand, H., Guillot, S., Villa, I.M., Keller, F., and Capiez, P., 2004, The south Ladakh ophiolites (NW Himalaya, India): an intra-oceanic tholeiitic origin with implication for the closure of the Neo-Tethys. Chemical Geology, v. 203, pp. 273–303.

Malpas, J., Zhou, M.F., Robinson, P.T., and Reynolds, P.H., 2003, Geochemical and geochronological constraints on the origin and emplacement of the Yarlung Zangbo ophiolites, Southern Tibet. In: Dilek, Y., Robinson, P.T. (Eds.), Ophiolites in Earth History. Geological Society, London, Special Publications, v. 218, pp. 191–206.

McDermid, I., Aitchison, J., Davis, A., Harrison, T., and Grove, M., 2002, The Zedong terrane: a Late Jurassic intra-oceanic magmatic arc within the Yarlung–Tsangpo suture zone, southeastern Tibet. Chemical Geology, v. 187, pp. 267–277.

Meschede, M., 1986, A method of discriminating between different types of mid-ocean ridge basalts and continental tholeiites with the Nb–Zr–Y diagram. Chemical Geology, v. 56, pp. 207–218.

Miller, C., Thöni, M., Frank, W., Schuster, R., Melcher, F., Meisel, T., Zanetti, A., 2003, Geochemistry and tectonomagmatic affinity of the Yungbwa ophiolite, SW Tibet. Lithos, v. 66, pp. 155–172.

Parkinson, I.J., and Pearce, J.A., 1998, Peridotites from the Izu–Bonin–Mariana Forearc (ODP Leg 125), Evidence for mantle melting and melt–mantle interaction in a supra-subduction zone setting. Journal of Petrology, v. 39, pp. 1577–1618.

Pearce, J., 2008, Geochemical fingerprinting of oceanic basalts with applications to ophiolite classification and the search for Archean oceanic crust. Lithos, v. 100, pp. 14–48.

Pedersen, R.B., Searle, M.P., and Corfield, R.I., 2001, U–Pb zircon ages

fromthe Spontang Ophiolite, Ladakh Himalaya. Journal of the Geological Society of London, v. 158, pp. 513–520.

Reuber, I., Colchen, M., and Mevel, C., 1987, The geodynamic evolution of the South-Tethyan margin in Zanskar, NW Himalaya, as revealed by the Spongtang ophiolitic melange. Geodinamica Acta, v. 1, pp. 283–296.

Reuber, I., Montigny, R., Thuizat, R., and Heitz, A., 1989, K–Ar ages of ophiolites and arc volcanics of the Indus Suture Zone: comparison with other Himalaya-Karakorum data. Eclogae Geologicae Helvetiae, v. 82, pp. 699–715.

Robinson, P.T., Bai, W.J., Malpas, J., Yang, J.S., Zhou, M.F., Fang, Q.S., Hu, X.F., Cameron, S., and Staudigel, H., 2004, Ultra-high pressure minerals in the Luobusa Ophiolite, Tibet, and their tectonic implications. In: Malpas, J., Fletcher, C.J.N., Ali, J., Aitchison, J.C. (Eds.), Aspects of the Tectonic Evolution of China: Geological Society of London Special Publications, v. 226, pp. 247–271.

Saccani, E., 2015, A new method of discriminating different types of post-Archean ophiolitic basalts and their tectonic significance using Th-Nb and Ce-Dy-Yb systematics. Geoscience Frontiers, v. 6, pp. 481–501.

Saccani, E., Dilek, Y., Marroni, M., and Pandolfi, L., 2015, Continental margin ophiolites of Neotethys: Remnants of ancient Ocean–Continent Transition Zone (OCTZ) lithosphere and their geochemistry, mantle sources and melt evolution patterns. Episodes, v. 38, No. 4, pp. 230-249, doi: 10.18814/epiiugs/2015/v38i4/82418.

Shi, R.D., Alard, O., Zhi, X.C., O'Reilly, S.Y., Pearson, N.J., Griffin, W.L., Zhang, M., and Chen, X.M., 2007, Multiple events in the Neo-Tethyan oceanic upper mantle: Evidence from Ru–Os–Ir alloys in the Luobusa and Dongqiao ophiolitic podiform chromitites, Tibet. Earth and Planetary Science Letters, v. 261, pp. 33–48.

Shervais, J.W., 1982, Ti–V plots and the petrogenesis of modern and ophiolitic lavas. Earth and Planetary Science Letters, v. 59, pp. 101–118.

Sihna, A.K., and Mishra, M., 1997, India–Eurasia tectonics, evidence of Cretaceous oceanic basalts along the ophiolitic mélange belt of Ladakh Himalaya, India. In: Sassi, F.P., Papnikolaou, D. (Eds.), Geodynamic Domains in the Alpine–Himalaya Tethys. Osford and IBH Publishing, New Delhi. pp 441.

Sun, L.X., Wan, X.Q., Wu, X.G., Jia, J.C., and Gao, L.F., 2005, Geochemical characteristics of basalt in a mélange zone in the central segment of the Yarlung Zangbo juncture. Geological bulletin of China, v. 24, pp. 65–71.

Sun, S.S., and McDonough, W.F., 1989, Chemical and isotopic systematic of oceanic basalts: implications for mantle composition and processes. In: Saunder, A.D., Norry, M.J. (Eds.), Magmatism in the Ocean Basins: The Geological Society of London, Special Publication, v. 42, pp. 313–345.

Wang, C.S., Liu, Z.F., and Hébert, R., 2000, The Yarlung–Zangbo paleo-ophiolite, southern Tibet: implications for the dynamic evolution of the Yarlung-Zangbo Suture Zone. Journal of Asian Earth Sciences, v. 18, pp. 651–661.

Wang, C.S., Liu, Z.F., Li, X.H., and Wan, X.Q., 1999. Xigaze Forearc Basin and Yarlung–Zangbo Suture Zone, Tibet. Beijing Geological Publishing House, China, pp. 237.

Wang, C.S., Li, X.H., Liu, Z.F., Li, Y.L., Jansa, L., Dai, J.G., and Wei, Y.S., 2012, Revision of the Cretaceous–Paleogene stratigraphic framework, facies architecture and provenance of the Xigaze forearc basin along the Yarlung Zangbo suture zone. Gondwana Research, v. 22, pp. 415–433.

Wang, R., Xia, B., Zhou, G., Zhang, Y., Yang, Z., Li, W., Wei, D., Zhong, L., and Xu, L., 2006, SHRIMP zircon U-Pb dating for gabbro from the Tiding ophiolite in Tibet. Chinese Science Bulletin, v. 51, pp. 1776–1779.

Wei, D.L., Xia, B., Zhou, G.Q., Wang, R., Zhong, L.F., and Wan, S.K., 2006a, Sm-Nd isochron age of Zedang ophiolite in Tibet and its significance. Acta Geoscientica sinica, v. 27, pp. 31–34.

Wei, Z.Q., Xia, B., Zhang, Y.Q., and Wang, R., 2006b, SHRIMP zircon dating of diabase in the Xiugugabu ophiolite in Tibet and its geological implications. Geotectonica et Metallogenia, v. 30, pp. 93–97.

Wen, D.R., Liu, D.Y., Chung, S.L., Chu, M.F., Ji, J.Q., Zhang, Q., Song, B., Lee, T.Y., Yeh, M.W., Lo, C.H., 2008a, Zircon SHRIMP U–Pb ages of the Gangdese Batholith and implications for Neotethyan subduction in southern Tibet. Chemical Geology, v. 252, pp. 191–201.

Wen, D.R., Chung, S.L., Song, B., Iizuka, Y., Yang, H.J., Ji, J., Liu, D., and Gallet, S., 2008b, Late Cretaceous Gangdese intrusions of adakitic geochemical characteristics, SE Tibet: petrogenesis and tectonic implications. Lithos, v. 105, pp. 1–11.

Wilson, M., 1989. Igneous Petrogenesis. Unwin Hyman, London.

Xia, B., Chen, G.W., Wang, R., and Wang, Q., 2008a, Seamount volcanism associated with the Xigaze ophiolite, Southern Tibet. Journal of Asian Earth Sciences, v. 32, pp. 396–405.

Xia, B., Li, J.F., Liu, L.W., Xu, L.F., He, G.S., Wang, H., Zhang, Y.Q., and Yang, Z.Q., 2008b, SHRIMP U-Pb dating for diabase in Sangsang ophiolite, Xizang, China: Geochronological constraint for development of eastern Tethys basin. Geochimica, v. 37, pp. 399–403.

Xia, B., Yu, H.X., Chen, G.W., Qi, L., Zhao, T.P., and Zhou, M.F., 2003, Geochemistry and tectonic environment of the Dazhuka ophiolite in the Yarlung Zangbo suture zone, Tibet. Geochemistry Journal, v. 37, pp. 311–324.

Xiong, F.H., Yang, J.S., Liang, F.H., Ba, D.Z., Zhang, J., Xu, X.Z., Li, Y., and Liu, Z., 2011, Zircon U-Pb ages of the Dongbo ophiolite in the western Yarlung Zangbo suture zone and their geological significance. Acta Petrologica Sinica, v. 27, pp. 3223–3238.

Xiong, F.H., Yang, J.S., Robinson, P.T., Xu, X.Z., Liu, Z., Li, Y., Li, J.Y., and Chen, S.Y., 2014, Origin of podiform chromitite, a new model based on the Luobusa ophiolite, Tibet. Gondwana Research, v. 27, pp. 525-542, doi: 10.1016/j.gr.2014.04.008.

Xu, D.M., Huang, G.C., and Li, Y.J., 2008, Sm-Nd ages and Nd-Sr-Pb isotope signatures of the Xiugugabu ophiolite, southwestern Tibet. Geology in China, v. 35, pp. 429–435.

Xu, G., Frey, F., Clague, D., Abouchami, W., Blichert-Toft, J., Cousens, B., and Weisler, M., 2007, Geochemical characteristics of West Molokai shield- and post shield-stage lavas: constraints on Hawaiian plume models. Geochemistry, Geophysics, Geosystems, v. 8, pp. 1–40.

Xu, X.Z., Yang, J.S., Ba, D.Z., Guo, G.L., Robinson, P.T., and Li, J.Y., 2011, Petrogenesis of the Kangjinla peridotite in the Luobusa ophiolite, Southern Tibet. Journal of Asian Earth Sciences, v. 42, pp. 553–568.

Xu, X.Z., Yang, J.S., Robinson, P.T., Xiong, F.H., Ba, D.Z., and Guo, G.L., 2014, Origin of ultrahigh pressure and highly reduced minerals in podiform chromitites and associated mantle peridotites of the Luobusa ophiolite, Tibet. Gondwana Research, v. 27, pp. 686–700.

Xu, Z.-Q., Dilek, Y., Yang, J.S., Liang, F.H., Liu, F., Ba, D.Z., Cai, Z.H., Li, G.W., Dong, H.W., and Ji, S.C., 2015a, Crustal structure of the Indus–Tsangpo suture zone and its ophiolites in southern Tibet. Gondwana Research, v. 27, pp. 507–524.

Xu, Z.-Q., Dilek, Y., Cao, H., Yang, J.-S., Robinson, P.T., Ma, C.-Q., Li, H.-Q., Jolivet, M., Roger, F., and Chen, X.J., 2015b, Paleo-Tethyan evolution of Tibet as recorded in the East Cimmerides and West Cathaysides. Journal of Asian Earth Sciences, v. 105, p. 320–337.

Yamamoto, H., Yamamoto, S., Kaneko, Y., Terabayashi, M., Komiya, T., Katayama, I., and Iizuka, T., 2007, Imbricate structure of the Luobusa Ophiolite and surrounding rock units, southern Tibet. Journal of Asian Earth Sciences, v. 29, pp. 296–304.

Yamamoto, S., Komiya, T., Hirose, K., and Maruyama, S., 2009, Coesite and clinopyroxene exsolution lamellae in chromites: In-situ ultrahigh-pressure evidence from podiform chromitites in the Luobusa ophiolite, southern Tibet. Lithos, v. 109, pp. 314–322.

Yang, J.S., Robinson, P.T., and Dilek, Y., 2014, Diamonds in Ophiolites. Elements, v. 10, p. 127–130.

Yang, J.S., Dobrzhinetskaya, L., Bai, W.J., Fang, Q.S., Robinson, P.T., Zhang, J.F., and Green H.W., 2007. Diamond- and coesite-bearing chromitites from the Luobusa ophiolite, Tibet. Geology, v. 35, pp. 875–878.

Yang, J.S., Meng, F.C., Xu, X.Z., Robinson, P.T., Dilek, Y., Makeyev, A.B., Wirth, R., Wiedenbeck, M., Cliff, J., 2015a, Diamonds, native elements and metal alloys from chromitites of the Ray-Iz ophiolite of the Polar Urals. Gondwana Research, v. 27, pp. 459–485

Yang, J.S., Robinson, P.T., and Dilek, Y., 2015b, Diamond-bearing ophiolites

and their geological occurrence. Episodes, v. 38, No. 4, pp. 344-364, doi: 10.18814/epiiugs/2015/v38i4/82430.

Yin, A., 2006. Cenozoic tectonic evolution of the Himalayan orogen as constrained by along-strike variation of structural geometry, exhumation history, and foreland sedimentation. Earth-Science Reviews, v. 76, pp. 1–131.

Yin, A., and Harrison, T.M., 2000, Geological evolution of Tibetan–Himalayan orogen. Annual Review of Earth and Planetary Sciences, v. 28, pp. 211–280.

Zhang, W.P., Mo, X.X., Zhu, D.C., Yuan, S.H., and Wang, L.Q., 2011, Chronology and geochemistry on gabbro and basalt of the ophiolite mélange in Lang County, Tibet, China. Journal of Chengdu University of Technology (Science & Technology Edition), v. 38, pp. 538–548.

Zhang, S.Q., Mahoney, J.J., Mo, X.X., Ghazi, A.M., Milani, L., Crawford, A.J., Guo, T.Y., and Zhao, Z.D., 2005. Evidence for a Widespread Tethyan Upper Mantle with Indian-Ocean-Type Isotopic Characteristics. Journal of Petrology, v. 46, pp. 829–858.

Zhang, K.J., and Tang, X., 2009. Eclogites in the interior of the Tibetan Plateau and their geodynamic implications. Chinese Science Bulletin, v. 54, pp. 2556–2567.

Zhang, Z., Zhao, G., Santosh, M., Wang, J., Dong, X., and Shen, K., 2010, Late Cretaceous charnockite with adakitic affinities from the Gangdese batholith, southeastern Tibet: evidence for Neo-Tethyan mid-oceanic ridge subduction? Gondwana Research, v. 17, pp. 615–631.

Zhong, L.F., Xia, B., Zhou, G.Q., Zhang, Y.Q., Wang, R., Wei, D.L., and Yang, Z.Q., 2006, SHRIMP age determination of Diabase in Luobusa ophiolite, southern Xizang (Tibet). Geological Review, v. 52, pp. 224–229.

Zhou, M.F., Robinson, P.T., Malpas, J., Edwards, S.J., and Qi, L., 2005, REE and PGE geochemical constraints on the formation of dunites in the Luobusa ophiolite, Southern Tibet. Journal of Petrology, v. 46, pp. 615–639.

Zhou, M.F., Robinson, P.T., Malpas, J., and Li, Z., 1996, Podiform chromitites in the Luobusa ophiolite (southern Tibet): implications for melt–rock interaction and chromite segregation in the upper mantle. Journal of Petrology, v. 37, pp. 3–21.

Zhou, M.F., Robinson, P.T., Su, B.X., Gao, J.F., Li, J.W., Yang, J.S., and Malpas, J., 2014, Compositions of chromite, associated minerals, and parental magmas of podiform chromite deposits: The role of slab contamination of asthenospheric melts in suprasubduction zone environments. Gondwana Research, v. 26, pp. 262–283.

Zhou, S., Mo, X.X., Mahoney, J.J., Zhang, S.Q., Guo, T.J., and Zhao, T.J., 2002, Geochronology and Nd and Pb isotope characteristics of gabbro dikes in the Luobusa ophiolite, Tibet. Chinese Science Bulletin, v. 47, pp. 143–146.

Zhou, S., 2002, Study on the Geochronology of pivotal regions of Gangdese magmatic and Yarlung Zangpo ophiolite belts, Tibet. Ph.D thesis, China University of Geosciences (Beijing) Beijing, pp. 75.

Zhu, D.C., Chung, S.L., Mo, X.X., Zhao, Z.D., Niu, Y.L., Song, B., and Yang, Y.H., 2009, The 132 Ma Comei–Bunbury large igneous province: remnants identified in present-day southeastern Tibet and southwestern Australia. Geology, v. 37, pp. 583–586.

Zhu, D.C., Mo, X.X., Wang, L.Q., Zhao, Z.D., and Liao, Z.L., 2008, Hotspot-ridge interaction for the evolution of Neo-Tethys: insights from the Late Jurassic-Early Cretaceous magmatism in southern Tibet. Acta Petrologica Sinica, v. 24, pp. 225–237.

Ziabrev, S.V., Aitchison, J.C., Abrajevitch, A., Badenzhu, Davis A.M., and Luo, H., 2003, Precise radiolarian age constraints on the timing of ophiolite generation and sedimentation in the Dazhuqu terrane, Yarlung-Tsangpo suture zone, Tibet. Journal of the Society of London, v. 160, pp. 591–599.

Ziabrev, S.V., Aitchison, J.C., Badengzhu, Davis, A.M., Luo, H., and Malpas, J., 1999, Radiolarian biostratigraphy of supra-ophiolite sequences in the Xigaze area, Yarlung Tsangpo suture, southern Tibet (preliminary report). Radiolaria, v. 17, pp. 13–19.

by Gianni Balestro [1], Andrea Festa [1], Yildirim Dilek [2], and Paola Tartarotti [3]*

Pre-Alpine extensional tectonics of a peridotite-localized oceanic core complex in the Late Jurassic, high-pressure Monviso ophiolite (Western Alps)

1 Dipartimento di Scienze della Terra, Università di Torino, Via Valperga Caluso, 35, 10125 - Torino, Italy
2 Department of Geology and Environmental Earth Science, Miami University, Oxford, OH 45056, USA
3 Dipartimento di Scienze della Terra, Università di Milano, Via Mangiagalli, 34, 20133 - Milano, Italy
[*] *Corresponding author: Andrea Festa. E-mail: andrea.festa@unito.it*

DOI: 10.18814/epiiugs/2015/v38i4/82421

The Late Jurassic Monviso ophiolite in the Western Alps is a multiply deformed, eclogite-facies meta-ophiolite that represents a remnant of the Alpine Tethyan oceanic lithosphere. The recent recognition of a pre-Alpine detachment fault in the Lower Tectonic Unit of this ophiolite has led to the discovery of an oceanic core complex, which developed during the initial stages of the tectonic evolution of the Alpine Tethys. The NNW-striking, 20–25-km-long shear zone (Baracun Shear Zone) contains ductilely to cataclastically deformed blocks and clasts of Fe-Ti and Mg-Al metagabbros in a matrix made of mylonitic serpentinite and talc-chlorite schist with high Ni–Cr concentrations and high Cl contents. Intensely sheared ophicarbonate rocks and brecciated serpentinite within this shear zone are deformed by the Alpine-phase S1 foliation and D2 folds, providing a critical age constraint for the timing of its formation. Metabasaltic–metasedimentary rocks in the hanging wall increase in thickness away from the shear zone, characteristic of syn-extensional rock sequences in supradetachment basins. A Lower Cretaceous post-extensional sedimentary sequence unconformably cover the syn-extensional strata, the detachment shear zone, and the ophiolitic footwall, establishing a strong structural evidence for the intraoceanic, seafloor spreading origin of the tectonic fabric of the Monviso ophiolite, prior to the onset of subduction zone tectonics in the Alpine Tethys. The Monviso ophiolite and the Baracun Shear Zone represent a peridotite-localized oceanic core complex, which survived both the subduction and continental collision tectonic stages of the Alpine orogeny. Intraoceanic detachment faults and oceanic core complexes may play a significant role in subduction initiation, and hence their recognition in orogenic belts is an important step in reconstructing the record of ocean basin collapse and closure.

Introduction

Discontinuous exposures of the Late Jurassic, eclogitic ophiolite massifs in the Western Alps (Fig. 1) have been widely used in various studies to constrain the paleogeography of the Alpine Tethys, evolved between Europe and Adria during the Mesozoic (Dilek and Robinson, 2003, and the papers therein). They, in particular, have been well utilized to determine the P-T-t trajectories of the Jurassic oceanic crust in a subduction-accretion system during the convergent–collision tectonic evolution of this orogenic belt (e.g., Frey et al., 1999). However, detailed, field-based structural, petrological and geochemical studies of the seafloor spreading and extensional tectonic history of these ophiolites have been scarce. This has been in part due to the strong overprint of the Alpine-stage subduction-collision related deformation–metamorphic events that obscures the previously developed rift-drift and seafloor spreading generated structures and mineral assemblages in these units.

In this paper, we document through detailed geological mapping, systematic structural and stratigraphic observations, petrographic and geochemical analyses the internal structure, tectonic fabric and evolution history of the Monviso ophiolite, one of the best preserved ophiolites in the Western Alps. We show that this ophiolite is an on-land exposure of an oceanic core complex, which formed through simple-shear seafloor spreading kinematics during the opening of the Ligurian–Piedmont ocean basin within the Alpine Tethys. This inferred

oceanic core complex origin of the Monviso ophiolite is significant in that: (1) it better explains the dismembered and highly attenuated crustal architecture of the ophiolites in the Western Alps; (2) it presents a first coherent documentation of the intraoceanic extensional tectonic history of the Jurassic oceanic lithosphere preserved in the Western Alps, demonstrating that it is possible "to see through" the subduction–collision induced metamorphic overprint in multiply deformed orogenic belts; and (3) it provides a regionally consistent tectonic framework for the rift-drift, seafloor spreading, and contractional episodes of the Ligurian – Piedmont ocean basin evolution. Our data and observations from the Monviso ophiolite complement the diverse datasets available from the modern oceanic core complexes, and provide further insights into the geometry, internal structure, and stratigraphy of supradetachment basin sequences, which are missing from in-situ oceanic core complexes.

Regional geology of the Western Alps and its Tethyan connection

The Western Alps (Fig. 1) developed due to the collision between Adria (upper plate) and Europe (lower plate) as the intervening oceanic lithosphere of the Jurassic Alpine Tethys Ocean was consumed (see e.g. Coward and Dietrich 1989; Laubscher 1991; Dilek, 2006). The collision zone (i.e. the axial section of the Alpine belt) involves an exhumed fossil subduction complex bounded by the Penninic front and the Insubric and Canavese lines (Fig. 1A). Tectonic units of this subduction complex are overthrust WNW onto the European foreland (Ricou and Siddans, 1986; Platt et al. 1989; Schmid and Kissling 2000; Butler et al. 2013). Different meta-ophiolite units (i.e. the Piedmont Zone; see e.g. Dal Piaz et al., 2003) are tectonically sandwiched between the European and Adriatic continental margin units (see Bigi et al., 1990), and display varying metamorphic facies conditions ranging from high-pressure (HP) to ultra high-pressure (UHP) (Frey et al., 1999 and reference therein). The Piedmont Zone is distinguished by eclogite-facies units (i.e. the Zermatt-Saas Zone *auct*.;Bearth, 1967) and blueschist-facies ones (i.e. the Combin Zone *auct.*, Fig. 1A).

The orogenic structural architecture of the Western Alps as seen in the field today (Fig. 1) was built up during three main phases of deformation-metamorphism events: (1) E-dipping subduction zone tectonics and eclogite-facies metamorphism in the Paleocene to middle Eocene, during which contractional deformation (D1) structures, mainly S1 foliation, were developed; (2) Continental collision tectonics in the late Eocene–early Oligocene that caused W-vergent folding and thrusting (D2). Blueschist- to greenschist-facies metamorphic re-equilibration took place during this event, producing S2 foliation; (3) Crustal exhumation (D3) and deep crust/mantle indentation in the middle Oligocene to Neogene. Updoming of the partially subducted European continental margin, the UHP Dora Maira, and the tilting of the Monviso ophiolite to the west (Fig. 1B) occurred during this late Alpine stage evolution of the Western Alps (see e.g. Lardeaux et al., 2006).

The meta-ophiolites in the Western Alps are the remnants of the Alpine Tethyan oceanic lithosphere, which developed as a result of its rift-drift and seafloor spreading evolution (Elter, 1971; Dal Piaz et al., 1972; Lemoine and Tricart., 1986; Stampfli and Marthaler, 1990; Michard et al., 1996; Dilek, 2003; Dilek and Furnes, 2011, 2014; Saccani et al., 2015). The timing of drifting and spreading has been constrained by U/Pb dating of ophiolitic gabbros between 165 and 150 Ma (Manatschal and Müntener, 2009 for a review), and by the ages of the initial post-rift sedimentary sequences (i.e. radiolarian chert) that overlap with the igneous ages of gabbros (see Bill et al, 2001, for a review). Paleo-spreading rates in the Alpine Tethys are inferred to have been slow- to ultraslow (~2 mm/yr) (see Lagabrielle, 2009, for a review), forming a Red Sea-type, embryonic ocean (Lombardo et al., 2002). This ultraslow-spreading origin interpretation is based, in part, on the occurrence of basaltic lava units directly resting on serpentinized peridotites. These spatial relationships between upper mantle peridotites and lavas with sedimentary intercalations and cover are well documented from modern oceanic core complexes, rifted continental margins, and some other Tethyan ophiolites (Dilek and Delaloye, 1992; Dilek and Eddy, 1992; Dilek et al., 1998; Miranda and Dilek, 2010; Manatschal et al., 2011; Festa et al., 2015a). Simple-shear extensional deformation in these tectonic settings is shown to have exhumed the lithospheric mantle rocks on the seafloor during the rift-drift and seafloor spreading stages of ocean basin evolution (Dilek and Thy, 1998; Dilek and Newcomb, 2003, and the papers therein).

Monviso ophiolite

The Monviso ophiolite occurs in the southern part of the Western Alps (Fig. 1), and is tectonically sandwiched between the Dora Maira Unit (Internal Cristalline Massif *Auct.*), which represents part of the subducted-exhumed European continental margin (e.g., Dal Piaz et al., 2003) and the Queyras Schistes Lustrés Complex (Lemoine, 1971; Lombardo et al., 1978; Lemoine and Tricart, 1986). The carbonate-rich metasedimentary sequence of *schistes lustrés* hosts large bodies of ophiolites, which comprise ophicarbonates and metaperidotites with gabbroic intrusions. This metasedimentary sequence includes discontinuous exposures of Middle-Late-Jurassic metachert horizons and laterally continuous Upper Jurassic marble layers covering the entire igneous basement (e.g., Tricart and Lemoine, 1991; Tricart and Schwartz, 2006).

The Monviso ophiolite consists mainly of serpentinized metaperidotites hosting large bodies of both Mg-Al and Fe-Ti metagabbros. These metagabbros have Middle–Late Jurassic crystallization ages (163± 2 Ma; Rubatto and Hermann, 2003). The upper mantle rocks are composed of lherzolite and minor harzburgite, and are overlain along tectonic contacts by tholeiitic pillow metalavas, and an Upper Jurassic – Lower Cretaceous meta-sedimentary sequence (Balestro et al., 2013). The Monviso ophiolite has been divided into two major tectonic units on the basis of their different Alpine-stage P-T metamorphic peaks (Fig. 1C). The *Lower Tectonic Unit* (LTU) includes the metaperidotites, metagabbros, metabasalts, and a shear zone made of mylonitic serpentinite and talc-chlorite schist. Overlying this unit along a WSW-dipping tectonic contact is the *Upper Tectonic Unit* (UTU), which is composed mainly of metabasaltic lavas and metagabbro intrusions. The LTU lithologies display peak metamorphic P-T conditions of 2.5 GPa – 550°C (Groppo and Castelli, 2010; Angiboust et al., 2012; Balestro et al., 2014). The UTU lithologies show, on the other hand, peak metamorphic P-T conditions of 2.2 GPa – 480°C (Angiboust et al., 2012). Thus, the ophiolite exhibits a major tectonic discontinuity separating two different metamorphic domains in it. Another major tectonic discontinuity occurs within the *Lower Tectonic Unit* (LTU), in which a NNW-striking, >20-km-long shear zone (Baracun Shear Zone, BSZ) separates the serpentinized

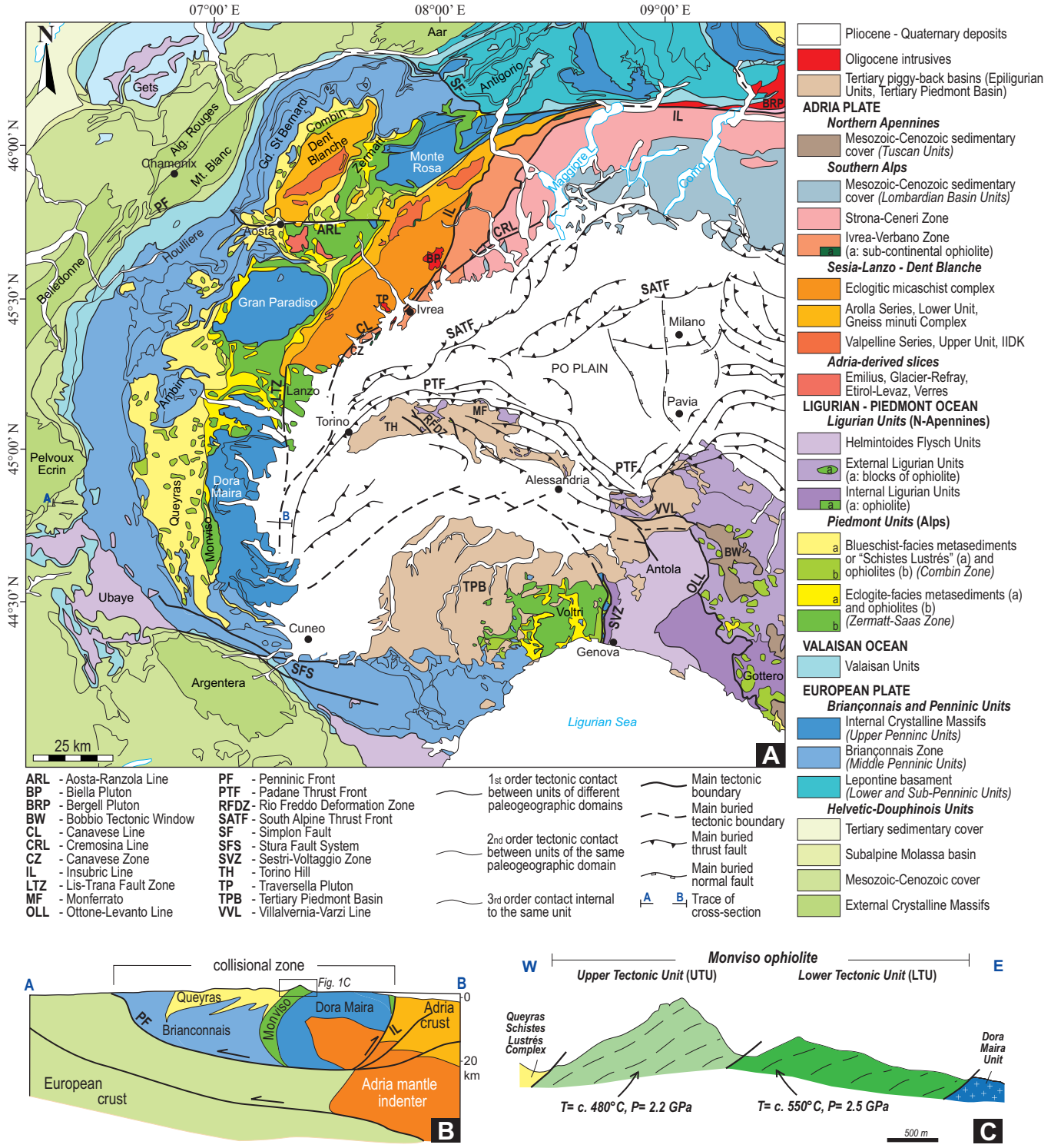

Figure 1 – (A) Tectonic map of the Western Alps and the Northern Apennines (modified from Bigi et al., 1990; Bousquet et al., 2012; Fantoni et al., 2003, 2004; Funicello et al., 1981; Ghibaudo et al., 2014; Ghielmi et al., 2013; Manzotti et al., 2014; Festa et al., 2015b, 2015c; Perrone et al., 2015). (B) Tectonic cross-section across the Western Alps (modified from Lardeaux et al., 2006). The box shows the westward titled Monviso ophiolite, enlarged in Figure 1C. (C) Simple structural cross section of the Monviso ophiolite, sandwiched between the UHP Dora Maira Unit and the Queyras Schistes Lustrés, and showing two different metamorphic domains (modified from Angiboust et al., 2012).

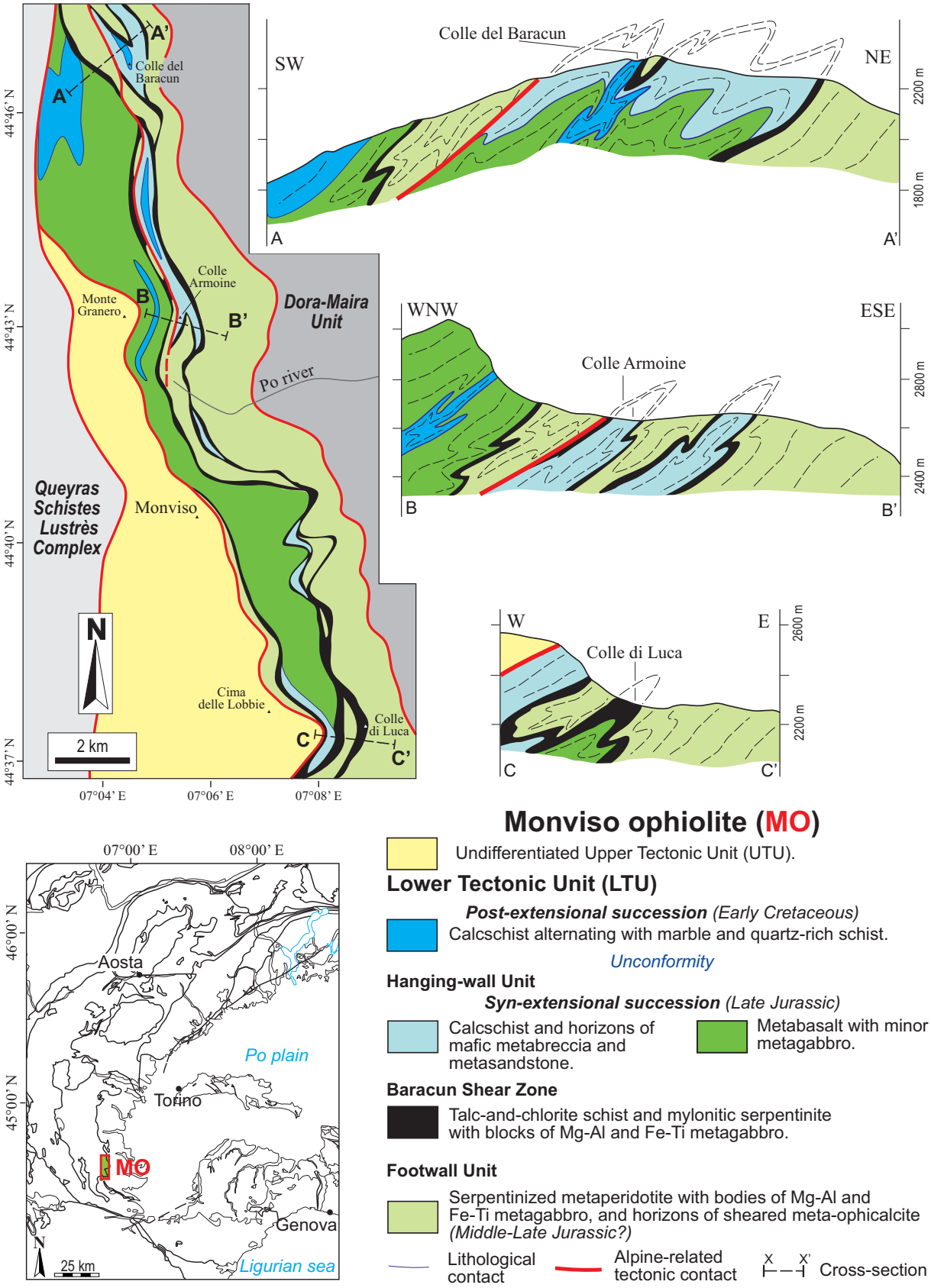

Figure 2. Geological map and structural cross-sections (A-A' through C-C") of the Lower Tectonic Unit (LTU) of the Monviso ophiolite (MO) (modified from Balestro et al., 2011, 2013, 2014, 2015), depicting the geometry of the Baracun Shear Zone (BSZ), its hanging wall and footwall units and the post-extensional metasedimentary sequence. The index map shows the location of the Monviso geological map and the geography of the Western Alps.

metaperidotites and metagabbros in its footwall from metabasalt and syn-extensional metasedimentary rocks in the hanging wall (Fig. 2). Both the footwall and hanging wall units are unconformably overlain by the Lower Cretaceous, post-extensional metasedimentary rocks (Festa et al., 2015a).

Structural architecture and stratigraphy of the LTU

Different lithologies and the BSZ in the LTU are pervasively folded during D2 deformation (see Balestro et al., 2014, 2015; Festa et al., 2015a for major details; Fig. 2), forming tight to isoclinal folds accompanied by a SW- to W-dipping axial planar foliation (i.e. the S2 foliation). These D2 folds deform the earlier formed S1 foliation and the primary surfaces (i.e. the S0 sedimentary bedding and magmatic foliation). Extensional normal faults, representing the D3 stage of deformation, are commonly localized along lithological contacts and the attenuated limbs of the D2 folds.

We describe below the structural architecture of the BSZ and the stratigraphy and structure of various tectonostratigraphic units in its footwall and hanging wall blocks. We also define and describe the post-extensional metasedimentary sequence that onlap all these tectonic entities in the LTU. These descriptions are based largely on our detailed structural work and observations in the Colle del Baracun, Colle Armoine, and Colle di Luca (Fig. 2) sections of the Monviso ophiolite.

Baracun Shear Zone (BSZ)

The BSZ is tens of meters thick and includes talc-chlorite schist and mylonitic serpentinite, containing blocks of metagabbro displaying a scale-independent block-in-matrix fabric (Figs. 3A-L; *sensu* Festa, 2011; Festa et al., 2012). Due to the macroscopic-scale folding (D2), the BSZ occurs at different structural levels within the ophiolite (Fig. 2). It does not contain any material derived from the lithological units in its hanging wall. It corresponds to the Lower Shear Zone of Angiboust et al. (2011) and to the Lago Superiore Shear Zone of Balestro et al. (2013).

In its type locality at Colle del Baracun, the BSZ includes a talc-chlorite schist matrix with distinct chlorite-, talc-, and amphibole-rich domains (Fig. 3C). The chlorite-rich domains consist of chlorite, magnetite, pistacite, and accessory apatite, magnetite, allanite and zircon, and mainly occur in rootless hinges of D2 folds, which folded the S1 foliation (Fig. 3M). Pre-D1 talc and chlorite lamellae are also included in apatite grains. Talc-rich domains in the talc-chlorite schist matrix are composed of talc and fine-grained magnetite, and occur in two different modes. In the first one, fine-grained aggregates of talc and magnetite appear within the D2 fold hinges. In the second mode, coarse-grained talc lamellae are oriented in the S2 foliation plane. Talc-rich domains are commonly folded together with chlorite-rich domains or form anastomosing crenulation cleavages with microlithons of the rock that contain S1 and S2 foliations (Fig. 3M; see also Fig. 3N). Amphibole-rich domains include fine-grained, light-green amphibole and minor chlorite. Calcite locally occurs between these different mineral domains in the matrix. In the Colle Armoine and Colle di Luca sections, the matrix consists of dm- to m-thick layers of talc-chlorite schist, which is interbedded within mylonitic serpentinite (Figs. 3D and 3E). The serpentinite consists mainly of antigorite and magnetite, with minor brucite, talc and carbonate.

Blocks of Fe-Ti metagabbro and Mg-Al metagabbro, ranging in size from few dm to several meters, widely occur within the talc-chlorite schist and in the mylonitic serpentinite matrix throughout the shear zone (Figs. 3A and 3D). These gabbro blocks are also folded by D2 folds, and locally occur as rootless fold hinges of D2 folds (Fig. 3B). Fe-Ti metagabbro blocks display a fine-grained, banded texture defining the S1 foliation and consisting of a mineral assemblage of garnet-omphacite-rutile eclogite with minor chlorite, Na-amphibole, albite, talc and quartz. Omphacite porphyroblasts locally preserve relics of the magmatic pyroxene and retain fine-grained intergrowths of quartz and amphibole. The amphibole is represented by Mg-hastingsitic hornblende replacing primary igneous

Figure 3. Images of the Baracun Shear Zone (BSZ) and structures at different scales: (A) Panoramic view of the BSZ at the Colle del Baracun, showing its block-in-matrix fabric. White arrows point tothe blocks of Fe-Ti and Mg-Al metagabbros, and to some rare blocks of metarenite embedded in a matrix of talc-chlorite schist. Yellow arrows indicate the younging direction of the primary sedimentary sequence, now folded by Alpine deformation. Post-extensional sedimentary rocks rest unconformably (dotted blue line) on both the syn-extensional sequence and the talc-chlorite schist of the BSZ; (B) Close-up photo of one of the larger metagabbro blocks embedded within the BSZ matrix (location in Fig. 3A).The shape of the block corresponds to the fold hinge of a D2 fold, which deformed the previously formed foliation S1. Note the mafic metabreccia enveloping the block (see also Figs. 3F, 3G, 3I, 3L). Hammer for scale; (C) Close-up of the structural fabric of the talc-chlorite schist matrix at Colle del Baracun (hammer as scale); (D) Close-up of of the block-in-matrix fabric of the BSZ at Colle di Luca. Rounded to elongated blocks of gabbro (black arrows) are embedded within a mylonitic serpentinite matrix affected by D2 foliation (dashed white lines); (E)Talc-chlorite schist matrix of the BSZ at Colle di Luca; (F) Close-up of a Fe-Ti metagabbro block within the BSZ, enveloped by a dm-thick horizon of a clast-supported mafic metabreccia outcrop (black arrows), with clasts of the same composition as in the main block (Colle del Baracun); (G) Close-up of the contact between the clast-supported mafic metabreccia enveloping the metagabbro blocks and the talc-chlorite schist matrix, embedding rounded blocks of metagabbro, centimeters to decimeters in size (Colle di Luca). Hammer as scale; (H and I) Close-up of the mafic metabreccia enveloping blocks of gabbro. Note that irregularly shaped clasts, centimeters to decimeters in size, preserve an earlier formed foliation, S1, folded by D2 deformation (Colle di Luca and Colle del Baracun, respectively); (L) Photomicrograph showing the clast/matrix relationship within the mafic metabreccia of Figure 3I (modified after Balestro et al., 2015). The matrix and the irregularly shaped clast (dashed blue line) are affected by S1 foliation (dashed red line), which is defined by an eclogite-facies mineral assemblage (i.e. garnet, omphacite, and rutile); (M) Photomicrograph of talc-chlorite schist in the BSZ at Colle del Baracun, showing amphibole- (Amp), chlorite- (Chl) and talc-rich (Tlc) domains folded by tight to isoclinal D2 folds. Note the folded S1 foliation (dashed white lines); (N) Close-up of a polished hand sample of the talc-chlorite schist matrix (Colle del Baracun), showing rootless D2 fold hinges in chlorite-rich (Chl) domains, overprinting the early S1 foliation (dashed white lines). S2 axial planar foliation (dashed black lines) occurs in talc-rich (Tlc) domains.

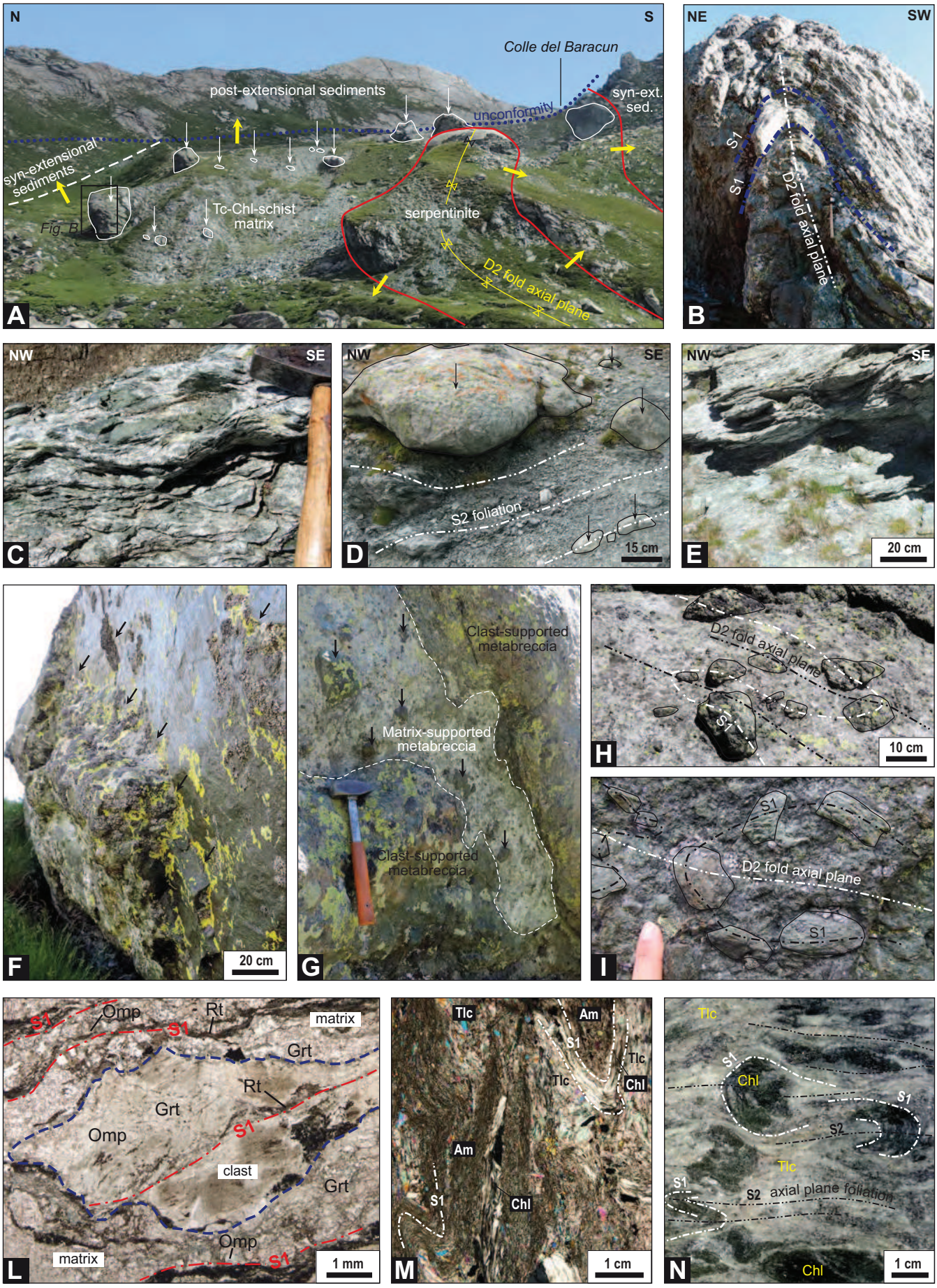
N
S
Colle del Baracun
post-extensional sediments
unconformity
syn-ext. sed.
syn-extensional sediments
Fig. B
Tc-Chl-schist matrix
serpentinite
D2 fold axial plane
A
NE
SW
S1
S1
D2 fold axial plane
B
NW
SE
C
NW
SE
S2 foliation
15 cm
D
NW
SE
20 cm
E
20 cm
F
Clast-supported metabreccia
Matrix-supported metabreccia
Clast-supported metabreccia
G
D2 fold axial plane
S1
10 cm
H
S1
D2 fold axial plane
S1
I
S1
Omp
Rt
matrix
Grt
Rt
Grt
Omp
S1
clast
Grt
Omp
matrix
S1
1 mm
L
Tlc
Am
S1
Tlc
Tlc
Chl
Am
S1
Chl
1 cm
M
Tlc
S1
Chl
S1
S2
Tlc
S1
S2 axial plane foliation
Chl
1 cm
N

pyroxene, and is a result of the pre-Alpine alteration of gabbroic rocks. Mg-Al metagabbro blocks are coarse-grained and more pervasively deformed in comparison to the Fe-Ti metagabbros. The mineral assemblages in these Mg-Al metagabbros include: (a) Cr-omphacite accompanied by actinolite, tremolite and chlorite, and replacing magmatic pyroxene, (b) aggregates of clinozoisite and albite pseudomorphs after the original plagioclase, and (c) aggregates of rutile and titanite pseudomorph after ilmenomagnetite.

Differently from the metagabbros in the footwall (see below), the metagabbro blocks embedded in the BSZ do not show metasomatic rims (i.e. rodingitic reactions) against the serpentinite wallrock and the talc-chlorite schist matrix. But, they are enveloped by dm-thick layers of a clast-supported metabreccia (Figs. 3F-I), in which clasts are made of the same gabbroic rocks as in the blocks. This metabreccia envelope around the metagabbro blocks within the BSZ occurs throughout the entire LTU, and is overprinted by S1 foliation and D2 folds (Figs. 3H and 3I). We observe these mesoscopic structures and deformation fabrics at microscopic scales, as well; both micro-clasts and the matrix are foliated along the S1 foliation planes (Fig. 3L). These observations indicate that brecciation, fragmentation of blocks, and embedding of micro-clasts within a matrix must have occurred before the Alpine-stage deformation and the associated metamorphic overprint (see, Balestro et al., 2015, for details).

BSZ footwall units

The footwall block of the BSZ consists of serpentinized metaperidotites and metagabbros (Figs. 2 and 4). The serpentinized metaperidotites derive from lherzolite and minor harzburgite (Fig. 5A), and consist of oriented aggregates of antigorite and magnetite (S2 foliation) with minor diopside, Mg-chlorite, tremolite and Ti-clinohumite. The original mineral assemblage is partly preserved in low-strain domains (e.g. in the cores of D2 folds exposed to the east of Colle Armoine), as evidenced by the relics of clinopyroxene and orthopyroxene porphyroclasts, and by olivine and spinel grains which are partially to entirely replaced by aggregates of antigorite and magnetite.

Metagabbro intrusions in the serpentinized metaperidotites form meters to hectometers thick and decameters to sub-kilometer long bodies. They range in texture from poorly foliated, coarse-grained pegmatitic gabbros (e.g. South of Colle Armoine; Fig. 5B) to pervasively foliated, anisotropic gabbros (Fig. 5C) (e.g. East of Colle del Baracun and West of Colle di Luca). Compositionally, they represent two sub-groups: Mg-Al and Fe-Ti metagabbros. The Mg-Al metagabbros are characterized by the occurrence of Cr-omphacite that replaced magmatic pyroxenes. The Fe-Ti metagabbros have a well-preserved garnet-omphacite-rutile eclogitic assemblage, which defines the S1 foliation. Contacts between the serpentinized metaperidotites and metagabbros are generally marked by rodingitic reaction rinds.

Serpentinite laced with irregular calcite vein networks (i.e., meta-ophicarbonate) is exposed along the contact between the footwall unit and the BSZ (Figs. 5D and 5E). Both in the Colle del Baracun and Colle Armoine sections, meta-ophicarbonate is few meters thick and shows a progressive transition from massive serpentinite to brecciated serpentinite with a white carbonate matrix, and up to a highly sheared meta-ophicarbonate rock (Fig. 5F). In the Colle di Luca section, the meta-ophicarbonate occurrence is no more than 30 m in thickness. Calcite veins in the meta-ophicarbonate rock are overprinted by S1 foliation and deformed by D2 folds, constraining the timing of hydrothermal activity that was responsible for the formation of ophicarbonates to a pre-Alpine stage (Festa et al., 2015a).

BSZ hanging wall unit

The hanging wall block of the BSZ includes metasedimentary and metabasaltic rocks spatially associated with minor metagabbro occurrences (Figs. 2 and 4). Metasedimentary units consist of calcschist layers interbedded with decimeters to sub-decameter thick horizons of mafic metasandstone and metabreccia (Figs. 2 and 4). The type locality of these rocks is at Colle del Baracun (Figs. 6A-C), where calcschist layers onlap the BSZ. The thickness of the entire calcschist unit increases from zero to 70 meters away from the shear zone (Figs. 2 and 4; see also Balestro et al., 2015; Festa et al., 2015a for details). At a regional scale and across the whole ophiolite, the thickness of the metasedimentary unit gradually decreases toward the south (i.e. between Colle Armoine and Colle di Luca sections). To the SW of Colle di Luca, a tens of meters – thick mafic metabreccia represents the syn-extensional unit.

The calcschist consists of subparallel layers of carbonate minerals (i.e. calcite, minor dolomite and ankerite), quartz and white mica, with subordinate chloritoid, Mg-Fe chlorite, zoisite, and textural relics of lawsonite with graphite flakes. A matrix-supported mafic metabreccia unit is interbedded with calcschist layers, and shows a fining-upward texture with sub-angular to angular clasts of gabbroic rocks (Fig. 6B). The metabreccia is laterally gradational into tens of meters – thick metasandstone, containing similar composition but much smaller size clasts (Figs. 4 and 6C). The matrix of the mafic metabreccia and metasandstone is made of angular to irregularly shaped micro-clasts and grains, composed of omphacite and aggregates of chlorite, Cr-rich white mica, and epidote (pistacite). All these grains are in turn embedded in a groundmass of zoisite, light-green amphibole, epidote, albite, chlorite, sphene, quartz and white mica. These textural relationships at various scales indicate the detrital sedimentary nature of the protoliths of the mafic metabreccia and metasandstone.

The metabasaltic unit in the hanging wall of the BSZ is well exposed in the Colle Armoine section. It gradually decreases in thickness from this locale both toward Colle del Baracun and Colle di Luca (Figs. 2 and 4), and tapers out near Colle di Luca in the south. Mg-Al metagabbro outcrops with fine-grained metabasaltic dikes are in contact with metabasalts north of Colle di Luca. The primary breccia texture is still visible and well preserved in the metabasalt (Fig. 6D) despite the strong overprint of a well developed S2 foliation, defined by alternating layers of light green-yellow albite, epidote, clinozoisite with minor white mica, and dark-green layers of Na-Ca amphibole, garnet and chlorite.

Post-extensional metasedimentary sequence

The footwall and hanging wall lithological units (syn-extensional metasedimentary and metabasaltic rocks) of the BSZ are unconformably overlain by a calcschist unit, which contains dm-thick marble beds (Figs. 2, 4, 7A and 7B), passing upward into layered-foliated quartz-schist devoid of any ophiolite-derived detrital material. On the basis of a regional correlation of this calc schist-marble-quartz schist unit with other metasedimentary rocks in the Western Alps,

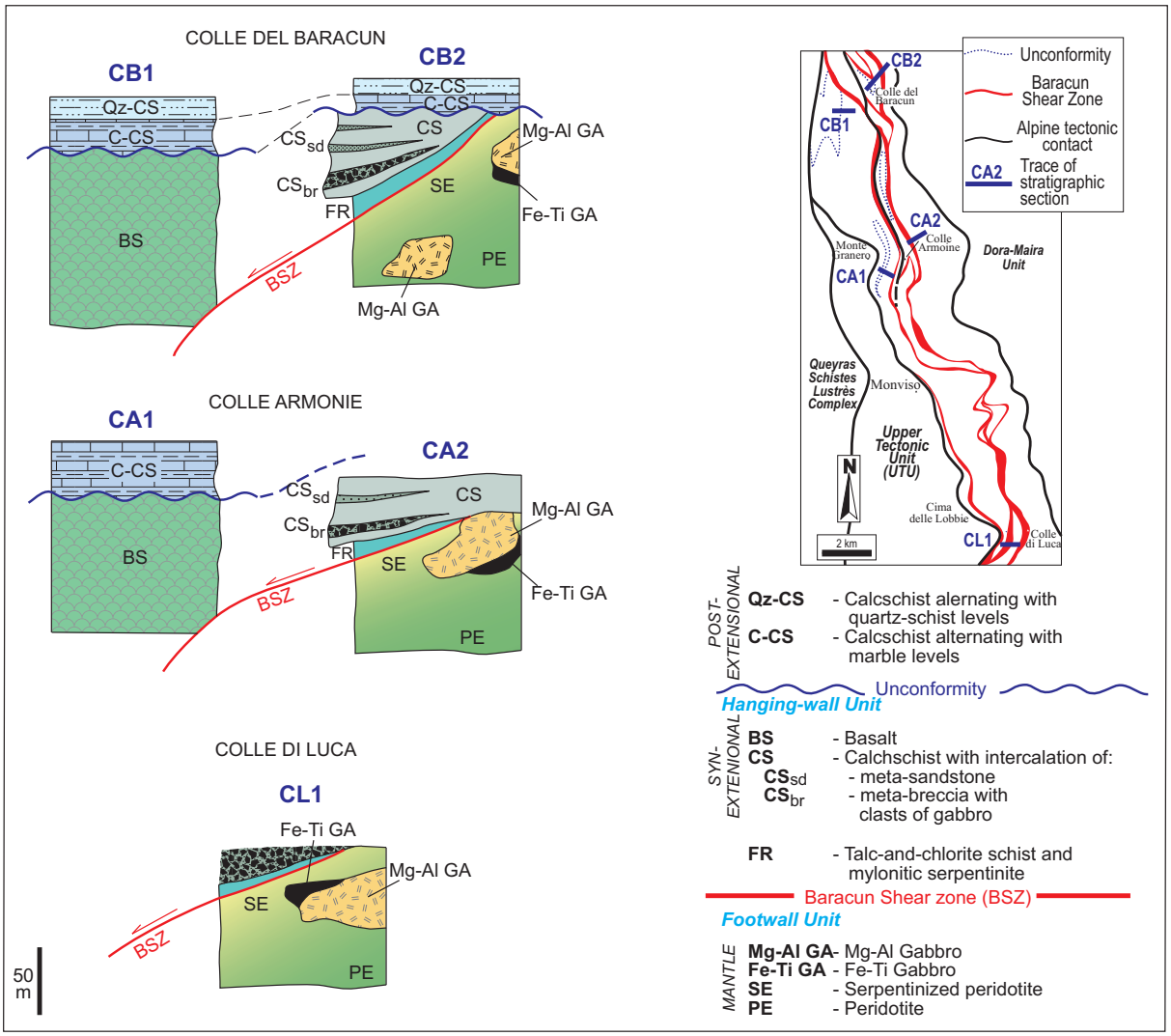

Figure 4 – Simplified stratigraphic columnar sections, showing the tectono-stratigraphic relationships between the hanging wall – footwall units and the BSZ (traces are shown in the simplified geological map).

Lagabrielle (1994) established the age of the calcschist and the overlying syn-extensional rocks as the Lower Cretaceous. Festa et al. (2015a) defined these metasedimentary rocks in the hanging wall of the BSZ as post- extensional depositional units. The thickness of the post-extensional metasedimentary sequence within the Monviso ophiolite is irregular (Fig. 2) and ranges from few meters to tens of meters.

The calcschist unit consists of calcite, and minor dolomite with ankerite, quartz and white mica, whereas the marble and quartz-rich schist are made of calcite and quartz, respectively. The contact between the post-extensional metasedimentary units and both the syn-extensional sedimentary sequence and the talc-chlorite schist of the BSZ is sharp and rugged (Figs. 7C-F), and corresponds to an original depositional surface as inferred from the lack of any mylonitic structure associated with it (Figs. 7E and 7F). This unconformity is folded together with the BSZ and the hanging wall and footwall units as seen at different structural levels in the field (Fig. 2).

Geochemistry and mineralogy of the BSZ

The composition of the talc-chlorite schist rocks within the BSZ was determined by major- and trace element chemistry analyses of selected rock samples, and by electron microprobe mineral analyses. The bulk rock geochemistry of the talc-chlorite schist was then compared with the compositional fields of the spatially associated serpentinite and metagabbro (Fig. 8). Compared to the serpentinite, the talc-chlorite schist rocks have higher values of SiO_2, Al_2O_3 and CaO, show lower values of MgO, and are characterized by particularly strong enrichment in TiO_2. On the other hand, compared to the metagabbro, the talc-chlorite schist is depleted in Al_2O_3, CaO, total Fe and Na_2O, enriched in MgO. The talc-rich rock also shows high absolute concentrations of Cr, Ni and V.

Electron microprobe mineral chemistry analyses reveal that chlorite in the talc-chlorite schist predominantly has a penninite (i.e., a Mg-rich solid solution between serpentine and amesite) composition (XMg=[0,83-0,89]), with minor pycnochlorite (XMg= 0,79) and clinochlore (XMg= 0,84-0,85) components. Some zoned chlorite grains are significantly enriched in Cr and in Ni in their centers. Chlorite also has relatively high chlorine content (up to 500 ppm).

Electron microprobe mineral chemistry analyses have shown that talc in the talc-chlorite schist is characterized by a negligible substitution of Mg by Fe (XFe=[0,04-0,09]), and that it contains high

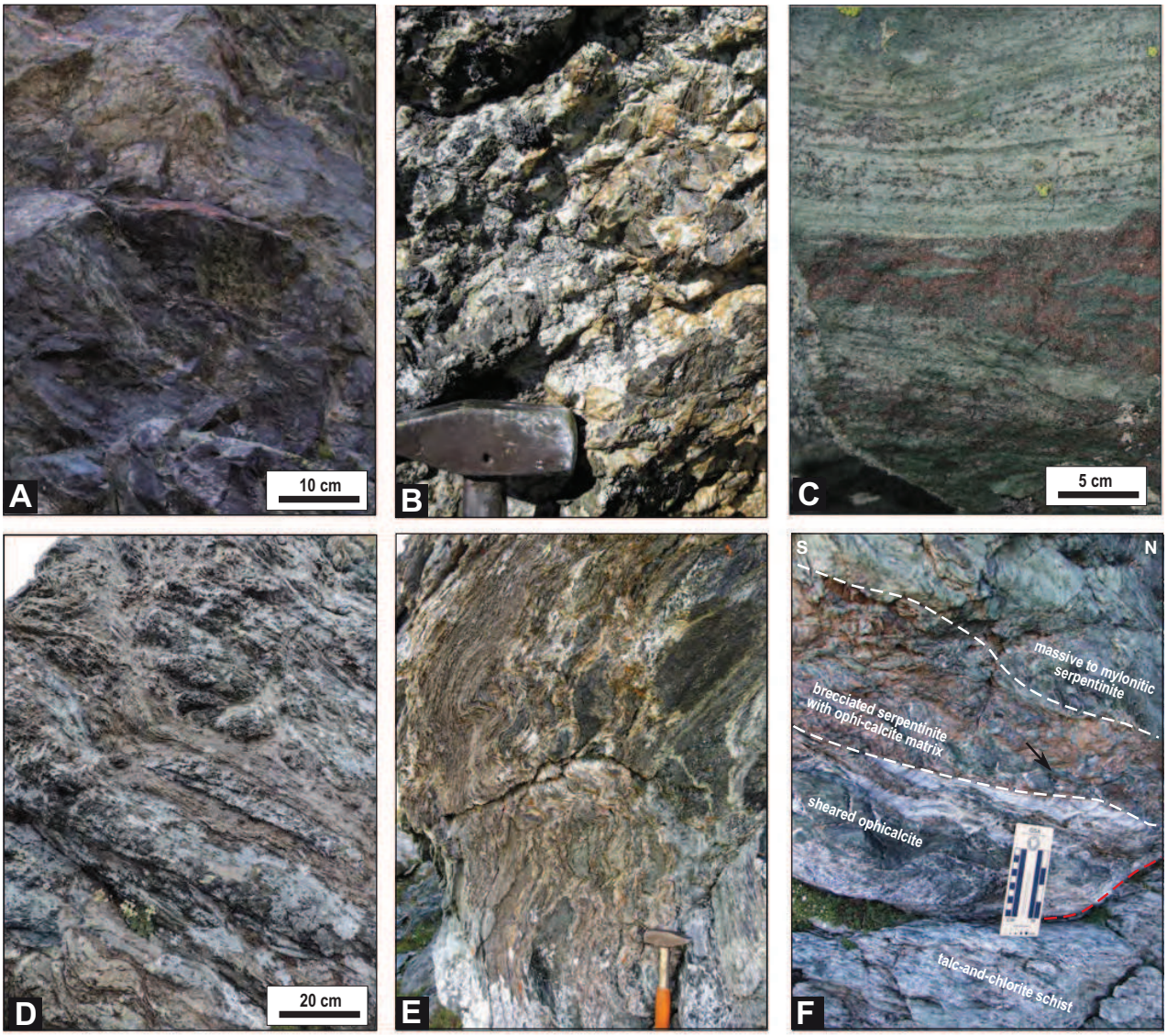

Figure 5. Field images of various lithologies and structures in the BSZ footwall unit: (A) Medium-grained, massive serpentinite with a lherzolitic protolith (East of Colle del Baracun); (B) Close-up of a pegmatitic, coarse-grained Mg-Al metagabbro (South of Colle Armoine). Hammer head as scale; (C) Close-up of a foliated, Mg-Al metagabbro with reddish Fe-Ti layers (W of Colle di Luca); (D) Sheared meta-ophicarbonate with light-brown carbonate layers, deformed by D2 folds (East of Colle Armoine); (E) Sheared meta-ophicarbonate marking the contact between the footwall sequence and the BSZ. Ophicarbonate rocks consists of serpentinite (dark green) meshed with white, cm- to mm-thick hydrothermal calcite veins (South of Colle di Luca); (F) Close-up view of the overturned tectonic contact between the massive serpentinite in the footwall unit and the talc-chlorite schist within the BSZ at the Colle del Baracun. Note the progressive transition from the massive serpentinite to the pervasively sheared talc-chlorite schist.

NiO concentrations (highest NiO= 0,32 wt% in talc lamellae included in apatite). Talc also has relatively high chlorine contents (up to 900 ppm).

Discussion

In this section, we discuss in a regional tectonic framework the significance of our structural, mineralogical and geochemical data, field observations, and interpretations from the Monviso ophiolite for: (1) its oceanic core complex origin, (2) the timing of this extensional tectonic episode and core complex development, and (3) the maturation of the Ligurian–Piedmont basin as a supradetachment depocenter within the Alpine Tethys.

Oceanic core complex origin of the Monviso ophiolite and the BSZ

The structural, textural and mineralogical evidence collectively indicate that the BSZ played a significant role in accommodating high-magnitude extension in young oceanic lithosphere and in the exhumation of lower crustal gabbros and upper mantle peridotites to the seafloor within the Ligurian-Piedmont ocean basin. This simple-shear extensional tectonics produced a Late Jurassic oceanic core complex, which is now represented by the multiply deformed Monviso ophiolite in the Western Alps (Figs. 9 and 10B). We infer that the mafic metabreccia within the BSZ and the talc-chlorite schist and mylonitic serpentinite matrix surrounding the metagabbro blocks

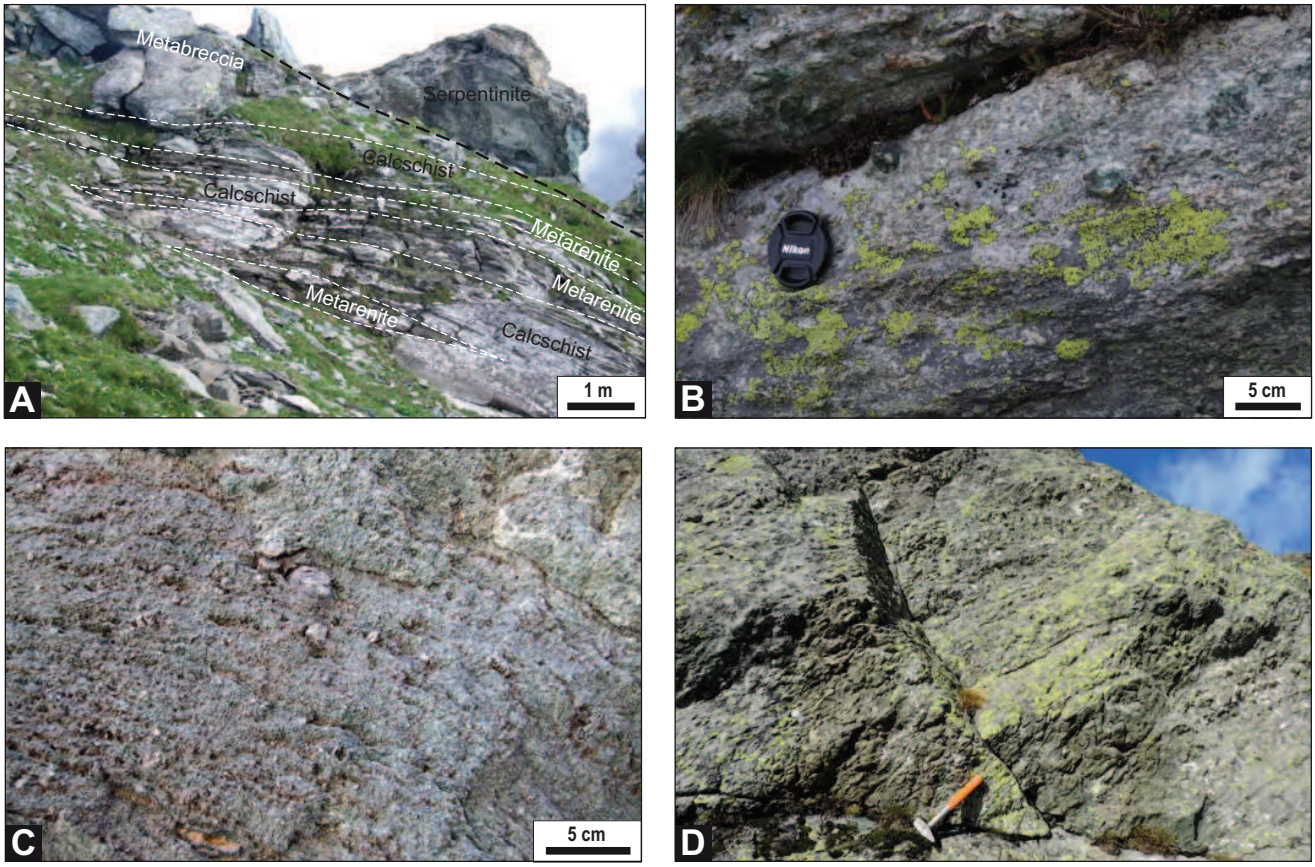

Figure 6 – Field images of various lithologies, contact relationships and structures in the BSZ hanging wall unit: (A) Panoramic view of the overturned mantle rocks and the cover sequence to the South of Colle del Baracun. Metasedimentary rocks consist of intercalations of mafic metabreccia and metasandstone horizons (dashed white lines), decimeters to several meters thick, that are interbedded with medium- to coarse-grained calcschist; (B) Close-up photo of the detrital texture of a matrix-supported mafic metabreccia layer characterized by rounded clasts, centimeters in size, embedded in the coarse-grained mafic matrix (NE of Colle del Baracun); (C) Close-up image of a fining-upward, matrix-supported, mafic metabreccia passing upward into a metasandstone rock (overturned sequence). Note the rounded shape of clasts (Colle del Baracun); (D) Metabasaltic rock with a relict brecciated texture (hammer for scale) (West of Colle Armoine).

represent a Late Jurassic intra-oceanic detachment fault. This low-angle detachment fault, which is now exposed along a 20-25-km-long (Fig. 2), NNW-striking and W-to SW-dipping shear zone (Baracun Shear Zone), controlled the seafloor spreading tectonics and the exhumation of upper mantle peridotites on the seafloor as an oceanic core complex (Fig. 9). The kinematics of detachment faulting and the mode of the inferred uplift and exhumation of the upper mantle rocks in the footwall of the BSZ (Figs. 9 and 10B) are analogous to those documented from the in-situ core complexes along the slow- (Atlantis Massif, Mid-Atlantic Ridge – MAR) and ultraslow-spreading (Atlantis Bank, Southwest Indian Ridge – SWIR) ridges (Cannat, 1993; Tucholke et al., 1998; Boschi et al., 2006; Karson et al., 2006; Dick et al., 2008; Miranda and Dilek, 2010).

Based on the results of the drilling and submersible studies of the Atlantis Bank (SWIR) and the Atlantis Massif (MAR), Miranda and Dilek (2010) defined gabbro-localized and peridotite-localized oceanic core complexes, respectively. In a gabbro-localized core complex, high-temperature, crystal-plastic deformation fabrics concentrate in the gabbros, and granulite-grade mylonitic rocks and shear zones appear to have formed the nucleation of detachment-related deformation in the presence of melt (Miranda and Dilek, 2010, and the references therein). In this type of oceanic core complex (such as SWIR), the footwall of the detachment fault includes widespread gabbroic intrusions in the serpentinized peridotites. In a peridotite-localized core complex, gabbroic intrusions in the footwall peridotites are less abundant in comparison to those in gabbro-localized core complexes, and the crystal-plastic deformation fabrics occur both in peridotites and gabbros with increasingly more abundant low-T°C fabric elements affecting the serpentinized peridotites. Detachment faulting appears to have nucleated mainly in the peridotites in which strain partitioning and formation of talc-amphibolite-chlorite schists were taking place at temperatures more than 500°C, following the emplacement of dispersed gabbros. The internal structure of the Monviso ophiolite and the BSZ detachment fault is more akin to that of a peridotite-localized oceanic core complex, such as the Atlantis Massif along the Mid-Atlantic Ridge (30° Latitude). We posit that emplacement of the Fe-Ti and Mg-Al gabbros in the Monviso ophiolite and serpentinization of the peridotites along syn-kinematic fracture networks promoted rheological weakening of the ultramafic rocks and the development of the low-angle BSZ (MacLeod et al., 2002).

The upper mantle peridotites and oceanic lower crustal units exposed on the seafloor along the MAR commonly occur in the footwalls of detachment faults, which are characterized by tens to hundreds of meters thick, ductile to cataclastic shear zones (Figs. 10A, 10C, and 10D; Boschi et al., 2006, and reference therein). These structural fabrics represent the artifacts of hydrothermal fluid flow

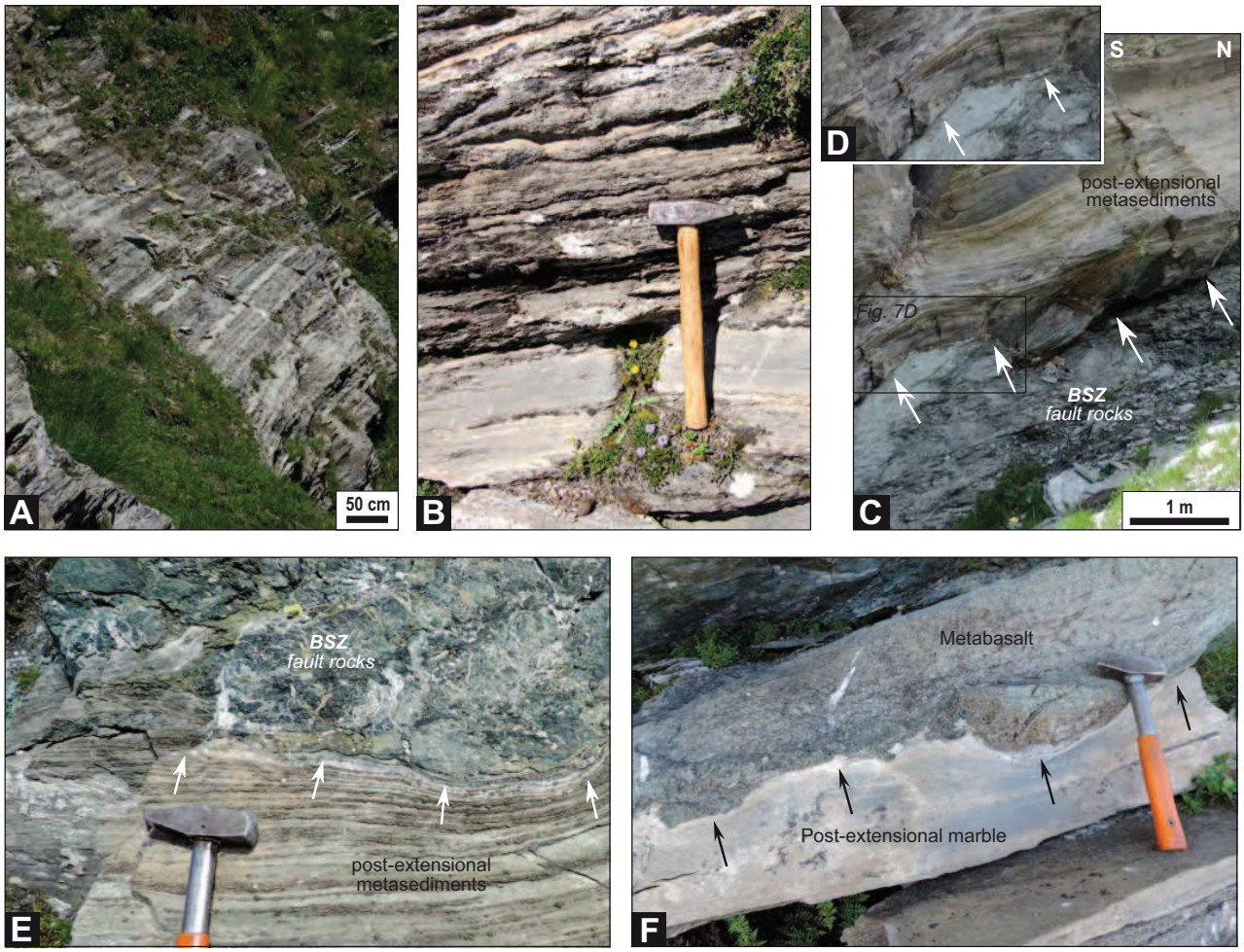

Figure 7 – Field images of various lithologies, contact relationships and structures in the post-extensional sedimentary sequence: (A) Panoramic view of the post-extensional sequence in the Colle del Baracun section, consisting of calcschist alternating with dm-thick marble layers; (B) Close-up of the outcrop in A, showing a dm-thick marble layer interbedded with calcschist (hammer for scale); (C, D, E) Different views of the post-extensional sequence, unconformably resting on the BSZ at Colle del Baracun. Note that the sequence is overturned in E; (F) Close-up photo of the overturned primary contact (black arrows) between a metabasalt and a white marble in the post-extensional sequence (hammer for scale) (West of Colle Armoine).

and associated metasomatism, greenschist to sub-greenschist facies metamorphism (Escartin et al., 2008), and strain partitioning in heterogeneously distributed rocks below the detachment surface. The ubiquitous occurrence of talc-chlorite schist provides a weakening mechanism to allow a low-angle normal fault to initiate and to localize strain over long periods of time (Escartin et al., 2008).

Our observations in the Monviso ophiolite indicate a progressive transition from massive serpentinites to meta-ophicarbonate rocks, and higher up to a talc-chlorite schist shear zone, which represents the Late Jurassic detachment fault (Figs. 10B, 10E and 10F). Low-angle faulting in this case was accompanied by extensive hydrothermal metasomatism. Our mircrostructural observations and mineral chemistry data suggest that the talc-chlorite schist along the BSZ was a result of rock–fluid interactions between the gabbros and serpentinite, and seawater-derived hydrothermal fluids. High Ni and Cr concentrations in this schist rock are compositionally similar to those of chlorite and talc documented from detachment zone fault rocks in both the modern (Boschi et al., 2006) and ancient (Manatschal et al., 2011) oceanic core complexes. The relatively high chlorine contents in the talc-chlorite schist along the BSZ highlight the role of seawater-derived hydrothermal fluids percolating along–across the shear zone. Talc-rich rocks may form at early stages of faulting by interaction of hydrothermal fluids with upper mantle rocks exhumed to shallow depths on their way to the seafloor. This metasomatic process is critical in rheological weakening and strain localization, and facilitates the propagation of deformation farther down into the footwall rocks beneath the detachment surface, resulting in thickening of the detachment-induced shear zone (Fig. 10). Further propagation of brittle faults and fractures into the peridotites and gabbros in the footwall must have provided preferential pathways for seawater penetration and attendant hydration and serpentinization of the ultramafic rocks. This serpentinization process was likely to have contributed to the footwall uplift and exhumation, as documented from the MARK (Mid-Atlantic Ridge at Kane Fracture Zone) area in the modern oceanic lithosphere (Dilek et al., 1997).

Timing of oceanic lithosphere formation in the Ligurian – Piedmont Ocean

Diachronous crystallization ages of gabbros in the ophiolites of the Western Alps have been widely used for reconstructing the tectonic history of the Ligurian – Piedmont ocean basin (e.g., Lombardo et

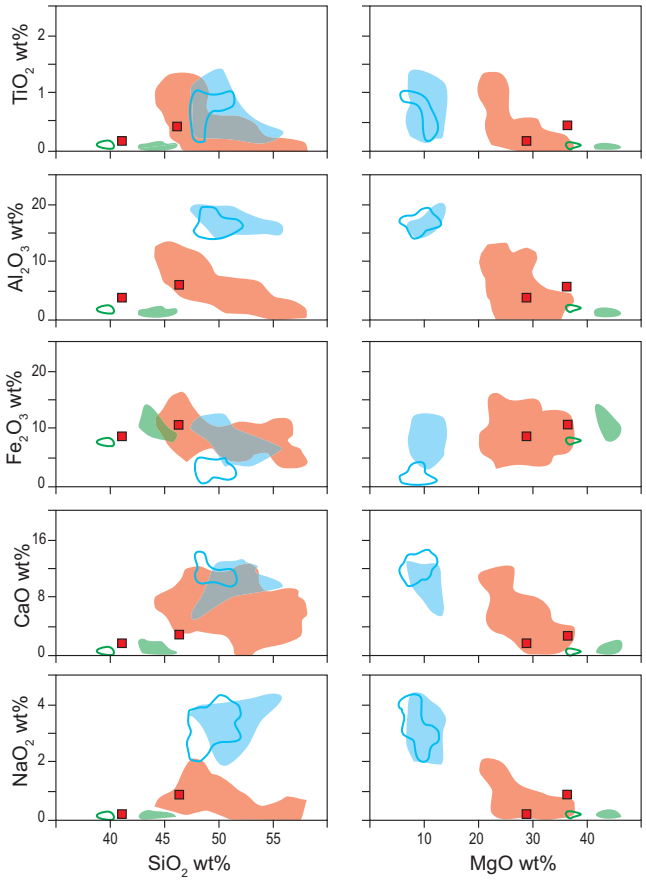

Figure 8 – Harker-type (SiO_2 and MgO) and major-element variation diagrams of the talc-chlorite schist (red square) of the BSZ matrix. Green, red and light blue shaded areas show the compositional ranges of serpentinite, talc-chlorite schist and gabbro from the Atlantis Massif, respectively (modified from Boschi et al., 2006). Green and light-blue lines show the compositional ranges of serpentinized metaperidotites and metagabbros from the Monviso ophiolite, respectively (modified from Lombardo et al., 1978, Lafay et al., 2013).

al., 2002; Piccardo, 2009; Manatchal and Müntener, 2009). Assuming that the igneous ages of the ophiolitic gabbros reflect the magmatic accretion of oceanic lithosphere, the seafloor spreading and the extensional tectonic history of the Ligurian-Piedmont oceanic lithosphere can be quantified temporally. The zircon U/Pb ages of the gabbro bodies within the Western Alps ophiolites (Fig. 11) range from 166±1 Ma (in Gets) to 155±1.2 Ma (in Antrona) (see, e.g., Lombardo et al., 2002 and Manatschal and Müntener, 2009, and reference therein), showing a close overlap with the biostratigraphic ages of the metaradiolarites spatially associated with the metabasalts. These ages collectively suggest that the oceanic lithosphere in the northern part of the Ligurian – Piedmont Ocean (Gets, 166±1 Ma) and in the Zermatt-Saas (Allain gabbro, 163±5 Ma) meta-ophiolites formed nearly 10 m.y. before than the oceanic lithosphere, now preserved in the Antrona section (155±2 Ma) to the north. Farther to the south in the Western Alps, the igneous ages of the gabbros (163±2 My, Rubatto and Hermann, 2003; and Lanzo massif, 162±2 Ma; Kaczmarek et al., 2008) are nearly coeval with those of the Voltri and Corsica ophiolite units (see, e.g., Piccardo, 2009; Fig. 11). Younger zircon U/Pb ages obtained from plagiogranites (Fig. 11) in the Monviso ophiolite (152±2 Ma, Lombardo et al., 2002) and in the Chenalliet ophiolite massif (153±3 Ma, Costa and Caby, 2001) likely represent a late-stage, off-axis magmatic episode in the igneous accretion history of the Ligurian – Piedmont oceanic lithosphere (see Lombardo et al., 2002). This latest pulse of magmatism in the Monviso ophiolite predated the unconformable deposition of the Lower Cretaceous post-extensional sediments overlying the intraoceanic Baracun detachment fault zone (BSZ).

The unconformity surface at the base of the Lower Cretaceous post-extensional sedimentary sequence seals the BSZ and onlaps both its hanging wall and footwall blocks. These stratigraphic relationships indicate that the structural architecture documented from the LTU of the Monviso ophiolite and the BSZ predates the deposition of these post-extensional rocks. Thus, the structural fabric elements and the primary mineral assemblages recorded in the rock units of the ophiolite and the BSZ reflect the rift-drift and seafloor spreading tectonic processes that took place during the opening of the Ligurian – Piedmont ocean basin prior to the Early Cretaceous.

The exhumation of the upper mantle peridotites in the footwall and the deposition of the syn-extensional sediments in the hanging wall of the BSZ occurred during the Late Jurassic. We can constrain the specific timing of this extensional phase as between post 163±2 Ma (Middle Callovian), which is the crystallization age of the gabbroic intrusions in the peridotites (Rubatto and Hermann, 2003) and the Early Cretaceous, which is the depositional age of the post-extensional sedimentary sequence above the unconformity. Meta-radiolarite rocks in the Queyras Schistes Lustrés Complex (Caby et al., 1987) represent the stratigraphic base of the post-extensional sequence and reveal a middle-late Oxfordian age for their deposition that is consistent with the age bracket we consider for the timing of simple-shear extension and detachment faulting.

The lack of any material or blocks within the BSZ derived from the hanging wall metasedimentary units or metabasaltic rocks also indicates that the main phase of detachment faulting must have occurred before the Alpine stage deformation. Although subduction- to exhumation-related tectonic reworking of the Ligurian – Piedmont oceanic lithosphere and the associated metamorphic overprints partly obliterated the seafloor spreading history of the BSZ, its pre-Alpine stage record can be well constrained by several lines of meso- to micro-scale structural evidence: (*1*) ophicarbonate rocks resting on the massive serpentinite indicate that the upper mantle peridotites were already exhumed on the seafloor prior to the onset of subduction zone tectonics within the ocean basin. (*2*) pre-D1 metabreccia enveloping the metagabbro blocks within the BSZ represents a fault rock that formed during detachment faulting and the associated cataclastic deformation. (*3*) talc-chlorite schist matrix in the BSZ represents a metamorphic assemblage, which typically develops along intraoceanic detachment fault zones (see e.g., Boschi et al., 2006, and reference therein) due to syn-kinematic alteration at the contact between serpentinized peridotites and gabbros.

Mature Ligurian–Piedmont ocean basin as a supradetachment depocenter

The lateral and vertical facies variations in the meta-sedimentary sequences of the Monviso ophiolite and the structural relationships of these sequences with the mantle peridotites provide important clues for the nature of their depocenter within the Ligurian-Piedmont ocean basin. Development of this depocenter and its accommodation space was strongly controlled by asymmetric extension and tectonically

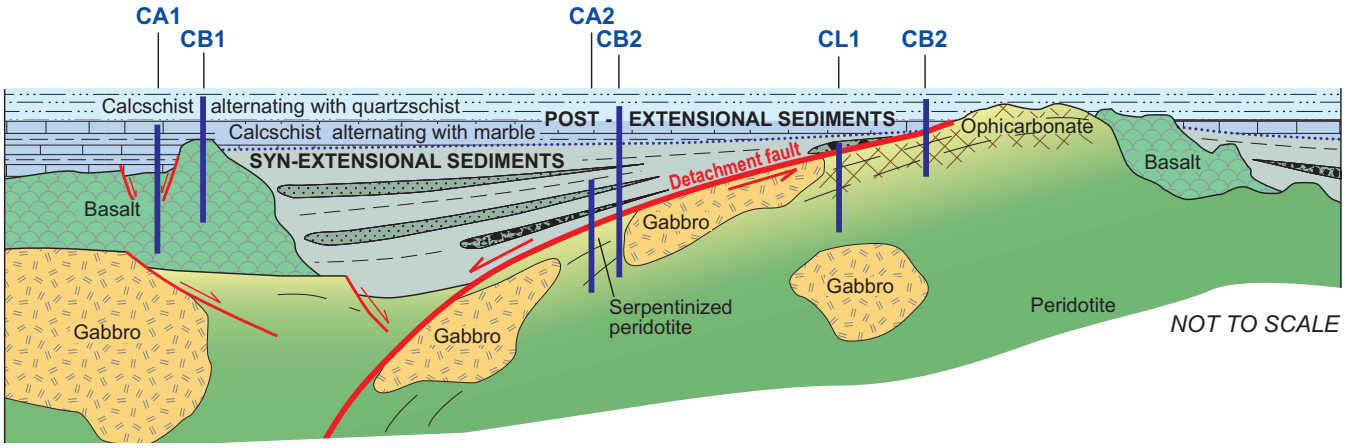

Figure 9 – Interpretive reconstruction of the Monviso ophiolite oceanic core complex, constrained by the analysis of the metasedimentary sequence and by the observed structural relationships between the hanging wall and footwall units of the extensional detachment fault (Baracun Shear Zone). Thick vertical blue lines (and related acronyms) indicate the approximate locations of the stratigraphic columnar sections shown in Figure 4.

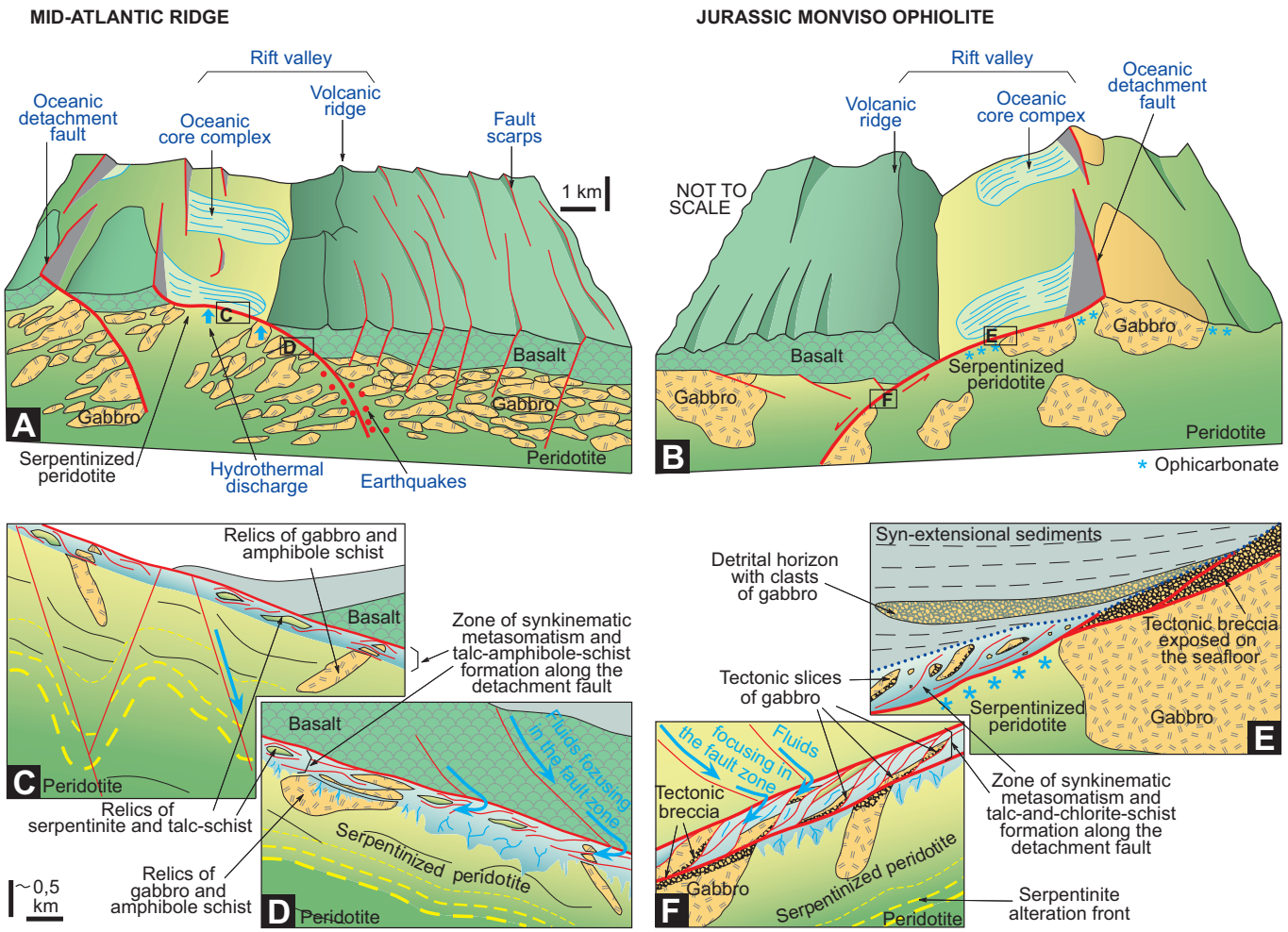

Figure 10 – Comparison between (A) an in-situ, intra-oceanic core complex along the Mid-Atlantic Ridge (modified from Escartin and Canales, 2011), and (B) the inferred Monviso oceanic core complex developed within the Jurassic Ligurian-Piedmont Ocean. (C-F) Close-up cross sections of a detachment fault system (location in Figs 10A and 10B) and associated metasomatic and tectonic- processes in modern (C-D; modified from Boschi et al., 2006) and ancient oceanic (E-F) settings, respectively.

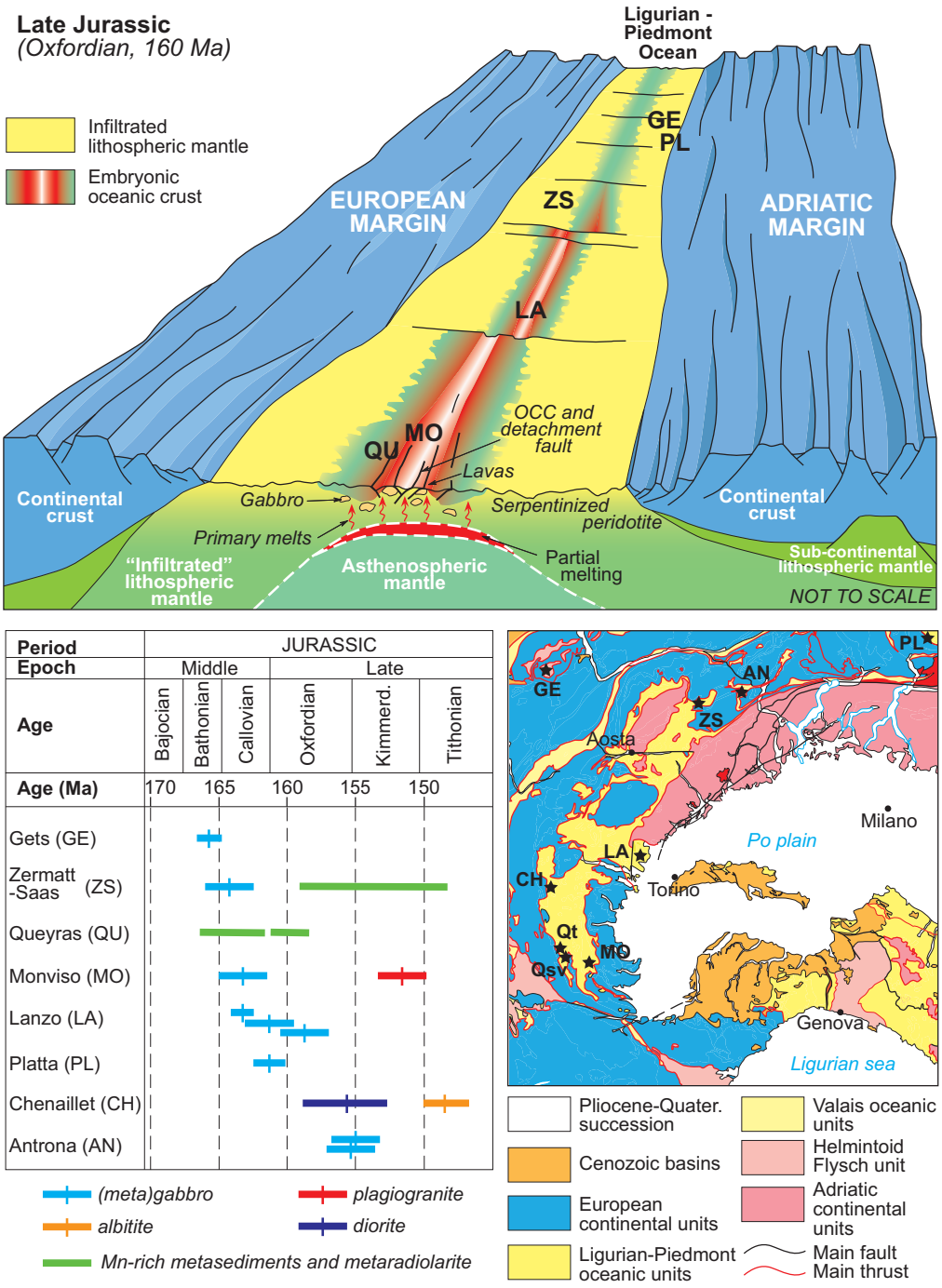

Figure 11 – Interpretive block diagram depicting the inferred paleogeography of the Monviso ophiolite ridge segment (MO) in the Ligurian-Piedmont Ocean in the Late Jurassic (Oxfordian, 160 Ma). Frontal cross-section modified from Dilek and Furnes (2011), Piccardo et al. (2009), Peron-Pinvidic and Manatschal (2009). Table in the lower left-side displays the known age ranges of mafic rocks, Mn-rich metasedimentary rocks, and meta-radiolarite from the Ligurian–Piedmont oceanic lithosphere (data sources: Borsi et al., 1996; Caby et al., 1987; Costa and Caby, 2001; De Wever and Beumagarter, 1995; Kaczmarek et al., 2008; Liati et al., 2005; Lombardo et al., 2002; Manatschal et al., 2006; Rubatto and Hermann, 2003; Rubatto et al., 1998; Stuki et al., 2003). Geological map of the Alps and the Northern Apennines shows the present-day location of the tectonostratigraphic units used in the entire figure.

controlled subsidence in the hanging wall of the low-angle Baracun detachment shear zone (Fig. 9). The Upper Jurassic syn-extensional sedimentary succession with abundant ophiolitic material onlaps the shear zone and its talc-chlorite schist rocks, and has a wedge shape geometry with its thickest section corresponding to the distal depocenter of the supradetachment basin.

The irregular thickness of the post-extensional sequence and its unconformable deposition on top of the footwall and hanging wall (metabasalts and metasediments) sequences and the BSZ rocks suggests an irregular seafloor bathymetry within the basin that was likely controlled by basement faulting and tectonic segmentation (Fig. 9). The thinner and incomplete sections of this sequence occur in the

eastern part of the ophiolite where the Lower Cretaceous carbonate-rich calcschists directly overlie the BSZ (Fig. 9). We interpret these bathymetric anomalies and the associated stratigraphic variations as tectonically controlled structural highs within a basin, which was deepening to the west (in the present coordinate system).

The initial input of continentally derived sediments within this basin did not occur until the deposition of the uppermost part of the post-extensional sequence that contains quartz-rich intercalations within the carbonate-rich calcschists. We postulate that this stage of deposition coincided with significant terrigenous input into the basin. In comparison with the analogous post-extensional sequences preserved in the unmetamorphosed Ligurian Units of the Northern Apennines (see, e.g., Decandia and Elter, 1972; Marroni et al., 2010; Festa et al., 2013, and references therein), we interpret these post-extensional deposits to represent distal carbonatic and mixed siliciclastic-carbonatic turbidites (i.e., Calpionella Limestone and/or Palombini Shale) which reworked a continental margin source area.

Conclusions

This study is a first systematic documentation, from the Western Alps, of the seafloor spreading and oceanic core complex development history of the Late Jurassic Monviso ophiolite, which experienced subduction zone deformation and high-P metamorphism following its magmatic construction. Our structural, stratigraphic, mineralogical and geochemical analyses of the footwall and hanging wall tectonostratigraphic units in the ophiolite indicate that the upper mantle peridotites and their Fe-Ti and Mg-Al gabbroic intrusions were uplifted and exhumed on the seafloor as in an intraoceanic core complex. Emplacement of gabbroic intrusions into the ultramafic rocks, widespread extensional fracturing and attendant serpentinization in the peridotites, and hydrothermal metasomatism associated with faulting were instrumental in the localization of a low-angle detachment shear zone in the upper mantle. Peridotite rocks within this shear zone experienced crystal-plastic fabric development, recrystallization of talc-chlorite schist, and cataclastic brecciation, as shown from the modern peridotite-localized core complexes along the Mid-Atlantic Ridge seafloor spreading environment.

The timing of intraoceanic core complex development in the Piedmont-Ligurian ocean basin, as preserved in the Monviso ophiolite, is well constrained to have taken place between Middle Callovian (163±2 Ma) and the middle-late Oxfordian. These ages reflect the timing of the emplacement of the gabbroic intrusions in the peridotites, and of the deposition of the post-extensional sedimentary sequence unconformably overlying the detachment shear zone and the syn-extensional deposits. Ophicarbonates and mafic breccias at the bottom of the syn-extensional deposits in the hanging wall record the early history of tectonically-induced sedimentation and accommodation space development above the shear zone. The wedge-shape geometry of the syn-extensional sequence, which thickens away from the Baracun shear zone, suggests a distal depocenter geometry as in a supradetachment basin configuration. Carbonate-rich calcschist with quartz-rich layers unconformably overlying the syn-extensional sequence and the ophiolite represent the post-extensional phase of deposition. The existence of continentally derived detrital material in this post-extensional sequence points to the proximal position of a continental margin to the Ligurian–Piedmont basin at this time.

The occurrence of a seafloor spreading originated oceanic core complex in the Monviso ophiolite is globally significant for two reasons: (1) Despite the strong overprint of subduction zone deformation and metamorphism, the simple-shear, intraoceanic extensional tectonic fabric is well preserved in the Late Jurassic oceanic lithosphere. This case study clearly demonstrates that not all shear zones, brittle-ductile and cataclastic structures, and highly dismembered ophiolites in high-pressure collisional belts generally represent the products of a subduction channel and subduction zone tectonics, as has been widely assumed in the literature pertaining to the Western Alps (i.e., Guillot et al., 2009; Angiboust et al., 2011). (2) Oceanic core complexes and their lithospheric-scale asymmetric shear zones (detachment faults) may be ideal tectonic settings for the localization of subduction initiation, as has been proposed from some other Tethyan ophiolites (i.e., Maffione et al., 2015). We think that inversion of extensional detachment faults into intraoceanic subduction zones under favorable geodynamic conditions provides a viable mechanism for basin collapse and closure without invoking other external driving forces in a given region.

Acknowledgements

This research has been supported by the following grants: (1) “ex 60%–2013 and 2014” Università degli Studi di Torino and PROGEO Piemonte (Universita degli Studi di Torino and Compagnia San Paolo) to A. Festa and G. Balestro, (2) the Italian Ministry of University and Research Cofin-PRIN 2010/2011(“GEOPROB–GEOdynamic Processes of Oceanic Basins” to A. Festa and P. Tartarotti, and (3) “Subduction and exhumationof continental lithosphere: Implications on orogenic architecture, environment and climate” to G. Balestro. We gratefully acknowledge these funds. We thank M. Marroni, J. Wakabayashi and several other colleagues for providing us with insightful feedback and comments on various aspects of our study in the Monviso ophiolite, as presented in this paper.

References

Angiboust, S., Agard, P., Raimbourgh, H., Yamato, P., and Huet, B., 2011, Subduction interface processes recorded by eclogite-facies shear zones (Monviso, W. Alps): Lithos, v. 127, pp. 222–238. doi:10.1016/j.lithos.2011.09.004

Angiboust, S., Langdon, R., Agard, P., Waters, D., and Chopin, C., 2012, Eclogitization of the Monviso ophiolite (W. Alps) and implications on subduction dynamics: Journal of Metamorphic Geology, v. 30, pp. 37–61. doi:10.1111/j.1525-1314.2011.00951.x

Balestro, G., Fioraso, G., and Lombardo, B., 2011, Geological map of the upper Pellice Valley (Italian Western Alps): Journal of Maps, 2011, pp. 634-654. doi: 10.4113/jom.2011.1213.

Balestro, G., Fioraso, G., and Lombardo, B., 2013, Geological map of the Monviso massif (Western Alps): Journal of Maps, v. 9(4), pp. 623-634. doi: 10.1080/17445647.2013.842507.

Balestro, G., Lombardo, B., Vaggelli, G., Borghi, A., Festa, A., and Gattiglio, M., 2014, Tectonostratigraphy of the northern Monviso Meta-ophiolite Complex (Western Alps): Italian Journal of Geosciences, v. 133 (3), pp. 409-426. Doi: 10.3301/IJG.2014.13

Balestro, G., Festa, A., and Tartarotti, P., 2015, Tectonic significance of different block-in-matrix structures in exhumed convergent plate margins: examples from oceanic and continental HP rocks in Inner Western Alps (northwest Italy): International Geology Review, v. 57, no. 5-8, pp. 581-605. http://dx.doi.org/10.1080/00206814.2014.943307.

Bearth, P., 1967, Die Ophiolithe der Zone von Zermatt-Saas Fee: Beiträge zur Geologischen Karte der Schweiz, Neue Folge, 132, 130 pp.

Bigi, G., Castellarin, A., Coli, M., Dal Piaz, G.V., Sartori, R., Scandone, P. and Vai, G.B., 1990, Structural Model of Italy, sheets 1-2: CNR, Progetto Fin. Geodinamica, SELCA Firenze

Bill, M., O'Dogherty, L., Guex, J., Baumgartner, P.O., Masson, H., 2001, Radiolarite ages in Alpine-Mediterranean ophiolites: constraints on the oceanic spreading and the Tethys-Atlantic connection: Geological Society of America Bulletin, v. 113, pp. 129–143.

Borsi, L., Schärer, U., Gaggero, L., and Crispini, L., 1996, Age, origin and geodynamic significance of plagiogranites in lherzolites and gabbros of the Piedmont-Ligurian ocean basin: Earth and Planetary Science Letters, v. 140, pp. 227–241.

Boschi, C., Früh-Green, G.L., and Delacour, A., 2006, Mass transfer and fluid flow during detachment faulting and development of an oceanic core complex, Atlantis Massif (MAR 30°N): Geochemistry, Gephysics, Geosystem, v. 7, doi: 10.1029/2005GC001074.

Bousquet, R., Schimid, S.M., Zeilinger, G., Oberhansli, R., Roseberg, C., Molli, G., Robert, C., Wiederkehr, M., Rossi, Ph., 2012, Tectonic framework of the Alps: CCGM/CGMW. 1 sheet.

Butler, J.P., Beaumont, C., and Jamieson, R.A., 2013, The Alps 1: A working geodynamic model for burial and exhumation of (ultra)high-pressure rocks in Alpine-type orogens: Earth and Planetary Science Letters, v. 377–378, pp. 114–131. doi:10.1016/j.epsl.2013.06.039

Caby R., Dupuy C. and Dostal J., 1987, The very beginning of the Ligurian Tethys in the Western Alps: Petrological and geochemical evidence from the oldest ultramafite-derived sediments in Queyras, Western Alps (France): Eclogae Geologicae Helvetiae, v. 80, pp. 223-240.

Cannat, M., 1993, Emplacement of mantle rocks in the seafloor at Mid-Ocean ridge: Journal of Geophysical Research, v. 98, B3, pp. 4163-4172.

Costa, S., and Caby, R., 2001, Evolution of the Ligurian Tethys in the Western Alps: Sm/Nd and U/Pb geochronology and rare-earth element geochemistry of the Montgenèvre ophiolite (France): Chemical Geology, v. 175, pp. 449–466.

Coward, M.P., and Dietrich, D., 1989, Alpine tectonics—an overview, in Coward M.P., Dietrich D., Park R.G., eds., Alpine tectonics: Geological Society of London Special Publications, v. 45, pp. 1–29. doi:10.1144/GSL.SP.1989.045.01.01

Dal Piaz, G.V., Bistacchi, A., and Massironi, M., 2003, Geological outline of the Alps: Episodes, v. 26, pp. 175–180.

Dal Piaz, G.V., Hunziker, J.C., and Martinotti, G., 1972, La zona Sesia–Lanzo e l'evoluzione tettonico metamorfica delle Alpi nordoccidentali interne: Memorie della Società Geologica Italiana, v. 11, pp. 433–460.

Decandia, F.A., and Elter, P., 1972, La "zona" ofiolitifera del Bracco nel settore compreso fra Levanto e la Val Graveglia (Appennino ligure): Memorie della Società Geologica Italiana, v. 11, pp. 503–530.

De Wever P. and Baumgartner P.O., 1995, Radiolarians from the base of the supra-ophiolitic Schistes Lustrés formation in the Alps (Saint-Véran, France and Traversiera Massif, Italy), in Baumgartner P.O. et al., eds., Middle Jurassic to Lower Cretaceous radiolaria of Tethys: occurrences, systematics, biochronology: Memoire Géologique, Lausanne, v. 23, pp. 725–730.

Dick, H.J.B., Tivey, M.A., and Tucholke, B.E., 2008, Plutonic foundation of a slow-spreading ridge segment: Oceanic core complex at Kane Megamullion, 23_300N, 45_200W: Geochemistry, Geophysics, Geosystems, v. 9, Q05014, doi:10.1029/2007GC001645.

Dilek, Y., 2003, Ophiolite pulses, mantle plumes and orogeny. Geological Society of London, Special Publications, v. 218, pp. 9-19.

Dilek,Y., 2006, Collision tectonics of the Eastern Mediterranean region:Causesandconsequences: Geological Society of America Special Paper, v. 409,pp.1-13.

Dilek, Y. and Delaloye, M., 1992, Structure of the Kizildag ophiolite, a slow-spread Cretaceous ridge segment north of the Arabian promontory: Geology, v. 20, pp. 19-22.

Dilek, Y. and Eddy, C.A., 1992, The Troodos (Cyprus) and Kizildag (S. Turkey) ophiolites as structural models for slow-spreading ridge segments: Journal of Geology, v. 100, pp. 305-322.

Dilek, Y., Coulton, A. and Hurst, S., 1997, Serpentinization and hydrothermal veining in peridotites at Site 920 in the MARK area (Leg153). *In:* Cannat, J. Karson, J. Miller and D. Elthon, eds., Proceedings of the Ocean Drilling Program, Scientific Results, v. 153: College Station, Texas (Ocean Drilling Program), pp.35-59.

Dilek, Y., Moores, E.M., and Furnes, H., 1998, Structure of modern oceanic crust and ophiolites and implications for faulting and magmatism at oceanic spreading centers: In, Buck, R., Karson, J., Delaney, P., and Lagabrielle, Y., eds., AGU Monograph on Faulting and Magmatism at Mid-Ocean Ridges, v. 106, pp. 219-266.

Dilek, Y. and Thy, P., 1998, Structure, petrology, and seafloor spreading tectonics of the Kizildag ophiolite (Turkey). In, Mills, R., and Harrison, K., eds., Modern Ocean Floor Processes and the Geological Record: Geological Society of London Special Publication, v. 148, pp. 43-69.

Dilek, Y. and Newcomb. S., 2003, Ophiolite Concept and the Evolution of Geological Thought: Geological Society of America Special Paper, v. 373, 504 pp. ISBN 0-8137-23736.

Dilek, Y. and Robinson, P.T., 2003, Ophiolites in Earth history. Geological Society, London, Special Publications, v. 218, pp. 1-8.

Dilek, Y. and Furnes, H., 2011, Ophiolite genesis and global tectonics: geochemical and tectonic fingerprinting of ancient oceanic lithosphere: The Geological Society of America Bulletin, v. 123, pp. 387-411, DOI: 10.1130/B30446.1.

Dilek, Y., and Furnes, H., 2014, Ophiolites and their origins: Elements, v. 10, p. 93–100, doi:10.2113/gselements.10.2.93.

Elter G., 1971, Schistes lustrés et ophiolites de la zone piemontaise entre Orco et Doire Baltée (Alpes Graies). Hypotèses sur l'origine des ophiolites: Gèologie Alpine, v. 47, pp. 147-169.

Escartin, J., and Canales, J.P., 2011, Detachments in oceanic lithosphere: Deformation, magmatism, fluid flow and ecosystems: Eos, Transactions, American Geophysical Union, v. 92, pp.31, http://dx.doi.org/10.1029/2011EO040003.

Escartýn, J., Smith, D.K., Cann, J., Schouten, H., Langmuir, C.H., and Escrig, S., 2008, Central role of detachment faults in accretion of slowspread oceanic lithosphere: Nature, v. 455, pp. 790–794, doi:10.1038/nature 07333.

Fantoni, R., Bersezio, R., and Forcella, F., 2004, Alpine structre and deformation chronology at the Southern Alps-Po Plain border in Lombardy: Bollettino della Società Geologica Italiana, v. 123, pp. 463-476.

Fantoni, R., Decarlis, A., and Fantoni, E., 2003, L'estensione mesozoica al margine occidentale delle Alpi meridionali (Piemonte settentrionale, Italia): Atti Ticinensi di Scienze della Terra, v. 44, pp. 97-110.

Festa, A., 2011, Tectonic, sedimentary, and diapiric formation of the Messinian mélange: Tertiary Piedmont Basin (northwestern Italy), inWakabayashi, J., and Dilek, Y., eds., Mélanges: Processes of Formation and Societal Significance: Geological Society of America Special Paper 480, pp. 215–232, doi:10.1130/2011.2480(10).

Festa A., Balestro, G., Dilek Y, and Tartarotti, P., 2015a, A Jurassic oceanic core complex in the high-pressure Monviso ophiolite (western Alps, NW Italy): Lithosphere, v. 7, pp. 646-652, Doi: 10.1130/L458.1.

Festa A., Dilek., Y., Codegone G., Cavagna, S., and Pini, G.A., 2013, Structural Anatomy of the Ligurian Accretionary Wedge (Monferrato, NW-Italy), and Evolution of Superposed Mélanges: Geological Society of America Bulletin, v. 125 (9/10), pp. 1580-1598. Doi: 10.1130/B30847.1

Festa, A., Dilek, Y., Pini, G.A., Codegone, G., and Ogata, K., 2012, Mechanisms and processes of stratal disruption and mixing in the development of mélanges and broken formations: redefining and classifying mélanges: Tectonophysics, v. 568-569, pp. 7-24. DOI: 10.1016/j.tecto.2012.05.021.

Festa A., Fioraso G, Bissacca E., and Petrizzo M.R., 2015b, Geology of the Villalvernia-Varzi Line between Scrivia and Curone valleys (NW Italy), in Zucali M., and Spalla, I., eds., Structural Mapping in the Mediterranean: bridging laboratory to lithosphere: Journal of Maps, v. 11 (1), pp. 39-55. Doi: 10.1080/17445647.2014.959569.

Festa, A., Ogata, K., Pini, G.A., Dilek, Y., and Codegone, G., 2015c, Late Oligocene – early Miocene olistostromes (sedimentary mélanges) as tectono-stratigraphic constraints to the geodynamic evolution of the exhumed Ligurian accretionary complex (Northern Apennines, NW Italy): International Geology Review, v. 57, no. 5-8, pp. 540-562. Doi: 10.1080/00206814.2014.931260.

Funicello, R., Parotto, M., Praturlon, A., and Bigi, G., 1981, Carta tettonica d'Italia – schema preliminare: CNR-Consiglio Nazionale delle Ricerche. Ed. Grafica editoriale cartografica, Roma. 1 sheet. 1:1.500.000 scale.

Frey, M., Desmons, J. and Neubauer, F., eds, 1999, The new metamorphic map of the Alps: Schweizrische Mineralogische und Petrogrographische Mitteilungen, v. 79, pp. 1-230.

Ghibaudo, G., Massari, F., and Chiambretti, I., 2014, Oligo-Miocene tectono-sedimentary evolution of the Langhe Sub-basin: from continental basinal setting (Tertiary Piedmont Basin – Northwestern Italy): Journal of Mediterranean Earth Sciences, v. 6, pp. 53-144.

Ghielmi, M., Minervini, M., Nini, C., Rogledi, S., and Rossi, M., 2013, Late Miocene – Middle Pleistocene sequences in the Po Plain – Northern Adriatic Sea (Italy): The stratigraphic record of modification phases affecting a complex foreland basin: Marine and Petroleum Geology, v. 42, pp. 50-81.

Groppo, C., and Castelli, D., 2010, Prograde P–T evolution of a lawsonite eclogite from the Monviso Meta-ophiolite (Western Alps): Dehydration and redox reactions during subduction of oceanic FeTi-oxide gabbro: Journal of Petrology, v. 51, pp. 2489–2514. doi:10.1093/petrology/egq065.

Guillot, S., Hattori, K., Agard, P., Schwartz, S., and Vidal, O., 2009, Exhumation processes in oceanic and continental subduction contexts: A review, in Lallemand, S., and Funiciello, F., eds., Subduction zone geodynamics: Berlin Heidelberg, Springer-Verlag, pp. 275.

Kaczmarek, M.-A., Müntener, O., Rubatto, D., 2008, Trace element chemistry and U–Pb dating of zircons oceanic gabbros and their relationship with whole rock composition (Lanzo, Italian Alps): Contributions to Mineralogy and Petrology, v. 155, pp. 295–312.

Karson J.A., Fruh-Green, G.L., Kelley, D.S., Williams,E.A., Yoerger, D.R. and Jakuba, M., 2006, Detachment shear zone of the Atlantis Massif core complex, Mid-Atlantic Ridge, 30°N: Geochemistry, Geophysics, Geosystems, v.7(6), Q06016, doi: 10.1029/20O5GC001109.

Lagabrielle, Y., 1994, Ophiolites of the southwestern Alps and the structure of the Tethyan oceanic lithosphere: Ofioliti, v. 19, 413–434.

Lagabrielle, Y., 2009, Mantle exhumation and lithosphere spreading: An historical perspective from investigations in the oceans and in the Alps-Apennines ophiolites: Italian Journal of Geosciences, v. 128 (2), pp. 279-293.

Lardeaux, J., Schwartz, S., Tricart, P., Paul, A., Guillot, S., Béthoux, N., and Masson, F., 2006, A crustal-scale crosssection of the south-western Alps combining geophysical and geological imagery: Terra Nova, v. 18, no. 6, pp. 412–422. doi:10.1111/j.1365-3121.2006.00706.x

Lafay, R., Deschamps, F., Scghwartz, S., Guillot, S., Godard, M., Debret, B., and Nicollet, C., 2013, High-pressure serpentinites, a trap-and-release system controlled by metamorphic conditions: Example from the Piedmont zone of the western Alps: Chemical Geology, v. 343, pp. 38-54.

Laubscher, H.P., 1991, The arc of Western Alps today: Eclogae Geologicae Helvetiae, v. 84, pp. 631–659.

Lemoine, M., 1971, Données nouvelles sur la série du Gondran près Briançon (Alpes Cottiennes). Réflexions sur les problèmes stratigraphique et paléogéographique de la zone piémontaise: Gèologie Alpine, v. 47, pp. 181-201.

Lemoine, M., and Tricart, P., 1986, Les schistes lustrés piémontais des Alpes occidentales: approche stratigraphique, structurale et sédimentologie: Eclogae Geologicae Helvetiae, v. 79, pp. 271–294.

Liati, A., Froitzheim, N., and Fanning, C.M., 2005, Jurassic ophiolites within the Valais domain of the Western and Central Alps: geochronological evidence for re-rifting of oceanic crust: Contributions to Mineralogy and Petrology, v. 149 (4), pp. 446–461.

Lombardo, B., Nervo, R., Compagnoni, R., Messiga, B., Kienast, J., Mevel, C., Fiora, L., Piccardo, G., and Lanza, R., 1978, Osservazioni preliminari sulle ofioliti metamorfiche del Monviso (Alpi Occidentali): Rendiconti Società Italiana Di Mineralogia E Petrologia, v. 34, pp. 253–305.

Lombardo, B., Rubatto, D., and Castelli, D., 2002, Ion microprobe U–Pb dating of zircon from a Monviso metaplagiogranite: Implications for the evolution of the Piedmont-Liguria Tethys in the Western Alps: Ofioliti, v. 27, pp. 109–117.

MacLeod, C.J., Escartin, J, Banerji, D., Banks, G.J., Gleeson, M., Irving, D.H.B., Lilly, R.M., McCaig, A.M., Niu, Y., Allerton, S., and Smith, D.K., 2002, Direct geological evidence for oceanic detachment faulting: The Mid-Atlantic Ridge, 15_450N: Geology, v 30, pp. 879–882.

Maffione, M., Thieulot, C., van Hinsbergen, D.J.J, Morris, A., Plumper, O., and Spakman, W., 2015, Dynamics of intra-oceanic subduction initiation. 1: Oceanic detachment fault inversion and the formation of forearc ophiolites: Geochemistry, Geophysics, Geosystems, v. 16 (6), pp. 1753-1770. doi:10.1002/2015GC005746.

Manatschal, M., and Müntener, O., 2009, A type sequence across an ancient magma-poor ocean–continent transition: the example of the western Alpine Tethys ophiolites: Tectonophysics, v. 473, pp. 4–19.

Manatschal, G., Engstrom, A., Desmurs, L., Schaltegger, U., Cosca, M., Müntener, O., and Bernoulli, D., 2006. What is the tectono-metamorphic evolution of continental break-up: the example of the Tasna Ocean–Continent Transition: Journal of Structural Geology, v. 28 (10), pp. 1849–1869.

Manatschal, G., Sauter, D., Karpoff, A.M., Masini, E., Mohn, G., and Lagabrielle, Y., 2011, TheChenaillet Ophiolite in the French/Italian Alps: an ancient analogue for an Oceanic Core Complex?: Lithos, v. 124, pp. 169–184. http://dx.doi.org/10.1016/j.lithos.2010.10.017.

Manzotti, P., Ballèvre, M., Zucali, M., Robyr, M. and Engi, M., 2014, The tectonometamorphic evolution of the Sesia-Dent Blanche nappes (internal Western Alps): review and synthesis: Swiss Journal of Geosciences, v.107, pp. 309-336.

Marroni, M., Meneghini, F., and Pandolfi, L., 2010, Anatomy of the Ligure-Piemontese subduction system: Evidence from Late Cretaceous–middle Eocene convergent margin deposits in the Northern Apennines, Italy: International Geology Review, v. 52, pp. 1160–1192.

Michard, A., Goffe, B., Chopin, C., and Henry, C., 1996, Did the Western Alps develop through an Oman-type stage? The geotectonic setting of high-pressure metamorphism in two contrasting Tethyan transects: Eclogae Geologicae Helvetiae, v. 89, pp. 43– 80.

Miranda, E.A. and Dilek, Y., 2010, Oceanic core complex development in modern and ancient oceanic lithosphere: Gabbro-localized versus peridotite-localized detachment models: Journal of Geology, v. 118, pp. 95-109, DOI: 10.1086/648460.

Péron-Pinvidic, G., and Manatschal, G., 2009, The final rifting evolution at deep magma-poor passive margins from Iberia-Newfoundland: a new point of view: International Journal of Earth Sciences, v. 98, pp. 1581-1597.

Perrone, G., Cadoppi, P., and Tallone, S., 2015, Geometry and impact of transpressional faulting in polyphasic metamorphic orogenic belts: the Viù Deformation Zone (inner Western Alps): International Geology Reviewv. 50 (11), pp. 1022-1039. doi: 10.1080/00206814.2015.1033655.

Piccardo, G., 2009, Evolution of the lithospheric mantle in an extensional setting: Insights from ophiolitic peridotites: Lithosphere, v.1, pp. 81-87.

Platt, J.P., Behrmann, J.H., Cunningham, P.C., Dewey, J.F., Helman, M., Parish, M., Shepley, M.G., Wallis, S., and Western, P.J., 1989, Kinematics of the Alpine arc and the motion history of Adria: Nature, v. 337, pp. 158–161.doi:10.1038/337158a0.

Ricou, L.E., and Siddans, W.B., 1986, Collision tectonics in the western Alps: Geological Society, London, Special Publications, v. 19, pp. 229–244. doi:10.1144/GSL.SP.1986.019.01.13.

Rubatto, D., and Hermann, J., 2003, Zircon formation during fluid circulation in eclogites (Monviso, Western Alps): implications for Zr and Hf budget in subduction zones: Geochimica et Cosmochimica Acta, v. 67 (12), pp. 2173–2187.

Rubatto, D., Gebauer, D., Fanning, M., 1998. Jurassic formation and Eocene subduction of the Zermatt–Saas-Fee ophiolites: implications for the geodynamic evolution of the Central and Western Alps: Contributions to Mineralogy and Petrology, v. 132, pp. 269–287.

Saccani, E., Dilek, Y., Marroni, M., and Pandolfi, L., 2015, Continental margin ophiolites of Neotethys: Remnants of ancient Ocean-Continent Transition Zone (OCTZ) lithosphere and their geochemistry, mantle sources and melt evolution patterns. Episodes, v. 38, No. 4, pp. 230-249, doi:10.18814/epiiugs/2015/v38i4/82418.

Schmid, S.M., and Kissling, E., 2000, The arc of the western Alps in the light of geophysical data on deep crustal structure: Tectonics, v. 19, pp. 62–85. doi:10.1029/1999TC900057.

Stampfli. G.M. and Marthaler. M., 1990, Divergent and convergent margins in the North-Western Alps confrontation to actualistic models: Geodinamica Acta, v. 4., pp. 159-184.

Stucki, A., Rubatto, D., and Trommsdorff, V., 2003, Mesozoic ophiolite relics in the Southern Steep Belt of the Central Alps.Schweizerische Mineralogische und Petrographische Mitteilungen, v. 83, pp. 285–299.

Tricart, P., and Lemoine, M., 1991, The Queyras ophiolite west of Monte Viso (Western Alps): indicator of a peculiar ocean floor in the Mesozoic Tethys: Journal of Geodynamics, v. 13, pp.163–181.

Tricart, P., and Schwartz, S., 2006, A north-south section across the Queyras Schistes lustrés (Piedmont zone, western Alps): Syn-collision refolding of a subduction wedge: Eclogae Geologicae Helvetiae, v. 99, pp. 429–442.

Tucholke, B., Lin, J. and Kleinrock, M.C., 1998, Megamullions and mullion structure defining oceanic metamorphic core complexes on the Mid-Atlantic Ridge: Journal of Geophysical Research, v. 103, pp. 9857-9866.

by Ki-Cheol Shin[1], Ryo Anma[2], Takanori Nakano[1], Yuji Orihashi[3] and Shin-ichi Ike[2,]*

The Taitao ophiolite-granite complex, Chile: Emplacement of ridge-trench intersection oceanic lithosphere on land and the origin of calc-alkaline I-type granites

[1] Research Institute for Humanity and Nature, Motoyama 457-4, Kamigamo, Kita-Ku, Kyoto 603-8047, Japan
[2] University of Tsukuba, Ten-nodai 1-1-1, Tsukuba 305-8572, Japan. *Corresponding author E-mail: amma.ryo.ge@u.tsukuba.ac.jp*
[3] Earthquake Research Institute, University of Tokyo, Yayoi 1-1-1, Bunkyo-Ku, Tokyo 113-0032, Japan
* Present address: Medical Device Supply Chain Asia Pacific, Johnson & Johnson K.K. Medical Company, 3-5-2 Nishikanda, Chiyoda-ku, Tokyo 101-0065, Japan

DOI: 10.18814/epiiugs/2015/v38i4/82424

The late Miocene – early Pliocene Taitao ophiolite is exposed ~30 km southeast of the Chile triple junction, where a spreading center of the Chile ridge system is subducting underneath the South America plate. This unique tectonic setting provides an excellent opportunity to study the emplacement mechanism of a ridge-trench intersection ophiolite and the complex magmatic interactions between the subducting ridge, overlying crust and sediments,and the mantle wedge. As a result of these interactions, several granitic plutons were formed contemporaneously with emplacement of the ophiolite. We review previous studies of the Taitao ophiolite and use new geochemical data to discuss the mechanism that formed juvenile magma of calc-alkaline I-type granites during ridge subduction. Our model implies that the magmas of the Taitao granites formed due to partial melting of hot oceanic crust adjacent to the subducting mid-oceanic ridge that has been contami-nated by deep crustal material and/or metasomatized sub-arc mantle. The partial melting took place under garnet-free amphibolite conditions. The juvenile magmas then incorporated different amounts of subducted sediments and/or continental material to form the I-type granites with various compositions. Subduction of fracture zones played an important role in these processes.

Introduction

Ophiolites are regarded as pieces of ancient oceanic lithosphere emplaced onto continental crust (Anonymous, 1972). Once it was presumed that this allochthonous material invariably formed at a mid-ocean spreading ridge. Today, most ophiolites are thought to form in supra-subduction zone (SSZ) settings in an island-arc or back-arc spreading environment (Miyashiro, 1973; Pearce and Robinson, 2010; Dilek and Furnes, 2011, 2014). However, even for extensively exposed and intensively studied examples like the Semail ophiolite, Oman, disagreement persists between ridge-origin scholars (Boudier *et al.*, 1996; MacLeod and Yaouancq, 2000; Miyashita *et al.*, 2003; Adachi and Miyashita, 2003; Boudier and Nicolas, 2011) and SSZ-origin scholars (Dilek and Flower, 2003; Dilek and Furnes, 2009; Dilek and Thy, 2009; Pearce and Robinson, 2010). One confounding factor is that all ophiolites must have experienced modification in SSZ environments just before their emplacement that may have obscured or obliterated primary features formed during their seafloor spreading origin (Tsuchiya *et al.*, 2013; Kanke and Takazawa, 2014; Yoshikawa *et al.*, 2015). Another factor may be that tectonic settings at the times of ophiolite formation and emplacement are ambiguous (Dilek and Robinson, 2003; Warren *et al.*, 2005).

The Taitao ophiolite, southern Chile (Fig. 1), is one of the few ophiolites for which the tectonic setting is clearly understood, because of its young age (< 6 Ma: Anma *et al.*, 2006) and the nearby presence of a subducting spreading-ridge segment of the Chile ridge system (Cande *et al.*, 1982, 1987; Cande and Leslie, 1986; Behrmann *et al.*, 1994). The plate configuration and plate kinematics before and after the oceanic lithosphere formed and was emplaced as an ophiolite can be well reconstructed from various data.

The thermal history of an ophiolite can be prolonged, especially one that formed at a spreading ridge far from land in a large ocean, migrated toward a continental margin and emplaced in a SSZ environment. However, in the case of the Semail ophiolite, its generation and emplacement took place in a short period: trondhjemite in the Semail ophiolite yielded zircon U-Pb ages of ~95.3 Ma, whereas amphibolite in the metamorphic sole yielded zircon U-Pb ages of ~94.5 Ma (Warren *et al.*, 2005). Tsuchiya *et al.* (2013)

also reported similar ages (~100 Ma) in both the quartz diorite that formed at the ridge axis and the late-stage tonalite that represents arc-like magmatism. However, progressive metamorphism continued after emplacement as obduction and subduction proceeded, and the peak metamorphism that resulted in eclogite formation took place at ~79 Ma (Warren *et al.*, 2005). Exhumation of blueschist in the southern part of the Semail ophiolite resulted in cooling of these rocks to the closing temperature of the zircon fission-track system (~250°C) at ~66–70 Ma (Yamato *et al.*, 2007). Jacobs *et al.* (2015) reported apatite fission-track and zircon and apatite (U-Th)/He ages of igneous rocks and the metamorphic sole from the section of the Semail ophiolite exposed in the UAE. They showed that the plutonic rocks were cooled to the closing temperatures of two of these three systems (zircon (U-Th)/He and apatite fission track) within 10 to 30 m (84.5–64.7 Ma and 87–62 Ma, respectively) of crust formation, whereas exhumation of metamorphic rocks took a longer period of time (until 63–31 Ma according to apatite fission-track ages). Both the plutonic and metamorphic rocks were cooled to the closing temperature of the apatite (U-Th)/He system in Miocene time (Jacobs *et al.*, 2015). Thus, during its prolonged thermal history, various modification processes could have affected the Semail ophiolite. This history can be compared with that, which is much more precisely determined for the Taitao ophiolite. It took only 1 my from the formation of the oceanic lithosphere through its emplacement and exhumation, as detailed in this paper (Fig. 1d).

The formation, emplacement and exhumation processes of ophiolites generate a wide range of geochemical variations (Flower and Dilek, 2003; Balestro et al., 2015; Fareeduddin and Dilek, 2015, Saccabu et al., 2015). In the case of the Semail ophiolite, the plutonic rocks range in chemical composition from ~48 wt.% SiO_2 in oceanic massive gabbro to ~75 wt.% SiO_2 in late-stage tonalite (Tsuchiya *et al.*, 2013). The chemical variation of the Taitao ophiolite-granite complex is similar, ranging from 48 to 74 wt.% SiO_2 for the plutonic rocks. However, in the Semail ophiolite, the late-stage felsic plutonic rocks are minor components. In contrast, in the Taitao ophiolite these rocks occupy as much as 10% of the exposure (Fig. 1c).

The advantage of studying the Taitao ophiolite and its related igneous rocks is that this area has a complete record of the magmatic history and the full range of chemical variation seen in ophiolites, with better tectonic and geochronological constraints than any other example in the world. Evidence of every process, from crustal formation to ophiolite emplacement, that took place over the span of 1 my was "frozen" into the geological record of this area. The Taitao ophiolite provides an excellent opportunity to study the emplacement mechanism of a ridge-trench intersection ophiolite, with its complex magmatic interactions between the subducting ridge, the overlying crust and sediments, and the mantle. Among these interactions, the mechanism that created voluminous intermediate to felsic magma in this area is of fundamental importance for understanding the processes that create continental crust (Kon *et al.*, 2013). In this study, we used chemical compositions and the Sr-Nd isotope system to ascertain the magmatic interactions during the formation and emplacement of the Taitao ophiolite.

Tectonic setting of the Taitao ophiolite and related rocks

The Taitao ophiolite is ~30 km southeast of the Chile triple junction, where a segment of the spreading Chile ridge system is subducting underneath the South America plate off the Taitao Peninsula, the westernmost promontory of the Chilean coast. The Chile ridge system, which separates the Nazca plate to the north and the Antarctica plate to the south, has a central axis trending north-northwest that consists of several segments separated by transform fracture zones trending east-northeast (Fig. 1a). The convergent rates of the Nazca and Antarctica plates with respect to the South America plate are 9 cm/y and 2 cm/y, respectively (Herron *et al.*, 1981; Cande *et al.* 1982; Tebbens and Cande, 1997; Tebbens *et al.*, 1997). The current plate configuration and plate kinematic data (Cande and Leslie 1986; Breitspecher and Thorkelson, 2009) allow us to deduce that short segments of this spreading center (< 100 km long) began subducting off the Taitao Peninsula at ~6 Ma and ~3 Ma. The formation and emplacement of the Taitao ophiolite are related to the first of these subduction events (Anma *et al.*, 2006).

The study area, in the westernmost part of the Taitao Peninsula, exposes four major rock suites (Fig. 1b): the Chonos metamorphic complex, the Chile Margin Unit (CMU), the Taitao ophiolite, and the Taitao granites (Forsythe *et al.*, 1986; Nelson *et al.*, 1993; Bourgois *et al.*, 1992; 1993; Guivel *et al.*, 1999). The Chonos metamorphic rocks, which mostly originated from siliciclastic and volcaniclastic protoliths, form the basement of the study area. Thomson and Herve (2002) determined Late Permian to Jurassic (258 to 207 Ma) fission-track and U-Pb ages from zircons in the basement rocks in the forearc region.

Chile Margin Unit

The CMU is a mixture of lava, pyroclastic rocks and semi-consolidated sediments (Fig. 1b, c). It was first defined by Bourgois *et al.* (1993) to distinguish it from the Main Volcanic Unit (see next section). The CMU directly overlies the pre-Jurassic basement, is of lower metamorphic grade, and appears to have deposited in the forearc area of the Chilean margin. Whole-rock K-Ar ages for the CMU range from 4.4 to 2.5 Ma (Mpodozis *et al.*, 1985). Volcanic rocks of the CMU have rather enriched compositions comparing with normal mid-ocean ridge basalt (N-MORB) (Lagabrielle *et al.*, 1994; Le Moigne *et al.*, 1996; Guivel *et al.*, 1999).

Anma and Orihashi (2013) dredged pyroclastic rocks resembling those of the CMU from the South Taitao Ridge, offshore from the Taitao ophiolite (Fig. 1b), and argued that the magmatic activity of the CMU started there at 5.2 Ma, migrated eastward at a rate of 2 to 5 cm/y, forming the CMU (Fig. 1c, d), and continued to the Pan de Azucar region (PA in Fig. 1b) where volcanic activity took place at 4.4 Ma based on zircon U-Pb data. All of these rocks contained inherited zircons that originated from subducted sediments. Anma and Orihashi (2013) suggested that the magmatic activity of the CMU is related to the subduction of a fracture zone separating segments of the Chile ridge system.

Taitao ophiolite

The Taitao ophiolite exposes the complete sequence of a Penrose-type oceanic lithosphere (Anonymous, 1972) (Fig. 1c). The top part, in the north, is represented by pillow lava and sheet flows interbedded with clastic deposits, which we refer to as the Main Volcanic Unit (MVU) after Bourgois *et al*. (1993). To the south are sheeted dikes, gabbros and ultramafic rocks (Forsythe *et al.* 1986; Kaeding *et al.*,

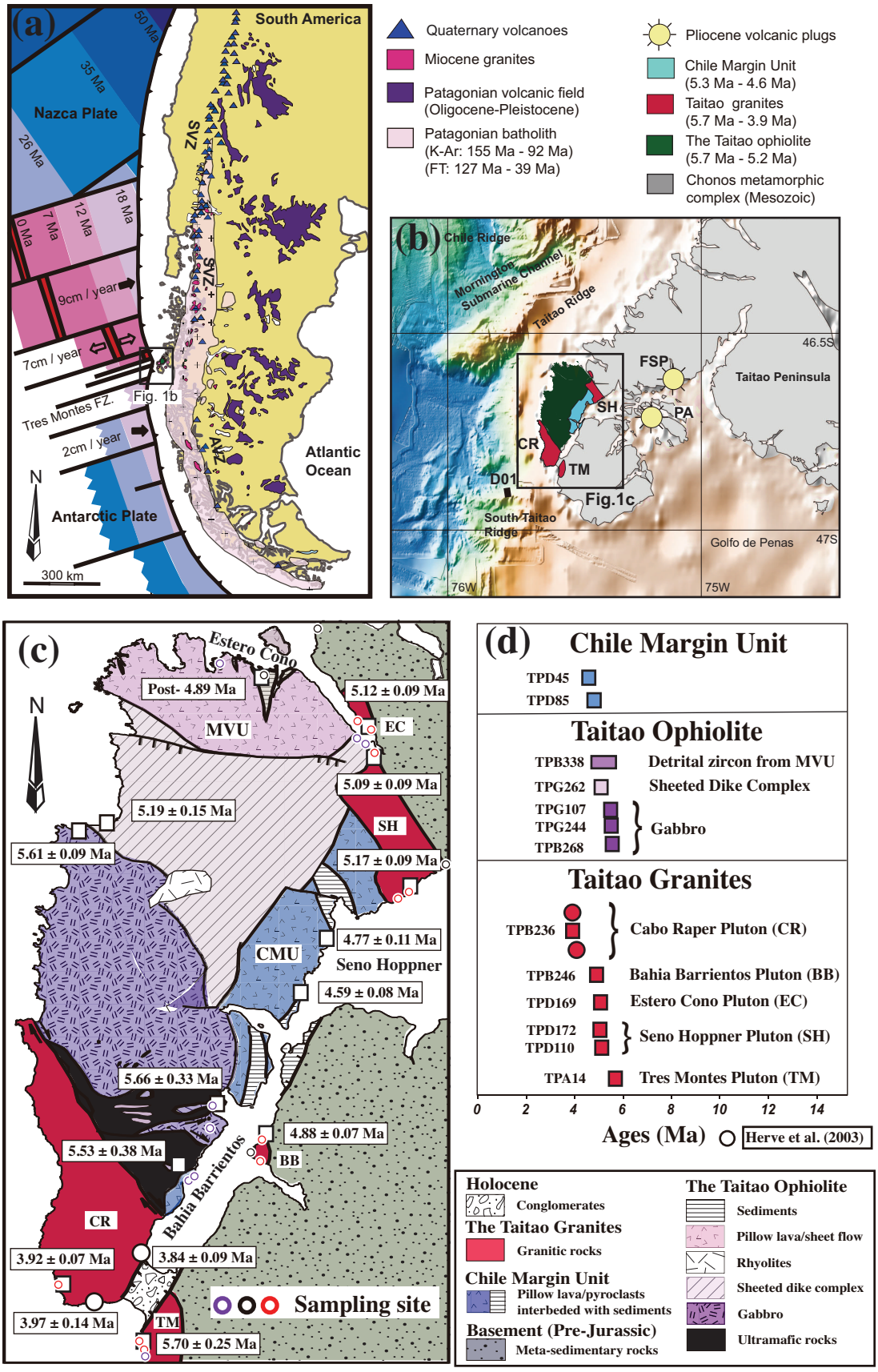

Figure 1. (a) Tectonics of the Chile Ridge subduction zone. (b) Distribution of the Taitao ophiolite and related igneous rocks together with detailed bathymetry. (c) Bedrock geology of the study area, modified from Anma et al. (2006), showing distribution of sampling sites for this study. MUV: Main Volcanic Unit, CMU: Chile Margin Unit, EC: Estero Cono Pluton, SH: Seno Hoppner pluton, BB: Bahia Barrientos intrusion, CR: Cabo Raper pluton, TM: Tres Montes pluton. (d) U-Pb age distribution of samples in this study.

1990; Nelson *et al.*, 1993; Bourgois *et al.*, 1993). The ophiolite shows evidence of hydrothermal alteration that is typical of ocean-floor metamorphism (Shibuya *et al.*, 2007). The ultramafic rocks provide evidence of at least two stages of melting, one that took place at ~1.6 Ga and the other of recent age related to magmatism in the Chile ridge (Schulte *et al.*, 2009). The gabbros have compositions similar to N-MORB, whereas the pillow basalts of the MVU have enriched compositions (Lagabrielle *et al.*, 1994; Le Moigne *et al.*, 1996; Guivel *et al.*, 1999) and isotopic compositions (Kaeding *et al.*, 1990) that suggest crustal contamination. Because of this compositional difference, the plutonic section has been referred to separately as the Bahia Barrientos ophiolite (Lagabrielle *et al.*, 1994; Le Moigne *et al.*, 1996; Guivel *et al.*, 1999). However, Schulte *et al.* (2009) reported that the ultramafic rocks and gabbros of the plutonic section also have a range of chemical and isotopic compositions that could be explained in terms of seawater contamination (for Sr isotopic ratios) and incorporation of sediment and basement rocks into the melt source of the Taitao ophiolite. Anma *et al.* (2006) explained the enriched composition of the MVU in terms of alteration along fracture zones or sub-segment boundaries, as reported previously from the Chile ridge (Klein and Karsten, 1995; Karsten *et al.*, 1996; Sherman *et al.*, 1997; Strum *et al.*, 1999, 2000), and considered the MVU to be a member of the Taitao ophiolite.

Previously reported U-Pb ages of the gabbros and sheeted dikes are ~5.6 Ma and ~5.2 Ma, respectively (Fig. 1c, d; Anma *et al.*, 2006). The sheeted dikes were thermally metamorphosed by the intrusion of the 5.1 Ma Seno Hoppner pluton (SH in Fig. 1c) (Shibuya *et al.*, 2007). Thus, the center of magmatic activities that formed the ophiolite migrated from south to north as a segment of the Chile ridge subducted obliquely against the Chilean continental margin (Anma *et al.*, 2006, 2009). Anma *et al.* (2009) reported U-Pb ages of zircons in clastic sediments in the MVU, of which 19 grains out of 24 yielded ages younger than 5.6 Ma, and concluded that their deposition postdated ~4.9 Ma. Veloso *et al.* (2007) argued that these clastic materials were derived from the south-southeast based on sedimentary structures and anisotropy of magnetic susceptibility fabrics. Thus, the post-5.6 Ma clastic zircons must have been derived from the plutonic section of the Taitao ophiolite and the Taitao granites, and by the time of deposition, most of these plutonic rocks must have been exposed subaerially (Anma *et al.*, 2009). Zircon fission-track ages from gabbros of the ophiolite that coincided with the U-Pb ages also attest to rapid exhumation and cooling of the plutonic section (Anma *et al.*, 2006).

The gabbros continued to fold even below their Curie temperature, as evidenced by macroscopic folding and Z-shaped demagnetization paths in the layered gabbros (Anma *et al.*, 2005; Veloso *et al.*, 2005), whereas the sheeted dike complex and the MVU rotated as rigid blocks as deformation proceeded (Veloso *et al.*, 2005, 2009). It was the eastern part of the subducted segment of the Chile ridge that was emplaced as the plutonic section of the Taitao ophiolite (Veloso *et al.*, 2005; Anma *et al.*, 2005, 2006). As the spreading center subducted obliquely, the center of magmatic activities migrated northward. During the time the midsection of the MVU was deposited, the plutonic section must have been subaerially exposed, supplying sediment to the subducting central valley (Anma *et al.*, 2006, 2009).

Taitao granites

The term "Taitao granites" collectively denotes the felsic plutonic rocks distributed around the Taitao ophiolite. These four plutons and a small body of granitic rocks exposed along the Bahia Barrientos (Fig. 1c) have zircon U-Pb ages that range from 5.7 Ma to 3.9 Ma (Fig. 1d) and compositions that range from trondhjemitic to granitic and tonalitic to granodioritic (Fig. 2b; Anma *et al.*, 2009). The plutons are the Tres Montes pluton (TM in Fig, 1c; 5.7 Ma) and Cabo Raper pluton (CR; 3.9 Ma) to the south of the Taitao ophiolite and the Seno Hoppner (SH) and Estero Cono (EC) plutons (5.2–5.1 Ma) to the northeast (Fig. 1). The Bahia Barrientos granite (BB in Fig. 1c; 4.9 Ma), intruded along the edge of the CMU, is thought to be related to CMU magmatism on the basis of its age (Anma and Orihashi, 2013).

The origin of the Taitao granites is controversial. Kaeding *et al.* (1990) were the first to recognize that the Cabo Raper pluton has a tonalitic to granodioritic composition with calc-alkaline I-type affinity, whereas the Seno Hoppner pluton has characteristics of S-type affinity. In contrast, Bourgois *et al.* (1996) suggested that the Cabo Raper pluton is a heavy rare earth element (HREE)-depleted trondhjemite-tonalite-granodiorite (TTG) that formed by slab melting under conditions of the amphibolite-eclogite transition. Guivel *et al.* (1999) reported that the Seno Hoppner pluton differs from the Cabo Raper and Seno Hoppner plutons in having a trondhjemite-granite composition and characteristics, typical of the calc-alkaline series. They also suggested that the Cabo Raper and Tres Montes plutons formed by slab melting under amphibolite-eclogite transition conditions.

Kon *et al.* (2013) recognized hornblende-bearing and hornblende-free members in the Seno Hoppner and Cabo Raper plutons. The hornblende-free members have trondhjemitic to granitic compositions whereas the hornblende-bearing members plot in the tonalitic to granodioritic compositional field along with the hornblende-bearing Cabo Raper pluton. The hornblende-free members have a pronounced negative Eu anomaly whereas the hornblende-bearing members have none or a small Eu anomaly. On the basis of trace-element compositions and tectonic constraints, they suggested that these granites were generated by partial melting of subducted oceanic crust with garnet-free-amphibolite conditions at depths shallower than 30 km.

The Tres Montes granodiorite includes numerous inherited zircons (7 of 15) with an age distribution similar to those from the CMU, whereas inherited zircons are rare in the Seno Hoppner and Cabo Raper granites (Herve *et al.*, 2003; Anma *et al.*, 2009). Thus, it has been proposed that the Tres Montes pluton originated with a strong influence from subducted sediments, whereas the Seno Hoppner and Cabo Raper plutons formed from juvenile granitic magmas (Anma *et al.*, 2009; Kon *et al.*, 2013). Kaeding *et al.* (1990) argued from Sr-Nd isotopic compositions that the Seno Hoppner and Cabo Raper granites formed by assimilation of basaltic magmas with 5–15% forearc sediments or metamorphic basement rocks.

Scope and analytical methods

To investigate the complicated magmatic processes resulting from the interaction between the spreading ridge and the subduction zone, and to test previous hypotheses, we conducted Sr-Nd isotopic analyses of this ridge-trench intersection ophiolite (Wakabayashi and Dilek, 2003; Dilek and Furnes, 2011, 2014) and its related rocks. The analyzed samples are described in Table 1 and their locations shown by circles in Figure 1c. Apart from 5 ophiolite and 10 granite samples, we measured two mafic volcanic rocks from the CMU and two mafic

Table 1. Geological unit and rock description of this study

Geological unit		Unit description	Sample ID	Age (Ma)*	Rock description
Mafic dikes in granite plutons		Estero Cono (EC) dike	TPD185	<5.2	basaltic dike intruded into the Seno Hoppner pluton
		Tres Montes (TM) dike	TPA009	<5.7	syn-plutonic basaltic dike intruded into the Tres Montes pluton
Chile Margin Unit (CMU)		Lavas and clastic rocks	TPB174	4.8 ~ 4.6	sheet flow: doleritic basalt
			TPB175		glass-rich hyaloclastite
Taitao Ophiolite	Main Volcanic Unit (MVU)	Lavas and clastic rocks	TPB345	< 5.2	basaltic pillow lava
			TPB347		basaltic massive sheet flow
	Estero Cono dike complex	Sheeted dike complex	TPD208	< 5.2	dolerite to basalt, metamorphosed by the intrusion of the Seno Hoppner pluton
	Plutonic complex	Gabbros and associated doleritic dikes	TPB020	5.6	medium-grained gabbro (massive)
			TPB024		fine-grained gabbro (mesocumulate)
Taitao Granites	Tres Montes (TM) pluton	Tonalite-granodiorite with syn-plutonic dikes	TPA007	5.7	hybrid rocks formed due to syn-plutonic mafic dike intrusion
			TPA014		fine to medium-grained biotite hornblende tonalite and granodiorite
	Seno Hoppner (SH) pluton	Leucocratic granite with mafic dike intrusion	TPD110	5.2 ~ 5.1	medium-grained hornblende biotite granite, thermal aureole contact in the ophiolite, mafic dike in the northern part.
			TPD115		
			TPD172		
	Estero Cono (EC) pluton	Tonalite-granodiorite	TPD168	5.1	fine to medium-grained biotite (hornblende) granodiorite
			TPD169		
	Bahia Barrientos (BB) pluton	Tonalite-trondhjemite	TPB243	4.9	fine to medium-grained biotite tonalite and trondhjemite
			TPB246		
	Cabo Raper (CR) pluton	Tonalite-granodiorite	TPB236	3.9	fine to medium-grained biotite hornblende granodiorite to tonalite
Others	Sediments	trench-slope sediments	TPB338	< 4.9	turbiditic sediment in the MVU
	Basement	meta-igneous rocks	TPD095	Jurassic**	felsic igneous rock (ryolitic)?
		meta-sedimentary rocks	TPB240	Jurassic**	sandstone/mudstone alternation
			TPB335		consolidated silici-clastic sediments
			TPD099		pelitic schist

* Age data from Anma et al. (2006, 2009) and Anma and Orihashi (2013), ** from Thomson et al. (2002)

dikes intruded into the granite plutons. One of the granite samples (TPA007) was a hybrid rock mixed with a syn-plutonic basaltic dike. We also measured samples of basement rocks and turbiditic sediments to estimate the respective influences of contamination from Jurassic wall rocks and sediments.

Major- and trace-element concentrations were measured using an X-ray fluorescence spectrometer and a laser ablation inductively coupled plasma mass spectrometer at the Earthquake Research Institute using conventional methods (Tani *et al.*, 2002; Orihashi and Hirata, 2003) (Table 2). The analytical results in Table 2 also include data for some granites reported in Anma *et al.* (2009). For whole-rock Sr and Nd isotopic analyses, approximately 100 mg of powdered sample was completely dissolved in a mixture of 38% HF (1.0 ml), 68% HNO_3 (0.7 ml), and 70% $HClO_4$ (0.3 ml) at 140ºC for 24 h using a hot plate. After evaporation, the residues were dissolved in 2 ml of 6M HCl and heated at 100ºC for 8 h. Sr and REEs were separated by conventional ion-exchange chromatography. Separation of Nd from REEs was facilitated using Ln Resin (Eichrom Tec. Inc).

The purified Sr was loaded with a Ta activator on preconditioned W filaments and was measured in single filament mode. Nd isotope ratios were measured in Ta-Re double filaments mode. Sr and Nd isotopic ratios were determined using a TRITON mass spectrometer (Thermo Fisher Scientific Co.) at the Research Institute for Humanity and Nature. Analytical precisions of isotopic ratio measurements are given as ±2ó standard errors. The measured $^{87}Sr/^{86}Sr$ and $^{143}Nd/^{144}Nd$ ratios were normalized to $^{86}Sr/^{88}Sr = 0.1194$ and $^{146}Nd/^{144}Nd = 0.7219$, respectively. The $^{87}Sr/^{88}Sr$ value of the NIST SRM 987 reference material throughout the analyses was 0.710264 ± 0.000014 (2σ, n = 14). The $^{143}Nd/^{144}Nd$ ratio of the La Jolla reference material was 0.511863 ± 0.000015 (2σ, n = 14). All samples were recalculated with reference to the values of reference materials. The results are listed in Table 3. We calculated the initial value of Sr and Nd isotope ratios (designated by the suffix *i*) using zircon U-Pb ages reported by Anma *et al.* (2006, 2009). The basement rock isotopic ratios were calculated assuming the age of incorporation to be 5.5 Ma.

Analytical results

The analytical results for major and trace elements are shown in Figs. 2 to 6, and results for isotopic compositions are shown in Figs. 7 and 8. Our analyses in general are in good agreement with previously reported results.

The mafic rocks had a basaltic to basaltic-andesitic composition (Fig. 2a) that could be divided into N-type to E-type (enriched) MORB

Table 2. Major and trace element compositions for the Taitao Ohpiolite, the Taitao granites, sediments and basement rocks

	Taitao Ophiolite					CMU		mafic dikes in granites		Taitao Granites										Sediment	Basement			
Locality	MVU		EC	gabbro						TM		SH			EC		BB		CR					
Sample	TPB	TPB	TPD	TPB	TPB	TPB	TPB	TPD	TPA	TPA	TPA	TPD	TPD	TPD	TPD	TPD	TPB	TPB	TPB	TPB	TPB	TPB	TPD	TPD
No.	345	347	208	020	024	174	175	185	009	007	014	110	115	172	168	169	243	246	236	338	335	240	095	099
SiO_2*	55.03	51.08	50.99	48.01	53.33	53.81	52.03	51.08	56.38	59.25	65.84	73.96	74.30	73.93	69.10	68.11	69.31	69.33	67.92	62.87	69.68	69.08	72.31	70.30
TiO_2	0.80	1.21	1.11	0.66	0.63	1.07	1.09	1.16	1.08	0.89	0.89	0.23	0.20	0.20	0.44	0.49	0.40	0.43	0.45	0.70	0.60	0.46	0.51	0.72
Al_2O_3	17.65	19.00	17.41	20.70	15.30	16.25	15.64	15.88	17.23	16.51	15.96	13.16	13.04	13.06	14.82	14.94	16.04	15.43	15.48	14.67	14.11	10.79	13.51	14.33
Fe_2O_3	5.67	6.54	8.34	6.46	8.70	7.55	8.02	9.41	7.84	6.71	5.64	2.25	2.16	2.29	2.78	3.21	2.51	3.05	3.01	5.42	4.55	6.78	3.55	4.96
MnO	0.10	0.10	0.08	0.10	0.14	0.12	0.14	0.11	0.14	0.12	0.08	0.03	0.03	0.03	0.05	0.05	0.04	0.11	0.05	0.10	0.07	0.04	0.06	0.07
MgO	6.41	6.55	6.47	11.46	7.41	6.21	9.43	7.74	4.50	4.27	2.18	0.34	0.27	0.20	1.61	1.83	1.78	1.54	1.96	2.42	1.70	1.64	1.30	1.85
CaO	8.64	9.22	11.67	10.16	10.96	7.62	5.72	11.18	8.37	6.60	3.54	1.14	0.97	1.08	3.44	3.58	3.00	2.75	3.64	5.18	2.92	1.69	2.34	0.98
Na_2O	4.15	4.31	3.07	2.24	3.65	5.77	3.04	2.81	3.58	4.10	3.94	4.59	4.62	4.71	3.95	4.09	4.59	4.40	4.20	3.51	2.71	2.55	3.57	2.57
K_2O	0.52	0.38	0.10	0.04	0.04	0.37	1.16	0.52	0.52	1.05	2.09	3.12	3.26	3.11	2.28	2.05	1.51	1.75	2.06	1.55	2.33	1.19	2.05	2.42
P_2O_5	0.11	0.17	0.12	0.04	0.05	0.13	0.12	0.11	0.14	0.11	0.20	0.04	0.03	0.04	0.08	0.09	0.10	0.09	0.11	0.17	0.14	0.09	0.14	0.17
Total	**99.07**	**98.55**	**99.34**	**99.86**	**100.20**	**98.88**	**96.38**	**100.00**	**99.78**	**99.61**	**100.35**	**98.87**	**98.87**	**98.64**	**98.55**	**98.44**	**99.28**	**98.87**	**98.88**	**96.58**	**98.80**	**94.30**	**99.32**	**98.35**
Sc**	26	30	33	15	44	30	30	39	28	27	16	5	6	6	10	10	7	7	10	17	13	9	9	10
V	143	196	203	108	209	194	188	223	186	162	128	15	9	11	51	54	43	44	59	119	97	67	68	86
Co	38	37	49	64	72	42	40	66	61	60	74	107	112	102	84	76	73	69	79	44	44	88	61	37
Zn	51	52	109	43	31	56	63	16	101	72	68	35	31	29	32	33	40	161	42	64	37	27	68	74
Ga	16	16	15	13	16	15	15	15	18	16	20	16	15	15	15	16	18	18	18	18	17	14	17	19
Rb	14	10	3.9	0.4	1.0	14	55	25	19	38	89	132	141	137	72	68	50	41	77	45	77	43	86	120
Sr	228	239	238	125	122	170	295	142	235	271	212	55	51	53	169	169	268	188	271	166	220	174	337	112
Y	17	25	25	12	25	26	26	25	22	29	29	36	37	39	20	23	13	19	17	23	26	17	28	32
Zr	83	105	83	35	42	105	107	77	100	155	215	217	219	223	161	168	129	160	157	170	157	153	235	286
Nb	4	6	4	0.8	0.6	5	5	3	6	7	12	10	8	9	6	7	4	7	8	7	9	8	11	16
Cs	1.6	1.4	2.9	1.6	1.8	1.6	11.5	3.9	1.8	1.0	5.2	9.2	10.6	6.4	8.1	3.6	3.5	1.4	3.4	3.7	8.3	4.0	5.6	6.4
Ba	95	90	41	10	16	66	109	60	151	229	424	475	470	459	525	465	285	489	377	204	479	203	441	422
La	6.25	7.45	3.45	0.55	1.0	7.69	6.76	3.43	11.6	15.5	25.3	31.9	39.1	37.4	14.7	12.1	13.0	8.66	18.0	18.9	22.7	20.2	38.3	44.3
Ce	13.4	17.1	9.16	2.68	3.8	16.9	17.6	9.76	23.4	34.8	48.9	71.3	84.6	71.5	34.0	27.8	31.0	20.1	37.7	41.1	46.0	40.6	80.4	89.5
Pr	1.70	2.20	1.34	0.49	0.79	2.15	2.28	1.47	2.97	4.05	5.68	7.66	8.25	7.67	3.55	3.04	3.13	2.02	4.01	4.66	5.20	4.39	8.27	9.91
Nd	7.48	10.1	6.83	2.74	4.9	11.0	10.2	8.06	13.3	17.5	24.5	28.1	29.4	28.2	13.6	12.7	12.1	7.51	14.8	18.8	19.7	17.3	30.2	35.0
Sm	1.89	3.09	2.33	0.98	2.21	3.03	2.97	2.74	3.07	4.34	5.06	6.21	5.52	5.75	2.94	2.77	2.54	1.41	3.03	4.01	4.08	3.52	5.65	7.28
Eu	0.95	1.25	0.89	0.67	0.94	1.09	1.06	1.14	1.38	1.25	1.30	0.68	0.77	0.78	0.66	0.67	0.77	0.34	1.00	1.05	0.90	0.88	1.10	1.55
Gd	2.28	3.05	2.89	1.41	2.55	3.45	3.35	3.73	3.43	4.04	4.52	5.86	6.33	5.71	3.26	2.67	1.91	1.44	2.33	3.32	4.07	3.06	5.22	5.70
Tb	0.41	0.56	0.50	0.23	0.50	0.55	0.62	0.60	0.58	0.65	0.81	0.98	0.99	0.95	0.44	0.46	0.30	0.26	0.39	0.56	0.59	0.42	0.74	0.97
Dy	2.55	3.21	3.27	1.59	3.53	3.78	3.73	3.47	3.52	4.64	4.99	6.18	5.54	6.06	2.80	3.07	1.81	1.31	2.41	3.31	2.94	2.75	3.87	5.50
Ho	0.50	0.74	0.71	0.34	0.82	0.88	0.80	0.80	0.73	0.93	1.05	1.25	1.23	1.43	0.55	0.65	0.43	0.30	0.57	0.70	0.72	0.51	0.82	1.12
Er	1.47	1.98	2.06	0.83	2.12	2.30	2.24	2.27	1.99	2.64	2.78	3.45	3.20	3.96	1.63	1.77	1.09	0.78	1.51	1.85	2.07	1.45	1.98	3.35
Tm	0.22	0.27	0.30	0.14	0.33	0.36	0.32	0.33	0.32	0.39	0.41	0.55	0.41	0.65	0.27	0.29	0.17	0.12	0.23	0.29	0.30	0.24	0.32	0.39
Yb	1.62	2.08	2.10	1.08	2.26	2.24	2.27	2.32	2.04	2.77	2.93	4.06	3.56	4.37	1.88	1.87	1.21	0.82	1.32	1.92	2.27	1.60	2.27	3.04
Lu	0.21	0.29	0.28	0.16	0.30	0.32	0.34	0.33	0.28	0.40	0.47	0.56	0.50	0.66	0.25	0.35	0.15	0.14	0.21	0.31	0.43	0.25	0.32	0.46
Hf	2.02	2.21	1.73	0.79	1.30	2.43	2.36	1.88	2.35	3.66	6.35	6.71	6.64	6.43	4.11	3.79	3.40	2.04	3.58	4.18	3.58	3.90	5.39	8.29
Ta	0.24	0.28	0.21	0.03	0.04	0.25	0.26	0.15	0.34	0.43	0.76	0.74	0.81	0.81	0.44	0.46	0.45	0.25	0.57	0.43	0.61	0.53	0.70	0.99
Pb	2.98	1.46	1.89	n.d.	0.26	2.19	2.11	0.37	17.5	5.10	15.7	11.2	13.6	12.1	12.4	10.7	10.8	9.17	10.7	10.3	7.34	6.35	18.5	17.7
Th	1.01	0.90	0.53	0.01	<0.04	1.61	1.37	0.51	3.53	4.74	8.41	11.9	11.3	15.4	7.28	5.94	5.39	3.81	6.56	6.17	7.00	5.94	12.3	13.1
U	0.42	0.37	0.23	0.01	<0.01	0.52	0.45	0.19	0.64	1.26	1.98	3.52	4.67	3.56	3.18	3.11	2.54	1.47	2.04	1.89	2.35	1.64	4.21	3.91
Mg#***	69.14	66.49	60.59	77.85	62.79	61.97	69.97	61.97	53.21	55.77	43.37	23.04	19.85	14.75	53.43	53.04	58.42	50.01	56.34	46.94	42.54	32.40	42.05	42.50
ASI****	0.76	0.78	0.66	0.93	0.59	0.68	0.94	0.62	0.80	0.83	1.05	1.01	1.01	1.00	0.97	0.97	1.10	1.09	0.98	0.87	1.15	1.26	1.09	1.66
T(Zr)	n.d.	n.d.	n.d.	n.d.	n.d.	n.d.	n.d.	n.d.	n.d.	n.d.	801	811	813	814	774	775	767	786	770	n.d.	n.d.	n.d.	n.d.	n.d.

*Compositions are quoted in weight %. Total Fe as Fe_2O_3. **Concentrations are in weight ppm. ***Mg#: 100× molar [Mg/(Mg+Fe)]. ****ASI: molar $Al_2O_3/(Na_2O+K_2O+CaO)$. The sample localities are shown in Fig. 1.

Table 3. Sr and Nd isotopic ratios for the Taitao Ophiolite, the Taitao granites, sediments, and basement rocks

Geological Unit			Sample ID	$^{87}Sr/^{86}Sr$	$^{87}Rb/^{86}Sr$	$^{87}Sr/^{86}Sri^{*}$	$^{143}Nd/^{144}Nd$	$^{147}Sm/^{144}Nd$	$^{143}Nd/^{144}Ndi$	εNdi^{**}
Mafic igneous rocks	Taitao Ophiolite	MVU	TPB345	0.703523 (±5)	0.173	0.703510	0.512957 (±4)	0.1526	0.512952	6.25
			TPB347	0.703408 (±5)	0.127	0.703399	0.513038 (±4)	0.1859	0.513031	7.81
		EC-SDC	TPD208	0.704236 (±5)	0.047	0.704233	0.51306 (±3)	0.2067	0.513053	8.22
		Gabbro	TPB020	0.702808 (±5)	0.009	0.702807	0.513162 (±5)	0.2168	0.513154	10.21
			TPB024	0.703175 (±5)	0.024	0.703173	0.513156 (±3)	0.2699	0.513146	10.05
		CMU	TPB174	0.705274 (±6)	0.230	0.705257	0.512909 (±3)	0.1661	0.512903	5.31
			TPB175	0.706713 (±4)	0.541	0.706674	0.512934 (±5)	0.1754	0.512928	5.79
	Mafic Dike	EC-dike	TPD185	0.703181 (±4)	0.503	0.703145	0.513119 (±4)	0.2054	0.513112	9.38
		TM-dike	TPA009	0.707171 (±5)	0.235	0.707154	0.512611 (±5)	0.1400	0.512606	-0.49
Felsic igneous rocks	Taitao Granites	TM	TPA007	0.708212 (±3)	0.402	0.708179	0.512448 (±3)	0.1500	0.512443	-3.68
			TPA014	0.707458 (±5)	1.214	0.707360	0.512705 (±19)	0.1251	0.512701	1.36
		SH	TPD110	0.704587 (±4)	6.992	0.704081	0.512839 (±3)	0.1339	0.512834	3.96
			TPD115	0.704795 (±3)	7.998	0.704216	0.512828 (±3)	0.1136	0.512824	3.76
			TPD172	0.704821 (±3)	7.493	0.704278	0.512797 (±5)	0.1233	0.512793	3.15
		EC	TPD168	0.705430 (±3)	1.242	0.705340	0.512661 (±4)	0.1305	0.512656	0.49
			TPD169	0.705440 (±3)	1.164	0.705356	0.512676 (±6)	0.1323	0.512671	0.79
		BB	TPB243	0.705155 (±3)	0.542	0.705117	0.512756 (±4)	0.1273	0.512751	2.35
			TPB246	0.705404 (±4)	0.630	0.705360	0.512667 (±9)	0.1135	0.512663	0.62
		CR	TPB236	0.704972 (±5)	0.820	0.704927	0.512714 (±4)	0.1238	0.512710	1.53
Contaminants	Sediment		TPB338	0.706549 (±3)	0.781	0.706495	0.512102 (±3)	0.1291	0.512097	-10.41
	Basement		TPB240	0.707882 (±5)	0.723	0.707830	0.512436 (±4)	0.1235	0.512432	-3.89
			TPB335	0.707408 (±5)	1.014	0.707335	0.512469 (±4)	0.1250	0.512465	-3.25
			TPD095	0.713521 (±5)	0.741	0.713467	0.512175 (±3)	0.1129	0.512171	-8.97
			TPD099	0.720999 (±5)	3.103	0.720774	0.512186 (±3)	0.1260	0.512181	-8.77

* Initial ratios (*i*) for the Sr and Nd isotopic ratios are calculated with the zircon age data from Anma et al., (2006, 2009), ** εNd*i*: deviation in parts per 10^4 from bulk earth values at their initial age (zircon age). Basement rocks are calculated with 5.1 Ma for comparison

(Figs. 4a and 5a). The gabbros had lower TiO_2, K_2O and P_2O_5 contents (Fig. 3) than other mafic rocks and had N-MORB signatures, being depleted in large ion lithophile elements (LILEs) such as Rb, Th and U (Fig. 4a). The other mafic rocks were relatively enriched in LILEs and slightly depleted in Ba, Nb and Ta. The mafic dike sample from the Tres Montes pluton (TM-dike in the figures and TPA009 in the tables) showed notable enrichment in Pb and Th, possibly due to the contamination of crustal rocks (Fig. 4a). Gabbros (Fig. 5a) had depleted light REE (LREE) contents with a positive Eu anomaly that implies accumulation of Ca-plagioclase. MVU samples and the TM-dike had less distinct positive Eu anomalies. Together with CMU samples, they had slightly LREE-enriched features. In the Estero Cono pluton, the samples from an isolated mafic dike (EC-dike; TPD185) and the sheeted dike complex (EC-SDC; TPD208) had a rather flat REE pattern. However, EC-SDC was slightly depleted in Rb, Ba and K and enriched in Pb compared to EC-dike, most likely due to alteration by the intrusion of the Seno Hoppner–Estero Cono pluton (Fig. 4a).

The gabbros and the EC-dike had the most primitive isotopic ratios among the mafic rocks we analyzed, ranging from 0.70281 to 0.70715 for $^{87}Sr/^{86}Sri$ and from 10.21 to –0.49 for åNd*i* values (Figs. 7 and 8). Compared to the gabbros, the MVU samples had slightly lower Nd isotopic ratios, whereas EC-SDC had a slightly higher $^{87}Sr/^{86}Sri$. The samples from CMU and TM-dike had higher Sr and lower Nd isotopic values than the other mafic rocks.

The Taitao granites plot in three distinct fields, except for one hybrid rock with a tonalitic composition (Fig. 2b). Each pluton has relatively homogeneous major-element compositions. The samples from the Seno Hoppner pluton plot in the field for true granite (Fig. 2b) and coincide with the hornblende-free granitoids of the Seno Hoppner–Estero Cono pluton reported by Kon *et al.* (2013) (Fig. 4b, 5b). They have the highest silica contents among the Taitao granites (Fig. 3) and low MgO and CaO contents with low Na_2O/K_2O and CaO/Na_2O ratios (1.4–1.5 and 0.2, respectively) (Table 2). The samples from the Estero Cono and Cabo Raper plutons plot on the boundary between the tonalite and granodiorite fields, coinciding with the hornblende-bearing granitoids of the Seno Hoppner–Estero Cono and Cabo Raper plutons reported by Kon *et al.* (2013) (Fig. 4b, 5b). The Tres Montes granodiorite plot in the same position as the hornblende-bearing granitoids (Fig. 2b), but has lower silica contents (Fig. 3). The samples from the Bahia Barrientos pluton have distinctive compositions, plotting on the boundary between the tonalite and trondhjemite fields (Fig. 2b). These samples have lower K_2O contents and higher aluminum saturation index (ASI) values (Table 2) than other granites.

In other respects, the Estero Cono, Cabo Raper and Bahia Barrientos plutons have similar major-element compositions with slight variations in Na_2O and K_2O contents. The Na_2O/K_2O ratios range from 1.7 to 3.0, and the CaO/Na_2O ratios range from 0.6 to 0.9. The ASI values (Table 2) indicate that the granites are metaluminous to slightly peraluminous and are classified as I-type granite (Chappell and White, 1974). All of the Taitao granites fall into the medium-K classification (Fig. 3). On the Sr/Y vs. Y diagram, all Taitao granites fell within the non-adakitic field (Fig. 6a). The Taitao granites range

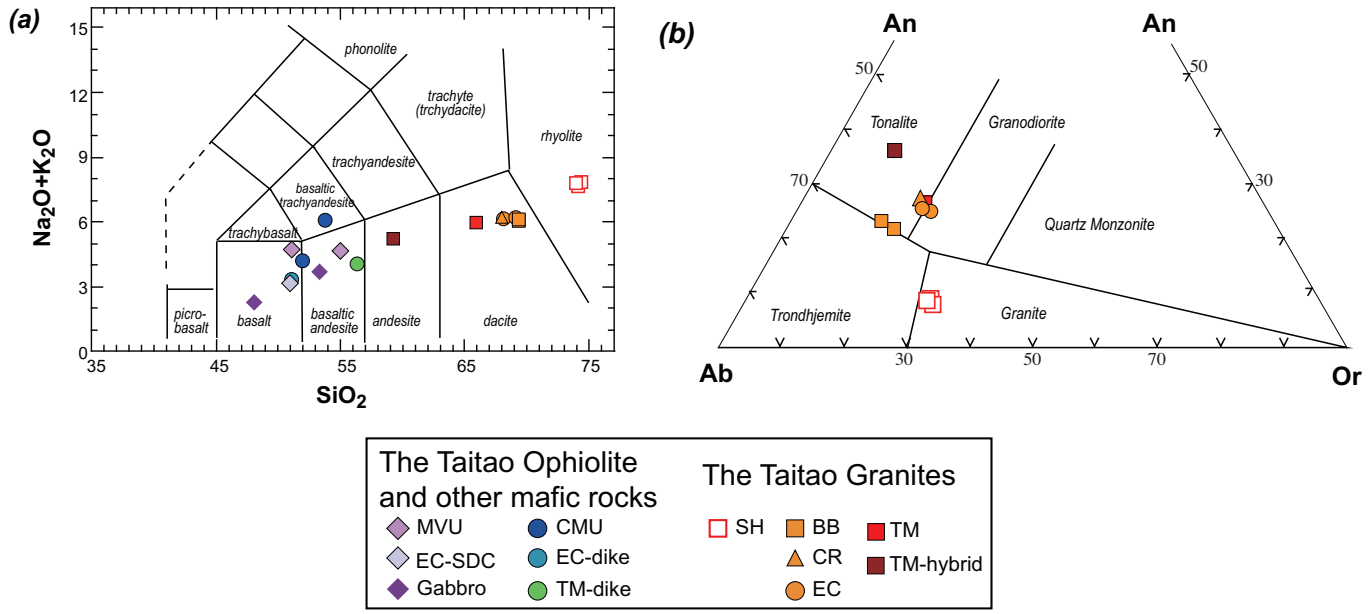

Figure 2. Chemical classification of the Taitao ophiolite and Taitao granites. (a) Total alkali vs. silica diagram after Le Maitre et al. (2005). (b) Normative anorthite (An)-albite (Ab)-orthoclase (Or) ternary diagram after Barker (1979).

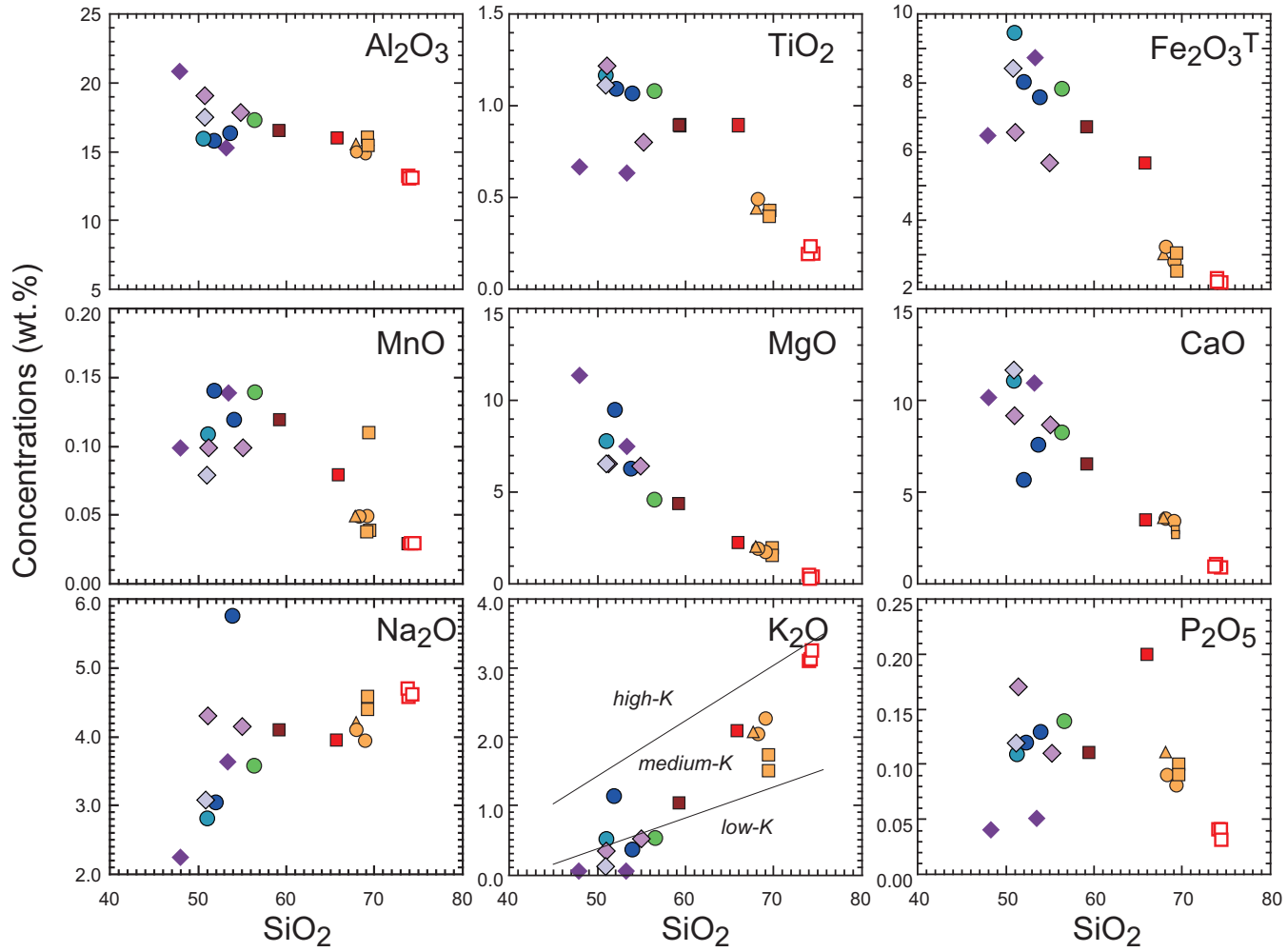

Figure 3. Harker variation diagrams for the Taitao ophiolite and Taitao granites. Symbols are the same as in Fig. 2.

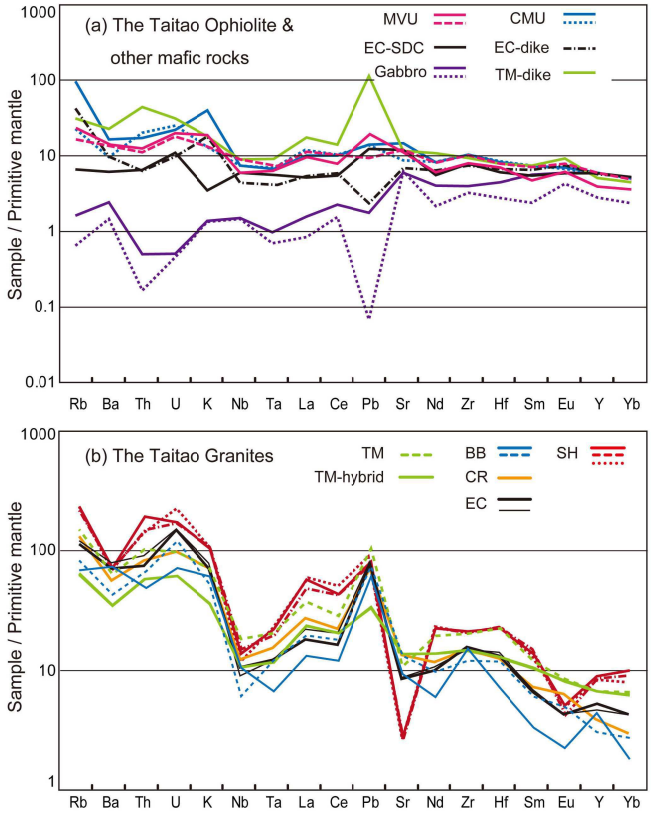

Figure 4. Trace-element variation diagrams for (a) the Taitao ophiolite and (b) the Taitao granites normalized with respect to primitive mantle (McDonough and Sun, 1995).

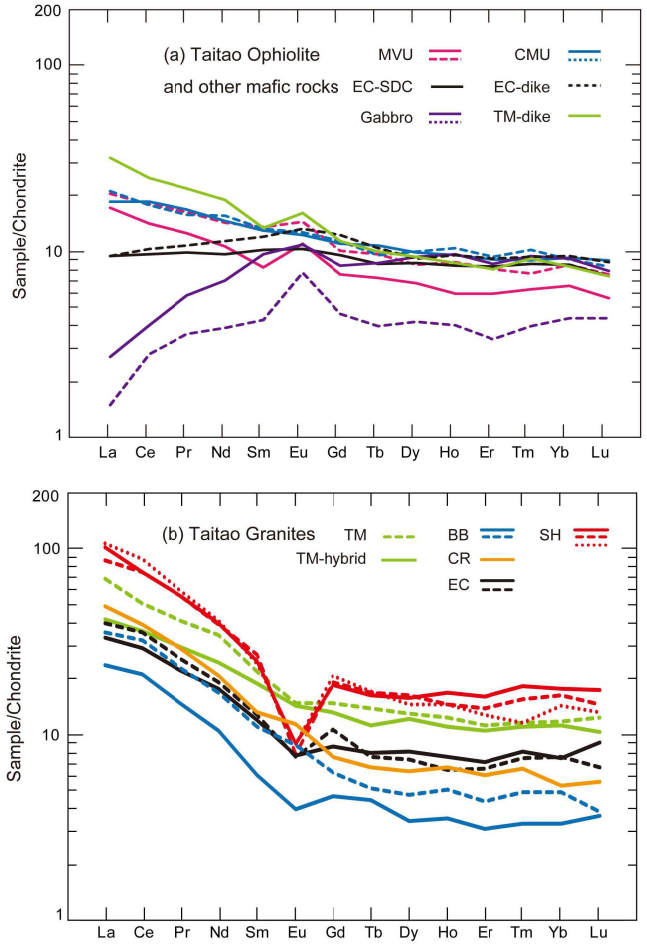

Figure 5. REE variation diagrams for (a) the Taitao ophiolite and (b) the Taitao granites normalized with respect to chondritic values (Taylor and McLennan, 1985).

in Y content from 17 ppm to 39 ppm, but the Seno Hoppner pluton has distinctly high Y contents among them.

In their trace-element profiles, the Taitao granites appear enriched in LILEs and Pb with respect to primitive mantle (Fig. 4b). The granites are depleted in Ba, Nb, Sr and Eu and showed wide variation in REEs. The Seno Hoppner samples are distinguished by higher contents of most trace elements and greater depletions in Sr and Eu. The Tres Montes samples do not show negative anomalies of Sr and Eu. Sample TPB246 from the Bahia Barrientos granite differs from the others in its enrichment in Ba, Zr and Y and depletion in Th, Ta and REEs. The chondrite-normalized REE patterns (Fig. 5b) confirm these geochemical features, showing relatively enriched and inclined LREE and flattened HREE patterns. The Eu anomaly is large in the Seno Hoppner pluton, but slight or absent in the other granites.

The Taitao granites also fall into three groups with restricted Sr and Nd isotopic values (Figs. 7 and 8). The Seno Hoppner granite, with the highest SiO_2 content of all felsic rocks in this area, has the most primitive isotopic composition: three $^{87}Sr/^{86}Sr_i$ values range from 0.7045 to 0.7048, and εNd_i values range from 3.15 to 3.96. The Tres Montes granodiorite, with the lowest SiO_2 content among the Taitao granites, has the highest $^{87}Sr/^{86}Sr_i$ value (0.7073) and a relatively low εNd_i value (1.36). Other plutons has intermediate $^{87}Sr/^{86}Sr_i$ values (0.7049–0.7053) and εNd_i values ranging from 0.49 to 2.35. The hybrid granite in the Tres Montes pluton has an intermediate composition between those of the mafic dike and the host granodiorite; however, it has the highest $^{87}Sr/^{86}Sr_i$ (0.7073) and the lowest εNd_i value (–3.68) among the Taitao granites.

The sediments in the MVU has the lowest Nd isotopic ratios (–10.41 for $\varepsilon Nd_{5.5}$) of all our samples. The basement rocks were divided into two groups by their $\varepsilon Nd_{5.5}$ values, one with values around –3 and the other with values around –9. The latter group of basement rocks has the highest $^{87}Sr/^{86}Sr_i$ values of our samples.

Magmatic interaction in the ridge-trench intersection environment

Our data indicate that the compositions of igneous rocks in the Taitao Peninsula area vary chemically and isotopically. Schulte *et al.* (2009) have demonstrated that gabbros and ultramafic rocks, which display rather restricted isotopic compositions in our data, have wider isotopic variations outside our study area ("reference data" in Fig. 8): most ultramafic rocks have $^{87}Sr/^{86}Sr_i$ values higher than those of N-MORB gabbros. The highest $^{87}Sr/^{86}Sr_i$ value was 0.708, and six of our eight ultramafic samples had high εNd_i values (9–10). Few gabbro samples plotted in that field (solid circles with $\varepsilon Nd_i > 9$ in Fig. 8; Schulte *et al.*, 2009). This trend implies alteration by seawater (indicated by arrow labeled "seawater alteration" in Fig. 8) with a $^{87}Sr/^{86}Sr$ value around 0.709.

Our data from the MVU basalts have lower εNd_i and slightly higher $^{87}Sr/^{86}Sr_i$ than the gabbros and the EC-dike with N-MORB

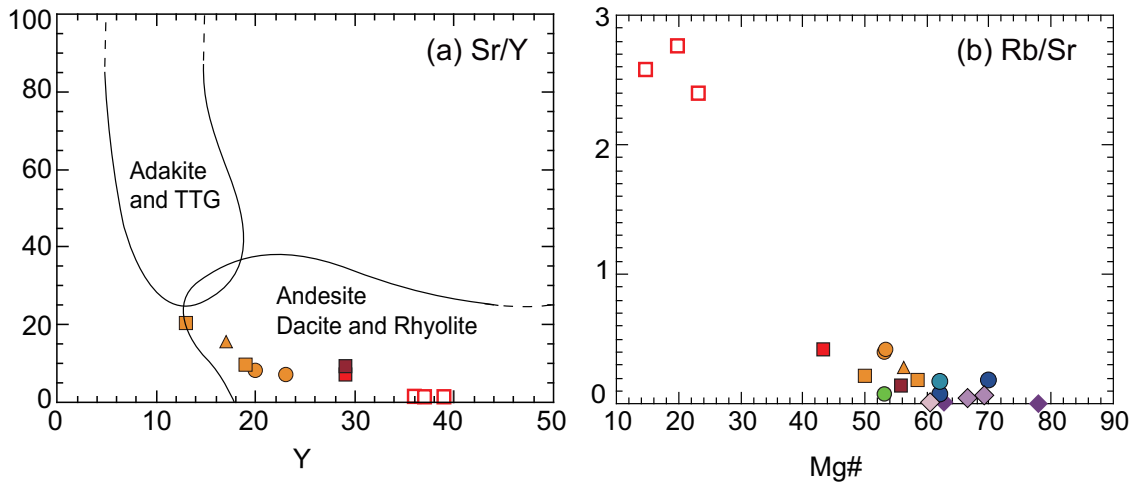

Figure 6. (a) Y vs. Sr/Y ratio diagram for the Taitao granites, and (b) Mg# vs. Rb/Sr plot for all analyzed rocks.

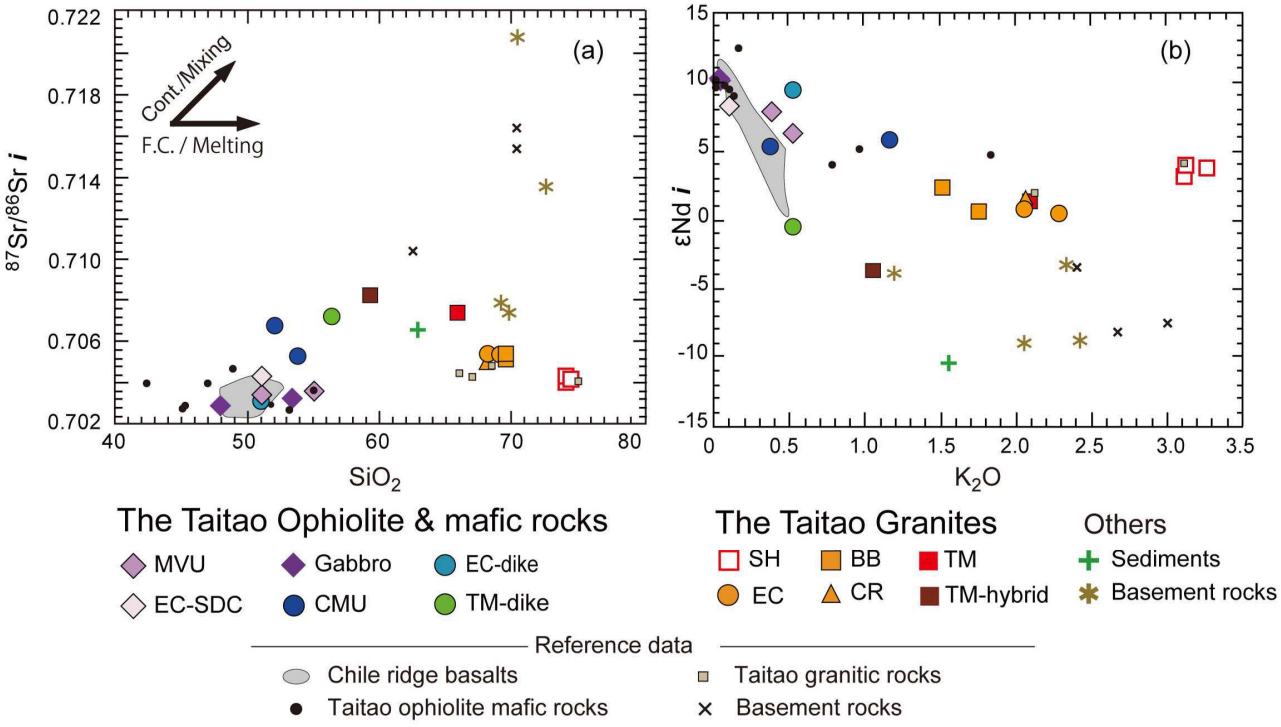

Figure 7. (a) SiO_2 vs. $^{87}Sr/^{86}Sr$i diagram and (b) K_2O vs. εNdi diagram for the Taitao ophiolite, Taitao granites, and basement rocks. Reference data sources: Klein and Karsten (1995) and Strum and Klein (1999) for Chile Ridge basalts, Kaeding et al. (1990) and Schulte et al. (2009) for Taitao ophiolite and granitic rocks.

composition. Some volcanic rocks from the Taitao ophiolite have been reported to have similar compositions (Kaeding *et al.*, 1990; solid circles with εNd*i* = 4–5 in Fig. 8). The distribution of these rocks nearly coincides with that of the basalts dredged from the Chile ridge segments (gray field in Fig. 8; Klein and Karsten, 1995; Strum *et al.*, 1999). Thus, these rocks were likely formed in a segment of the Chile ridge that had already subducted (segment –2 in Fig. 9a).

The volcanic rocks from the Chile ridge and from the Taitao ophiolite both plotted in a wider field that extends to lower εNd*i* values than the N-MORB field (Fig. 8). This isotopic variation implies that the source material of these rocks in the upper mantle was contaminated by crustal material with lower εNd value. The most probable candidate for such material is lower crust that has experienced partial melting (indicated by arrow labeled "deep crustal contamination" in Fig. 8). To introduce such material into the sub-ridge area, Strum *et al.* (2000) suggested a mechanism in which suboceanic lithospheric mantle material foundered during subduction and was brought beneath the spreading ridge entering the subduction zone by mantle upwelling (Fig. 10a), or one in which old continental crust or metasomatized mantle beneath the arc communicated with mantle beneath the ridge through a slab window (Fig. 10b). The contaminant must have had an isotopic composition similar to the sediment in the MVU (TPB338; green cross in Fig. 8). However, this sample contained clastic zircons of the same age as the Taitao granites, and there is no rational explanation for the extremely low εNd value of this sediment.

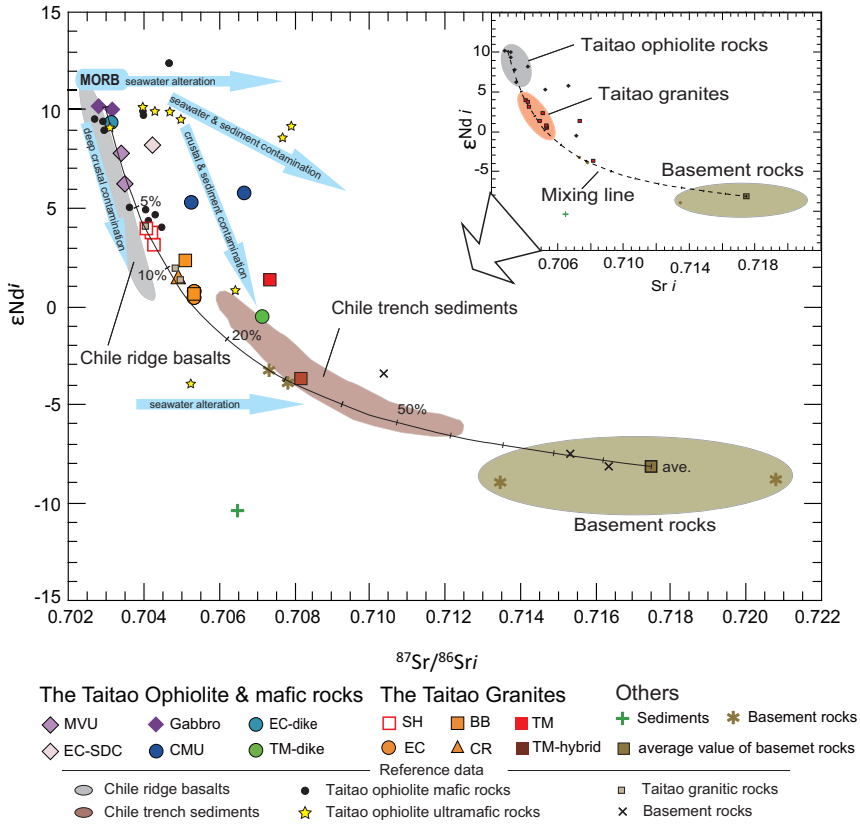

Figure 8. $^{87}Sr/^{86}Sri$ vs. εNdi diagram for the Taitao ophiolite, Taitao granites, and basement rocks and sediments. The thin solid line is a mixing line that ties isotopic composition of average gabbro and average basement rocks. Reference data sources: Kilian and Behrmann (2003) for the Chile trench sediments, Klein and Karsten (1995) and Strum and Klein (1999) for Chile Ridge basalts, Kaeding et al. (1990) and Schulte et al. (2009) for Taitao ophiolite and granitic rocks. CHUR(0) = 0.512638 (Wasserburg et al., 1981) was used for the calculation of εNdi.

Alteration of the source mantle by deep crustal material and seawater must have been proceeding when segments of the Chile ridge were entering the subduction zone. The ultramafic section of the ophiolite underwent severe alteration by seawater, but no basaltic rocks from the Chile ridge and only a few gabbros of the Taitao ophiolite exhibited such evidence. In contrast, evidence for contamination of the sub-ridge mantle by deep crustal material has been observed in both the ridge and the ophiolite. Thus, pervasive contamination by deep crustal material must have been taking place before seawater alteration started as the ridge approached the subduction zone.

Anma *et al.* (2013) have shown that the magmatism that formed the 4.6 Ma CMU started in the South Taitao Ridge (Fig. 1b) at around 5.3 Ma and migrated eastward. They attributed this phenomenon to the subduction of the Tres Montes fracture zone. They also have reported evidence for the incorporation of trench-fill sediment that was brought to the upper mantle with the subducting fracture zone, then returned to the surface by volcanic activities of the CMU. Our new isotopic data support this model in that the mafic volcanic rocks of the CMU and TM-dike have higher $^{87}Sr/^{86}Sri$ values than the Chile ridge basalts. The isotopic composition of the CMU may be explained in terms of marine alteration of basaltic rocks that were contaminated by deep crustal material (trajectory 1 in Fig. 8), contamination by trench-fill sediment of mantle that was altered by seawater (trajectory 3 in Fig. 8), or the combined influence of seawater alteration and sediment contamination of N-MORB magmas (trajectory 2 in Fig. 8). Alteration of mantle by seawater was most likely to occur along a fracture zone (Fig. 9a–d). As the fracture zone approached the subduction zone, sediment from the forearc area was carried onto it through submarine canyons. This fracture-filling sediment, accompanied by seawater, may have penetrated the crust during shear along the fracture zone and altered the mantle (Fig. 10c). The influence of slab tearing that resulted from buoyancy differences between the subducting slab segments may have enhanced this penetration.

Origin of calc-alkaline I-type granites

The fact that the Taitao granites are restricted to the vicinity of the Taitao ophiolite implies that the plutonism was related to the subduction of the hot ridge. The Taitao granites are calc-alkaline, meta-aluminous to slightly peraluminous (0.83 < ASI < 1.1), I-type granites. Such granites are generally considered to form by partial melting of an igneous source material. In the Taitao Peninsula region, possible source materials are limited to the subducting oceanic crust or igneous crustal material in the forearc region, if any. The low Sr*i* ratios and high εNd ratios support the oceanic crustal origin of the granitic melts. However, contamination by sediment or other continental crustal material did occur, especially in the Tres Montes granodiorite, which contains over 40% recycled zircon of Cretaceous to Late Proterozoic ages (Anma *et al.*, 2009).

The mixing line in Figure 8 represents a petrogenetic model based on Sr-Nd isotopic compositions. Most Taitao granites plot on the mixing line between the average composition of gabbros, with primitive N-MORB isotopic compositions, and the average composition of metasedimentary basement rocks with the lowest εNd values, chosen as an extreme end-member. Taking N-MORB as the source material of the granite melts, our calculations indicate that the Seno Hoppner granite (with the most depleted isotopic composition) requires incorporation of no more than 5–10% of contaminant. Other plutons, except the Tres Montes pluton, would require slightly more contamination to yield a result concordant with the calculation by Kaeding *et al.* (1990). Because recycled zircon is rare in these plutons, the contaminant could also be lower crustal material originating from a foundering slab or from sub-arc mantle that had experienced partial melting (Strum *et al.* 2000). Conversely, the major- and trace-element compositions of our samples favor contamination by sediment or basement of the upper crust. To produce the Tres Montes granodiorite requires a significant alteration by seawater or incorporation of sediment, most probably related to the subduction of the Esmeralda fracture zone (Fig. 9b, c).

The Taitao ophiolite has undergone low-pressure metamorphism at zeolite to amphibolite facies conditions (Shibuya *et al.*, 2007). Experimental studies at less than 1 GPa suggest that decomposition of amphiboles in hot oceanic crust could result in K-poor partial melts

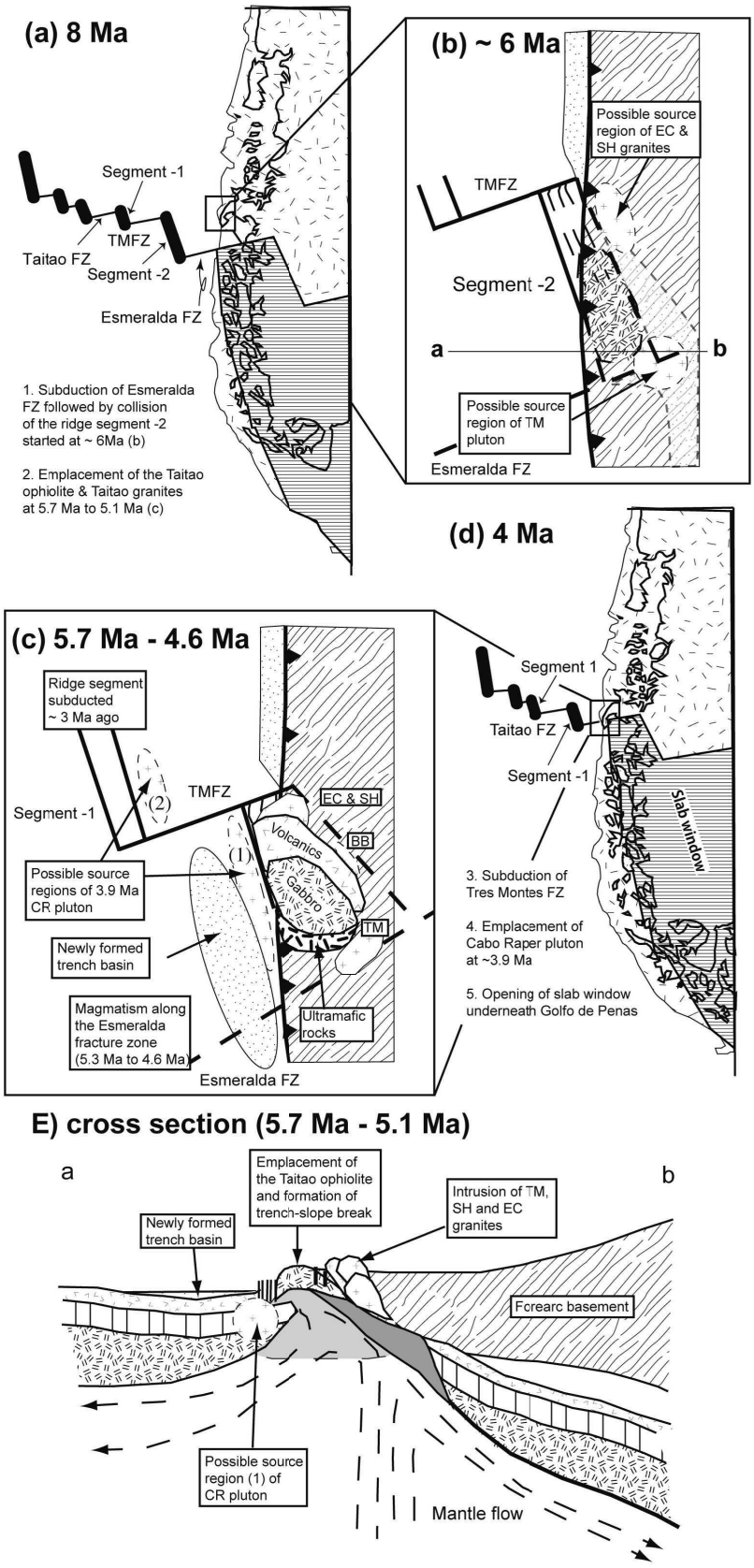

Figure 9. (a) Migration and subduction of the Chile ridge at 8 Ma. (b) Emplacement of the Taitao ophiolite and Taitao granites at ~6 Ma. (c) Emplacement of the Taitao ophiolite and Taitao granites at 5.7–4.6 Ma. (d) Migration and subduction of the Chile ridge at 4 Ma. (e) Cross section of ophiolite and granite emplacement at 5.7–5.1 Ma; location in (b). Figures are modified from Anma et al. (2006, 2013).

with tonalitic, trondhjemitic or granodioritic compositions (Beard and Lofgren, 1990; Rapp *et al.*, 1991; Patino Douce, 1995; Rapp and Watson, 1995; Springer and Seck, 1997; Sisson *et al.*, 2005). The juvenile magmas that constitute the principal component of the Taitao granites, with unfractionated HREE patterns and low La/Yb ratios, could be explained by partial melting of amphibolite in the absence of garnet (Kon *et al.*, 2013).

The high K content and lower MgO and CaO contents in the Seno Hoppner granite imply partial melting of oceanic crust at a higher temperature than other plutons. This temperature contrast is reasonable because the 5.2 Ma Seno Hoppner pluton is farther from the trench, hence the subducting slab underneath it was deeper and hotter than was the case for the 5.2 Ma Estero Cono pluton and the 5.7 Ma Tres Montes pluton near the trench. Zircon saturation temperatures (Hanchar and Watson, 2003) calculated for the granites support the higher temperatures (over 810°C) for the Seno Hoppner granite compared to the others (down to 770 °C). Partial melting of K-rich basaltic rocks of the Chile Ridge (Klein and Karsten, 1995; Sherman *et al.*, 1997) could have formed such granitic melts (Sisson *et al.*, 2005). Nevertheless, producing high-K granitic melts with 74% SiO_2 content is not easy and may require further processing. The Seno Hoppner granite has a prominent negative Eu anomaly that implies fractional crystallization by settlement of Ca-plagioclase, whereas the hypothesized source gabbros with N-MORB composition have positive Eu anomalies. Considering that REE concentrations in our samples were about 10 times greater in granite than in gabbro, the granitic melts must have collected material from a vast amount (10 times their volume) of gabbro that was continually brought into the subduction zone with the moving plate.

Lagabrielle et al. (2003) emphasized the importance of repeated passages of several ridge segments to develop high thermal gradients that allow partial melting of oceanic lithosphere at temperatures of 800–900°C and low pressures corresponding to depths of 10–20 km, and to form Quaternary calc-alkaline acidic magmatism in the Chile triple junction area. It is noteworthy that the I-type calc-alkaline magmatism took place during the first ridge subduction event (Fig. 9a, b).

Implication for ophiolite tectono-magmatism

The tectonomagmatic processes we report here, especially the formation of the calc-alkaline granites at this ridge-trench intersection environment, have important implications for constructing tectono-magmatic models of ophiolites. Presence of the calc-alkaline granites is usually interpreted as a supra-subduction zone signature. Our study shows that the

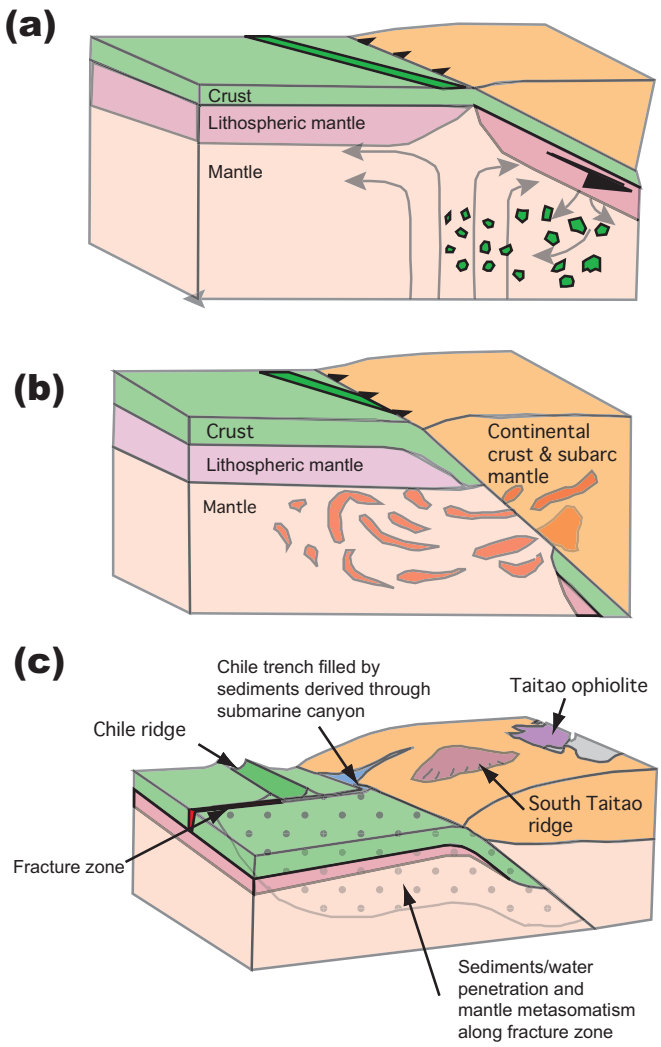

Figure 10. Models for the contamination of oceanic mantle by continental material (a) through incorporation of foundered slab material (Strum et al., 2000), (b) through a slab window connecting sub-arc mantle and sub-ridge mantle (Strum et al., 2000), and (c) through incorporation of seawater and sediment penetrating a fracture zone (this study).

calc-alkaline magmas might be generated at mid-ocean ridge segments that are about to be subducted.

As exemplified in introduction, the Taitao ophiolite-granite complex has a full range of chemical variations that is comparable to the Semail ophiolite, which had a rather prolonged tectonomagmatic history. In the case of the Semail ophiolite, the history from the generation of ophiolitic rocks to magmatism and modification at an arc environment is supported by age constraints. However, if such history relies only on geochemical signatures, then it may result in misinterpretation of the rock record of many ophiolites by mistaking what are essentially of mid-oceanic segment origin for an apparent supra-subduction zone signature.

Compared to the Semail ophiolite, the Taitao ophiolite-granite complex has a significantly greater fraction of granitic rocks. Previous have argued for for heating of the forearc region as evidenced by high geothermal gradient metamorphism in this region (Lagabrielle et al., 2000; Shibuya et al., 2007; Kon et al., 2013). Such evidence for a high geothermal gradient is lacking in the generally cold settings of emplacement for ophiolites such as Semail (Wakabayashi et al., 2010), with minor exception of the metamorphic sole that indicates a ridge subduction origin. Perhaps, the amount of calc-alkaline granites incorporated into ophiolites depends on whether the concerned oceanic lithosphere was young and hot: in the case of Semail with a prolonged history, the place of origin of ophiolitic rocks and the obducted margin were far enough such that the Cretaceous oceanic lithosphere was cooled sufficiently before obduction. This process might have resulted in a distinctive arc-type magmatism and a less amount of granitic rocks.

Summary

The late Miocene – early Pliocene Taitao ophiolite provides an excellent opportunity to study the emplacement mechanism of a ridge-trench intersection ophiolite and the complex magmatic interactions between the subducting ridge, overlying crust and sediments, and mantle. The MORB erupted near the ridge subduction zone appears to have been contaminated by a lower crustal material that has experienced partial melting. Such material could have been delivered to the sub-ridge mantle through a slab window from the sub-arc mantle, or it could have originated from sub-oceanic lithospheric mantle that had foundered during subduction and been brought to the spreading ridge by mantle upwelling. Alteration of mantle material by seawater along fracture zones and contamination by fracture zone-fill sediments are other important factors that may control magmatic interactions in a ridge-trench intersection environment. As a result of ridge subduction, juvenile magmas of calc-alkaline I-type granites were formed by partial melting of young and hot oceanic ridge lithosphere under garnet-free-amphibolite conditions. The magmas were then contaminated by subducted sediment or upper crustal components. Fractional crystallization of Ca-plagioclase favored production of granitic melt with high K_2O and SiO_2 contents.

Acknowledgements

This work was supported by grant-in-aid for Science Research 13373004 and 15H02630 by the Ministry of Education, Culture, Sports, Science and Technology of Japan. RA thanks Y. Kaneko (Meisei University), M. Terabayashi (Kagawa University), T. Komiya (University of Tokyo), S. Kagashima (Yamagata University), I. Katayama (Hiroshima University), F. Herve (University of Chile), T. Nishimura (NICHIMAR), S. Maruyama (TiTech), T. Ota (Okayama University), E. E. Veloso (Universidad Catolica del Norte), M. Schilling (Universidad Austral de Chile), S. Yamamoto (TiTech), Y. Kon (AIST), and T. Shibuya (JAMSTEC) for their field support. Our thanks go to J. Wakabayashi of California State University and an anonymous reviewer for the careful review and constructive ideas that helped to improve the manuscript. We thank Y. Dilek of Miami University for the opportunity to publish this paper and for his editorial help and improvements.

References

Adachi, Y. and Miyashita, S., 2003, Geology and petrology of the plutonic complexes in the Wadi Fizh area: Multiple magmatic events and segment structure in the northern Oman ophiolite: Geochemistry Geophysics Geosystems, v. 4, doi: 10. 1029/2001GC000272.

Anma, R. and Orihashi, Y., 2013, Shallow-depth melt eduction due to ridge subduction: LA-ICPMS U-Pb igneous and detrital zircon ages from the Chile Triple Junction and the Taitao Peninsula, Chilean Patagonia: Geochemical Journal, v. 47, pp. 149-165.

Anma, R., Veloso-Espinosa, E. A. and the CHRISTMASSY Project-Taitao Ophiolite Study Group, 2005, Tectonic Evolution of the Taitao ophiolite-an ophiolite formed by ridge collision event: Gekkan Chikyu, v. 312, pp. 428-437. (in Japanese)

Anma, R., Armstrong, R., Danhara, T., Orihashi, Y. and Iwano, H., 2006, Zircon sensitive high mass-resolution ion microprobe U-Pb and fission-track ages for gabbros and sheeted dykes of the Taitao ophiolite, Southern Chile, and their tectonic implications: Island Arc, v. 15, pp. 130-142.

Anma, R., Armstrong, R., Orihashi, Y., Ike, S., Shin, K-C., Kon, Y., Komiya, T., Ota, T., Kagashima, S., Shibuya, T., Yamamoto, S., Veloso, E. E., Fannin, M. and Herve, F., 2009, Are the Taitao granites formed due to subduction of the Chile ridge? Lithos, v. 113, pp. 246-258.

Anonymous, 1972, Penrose field conference on ophiolites: Geotimes, v. 17, pp. 24-25.

Balestro, G., Festa, A., Dilek, Y. and Tartarotti, P., 2015, Pre-Alpine Extensional tectonics of a peridotite-localized oceanic core complex in the late Jurassic, high-pressure Monviso ophiolite (Western Alps). Episodes, v. 38, No. 4, pp. 266-282, doi:10.18814/epiiugs/2015/v38i4/82421.

Barker, F., 1979, Trondhjemite: definition, environment and hypothesis of origin: in Baker, F. (ed), Trondhjemite, Dacite and Related Rocks: Development in Petrology, v. 6, pp. 1-12.

Beard, J.S. and Lofgren, G.E., 1990, Dehydration melting and water-saturated melting of basaltic and andestic greenstones and amphibolites at 1, 3, and 6.9 kb: Journal of Petrology, v. 32, pp. 365–401.

Behrmann, J. H., Lewis, S. D., Cande, S. C. and ODP Leg 141 Scientific Party, 1994, Tectonic and geology of spreading ridge subduction at Chile Triple Junction: a synthesis of results from Leg 141 of the Ocean Drilling Program: Geologische Rundschau, v. 83, pp. 832-852.

Boudier, F. and Nicolas, A., 2011, Axial melt lenses at oceanic ridges – A case study in the Oman ophiolite: Earth and Planetary Science Letters, v. 304, pp. 313-325.

Boudier, F., Nicolas, A. and Ildefonse, B., 1996, Magma chambers in the Oman ophiolite: fed from the top and the bottom: Earth and Planetary Science Letters, v. 304, pp. 313-325.

Bourgois, J., Lagabrielle, Y., Maury, R., Le Moigne, J., Vidal, P., Cantagrel, J. M. and Urbina, O., 1992, Geology of the Taitao peninsula (Chile margin triple junction area, 46-47°S); Miocene to Pleistocene obduction of the Bahia Barrientos Ophiolite: EOS, v. 73, (43) 592.

Bourgois, J., Lagabrielle, Y., Le Moigne, J., Urbina, O., Janin, M-C., Beuzart, P., 1993, Preliminary results of a field study of the Taitao ophiolite (southern Chile): Implications for the evolution of the Chile triple junction: Ofioliti, v. 18, pp. 113-129.

Bourgois, J., Martin, H., Lagabrielle, Y., Le Moigne, J. and Frutos Hara, J., 1996, Subduction erosion related to spreading-ridge subduction: Taitao peninsula (Chile margin triple junction area): Geology, v. 24, pp. 723-726.

Breitsprecher, K. and Thorkelson, D. J., 2009, Neogene kinematic history of Nazca-Antarctica-Phoenix slab windows beneath Patagonia and the Antarctic Peninsula: Tectonophysics, v. 464, pp. 10-20.

Cande, S. and Leslie, B., 1986, Late Cenozoic tectonics of southern Chile trench: Journal of Geophysical Research, v. 91 (B1), pp. 471-96.

Cande, S., Herron, E. and Hall, B., 1982, The early Cenozoic tectonic history of the southeast Pacific: Earth Planetary Science Letters, v. 57, pp. 63-74.

Cande, S. C., Leslie, R. B., Parra, J. C. and Hobart, M., 1987, Interaction between the Chile ridge and Chile trench: Geophysical and geothermal evidence: Journal of Geophysical Research, v. 92 (B1), pp. 495-520.

Chappell, B. W. and White, A. J. R., 1974, Two contrasting granite types: Pacific Geology, v. 8, pp. 173-174.

Dilek, Y. and Newcomb, S., 2003, Ophiolite concept and the evolution of geological thought: The Geological Society of America Special Paper, vol. 373, ISBN 0-8137-2373-6.

Dilek, Y. and Flower, M.F.J., 2003, Arc-trench rollback and forearc accretion: 2. A model template for ophiolites in Albania, Cyprus, and Oman: The Geological Society of London Special Publications, v. 218, pp. 43-68.

Dilek, Y. and Robinson, P.T., 2003, Ophiolites in Earth history. Geological Society, London, Special Publication, v. 218, pp. 1-8.

Dilek, Y. and Furnes, H., 2009, Structure and geochemistry of Tethyan ophiolites and their petrogenesis in subduction rollback systems: Lithos, v. 113, pp. 1-20.

Dilek, Y. and Furnes, H., 2011, Ophiolites genesis and global tectonics: Geochemical and tectonic fingerprinting of ancient oceanic lithosphere: Geological Society of America Bulletin, v. 123, pp. 387-411.

Dilek, Y. and Furnes, H., 2014, Ophiolites and their origins: Elements, v. 10, pp. 93-100.

Fareeduddin and Dilek, Y., 2015, Structure and petrology of the Nagaland-Manipur Hill ophiolite melange zone, NE India: A fossil Tethyan subduction channel at the India-Burma plate boundary. Episodes, v. 38, No. 4, pp. 298-314, doi:10.18814/epiiugs/2015/v38i4/82426.

Flower, M.J.F, and Dilek, Y., 2003, Arc-trench rollback and forearc accretion: 1. A collision-induced mantle flow model for Tethyan ophiolites: The Geological Society of London Special Publications 2003, v. 218, pp. 21-41.

Forsythe, R., Nelson, E., Carr, M., Kaeding, M. E., Herve, M., Mpodozis, C., Soffia, J. M. and Harambour, S., 1986, Pliocene near-trench magmatism in southern Chile: A possible manifestation of the ridge collision. Geology, v. 14, pp. 23-27.

Guivel, C., Lagabrielle, Y., Bourgois, J., Maury, R. C., Fourcade, S., Martin, H. and Arnaud, N., 1999, New geochemical constraints for the origin of ridge-subduction-related plutonic and volcanic suites from the Chile triple junction (Taitao peninsula and Site 862, LEG ODP141 on the Taitao ridge): Tectonophysics, v. 311, pp. 83-111.

Hanchar, J. M. and Watson, E. B., 2003, Zircon Saturation Thermometry: Reviews in Mineralogy and Geochemistry, v. 53, pp. 89-112.

Herron, E. M., Cande, S. C. and Hall, B. R. (1981) An active spreading center collides with a subduction zone: A geophysical survey of the Chile Margin triple junction. Geol. Soc. Am. Memoir 154, 683-701.

Herve, F., Fanning, M. C., Thomson, S. N., Pankhurst, R. J., Anma, R., Veloso, E. E. and Herrera, C., 2003, SHRIMP U-Pb and FT Pliocene ages of near-trench granites in Taitao peninsula, Southern Chile: Short Papers – IV South American Symposium on Isotope Geology, pp. 190-193.

Jacobs, J., Thomas, R. J., Ksienzky, A. K. and Dunkl, I., 2015, Tracking the Oman Ophiolite to the surface – New fission track and (U-Th)/He data from the Aswad and Khor Fakkan Blocks, United Arab Emirates: Tectonophysics, v. 644-645, pp. 68-80.

Kaeding, M., Forsythe, R. and Nelson, E., 1990, Geochemistry of the Taitao ophiolite and near-trench intrusions from the Chile margin triple junction: Journal of South American Earth Science, v. 3, pp. 161-177.

Kanke, N., and Takazawa, E., 2014, A kilometer-scale highly refractory harzburgite zone in the mantle section of the northern Oman Ophiolite (Fizh Block): implications for flux melting of oceanic lithospheric mantle: Geological Society, London, Special Publications, v. 392, pp. 229-246.

Karsten, J. L., Klein E. M. and Sherman, S. B., 1996, Subduction zone geochemical characteristics in ocean ridge basalts from the southern Chile Ridge: implications of modern ridge subduction systems for the Archean: Lithos, v. 37, pp. 143-161.

Kilian, R. and Behrmann, J. H. (2003) Geochemical constraints on the sources of Southern Chile Trench sediments and their recycling in arc magmas of the Southern Andes. J. Geol. Soc., London, v. 160, pp. 57-70.

Klein, E. M. and Karsten, J. L., 1995, Ocean-ridge basalts with convergent-margin geochemical affinities from the Chile ridge: Nature, v. 374, pp. 52-57.

Kon, Y., Komiya, T., Anma, R., Hirata, T., Shibuya, T., Yamamoto, S. and Maruyama, S., 2013, Petrogenesis of the ridge subduction-related granitoids from the Taitao Peninsula, Chile Triple Junction area: Geochemical Journal, v. 47, pp. 167-183.

Lagabrielle, Y., Guivel, C., Maury, R., Bourgois, J., Fourcade, S. and Martin, H., 2000, Magmatic-tectonic effects of high thermal regime at the site of active ridge subduction: The Chile triple junction model. Tectonophysics, v. 326, pp. 255-268.

Lagabrielle, Y., Le Moigne, J., Maury, R., Cotton, J. and Bourgois, J., 1994, Volcanic record of the subduction of an active spreading ridge, Taitao peninsula (southern Chile): Geology, v. 22, pp. 515-518.

Le Maitre, R. W., Streckeisen, A., Zanettin, B., Le Bas, M. J., Bonin, B., Bateman, P., Bellieni, G., Dudek, A., Efremova, S., Keller, J., Lameyre, J., Sabine, P. A., Schmid, R., Sorensen, H. and Woolley, A. R., 2005, Igneous Rocks: A Classification and Glossary of Terms (2nd Edition): Cambridge University Press, Cambridge, 256 pp.

Le Moigne, J., Lagabrielle, Y., Whitechurch, H., Girardeau, J., Bourgois, J. and Maury, R. C., 1996, Petrology and geochemistry of the ophiolitic and volcanic suites of the Taitao peninsula-Chile triple junction area: Journal of South American Earth Science, v. 9, pp. 43-58.

MacLeod, C. J. and Yaouancq, G., 2000, A fossil melt lens in the Oman ophiolite: Implications for magma chamber processes at fast spreading ridges: Earth and Planetary Science Letters, v. 176, pp. 357-373.

McDonough, W. F. and Sun, S.-S., 1995, The composition of the Earth: Chemical Geology, v. 120, pp. 223-225.

Miyashiro, A., 1973, The Troodos ophiolitic complex was probably formed in an island arc: Earth and Planetary Science Letters, v. 19, pp. 218-224.

Miyashita, S., Adachi, Y. and Umino, S., 2003, Along-axis magmatic system in the northern Oman ophiolite: Implications of compositional variation of the sheeted dike complex: Geochemistry Geophysics Geosystems, v. 4, doi: 10. 1029/2001GC000235.

Mpodozis, C., Herve, M., Nasi, C., Soffia, J., Forsythe, R. and Nelson, E., 1985, El magmatismo plioceno de la península Tres Montes y su relación con la evolución del punto triple de Chile: Revista Geolgica de Chile, v. 25-26, pp. 13-28.

Nelson, E., Forsythe, R., Diemer, J., Allen, M. and Urbina, O., 1993, Taitao ophiolite: A ridge collision ophiolite in the forearc of southern Chile (46ºS): Revista Geolgica de Chile, v. 20, pp. 137-166.

Orihashi, Y. and Hirata, T., 2003, Rapid quantitative analysis of Y and REE abundances in XRF glass bead for selected GSL reference rock standards using Nd-YAG 266 nm UV laser ablation ICP-MS: Geochemical Journal, v. 37, pp. 401-412.

Patino Douce, A.E., 1995, Experimental generation of hybrid silicic melts by reaction of high-Al basalt with metamorphic rocks: Journal of Geophysical Research, v. 100 (B8), pp. 15623–15639.

Pearce, J. A. and Robinson, P. T., 2010, The Troodos ophiolitic complex probably formed in a subduction initiation, slab edge setting: Gondwana Research, v. 18, pp. 60-81.

Rapp, R.P., Watson, E.B. and Miller, C.F., 1991, Partial melting of amphibolite/eclogite and the origin of Archean trondhjemites and tonalities: Precambrian Research, v. 51, pp. 1–25.

Rapp, R.P. and Watson, E.B., 1995, Dehydration melting of metabasalt at 8–32 kbar: implications for continental growth and crust–mantle recycling: Journal of Petrology, v. 36, pp. 891–931.

Saccani, E., Dilek, Y., Marroni, M., and Pandolfi, L., 2015, Continental margin ophiolites of Neotethys: Remnants of ancient Ocean-Continent Transition Zone (OCTZ) lithosphere and their geochemistry, mantle sources and melt evolution patterns. Episodes, v. 38, No. 4, pp. 230-249, doi:10. 18814/epiiugs/2015/v38i4/82418.

Schulte, R. F., Schilling, M., Anma, R., Farquhar, J., Horan, M., Komiya, T., Piccoli, P. M., Pitcher, L. and Walker, R., 2009, Chemical and chronologic complexity in the convecting upper mantle: Evidence from the Taitao ophiolite, southern Chile: Geochimica Cosmochimica Acta, v. 73, pp. 5793-5819.

Sherman, S. B., Karsten, J. L. and Klein, E. M., 1997, Petrogenesis of axial lavas from the southern Chile ridge: major element constraints: Journal of Geophysical Research, v. 102, B7, pp. 14963-14990.

Shibuya, T., Komiya, T., Anma, R., Ota, T., Omori, S., Kon, Y., Yamamoto, S. and Maruyama, S., 2007, Progressive metamorphism of the Taitao ophiolite; Evidence for axial and off-axis hydrothermal alterations: Lithos, v. 98, pp. 233-260.

Sisson, T.W., Ratajeski, K., Hankins, W.B., Glazner, A.F., 2005, Voluminous granitic magmas from common basaltic sources: Contributions to Mineralogy and Petrology, v. 148, pp. 635–661.

Springer, W. and Seck, H.A., 1997, Partial fusion of basic granulites at 5 to 15 kbar: implications for the origin of TTG magmas: Contributions to Mineralogy and Petrology, v. 127, pp. 30–45.

Strum M. E., Klein, E. M., Graham, D. W. and Karsten, J., 1999, Age constraints on crustal recycling to the mantle beneath the southern Chile Ridge: He-Pb-Sr-Nd isotope systematics: Journal of Geophysical Research, v. 104, B3, pp. 5097-5114.

Strum M. E., Klein, E. M., Karsten, J. and Karson, J. K., 2000, Evidence for subduction-related contamination of the mantle beneath the southern Chile Ridge: Implications for ambiguous ophiolite compositions: In, Dilek, Y. and others (Editors), Geological Society of America, Special Paper, v. 349, pp. 13-20.

Tani, K., Orihashi, Y. and Nakada, S., 2002, Major and trace component analysis of silicate rocks using fused glass bead by X-ray Fluorescence spectrometer: Evaluation of analytical precision for third, sixth and eleventh dilution fused glass beads. Technical Research Report, Earthquake Research Institute, University of Tokyo, v. 8, pp. 26–36.

Taylor, S. R. and McLennan, S. M., 1985, The Continental Crust: Its Composition and Evolution: Blackwell, Oxford, 312 pp.

Tebbens, S. F. and Cande, S. C., 1997, Southeast pacific tectonic evolution from early Oligocene to Present: Journal of Geophysical Research, v. 102, pp. 12061-12084.

Tebbens, S. F., Cande, S. C., Kovacs, L., Parra, J. C., LaBrecque, J. L. and Vergara, H., 1997, The Chile ridge: A tectonic framework: Journal of Geophysical Research, v. 102, pp. 12035-12059.

Thomson, S. N. and Herve, F., 2002, New time constraints for the age of metamorphism at the ancestral Pacific Gondowana margin of southern Chile (42°–52°S): Revista Geologica de Chile, v. 29, pp. 255-271.

Tsuchiya, N., Shibata, T., Yoshikawa, M., Adachi, Y., Miyashita, S., Adachi, T., Nakano, N. and Osanai, Y., 2013, Petrology of Lasail plutonic complex, northern Oman ophiolite, Oman: An example of arc-like magmatism associated with ophiolite detachment: Lithos, v. 156-159, pp. 120-138.

Veloso, E. E., Anma, R. and Yamazaki, T., 2005, Tectonic rotations during the Chile ridge collision and obduction of the Taitao ophiolite (Southern Chile): Island Arc, v. 14, pp. 599-615.

Veloso, E. E., Anma, R., Ota, T., Komiya, T., Kagashima, S. and Yamazaki, T., 2007, Paleocurrent patterns of the sedimentary sequence of the Taitao ophiolite constrained by anisotropy of magnetic susceptibility and paleomagnetic analyses. Sedimentary Geology, v. 201, pp. 446-460.

Veloso, E. E., Anma, R. and Yamaji, A., 2009, Ophiolite emplacement and the effects of the subduction of the Chile Ridge System: Heterogeneous paleostress regimes recorded in the Taitao ophiolite (Southern Chile): Andean Geology, v. 36, pp. 3-16.

Wakabayashi, J., Ghatak, A. and Basu, A. R., 2010, Tectonic setting of supra-subduction zone ophiolite generation and subduction initiation as revealed through geochemistry and regional field relationships: Geological Society of America Bulletin, v. 122, pp. 1548-1568.

Wakabayashi, J. and Dilek, Y., 2003, What constitutes 'emplacement' of an ophiolite?: mechanism and relationship to subduction initiation and formation of metamorphic soles: Geological Society, London, Special Publications, v. 218, pp. 427-447.

Warren, C. J., Parrish. R. R., Waters, D. L. and Seale, M. P., 2005, Dating the geologic history of Oman's Semail ophiolite: insights from U-Pb geochronology: Contribution to Mineralogy and Petrology, v. 150, pp. 403-422.

Wasserburg, G.J., S.B. Jacobsen, D.J. DePaolo, M.T. McCulloch, and T. Wen, 1981, Precise determination of Sm/Nd ratios, Sm and Nd isotopic abundances in standard solutions: Geochimica Cosmochimica Acta, v. 45, pp. 2311-2323.

Yamato, P., Agard, P., Goffe, B., De Andrade, V., Vidal, O. and Jolivet, L., 2007, New, high-precision P-T estimates for Oman blueschists: implications for obduction, nappe stacking and exhumation processes: Journal of Metamorphic Geology, v. 25, pp. 657-682.

Yang, G.X. and Dilek, Y., 2015, OIB- and P-Type ophiolites along the Yarlung-Zangbo Suture Zone (YZSZ), southern Tibet: Polyphase melt history and mantle sources of the Neotethyan oceanic lithosphere. Episodes, v. 38, No. 4, pp. 250-265, doi:10.18814/epiiugs/2015/v38i4/82420.

Yoshikawa, M., Python, M., Tamura, A., Arai, S., Takazawa, E., Shibata, T., Ueda, A. and Sato, T., 2015, Melt extraction and metasomatism recorded in basal peridotites above the metamorphic sole of the northern Fizh massif, Oman ophiolite: Tectonophysics, v. 650, pp. 53-64.

by Fareeduddin[1] and Yildirim Dilek[2]

Structure and petrology of the Nagaland-Manipur Hill Ophiolitic Mélange zone, NE India: A Fossil Tethyan Subduction Channel at the India – Burma Plate Boundary

[1] Geological Society of India, Bangalore – 560 019, India. *Corresponding author E-mail: fareedromani@gmail.com*
[2] Department of Geology & Environmental Earth Science, Miami University, Oxford, OH 45056, USA

DOI: 10.18814/epiiugs/2015/v38i4/82426

The Nagaland–Manipur Hill ophiolite belt in NE India represents the southern extension of the Neotethyan Yarlung-Zhangbo suture zone in Southern Tibet, and connects this on-land exposure of the late Mesozoic collision front in the north with a modern trench-arc system in the Andaman Sea region in the south. Ophiolitic subunits in the Nagaland–Manipur Hill area in the Indo-Myanmar Ranges occur as blocks or thrust sheets within a mélange with a serpentinite or fine-grained greywacke matrix, and are spatially associated with eclogitic and blueschist rock assemblages. This ophiolitic mélange zone is tectonically sandwiched between an older (Triassic – Cretaceous) accretionary prism complex (Nimi Flysch) to the east and a younger (Late Cretaceous –Miocene) accretionary wedge (Disang Flysch) to the west. The Nagaland–Manipur Hill ophiolitic mélange is thus part of a progressively westward migrated subduction-accretion complex, and it represents a typical subduction channel mélange evolved during the fast subduction of the Neotethyan oceanic lithosphere beneath Asia – Sundaland. The exhumation of this mélange was facilitated by return flow within a subduction channel at the plate interface between the downgoing Indian continental margin, subducting at a shallow angle during the Eocene, and the Triassic – Early Cretaceous accretionary prism of the overlying Burma plate. The Upper Eocene – Miocene Pokhpur sedimentary strata uncomformably overlying the ophiolitic mélange and the accretionary prism metasedimentary rocks constitute a wedge-top or slope-basin sequence, rather than a post-collisional molasse deposit. The occurrence of ophiolitic subunits in the Nagaland–Manipur Hill area represents an accretionary-type ophiolite, derived mainly from the downgoing plate, and does not characterize a Penrose-type, complete ophiolite sequence.

Introduction

Jurassic – Cretaceous ophiolites and ophiolitic mélanges occur discontinuously along a series of suture zones and major fault systems around the periphery of the Indian sub-continent (Figs. 1 and 2). The Bela, Muslim Bagh, Zhob and Waziristan ophiolites along the N-S-trending, western edge of the Indian continental margin (Sarwar, 1992; Kakar et al., 2014), the ophiolites of the E-W-trending Yarlung-Zhangbo suture zone along its northern periphery in southern Tibet (Xu et al., 2015; Yang and Dilek, 2015; Yang et al., 2015), and the N-S trending ophiolites and mélanges along its eastern edge in India and Myanmar (Sengupta et al., 1990; Mitchell et al., 2012; Soibam et al., 2015) represent the remnants of the Neotethyan oceanic lithosphere. These peri-Indian ophiolites are highly diverse in their geochemical compositions, internal structures, igneous and metamorphic ages, and emplacement mechanisms. Hence, numerous tectonic models have been developed in the literature regarding the tectonic environment(s) of their magmatic construction, the paleogeography of the Neotethyan seaways in which they evolved, and the nature and kinematics of plate boundaries and plate boundary interactions through which they were accreted into the continental margins of India.

Along the peri-Indian ophiolites, those occurring along the eastern margin of India are the least known ones in terms of their internal structures, geochemical makeups and emplacement mechanisms. Yet, their tectonic position between the collisional front and a late Mesozoic suture zone (Yarlung-Zhangbo suture zone) in the north and the active suprasubduction zone seafloor spreading system in the Andaman Sea to the south (Figures 1 and 2; Morley, 2009) makes them an ideal laboratory for investigating a diverse range of ophiolite problems. The active eastward subduction of the Bay of Bengal crust and the Indian continental margin beneath the Indo-Myanmar Ranges also provides an excellent opportunity to examine the *in-situ* structural, sedimentological, and tectonic processes associated with accretionary

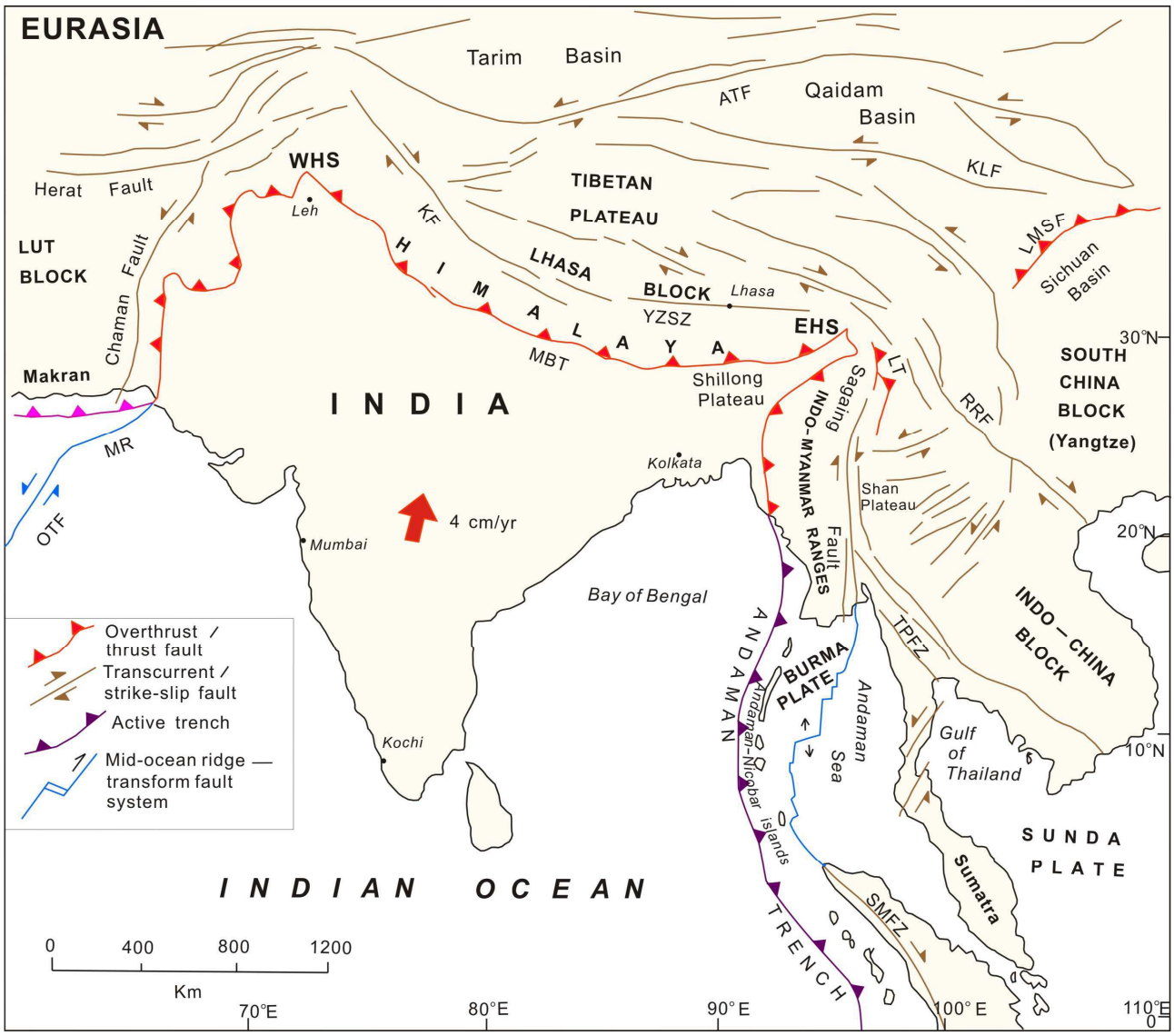

Figure 1. Tectonic map of the peri-Indian region, showing the current plate boundaries and plate distributions, major continental blocks, suture zones, and salient fault systems. Data from: Curray (2005); Morley (2009); Maurin and Rangin (2009). Key to symbols: ATF: Altyn Tagh Fault; EHS: Eastern Himalaya Syntaxis; KF: Karakorum Fault; KLF: Kunlun Fault; LMSF: Longmen Shan Fault; LT: Lohit Thrust; MR: Murray Ridge; OTF: Owen Transform Fault; RRF: Red River Fault; SMFZ: Sumatran Fault Zone; TPFZ: Three Pagodas Fault Zone; WHS: Western Himalaya Syntaxis; YZSZ: Yarlung-Zangbo suture zone.

prism development and related ophiolite emplacement mechanisms.

In this paper, we document the internal structure of the Nagaland-Manipur Hill ophiolite belt in the central part of the Burma plate, present petrographic and petrological data on both the ophiolitic rocks and the blueschist assemblages spatially associated with them, and present a new tectonic model for the evolution and accretion of this ophiolite belt within the Neotethyan realm. This study is the first account of defining the previously described ophiolitic occurrences in the region as part of an ophiolitic mélange and shear zone within a broad accretionary prism complex, which constitutes the Indo-Myanmar Ranges. We show that the Nagaland-Manipur Hill ophiolite belt does not display a coherent ophiolite stratigraphy, but that it rather has all the characteristic features of a subduction channel mélange. In light of the new ophiolite classification scheme of Dilek and Furnes (2011) we classify the Nagaland-Manipur Hill ophiolites as accretionary-type ophiolites.

Regional Geology

The regional geology of the Indo-Myanmar Ranges includes seven major tectonostratigraphic units (1) a Triassic-Jurassic accretionary complex with meta-sedimentary rocks with thrust wedges of serpentinites and volcanic rocks; (2) a mid-Cretaceous –early Tertiary volcanic arc sequence (Wuntho-Popa arc) of Central Myanmar; (3) latest Cretaceous to early Tertiary felsic (granitoid) and mafic (diorite) plutons; (4) fault bounded slivers of Late Cretaceous–Eocene ophiolites and ophiolitic melanges of Neotethyan origin; (5) low-P / low-T and high-P /low-T metamorphic assemblages; (6) Jurassic – Eocene deep sea pelagic sedimentary rocks, and (7) Late Cretaceous – Eocene accretionary complex with meta-sedimentary rocks and blueschist assemblages. These tectono-stratigraphic units were brought together and juxtaposed as a result of complex interplay of plate boundary interactions and associated

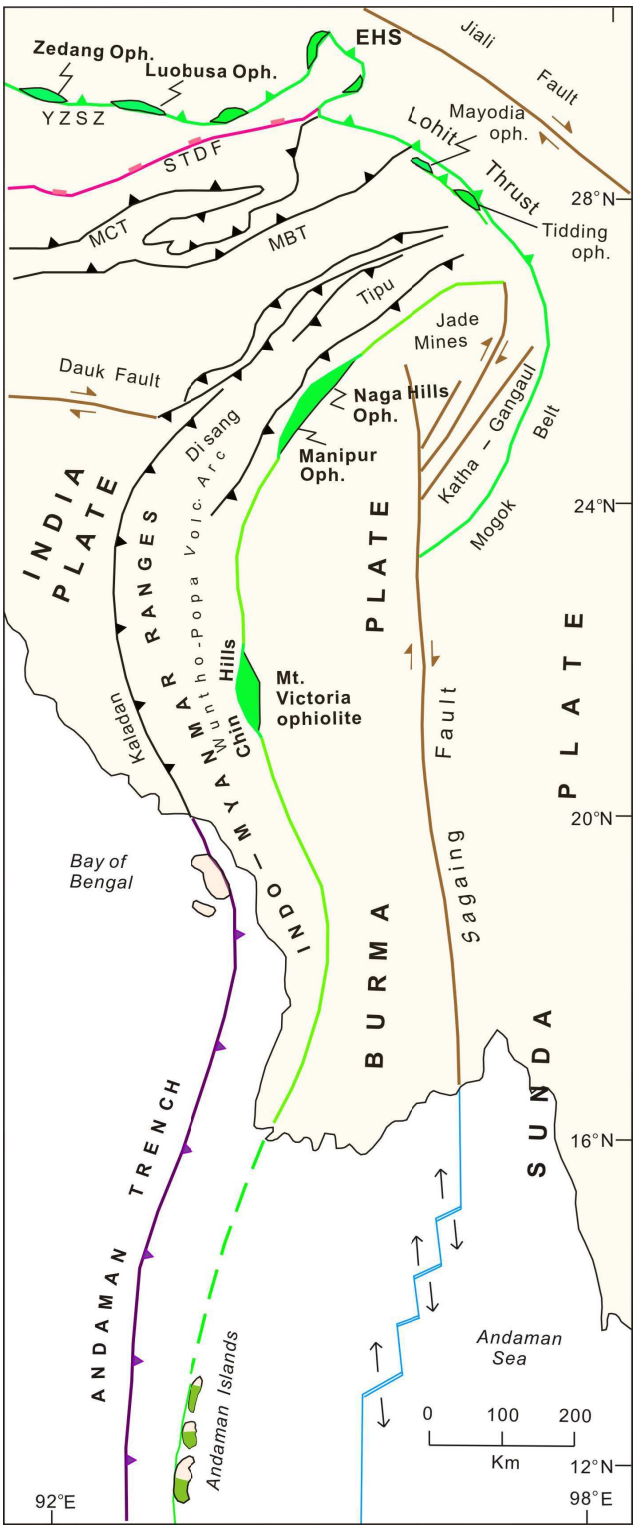

Figure 2: Simplified tectonic map of the eastern margin of India and the plate boundary interactions between India, Burma and Sunda. Also shown are the Eastern Syntaxis of Himalaya (EHS), the eastern end of the Yarlung-Zangbo suture zone (YZSZ), the seafloor spreading system in the Andaman backarc basin, and the Nagaland–Manipur Hills ophiolite belt as the southern continuation of the YZSZ. Key to symbols: EHS: Eastern Himalaya Syntaxis; MBT: Main Boundary Thrust; MCT: Main Central Thrust; STDF: South Tibetan Detachment Fault; YZSZ: Yarlung-Zangbo suture zone. Data from: Ghose et al. (2014).

deformation-metamorphic events within a broad zone of convergence, involving the India and Burma plates (Fig. 2) and the intervening Neotethyan oceanic lithosphere between them.

Tectonic processes associated with two major subduction zone events have played a significant role in the tectonic evolution of the region: (1) Neotethyan oceanic lithosphere subduction beneath an island arc system (Wuntho-Popa arc), and (2) Indian Ocean lithosphere subduction beneath the Burma plate (Bhattacharjee, 1991; Mitchell, 1993; Curray, 2005; Maurin and Rangin, 2009). Recently obtained SHRIMP U–Pb zircon date of 146.5 ± 3.4 Ma from the jadeitites of the *Jade Mines* area to the northeast of the Nagaland-Manipur Hills ophiolitic mélange zone (Fig. 2) indicates that the onset of first subduction event within Neotethys might have taken place as early as in the latest Jurassic (Shi et al., 2008).The eastern margin of India has been underplating the Burma plate since the closure of Neotethys in the early Cenozoic, and the current plate boundary is marked by a broad zone of dextral, lithospheric-scale transpressional deformation (Maurin and Rangin, 2009). Subduction zone tectonic evolution of the region throughout the Mesozoic is supported by the occurrence of eclogitic and blueschist rock assemblages within the accretionary wedge complexes.

Late Mesozoic ophiolitic rocks occur in two ~N-S-trending, sub-parallel belts along the eastern margin of India (Sengupta et al., 1990). The eastern belt going through central Burma, Sumatra and Java coincides with a high-gravity anomaly, caused by thick slab(s) of mafic-ultramafic rocks at depth; the western belt going through the Nagaland-Manipur Hills region in eastern India, western Burma and the Andaman Sea includes rootless bodies of mafic-ultramafic rocks within a flysch complex, which is represented by a negative gravity anomaly zone (Sengupta et al., 1990). The western belt exposures in NE India occur as a NNE-SSW trending, discontinuous curvilinear belt for about 200 km from the northeast in Nagaland to the south-west in Manipur Hill in the Indo-Myanmar Ranges (Fig. 2). Extensive geological mapping by the Geological Survey of India in the Nagaland-Manipur Hill area (Chattopadhyaya et al., 1983; Acharaya, 2010) has revealed the occurrence of discrete ophiolite complexes in a ~10-km-wide ophiolitic mélange zone (Fig. 2). These dismembered ophiolites are tectonically intercalated to the east with a thick sequence of low-grade meta-sedimentary rocks, known as the Naga metamorphic unit, which includes the Saramati and Nimi Formations (Chattopadhyaya et al., 1983; Ghose et al., 2014). The inferred age of the Saramati Formation isProterozoic; the age of the Nimi Formation has been interpreted as the Maastrichtian based on fossil evidence and biostratigraphy (Acharya, 2006).

The ophiolitic mélange belt is bounded on the west by a thick, folded sequence of very low-grade meta-sedimentary rocks (slate, phyllite, siltstone, and fine-grained quartz-arenite). These meta-sedimentary rocks make up the Disang Formation (Fig. 3), which includes the Barail and Tipam Groups unconformably resting on them. Pelagic sedimentary rocks (chert, claystone and limestone) of the Salumi Formation overlie the ophiolitic mafic-ultramafic rock units, and are in turn unconformably overlain by an Eocene-Miocene sedimentary sequence (Figs. 3 and 4; Jopi and/or Phokphur Formations; Acharyya, 2007) with abundant ophiolite-derived material. A series of NNE-SSW to NE-SW-oriented, sub-parallel thrust sheets traverse both along the contacts and within each of these tectono-stratigraphic units. Tectonic slivers of the Naga metamorphic rock assemblages, bounded by major shear zones, also occur within the ophiolitic mélange zone.

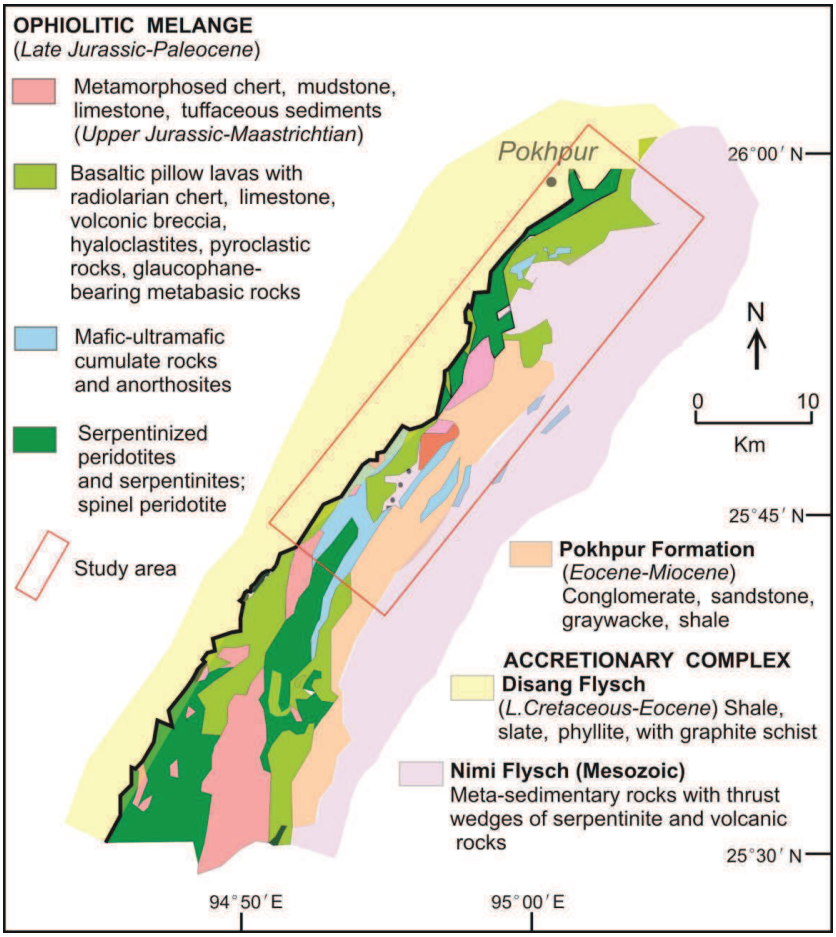

Figure 3: Geological map of the northern part of the Naga Hills ophiolitic mélange zone near Pohkpur - Pungro. Red box denotes the study area depicted in Figure 4.

Nagaland-Manipur Hill ophiolitic mélange zone

The NE-SW-trending and nearly 200-km-long belt of ophiolitic rocks and an ophiolitic mélange zone is known in the literature as the Nagaland-Manipur Hill Ophiolites (NMHO).The Nagaland-Manipur Hill Ophiolite belt comprises: (1) extensively tectonized and partially serpentinized upper mantle peridotites, composed of dunite, harzburgite and minor lherzolite. Chromitites in the harzburgitic peridotites in the Manipur Hill area appear to have boninitic and mixed boninitic – island arc tholeiitic (IAT) affinities (Pal, 2014); (2) ultramafic to mafic intrusions consisting of discontinuous pods of dunite, wehrlite, gabbro, norite, plagiogranite and pyroxenites; (3) mafic to intermediate composition volcanic rocks with MORB-like geochemical signatures that are intercalated with felsic to intermediate composition extrusive rocks (trachyte, andesite, dacite, rhyolite commonly with pyroclastic units). This sequence of mafic to intermediate volcanic rocks are overlain by pyroclastic deposits; (4) minor dolerite dikes that are intrusive into the mafic-ultramafic rocks; (5) agglomerates and tuffaceous rocks; (6) pelagic sedimentary rocks, mainly pale green to dark reddish brown cherts, tectonically interleaved with mafic and ultramafic rocks. These sedimentary rocks collectively make up the Salumi Formation. Sinha et al. (1982) and Chattopadhyay et al. (1983) have reported the occurrence of marine invertebrate, radiolarian, coccolithosphporid and related nano-plankton fossils in these sedimentary units of the Salumi Formation. All these ophiolitic units are bounded by west-directed thrust faults, which are commonly associated with sheared serpentinite with thicknesses ranging from several meters to 100s of meters.

Eclogites and blueschist-bearing rocks are ubiquitous within the mélange zone and commonly occur as tectonic slices and lenses interleaved with basaltic and ultramafic rock units. These high-P rock units have bulk rock chemistry similar to that of abyssal tholeiites and to the high-Ti basaltic volcanic rocks in the ophiolitic mélange zone (Agrawal and Ghose, 1986; Ghose et al., 1986; Chatterjee and Ghose, 2010). Eclogite lenses are surrounded by layers of garnet-blueschist, glaucophane-schist and greenschist, and consist mainly of barroisite, epidote, chlorite and phengite as well as the typical garnet–omphacite association (Chatterjee and Ghose, 2010). Glaucophane growth along the rims of barroisite is widespread. Preferred alignment of amphibole ± phengite ± chlorite, and the alternating amphibole-rich and epidote-rich layers collectively define the weak foliation planes in these eclogitic rocks. The P–T estimates of the Nagaland eclogites indicate a clockwise P–T path with prograde metamorphism beginning at 1.3 GPa and 525° C, and peaking at 1.7–2.0 GPa and 580º–610ºC (Chatterjee and Ghose, 2010). The occurrence of late albite veins and amphibole, actinolite and epidote rims around the garnet and omphacite suggests that these eclogites were retrogressed to 1.1 GPa and 540ºC. Eclogitic lenses surrounded by serpentinized ultramafic rocks display actinolite rims around them, suggesting advanced fluid – rock interaction during their low-temperature retrogression as also documented from other subduction-zone mélanges (Bebout and Barton, 2002; Errico et al., 2013). Some of the late-stage albite veins are commonly undeformed and crosscut weakly foliated to unfoliated hosts, indicating their post-kinematic origin in a relatively brittle conditions. Numerical thermal modeling of these P-T conditions suggests that the Nagaland eclogites may have formed near the top of the subducting Neotethyan oceanic lithosphere, with estimated fast convergence rates of 100 to 55 km/my (Chatterjee and Ghose, 2010).

The Nagaland-Manipur Hill ophiolitic mélange zone is bounded by narrow strips of sheared and mylonitic serpentinite, separating it from the Disang meta-sedimentary rocks to the west and the Naga metamorphic assemblage to the east (Acharya, 2010; Fig.2). The Disang Formation in the west includes shale, sandstone, slate, phyllite, sub-greywacke with thin intercalations of calcareous shale and carbonate rocks, and all these lithologies display a well-developed, NNE-SSW-striking foliation with variable dips. Adjacent to the sheared serpentinite boundary the Disang rock units are penetratively cleaved, sheared and ductilely deformed, whereas away from it the rocks show progressively less deformation effects and exhibit well defined sedimentary features, such as bedding, graded bedding and load-cast structures. The 40-50-m-thick sheared serpentinite zone between the ophiolitic mélange zone and the Disang Formation comprises fragments of harzburgite, dunite, gabbro-anorthosite, and

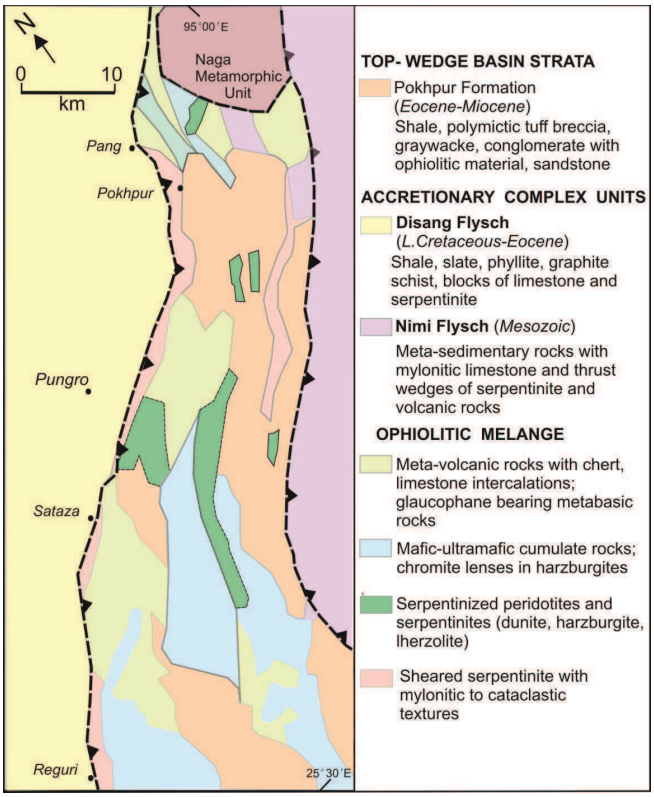

Figure 4: Detailed geological map, showing the internal structure of the ophiolitic mélange zone and the distribution of ophiolitic units, blueschist–bearing rocks. The contacts between these units are mostly tectonic (thrust and oblique-slip faults). Coarse-grained sedimentary rocks of the Eocene – Miocene Pohkpur Formation locally rest on the mélange units uncomformably. The Nimi and Disang Flysch formations tectonically overlie and underlie, respectively, the ophiolitic mélange zone along west-directed thrust faults (modified after Acharyya, 2010).

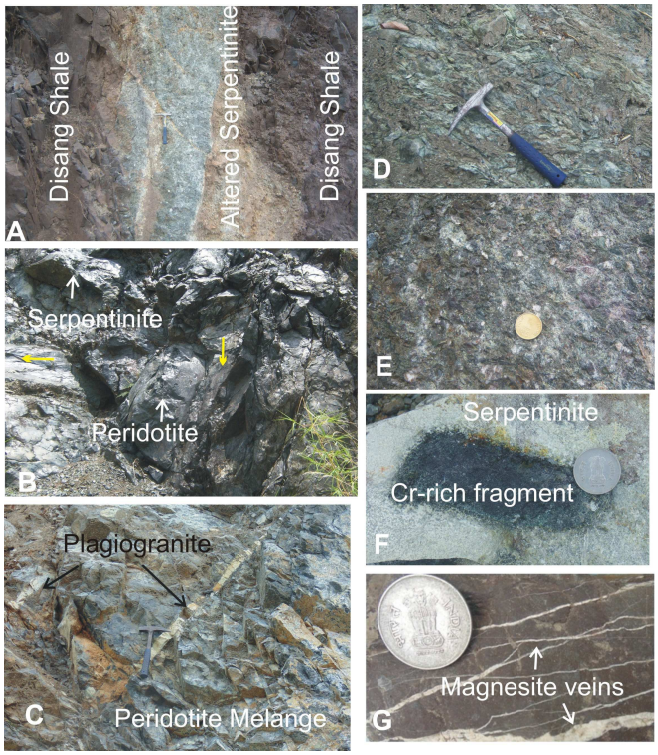

Figure 5: Outcrop photos of various unots in the ophiolitic mélange zone. A- Serpentinite – shale tectonic intercalation in the Disang Flysch near Pohkpur. Hammer for scale. B- Lherzolitic peridotite boudins in a cataclastically deformed and highly sheared serpentinite. Slickenside lineation orientations (shown by yellow arrows) in the serpentinite vary significantly. Width of the image is ~8 meters. Location: 1 km SW of Luthur village, along the Pungro-Salumi Road. C- Thin dikelets and veins of plagiogranite crosscutting the sheared serpentinite matrix in the mélange. Location: 1 km SW of Luthur Village. D- Reworked, angular clasts of serpentinite in a very fine-grained, serpentinite-shale matrix. Note the strong deformation fabric defined by the extreme flattening in coarser clasts and a schistosity in the inter-clast matrix. Location: About 500 m southwest of Luthur village. E- Volcaniclastic rocks in the Pokhpur Formation, overlying the mélange units. Location: 1 km east of Pokhpur Village. F- Chromite lens in serpentinized peridotite. Location: About 500 m southwest of Luthur Village. G- Networks of magnesite veinlets in a chromitite band. Location: About 750 m southwest of Luthur Village.

mafic volcanic rocks in a finely pulverized matrix composed mainly of serpentinite. Lenses and pods of highly altered and deformed ultramafic rocks are tectonically intercalated with steeply dipping Disang Shales along high-angle faults within this sheared serpentinite zone (Fig. 5A). Thin veinlets of dark grey, ultra-fine pseudotachylites are common in the matrix of the sheared serpentinite zone, crosscutting the early generation fold structures (F1 folds) (Fig. 5B).

In the Pungro-Salumi-Penkim section of the ophiolitic mélange belt, the sheared serpentinite zone encompasses tectonic slices of peridotites, cumulates and volcanic rocks within the Naga metamorphic assemblage (Saramati Formation) to the east. A narrow strip of this sheared serpentinite with very thin intercalations of mafic meta-volcanic rocks also occurs along the contact between the Naga metamorphic assemblage and the Disang Shale (Chattopadyaya et al., 1983). About 1 km SW of Luthur village, along the Pungro-Salumi Road section, the sheared serpentinite zone shows angular and phacoidal shaped fragments of various ophiolitic units (mostly peridotites) tectonically intermixed, along brittle-ductile shear zones, with very fine-grained cataclastic material, forming the inter-clast groundmass (Fig.6). The main rock types observed in this melange zone are sheared and boudinaged serpentinized dunite, lherzolite, pyroxenite, gabbro (locally anorthositic), chromitites, and blueschist rocks. None of these lithologies possesses any appreciable along-strike continuity in the outcrop. These NNE-SSW-oriented lithological units show highly variable but commonly steep dip angles, and down-dip stretching lineations. A series of parallel to sub-parallel fault zones, exhibiting variably oriented slickensides and ultrafine cataclasites and pseudotachylite veins characterize this melange zone. Fine-grained serpentinized dunites show strong foliation fabric (Fig.5D). Towards the easternmost part of the mélange zone both the mélange matrix and the blocks and fragments are crosscut by fine-to medium-grained, several meter thick, plagiogranite intrusions, which continue laterally for few 10's of meters (Fig. 5C). The intensely brecciated zone also includes very thin (few 10s of centimetres) layers of graphite-schist. Lenses of chromite fragments are rare, but when present they are laced with a fine network of white magnesite veinlets (Fig. 5G).

Figure 6: Field photograph showing the serpentinite mélange 1 km SW of Luthur village along Pungro-Salumi road section showing intensely intermixed and brecciated rock components due to polyphase fracturing and faulting (brittle deformation) events.

Petrology and Mineral Chemistry

We carried out detailed petrological and electron microprobe studies of different mafic-ultramafic units in the ophiolitic melange zone in order to quantify their mineralogy and mineral chemistry. Minerals were analyzed by wavelength-dispersive spectrometry (WDS) using CAMECA SX100 electron microprobe instrument at National Centre for Excellence in Geoscience Research, Geological Survey of India, Bangalore. These analyses were carried out at an accelerating potential of 15kV and 5-20 nA using 1 to 5 mm diameter electron beam depending on the nature of the mineral. Natural and synthetic standards were used.

Serpentinized dunite

This is the most abundant rock in the mélange zone and occurs as either dark grey to greenish grey massive rock or dark green, highly boudinaged and sheared rock with penetrative schistosity (Fig. 5D). In thin section, the massive dunite exhibits a mesh texture with relict granular olivine grains and local specs of spinels. The sheared dunite is almost entirely made of serpentine minerals showing a ribbon texture and rarely with asbestiform streaks and lenses. Disseminated spinels locally constitute thin layers in the rock (Fig. 7A). Representative mineral chemistry of the constituent minerals in the sheared dunite is presented in Table 1. MgO makes up nearly 40 wt.% of the analyzed dunite. Spinels in dunite are of two types (1) microcrystic (< 1mm size), subhedral to sub-rounded Cr-spinels with a distinct rim of magnetite (Fig. 7A), and (2) large anhedral, mesocrystic (>1mm, up to 10 mm) grains with a poly-crystalline texture (Fig. 7B) and with a uniform core-rim chemistry. The spinel microcrysts are Al-bearing with average chrome content of about 50 wt.%. The poly-crystalline spinels contain on average 63 wt.% Cr_2O_3 and a much lower content of alumina (~ 7 wt.%).

Harzburgitic peridotite

The harzburgitic peridotite contains granular grains of orthopyroxene, olivine, clinopyroxene and minor spinel, collectively displaying an interlocking mesh texture (Fig. 8). Coarse grains of fresh, feebly pleochroic to non-pleochroic orthopyroxenes occur as a distinct cumulate phase, commonly showing strain shadows. Granular, subhedral olivine is fractured extensively with ubiquitous serpentinization along the fracture crevices. Colourless to pale green clinopyroxene grains (diopside) show bent twin lamellae and undulose extinction. Serpentine forms alteration rims along the grain boundaries of orthopyroxenes with clinopyroxene and those of pyroxenes with olivine (Fig. 8). Spinel occur as: (i) small size, discrete grains disseminated uniformly in the rock, (ii) embayed crystals forming inclusions within the clinopyroxene (Fig. 8D), (iii) trails along spinel-cpx grain boundaries, and (iv) thin, healed fracture trails in pyroxenes. A few grains of sulfides, mainly pyrrhotite, are also observed in the harzburgites.

Electron microprobe analyses of the constituent minerals (Table 2) suggest that the clinopyroxene and orthopyroxene are represented by diopside and hypersthene, respectively. Among the spinels, those occurring in paragenesis (i) and (ii) are distinctly Mg-Cr-Fe bearing aluminous spinels, whereas those occurring in paragenesis (iii) are chromiferous magnetite, and those occurring within fractures

Table 1. Mineralogy and summary petrography of representative rock samples from the Nagaland-Manipur Hill mélange zone

Sl. No.	Sample No.	Rock type	Mineralogy	Brief petrographic description
1	F/NHO/1	Serpentinized dunite	Serpentine, Cr-spinel with relict olivine	Exhibits a schistose texture with extensively flattened serpentine grains; spinel is disseminated ubiquitously.
2	F/NHO/2	Peridotite	Clinopyroxene (Cpx), orthopyroxene (Opx), olivine, spinels, magnetite, serpentine, and chlorite	Exhibits an interlocking mesh texture. Coarse grains of Opx, Cpx, and olivine show strain shadows. Spinels are disseminated. Serpentine and chlorite are the main alteration products.
3	F/NHO/3	Websterite	Opx, Cpx, serpentine, chlorite and spinels	Exhibits a cumulus texture with coarse-grained Opx cumulates surrounded by Cpx grains.
4	F/NHO/4	Glaucophane schist	Chloritised actinolite, glaucophane, albite, and epidote	Schistose texture with fibrous chlorite, prismatic glaucophane, acicular chloritized actinolite, and stretched aggregates of albite and quartz.
5	F/NHO/7	Matrix in the melange zone	Glaucophane, chlorite, epidote, plagioclase (labradorite), albite, magnetite, ilmenite and chromite	Ultra fine-grained mineral fragments caught up in an ultra-fine pseudotachylitic groundmass.

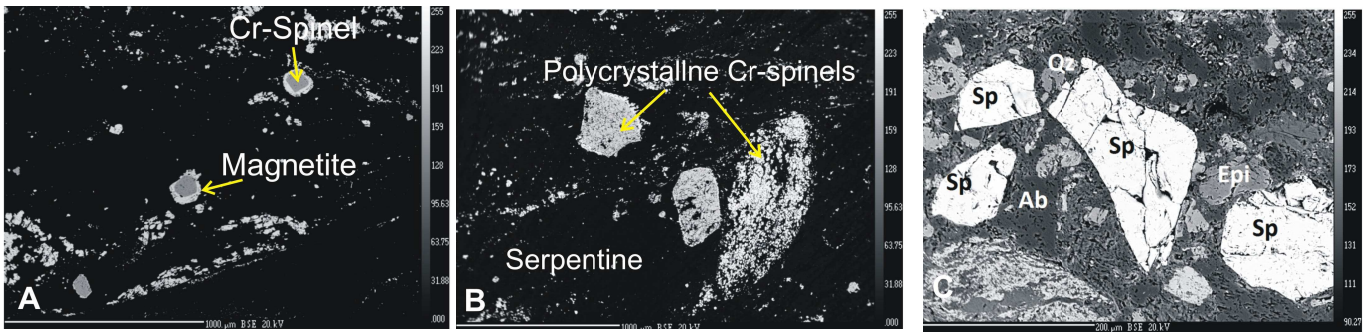

Figure 7: Back-scattered electron microscopy (BSE) images of different types of spinels from various units in the ophiolitic mélange zone. A-Square shaped microcrystic grains of Al-bearing Cr-spinel with a distinct rim of Cr-bearing magnetite in a serpentinized dunite peridotite. Dark area in the image largely represents serpentine minerals. B-Polycrystalline aggregates of Cr-spinels. Such grains do not show any perceptible difference between the core and rim chemistry. C-Angular disintegrated clusters of Cr-spinel grains, together with albite, epidote and quartz in a brecciated rock. These spinels are interpreted to have been disintegrated from a chromitite rock.

(paragenesis -iv) are distinctly magnetites. Pyroxene grains are mostly altered to Fe-bearing serpentinites.

Websterite

The Websterite with clinopyroxene and orthopyroxene grains shows a cumulus texture with coarser plates of cumulus orthopyroxene (Fig. 8A) generally surrounded by inter-cumulus clinopyroxene (Fig. 8B). Serpentine occurs either as a fracture-filling material or as an alteration product along the grain boundaries of pyroxenes. Electron microprobe analyses (Table 3) show that the clinopyroxenes are composed of homogeneous diopside with no variations in their core and rim compositions. The orthopyroxene in websterite has chemical composition similar to that of hypersthene. Similar to the clinopyroxenes, the core and the rim compositions of the orthopyroxene grains are nearly the same and do not show any distinct chemical variation.

Blueschist facies rocks

Outcrops with blueschist assemblages occur as pale bluish grey, thin streaks or extensively flattened schistose units within dark grey, fine-size, matrix-rich portions with apparently no boundary between schistose rock and the surrounding groundmass of the mélange zone. Blueschist assemblages comprise fibrous chlorite, prismatic glaucophane, acicular chloritised actinolite, and stretched aggregates of albite and quartz. The majority of the glaucophane analyses (Table 4) plot in its designate field of Na vs Si binary diagram (Fig. 9), but few of the analyses show transition to winchite. Chlorite is an iron-rich, Mg-poor variety.

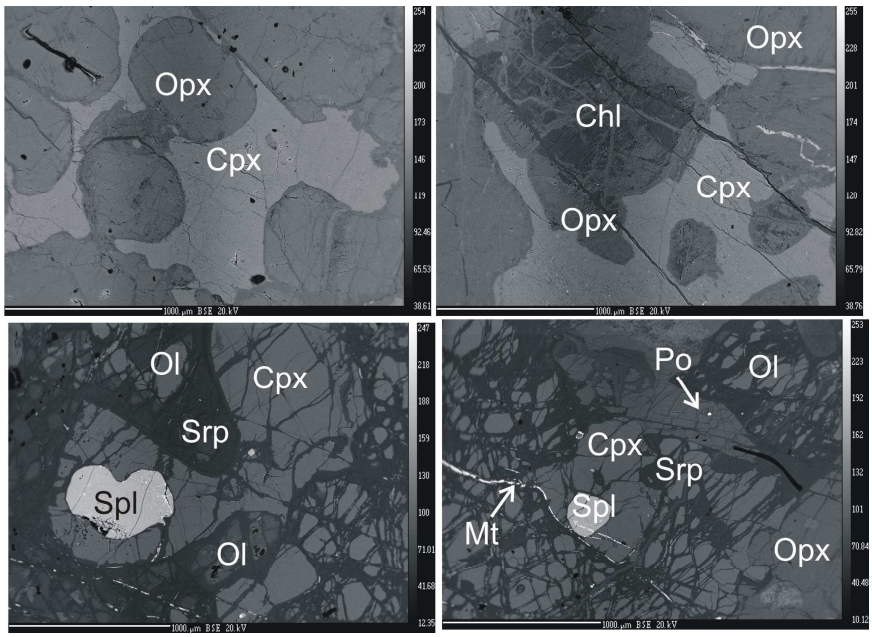

Figure 8: Back-scattered electron microscopy (BSEM) images showing different mineral phases in representative wehrlite (A and B) and lherzolite (C and D) samples from the ophiolitic mélange zone. A- Cumulate texture in wehrlite with well-rounded and partially disintegrated orthopyroxene grains surrounded by inter-cumulus clinopyroxene. B - Same rock as in A. Cores of the orthopyroxene grains are altered to chlorite and crosscut by fractures that are filled with serpentine minerals. C- Intensely fractured lherzolite with large clinopyroxene (Cpx) grains containing large Cr-spinel inclusions. Subhedral, oval-shaped olivine (Ol) occurs adjacent to the Cpx grains. Fractures and fracture networks in all mineral grains are healed by fine serpentine mass. D- Same rocks as in A. Thin magnetite (Mt) veinlets and disseminated pyrrhotite (Po) grains occur in all minerals.

Glaucophane bearing mafic rocks

Clasts of epidote-chlorite-plagioclase-glaucophane rock occurs either as (i) dismembered and disintegrated mineral clusters (Fig. 10A), or (ii) fragments caught-up in a dark-grey, opaque pseudotachylite groundmass (Fig. 10B). The rock shows a granoblastic, recrystallization texture with triple junction boundaries among the constituent minerals. Epidotes in such clasts display two distinct phases of development: the earlier phase epidote is made of anhedral to subhedral grains, showing a patchy development of glaucophane along the margins of epidote, whereas the late phase epidote is subhedral to euhedral, and largely free of glaucophane. The epidote-glaucophane assemblage, also reported from different parts of the Nagaland ophiolites by Chatterjee and Ghose (2010), is interpreted to represent prograde

Table 2. Mineral chemistry data of representative dunite samples from the Nagaland-Manipur Hill ophiolitic mélange zone

	Spinels												Polycrystalline Chromites			Serpentine		
	1C	1R	2C	2R	3C	3R	4C	4R	5C	5R	6C	6R	24	29	30	7	8	14
SiO_2	0.06	0.16	0.08	0.07	0.07	0.08	0.09	0.56	0.06	0.15	0.07	0.87	0.07	0.03	0.07	42.8	42.91	43.1
TiO_2	0.15	0	0.15	0.04	0.15	0	0.15	0.03	0.18	0.02	0.14	0.06	0.07	0.07	0.05	0.02	0.01	0.02
Al_2O_3	10.77	0	10.09	0	10.91	0	11.17	0.05	11.15	0	11.27	2.07	5.62	9.32	9.39	0.62	0.07	0.04
Cr_2O_3	49.52	0.63	49.12	0.15	47.38	0.01	50.52	1.61	49.72	0.03	47.25	11.14	65.24	60.09	59.8	0.07	0.02	0.04
FeO^T	29.62	90.22	29.99	89.91	30.79	90.57	28.8	86.81	29.11	88.42	31.69	71.21	15.28	18.6	19.26	2.57	1.06	2.17
MnO	0.4	0.17	0.48	0	0.41	0.21	0.42	0.16	0.42	0.16	0.38	0.47	0.29	0.36	0.31	0.05	0.03	0.03
MgO	6.98	0.26	6.49	0.33	6.46	0.21	7.26	0.32	7.24	0.26	5.63	1.81	10.93	9.39	8.87	38.09	40.45	39.36
CaO	0.02	0	0.02	0	0	0.01	0.01	0.09	0.04	0.04	0.05	0.2	0.06	0.01	0.04	0.01	0.03	0.08
Total	**97.56**	**91.48**	**96.47**	**90.5**	**96.22**	**91.15**	**98.47**	**89.7**	**97.94**	**89.1**	**96.5**	**87.88**	**97.62**	**97.92**	**97.83**	**84.27**	**84.63**	**85.06**
Si	0.00	0.01	0.00	0.00	0.00	0.00	0.00	0.02	0.00	0.01	0.00	0.03						
Al	0.43	0.00	0.41	0.00	0.45	0.00	0.45	0.00	0.45	0.00	0.46	0.10						
Cr	1.34	0.02	1.35	0.00	1.30	0.00	1.35	0.05	1.34	0.00	1.30	0.35						
Fe^{+3}	0.22	1.97	0.22	1.99	0.24	2.00	0.19	1.91	0.20	1.99	0.22	1.48						
Fe^{+2}	0.63	0.98	0.65	0.98	0.65	0.97	0.62	0.98	0.62	0.98	0.70	0.90						
Mn	0.01	0.01	0.01	0.00	0.01	0.01	0.01	0.01	0.01	0.01	0.01	0.02						
Mg	0.36	0.02	0.34	0.02	0.33	0.01	0.37	0.02	0.37	0.02	0.29	0.11						
Total	**3.00**	**3.00**	**3.00**	**3.00**	**3.00**	**3.00**	**3.00**	**3.00**	**3.00**	**3.00**	**3.00**	**3.00**						
Mol. per cent end-members																		
Spinel	20.62	0.00	19.61	0.00	21.08	0.00	21.26	0.08	21.25	0.00	21.90	3.57						
Mg.Ulv.Spi	0.55	0.00	0.56	0.12	0.55	0.00	0.55	0.09	0.66	0.06	0.52	0.20						
Mn.Ulv.Spi	0.00	0.00	0.00	0.00	0.00	0.00	0.00	0.00	0.00	0.00	0.00	0.00						
Ulvospinel	0.00	0.00	0.00	0.00	0.00	0.00	0.00	0.00	0.00	0.00	0.00	0.00						
Mn.Chromite	1.10	0.38	1.34	0.00	1.14	0.01	1.15	0.37	1.15	0.03	1.06	1.17						
Mg.Chromite	12.45	0.28	11.55	0.16	9.75	0.00	12.96	1.09	12.77	0.00	5.08	4.06						
Chromite	50.06	0.00	51.15	0.00	50.52	0.00	50.39	0.27	49.63	0.00	55.46	7.66						
Magnetite	15.22	99.34	15.78	99.72	16.95	99.99	13.70	98.11	14.54	99.91	15.97	83.34						

C = Analysis of the core M = Analysis of the rim

Table 3. Mineral chemistry data of representative peridotite samples from the Nagaland-Manipur Hill ophiolitic mélange zone

	Clinopyroxene										Orthopyroxene		Olivine			
	1	2	3	4	5	6	7	8	9	10	1	2	1	2	3	4
SiO_2	52.15	51.51	51.3	51.29	51.39	51.58	50.8	50.92	51.08	51.33	54.02	54.03	38.48	38.83	38.85	39.03
TiO_2	0.18	0.33	0.31	0.34	0.27	0.15	0.27	0.26	0.21	0.16	0.04	0.1	0	0	0.01	0.03
Al_2O_3	2.24	3.71	3.76	3.92	3.44	2.88	3.59	3.74	3.34	2.98	2.73	2.83	0	0	0	0
Cr_2O_3	0.25	0.52	0.57	0.46	0.47	0.48	0.42	0.57	0.48	0.26	0.25	0.21	0	0	0	0.02
FeO	4.83	5.71	5.54	5.79	5.5	4.82	5.14	5.68	4.93	5.25	13.24	13.27	20.93	20.71	20.33	20.38
MnO	0.12	0.19	0.11	0.14	0.23	0.09	0.19	0.2	0.09	0.12	0.35	0.25	0.25	0.22	0.28	0.43
CaO	23.56	22.69	23.3	22.5	23.04	23.54	23.22	22.1	23.53	23.01	0.67	0.83	0.01	0	0.02	-0.01
MgO	15.7	15.44	15.2	14.97	15.72	15.7	15.43	15.36	15.59	15.8	28.75	28.52	40.73	40.6	39.97	40.41
K_2O	0	0	0	0	0	0	0.01	0	0.01	0.02	0.02	0	0	0	0	0
Na_2O	0.21	0.22	0.25	0.25	0.2	0.18	0.18	0.21	0.22	0.2	0.02	0	0	0	0.03	0.02
Total	**99.24**	**100.32**	**100.34**	**99.66**	**100.26**	**99.44**	**99.25**	**99.03**	**99.49**	**99.13**	**100.08**	**100.03**	**100.4**	**100.37**	**99.48**	**100.32**

	Spinel					Magnetite			Serpentine								
	1	2	3	4	5	1	2	3	1	2	3	4	5	6	7	8	9
SiO_2	0.05	0.03	0	0.05	0.06	0.04	0	0.08	41.25	42.64	38.52	40.6	39.27	41.18	39.37	40.39	37.65
TiO_2	0.58	0.47	0.35	0.3	0.25	2.75	3.57	3.39	0.01	0.02	0.25	0.03	0.03	0.02	0.13	0.1	0.02
Al_2O_3	31.96	33.37	34.72	33.33	34.2	3.95	2.7	3.36	2.39	1.11	5.08	1.39	4.41	1.19	1.62	1.59	7.56
Cr_2O_3	19.48	19.17	18.78	19.39	18.81	15.69	13.89	14.3	0.04	0	0.28	0.01	0.01	0.02	0.55	0.47	0
FeO	37.83	36.46	34.78	37.86	37.44	68.26	71.78	69.86	17.77	6.78	18.43	10.26	13.56	11.37	8.9	9.49	12.77
MnO	0.35	0.27	0.19	0.19	0.34	0.43	0.24	0.31	0.18	0.05	0.24	0.04	0.15	0.13	0.12	0.11	0.14
CaO	0	0.06	0.05	0	0.08	0.04	0.01	0.03	0.37	0.12	0.55	0.13	0.17	0.12	0.14	0.05	0.24
MgO	8.27	8.38	9	8.08	7.96	1.77	1.55	1.75	26.21	36.05	23.3	33.64	28.47	31	34.83	35.21	27.94
K_2O	0.02	0	0.01	0	0	0	0	0	0.05	0.02	0.05	0.02	0.04	0.01	0.02	0	0.03
Na_2O	0.01	0	0	0.03	0	0	0	0	0.08	0.01	0.05	0.06	0.02	0.02	0.01	0	0.04
Total	**98.55**	**98.22**	**97.9**	**99.22**	**99.14**	**92.94**	**93.8**	**93.08**	**88.36**	**86.8**	**86.76**	**86.19**	**86.14**	**85.05**	**85.69**	**87.41**	**86.39**

Table 4. Mineral chemistry data of representative websterite samples from the Nagaland-Manipur Hill ophiolitic mélange zone

Clinopyroxene

	1 C	1 M	2 C	2 M (i)	2 M (ii)	3C	3 M (i)	3 M(ii)	4 C	4 M	5 C	5 M	6 C	6 M	7 C	7 M
SiO_2	53.23	53.23	53.69	52.16	53.1	53.58	52.82	53.55	52.41	52.39	52.25	52.87	52.67	52.09	53.43	53.4
TiO_2	0.07	0.05	0.05	0.08	0.08	0.06	0.04	0.07	0.07	0.11	0.13	0.09	0.16	0.15	0.08	0.07
Al_2O_3	1.95	0.99	1.54	1.64	1.52	1.4	0.82	1.37	1.74	1.61	2	1.52	1.71	1.37	1.29	1.52
Cr_2O_3	0.64	0.33	0.64	0.58	0.6	0.66	0.36	0.58	0.4	0.41	0.48	0.42	0.41	0.37	0.61	0.43
FeO	4.03	3.89	4.58	4.65	4.42	4.71	4.08	4.77	4.84	4.56	4.82	4.96	4.41	4.61	4.28	4.86
MnO	0.02	0.14	0.03	0.08	0.2	0.16	0.13	0.17	0.15	0.19	0.17	0.07	0.22	0.09	0.17	0.12
MgO	18.04	16.52	18.29	16.82	16.6	16.95	16.63	17.45	17.69	16.38	16.73	16.75	16.76	16.82	17.37	17.29
CaO	19.88	23.76	21.25	22.57	22.62	22.17	23.87	21.95	20.84	22.82	21.74	22.13	22.21	21.84	21.99	22.26
K_2O	0.04	0.01	0.02	0.01	0.01	0	0.01	0.01	0.04	0	0.01	0	0	0	0	0.02
Na_2O	0.31	0.13	0.19	0.18	0.27	0.26	0.16	0.25	0.34	0.24	0.27	0.34	0.25	0.32	0.21	0.22
Total	**98.21**	**99.05**	**100.27**	**98.76**	**99.41**	**99.95**	**98.92**	**100.17**	**98.52**	**98.72**	**98.6**	**99.17**	**98.8**	**97.66**	**99.43**	**100.2**

Orthopyroxene

	1 C	1 M (i)	1 M (ii)	2 C	2 M	3 C	3 M	4 C	4 M	4 M (ii)	5 C	5 M	6 C	6 M
SiO_2	55.9	55.55	54.7	55.06	52.91	54.64	55.23	55.49	51.15	54.9	55.11	54.71	55.41	55.46
TiO_2	0.06	0.03	0.02	0.02	0.03	0.03	0.06	0.01	0.06	0.04	0.01	0.06	0.04	0.04
Al_2O_3	1.03	1.11	1.04	1.08	1.09	1.14	0.8	1.02	1.79	1.07	1.11	1.2	1.13	0.88
Cr_2O_3	0.43	0.32	0.26	0.33	0.3	0.26	0.32	0.27	0.33	0.22	0.26	0.3	0.27	0.37
FeO	10.34	10.37	10.14	10.02	10.61	9.97	10.83	10.82	10.37	11	10.97	11.12	10.45	9.49
MnO	0.21	0.19	0.27	0.2	0.21	0.26	0.29	0.26	0.26	0.26	0.19	0.25	0.21	0.24
MgO	30.83	30.5	30.35	30.72	29.59	29.96	30.55	29.93	27.84	29.6	29.55	29.83	30.51	30.27
CaO	1.45	1.38	1.57	1.59	1.45	2.03	0.97	1.69	3.61	1.04	1.33	1	1.24	2.61
K_2O	0	0	0.02	0.01	0.03	0.01	0.01	0.01	0.02	0.02	0.13	0.01	0.01	-0.01
Na_2O	0	0.02	0.06	0	0.02	0.01	0.02	0.03	0.05	0.04	0.21	0	0.03	0.04
Total	**100.24**	**99.46**	**98.41**	**99.06**	**96.25**	**98.31**	**99.07**	**99.54**	**95.48**	**98.19**	**98.86**	**98.48**	**99.3**	**99.4**

Serpentine

	1	2	3	4	5	6	7
SiO_2	47.86	42.73	42.74	44.12	44.11	43.45	43.04
TiO_2	0.05	0.07	0.03	0.02	0.01	0.04	0.06
Al_2O_3	1.16	1.05	1.34	1.44	1.42	1.47	1.54
Cr_2O_3	0.36	0.36	0.48	0.65	0.4	0.54	0.53
FeO	11.18	13.51	10.51	10.47	12.33	10.3	10.85
MnO	0.36	0.29	0.07	0.18	0.25	0.11	0
MgO	26.07	27.25	30.52	30.21	28.28	32.1	30.9
CaO	4.02	2.05	0.25	2.01	0.95	0.25	0.82
K_2O	0.04	0.02	0.02	0.03	0.03	0.03	0.03
Na_2O	0.02	0.05	0.04	0.08	0.03	0.05	0.03
Total	**91.13**	**87.38**	**85.99**	**89.2**	**87.8**	**88.33**	**87.78**

C= Analysis of the core M = Analysis of the rim

reactions related to eclogite-blueschist facies of metamorphism (representing a reaction Tremolite + Chlorite + Albite = Glaucophane + Epidote + H_2O).

Electron microprobe analyses of the glaucophanes (Table 4) from this assemblage show that these glaucophanes differ in their chemistry from those glaucophanes observed in schistose, glaucophane-bearing rocks; the glaucophane-epidote assemblages are more calcic than the schistose glaucophane rocks. In a Si vs Na (B) plot, which discriminates different fields of alkali amphiboles (Fig. 9), analyses from the both parageneses plot in the glaucophane field, albeit maintaining distinct clusters. The glaucophane from the glaucophane-epidote assemblage compares well with the published glaucophane analyses from other sectors of glaucophane bearing eclogite and blueschist rocks (Fig.9; Chatterjee and Ghose, 2010).

Matrix of the mélange zone

The matrix in the ophiolitic mélange zone is of two types, each of which represents different degrees of grain size reduction in the minerals and rocks. The less deformed, Type-1 matrix is grey to brown in color with sand-size grains cemented in a fine-grained, dark grayish graywacke material (Fig. 11A), whereas the Type-2 matrix is ultra-fine, dark brown to black colored, massive glassy in nature, similar to a pseudotachylitic mass (Fig. 11B). The latter contains mineral and rock fragments of varying sizes. Millimeter to less than half-centimeter size, sub-angular to sub-rounded rock fragments in Type-1 matrix are composed of metachert, phengite-bearing quartzites (Fig. 11C), argillite, serpentinite, plagiogranite, and mafic cumulates (layered gabbros). Most of these rock fragments show embayed grain margins, which may have resulted from their interaction with the ultra-fine pseudotachylitic material. The phengite in phengitic quartzite shows 'mica fish' structures, and recrystallized quartz in the metachert exhibits a strong preferred orientation fabric as an evidence of strong ductile shearing of their protolith is before and during their recrystallization. Mineral fragments of variable shapes and sizes identified in the matrix are made of chromite, quartz, epidote, zoisite and plagioclase. Both the matrix and the mineral/rock fragments are locally crosscut by ubiquitous veins of quartz, chlorite, and albite.

Plagioclase fragments

Tabular plagioclase grains in the matrix are of labradorite to

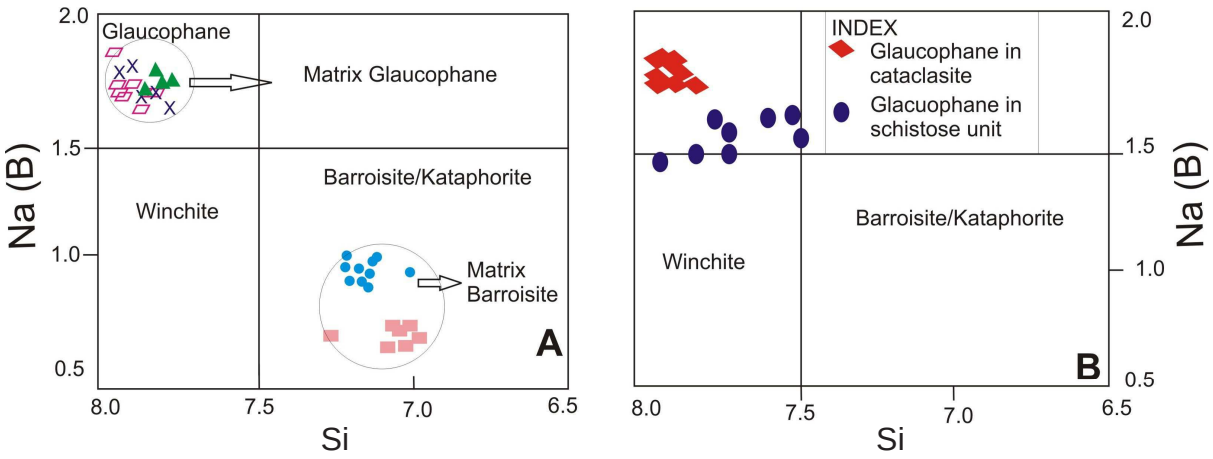

Figure 9: A- Si vs. Na diagram (after Leak et al. 1997) for the amphiboles from the Nagaland section of the ophiolitic mélange zone (*after Chatterjee and Ghose, 2010). Explanation for symbols: Green triangles – glaucophane in garnet; pink open boxes and blue crosses represent glaucophane in matrix in two different samples. Blue filled cirlcles and pink filled boxes represent barroiste from the matrix rock. B- Si vs. Na diagram for the amphiboles from the mélange zone. Glaucophane in the cataclasites are compositionally similar to the glaucophane from the matrix as reported by Chatterjee and Ghose (2010), whereas those glaucuphanes from the schistose serpentinite unit are less sodic than those from the cataclasite matrix.***

bytownite composition. Such coarse fragments of feldspar represent disintegrated grains of precursor cumulate rocks (gabbro/anorthosites).

Cr-spinels in matrix

Cr-spinels are common in Type-1 matrix (Fig. 12), and are of two distinct types: (i) angular, reddish brown Cr-spinels that occur either in rows or in clusters in close proximity to each other; they are, therefore, interpreted as disintegrated grains from chromitite layers. Chemically these chromites are rich in Cr_2O_3 (Table 6; mean = 60.20 wt.% highest among the chrome-spinels analyzed from this unit), and moderately low MgO (mean = 10.36 wt.%) and FeO (~10 wt.%). (ii) subangular to sub-rounded, dark grey-black Cr-spinels that are sparsely disseminated throughout the matrix. These Cr-spinels are moderately low in Cr_2O_3 (mean ~40 wt.%), moderate to high in FeO (mean ~ 30 wt.%), and low in MgO (mean ~ 8.4 wt.%).

The mineral chemistry of chromites from dunite, lherzolite, chromitite and disseminated Cr-spinels in the latter group shows important variations (Tables 5 and 6). When plotted in a Cr-Fe^3-Al diagram (Fig. 12A), these chromites define three separate clusters within the Al-chromite field and the cluster characterized by the

Table 5. Mineral chemistry data of representative glaucophane schist samples from the Nagaland-Manipur Hill ophiolitic mélange zone

	Glaucophane								Chlorite				Epidote	Albite
	1	2	3	4	5	6	7	8	1	2	3	4	1	1
SiO_2	54.62	53.94	55.05	54.91	53.02	53.5	52.94	54.33	26.84	26.54	30.38	30.43	36.62	68.69
TiO_2	0.03	0.01	0.08	0.2	0.06	0.07	0.04	0.05	0.06	0.04	0.03	0.01	0.13	0.01
Al_2O_3	4.54	2.45	3.7	6.78	6.83	2.49	2.63	3.52	17.66	17.65	18.94	18.6	22.97	20.01
Cr_2O_3	0.05	0.06	0.07	0.01	0.06	0.02	0	0	0.09	0.07	0.15	0.16	0.05	0.04
Fe_2O_3	9.12	12.90	9.89	6.27	11.29	13.70	11.15	11.16						
FeO	11.23	9.98	12.10	11.56	7.61	12.05	12.99	10.61	24.49	23.56	13.64	13.89	11.16	0.01
MnO	0.1	0.22	0.23	0.09	0.29	0.19	0.3	0.47	0.2	0.19	0.42	0.58	0.22	0
MgO	8.07	8.62	8.46	7.92	8.62	7.07	7.08	8.18	16.53	16.62	21.62	22.1	0.07	0.01
CaO	0.36	1.01	1.08	0.99	1.6	0.75	1.4	0.87	0.03	0.02	0.17	0.14	23.28	0
Na_2O	7.04	6.47	7.14	6.43	5.63	6.58	6.21	6.6	0.05	0.05	0.07	0.03	0.01	11.08
K_2O	0.03	0.07	0.05	0	0.03	0.02	0.03	0.02	0.01	0.01	0.09	0.05	0	0.02
Total	**95.18**	**95.72**	**97.85**	**95.16**	**95.04**	**96.44**	**94.77**	**95.81**	**85.98**	**84.73**	**85.52**	**85.99**	**94.51**	**99.87**
Structural formulae														
Si	8.03	7.97	7.96	7.99	7.73	7.94	7.99	7.99						
Al^{iv}	0.00	0.03	0.04	0.01	0.27	0.06	0.01	0.01						
Al^{vi}	0.79	0.40	0.59	1.15	0.91	0.38	0.46	0.60						
Ti	0.00	0.00	0.01	0.02	0.01	0.01	0.00	0.01						
Cr	0.01	0.01	0.01	0.00	0.01	0.00	0.00	0.00						
Fe^{3+}	1.01	1.43	1.08	0.69	1.24	1.53	1.27	1.23						
Fe^{2+}	1.38	1.23	1.46	1.41	0.93	1.50	1.64	1.31						
Mn	0.01	0.03	0.03	0.01	0.04	0.02	0.04	0.06						
Mg	1.77	1.90	1.82	1.72	1.87	1.56	1.59	1.79						
Ca	0.06	0.16	0.17	0.15	0.25	0.12	0.23	0.14						
Na	2.01	1.85	2.00	1.81	1.59	1.89	1.82	1.88						
K	0.01	0.01	0.01	0.00	0.01	0.00	0.01	0.00						
Total	**17.07**	**17.03**	**17.18**	**16.97**	**16.85**	**17.02**	**17.05**	**17.02**						

Table 6: Mineral chemistry data of representative samples of the ultracataclastite matrix from the Nagaland-Manipur Hill ophiolitic mélange zone

	Glaucophane									Chlorite						
	1	2	3	4	5	6	7	8	9	1	2	3	4	5	6	7
SiO_2	52.38	51.65	51.5	51.39	54.57	59.29	54.31	53.46	54.77	28.63	30.24	32.83	33.52	32.51	39.31	41.18
TiO_2	0.19	0.11	0.09	0.1	0.02	0.11	0.05	0.19	0.07	0.09	0.02	0.03	0.03	0	0.02	0.04
Al_2O_3	5.18	4.76	4.52	4.65	3.11	3.49	3.39	5.54	2.21	17.58	19.42	17.86	19.82	20.61	16.44	15.6
Cr_2O_3	0.02	0.03	0.02	0.34	0.03	0.01	0.03	0.02	0.05	0.05	0.17	0.25	0.71	0.19	0.07	0.92
FeO	21.96	22.07	22.35	20.86	21.23	20.05	23.41	21.11	19.21	24.48	14.74	13.43	16.06	11.33	14.5	13.6
MnO	0.32	0.42	0.5	0.57	0.34	0.22	0.38	0.3	0.56	0.87	0.52	0.3	0.43	0.34	0.44	0.5
MgO	6.94	8.89	7.19	8.97	8.93	6.74	6.66	6.82	10.34	15.83	20.86	20.49	17.27	21.21	19.11	16.38
CaO	2.49	1.43	3.29	2.31	1.29	1.39	0.91	1.42	3.67	0.13	0.09	0.15	0.45	0.26	0.14	0.19
Na_2O	6.26	5.55	5.71	5.76	6.75	4.96	6.95	6.78	5.46	0.04	0.03	0.07	0.3	0.06	0.05	0.08
K_2O	0.08	0.02	0.16	0.07	0.01	0.04	0.02	0.05	0.05	0.05	0.03	0.08	0.53	0.09	0.05	0.21
Total	**95.8**	**94.92**	**95.34**	**95.02**	**96.28**	**96.3**	**96.12**	**95.69**	**96.4**	**87.74**	**86.11**	**85.48**	**89.12**	**86.6**	**90.12**	**88.7**

	Epidote					Magnetite		Ilmenite				Plagioclase
	1	2	3	4	5	1	2	1	2	3	4	1
SiO_2	37.39	38.18	37.66	37.44	37.39	0.14	0.05	0.04	0.12	0.04	0.12	51.03
TiO_2	0.11	0.2	0.24	2.67	0.1	1.46	5.26	59.16	65.46	59.16	65.46	0.02
Al_2O_3	23.35	25.26	24.72	21	22.46	0.28	3.38	0.03	0.08	0.03	0.08	27.94
Cr_2O_3	0.03	0.04	0.01	0	0.04	0.27	0.96	0.02	-0.01	0.02	-0.01	0
FeO	11.76	10.11	10.21	12.25	12.7	86.11	77.92	36.6	23.7	36.6	23.7	2.47
MnO	0.39	0.32	0.26	0.24	0.33	0.05	0	0.31	1.19	0.31	1.19	0.06
MgO	0.04	0.22	0.29	0	0.02	0.01	0.01	0.63	1.15	0.63	1.15	0.01
CaO	23.41	23.67	23.1	24.52	23.53	0.03	0.04	0.03	0.07	0.03	0.07	14.65
Na_2O	0.03	0.09	0.04	0.02	0.03	0.06	0.04	0.02	0.06	0.02	0.06	4.62
K_2O	0.01	0.03	0.01	0.01	0.01	0	0.01	0.01	0.02	0.01	0.02	0.04
Total	**96.52**	**98.1**	**96.54**	**98.15**	**96.62**	**88.41**	**87.66**	**96.84**	**91.85**	**96.84**	**91.85**	**100.86**

Spinel

	Disseminated spinels in the matrix							Chrome-spinels in chromitite fragments				
	1	2	3	4	5	6	7	1	2	3	4	5
SiO_2	0.07	0.06	0.08	0.07	0.06	0.15	0.04	0.11	0.07	0.07	0.03	0.07
TiO_2	0.35	0.40	0.15	0.16	0.46	0.48	0.27	0.28	0.06	0.07	0.07	0.05
Al_2O_3	19.10	17.97	26.58	25.42	18.64	18.38	13.75	16.98	5.62	5.62	9.32	9.39
Cr_2O_3	37.23	38.04	35.79	37.60	42.62	42.11	49.87	50.63	65.51	65.24	60.09	59.80
FeO^T	34.25	35.05	25.69	26.42	28.75	28.72	25.24	17.00	15.77	15.28	18.60	19.26
MnO	0.39	0.47	0.30	0.39	0.41	0.42	0.17	0.23	0.20	0.29	0.36	0.31
MgO	7.30	6.67	10.84	10.34	7.78	7.25	9.33	11.62	10.97	10.93	9.39	8.87
CaO	0.01	0.02	0.00	0.02	0.02	0.01	0.01	0.02	0.03	0.06	0.01	0.04
Na_2O	0.03	0.04	0.03	0.05	0.01	0.07	0.02	0.00	0.04	0.03	0.03	0.02
K_2O	0.00	0.00	0.00	0.00	0.00	0.00	0.00	0.01	0.00	0.04	0.01	0.01
NiO	0.00	0.00	0.00	0.00	0.00	0.00	0.00	0.00	0.00	0.00	0.00	0.00
Total	98.73	98.73	99.46	100.47	98.74	97.59	98.71	96.88	98.27	97.62	97.92	97.83
Fe_2O_3	11.85	11.98	6.95	6.98	6.57	6.23	6.17	1.00	0.44	0.27	0.56	0.33
FeO	23.59	24.27	19.44	20.14	22.84	23.12	19.69	16.10	15.37	15.04	18.10	18.96
Total	**99.92**	**99.92**	**100.16**	**101.17**	**99.41**	**98.21**	**99.32**	**96.98**	**98.31**	**97.66**	**97.97**	**97.85**
Cations:	4(O)	4(O)	4(O)	4(O)	4(O)	4(O)	4(O)	4(O)	4(O)	4(O)	4(O)	4(O)
Si	0.00	0.00	0.00	0.00	0.00	0.00	0.00	0.00	0.00	0.00	0.00	0.00
Ti	0.01	0.01	0.00	0.00	0.01	0.01	0.01	0.01	0.00	0.00	0.00	0.00
Al	0.73	0.70	0.96	0.92	0.72	0.72	0.53	0.65	0.22	0.23	0.37	0.38
Cr	0.96	0.99	0.87	0.91	1.10	1.10	1.30	1.30	1.76	1.76	1.61	1.61
Fe^{+3}	0.29	0.30	0.16	0.16	0.16	0.15	0.15	0.02	0.01	0.01	0.01	0.01
Fe^{+2}	0.64	0.67	0.50	0.52	0.62	0.64	0.54	0.44	0.44	0.43	0.51	0.54
Mn	0.01	0.01	0.01	0.01	0.01	0.01	0.00	0.01	0.01	0.01	0.01	0.01
Mg	0.35	0.33	0.50	0.47	0.38	0.36	0.46	0.56	0.56	0.56	0.47	0.45
Ca	0.00	0.00	0.00	0.00	0.00	0.00	0.00	0.00	0.00	0.00	0.00	0.00
Na	0.00	0.00	0.00	0.00	0.00	0.00	0.00	0.00	0.00	0.00	0.00	0.00
K	0.00	0.00	0.00	0.00	0.00	0.00	0.00	0.00	0.00	0.00	0.00	0.00
Ni	0.00	0.00	0.00	0.00	0.00	0.00	0.00	0.00	0.00	0.00	0.00	0.00
Total	**3.00**	**3.00**	**3.00**	**3.00**	**3.00**	**3.00**	**3.00**	**3.00**	**3.00**	**3.00**	**3.00**	**3.00**
Mol. per cent end-members :												
Spinel	33.12	30.62	46.19	44.19	34.24	34.31	25.65	32.30	11.23	11.35	18.57	18.82
Mg.Ulv.Spi	0.00	0.00	0.50	0.53	1.43	0.00	0.96	1.02	0.23	0.27	0.27	0.19
Mn.Ulv.Spi	0.75	0.92	0.00	0.00	0.19	0.85	0.00	0.00	0.00	0.00	0.00	0.00
Ulvospinel	0.45	0.47	0.00	0.00	0.00	0.87	0.00	0.00	0.00	0.00	0.00	0.00
Mn.Chromite	0.00	0.00	0.75	0.97	0.83	0.00	0.46	0.63	0.57	0.84	1.03	0.89
Mg.Chromite	0.00	0.00	0.79	0.57	0.00	0.00	17.09	22.25	43.93	44.11	28.40	25.89
Chromite	44.79	46.32	40.18	42.30	51.68	52.85	44.86	41.72	43.34	43.08	50.88	53.62
Magnetite	20.89	21.67	11.59	11.43	11.63	11.12	10.98	2.08	0.70	0.35	0.85	0.58

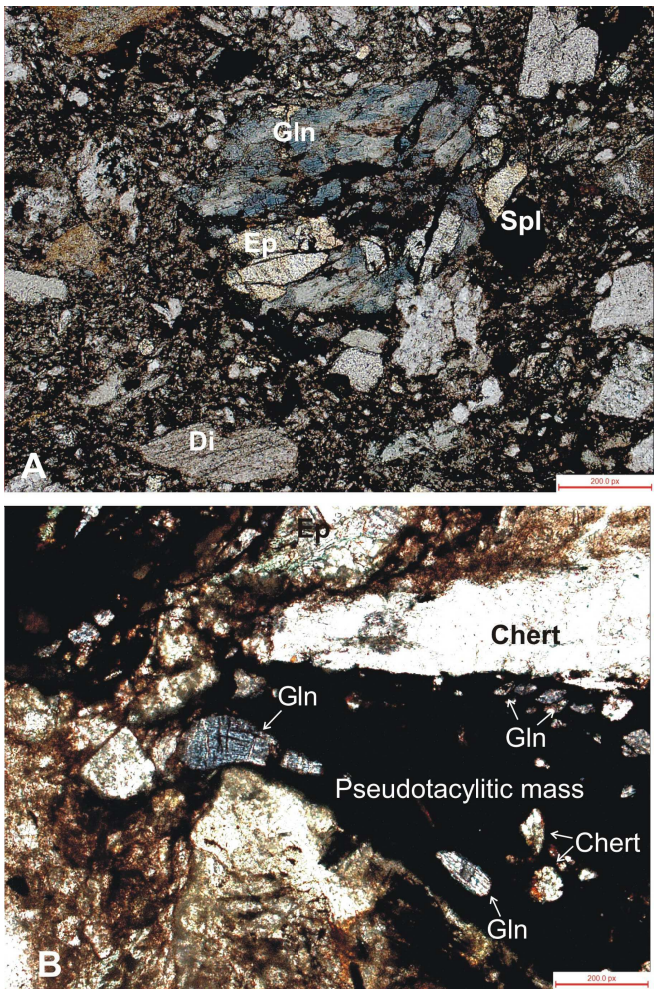

Figure 10: A-Photomicrograph of a mafic, cataclastic breccia, showing patchy growth of glaucophane on an epidote grain. Other minerals that are present in the field of view include: Ep = subhedral grains of epidote free of glaucophane growth; Di = subhedral grains of diopside; Spl = granular grains of spinel; and Ser = anhedral mass of serpentine. All these mineral phases are interpreted to represent disintegrated grains from a mafic rock. Plane polarized light. B- Photomicrograph of a mafic, cataclastic breccia with disintegrated fragments of glaucophane, chert and epidote in a dark brown pseudotachylitic groundmass. Plane polarized light.

chromitite field resembles the chromites from the Manipur area. However, in a Mg# vs Cr binary plot (Fig. 12B) the chromites of the all three clusters plot away from the field of Manipur chromitites, but correlate closely with the chromites of forearc peridotites. In a Cr# vs TiO_2 diagram (Fig. 12C), the analyzed chromites show distinctly different source characteristics. The chromites from the dunites and chromitites show reaction trends closer to those showing boninitic affinities, whereas the chromites from the chromitites display trends similar to those of the island arc tholeiitic melts.

Tectonic Interpretations and Model: Discussion and Conclusions

We present a new tectonic model for the origin and development of the Nagaland-Manipur Hill ophiolitic mélange zone within the framework of the regional geology (Fig. 13). In this model we infer

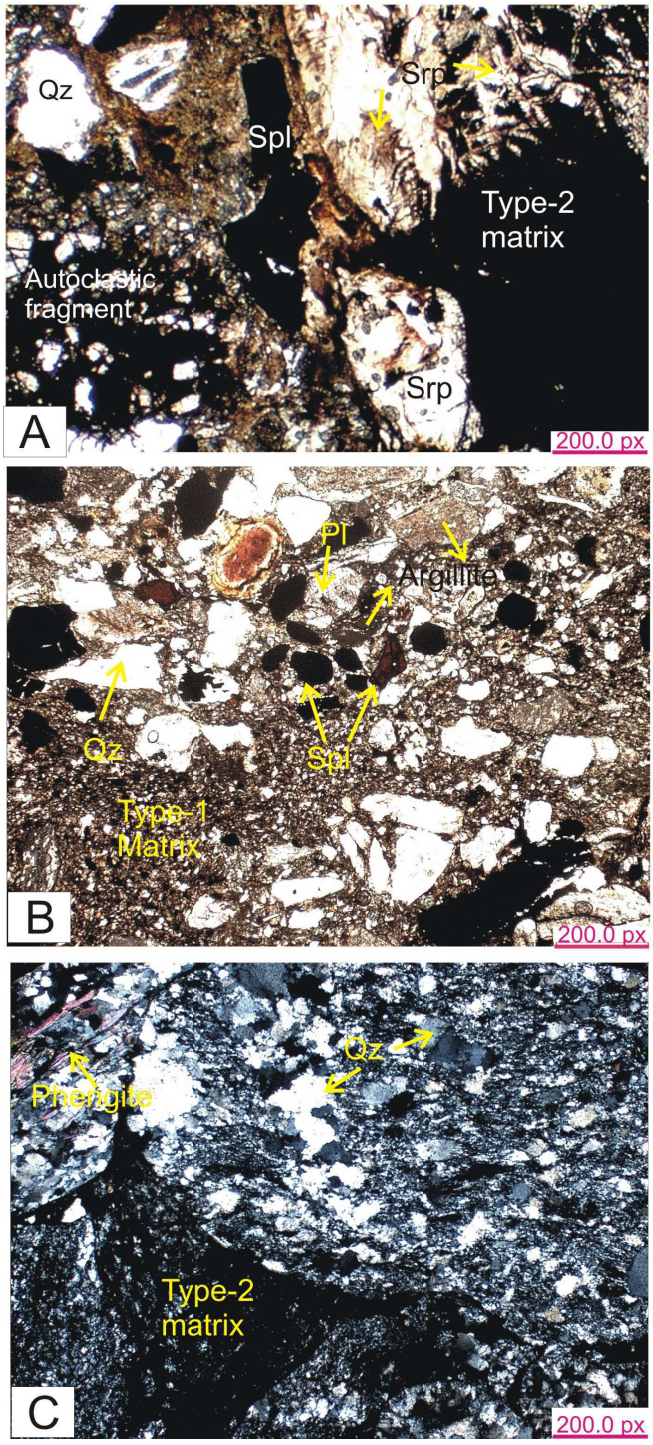

Figure 11: Photomicrographs in plane-polarized light (A and B) and under crossed nicols (C) showing two types of matrix in cataclastic breccia rocks. See text for discussion.

that the ophiolitic mélange zone and the discontinuous exposures of the dismembered ophiolites in the Indo-Myanmar Ranges represent the southern continuation of the latest Jurassic – early Cretaceous South Tibetan ophiolites exposed along the Yarlung-Zhangbo suture zone, and that all these ophiolites collectively formed in a subduction-accretion system within a Neotethyan seaway between India and Asia during the Mesozoic (Fig. 13A). The current ~N-S orientation of this Neotethyan ophiolite belt south of the Eastern Himalaya Syntaxis

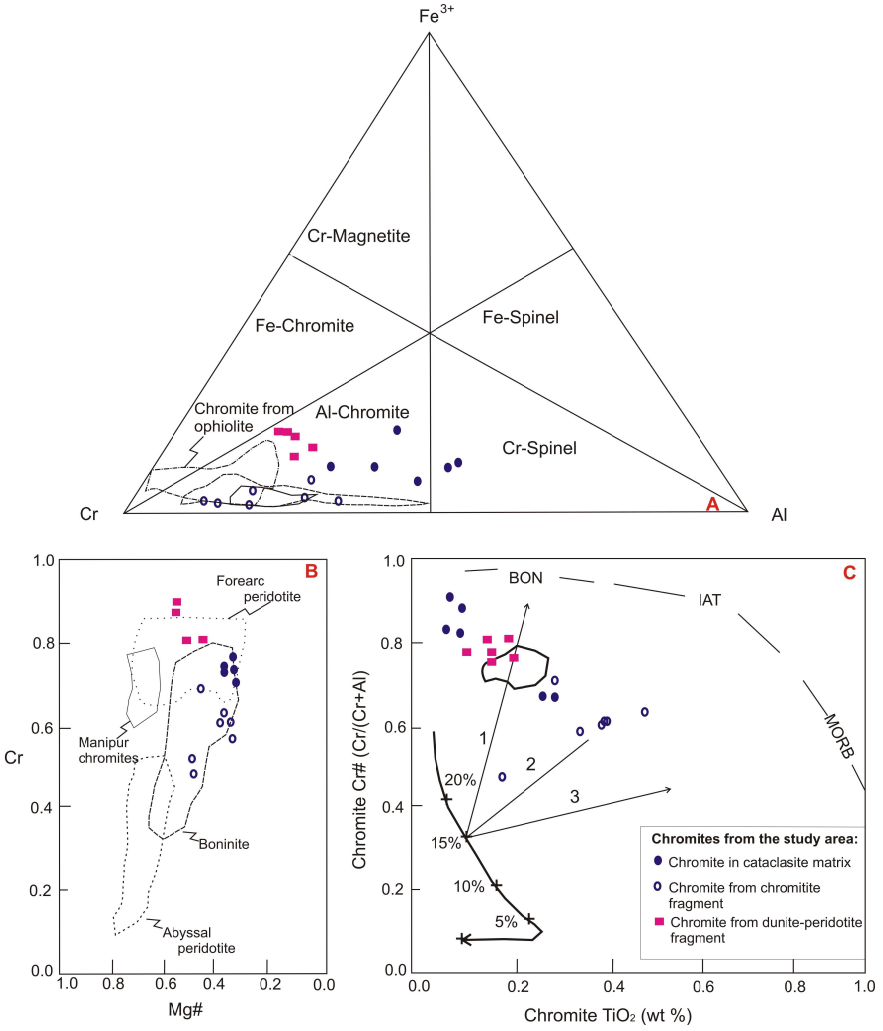

Figure 12: Compositional plots for chromite ocurrences in different peridotites in the ophiolitic mélange zone. A- Cr-Fe^{3+}-Al diagram (after Stevens, 1944; Barnes and Roeder, 2001). Note that all the chromites are Al-bearing chromites, but plot within distinctly different clusters. Only the chromites from the dunite-peridotite samples show compositional similarities with the ophiolitic chromites, whereas those from the matrix are more akin to the chromites from the Manipur Hill area chromitites (data for the Manipur area chromitites are from Pal et al. 2014). B- Mg# vs Cr diagram for different chromite types in the sudy area. Dunite-peridotite samples from our study area have chromites that are compositionally similar to the abyssal peridotites, whereas the other two types of chromites are analogous to the chromitites in boninitic series peridotites. C- Cr# vs TiO_2 plot for chromites (after Pearce et al., 2000) discriminating the upper mantle peridotites generated by different degrees of partial melting of fertile MORB mantle (FMM). Distribution of different chromite types on this diagram shows that the chromites in the cataclasitic matrix and the dunite-peridotite samples are reminiscent of those formed as a result higher degree of partial melting (~15%) with a crystallization trend similar to that of boninitic melts.

(Figs. 1 and 2) is a result of the clockwise rotation of Indo-China after the initial impingement and collision of the proto-India continent with the intraoceanic arc-trench system in the latest Cretaceous (Fig. 13A; Curray et al., 1979). The dextral fault system between India and the intraoceanic arc-trench system in this figure represents the initial stage of the Sagaing Fault, which separates the Burma plate to the west from the Indo-China Block (Sunda plate) to the east in present time. A broad zone of dextral shearing has been in existence in the inner part of the Indo-Burmese Wedge since the late Miocene (Maurin and Rangin, 2009).

Accretionary prism tectonics of the Indo-Burma Ranges

We interpret the Burma plate as an intra-oceanic arc-trench system that grew westward in time throughout the Mesozoic and early Cenozoic. In this model, the volcanic-plutonic sequence in the east-central part of the Burma plate constitutes an island arc system with a well developed forearc basin, Central Basin, to its west (Fig. 13B). The Central Basin is underlain by a mafic-ultramafic slab representing a forearc ophiolite complex, which we think may have formed the Nagaland-Manipur Hill ophiolite and its equivalents in the latest Cretaceous. The N-S-trending high gravity anomaly in the eastern part of the Indo-Burma Ranges and along the eastern edge of the Central Basin (Sengupta et al., 1990) is an artifact of this forearc ophiolitic basement. Both the Nimi and Disang Flysch complexes, which constitute much of the Indo-Myanmar Ranges in present time, developed as a westward migrating and growing trench–accretionary wedge system (Figs. 13B and C).

The Nimi Flysch to the east represents the older (latest Triassic-Cretaceous) and the Disang Flysch to the west the younger (latest Cretaceous – Eocene and Miocene) components of this trench–accretionary wedge system (Fig. 13C). The metamorphic grade in the accretionary prism meta-sedimentary and meta-felsic and meta-mafic rock assemblages decreases from amphibolite facies (>500°C) in the Nimi Flysch in the older accretionary wedge in the east to lower greenschist facies and unmetamorphosed rocks in the Disang Flysch in the west (Ghose et al., 2014). The Nimi Flysch consists mainly of phyllite, feldspathic quartzite, quartz-sericite schist, mylonitic limestone, locally intercalated with thrust slices of meta-volcanic rocks and meta-serpentinites. These rocks are tightly to isoclinally folded and generally overturned to the west with steeply E-SE-dipping axial surfaces. Tectonic slices of garnet-staurolite-biotite-muscovite schist are common within this folded, meta-sedimentary package. Previous studies have interpreted the Nimi Flysch as an accretionary prism complex, developed above an east-dipping subduction zone, and accreted progressively into the overriding Burma plate (Roy, 1989).

The latest Cretaceous – Miocene Disang Flysch is estimated to be more than 3000 meters in thickness and is composed mainly of slate, graphite-bearing slate, phyllite, siltstone and sandstone (Ghose et al., 2014). These rocks display rhythmic alternation and graded bedding – cross-bedding sedimentary features (Agrawal and Ghose, 1986), and the fine-grained rocks show bedding-parallel slaty cleavage. Similar to the Nimi Flysch, the Disang Flysch sedimentary units also include tectonic slices of serpentinites and basaltic volcanic rocks (Vidyadharan et al., 1989). All these rocks exhibit

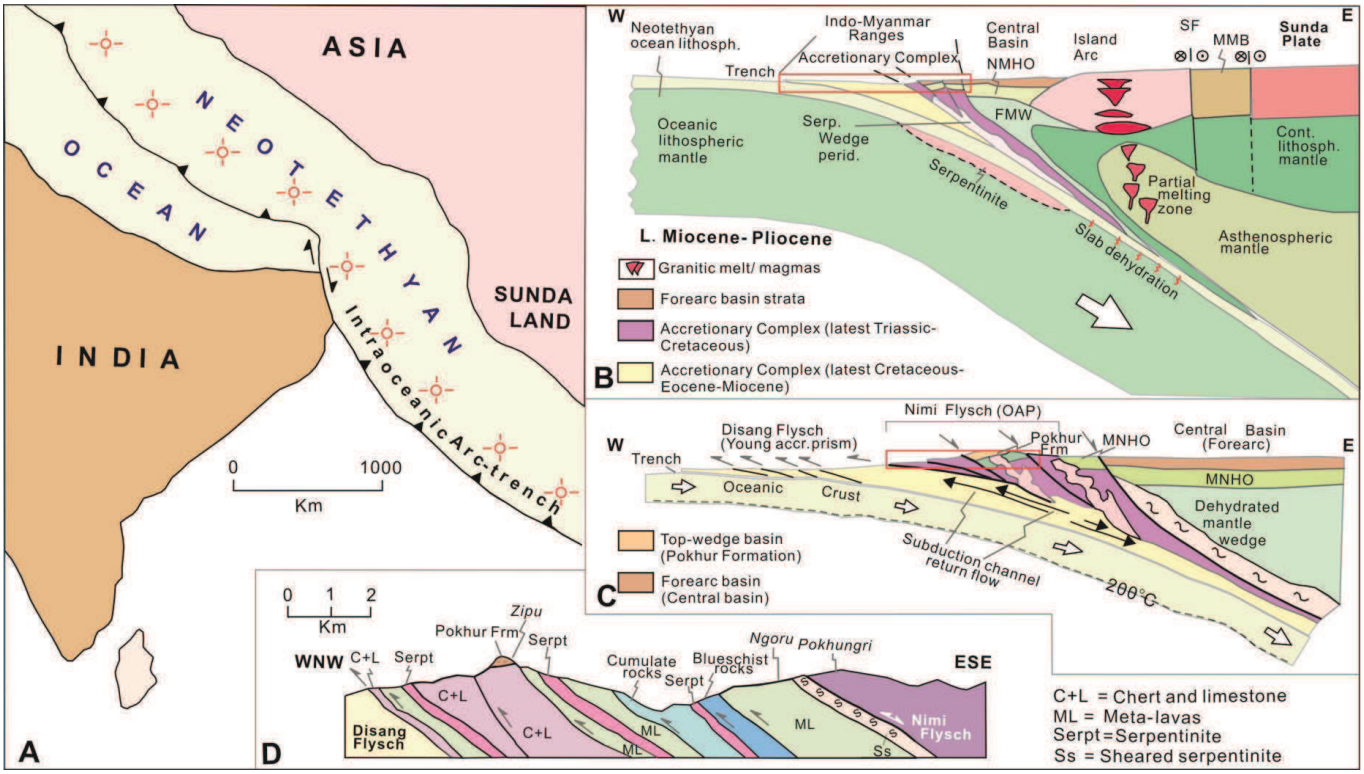

Figure 13: Interpretive reconstructions of the tectonic and metamorphic evolution of the Nagaland-Manipur Hill ophiolitic melange zone. A- Occurrence of a Cretaceous intra-oceanic arc-trench system in a Neotethyan seaway between India and Asia–Sundaland and the oblique collision of the NE edge of the Indian continent with this arc-trench system in the late Cretaceous. The initial dextral transform plate boundary between India and Asia in this configuration evolves into the dextral Sagaing Fault with further indentation of the Indian plate into the Neotethyan realm and the clockwise rotation of Sundaland. B- E-W–oriented tectonic cross section (at the ~23° North Latitude in present-day configuration) across the late Miocene – Pliocene active margin between Asia and the Neotathyan seaway, east of India. The Indo-Myanmar Ranges represent a westward growing accretionary wedge with oldest accreted sediments in the eastern part of the prism, faulted against the forearc sedimentary basin strata of the Central Basin. The igneous basement beneath the forearc basin represents a suprasubduction zone oceanic lithosphere with MORB-like, IAT and boninitic geochemical affinities (Dilek and Furnes, 2011, 2014). The active volcanic arc to the east of the forearc basin constitutes a backstop and is represented by the Wuntho-Popa arc (data from Morley, 2009; Soibam et al., 2015). Key to lettering: FMW = Forearc mantle wedge; MMB = Mogoc metamorphic belt; NMHO = Nagaland-Manipur Hill ophiolite; SF = Sagaing Fault. C- Close-up of the trench-accretionary prism complex depicted in B. The older (Nimi Flysch) and younger (Disang Flysch) accretionary prisms are separated by an ophiolitic mélange zone, which includes highly dismembered and metamorphosed ophiolitic rocks, blueschist rocks and minerals, and low-grade sedimentary rocks in a sheared serpentinite and cataclastic breccia matrix. This mélange zone represents an exhumed subduction zone channel, in which the subducted oceanic lithosphere fragments and sediments were returned to the shallow depths within the dynamic accretionary wedge. Faulted and folded conglomeratic rocks of the Pohkur Formation (wedge-top or slope basin sedimentary sequence, reminiscent of the wedge-top basin strata in the Apennines and Calabria in Italy; Barone et al., 2008; Conti et al., 2008) unconformably overlie the ophiolitic mélange. The red box depicts the cross-section area in E. D- Structural cross section of the ophiolitic mélange zone (modified after Agrawal and Ghose, 1986). Different ophiolitic units, meta-sedimentary rocks, and blueschist assemblages are separated by W-vergent thrust faults, which are commonly associated with several-meters-thick, sheared serpentinite.

close to tight folds with NNE-trending fold axes, and are crosscut by low- to high-angle thrust faults and local normal faults. Olistholiths and olistostromal blocks and deposits with sizes well over 500 meters are widespread in the upper parts of the Disang Flysch, reminiscent of similar chaotic deposit occurrences in both modern and ancient accretionary prisms (Festa et al., 2010, 2012). These chaotic deposits, derived from the ophiolitic basement rocks in high elevations on the wedge slope, likely formed as gravity-driven accumulations in slope basins perched on top of the accretionary wedge. Foraminiferal fossil assemblages recovered from these olistolith and olistostromal deposits have revealed biostratigraphic ages of Maastrichtian, Paleocene and Eocene (Mitra et al., 1986; Acharyya et al., 1986; Lukram and Kachhara, 2010). The accretionary prism turbiditic sedimentary packages and olistostromal deposits are stratigraphically overlain by Oligocene-Miocene, shallow marine and fluvial sedimentary rocks (Barail Formation) (Vidyadharan et al., 1989).

Subduction channel mélange

The Nagaland-Manipur Hill ophiolitic mélange zone bounded by the exhumed accretionary prism wedges on both sides represents a subduction channel shear zone (Fig. 13C). The lack of an intact ophiolite pseudostratigraphy, the occurrence of sheared contacts

between different ophiolitic units, slivers of sheared serpentinite within and between ophiolitic units, and the existence of blueschist blocks throughout the mélange zone indicate a characteristic subduction zone mélange, reminiscent of the Franciscan mélange in California (Cloos, 1986; Cloos and Shreve, 1988; Ukar, 2012; Ogawa et al., 2014; Ernst, 2015).

We infer that with the continued eastward subduction of the Neotethyan oceanic lithosphere mid-ocean generated basaltic lavas and small volumes of sediments were metamorphosed to eclogites and metasedimentary rocks, and were subsequently accreted to the bottom of the peridotites of the mantle wedge in the overlying plate. They continued to grow as blocks of garnet eclogites in the mantle wedge. The refrigeration effect of the subducting cold lithosphere resulted in retrograde bluschist metamorphism overprinting the eclogitic blocks and fragments. Migration of subduction-derived fluids into the mantle wedge triggered extensive hydration and serpentinization of the peridotites surrounding the eclogite – blueschist rocks, and formed actinolitic rinds between the peridotites and high-pressure blocks, as well as extensive networks of chlorite, epidote and quartz veins crosscutting these lithologies and the serpentinized peridotites. Extensive serpentinization of the peridotites at the bottom of the mantle wedge and along the plate interface may have developed a serpentinite matrix mélange, as predicted in numerical modeling of subduction channels (Gerya et al., 2002). We interpret these processes to have taken place throughout the latest Cretaceous and Paleocene.

We posit that with the approach of the Indian continental margin at and its collision with the Cretaceous-Paleocene trench-accretion system in the early Eocene, the convergence rate decreased from ~100 mm/yr to ~60 mm/yr by 44 Ma (Morley, 2009), and the subduction angle of the downgoing Neotethyan lithosphere became shallow. These significant changes in the subduction parameters resulted in subduction erosion at the base of the upper plate and uplift of the older Nimi accretionary prism and the Cretaceous-Paleocene arc plutons in the Central Belt to the east. The combination of these processes caused the exhumation of high-pressure meta-mafic rocks and metasedimentary rocks as blocks and the incorporation of these exhumed blocks into the subduction channel shear zone along the plate interface. The upward return flow within this shear zone resulted in metasomatism, extensive cataclastic deformation, extensional shearing, and contractional deformation and tectonic imbrication within the mélange. Sheared serpentinite, derived from the mélange matrix, was injected along the thrust faults during further exhumation and upwelling of the ophiolitic mélange zone. Incorporation of coherent ophiolite blocks from the overlying forearc oceanic lithosphere into the trench deposits and into the accretionary wedge at the surface may also have contributed to the occurrence of less deformed ophiolitic rocks in the mélange. The resulting crustal structure of this subduction channel shear zone is depicted in Figure 13D.

Ophiolitic units and ophiolite blocks in the Nagaland-Manipur Hill ophiolite melange zone do not represent an intact ophiolite sequence, as commonly observed in Penrose-type ophiolites that have a petrological Moho and crustal – upper mantle peridotites showing a melt-residua relationship (Dilek and Eddy, 1992; Dilek and Thy, 1998; Dilek and Furnes, 2014). They are also distinctly different from Hess-type ophiolites commonly observed in ocean – continent transition zones (Dilek and Newcomb, 2003, and references therein; Dilek and Robinson and references therein; Saccani et al., 2015; Balestro et al., 2015). In all these ophiolite types primary igneous and sedimentary contact relationships between different ophiolitic subunits are well preserved, and there are no significant metamorphic gradients within and across the ophiolitic subunits. The contacts between all ophiolitic subunits in the Nagaland-Manipur Hill ophiolite melange zone are thrust faulted, and most of the rocks display various degrees of subduction zone metamorphic overprint. Based on these characteristic features and following the recent ophiolite classification terminology by Dilek and Furnes (2011), we classify the Nagaland-Manipur Hill ophiolite occurrences as accretionary-type, derived mostly from the downgoing plate (Dilek and Furnes, 2014).

Acknowledgements

The first author thanks the Director General, Geological Survey of India for sending him to the Pungro-Pokpur sector of Nagaland to explore the possibility of declaring the ophiolite melange zone of this region as a National Geoheritage site. Help rendered by Dr. Dipayan Guha, Director and Mr. N. Meripebumu, Sr. Geologist during fieldwork and Mr. Mahesh Korkoppa, Sr. Geologist, during laboratory studies is gratefully acknowledged and greatly appreciated. Our discussions with Prof. N.C Ghose, on the geology of the Nagaland-Manipur Hill region have been most helpful for our interpretations of the structure, petrology and tectonics of the accretionary prism complexes and ophiolitic occurrences, as presented in this paper.

References

Acharyya, S.K., 1986, Tectono-stratigraphic history of Naga Hill Ophiolites. Geological Survey of India, Memoirs, v. 119, pp. 94-103.

Acharyya, S.K., 2006, Collisional emplacement history of the Naga-Andaman ophiolites and the position of the eastern Indian suture. Journal of Asian Earth Sciences, v. 29, pp. 229–242.

Acharyya, S.K., 2010, Tectonic evolution of Indo-Burma Range with special reference to Naga-Manipur Hills. In, Soibam Ibotombi (Ed.), Indo-Myanmar Ranges in the Tectonic Framework of the Himalaya and Southeast Asia. Memoir Geological Society of India, No. 75, pp. 25-43.

Agrawal, O.P. and Ghose, N.C., 1986, Geology and stratigraphy of the Naga Hills ophiolite between Meluri and Awankhoo, Phek District, Nagaland, India. In, Ghose, N.C. and Varadarajan, S. (Eds.), Ophiolites and Indian Plate Margin. Sumna Publishers, Patna, pp. 163-195.

Balestro, G., Festa, A., Dilek, Y., and Tartarotti, P., 2015, Pre-Alpine Extensional Tectonics of a Peridotite-Localized Oceanic Core Complex in the Late Jurassic, High-Pressure Monviso ophiolite (Western Alps). Episodes, v. 38, No. 4, pp. 266-282,doi: 10.18814/epiiugs/2015/v38i4/82421

Barnes, S.J. and Roeder, P.L., 2001, The range of spinel compositions in terrestrial mafic and ultramafic rocks. Journal of Petrology, v. 42, pp. 2279-2302.

Barone, M., Dominici, R., Muto, F., and Critelli, S., 2008, Detrital modes in a late Miocene wedge-top basin, northeastern Calabria, Italy: Compositional record of wedge-top partitioning. Journal of Sedimentary Research, v. 78, pp. 693-711.

Bebout, G.E. and Barton, M.D., 2002, Tectonic and metasomatic mixing in a high-T, subduction-zone mélange – insights into the geochemical evolution of the slab-mantle interface. Chemical Geology, v. 187, pp. 79-106.

Bhattacharjee, C.G. (1991) The ophiolites of northeast India – a subduction zone ophiolite complex of the Indo-Burman orogenic belt. Tectonophysics, v. 191, pp. 213-222.

Chattopadhyaya, B., Venkataramana,, P., Roy, D.K., Bhattacharyya, S. and Ghosh, S., 1983, Geology of Naga Hills Ophiolites. Geological Survey of India, v. 112, pp. 59-115

Chatterjee, N. and Ghose, N.C., 2010, Metamorphic evolution of the Naga Hills eclogite and blueschist,Northeast India: implications for early

subduction of the Indian plate under the Burma microplate. Journal of Metamorphic Geology, v. 28, pp. 209-225.

Cloos, M., 1986, Bluschists in the Franciscan Complex of California: petrotectonic constraints on uplift mechanisms. Geological Society of America Memoir, v. 164, pp. 77-93.

Cloos, M. and Shreve, R.L., 1988, Subduction-channel model of prism accretion, mélange formation, sediment subduction, and subduction erosion at convergent plate margins: 1. Background and description. Pure and Applied Physics, v. 128, pp. 455-500.

Conti, S., Fontana, D., and Lucente, C.C., 2008, Sedimentary filling of a wedge-top basin and relationship with the foredeep (Middle Miocene Marnoso-arenacea Formation, northern Apennines). Facies, v. 54, p. 479-498.

Curray, J.R., 2005, Tectonics and history of the Andaman Sea region. Journal of Asian Earth Sciences, v. 25, pp. 187-232.

Curray, J.R., Moore, D.G., Lawyer, L.A. et al., 1979, Tectonicsof the Andaman Sea and Burma. In, Watkins, J., Montadert, L. and Dickinson, P. (Eds.), Geological and Geophysical Investigations of Continental Slopes and Rises. Memoirs of the American Association of Petroleum Geologists, v. 29, pp. 189–198.

Dilek, Y., and Eddy, C., 1992, The Troodos (Cyprus) and Kizildag (S. Turkey) ophiolites as structural models for slow-spreading ridge segments. Journal of Geology, v. 100, pp. 305-322.

Dilek, Y. and Thy, P., 1998, Structure, petrology and seafloor spreading tectonics of the Kizildag ophiolite, Turkey.Geological Society of London, Special Publication, v. 148, pp. 43-69.

Dilek, Y. and Newcomb, S., 2003, Ophiolite concept and the evolution of geological thought. Geological Society of America Special Papers, v. 373, The Geological Society of America, Boulder, CO 80301, ISBN 0-8137-2373-6.

Dilek, Y. and Robinson, P.T., 2003, Ophiolites in Earth history. Geological Society, London, Special Publications, v. 218, pp. 1-8.

Dilek, Y., 2003, Ophiolite pulses, mantle plumes and orogeny. In, Geological Society, London, Special Publications, v. 218, pp. 9-19.

Dilek, Y., and Furnes, H., 2011, Ophiolite genesis and global tectonics: Geochemical and tectonic fingerprinting of ancient oceanic lithosphere. Geological Society of America Bulletin, v. 123, pp. 387–411.

Dilek, Y., and Furnes, H., 2014, Ophiolites and their Origins. Elements, v. 10, pp. 93-100.

Ernst, W.G., 2015, Franciscan geologic history constrained by tectonic/olistostromal high-grade metamafic blocks in the iconic California Mesozoic-Cenozoic accretionary complex. American Mineralogist, v. 100, pp. 6-13.

Errico, J.C., Barnes, J.D., Strickland, A., and Valley, J.W., 2013, Oxygen isotope zoning in garnets from Franciscan ecologite blocks: evidence for rock-buffered fluid interaction in the mantle wedge. Contributions to Mineralogy and Petrology, v. 166, pp. 1161-1176.

Festa, A., Pini, G.A., Dilek,Y., and Codegone, G., 2010 Mélanges and mélange forming processes: historical overview and new concepts: International Geology Review, v. 52, No.10-12, pp.1040-1105, DOI:10.1080/00206810903557704.

Festa, A., Dilek, Y., and Pini, G.A., 2012 Mechanisms and processes of stratal disruption and mixing in the development of mélanges and broken formations: Redefining and classifying mélanges: Tectonophysics, v. 568-569, pp. 7-24, DOI:10.1016/j.tecto2012.05.021.

Gerya, T.V., Stockhert, B., and Perchuk, A.L., 2002, Exhumation of high-pressure metamorphic rocks in a subduction channel: a numerical simulation. Tectonics, v. 21, p. 1056, doi: 10.1029/2002TC001406 (19 p).

Ghose, N.C., Agrawal, O.P., and Chatterjee, N., 2010, A geological and mineralogical study of eclogite and glaucophane schists in the Naga Hills ophiolite, Northeast India. Island Arc, v. 19, pp. 336-356.

Ghose, N.C., Agrawal, O.P. and Singh, R.N., 1986, Geochemistry of the ophiolite belt of Nagaland, N.E. India. *In:* Ophiolites and Indian Plate Margin. Ghose, N.C. & Varadarajan, S. (eds,). Sumna Publishers, Patna, India, pp. 241–294.

Ghose, N.C, Chatterjje, N., and Fareeduddin, 2014, A petrographic atlas of ophiolite: An example from the eastern India-Asia Collision Zone. Springer, 234 p.

Kakar, M.I., Kerr, A.C., Mahmood, K., Collins, A.S., Khan, M., and McDonald, I., 2014, Supra-subduction zone tectonic setting of the Muslim Bagh Ophiolite, northwestern Pakistan: Insights from geochemistry and petrology. Lithos, v. 202–203, pp. 190-206.

Leake, B., Woolley, A.R., Arps, C.E.S. et al., 1997. Nomenclature of amphiboles: Report of the subcommittee on amphiboles of the International Mineralogical Association,Commission on new minerals and mineral names. Canadian Mineralogist, v. 35, pp. 219–246.

Lin, T.-H.,Chung, S.-L.,Kumar, A., Wu, F.-Y., Chiu, H.-Y., and Lin, I.-J., 2013, Linking a prolonged Neo-Tethyan magmatic arc in South Asia: Zircon U-Pb and Hf isotopic constraints from the Lohit Batholith, NE India. Terra Nova, v. 25, pp. 453-458.

Lukram, J.S. and Kachhara, R.P., 2010, Molluscan Biostratigraphy of the Disang Group of rocks in parts of Manipur, India. In, Soibam Ibotombi (Ed) Indo-Myanmar Ranges in the Tectonic Framework of the Himalaya and Southeast Asia. Memoir Geological Society of India, No. 74, pp. 149-164.

Maurin, T., and C. Rangin, 2009, Structure and kinematics of the Indo-Burmese Wedge: Recent and fast growth of the outer wedge.Tectonics, v. 28/2, 21 p. doi.org/10.1029/2008TC0022876.

Mitchell, A.H.G., 1993, Cretaceous-Cenozoic tectonic events in the western Myanma (Burma-Assam region. Journal of the Geological Society of London, v. 150, pp. 1012-1089.

Mitchell. A.H.G., Chung, S.L., Oo, T., Lin, T.H., and Hung, C.H., 2012, Zircon U/Pb ages in Myanmar: magmatic-metamorphic events and the closure of a neo-Tethys ocean? Journal of Asian Earth Sciences, v. 56, pp. 1-23.

Mitra, N.D., Vidyadharan, K.T., Gaur, M.P., Singh, S.K., Mishra, U.K., Joshi, A., Khan, I.K., and Ghosh, S. 1986, A note on the olistrostromal deposits of Manipur. Records Geological Survey of India, v. 114, pp. 61-76.

Morley, C.K., 2009, Evolution from an oblique subduction back-arc mobile belt to a highly oblique collisional margin: the Cenozoic tectonic development of Thailand and eastern Myanmar. In, Cawood, P.A. and Kröner, A. (Eds.), Earth Accretionary Systems in Space and Time, The Geological Society of London Special Publication, v. 138, pp. 373-403.

Ni, J.F., Guzman-Speziale, M., Bevis, M., Holt, W.E., Wallace, T.C. and Seager, W.R., 1989. Accretionary tectonics of Burma and the three-dimensional geometry of the Burma subduction zone. Geology, v. 17, pp. 68-71.

Ningthoujam, P.S., Dubey, C.S., Guillot, S., Fagion, A.-S., and Shukla, D.P., 2012, Origin and serpentinization of ultramafic rocks of Manipur ophiolite complex in the Indo-Myanmar subduction zone, Northeast India. Journal of Asian Earth Sciences, v. 50, pp. 128-140.

Ogawa, Y., Mori, R., Tsunogae, T., Dilek, Y. and Harris, R., (2014) New interpretation of the Franciscan melange at San Simeon coast, California: tectonic intrusion into an accretionary prism. International Geology Review. doi:10.1080/00206814.2014.968813.

Pal, T., Bhattacharya, A.,Nagendran, G., Yanthan, N.M., Singh, R., Raghumani, N., 2014, Petrogenesis of chromites from the Manipur ophiolite belt, NEIndia: evidence for a supra-subduction zone setting prior to Indo-Myanmar collision. Mineralogy and Petrology, DOI 10.1007/s00710-014-0320-z.

Pearce, J.A., Barker, P.E., Edwards, S.J., Parkinson, I.J. & Leat, P.T. 2000. Geochemistry and tectonic significance from the South Sandwich arc–basin system, South Atlantic. Contributions to Mineralogy and Petrology, v. 139, pp. 36–53.

Roy, R.K., 1986, Ophiolites and geodynamic developments on the northern and eastern margins of the Indian subcontinent. In Ghose, N.C. and Varadarajan, S. (Eds), Ophiolites and Indian Plate Margin, Sumna Pubications, pp.223-240.

Saccani, E., Dilek, Y., Marroni, M., and Pandolfi, L., 2015, Continental Margin Ophiolites of Neotethys: Remnants of Ancient Ocean–Continent Transition Zone (OCTZ) Lithosphere and Their Geochemistry, Mantle

Sources and Melt Evolution Patterns. Episodes, v. 38, No. 4, pp. 230-249, doi: 10.18814/epiiugs/2015/v38i4/82418.

Sarwar, G., 1992, Tectonic setting of the Bela ophiolites, southern Pakistan. Tectonophysics, v. 207, pp. 359-381.

Sengupta, S., Ray, K.K., Acharyya, S.K., and de Smeth, J.B., 1990, Nature of ophiolite occurrences along the eastern margin of the Indian plate and their tectonic significance. Geology, v. 18, pp. 439-442.

Sinha, N.K., Chatterjee, B.P and Satsangi, P.P., 1982, Status of palaeontology research in northeast Region. Rec. Geol. Surv. India, v. 112,

Soibam, I., Khuman, M.Ch., and Subhamonon, S.S., 2015, Ophiolitic rocks of the Indo-Myanmar Ranges, NE India: relicts of an inverted and tectonically imbricated hyper-extended continental margin basin? doi:10.1144/SP413.12.

Stevens, R.E., 1944, Compostion of some chromites of the Western Hemisphere. American Mineralogist, v. 29, pp. 1-34.

Ukar, E., 2012, Tectonic significance of low-temperature blueschist blocks in the Franciscan mélange at San Simeon, California. Tectonophysics, v. 568-569, pp. 154-169.

Vidyadharan, K.T., Joshi, A., Ghosh, S., Gaur, M.P. and Shukla, R. (1989), Manipur Ophiolites: Its Geology, Tectonic Setting and Metallogeny. In Ghose, N.C. (Ed), Phanerozoic Ophiolites of India. Sumna Publications, Patna, pp. 197-212.

Xu, Z.Q., Dilek, Y., Cao, H., Yang, J.S., Robinson, P., Ma, C.Q., Li, H., Jolivet, M., Roger, F., Chen, X.J., 2015, Paleo-Tethyan Evolution of Tibet as Recorded in the East Cimmerides and West Cathaysides: Journal of Asian Earth Sciences, v. 105, pp. 320-337, doi: 0.1016/j.jseaes.2015.01.021.

Yang, G.X. and Dilek, Y., 2015, OIB- and P-Type Ophiolites Along the Yarlung Zangbo Suture Zone (YZSZ), Southern Tibet: Poly-Phase Melt History and Mantle Sources of the Neotethyan Oceanic Lithosphere. Episodes, v. 38, No. 4, pp. 250-265, doi: 10.18814/epiiugs/2015/v38i4/82420.

Yang, J.S., Robinson, P.T., and Diley, Y. (2015), Diamond-bearing ophiolites and their geological occurrence. Episodes, v. 38, No. 4, pp. 344-364, doi: 10.18814/epiiugs/2015/v38i4/82430.

by Ricardo Arenas and Sonia Sánchez Martínez

Variscan ophiolites in NW Iberia: Tracking lost Paleozoic oceans and the assembly of Pangea

Departamento de Petrología y Geoquímica e Instituto de Geociencias (UCM, CSIC), Universidad Complutense, 28040 Madrid, Spain.
E-mail: arenas@geo.ucm.es

DOI:10.18814/epiiugs/2015/v38i4/82427

In the Galicia Region of the NW Iberian Massif several allochthonous complexes (Cabo Ortegal, Órdenes and Malpica-Tui) contain a rootless Variscan suture that can be traced along the belt, from Iberia to the Bohemian Massif in Central Europe. Within these allochthonous complexes are several ophiolite zones bounded by two different continental terranes. There exist in NW Iberia two different ophiolite groups with different chemical compositions, isotopic signatures and structural positions. The Bazar and Vila de Cruces ophiolites, characterized by c. 500 Ma protolith ages, represent the Lower Group, whereas the Careón, Purrido and Moeche ophiolites containing 395 Ma maficultramafic sequences represent the Upper Group. This younger group constitutes the most widespread ophiolites in the Variscan Belt. A thick serpentinite mélange (Somozas Mélange) occurring at the base of the Cabo Ortegal Complex also belongs to the ophiolite zones of the Variscan suture. In this paper we describe the Galician ophiolites of the Variscan suture and discuss their tectonic setting of formation. We interpret the generation of the Galician ophiolites within the geodynamic and paleogeographic evolution of the Rheic Ocean and the Pangea supercontinent.

Introduction

In the Variscan Belt, a long suture zone is outlined by thick sequences of mafic and ultramafic rocks that are interpreted as ophiolites. These formed during the closure of at least one oceanic domain during the main stage of Pangea assembly. They are included in allochthonous complexes of several exotic terranes that were, in some cases, affected by high pressure metamorphic events (Martínez Catalán et al., 2007; Fig. 1). It is accepted that the Rheic Ocean was the main oceanic domain closed during the collision of Gondwana and Laurussia in Late Devonian and Carboniferous times (Matte, 2001; Stampfli and Borel, 2002; Winchester et al., 2002) but other, minor, oceanic domains also participated in the formation of Pangea (Arenas et al., 2014a). The Rheic Ocean was the largest ocean during the Paleozoic, in Middle Cambrian-Early Ordovician times, formed during the rifting and later drifting of Avalonia and other minor terranes away from Gondwana (Murphy et al., 2006; Nance et al., 2010; van Staal et al., 2012).

Several recent papers have described the lithologies, chemical compositions and isotopic geochronology of the ophiolites of NW Iberia (Arenas et al., 2007a; Sánchez Martínez et al., 2009). It is now well-known that their igneous protoliths correspond to two age groups which cannot be linked to one stage in the evolution of a single oceanic domain. These ophiolites provide information about the oceanic domains located along the periphery of Gondwana in pre-Ordovician times as well as the oceanic domains involved in the final assembly of Pangea. Two groups of ophiolites can be distinguished: an older group containing Cambrian meta-igneous rocks while a second younger group includes Devonian gabbroic rocks. Moreover, a thick serpentinite mélange forms part of these groups of mafic-ultramafic units.

The long Variscan-Appalachian-Alleghenian Orogen, which extends through parts of Europe and eastern North America, contains key information for reconstructing the amalgamation history of the Pangea supercontinent. In the Variscan Belt, the oldest tectono-thermal events are preserved in the complex suture zone that can be traced from the Iberian Peninsula to the Bohemian Massif (Fig. 1). Two different events of high pressure metamorphism appear to have occurred, relatively close in time although separated by the development of oceanic basins. This evolution is unusual in large collisional belts in which tectono-thermal evolution is commonly interpreted as reflecting a single high-P (HP) or ultra-high-P (UHP) metamorphic event associated with subduction of one of the colliding continental margins (Platt, 1986; Beaumont et al., 2009). In the Variscan Belt, both HP events and the development of some of the oceanic domains occurred after the earliest Devonian and are thus broadly coeval with the initial stages of the assembly of Pangea.

This paper presents a short overview of the features and origin of the ophiolites along the Variscan suture of NW Iberia, and provides a conceptual model within the context of Pangea assembly. These ophiolites are interpreted in relation to the origin and tectonothermal evolution of the other allochthonous terranes in the region. The geological section exposed in the NW Iberian Massif is taken as an example, but allochthonous terranes are fairly continuous along

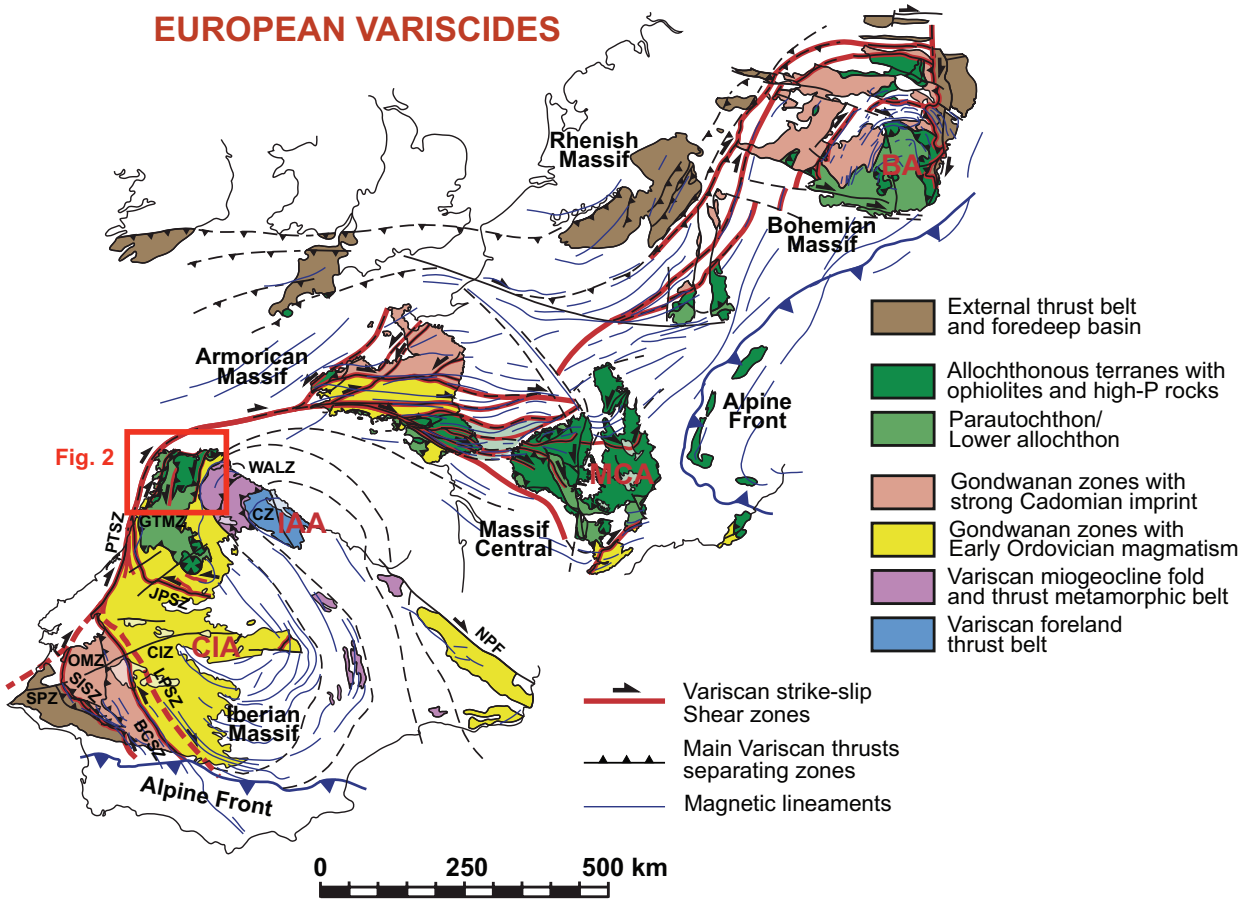

Fig.1. Terranes and oroclines of the Variscan belt (Martínez Catalán, 2011). Arcs: BA, Bohemian; CIA, Central Iberian; IAA, Ibero-Armorican; MCA, Massif Central. Zones of the Iberian Massif: CIZ, Central Iberian; CZ, Cantabrian; GTMZ, Galicia-Trás-os-Montes; OMZ, Ossa-Morena; SPZ, South Portuguese; WALZ, West Asturian-Leonese. Shear zones and faults: BCSZ, Badajoz-Córdoba; JPSZ, Juzbado-Penalva; LPSZ, Los Pedroches; NPF, North Pyrenean; PTSZ, Porto-Tomar; SISZ, Southern Iberian. Location of the geological map and section presented in Fig. 2 is also shown.

the suture and are largely comparable throughout the European Variscan Belt (Faryad and Kachlik, 2013; Kroner and Romer, 2013; Ballèvre et al., 2014; Von Raumer et al., 2015). Recent isotopic and geochronological data on the origin of these ophiolites and U-Pb geochronological constraints on the HP events provide new insights into the early events involved in the formation of Pangea. We infer that the history of convergence and collision was probably longer and more complex than previously described, and that the origin and evolution of the most common ophiolites in the Variscan belt were related to the amalgamation of the supercontinent Pangea.

Terranes incorporated into the Variscan suture of NW Iberia

The NW Iberian section of the Variscan Belt contains terranes with contrasting origins and tectono-thermal evolutions (Arenas et al., 1986; Martínez Catalán et al., 2009). The Central Iberian Zone is the lowest sequence and, together with a parautochthonous domain (Parautochthon or Schistose Domain), defines the main section of the Gondwanan margin involved in the Variscan Orogen (Martínez Catalán et al., 2009) (Figs. 1 and 2). Above that sequence, a set of terranes of allochthonous and alleged exotic origin forms a nappe stack representating the rootless suture zone (Figs. 1 and 2). The origins of the allochthonous complexes have been extensively discussed (Martínez Catalán et al., 2009). Three main groups of terranes have been identified, two of which show continental crustal affinities (Basal and Upper Units). These are separated by ophiolites representing the suture itself (ophiolitic units; Fig. 2).

Located immediately below the suture, the Basal Units contain metasedimentary rocks (comprised of a thick pile of metagreywackes with minor metapelites, graphitic schist, calc-silicate lenses, metacherts and quartzites), calc-alkaline to alkaline-peralkaline metagranitoids, and some mafic rocks. Maximum depositional ages for the metasedimentary series range between Ediacaran and Early Ordovician (Díez Fernández et al., 2010, 2012a) with Nd model ages of between 1.78 and 2.22 Ga (Fuenlabrada et al., 2012). Major and trace element geochemistry of the metagreywackes suggests deposition in association with a peri-Gondwanan arc system built upon a thinned continental margin. Calc-alkaline (c. 493 Ma; Abati et al., 2010) and alkaline-peralkaline (c. 475-470 Ma; Díez Fernández et al., 2012b) granitoids were generated within this arc, suggesting a change over time from convergence to continental rifting. The Basal Units are considered to represent a section of the most external margin of Gondwana originally located somewhere between the West African and Saharan cratons (Díez Fernández et al., 2010). The first tectono-thermal event recorded in these units is a HP and low- to intermediate-

T (LIT) event dated at c. 370 Ma (Rodríguez et al., 2003; Abati et al., 2010). A variety of HP mica schists and orthogneisses, C-type eclogites (Coleman et al., 1965) and some blueschists were formed at that time (Arenas et al., 1995, 1997; Rodríguez et al., 2003; López Carmona et al., 2013, 2014).

Resting above this suture zone, the Upper Units consist of a 10-12 km thick pile of: metasedimentary rocks (mainly metagreywackes) and large massifs of calc-alkaline orthogneisses, and gabbros, with compositions of island-arc tholeiites, together with medium to high-grade mafic rocks, including B-type eclogites (Coleman et al., 1965), HP granulites, and some ultramafic massifs. The structurally highest low grade metagreywackes have a Middle Cambrian maximum depositional age (Fernández-Suárez et al., 2003), with Nd model ages ranging between 0.72 and 1.22 Ga, and major and trace element compositions typical of active margin settings (Fuenlabrada et al., 2010). Protolith ages for the gabbros and granitoids range between 490 and 520 Ma (Fernández-Suárez et al., 2007; Andonaegui et al., 2012). These units were probably part of a Cambrian peri-Gondwanan magmatic arc located in the periphery of the West African Craton, to the West of the external margin section represented by the Basal Units (Díez Fernández et al., 2010; Fuenlabrada et al., 2010; Albert et al., 2015). The Upper Units may be divided into two groups based on metamorphic criteria. An uppermost section shows intermediate-P (IP) metamorphism ranging from chlorite to granulite facies. The main tectono-thermal events recorded in this uppermost section are Cambrian in age and were probably developed in response to the accretionary dynamics of the peri-Gondwanan arc system (Abati et al., 1999, 2007; Díaz García et al., 2010). A lower section is characterized by HP and high-T (HT) metamorphism dated at c. 400-390 Ma (Ordóñez Casado et al., 2001; Fernández-Suárez et al., 2007). The latter metamorphic event reached UHP conditions in other domains of the Variscan belt (Lardeaux et al., 2001).

The ophiolites of NW Iberia consist of a diverse group of mafic-ultramafic sequence making up five different ophiolites and a serpentinite mélange (Fig. 2). Two groups of ophiolitic units have been distinguished (Fig. 2): an older group (Lower Ophiolitic Units) containing meta-igneous rocks of Late Cambrian age (c. 497-495 Ma), and a younger group (Upper Ophiolitic Units) including gabbroic rocks of Devonian age (Emsian-Eifelian; c. 395 Ma). The Lower Ophiolitic Units are interpreted as a series of mafic complexes linked to the dynamics affecting the most external margin of Gondwana in Cambrian-Early Ordovician times. The Middle Devonian ophiolites are the most abundant group found in the Variscan suture (Díaz García et al., 1999; Murphy et al., 2011; Arenas et al., 2014b). The origin of this group of ophiolites has been the subject of different interpretations. The most relevant features of the Galician ophiolites are described in the following sections.

Ophiolitic units

According to a typical Wilson Cycle, a collisional orogen should contain a single ophiolitic belt, representative of the consumed oceanic domain. However, it is known that preservation of ancient N-MORB type oceanic lithosphere is extremely difficult, since its thermal structure favors complete elimination by subduction. In contrast, many of the ophiolites emplaced in orogenic belts are sequences typically generated in supra-subduction zone settings, either during the last stages of the closure of the ocean or during the opening of more-or-less ephemeral basins (Leitch, 1984; Pearce et al., 1984; Dilek and Furnes, 2011). Ophiolitic belts generated in connection with pull-apart ephemeral basins have also been described (Murphy et al., 2011). These buoyant oceanic lithospheres show greater resistance to subduction and can be easily thrust over continental margins instead (Murphy et al., 2011). Moreover, the dynamics of the collision and the eventual development of a high rate of lateral convergence may allow the incorporation of oceanic sections of different ages and characteristics into the orogen. Hence, the real dynamic context may generate situations that tend to increase the variety of ophiolitic belts incorporated into an orogen which rarely contains a simple ophiolite generated at one particular time. In the Variscan Belt recent studies have described a variety of ophiolites with significant differences in lithological constitution and age. Such diversity responds to a variety of dynamic settings of generation. Proper understanding of these would improve knowledge of paleogeographic evolution in pre-Variscan and Variscan times.

In the NW Iberian Massif, a set of tectono-stratigraphic units comprising mafic and ultramafic lithologies, and almost devoid of metasedimentary rocks, were interpreted as ophiolites included in the allochthonous complexes (Arenas et al., 1986). Two groups of ophiolitic units are distinguished in Galicia (Arenas et al., 2007a) (Fig. 2), which can be generally correlated with equivalent groups along the entire belt. The Upper Ophiolitic Units are Devonian in age and according to their chronology they represent the most common type of ophiolites in the Variscan suture (Díaz García et al., 1999; Murphy et al., 2011; Arenas et al., 2014b). Ophiolites of this age have also been described in Cornwall (Lizard Ophiolite; Clark et al., 1998; Nutman et al., 2001), Armorican Massif (Drain Ophiolite; Ballèvre et al., 2009, 2014) and the Bohemian Massif (Sleza Ophiolite; Dubinska et al. 2004; Kryza and Pin 2010). These ophiolites have been traditionally considered to be related to the evolution of the Rheic Ocean, their origin coinciding with the final stages of its development (Díaz García et al., 1999; Sánchez Martínez et al., 2007a). However, new geochronology and isotope geochemistry data question the relationship of the Devonian ophiolites with this ocean, suggesting that they are more likely to be related to the opening of minor ephemeral oceanic domains (Arenas et al., 2014a). The Lower Ophiolitic Units include Cambrian mafic-ultramafic sequences which developed in different dynamic contexts. Their origin may be related either to the opening of the Rheic Ocean (Arenas et al., 2007b) or to a geodynamic regime that occurred prior to the opening of this ocean (Sánchez Martínez et al., 2012).

In the NW Iberian Massif in Galicia, five ophiolitic units have been delineated. The Lower Ophiolitic Units comprise the Vila de Cruces and Bazar ophiolites while the Upper Ophiolitic Units are represented by the Careón, Purrido and Moeche ophiolites. A thick mélange of serpentinite, the Somozas Mélange, can be included among the ophiolitic and related sequences of NW Iberian Massif.. Other different ophiolitic units of similar age and setting have also been described in the neighboring region of Trás-os-Montes, Portugal (Pin et al., 2006). The ophiolitic units of Galicia will be described separately, as they show different lithologic constitutions and tectono-thermal evolutions.

Lower Ophiolitic Units

Bazar Ophiolite

The Bazar Ophiolite, located in the westernmost part of the

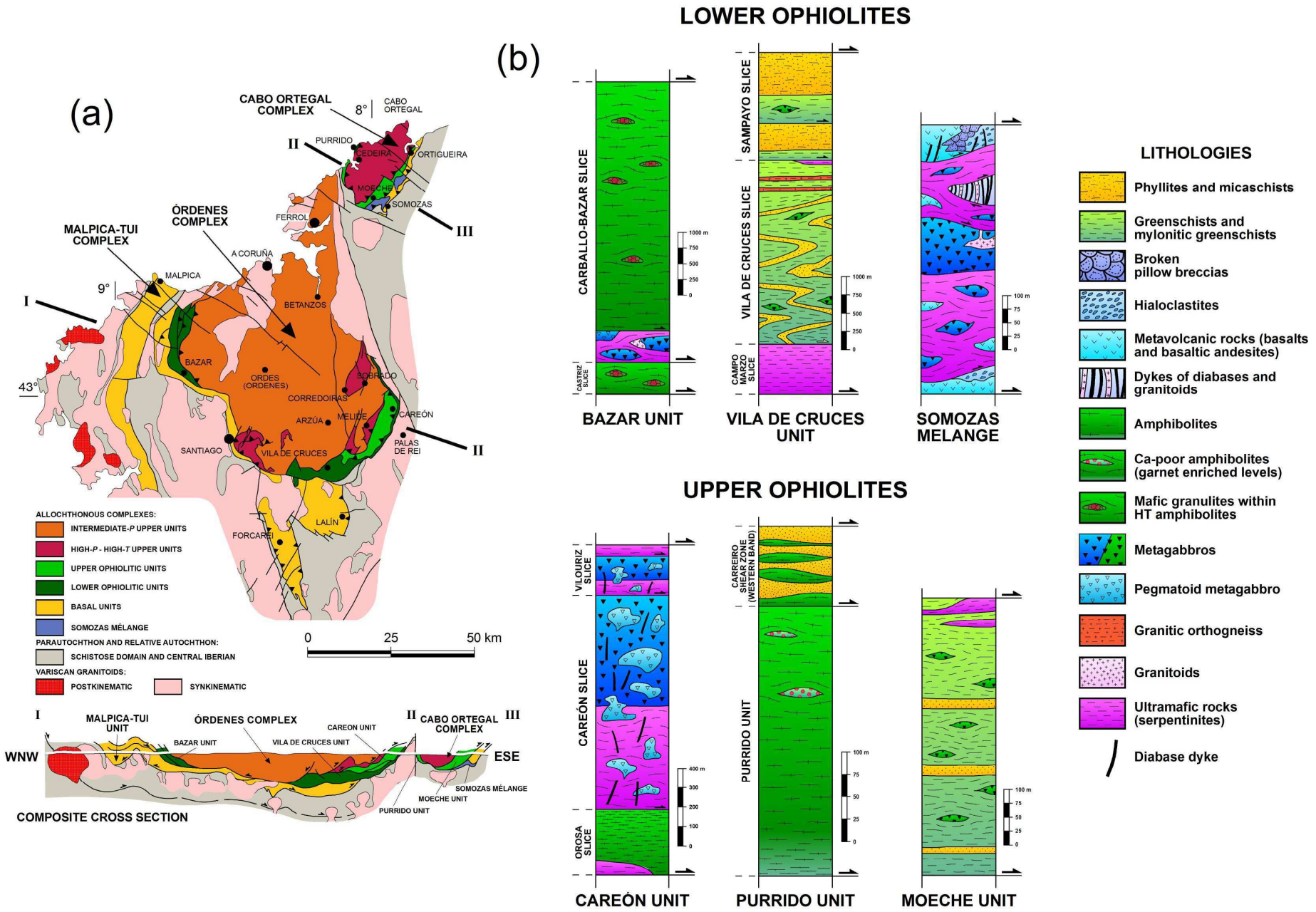

Fig.2. (a) Geological map and cross section of the allochthonous complexes of the NW Iberian Massif (Galicia region). These show the distribution and general structure of the terranes involved in the Variscan suture. The locations and names of the ophiolites are also indicated. (b) Schematic columns showing the lithological constitution of the ophiolites from Galicia.

Órdenes Complex (Fig. 2), consists of an imbricate of tectonic slices, c. 5000 m thick, containing metagabbroic rocks and a minor proportion of ultramafic rocks at the base of the ophiolite (Díaz García, 1990). The main tectonic slice (Carballo-Bazar; Sánchez Martínez et al., 2009, 2012; Fig. 2) is c. 4000 m thick and is composed of amphibolites and foliated metagabbros with an HT foliation, which evolved from an initial granulite-facies tectono-thermal event (Fig. 3). Scarce metre-sized boudins of mafic granoblastic granulites are preserved within the metagabbros (Fig. 3). They are wrapped by the HT foliation and their mineral association is transitional between low and intermediate pressure conditions (plagioclase-clinopyroxene-orthopyroxene-hornblende-ilmenite±garnet±olivine). The lower part of the main slice consists of relatively well-preserved gabbros and ultramafic rocks, with minor leucogabbros and tonalites (Fig. 2). The geochemical features of the most representative lithologies of the Bazar Ophiolite are variable. The common amphibolites, which are the most abundant lithological type, and the metagabbros, show compositions equivalent to island-arc tholeiites or N-MORB (Fig. 4a). However, the mafic granulites seem to be transitional between MOR (mid-ocean ridge) and WP (within-plate) basalts, with normalized trace element patterns similar to those of T-MORB generated by plume-ridge interactions (Pearce, 1996) (Fig. 4a).

Zircon grains obtained from an amphibolite sample have an internal structure characterized by the presence of a magmatic core surrounded by a very irregular overgrowth rim (Fig. 5a). Their analysis yielded two different groups of U-Pb concordant ages (Fig. 5b) which are significant according to their contrasting $^{176}Yb/^{177}Hf$ ratios (Fig. 5c). The first group corresponds to an average age of 495 ± 2 Ma interpreted as the intrusive age of the gabbroic protoliths. The second group yields an average age of 475 ± 2 Ma and is interpreted to date the high-T metamorphic event (Sánchez Martínez et al., 2012). The Hf isotope composition of the zircons from this amphibolite sample reveals the juvenile signature of the mafic protoliths of this unit and a lack of interaction with old crustal components (Fig. 5d). These features, combined with the trace element composition of the mafic rocks, suggest that the protoliths of the Bazar Ophiolite were generated in an oceanic setting, although the mafic rocks are compositionally heterogeneous.

The compositional features, age and tectono-thermal evolution of the Bazar Ophiolite indicate that it may represent a lithospheric section of the Cambrian peri-Gondwanan ocean. The specific dynamic setting in which the mafic rocks originated is uncertain, but the presence of metagabbros with N-MORB composition suggests that it involved the participation of a mid-ocean ridge. The oceanic lithosphere represented by the Bazar Ophiolite should have been buoyant, given the small time difference (c. 20 Ma) between the ages of protoliths and HT metamorphism, and was accreted under the peri-Gondwana system of magmatic arcs. The development of a low-medium-P granulitic metamorphism is compatible with overheating associated with the base of the magmatic arc, but could also be caused

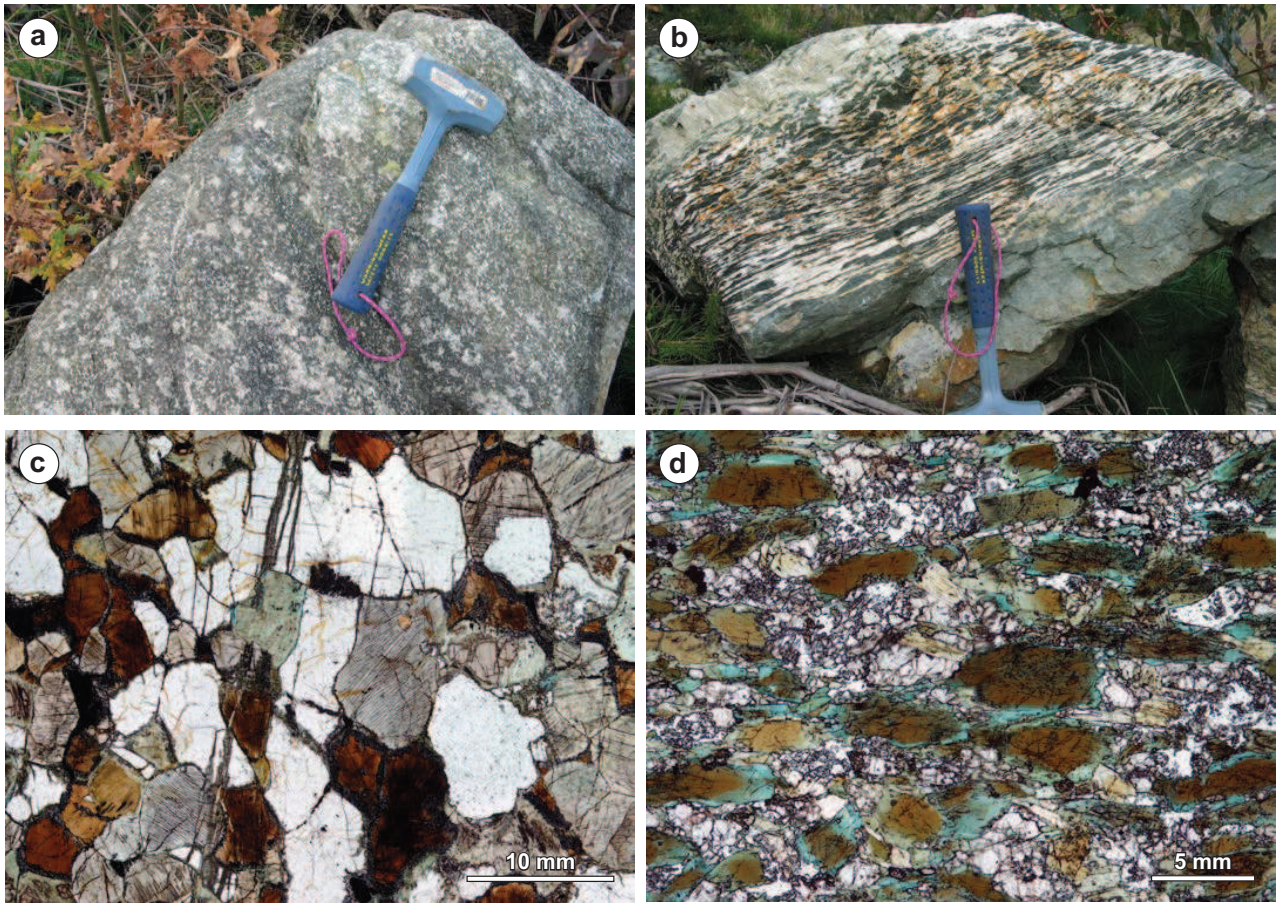

Fig. 3. Field and petrographic aspects of the Bazar Ophiolite. (a) Coarse-grained gabbro. (b) Strongly sheared metagabbro. (c) Low to intermediate-P mafic granulite composed of clinopyroxene, orthopyroxene, plagioclase, brown hornblende, biotite and very thin garnet coronas, occasional olivine crystals can also appear. (d) HT amphibolite developed after the granulites. It shows a first generation of brown hornblende subsequently replaced by blue-green amphibole.

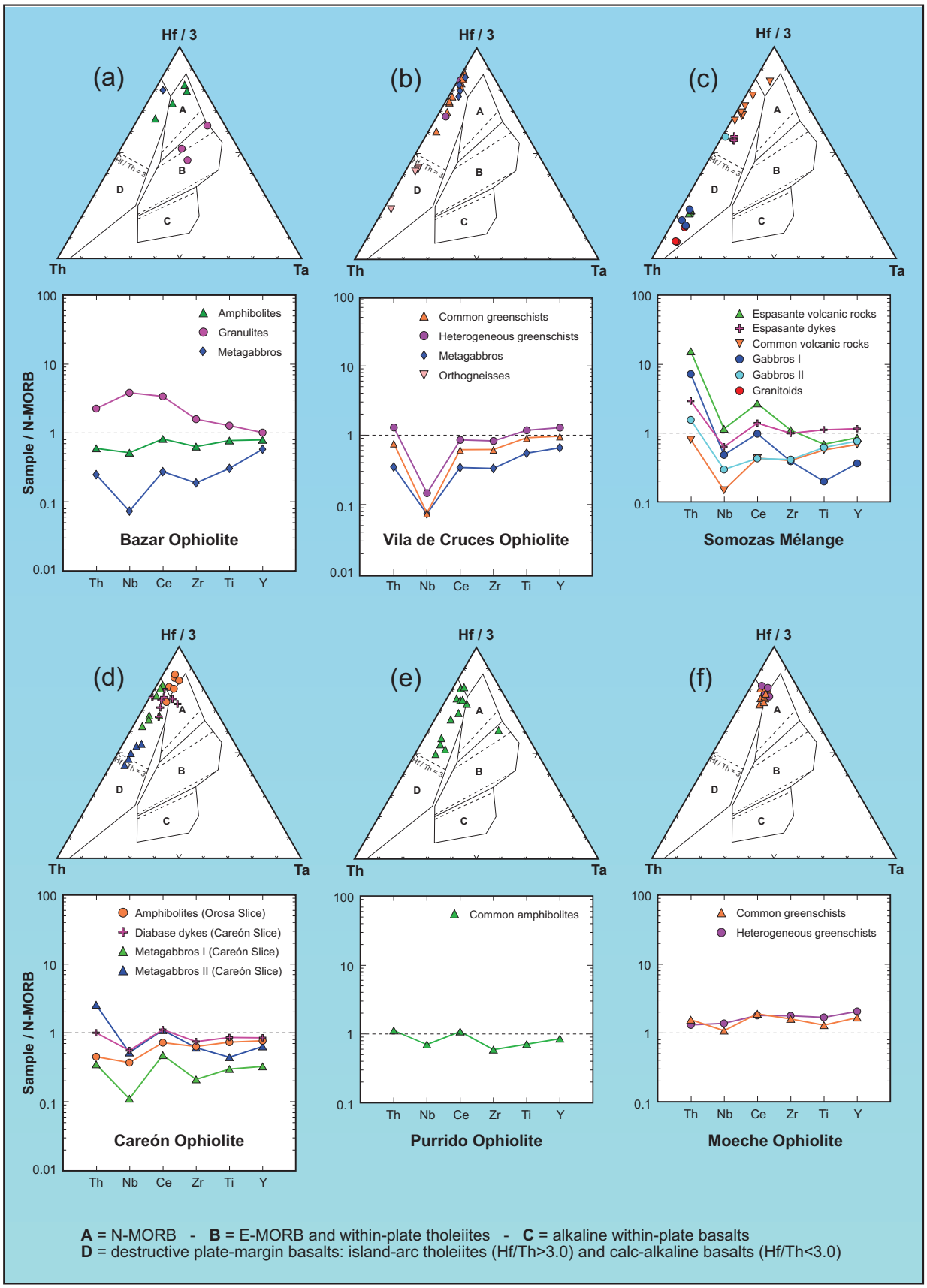

Fig. 4. Th-Hf-Ta diagrams (Wood, 1980) and N-MORB-normalized trace-element patterns (selected elements and normalizing values according to the criteria of Pearce, 1996) for the most representative lithologies of the ophiolites included in the allochthonous complexes of Galicia. (a) Bazar Ophiolite. (b) Vila de Cruces Ophiolite. (c) Somozas Mélange. (d) Careón Ophiolite. (e) Purrido Ophiolite. (f) Moeche Ophiolite.

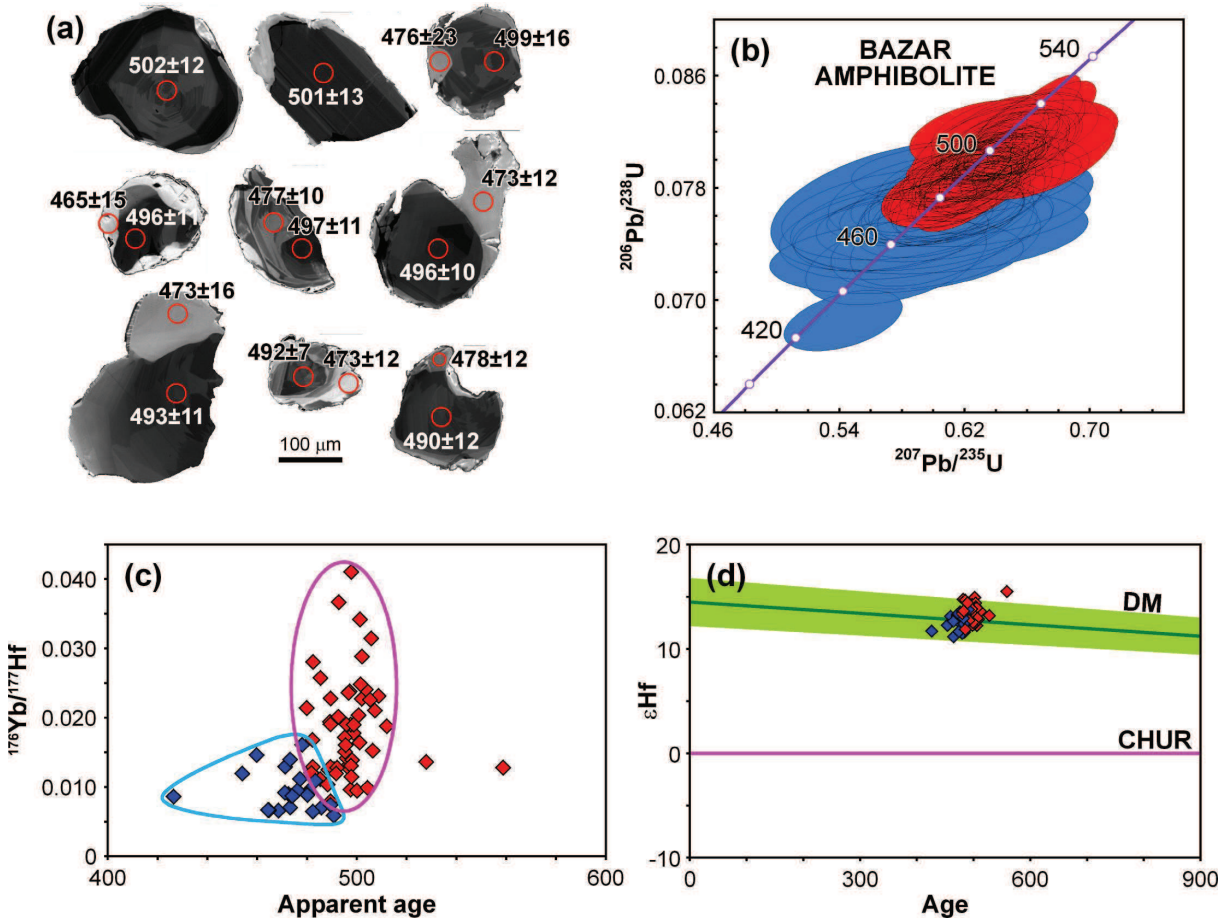

Fig. 5. U-Pb dating and Lu-Yb-Hf isotope data of a metagabbroic amphibolite sample from the Bazar Ophiolite. (a) Cathodo-luminiscence images of selected zircons, circles representing the spot size of U-Th-Pb analyses. (b) Concordia diagram showing the results of the U-Pb analyses, with two statistically coherent groups of data. (c) $^{176}Yb/^{177}Hf$ versus apparent age diagram, the different trends of each group of analyses appearing encircled. (d) εHf versus apparent age plot; the depleted mantle array (DM) is extrapolated from average modern-day values of mid-ocean ridge basalts (Chauvel and Blichert-Toft, 2001), assuming a linear behaviour from εHf = 2 at 4000 Ma (Vervoort and Blichert-Toft, 1999). Red symbols = zircon cores, blue symbols = zircon overgrowths-recrystallized domains. Modified after Sánchez Martínez et al. (2012).

by the subduction of a section of a mid-ocean ridge and the opening of an ephemeral asthenospheric window (Fig. 6).

Vila de Cruces Ophiolite

Located SE of the Órdenes Complex, the Vila de Cruces Ophiolite has a complex structure characterized by the presence of at least two superimposed tectonic slices with a total thickness of c. 4000 m (Fig. 2). The main lithologies are greenschist rocks of possible metavolcanic origin, alternating with abundant layers of phyllites, mica schists and schists with albite and garnet porphyroblasts, and scarce metachert bands. Lenticular intercalations of metagabbros and two bodies of tonalitic orthogneisses, transitional to metagabbroic types, can also be identified. Thin serpentinite bands occur along the contact between the main slices. Immobile trace element abundances of both the mafic types and the tonalitic orthogneisses are typical of magmas generated at destructive plate margins (Fig. 4b). Greenschists and metagabbros have compositions characteristic of island-arc tholeiites. The presence of a strong negative Nb anomaly compared to N-MORB (Fig. 4b) is also compatible with the supra-subduction zone setting proposed for this ophiolite (Arenas et al., 2007b).

The orthogneisses from this ophiolite are dated at 497 ± 4 Ma (U-Pb in zircon; Arenas et al., 2007b). However this unit was interpreted as a composite terrane instead of a simple ophiolite (Sánchez Martínez, 2009; Sánchez Martínez et al., 2009) based on the discovery of zircon populations of imprecise Mesoproterozoic ages (1168–1176 Ma) in two samples of metagabbros. New U-Pb zircon dating has provided very consistent ages of c. 500 Ma in a sample of metagabbros and three samples of orthogneiss (Sánchez Martínez et al., 2013). That is now considered to be the igneous protolith age of the Vila de Cruces Ophiolite. As in the Upper Ophiolitic Units, discussed below, the presence of Mesoproterozoic zircons is considered to be evidence of interaction between the igneous protoliths and the continental crust.

The Vila de Cruces Ophiolite has a penetrative regional foliation, which transects a previous schistose fabric. Both schistosities are associated with different generations of mappable-scale recumbent folds (Arenas et al., 2007b). The regional metamorphic conditions correspond to the greenschist facies, but they can reach amphibolite facies or transitional conditions to that facies in the upper levels. There, the micaschists contain a mineral assemblage with garnet-chlorite-white mica but lack biotite, suggesting that the unit underwent

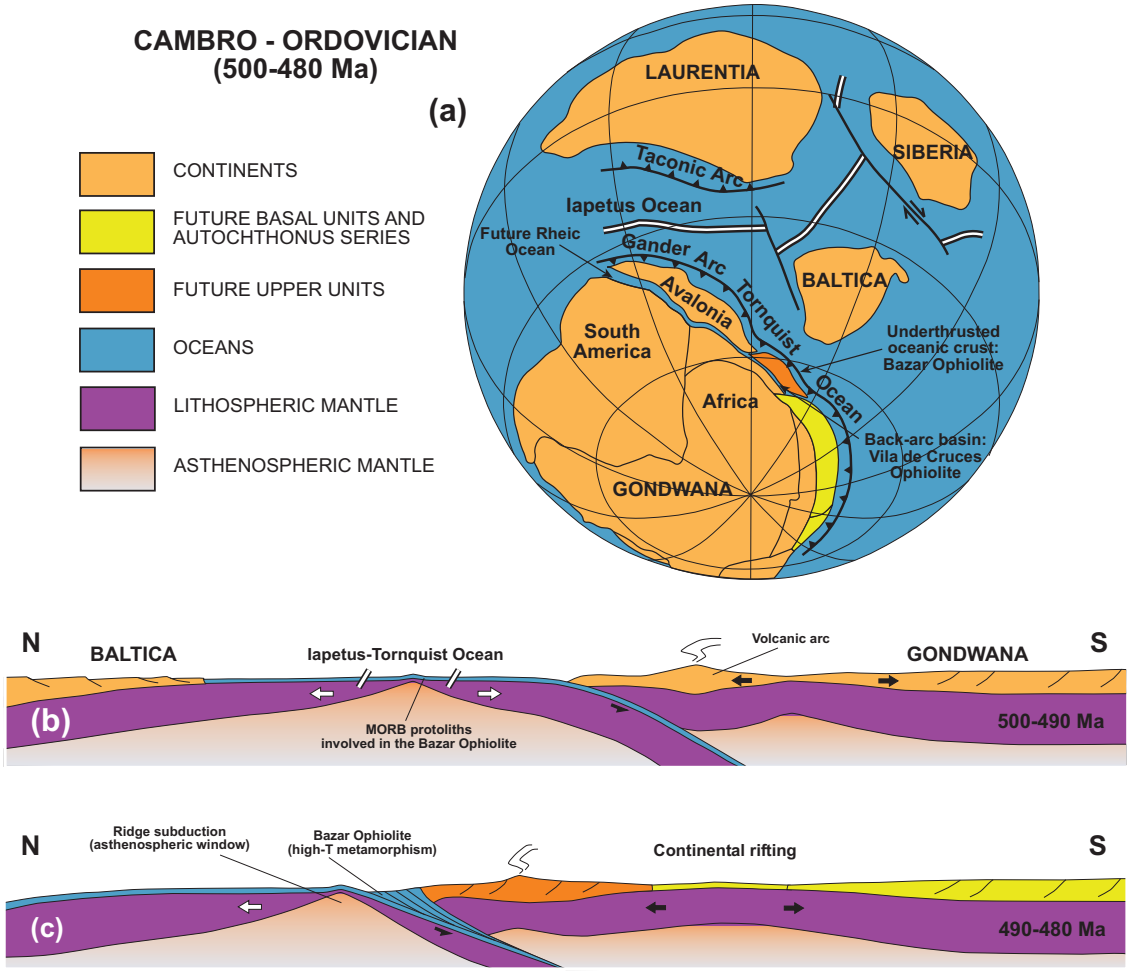

Fig. 6. A paleogeographic reconstruction (a) and interpretive tectonic cross sections of the Iapetus realm during the Cambro-Ordovician (b and c). These diagrams show the tectonic setting for a time immediately prior to the opening of the Rheic Ocean. The Bazar Ophiolite probably represents a remnant of the peri-Gondwanan oceanic lithosphere accreted below a volcanic-arc system, whereas the Vila de Cruces Ophiolite contains the remnants of an incipient backarc basin. Based on Winchester et al. (2002), Arenas et al. (2007b), Gómez Barreiro et al. (2007) and Sánchez Martínez et al. (2012).

an initial HP metamorphic event. The age of the regional foliation is estimated at 363-367 Ma, according to $^{40}Ar/^{39}Ar$ dating of white mica concentrates from two phyllite samples (Dallmeyer et al., 1997).

Because the chemical composition of the mafic and felsic rocks is typical of magmatic arcs, and the abundance of sedimentary rocks, the Vila de Cruces Ophiolite is considered to be a supra-subduction zone sequence generated in a Cambrian back-arc basin opened at the periphery of Gondwana (Arenas et al., 2007b) (Fig. 6). It therefore represents a transitional crust domain where magmas of juvenile mantle provenance interacted with a thinned continental crust.

Upper Ophiolitic Units

Careón Ophiolite

This ophiolitic unit contains the best preserved meta-igneous succession in the NW Iberian Massif (Fig. 2). It consists of three imbricated sheets that repeat the mantle-crust transition with a total thickness of c. 1500 m (Figs. 7 and 8). The thickest slice is the c. 1000 m thick Careón Sheet, which consists mainly of serpentinized ultramafic rocks and isotropic metagabbros, with abundant stocks of pegmatoid metagabbros emplaced at all levels as well as scarce wehrlite sills. Diabase and late diabase dykes cut all exposed levels, from the deepest mantle section to the most superficial crustal sections.

The lithological constitution of the Careón Ophiolite differs significantly from the classical HOT and LOT ophiolitic types defined by Nicolas (1989, 1995) (Fig. 8). Therefore, it was interpreted as an ophiolite generated in a supra-subduction zone setting by Díaz García et al. (1999). The intrusion of abundant diabase dikes at all levels of the Careón Sheet suggests the development of this ophiolite via extension and thinning, in the upper plate of a subduction zone. Immobile trace element abundances (Wood, 1980) (Fig. 4d) are typical of island-arc tholeiitites, and the youngest diabase dykes have compositions transitional to N-MORB. All lithologies present in the Careón Ophiolite display a negative Nb anomaly compared to N-MORB, which is compatible with generation in an active supra-subduction zone setting (Sánchez Martínez et al., 2007a) (Fig. 4d).

The Careón Ophiolite was the first ophiolite to be dated by isotope geochronology in the NW Iberian Massif. U-Pb zircon dating of a sample of pegmatoid metagabbro from the Careón Sheet yielded a

Fig. 7. Field aspects of the Careón Ophiolite. (a) Layered ultramafic rocks. (b, c) Complex intrusive relationships with local development of mingling processes.

protolith age of c. 395 Ma (Díaz García et al., 1999). Similar U-Pb ages were obtained later by analyzing zircons from a similar metagabbro sample from the same sheet (Pin et al., 2002). The three imbricated sheets have a penetrative foliation with evidence of increasing temperature towards the top of each sheet, reaching the highest temperatures close to the contact with the ultramafic rocks of each overlying sheet. There, the gabbroic rocks were transformed into garnet amphibolites. There are also higher temperature metamorphic soles with very local development of metre-scale corundum-rich layers (Fig. 8). The P-T conditions reached during the deep imbrication of the ophiolitic sheets are estimated as 11.5 Kbar and 650 °C in the garnet amphibolites from the upper part of the Careón Sheet (Fig. 8). The mineral lineation in the amphibolites has a consistent E-W orientation, with an associated top-to-the-east sense of shearing (Gómez Barreiro et al., 2010). The imbrication occurred at c. 377 Ma, according to the $^{40}Ar/^{39}Ar$ dating of hornblendes from the amphibolitic foliation (Dallmeyer et al., 1997).

The Careón Ophiolite was initially interpreted as having been generated in an intra-Rheic Ocean supra-subduction zone (Díaz García et al., 1999; Sánchez Martínez et al., 2007a), beneath which was subducted almost all of the old dense oceanic lithosphere of the Rheic Ocean. Thus, common N-MORB compositional types have not been clearly described so far in the Variscan Belt. The youngest lithosphere generated in this intra-Rheic subduction zone at c. 395 Ma would have been buoyant, and was accreted shortly after its formation at c. 377 Ma, below the southern margin of Laurussia. These are now the most common ophiolites in the Variscan suture. This initial interpretation will be discussed in the following sections in the light of new data obtained from the other Upper Ophiolitic Units.

Purrido Ophiolite

Located at the westernmost limit of the Cabo Ortegal Complex, the Purrido Ophiolite consists of c. 300 m of monotonous amphibolites and garnet-bearing amphibolites of metagabbroic origin (Figs. 2 and 9). Unlike the Careón Ophiolite, well preserved igneous features are not seen but the amphibolite types that appear within both units are very similar from mineralogical and compositional points of view, so both of these ophiolites have been traditionally correlated (Sánchez Martínez et al., 2007b). The mafic rocks have compositions typical of island-arc tholeiites, with slight negative Nb anomalies (Sánchez Martínez et al., 2007b) (Fig. 4e).

U-Pb dating of an amphibolite with a dominant zircon population of c. 1160 Ma was originally interpreted as the age of the gabbroic protolith but with minor populations ranging between 1.2-1.6 Ga considered to be inherited grains (Sánchez Martínez et al., 2006). However, subsequent U-Pb zircon dating of two amphibolite samples provided a single consistent age at c. 395 Ma, interpreted as the actual protolith age thus coinciding with the age previously obtained in the Careón Ophiolite (Sánchez Martínez et al., 2011). The Lu-Hf isotope geochemistry in zircons from this ophiolite demonstrate complex evolution, clearly indicating participation of Paleo-Proterozoic isotopic sources and mixing with juvenile material at c. 395 Ma (Fig. 10). Whole rock Sm-Nd isotope geochemistry of the amphibolitic rocks also indicates important isotopic heterogeneity of the mafic material (Murphy and Gutierrez-Alonso, 2008; Sánchez Martínez et al., 2011). The Purrido amphibolites show intense plano-linear foliation development in the amphibolite facies which has been dated at 391.3 ± 6.6 Ma ($^{40}Ar/^{39}Ar$ in hornblendes; Dallmeyer et al., 1997).

The geochemical and geochronological data provided by the Purrido Ophiolite are interpreted as reflecting interaction between Devonian gabbroic magmas and continental crust. This interpretation calls into question the initially proposed origin for the Upper Ophiolitic Units in an intra-Rheic Ocean subduction zone, seeming to indicate a different tectonic and paleogeographic setting. This new interpretation will be discussed below in the context of a new model for the origin and tectono-thermal evolution of the terranes incorporated in the Variscan suture.

Moeche Ophiolite

The Moeche Ophiolite crops out widely in the eastern part of Cabo Ortegal Complex (Fig. 2). The Moeche and Purrido ophiolites are in contact in a small coastal section to the West of Cedeira village, where the Moeche Ophiolite occupies the lower structural position. This ophiolitic unit consists of c. 500 m of greenschists with abundant intercalations of phyllites and mica schist and scarce metagabbros and serpentinites (Fig. 9). Th-Hf-Ta plots for the metabasites (Wood, 1980) indicate chemical compositions transitional between N-MORB and island-arc tholeiites. They show a slight enrichment of trace element abundances relative to N-MORB (Sánchez Martínez et al., 2007b) (Fig. 4f).

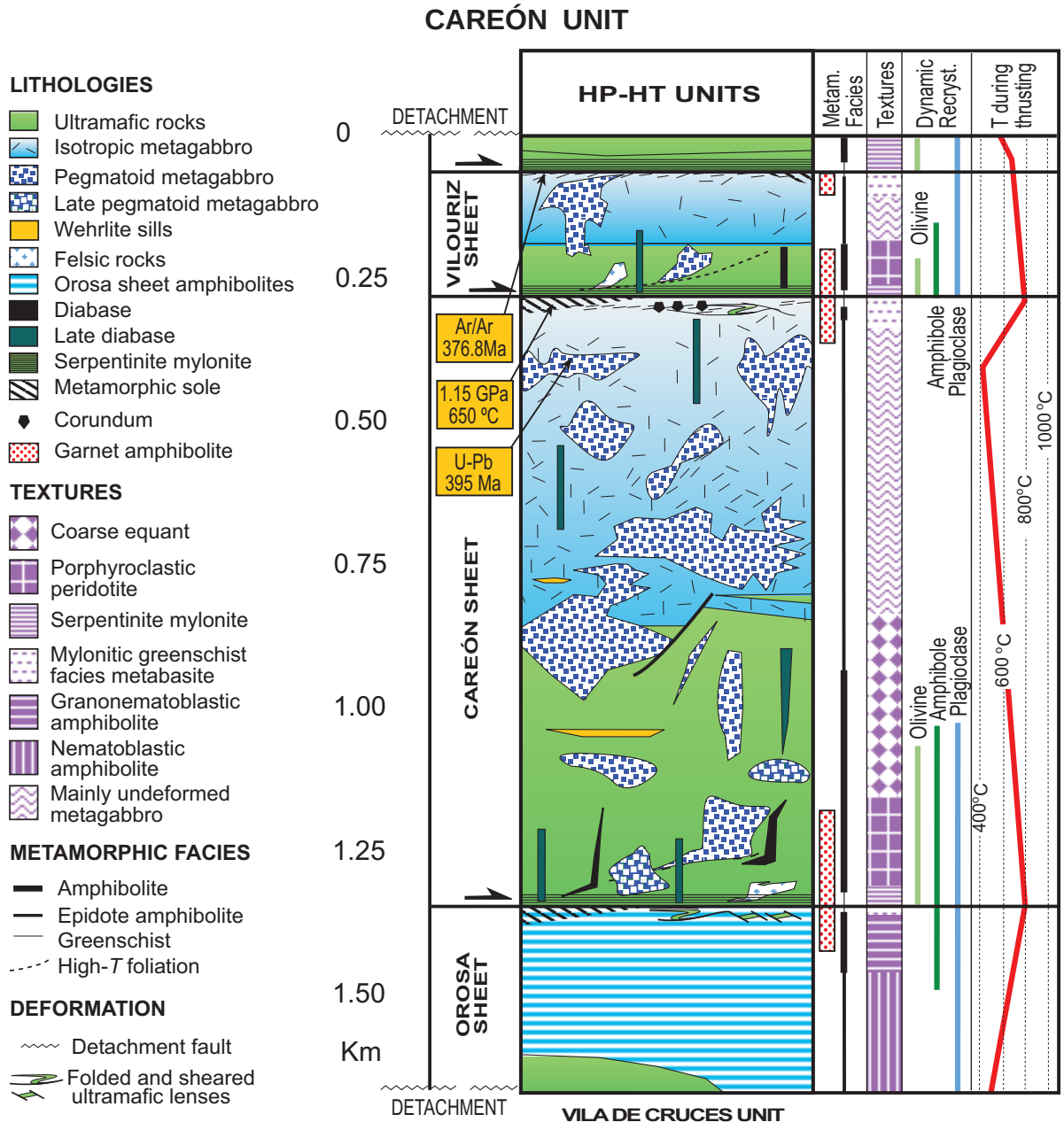

Fig. 8. Synthetic column of the Careón Ophiolite showing the main lithologies and imbricates, distribution of metamorphic facies, textures, levels where dynamic recrystallization of main components occurred, and the saw-tooth thermal gradients developed during the earliest stages of thrusting. The U-Pb age of the gabbroic protoliths, $^{40}Ar/^{39}Ar$ age of hornblende in metamorphic soles and the peak P-T conditions reached during the accretion are also shown. Modified from Díaz García et al. (1999).

U-Pb dating of zircons from a mylonitic greenschist yield an age of 400 ± 3 Ma (Arenas et al., 2014b) which is comparable to the ages obtained in Careón and Purrido ophiolites. Lu-Hf isotope signatures of the zircons clearly indicate contributions from a continental source. εHf values in the analyzed zircons are negative (generally below εHf = -5), and hence they are not compatible with crystallization from a juvenile mantle source (Fig. 10). Isotopic Hf data from the zircons of the Moeche Ophiolite are similar to those from the Purrido Ophiolite. These data are again incompatible with formation in an oceanic setting far from continental domains.

The internal structure of the Moeche Ophiolite is poorly known. It displays a regional foliation in greenschist facies conditions which generally has mylonitic-ultramylonitic character. This hinders the recognition of the original nature of the mafic igneous protoliths which have been regarded as both basaltic and gabbroic. The regional foliation is axial planar to tight outcrop-scale recumbent folds. $^{40}Ar/^{39}Ar$ dating of the mylonitic foliation in the phyllite intercalations has provided an age of c. 364 Ma (whole rock analysis; Dallmeyer et al., 1997), which is slightly younger than the other regional fabrics dated in the Upper Ophiolitic Units.

Somozas Mélange

The lowest part of Cabo Ortegal Complex includes a thick tectonic mélange which is only represented in this part of the allochthonous complexes of the NW Iberian Massif (Fig. 2). This tectonic mélange

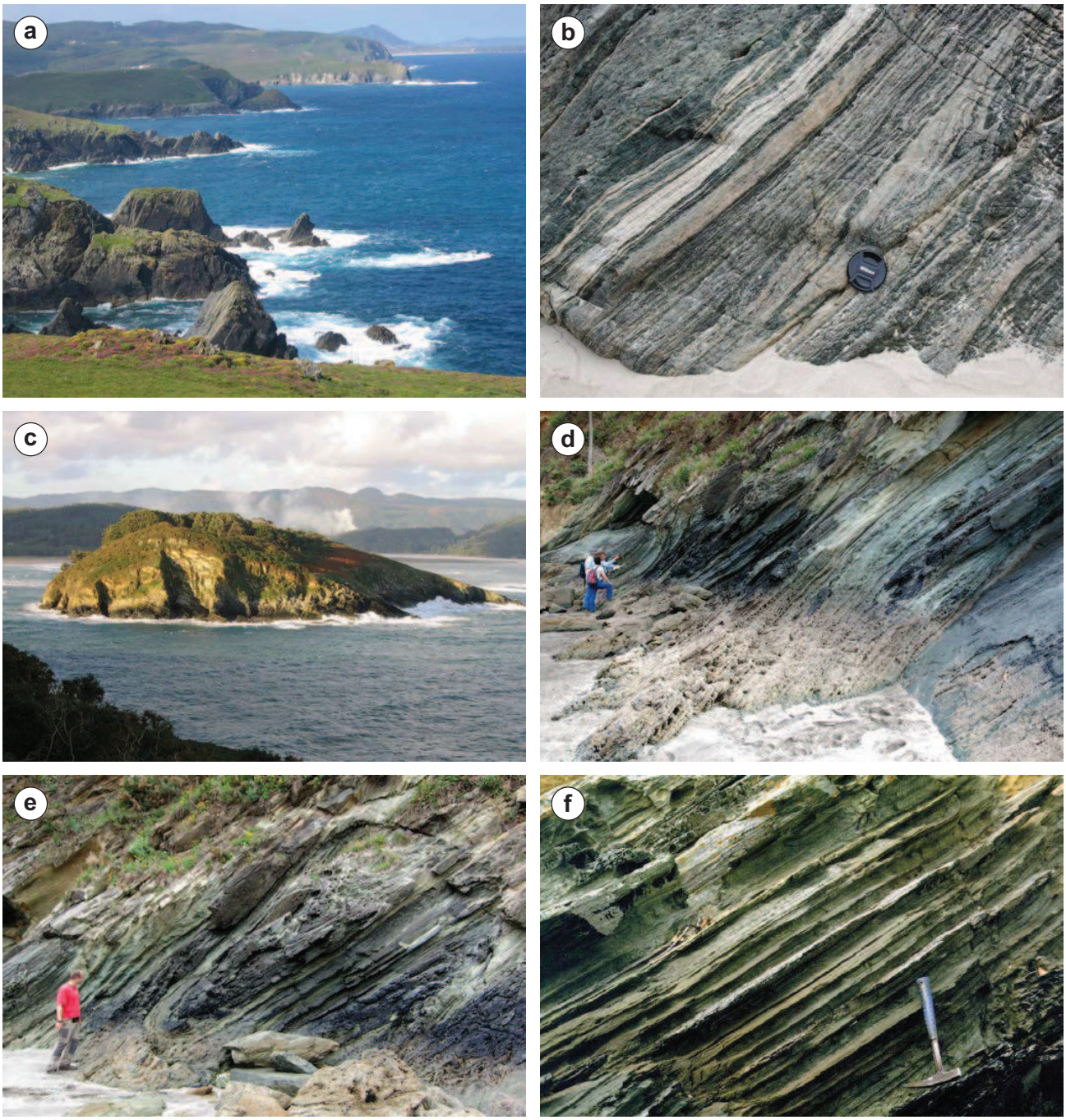

Fig. 9. Field aspects of the Purrido and Moeche ophiolites. (a) Exposures of the Purrido Ophiolite in the western coastal sections of the Cabo Ortegal Complex (foreground). (b) Banded Purrido amphibolites in Baleo beach; these show thick intra-foliation folds. (c) Moeche Ophiolite exposed in San Vicente Island, in the eastern section of the Cabo Ortegal Complex. (d, e, f) Typical mylonitic greenschists of the Moeche Ophiolite in San Vicente island. Observe the large recumbent folding present in this unit, well shown in photograph (e).

is located in the advancing front of the large thrust sheet represented by the allochthonous complexes. The Somozas Mélange was initially described by Arenas et al. (1986), Arenas (1988) and Marcos et al. (2002). More recently, Arenas et al. (2009) presented a detailed map of the mélange in addition to whole-rock geochemical data of the igneous rocks and some U-Pb zircon ages.

The Somozas Mélange is better exposed in the southern part of Cabo Ortegal Complex, where it comprises a c. 1800 m thick unit composed of two contrasting members (Fig. 2). The upper member is c. 800 m thick and is a mélange with a strongly sheared serpentinite matrix. This matrix surrounds tectonic blocks ranging from metre-hectometre to kilometre sizes. The tectonic blocks consist of gabbro, diabase, granitoid, metabasalt, andesitic basalt, pillow breccia, pillow lava, hyaloclastite, marble, phyllite, sandstone and conglomerate, together with HT metamorphic rocks including orthogneisses, common amphibolite and zoisite-rutile rich metabasites (Fig. 11). Many of these tectonic blocks are exotic: their source rocks have not been identified in the allochthonous complexes or the Parautochthon. The lower member is c. 1000 m thick and it is composed of a mélange with a matrix of ochre colored phyllites or

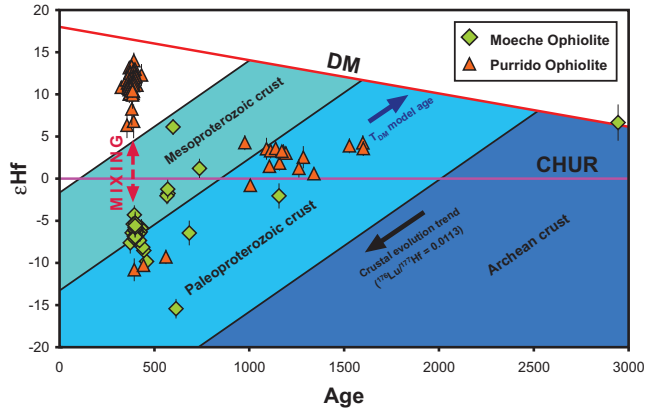

Fig. 10. εHf versus age diagram combining the U-Pb and Lu-Hf isotope data of zircons from the Purrido and Moeche ophiolites. Crustal evolution trends ($^{176}Lu/^{177}Hf$ = 0.0113) for the Archean, Paleoproterozoic and Mesoproterozoic crusts are also shown. Based in Sánchez Martínez et al. (2011) and Arenas et al. (2014b).

blue colored phyllonites surrounding tectonic blocks of the lithologies incorporated into the serpentinite mélange. No HP rocks have been described so far in the Somozas Mélange, although some of the high-T tectonic blocks reached at least the highest pressure conditions of the amphibolite facies. However, a detailed study of all mineral assemblages has not yet been made.

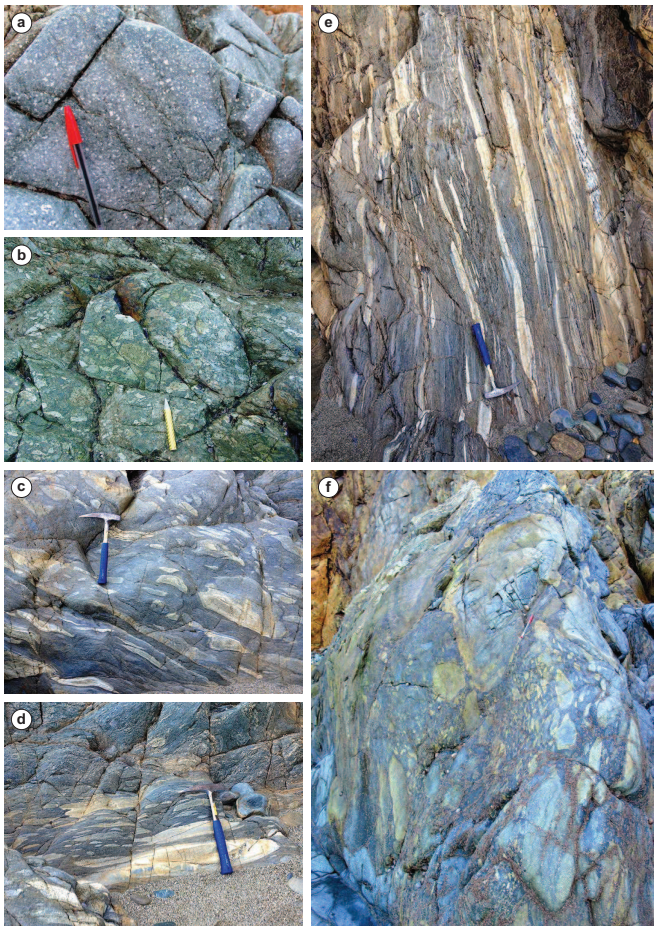

Fig. 11. Field aspects of tectonic blocks in the Somozas Mélange. (a) Massive basaltic andesites. (b) Broken pillow-breccia. (c, d) Sheared pillow breccias with local presence of intrusive diabase dykes. (e) Strongly sheared pillow breccias. (f) Undeformed pillow breccia with preserved large whole pillows.

U-Pb zircon dating was undertaken on a tonalitic orthogneiss from a large high-T tectonic block and on two few deformed granitoids affected by low-grade recrystallization (Arenas et al., 2009). The HT orthogneiss yields an age of c. 485 Ma (SHRIMP), and the two granitoids yield ages of c. 499 Ma (SHRIMP) and c. 527 Ma (LA-ICP-MS). Whole rock geochemistry of all the igneous rocks in the mélange, whether volcanic, plutonic or dykes, points to a volcanic arc setting (Fig. 4c). A negative Nb anomaly is exhibited by all lithologies, a feature considered an indication of a supra-subduction zone setting (Fig. 4c). Furthermore, the U-Pb ages of detrital zircon populations present in a block of conglomerate indicate a maximum age of sedimentation at about the Early-Middle Ordovician boundary and deposition at the paleo-margin of Gondwana with a typical West-African provenance (Arenas et al., 2009).

U-Pb geochronology and whole rock geochemistry data indicate that the Somozas Mélange contains abundant materials derived from a peri-Gondwanan magmatic arc. This observation suggests that the margin of Gondwana itself might have participated in the formation of the mélange, although the exact time of mélange formation is unknown. However, the position of the mélange also suggests a relationship with the subduction and accretion that affected the Basal Units. The upper section of the Somozas Mélange is a typical serpentinite mélange. Its formation implies the existence of active subduction for a protracted period, with generation of a low viscosity channel in the overlying mantle (Gerya et al., 2002; Hebert et al., 2009). The lower section of the mélange was developed later and represents an imbrication zone of the upper serpentinite melange with the higher levels of the Parautochthon. Thus the time of formation of the Somozas Mélange can be roughly constrained between the age of the subduction, which affected the Basal Units (c. 370 Ma; Abati et al., 2010), and the age of the imbrication with the Parautochthon. That date is, at present, unknown, but logically should be similar to or slightly earlier than the age estimated for the basal thrust of the Parautochthon above the Central Iberian Zone (c. 343 Ma; Dallmeyer et al., 1997).

Paleozoic oceans and the assembly of Pangea

Based on the U-Pb chronology obtained for their most representative lithologies, the ophiolites of NW Iberian Massif are of two main age groups: Cambrian (Lower Ophiolitic Units) and Devonian (Upper Ophiolitic Units). The Somozas Mélange is a separate unit, the age of which is not known precisely. The main Ophiolitic Units (excepting the Bazar Ophiolite) show chemical compositions related to supra-subduction zones or pull-apart basins. This interpretation is also compatible with the lithological features of the best preserved ophiolitic sections, such as the Careón Ophiolite. Thus, the age of the ophiolites involved in the Variscan suture spans much of the Paleozoic; significantly, the time range between the opening and closure of the main Paleozoic ocean generated in the peri-Gondwana context (the Rheic Ocean). Moreover, the youngest ophiolites are approximately coeval with the first tectono-thermal events related to the assembly of Pangea. The Variscan suture therefore has specific features that throw light on the relationship between the opening and closure of a large oceanic domain, and complex tectono-

thermal episodes culminating in the final assembly of a supercontinent.

The Upper Units of the allochthonous complexes have been interpreted as a section of a peri-Gondwanan arc, rifted from the mainland in Cambrian-Early Ordovician times during the opening of the Rheic Ocean (Fig. 12). That rifting should be contemporary with that of the Avalonia microcontinent (Murphy et al., 2006), although the terrane represented by the Upper Units had a distinct identity and provenance from further east along the paleomargin of Gondwana (Abati et al., 2007; Gómez Barreiro et al., 2007) (Fig. 12). The HP-UHP metamorphism affecting the lower part of the Upper Units at c. 400-390 Ma would have developed during the accretion of this terrane to the southern margin of Laurussia and would have defined the change to a convergent regime in the Rheic Ocean domain (Gómez Barreiro et al., 2007; Sánchez Martínez et al., 2007a). The evolution proposed for the Upper Units implies that the Variscan suture ophiolites were generated within the Rheic Ocean realm. The Cambrian ophiolites, excepting the Bazar Ophiolite, would be linked to the initial stages of the opening of this ocean reminiscent of the Western Alps Tethys (Dilek and Furnes, 2014; Balestro et al. 2015; Saccani et al. 2015), whereas the Devonian ophiolites would have originated during the final stages of its closure (Arenas et al., 2007a) analogous to many supra-subduction zone ophiolites (Dilek, 2003; Dilek and Furnes, 2011; Yang et al. 2015). The Devonian ophiolites, the commonest in the Variscan suture, have been interpreted as supra-subduction zone ophiolites generated at the intra-Rheic subduction zone located near the Southern margin of Laurussia (Díaz García et al., 1999; Sánchez Martínez et al., 2007a). This subduction zone would have generated buoyant oceanic lithosphere that would have accreted soon after, below the Upper Units then constituting the Southern margin of Laurussia, and later thrust above the most external margin of Gondwana (Basal Units), at the onset of the Variscan deformation (c. 370 Ma). The activity of the intra-Rheic Ocean subduction zone also would explain the widespread absence in the Variscan Belt of N-MORB-type oceanic lithosphere typical of the Rheic Ocean, which would have been completely eliminated by subduction.

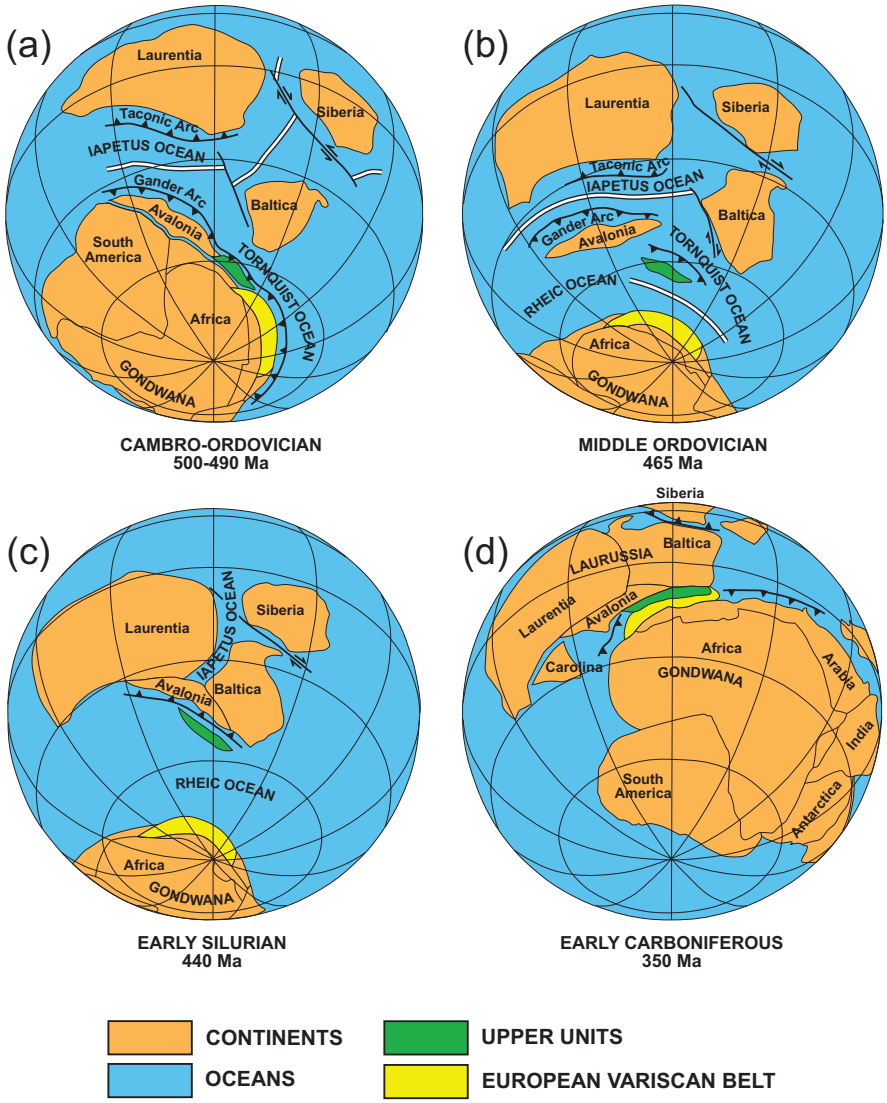

Fig. 12. Paleozoic paleogeography showing the distribution of terranes in the peri-Gondwanan realm and the main stages involved in the assembly of Pangea. This model interpreted the Upper Units of NW Iberia as a far traveled terrane drifted from Gondwana and finally accreted to the southern margin of Laurussia later than Avalonia. The Rheic Ocean opened in Late Cambrian-Early Ordovician times and widened during drifting to the North of Avalonia and the NW Iberia Upper Units. Based on Winchester et al. (2002), Arenas et al. (2007b), Gómez Barreiro et al. (2007)

It is implausivle, however, to interpret in this model the Devonian ophiolites as remnants of oceanic lithosphere formed in open oceanic domains. The new isotope geochemistry data indicate that the gabbroic protolith interacted with ancient continental crust. Many existing zircons in mafic rocks of the Purrido and Moeche ophiolites show a Lu-Hf isotope composition that is only compatible with a continental origin. Therefore, they must be interpreted as inherited zircons in the mafic magma (Sánchez Martínez et al., 2011; Arenas et al., 2014b). However, there is no conclusive data to connect the generation of the Devonian ophiolites with the evolution of the Rheic Ocean, therefore it is not possible to assert that the suture zone they define was a consequence of its closure. If the suture zone of NW Iberia is not linked to the evolution of the Rheic Ocean, the main argument for considering the Upper Units as a terrane drifted to the North from Gondwana during the opening of this oceanic domain is not supported. However, there are also problems for the possible development of an episode of HP-UHP metamorphism in a small peri-Gondwana terrane colliding with Laurussia. That type of tectono-thermal evolution is generally associated with deep subduction of the thinned margin of a large continental landmass (Warren et al., 2008; Beaumont et al., 2009).

Regarding the HP-UHP event of the Upper Units, the existing U-Pb geochronological data indicate that it took place at c. 400-390 Ma (Ordóñez Casado et al. 2001; Fernández Suárez et al. 2007) approximately coincident with the age of the mafic rocks of the

Upper Ophiolitic Units, which has been repeatedly dated by U-Pb geochronology at c. 400-395 (Díaz García et al., 1999; Pin et al., 2002, 2006; Sánchez Martínez et al., 2011; Arenas et al., 2014b). For the HP metamorphic event, the U-Pb geochronology may reflect the age of zircon growth that took place at high temperatures and therefore would have occurred later than the onset of deformation and the metamorphism itself. The subduction affecting this section of the volcanic arc would logically have started before 400-390 Ma, although it is not possible to know the precise age and, therefore, must have occurred prior to the generation of the Devonian ophiolites.

The recently obtained data, especially the Lu-Hf isotope data from the zircons of the Devonian ophiolites and detailed U-Pb geochronology of the HP metamorphic events, favor an alternative interpretation to that initially proposed for the allochthonous terranes of the Variscan suture of the NW Iberian Massif. These data suggest two successive stages of collision between Gondwana and Laurussia, which took place in a context of dextral convergence, separated in time by the opening of a relatively wide, probably a pull-apart, oceanic basin (Arenas et al., 2014a).

The Upper Units are considered the most external part of the continental platform of Gondwana. That platform was probably very wide and composed of a thick turbidite series intruded by large bodies of gabbros and granitoids. Its origin was related to the activity of a volcanic arc during Cambrian-Early Ordovician times that later underwent strong extension and subsequent thinning. As evidence of renewed igneous or deformational activity was not preserved in the platform until the beginning of the Devonian HP-UHP metamorphic event, this must have been a typical passive margin during much of Ordovician and Silurian times, with no evidence for its separation from the mainland. Convergence between Gondwana and Laurussia favored the development of a first collision and subduction to the north of the most external section of the platform which underwent the HP-UHP event prior to c. 400-390 Ma. The interaction between the two large continents allowed the deep subduction of the thinned prograde margin of Gondwana. The southern margin of Laurussia acted as a retro-continent and the most important collision probably took place along the eastern part of Avalonia and, perhaps, along the margin of Baltica (Fig. 13).

Continued dextral convergence favored the fast development of a wide pull-apart basin during the Lower Devonian, in which mafic rocks would have been generated at c. 395 Ma constituting, later, the typical ophiolites of the Variscan suture (Fig. 13). A modern equivalent for this setting can be found in the pull-apart basin generated between the North American Plate and the Caribbean Plate, although in that case the continental convergence shows sinistral motion. There, the Gonâve microplate, occupying the pull-apart basin, is comprised of oceanic-type lithosphere, generated by the activity of the Mid-Caiman Spreading Centre, and scarce or nonexistent

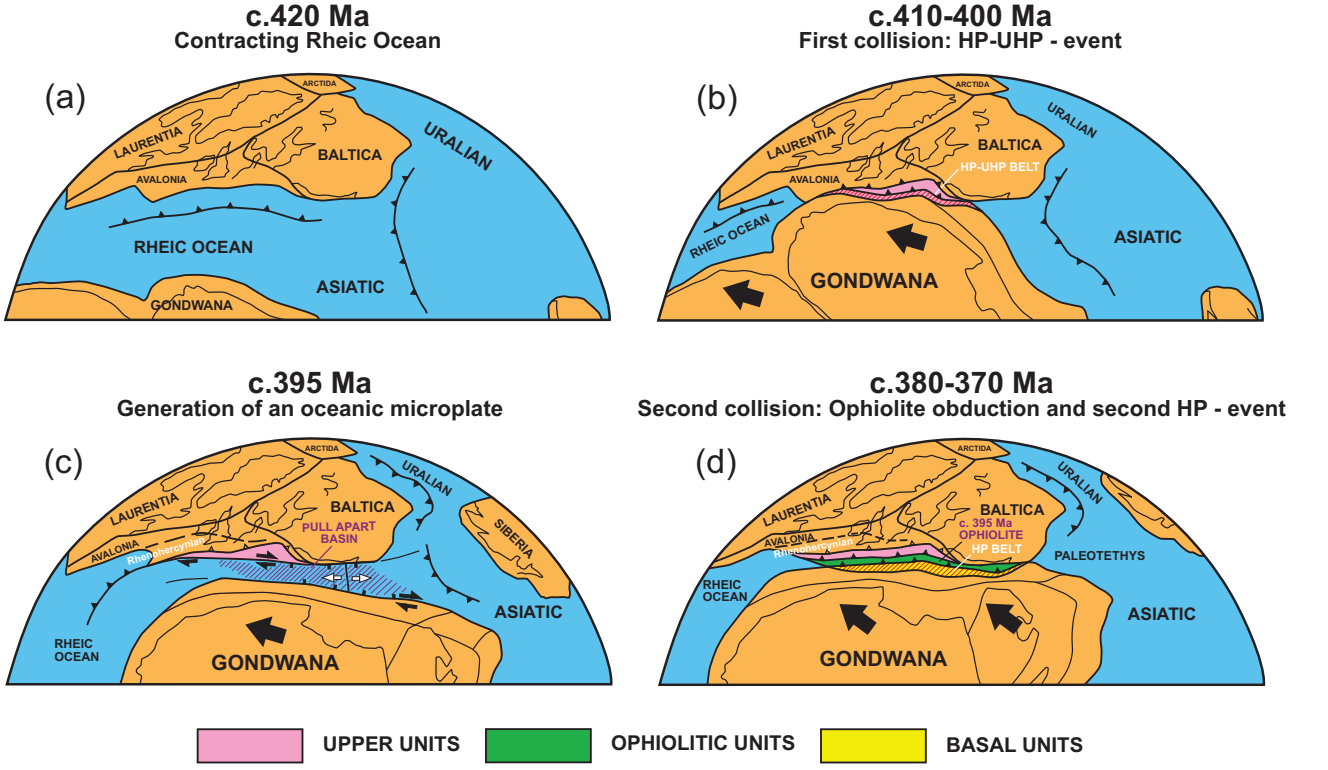

Fig. 13. Reconstruction of the Rheic Ocean realm at the Silurian-Devonian boundary (a), and the initial collision between Gondwana and Laurussia at c. 410-400 Ma following the complete closure of the Rheic Ocean (b). This collision caused subduction of a section of the margin of Gondwana and generated the HP-UHP metamorphic belt preserved in the allochthonous Upper Units exposed in the Variscan suture. The true Rheic Ocean suture is not represented in NW Iberia. Dextral motion between Gondwana and Laurussia favored the opening of a rather ephemeral pull-apart basin at c. 395 Ma with generation of new oceanic lithosphere (c). The second and final collision at c. 380-370 Ma caused the accretion of buoyant oceanic lithosphere followed by new subduction affecting the margin of Gondwana, thereby developing a second HP-LIT metamorphic belt (d). The two different HP belts and the ophiolitic units dated at c. 395 Ma can be identified in the allochthonous terranes which outline the Variscan suture from Iberia to the Bohemian Massif. Modified after Arenas et al. (2014a).

sedimentary cover (Brink et al., 2002). In this modern example, as apparently occurred in the inception of Pangea, the pull-apart basin was generated after an initial collision event between the two plates that currently limit the basin (García Casco et al., 2008; Sommer et al., 2011).

The dextral convergence of Gondwana finally facilitated the closure of the basin and the initial accretion of buoyant oceanic lithosphere below the northern continent after c. 380 Ma; the age of the prograde foliation in the Careón and Purrido ophiolites (Dallmeyer et al., 1997). This lithosphere escaped the renewed subduction while undergoing amphibolite facies regional metamorphism, although some metamorphic soles with local growth of corundum indicate the local occurrence of high thermal gradients (Díaz García et al., 1999). The imbrication of new mafic sheets took place under a lower greenschist facies thermal regime, favoring the accretion of the other sheets of Devonian ophiolites (Moeche Ophiolite) and other older mafic sequences generated by the activity of the peri-Gondwanan magmatic arc (Vila de Cruces Ophiolite). The result was a complex suture zone developed during protracted dextral convergence and containing two ophiolitic belts of different ages, the Cambrian Lower Ophiolitic Units and Devonian Upper Ophiolitic Units. The existence of a thick serpentinitic mélange at the base of the allochthonous pile, the Somozas Mélange, has also been interpreted in the context of dextral convergence (Arenas et al., 2009).

The final collision between Laurussia and Gondwana, as a consequence of oblique convergence, took place at c. 370Myr (Díez Fernández et al., 2012c). It initiated a renewed north-directed subduction of the outer section of the most external thinned margin of Gondwana, this time with easternmost provenance (Basal Units; Díez Fernández et al., 2010; Fuenlabrada et al., 2012). Thus a second HP metamorphic event was generated, in this instance of LIT, originating C-Type eclogites, blueschists and HP metapelites (Fig. 13). The convergence went on during a long period of progressive intra-continental deformation, which propagated to the south, thereby affecting the margin of Gondwana and reaching the external Variscan areas about 40-50 Ma later (Dallmeyer et al., 1997).

Classification of the NW Iberia ophiolites

Dilek and Furnes (2011, 2014) presented a new classification of ophiolites according to their geochemical signature and internal structure. They distinguished two first order groups: subduction-unrelated and subduction-related ophiolites. The first type includes continental margin (CM), mid-ocean ridge (MOR) and plume-type (P) ophiolites. CM ophiolites are formed during continental rifting and generation of an incipient ocean. In subsequent stages of lithospheric extension and seafloor spreading the resulting ophiolite type is MOR, whose features may vary depending on the spreading rate at the ridge (fast, intermediate or slow spreading ridges). P type ophiolites form at plume-proximal oceanic ridges or as part of oceanic plateaus. Subduction related ophiolites include supra-subduction zone (SSZ) and volcanic arc (VA) ophiolites. SSZ ophiolites represent oceanic lithosphere formed in the extended upper plates of subduction zones (Dilek and Furnes, 2011). The tectonic setting for the oceanic crust forming these ophiolites includes the fore-arc, the back arc and the incipient arc. Within back-arc tectonic environments it is possible to distinguish trench-proximal or trench-distal spreading centers depending on the extent of subduction influence. Furthermore, it would be possible to differentiate SSZ oceanic or continental back-arc basin ophiolites whether they resulted from seafloor spreading in "ensimatic" or "ensialic" settings. VA ophiolites differ from SSZ in a thicker and more fully developed arc crust with calc-alkaline geochemical signatures and the presence of more varied igneous lithologies.

In the case of the NW Iberia ophiolites, the Bazar ophiolite is the only one which does not record a clear influence of a subduction zone in the generation of its igneous protoliths (Fig. 4). Consequently it can be classified as an ophiolite unrelated to subduction, most probably of the MOR type (Fig. 6). As discussed before, it probably represents Cambrian (c. 495 Ma) peri-Gondwanan oceanic lithosphere, accreted during Early Ordovician times (c. 475 Ma), shortly after its generation at the ridge. Given this particular evolution mode and the geochemical features of its lithologies as transitional between N-MORB and E-MORB similar to the trench-proximal Taitao ophiolite in Southern Chile (Le Moigne et al., 1996), it is not possible to discard the possibility that part of the oceanic lithosphere was generated while the ridge was subducted (ridge-subduction ophiolite, according to the classification of Pearce, 2014) (Fig. 6).

The igneous lithologies of the Vila de Cruces ophiolite (c. 500 Ma) show geochemical features clearly indicative of an origin related with the activity of a subduction zone (Fig. 4). It can be classified as a subduction-related SSZ type of ophiolite generated in a back-arc basin (Fig. 6). The significant negative Nb anomalies suggest a trench proximal position of the basin, and, given the important amount of sediment contained in the ophiolite (Fig. 2), as well as the evidence of interaction between the igneous protoliths and the continental crust, it would probably represent a continental backarc basin (Dilek and Robinson, 2003, and references therein).

The classification of the Devonian (c. 395 Ma) ophiolites (Careón, Purrido and Moeche) following the guidelines of Dilek and Furnes (2011, 2014) is more complicated. We have interpreted the tectonic setting where the oceanic lithosphere formed as a pull-apart basin formed after a first collision between Gondwana and Laurussia (Fig. 13). Nevertheless, it is clear that subduction zone influence does exist as it is recorded by the geochemistry of the associated mafic rocks (Fig. 4). It is noticeable that such subduction components vary from one ophiolite to another, being more significant in Careón and progressively attenuating in Purrido and even more in Moeche. The most plausible interpretation of this observation is that this pull-apart basin opened within a back-arc basin, which persisted after the initial collision. In this context, variation of the influence of the subduction zone depended on the proximity of the spreading ridge of the pull-apart basin to the original trench. Thus, applying the new ophiolite classification, it is clear that the Devonian ophiolites are in general terms of subduction-related SSZ type.

Finally, to apply the new ophiolite classification to the Somozas Mélange, we should first address the problem of the origin of that unit. The development of the mélange itself was distinct from the origin of the igneous lithologies forming part of the tectonic blocks. They should represent at least in part sections of an oceanic sequence, as the development of a low viscosity channel in the lithospheric mantle implies dehydration of its mafic components during subduction. The compositions of the mafic lithologies (c. 527-485 Ma) present in the mélange show a clear participation of a subduction component (Fig. 4). Therefore, the ophiolitic components included in this serpentinite mélange are of SSZ type, and were developed in relation to a Cambrian subduction zone active in the peri-Gondwanan realm.

Conclusions

In the NW Iberian Massif, two main groups of ophiolites are preserved in the Variscan suture: Cambrian (c. 500 Ma; Lower Ophiolitic Units) and Devonian (c. 395 Ma; Upper Ophiolitic Units). A thick serpentinitic mélange of uncertain age and origin is also present. These ophiolites are composed of mafic sequences with minor strongly deformed ultramafic rocks metamorphosed from greenschist to low-P granulites facies. Although the primary mineralogy is not preserved, the plutonic, intrusive and volcanic textures and structures are frequently observed. Sedimentary rocks are rather scarce and it is unclear whether their presence in the ophiolite has tectonic significance.

The lithological and geochemical features of most of these ophiolites show that they are not of common MOR types. They instead formed in a supra-subduction zone setting (SSZ) or during the opening of pull-apart type ephemeral basins. Perhaps, the only exception is the Bazar Ophiolite, which has a more representative oceanic composition that seems to reflect a Cambrian accretion zone of peri-Gondwanan oceanic material below a magmatic arc system. This, together with the Vila de Cruces Ophiolite, also generated during Cambrian times in relation to the opening of a back-arc basin, reflects, to some extent, the earliest stages of the opening of the Rheic Ocean, the largest Paleozoic ocean generated in the peri-Gondwanan setting.

The Devonian ophiolites (Careón, Purrido and Moeche ophiolites) were previously interpreted to have been generated at an intra-Rheic Ocean supra-subduction zone. This subduction zone would have been responsible for the removal of almost all the lithosphere of the Rheic Ocean. However, recent isotopic data (Lu-Hf in zircon) clearly indicates that the source of the mafic rocks of these ophiolites interacted with continental crust. Therefore they are better interpreted as remnants of an oceanic lithosphere generated in an ephemeral basin, probably of a pull-apart type, developed during dextral convergence. That basin probably opened at c. 400-390 Ma, apparently after a first interaction between the continental margins, which triggered the HP-UHP metamorphism in the subducted margin of Gondwana. Its total closure occurred at c. 370 Ma, when the Gondwana margin underwent a second event of subduction and HP metamorphism. The buoyant oceanic crust of this ephemeral basin was accreted at high-T, below the terrane which currently constitutes the Upper Units of NW Iberian Massif.

The two ophiolitic belts in Galicia preserve evidence for the complex tectono-thermal events that occurred during the assembly of Pangea. This collision was not simple, but occurred in at least two distinct events separated by the opening of pull-apart basins. In addition, the tectono-thermal events related to the assembly of Pangea seem to start by c. 390 Ma, considerably earlier than previously considered, and thus they lasted longer. Therefore, the conclusions presented in this paper indicate that the early events in the assembly of Pangea are more complex than previously described. Nevertheless, these findings are not surprising since the history of convergence and collision between two large continental masses is commonly not simple, and complexity is the norm rather than the exception, as can be observed in some modern examples of continental convergence.

Acknowledgements

Financial support has been provided by the Spanish project CGL2012-34618 (Ministerio de Economía y Competitividad). Insightful reviews by Brendan Murphy and J.A. Winchester are kindly acknowledged.

References

Abati, J., Dunning, G.R., Arenas, R., Díaz García, F., González Cuadra, P., Martínez Catalán, J.R. and Andonaegui, P, 1999, Early Ordovician orogenic event in Galicia (NW Spain): evidence from U-Pb ages in the uppermost unit of the Ordenes Complex: Earth and Planetary Science Letters, v. 165, pp. 213-228.

Abati, J., Castiñeiras, P., Arenas, R., Fernández-Suárez, J., Gómez-Barreiro, J. and Wooden, J., 2007, Using SHRIMP zircon dating to unravel tectonothermal events in arc environments. The early Palaeozoic arc of NW Iberia revisited: Terra Nova, v. 19, pp. 432-439.

Abati, J., Gerdes, A., Fernández-Suárez, J., Arenas, R., Whitehouse, M.J. and Díez Fernández, R., 2010, Magmatism and early-Variscan continental subduction in the northern Gondwana margin recorded in zircons from the basal units of Galicia, NW Spain: Geological Society of America Bulletin, v. 122, pp. 219-235.

Albert, R., Arenas, R., Gerdes, A., Sánchez Martínez, S., Fernández-Suárez, J. and Fuenlabrada, J.M., 2015, Provenance of the Variscan Upper Allochthon (Cabo Ortegal Complex, NW Iberian Massif): Gondwana Research. Gondwana Research, v. 28, pp. 1434-1448. DOI.org/10.1016/j.gr.2014.10.016

Andonaegui, P., Castiñeiras, P., González Cuadra, P., Arenas, R., Sánchez Martínez, S., Abati, J., Díaz García, F. and Martínez Catalán, J.R., 2012, The Corredoiras orthogneiss (NW Iberian Massif): Geochemistry and geochronology of the Paleozoic magmatic suite developed in a peri-Gondwanan arc: Lithos, v. 128-131, pp. 84-99.

Arenas, R., 1988, Evolución petrológica y geoquímica de la unidad alóctona inferior del Complejo Metamórfico Básico – Ultrabásico de Cabo Ortegal (Unidad de Moeche) y del Silúrico Parautóctono (NW de España): Corpus Geologicum Gallaeciae, v. 4, 543 p.

Arenas, R., Gil Ibarguchi, J.I., González Lodeiro, F., Klein, E., Martínez Catalán, J.R., Ortega Gironés, E., Pablo Maciá, J.G. de and Peinado, M., 1986, Tectonostratigraphic units in the complexes with mafic and related rocks of the NW of the Iberian Massif: Hercynica, v. 2, pp. 87-110.

Arenas, R., Rubio Pascual, F.J., Díaz García, F. and Martínez Catalán, J.R., 1995, High-pressure microinclusions and development of an inverted metamorphic gradient in the Santiago Schists (Órdenes Complex, NW Iberian Massif, Spain): evidence of subduction and syn-collisional decompression: Journal of Metamorphic Geology, v. 13, pp. 141-164.

Arenas, R., Abati, J., Martínez Catalán, J.R., Díaz García, F. and Rubio Pascual, F.J., 1997, P-T evolution of eclogites from the Agualada Unit (Órdenes Complex, NW Iberian Massif, Spain): Implications for crustal subduction: Lithos, v. 40, pp. 221-242.

Arenas, R., Martínez Catalán, J.R., Sánchez Martínez, S., Díaz García, F., Abati, J., Fernández-Suárez, J., Andonaegui, P. and Gómez-Barreiro, J., 2007a, Paleozoic ophiolites in the Variscan suture of Galicia (northwest Spain): distribution, characteristics and meaning, in Hatcher, R.D. Jr., Carlson, M.P., McBride, J.H. and Martínez Catalán, J.R., eds, 4-D Framework of Continental Crust: Geological Society of America Memoir, v. 200, pp. 425-444.

Arenas, R., Martínez Catalán, J.R., Sánchez Martínez, S., Fernández-Suárez, J., Andonaegui, P., Pearce, J.A. and Corfu, F., 2007b, The Vila de Cruces Ophiolite: A remnant of the early Rheic Ocean in the Variscan suture of Galicia (NW Iberian Massif): Journal of Geology, v.115, pp.129-148.

Arenas, R., Sánchez Martínez, S., Castiñeiras, P., Jeffries, T.E., Díez Fernández, R. and Andonaegui, P., 2009, The basal tectonic mélange of the Cabo Ortegal Complex (NW Iberian Massif): a key unit in the suture of Pangea: Journal of Iberian Geology, v. 35, pp. 85-125.

Arenas, R., Díez Fernández, R., Sánchez Martínez, S., Gerdes, A., Fernández-Suárez, J. and Albert, R., 2014a, Two-stage collision: Exploring the birth of Pangea in the Variscan terranes: Gondwana Research, v. 25, pp. 756-763.

Arenas, R., Sánchez Martínez, S., Gerdes, A., Albert, R., Díez Fernández, R. and Andonaegui, P., 2014b, Re-interpreting the Devonian ophiolites involved in the Variscan suture: U-Pb and Lu-Hf zircon data of the Moeche Ophiolite (Cabo Ortegal Complex, NW Iberia): International Journal of Earth Sciences, v. 103, pp. 1385-1402.

Balestro, G., Festa, A., Dilek, Y. and Tartarotti, P., 2015, Pre-Alpine Extensional tectonics of a peridotite-localized oceanic core complex in the late Jurassic, high-pressure Monviso ophiolite (Western Alps). Episodes, v. 38, no.4, pp. 266-282, doi:10.18814/epiiugs/2015/v38i4/82421.

Ballèvre, M., Bosse, V., Ducassou, C. and Pitra, P., 2009, Palaeozoic history of the Armorican Massif: Models for the tectonic evolution of the suture zones: Comptes Rendus Geoscience, v. 341, pp. 174-201.

Ballèvre, M., Martínez Catalán, J.R., López Carmona, A., Abati, J., Díez Fernández, R., Ducassou, C., Pitra, P., Arenas, R., Bosse, V., Castiñeiras, P., Fernández-Suárez, P., Gómez Barreiro, J., Paquette, J.L., Peucat, J.J., Poujol, M., Ruffet, G. and Sánchez Martínez, S., 2014, Correlation of the nappe stack in the Ibero-Armorican arc across the Bay of Biscay: a joint French-Spanish project, in Schulmann, K., Martínez Catalán, J.R., Lardeaux, J. M., Janousìk, V. and Oggiano, G., eds, The Variscan Orogeny: Extent, Timescale and the Formation of the European Crust: Geological Society of London, Special Publication, v. 405, pp. 77-113.

Beaumont, C., Jamieson, R.A., Butler, J.P and Warren, C.J., 2009, Crustal structure: A key constraint on the mechanism of ultra-high-pressure rock exhumation: Earth and Planetary Science Letters, v. 287, pp. 116-129.

Brink, U.S. ten, Coleman, D.F. and Dillon, W.P., 2002, The nature of the crust under Cayman Trough from gravity: Marine and Petroleum Geology, v. 19, pp. 971-987.

Chauvel, C. and Blichert-Toft, J., 2001, A hafnium isotope and trace element perspective on melting of the depleted mantle: Earth and Planetary Science Letters, v. 190, pp. 137-151.

Clark, A.H., Scott, D.J., Sandeman, H.A., Bromley, A.V. and Farrar, E., 1998, Siegenian generation of the Lizard ophiolite: U-Pb zircon age data for plagiogranite, Porthkerries, Cornwall: Journal of de Geological Society, London, v. 155, pp. 595-598.

Coleman, R.G., Lee, D.E., Beatty, L.B. and Brannock, W.W., 1965, Eclogites and eclogites - their differences and similarities: Geological Society of America Bulletin, v. 76, pp. 483-508.

Dallmeyer, R.D., Martínez Catalán, J.R., Arenas, R., Gil Ibarguchi, J.I., Gutiérrez Alonso, G., Farias, P., Aller and J., Bastida, F., 1997, Diachronous Variscan tectonothermal activity in the NW Iberian Massif: evidence from $^{40}Ar/^{39}Ar$ dating of regional fabrics: Tectonophysics, v. 277, pp. 307-337.

Díaz García, F., 1990, La geología del sector occidental del Complejo de Órdenes (Cordillera Hercínica, NW de España): Nova Terra, v. 3, 230 p.

Díaz García, F., Arenas, R., Martínez Catalán, J.R., González del Tánago, J. and Dunning, G.R., 1999, Tectonic evolution of the Careón Ophiolite (northwest Spain): a remnant of oceanic lithosphere in the Variscan Belt: Journal of Geology, v. 107, pp. 587-605.

Díaz García, F., Sánchez Martínez, S., Castiñeiras, P., Fuenlabrada, J.M. and Arenas, R., 2010, A peri-Gondwanan arc in NW Iberia. II: Assessment of the intra-arc tectonothermal evolution through U-Pb SHRIMP dating of mafic dykes: Gondwana Research, v. 17, pp. 352-362.

Díez Fernández, R., Martínez Catalán, J.R., Gerdes, A., Abati, J., Arenas, R. and Fernández-Suárez, J., 2010, U-Pb ages of detrital zircons from the basal allochthonous units of NW Iberia: Provenance and paleoposition on the northern margin of Gondwana during the Neoproterozoic and Paleozoic: Gondwana Research, v. 18, pp. 385-399.

Díez Fernández, R., Martínez Catalán, J.R., Arenas, R., Abati, J., Gerdes, A. and Fernández-Suárez, J., 2012a, U-Pb detrital zircon analysis of the lower allochthon of NW Iberia: age constraints, provenance and links with the Variscan mobile belt and Gondwana cratons: Journal of the Geological Society, London, v. 169, pp. 655-665.

Díez Fernández, R., Castiñeiras, P. and Gómez Barreiro, J., 2012b, Age constraints on Lower Paleozoic convection system: magmatic events in the NW Iberian Gondwana margin: Gondwana Research, v. 21, pp. 1066-1079.

Díez Fernández, R., Martínez Catalán, J.R., Arenas, R. and Abati, J., 2012c, The onset of the assembly of Pangaea in NW Iberia: Constraints on the kinematics of continental subduction: Gondwana Research, v. 22, pp. 20-25.

Dilek, Y., 2003, Ophiolite pulses, mantle plumes and orogeny. Geological Society of London, Sepcial Publications, v. 218, pp. 9-19.

Diley, Y. and Robinson, P.T., 2003, Ophiolites in Earth history. Geological Society, London, Special Publication, v. 218, pp. 1-8.

Dilek, Y. and Furnes, H., 2011, Ophiolite genesis and global tectonics: Geochemical and tectonic fingerprinting of ancient oceanic lithosphere: Geological Society of America Bulletin, v. 123, pp. 387-411.

Dilek, Y. and Furnes, H., 2014, Ophiolites and their origins: Elements, v. 10, pp. 93-100.

Dubinska, E., Bylina, P., Kozlowski, A., Dörr, W., Nejbert, K. 2004. U-Pb dating of serpentinization: Hydrothermal zircon from a metasomatic rodingite shell (Sudetic ophiolite, SW Poland). Chemical Geology, v. 203, pp. 183-203.

Faryad, S.W. and Kachlík, V., 2013, New evidence of blueschist facies rocks and their geotectonic implication for Variscan suture (s) in the Bohemian Massif: Journal of metamorphic Geology, v. 31, pp. 63-82.

Fernández-Suárez, J., Díaz García, F., Jeffries, T.E., Arenas, R. and Abati, J., 2003, Constraints on the provenance of the uppermost allochthonous terrane of the NW Iberian Massif: Inferences from detrital zircon U-Pb ages: Terra Nova, v. 15, pp. 138-144.

Fernández-Suárez, J., Arenas, R., Abati, J., Martínez Catalán, J.R., Whitehouse, M.J. and Jeffries, T.E., 2007, U-Pb chronometry of polymetamorphic high-pressure granulites: An example from the allochthonous terranes of the NW Iberian Variscan belt, in Hatcher, R.D. Jr., Carlson, M.P., McBride, J.H. and Martínez Catalán, J.R., eds, 4-D Framework of Continental Crust: Geological Society of America Memoir, v. 200, pp. 469-488.

Fuenlabrada, J.M., Arenas, R., Sánchez Martínez, S., Díaz García, F. and Castiñeiras, P., 2010, A peri-Gondwana arc in NW Iberia. I: Isotopic and geochemical constraints on the origin of the arc – A sedimentary approach: Gondwana Research, v. 17, pp. 338-351.

Fuenlabrada, J.M., Arenas, R., Díez Fernández, R., Sánchez Martínez, S., Abati, J. and López Carmona, A., 2012, Sm-Nd isotope geochemistry and tectonic setting of the metasedimentary rocks from the basal allochthonous units of NW Iberia (Variscan suture, Galicia): Lithos, v. 148, pp. 196-208.

García-Casco, A., Iturralde-Vinent, M.A. and Pindell, J., 2008, Latest Cretaceous collision/accretion between the Caribbean plate and Caribeana: Origin of metamorphic terranes in the Greater Antilles: International Geology Review, v. 50, pp. 781-809.

Gerya, T.V., Stöckhert, B. and Perchuk, A.L., 2002, Exhumation of high-pressure metamorphic rocks in a subduction channel: A numerical simulation: Tectonics, v. 21, pp. 6-1-19.

Gómez-Barreiro, J., Martínez Catalán, J.R., Arenas, R., Castiñeiras, P., Abati, J., Díaz García, F. and Wijbrans, J.R., 2007, Tectonic evolution of the upper allochthon of the Órdenes complex (northwestern Iberian Massif): Structural constraints to a polyorogenic peri-Gondwanan terrane, in Linneman, U., Nance, R.D., Kraft, P. and Zulauf, G., eds, The evolution of the Rheic Ocean: From Avalonian-Cadomian active margin to Alleghenian-Variscan collision: Geological Society of America Special Paper, v. 423, pp. 315-332.

Gómez Barreiro, J., Martínez Catalán, J.R., Prior, D., Wenk, H.-R., Vogel, S., Díaz García, F., Arenas, R., Sánchez Martínez, S. and Lonardelli, I., 2010, Fabric development in a Middle Devonian intra-oceanic subduction regime: the Careón ophiolite (NW Spain): Journal of Geology, v. 118, pp. 163-186.

Hebert, L.B., Antoshechkina, P., Asimow, P and Gurnis, M., 2009, Emergence of a low-viscosity channel in subduction zones through the coupling of mantle flow and thermodynamics: Earth and Planetary Science Letters, v. 278, pp. 243-256.

Kroner, U. and Romer, R.L., 2013, Two plates–Many subduction zones: The Variscan orogeny reconsidered: Gondwana Research, v. 24, pp. 298-329.

Kryza, R. and Pin, C., 2010, The Central-Sudetic ophiolites (SW Poland): Petrogenetic issues, geochronology and palaeotectonic implications: Gondwana Research, v. 17, pp. 292-305.

Lardeaux, J.M., Ledru, P., Daniel, I. and Duchene, S., 2001, The Variscan French Massif Central-a new addition to the ultra-high pressure metamorphic 'club': exhumation processes and geodynamic consequences: Tectonophysics, v. 332, pp. 143-167.

Le Moigne, J., Lagabrielle, Y., Whitechurch, H., Girardeau, J., Bourgois, J. and Maury, R.C., 1996, Petrology and geochemistry of the ophiolitic and volcanic suites of the Taitao Peninsula–Chile Triple Junction Area: Journal of South American Earth Sciences, v. 9, pp. 43-58.

Leitch, E.C., 1984, Island arc elements and arc-related ophiolites: Tectonophysics, v. 106, pp. 177-203.

López Carmona, A., Pitra, P. and Abati, J., 2013, Blueschist-facies metapelites from the Malpica-Tui Unit (NW Iberian Massif): phase equilibria modelling and H_2O and Fe_2O_3 influence in high-pressure assemblages: Journal of Metamorphic Geology, v. 31, pp. 263-280.

López Carmona, A., Abati, J., Pitra, P., and Lee, J.K.W., 2014, Retrogressed lawsonite blueschists from the NW Iberian Massif: P-T constraints from numerical modelling and $^{40}Ar/^{39}Ar$ geochronology: Contributions to Mineralogy and Petrology, v. 167, 987, pp. 1-20.

Marcos, A., Farias, P., Galán, G., Fernández, F.J., and Llana-Fúnez, S., 2002, Tectonic framework of the Cabo Ortegal Complex: A slab of lower crust exhumed in the Variscan orogen (northwestern Iberian Peninsula), in Martínez Catalán, J.R., Hatcher, R.D. Jr., Arenas, R. and Díaz García, F., eds, Variscan-Appalachian dynamics: the building of the Late Paleozoic basement: Geological Society of America Special Paper, v. 364, pp. 143-162.

Martínez Catalán, J.R., 2011, Are the oroclines of the Variscan belt related to late Variscan strike-slip tectonics? Terra Nova, v. 23, pp. 241-247.

Martínez Catalán, J.R., Arenas, R., Díaz García, F., González Cuadra, P., Gómez-Barreiro, J., Abati, J., Castiñeiras, P., Fernández-Suárez, J., Sánchez Martínez, S., Andonaegui, P., González Clavijo, E., Díez Montes, A., Rubio Pascual, F.J. and Valle Aguado, B., 2007, Space and time in the tectonic evolution of the northwestern Iberian Massif: Implications for the Variscan belt, in Hatcher, R.D. Jr., Carlson, M.P., McBride, J.H. and Martínez Catalán, J.R., eds, 4-D Framework of Continental Crust: Geological Society of America Memoir, v. 200, pp. 403-423.

Martínez Catalán, J.R., Arenas, R., Abati, J., Sánchez Martínez, S., Díaz García, F., Fernández-Suárez, J., González Cuadra, P., Castiñeiras, P., Gómez Barreiro, J., Díez Montes, A., González Clavijo, E., Rubio Pascual, F.J., Andonaegui, P., Jeffries, T.E., Alcock, J.E., Díez Fernández, R. and López Carmona, A., 2009, A rootless suture and the loss of the roots of a mountain chain: The Variscan belt of NW Iberia: Comptes Rendus Geoscience, v. 341, pp. 114-126.

Matte, Ph., 2001, The Variscan collage and orogeny (480-290 Ma) and the tectonic definition of the Armorica microplate: a review: Terra Nova, v. 13, pp. 122-128.

Murphy, J.B., Gutiérrez-Alonso, G., Nance, R.D., Fernández-Suárez, J., Keppie, J.D., Quesada, C., Strachan, R.A. and Dostal, J., 2006, Origin of the Rheic Ocean: rifting along a Neoproterozoic suture?: Geology, v. 34, pp. 325-328.

Murphy, J.B., Gutiérrez-Alonsi, G., 2008, The origin of the Variscan upper allochthons in the Ortegal Complex, northwestern Iberia: Sm-Nd isotopic constraints on the closure of the Rheic Ocean. Canadian Journal of Earth Sciences, v. 45, pp. 651-668.

Murphy, J.B., Cousens, B.L., Braid, J.A., Strachan, R.A., Dostal, J., Keppie, J.D. and Nance, R.D., 2011, Highly depleted oceanic lithosphere in the Rheic Ocean: Implications for Paleozoic plate reconstructions: Lithos, v. 123, pp.165-175.

Nance, R.D., Gutiérrez-Alonso, G., Keppie, J.D., Linnemann, U., Murphy, J.B., Quesada, C., Strachan, R.A. and Woodcock, N.H., 2010, Evolution of the Rheic Ocean: Gondwana Research, v, 17, pp. 194-222.

Nicolas, A., 1989, Structures of ophiolites and dynamics of oceanic lithosphere: Kluwer Academic Publishers, 367 p.

Nicolas, A., 1995, The mid-oceanic ridges. Mountains below sea level: Springer-Verlag. 200 p.

Nutman, A.P., Green, D.H., Cook, C.A., Styles, M.T. and Holdsworth, R.E., 2001, SHRIMP U-Pb zircon dating of the exhumation of the Lizard Peridotite and its emplacement over crustal rocks: Constraints for tectonic models: Journal of the Geological Society, London, v. 158, pp. 809-820.

Ordóñez Casado, B., Gebauer, D., Schäfer, H.J., Gil Ibarguchi, J.I. and Peucat, J.J., 2001, A single Devonian subduction event for the HP/HT metamorphism of the Cabo Ortegal complex within the Iberian Massif: Tectonophysics, v. 332, pp. 359-385.

Pearce, J.A., 1996, A users guide to basalt discrimination diagrams, in Wyman, D.A., ed, Trace Element Geochemistry of Volcanic Rocks: Application for Massive Sulphide Exploration: Short Course Notes, Geological Association of Canada, v. 12, pp. 79-113.

Pearce, J.A., 2014, Immobile element fingerprinting of ophiolites: Elements, v. 10, pp. 101-108.

Pearce, J.A., Lippard, S.J. and Roberts, S., 1984, Characteristics and tectonic significance of supra-subduction zone ophiolites, in Kokelaar, B.P. and Howells, M.F., eds, Marginal Basin Geology: Geological Society, London, Special Publications, v. 16, pp. 77-94.

Pin, C., Paquette, J.L., Santos Zalduegui, J.F. and Gil Ibarguchi, J.I., 2002, Early Devonian supra-subduction zone ophiolite related to incipient collisional processes in the Western Variscan Belt: The Sierra de Careón unit, Órdenes Complex, Galicia, in Martínez Catalán, J.R., Hatcher, R.D. Jr., Arenas, R. and Díaz García, F., eds, Variscan-Appalachian dynamics: the building of the Late Paleozoic basement.: Geological Society of America Special Paper, v. 364, pp. 57-71.

Pin, C., Paquette, J.L., Ábalos, B., Santos, J.F. and Gil Ibarguchi, J.I., 2006, Composite origin of an early Variscan transported suture: Ophiolitic units of the Morais Nappe Complex (north Portugal): Tectonics, v. 25, pp. 1-19.

Pin, C., Paquette, J.L., Santos Zalduegui, J.F. and Gil Ibarguchi, J.I., 2002, Early Devonian supra-subduction zone ophiolite related to incipient collisional processes in the Western Variscan Belt: The Sierra de Careón unit, Órdenes Complex, Galicia, in Martínez Catalán, J.R., Hatcher, R.D. Jr., Arenas, R. and Díaz García, F., eds, Variscan-Appalachian Dynamics: the building of the Late Paleozoic Basement: Geological Society of America Special Paper, v. 364, pp. 57-71.

Pin, C., Paquette, J.L., Ábalos, B., Santos, J.F. and Gil Ibarguchi, J.I., 2006, Composite origin of an early Variscan transported suture: Ophiolitic units of the Morais Nappe Complex (north Portugal): Tectonics, v. 25, pp. 1-19.

Platt, J.P., 1986, Dynamic of orogenic wedges and the uplift of high-pressure metamorphic rocks: Geological Society of America Bulletin, v. 97, pp. 1037-1053.

Rodríguez, J., Cosca, M.A., Gil Ibarguchi, J.I. and Dallmeyer, R.D., 2003, Strain partitioning and preservation of $^{40}Ar/^{39}Ar$ ages during Variscan exhumation of a subducted crust (Malpica-Tui complex, NW Spain): Lithos, v. 70, pp. 111-139.

Saccani, E., Dilek, Y., Marroni, M., and Pandolfi, L., 2015, Continental margin ophiolites of Neotethys: Remnants of ancient Ocean-Continent Transition Zone (OCTZ) lithosphere and their geochemistry, mantle sources and melt evolution patterns. Episodes, v. 38, no. 4, pp.230-249, doi:10.18814/epiiugs/2015/v38i4/82418.

Sánchez Martínez, S., 2009, Geoquímica y geocronología de las ofiolitas de Galicia: Nova Terra, v. 37, 351 p.

Sánchez Martínez, S., Jeffries, T., Arenas, R., Fernández-Suárez, J. and García-Sánchez, R., 2006, A pre-Rodinian ophiolite involved in the Variscan suture of Galicia (Cabo Ortegal Complex, NW Spain): Journal of the Geological Society, London, v. 163, pp. 737-740.

Sánchez Martínez, S., Arenas, R., Díaz García, F., Martínez Catalán, J.R., Gómez Barreiro, J. and Pearce, J., 2007a, The Careón Ophiolite, NW Spain: supra-subduction zone setting for the youngest Rheic Ocean floor: Geology, v. 35, pp. 53-56.

Sánchez Martínez, S., Arenas, R., Andonaegui, P., Martínez Catalán, J.R. and Pearce, J.A., 2007b, Geochemistry of two associated ophiolites from

the Cabo Ortegal Complex (Variscan belt of northwest Spain), in Hatcher, R.D. Jr., Carlson, M.P., McBride, J.H. and Martínez Catalán, J.R., eds, 4-D Framework of Continental Crust: Geological Society of America Memoir, v. 200, pp. 445-467.

Sánchez Martínez, S., Arenas, R., Fernández-Suárez, J. and Jeffries, T.E., 2009, From Rodinia to Pangaea: ophiolites from NW Iberia as witness for a long-lived continental margin, in Murphy, J.B., Keppie, J.D. and Hynes, A.J., eds, Ancient Orogens and Modern Analogues: Geological Society, London, Special Publications, v. 327, pp. 317-341.

Sánchez Martínez, S., Arenas, R., Gerdes, A., Castiñeiras, P., Potrel, A. and Fernández-Suárez, J., 2011, Isotope geochemistry and revised geochronology of the Purrido Ophiolite (Cabo Ortegal Complex, NW Iberian Massif): Devonian magmatism with mixed sources and involved Mesoproterozoic basement: Journal of the Geological Society, London, v. 168, pp. 733-750.

Sánchez Martínez, S., Gerdes, A., Arenas, R. and Abati, J., 2012, The Bazar Ophiolite of NW Iberia: a relic of the Iapetus-Tornquist Ocean in the Variscan suture: Terra Nova, v. 24, pp. 283-294.

Sánchez Martínez, S., Arenas, R., Albert, R., Gerdes, A. and Potrel, A., 2013, Detailed re-dating of the Vila de Cruces Ophiolite (allochthonous complexes of NW Iberia): The opening of a back-arc basin in the Gondwana shelf, in •ák, J., Zulauf, G. and Röhling, H.-G., eds, Crustal evolution and geodynamic processes in Central Europe (abs): Proceedings of the Joint conference of the Czech and German geological societies, Pilsen, Czech Republic, v. 82, pp. 95.

Shin, K.-C., Anma, R., Nakano, T., Orihashi, Y., and Ike, S.-I., 2015, TheTaitao ophiolite-granite complex, Chile: Emplacement of ridge-trench intersection oceanic lithosphere on land and origin of calc-alkaline I-type granites. Episodes, v. 38, no. 4, pp. 283-297, doi: 10.18814/epiiugs/2015/v38i4/82424.

Sommer, M., Hüneke, H., Meschede, M. and Cobiella-Reguera, J., 2011, Geodynamic model of the northwestern Caribbean: scaled reconstruction of Late Cretaceous to Late Eocene plate boundary relocation in Cuba: Neues Jahrbuch für Geologie und Paläontologie, Monatschefte, v. 259, pp. 299-312.

Stampfli, G.M. and Borel, G.D., 2002, A plate tectonic model for the Paleozoic and Mesozoic constrained by dynamic plate boundaries and restored synthetic oceanic isochrones: Earth and Planetary Science Letters, v. 196, pp. 17-33.

Van Staal, C.R., Barr, S.M. and Murphy, J.B., 2012. Provenance and tectonic evolution of Ganderia: Constraints on the evolution of the Iapetus and Rheic oceans: Geology, v. 40, pp. 987-990.

Vervoort, J.D. and Blichert-Toft, J., 1999, Evolution of the depleted mantle: Hf isotope evidence from juvenile rocks through time: Geochimica et Cosmochimica Acta, v. 63, pp. 533-556.

Von Raumer, J.F., Stampfli, G.M., Arenas, R. and Sánchez Martínez, S., 2015, Ediacaran to Cambrian oceanic rocks of the Gondwana margin and their tectonic interpretation: International Journal of Earth Sciences, v. 104, pp. 1107-1121. DOI 10.1007/s00531-015-1142-x

Warren, C.J., Beaumont, C. and Jamieson, R.A., 2008, Modelling tectonic styles and ultra-high pressure (UHP) rock exhumation during the transition from oceanic subduction to continental collision: Earth and Planetary Science Letters, v. 267, pp. 129-145.

Winchester, J.A., Pharaoh, T.C. and Verniers, J., 2002, Palaeozoic amalgamation of Central Europe: an introduction and synthesis of new results from recent geological and geophysical investigations, in Winchester, J.A., Pharaoh, T.C. and Verniers, J., eds, Palaeozoic Amalgamation of Central Europe: Geological Society, London, Special Publications, v. 201, pp. 1-18.

Wood, D.A., 1980, The application of a Th-Hf-Ta diagram to problems of tectomagmatic classification and to establishing the nature of crustal contamination of basaltic lavas of the British Tertiary Volcanic Province: Earth and Planetary Science Letters, v. 50, pp. 11-30.

Yang, G.X. and Dilek, Y., 2015, OIB- and P-Type ophiolites along the Yarlung-Zangbo Suture Zone (YZSZ), Southern Tibet: Poly-phase melt history and mantle sources of the Neotethyan oceanic lithosphere. Episodes, v. 38, no. 4, pp. 250-265, DOI: 10.18814/epiiugs/2015/v38i4/82420.

by Angélica Isabel Llanes Castro[1], Joquín Antonio Proenza[2], Federica Zaccarini[3], Giorgio Garuti[3], María Santa Cruz Pacheco Sarlabous[1]

Al- and Cr-rich chromitites from the Eastern Havana-Matanzas ophiolites (Western Cuba)

[1] Departamento de Petrología y Mineralogía, Instituto de Geología y Paleontología, Cuba. *Corresponding author E- mail: isa@igp.minem.cu*
[2] Departament de Crystallografia, Mineralogia i Depòsits Minerals, Universitat de Barcelona, España
[3] Department Angewandte Geowissenschaften und Geophysik, Montanuniversität Leoben, Austria

DOI: 10.18814/epiugs/2015/v38i4/82429

Chromite deposits in the Havana-Matanzas ophiolites of Western Cuba include both Al- ([Cr/(Cr+Al)=0.44-0.46]) and Cr-rich ([Cr/(Cr+Al) = 0.65-0.74] chromitites that commonly occur in the upper part of mantle ectonites near the mantle-crust transition zone. These chromitites generally form small lenticular bodies spatially associated with strongly serpentinized dunite. Platinum group minerals (PGM) are found only in the Cr-rich chromitites, as euhedral or subeuhedral, very small (less than 10 µm long) crystals. The most abundant PGM is laurite, accompanied by minor osmium, cuproiridsite, iridium and an unnamed phase composed of Ir-Ni-Fe-S, all of which are magmatic in origin. These magmatic PGMs and amphiboles crystallized at high temperatures (~1300 ºC) and at relatively high sulphur fugacities from fluid-rich magmas. The chromite mineral chemistry suggests that melts that were in equilibrium with Cr-rich and Al-rich chromitites had island-arc tholeiite – boninite and backarc basin basalt (BABB) affinities, respectively.

Introduction

Chromitites in ophiolites display a wide compositional range from Al-rich (refractory-grade) to Cr-rich chromite (metallurgical-grade) (Stowe, 1994; Uysal et al., 2005). The origin of these compositional variations is interpreted to have resulted from the crystallization of chromite from parental melts generated by different degrees of partial melting, progressive fractionation, variable degrees of melt-rock reactions, nature of the host peridotite, different magmatic sources and geodynamic settings (Dilek and Furnes, 2014, and the references therein; Uysal et al., 2012). In general, Cr-rich chromitites occur in the deeper parts of the upper mantle sequence of ophiolites, whereas Al-rich chromitites in the mantle-crust transition zone (e.g. Flint et al., 1948; Thayer, 1942, 1946; Leblanc and Violette, 1983; Leblanc and Nicolas, 1992; Zhou and Bai, 1992; Graham et al., 1996; Melcher et al., 1997; Proenza et al., 1999, Uysal et al., 2007; Rollinson, 2008; González-Jiménez et al., 2014 and references therein). However, the coexistence of high-Cr and high-Al chromitites in a small area within a single ophiolite massif has been documented only from a few ophiolites earlier (e.g. Thayer, 1942, 1964; Proenza et al., 1999, 2003; Zaccarini et al., 2011; González-Jiménez et al., 2011).

The Cuban ophiolites host some of the world's richest chromite ore deposits, especially refractory-grade chromite in the Moa-Baracoa and Camagüey ophiolite massifs (Proenza et al., 1999, 2002, 2003; Henares et al., 2010; González-Jiménez et al., 2011; Butjosa et al., 2015). Also, high-Cr and high-Al chromitites bodies are distributed in a relatively small area (from 2 km to around 10 km in length) within the eastern part of the Havana-Matanzas ophiolites in western Cuba (Thayer, 1942; Lavandero et al., 1988, 1995) (Fig. 1; Table 1). These chromite deposits were extensively exploited in the past (before and during World War II).

In this paper, we present the results of a new, detailed study of chromian spinel compositions in selected chromite deposits (three Cr-rich and one Al-rich) of the Havana-Matanzas ophiolites in Western Cuba (Fig. 1). We use the chromian spinel compositions to decipher the nature of parental melts, which resulted in the chromitite formation and in the modification of the upper mantle peridotites in these ophiolites.We describe the platinum group minerals (PGM) in the chromitites and discuss their paragenesis. We then present a model for the tectonic setting of the formation of the Havana-Matanzas ophiolites and their chromitite deposits. This paper provides the first systematic classification of chromitite occurrences in the Western Cuban ophiolites.

Geological setting

The largest Caribbean ophiolites crop out in the northern part of the Island of Cuba, along the Northern Ophiolite Belt (NOB; Iturralde-Vinent, 1996, 1998; Lewis et al., 2006; Fig. 1), which is an ~E-W-trending, ~1000-km-long belt comprising dismembered mafic–ultramafic rock bodies (Fonseca et al., 1985; Iturralde-Vinent 1996) (Fig. 1). The NOB is part of the Cuban orogenic belt, formed during the Cretaceous–Tertiary convergence and collision of the Caribbean oceanic plate with the Bahamas platform (Iturralde-Vinent, 1996, 1998) or the Caribeana terrane (García-Casco et al., 2008; Iturralde-Vinent et al., 2008). This collision in the latest Cretaceous–early

Tertiary facilitated the tectonic emplacement of ophiolites, oceanic volcanic arcs, subduction-accretion mélanges, and flysch deposits onto the southern paleo-margin of North America (Iturralde-Vinent, 1998; García-Casco et al.,2008). In the western part of the NOB, the Havana-Matanzas ophiolites are tectonically imbricated with Cretaceous intra-oceanic volcanic arc units and Campanian-Maastrichtian sedimentary sequences as part of a tectonic mélange (Fig. 1). This mélange belt extends in a WNW – ESE direction and covers an area of up to30 km^2.

A reconstructed Havana-Matanzas ophiolite sequence is ~4 km-thick (Fig. 2) and consists of a lower unit of upper mantle peridotites, a Moho transition zone, and a crustal section composed of massive gabbros, dolerite and pillow lavas, and sedimentary rocks, mainly made of radiolarite, lutite and mudstone (Fonseca et al., 1985; Llanes et al., 2001).

The upper mantle tectonites consist mainly of serpentinized harburgites with strongly deformed orthopyroxene porphyroclasts, and contain ubiquitous pyroxenite veins. Minor dunites occur as sub-concordant layers in the harzburgites and as the wallrock of chromitite bodies. Ultramafic rocks in the mantle–crust transition zone above the tectonites are rich in plagioclase and clinopyroxene, and commonly contain gabbro sills, and gabbro and pegmatitic gabbro dikes (Llanes et al., 2001).The poorly exposed crustal section in the Havana-Matanzas ophiolites, and is composed mainly of massive (isotropic) gabbros and basalts overlain by sedimentary rocks (Fig. 2; Llanes et al., 2001). Plagiogranite dikes locally intrude massive gabbros. Doleritic dike rocks occur as blocks in the mélange but are not observed to form a separate sheeted dike complex in the ophiolite although the presence of sheeted dikes has been reported previously (Fonseca et al., 1985).

Serpentinized peridotites are juxtaposed tectonically against the Cenomanian-Turonian (88–99 Ma) volcanic rocks of the Margot

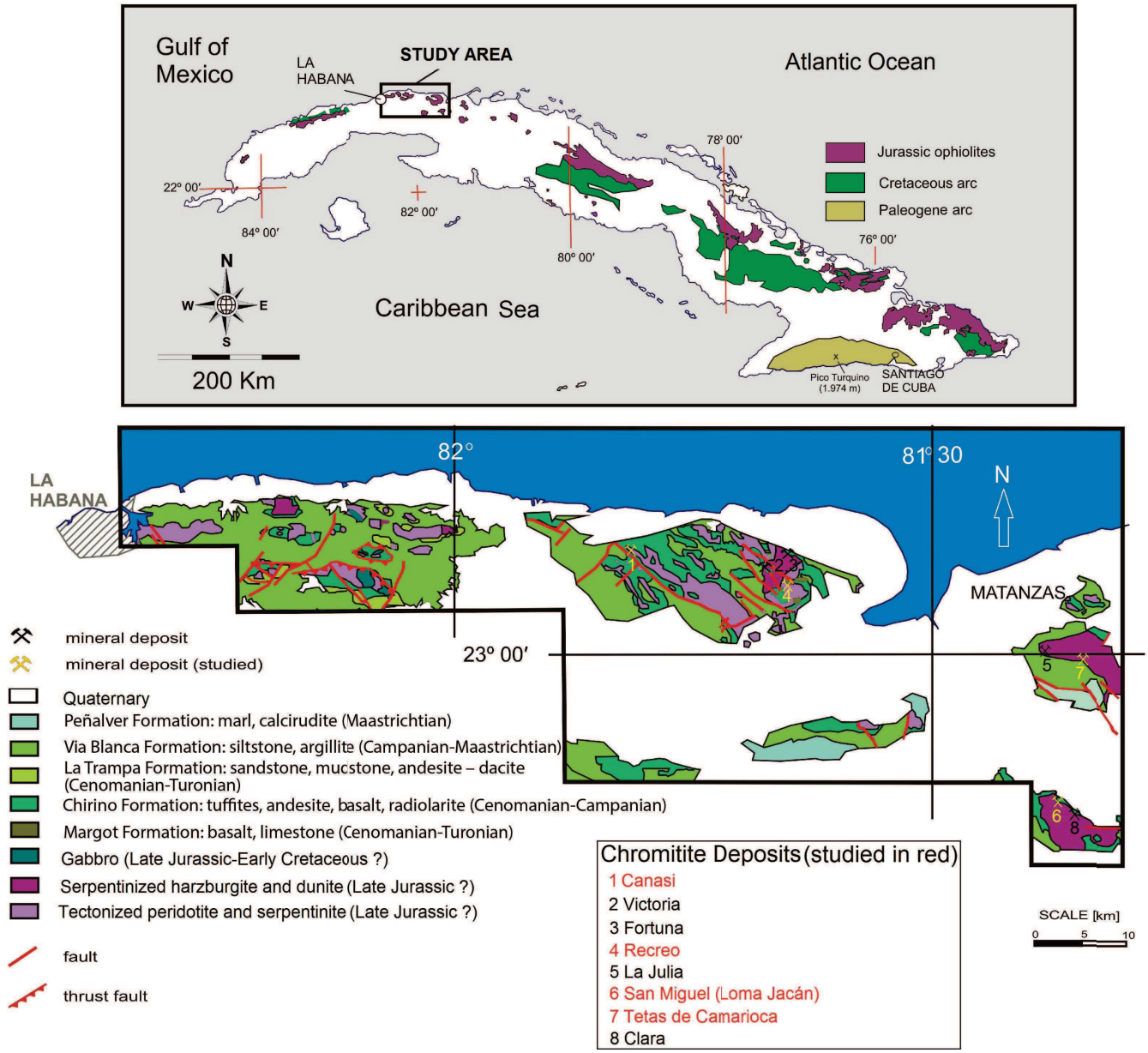

Figure 1. Location of the Havana-Matanzas Ophiolites within the Northern Cuban Ophiolitic belt, and simplified geological map with location of the studied chromitites.

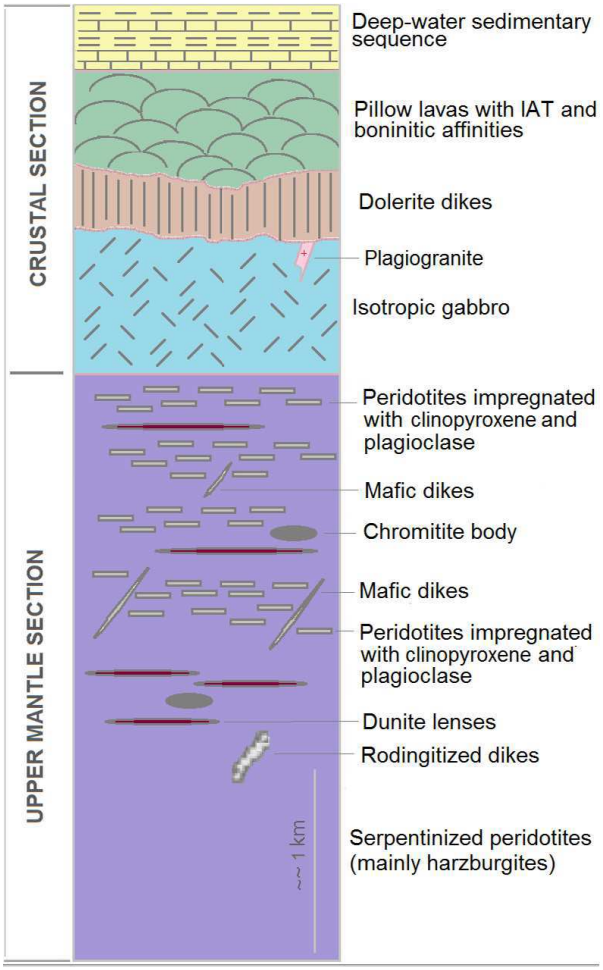

Figure 2. Idealized stratigraphic columnar section of the Havana-Matanzas ophiolites.

Formation (Pszczólkowski, 2002). These volcanic rocks mainly consist of pillow basalts with N-MORB and E-MORB affinities (Llanes et al., 2001), interbeded with chert and fine-grained limestone. Kerr et al. (1999) suggested an oceanic intra-plate tholeiitic affinity for the origin of the Margot basalts, as remnants of an oceanic plateau. However, in some other areas (e.g. Campo Florido, América mine) within the Havana-Matanzas region basaltic pillow lavas of the Margot Formation consist of low-Ti, island arc tholeiites and boninites. These volcanic rocks have been interpreted to represent the upper crust of a forearc oceanic lithosphere (Llanes et al., 2015).

Sampling and analytical techniques

The chromitite samples analyzed in this study are from the eastern part of the Havana-Matanzas ophiolites (western Cuba), collected from four separate chromite deposits **(**Table 1; Fig. 1**)**. We sampled these chromitite bodies based on the availability of fresh outcrops and the distribution of deposit types in the study area. Petrographic studies as well as analyses of chromian spinel, silicate and PGM were performed on 8 polished thin sections and 12 polished sections.

The chromian spinel composition has been determined by electron microprobe analysis, using a CAMECA SX50 instrument in wavelength dispersive mode, at the Serveis Científics i Tecnòlogics, University of Barcelona, Spain. The analytical conditions were: accelerating voltage 20 kV, beam current 20 nA, beam diameter 2 µm, and a counting time of 10 seconds per element. Calibrations were performed using natural and synthetic reference materials: chromite (Cr, Al, Fe), periclase (Mg), rhodonite (Mn), rutile (Ti), NiO (Ni) and metallic V. The proportion of Fe^{3+} in chromian spinel was calculated assuming stoichiometry.

The PGM were investigated *in-situ* by scanning electron microscopy (SEM), and were analyzed by electron microprobe (EMP), using a Jeol JXA 8200 Superprobe at the Eugen F. Stumpfl Laboratory at the University of Leoben, Austria. The instrument operated in WDS mode, at 20 kV accelerating voltage, 10 nA beam current and with a beam diameter of less than 1 ìm. The counting time on peak and backgrounds were 20 and 10 seconds, respectively. All possible peak overlaps among the selected X -ray emission lines were checked and automatically corrected, using the on-line procedure. Pure metals were the reference material for Os Ir, Ru, Rh, Pt, and Pd. The natural minerals chalcopyrite and synthetic nickeline were used to calibrate Cu, Fe, S, Ni and As. The following X-ray lines were used: Ka for S, Fe, Cu, and Ni; La for Ir, Ru, Rh, Pt, Pd and As; and Ma for Os.

Chromitites and host rocks

About 10 chromitite occurrences have been described in the Havana-Matanzas ophiolites (Thayer, 1942; Murashko and Lavandero 1989; Lavandero et al., 1995). They are spatially related to the mantle tectonites close to the mantle-crust transition zone (Fig. 2). The ore bodies are small (0.5-m-wide and 2-m-long) and have tabular to lenticular shapes, enclosed in deformed, serpentinized dunite hosted by strongly serpentinized harzburgites (Table 1). The contact between the chromitite and dunite occurs along a zone of disseminated ore. The majority of the studied chromitite bodies are concordant with

Table 1. Chromitite deposits from the Havana-Matanzas district, NW Cuba

Deposit/Type/Tectonic structure	Host rocks	Morphology / structure
Recreo / Al- Rich Chromitite Tectonic mega-block of Matanzas	Serpentinized harzburguites and dunites (base of the mantle-crust transition zone)	Pods of massive and nodular chromite enclosed in deformed serpentinized dunite
Canasí / Cr- Rich Chromitite Tectonic mega-block of Matanzas	Serpentinized harzburguites and dunites (base of the mantle-crust transition zone)	Pods of massive chromite enclosed in deformed serpentinized dunite
San Miguel / Cr- Rich Chromitite Tectonic block of Coliseo	Serpentinized clinopyroxene-harzburguite, impregnated peridotite with clinopyroxene and plagioclase (mantle-crust transition zone in the upper part of the mantle sequence).	Pods of massive chromite (~ 0.5 m-wide, 2 m-long), enclosed in deformed serpentinized dunite
Tetas de Camarioca / Cr- Rich Chromitite Tectonic block of Camarioca	Serpentinized harzburguites and dunites (base of the mantle-crust transition zone), with clinopyroxenite dikes/sills	Irregular bodies with sub-vertical dips

the foliation in the host peridotites, except in the Tetas de Camarioca body in which they are clearly discordant.

Some Cr-rich deposits (e.g. San Miguel) are hosted by weakly depleted, clinopyroxene-rich harzburgite and peridotite impregnated with clinopyroxene and plagioclase. The Recreo Al-rich chromitites are hosted, on the other hand, by more depleted harzburgite (without clinopyroxene). Similar relationships have been described in the chromitites of the Sagua de Tánamo district in the Mayari-Baracoa ophiolite belt (eastern Cuba), where harzburgites hosting Al-rich chromitites are relatively more depleted than the harzburgites hosting Cr-rich chromitite bodies (Proenza et al., 2003; González-Jiménez et al., 2011).

Mineralogy and chromitite textures

The Havana-Matanzas chromitites display predominantly massive textures (Fig. 3a-c). However, disseminated ores are also common near the contacts with the host dunite (Fig. 3d). Nodular texture has been observed only in the Al-rich Recreo deposit. In general, the late-stage orogenic deformation associated with shearing and faulting obliterated primary magmatic textures in the chromitites, and produced instead mylonitic, cataclastic and brecciated textures (Fig. 3e, f).

Chromian spinel as the main ore mineral represents 85-95 vol.% of the chromitites, and shows anhedral to subhedral habits with grain sizes reaching up to 5 mm (Fig. 3). A thin rim of ferrian chromite is observed along grains boundaries and cracks (Fig. 3c). Clinochlore and serpentine with traces of Fe-Ni sulfides (heazlewoodite, millerite, pentlandite) and Fe-Ni alloys (mainly awaruite) occur as main inter-granular phases. Clinopyroxene, amphibole (mainly pargasite), serpentine, clinochlore, Fe-Ni sufides, and platinum-group minerals (PGM) make up the main solid inclusions in chromian spinel.

PGM were found only in the Cr-rich chromitites of the Tetas de Camarioca and Arco de Canasí deposits. They are very small, less than 10-µm-long, and occur as euhedral to subeuhedral crystals, included in chromian spinel. They form poly-phase grains composed of different PGM and silicates, which are made mainly clinopyroxene and amphibole. The most abundant PGM is laurite [$(Ru,Os,Ir)S_2$] (Fig. 4) forming polyphase grains with cuproiridisite ($CuIr_2S_4$), native Os (Fig. 4a), and an unidentified phase composed of Ir-Ni-Fe-S (Fig. 4d, e). Laurite also forms composite inclusions with primary silicates (clinopyroxene and amphibole) (Fig. 4 a, c, d, e, f), or with secondary mineral (Fe-Cu sulfide) (Fig. 4f). Native Os was found as minute particles (<1 µm) attached to the external border of the laurite (Fig. 4a). The composition of laurite, in terms of Ru-Os-Ir (at%) is similar to that of the laurite occurrences in both the Tetas de Camarioca and Arco de Canasi chromitites (Fig. 5; Table 2).

Chromian spinel chemistry

The chemistry of chromian spinel in the Havana-Matanzas chromitites shows a wide compositional range, from Cr-rich (San Miguel, Canasí and Tetas de Camarioca) to Al-rich (Recreo) (Fig. 6; Table 3). As a whole, Cr# [Cr/(Cr+Al)] varies from 0.44 to 0.75 (corresponding to 38-57 wt.% Cr_2O_3 and 13-30 wt.% Al_2O_3) and Mg#[Mg/(Mg+Fe^{2+})] from 0.66 to 0.74 (corresponding to 10.8-14.4 wt.% FeO and 13.3-17.1 wt.% MgO). The TiO_2 contents range between 0.15 and 0.44 wt.% and the Fe_2O_3 values between 3.64 and 4.78 wt.%. Minor amounts of V_2O_3 (0.1–0.3 wt. %), MnO (0.1-0.3 wt.%), NiO (0.1–0.3 wt.%) and ZnO (<0.2 wt.%) were also detected in chromian spinels of the both chromite types. The TiO_2 contents in

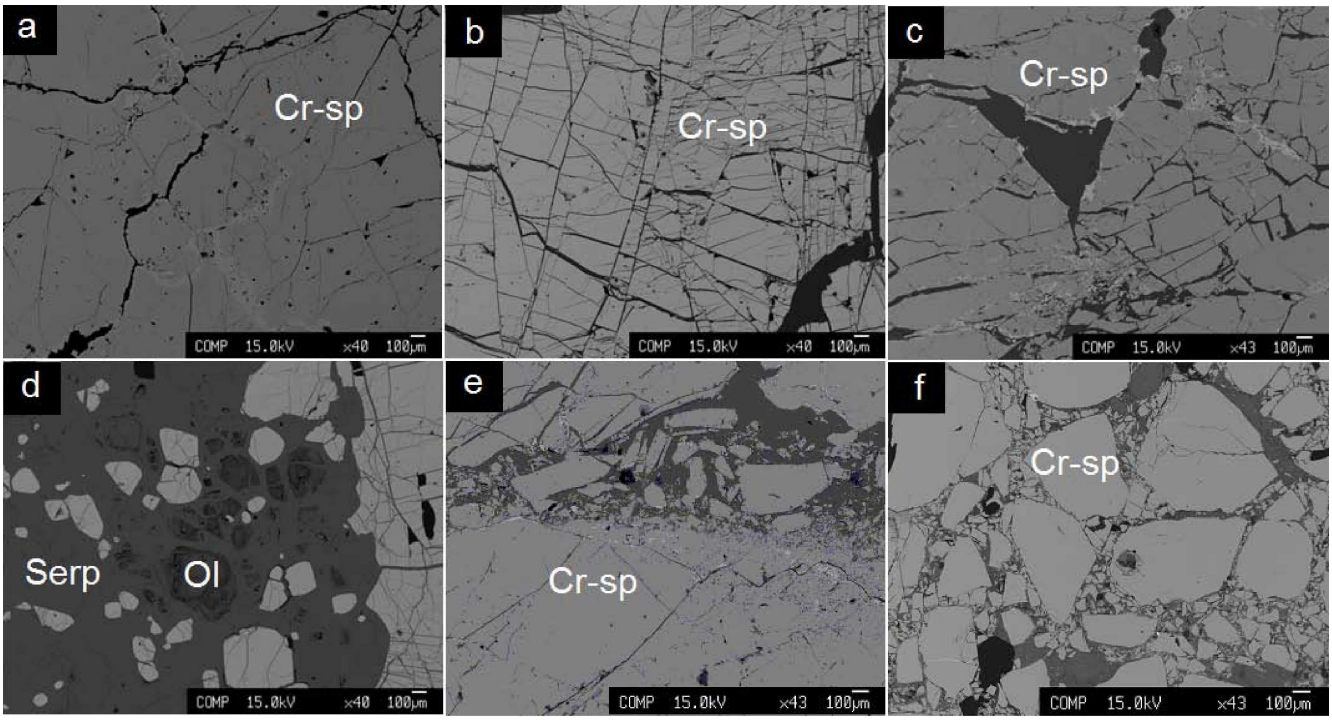

Figure 3. Back-scattered electron microscopy images of the investigated chromitites, showing different textures. (a) and (b) Massive chromitites from the high-Cr chromitite of Tetas de Camarioca and San Miguel, respectively. (c) Massive chromitite from the high-Al chromitite of Recreo. (d) Disseminated chromitite from the high-Al chromitite of Recreo. (e) Cataclastic chromitite from the high-Al chromitite of Recreo. (f) Brecciated chromitite from the high-Cr chromitite of Canasi. Cr-sp: chromian spinel, Ol: olivine, Serp: serpentine.

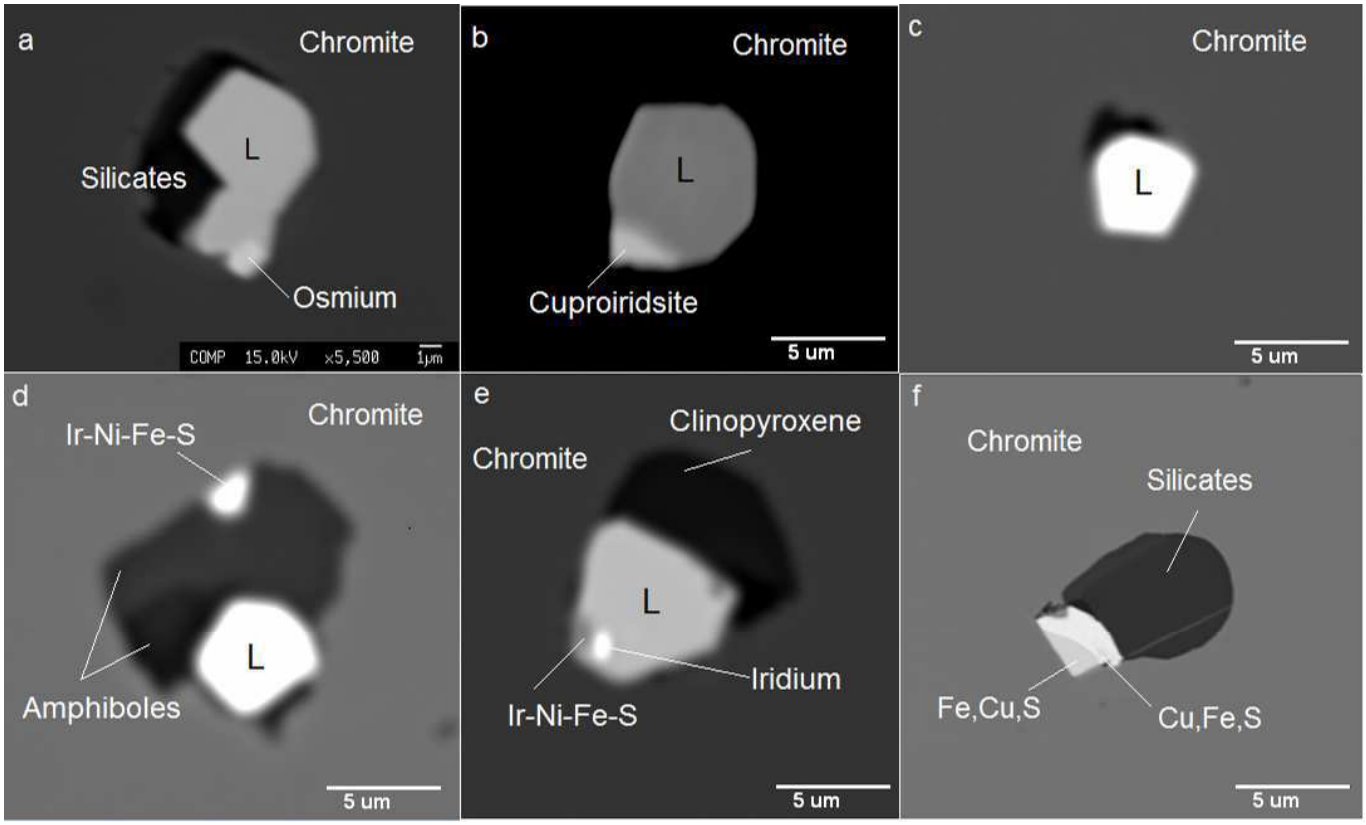

Figure 4. Backscattered-electron microscopy images showing the morphology, texture and mineral assemblages of PGM in the Western Cuban ophiolites. L: laurite.

chromian spinel of the Al-rich chromitite ranges between 0.32 and 0.42 wt. %, similar to the contents observed in chromian spinel from the Arcos de Canasí and Tetas de Camarioca Cr-rich chromitites (Fig. 6).

All chromian spinel from the studied chromitites at Havana-Matanzas plot within the podiform (ophiolitic) chromitite field (Fig. 6A). In the Cr# vs. TiO_2 plot (Fig. 6B), the chromian spinel compositions of the San Miguel chromitites plot within the field defined by boninites, whereas the Recreo chromitites plot in the field defined by mid-oceanic ridge basalts (MORB) (Arai, 1997). On the other hand, the Canasí and Tetas de Camariocas chromian spinel compositions fall between these two fields and within the compositional range defined by the chromitites from the Sagua de Tánamo district in eastern Cuba (Proenza et al., 1999, 2003; González-Jiménez et al., 2011).

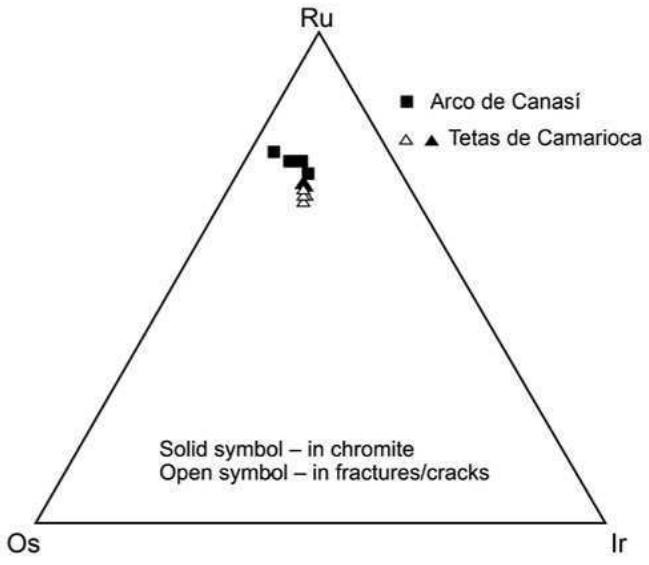

Figure 5. Compositional variations (at.%) of the analyzed laurite from the Havana-Matanzas Ophiolites.

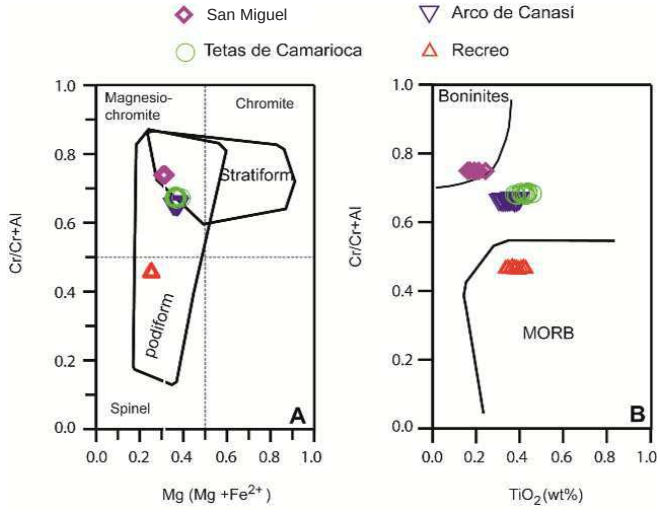

Figure 6. (A) #Cr[Cr/(Cr + Al)] versus #Mg[Mg/(Mg + Fe)], and (B) #Cr versus TiO_2 content for chromian spinel in chromitites of the Havana-Matanzas ophiolites: The fields labeled "podiform" and "stratiform" are after Irvine (1967) and Leblanc and Nicolas (1992), respectively. Boninitic and MORB fields were defined by Arai (1997).

Table 2 Compositions of representative laurite samples in chromitites from the Havana-Matanzas ophiolites, NW Cuba

Wt.%	S	As	Os	Ir	Ru	Rh	Pt	Pd	Fe	Ni	Cu	Total
Tetas de Camarioca												
1-3ap1an1	34,52	0,94	15,70	11,17	31,56	2,02	0,00	2,20	1,08	0,20	0,14	99,52
1-3ap1an2	34,27	1,01	16,24	11,41	32,34	2,11	0,00	2,18	1,03	0,21	0,12	100,94
1-3ap2an1	33,69	0,99	16,59	11,68	31,36	1,68	0,00	1,97	0,93	0,17	0,11	99,17
1-3ap2an2	33,97	0,93	16,50	12,55	30,50	1,68	0,00	2,09	0,93	0,20	0,07	99,41
1-3ap2an3	32,86	0,89	16,82	12,28	30,88	1,68	0,00	1,95	0,93	0,18	0,13	98,60
1-3ap3an1	32,69	0,75	17,14	12,02	29,07	1,80	0,00	1,97	1,49	0,05	0,08	97,06
Arco de Canasi												
1-61-1ap3an1	32,95	1,03	16,05	7,52	34,05	1,67	0,00	2,02	1,85	0,05	0,11	97,29
1-61-1ap3an2	33,16	1,07	16,03	7,77	34,61	1,64	0,00	2,12	1,43	0,10	0,06	97,99
1-61-5ap1an1	34,71	1,04	14,77	11,25	33,92	1,95	0,00	2,18	0,86	0,06	0,14	100,88
1-61-5ap1an2	33,44	1,15	14,70	11,31	33,69	2,00	0,00	2,21	0,85	0,06	0,06	99,48
1-61-5ban1	36,09	0,82	15,99	3,44	31,76	1,03	0,00	1,53	5,02	0,03	2,15	97,87
1-61-5bp2an1	33,96	1,05	15,33	8,95	35,15	1,96	0,00	2,31	1,08	0,18	0,16	100,12
1-61-5bp2an2	33,58	1,18	14,57	9,46	35,01	1,95	0,00	2,29	1,15	0,23	0,16	99,58
At%	S	As	Os	Ir	Ru	Rh	Pt	Pd	Fe	Ni	Cu	Total
Tetas de Camarioca												
1-3ap1an1	66,98	0,78	5,14	3,61	19,43	1,22	0,00	1,29	1,20	0,21	0,14	100
1-3ap1an2	66,30	0,84	5,30	3,68	19,85	1,27	0,00	1,27	1,14	0,22	0,12	100
1-3ap2an1	66,58	0,84	5,53	3,85	19,66	1,03	0,00	1,17	1,06	0,18	0,11	100
1-3ap2an2	66,94	0,79	5,48	4,12	19,07	1,03	0,00	1,24	1,05	0,21	0,07	100
1-3ap2an3	66,07	0,77	5,70	4,12	19,70	1,05	0,00	1,18	1,08	0,20	0,13	100
1-3ap3an1	66,44	0,65	5,87	4,07	18,74	1,14	0,00	1,21	1,74	0,06	0,08	100
Arco de Canasi												
1-61-1ap3an1	65,34	0,87	5,37	2,49	21,42	1,03	0,00	1,21	2,11	0,05	0,11	100
1-61-1ap3an2	65,46	0,90	5,33	2,56	21,68	1,01	0,00	1,26	1,63	0,11	0,06	100
1-61-5ap1an1	66,57	0,85	4,78	3,60	20,64	1,16	0,00	1,26	0,95	0,06	0,14	100
1-61-5ap1an2	65,79	0,97	4,87	3,71	21,03	1,22	0,00	1,31	0,96	0,06	0,06	100
1-61-5ban1	66,15	0,64	4,94	1,05	18,47	0,59	0,00	0,85	5,28	0,03	1,99	100
1-61-5bp2an1	65,64	0,87	4,99	2,89	21,55	1,18	0,00	1,34	1,20	0,19	0,15	100
1-61-5bp2an2	65,34	0,99	4,78	3,07	21,61	1,18	0,00	1,34	1,29	0,25	0,16	100

Discussion

Chromite compositions and tectonic setting of the chromitites

The origin of the close association of high-Cr and high-Al chromitites in some ophiolite complexes has been extensively debated, and several genetic models have been proposed for their origin (Zhou and Robinson, 1994; 1997; Arai, 1997; Leblanc, 1995; Malpas et al., 1997; Melcher et al., 1997; Robinson et al., 1997; Proenza et al., 1999, 2003; Zaccarini et al., 2011; González-Jiménez et al., 2011; Dilek and Newcomb, 2003, and references therein; Yang et al., 2015). In general, Cr-rich and Al-rich ophiolitic chromitites are interpreted to have originated from melts, formed by high- and low-degrees of partial melting, respectively. The high-degrees of mantle depletion have been linked to suprasubduction zone environments, where partial melting of the mantle wedge peridotites is enhanced by the addition of volatiles from the downgoing slab (Pearce et al., 1984; Dilek and Robinson, 2003; Dilek and Furnes, 2009, 2011; Dilek and Thy, 1998, 2009). Thus, the melt-rock reaction removes both clinopyroxene and orthopyroxene, leaving behind a residuum of dunite, enveloping the chromitite bodies (Zhou et al., 1994; Arai, 1997; Morishita et al., 2011; Yang et al., 2014). The main controlling factor in this process is the degree of melt-rock interaction related to the percolation of melts through variably depleted peridotites (Zhou et al., 1994; Melcher et al., 1997; Zhou and Robinson, 1997; Robinson et al., 1997; Brough et al., 2015).

Llanes et al. (2001) concluded previously that the Havana-Matanzas Cr-rich chromitites that are hosted in depleted peridotites were crystallized from highly magnesian magmas, whereas Al-rich chromitites were derived from magmas precipitated from tholeiitic melts under moderate to high grades of partial melting. However, the San Miguel Cr-rich deposit is hosted in weakly depleted harzburgites and peridotites impregnated with clinopyroxene and plagioclase, whereas the Recreo Al-rich chromitites are hosted in more depleted harzburgites and dunite. Thus, the factors controlling the chromite compositions and the spatial relationships of chromitites to their host rocks are still unclear regarding the Cuban ophiolites.

Based on the chromian spinel chemistry and regression lines developed by Zaccarini et al. (2011) and using the data of Kamenetsky et al. (2001), we infer that the calculated melts that were in equilibrium with Cr-rich and Al-rich Havana-Matanzas chromitites had island-arc tholeiite (IAT) – boninite and mid-ocean ridge tholeiite (MORB)/backarc basin basalt (BABB) affinities, respectively. We observe the same distinct geochemical affinities for the Cr-rich and Al-rich Havana-Matanzas chromitites on the TiO_2 versus #Cr [Cr/(Cr + Al)] discrimination diagram (Fig. 7). Collectively, these geochemical data and observations indicate that the Havana-Matanzas chromitites and

Table 3. Representative electron-microprobe analyses of chromian spinel from chromitites of the Havana-Matanzas district

Canasí deposit

Sample	TiO_2	Al_2O_3	Cr_2O_3	Fe_2O_3	FeO	V_2O_3	MnO	MgO	NiO	Total	Ti	Al ^{VI}	V	Fe^{3+}	Mn^{2+}	Fe^{2+}	Ni	# Cr	# Mg
I-61-1-1	0,32	17,84	49,65	5,17	14,50	0,25	0,21	13,61	0,12	101,81	0,007	0,648	0,01	0,12	0,01	0,37	0,003	0,65	0,63
I-61-1-2	0,37	17,95	49,41	4,40	14,41	0,12	0,24	13,42	0,22	100,71	0,009	0,658	0,00	0,10	0,01	0,38	0,006	0,65	0,62
I-61-1-3	0,36	17,88	49,47	4,78	14,09	0,12	0,26	13,66	0,13	100,95	0,008	0,653	0,00	0,11	0,01	0,37	0,003	0,65	0,63
I-61-1-4	0,29	17,96	49,39	5,00	14,01	0,19	0,18	13,69	0,21	101,15	0.007	0,655	0,01	0,12	0,01	0,36	0,005	0,65	0,64
I-61-1-5	0,35	17,96	49,57	4,86	14,35	0,19	0,21	13,61	0,20	101,50	0.008	0,653	0,01	0,11	0,01	0,37	0,005	0,65	0,63
I-61-1-6	0,34	18,04	49,47	5,17	13,91	0,19	0,27	13,89	0,18	101,63	0.008	0,654	0,01	0,12	0,01	0,36	0,004	0,65	0,64
I-61-1-7	0,30	17,97	49,20	5,35	13,89	0,22	0,23	13,84	0,26	101,37	0.007	0,653	0,01	0,12	0,01	0,36	0,006	0,65	0,64
I-61-1-8	0,38	17,88	49,63	5,10	14,16	0,16	0,27	13,72	0,29	101,75	0.009	0,649	0,00	0,12	0,01	0,37	0,007	0,65	0,63
I-61-1-9	0,36	18,13	49,43	5,08	14,37	0,17	0,23	13,70	0,18	101,86	0.008	0,656	0,00	0,12	0,01	0,37	0,004	0,65	0,63
I-61-1-10	0,33	17,98	49,46	4,75	14,14	0,14	0,21	13,66	0,22	101,00	0.008	0,656	0,00	0,11	0,01	0,37	0,006	0,65	0,63
I-61-5-1	0,37	18,09	49,65	4,53	14,57	0,19	0,25	13,48	0,21	101,50	0.009	0,658	0,01	0,11	0,01	0,38	0,005	0,65	0,62
I-61-5-2	0,30	17,83	49,91	4,18	14,59	0,19	0,22	13,32	0,18	100,78	0.007	0,654	0,01	0,10	0,01	0,38	0,004	0,65	0,62
I-61-5-3	0,38	17,62	49,81	4,66	14,49	0,11	0,27	13,43	0,17	101,08	0.009	0,654	0,00	0,11	0,01	0,38	0,004	0,65	0,62
I-61-5-4	0,36	18,22	49,36	4,60	14,53	0,20	0,29	13,52	0,20	101,40	0.008	0,663	0,01	0,11	0,01	0,38	0,005	0,64	0,62
I-61-5-5	0,33	18,05	49,82	4,53	14,58	0,24	0,21	13,55	0,22	101,67	0.008	0,655	0,01	0,11	0,01	0,38	0,006	0,65	0,62
I-61-5-6	0,35	17,93	49,59	4,72	14,68	0,16	0,19	13,45	0,17	101,40	0.008	0,653	0,00	0,11	0,01	0,38	0,004	0,65	0,62
I-61-5-7	0,34	17,61	50,04	4,69	14,74	0,19	0,31	13,38	0,11	101,58	0.008	0.642	0,01	0,11	0,01	0,38	0,003	0,66	0,62
I-61-5-8	0,37	18,14	49,48	4,76	14,45	0,09	0,27	13,55	0,24	101,47	0.009	0.66	0,00	0,11	0,01	0,37	0,006	0,65	0,63
I-61-5-9	0,32	18,16	49,59	4,29	14,59	0,21	0,24	13,42	0,20	101,21	0.007	0.662	0,01	0,10	0,01	0,38	0,005	0,65	0,62
I-61-5-10	0,30	18,06	49,60	4,99	14,52	0,16	0,23	13,52	0,20	101,75	0.007	0.650	0,00	0,12	0,01	0,37	0,005	0,65	0,62

Recreo deposit

Sample	TiO_2	Al_2O_3	Cr_2O_3	Fe_2O_3	FeO	V_2O_3	MnO	MgO	NiO	Total	Ti	Al ^{VI}	V	Fe^{3+}	Mn^{2+}	Fe^{2+}	Ni	# Cr	# Mg
REC-1	0,35	29,34	37,66	4,08	10,82	0,14	0,15	16,81	0,21	99,66	0.002	1.014	0,003	0,09	0,004	0,265	0,005	0,46	0,74
REC-2	0,38	29,82	37,06	4,41	10,79	0,19	0,2	16,97	0,18	100,07	0.001	1.025	0,005	0,097	0,005	0,263	0,004	0,45	0,74
REC-3	0,39	29,64	37,4	4,89	10,63	0,18	0,15	17,15	0,19	100,78	0.001	1.013	0,004	0,107	0,004	0,258	0,004	0,46	0,74
REC-4	0,36	30,38	37,8	3,99	11,11	0,18	0,16	17,09	0,19	101,36	0.002	1.03	0,004	0,086	0,004	0,267	0,004	0,46	0,73
REC-5	0,41	30,06	37,82	4,32	11,01	0,13	0,18	17,12	0,15	101,35	0.001	1.021	0,003	0,094	0,005	0,265	0,003	0,46	0,74
REC-6	0,32	29,96	37,78	4,55	10,66	0,18	0,17	17,28	0,21	101,19	0.002	1.018	0,004	0,099	0,004	0,257	0,005	0,46	0,74
REC-7	0,34	30,14	37,63	4,45	11,05	0,19	0,22	16,96	0,32	101,45	0.002	1.023	0,004	0,096	0,005	0,266	0,007	0,46	0,73
REC-8	0,4	29,76	37,9	4,21	10,78	0,28	0,2	17,1	0,3	101,08	0.002	1.014	0,006	0,092	0,005	0,261	0,007	0,46	0,74
REC-9	0,33	29,72	37,69	4,88	10,57	0,18	0,21	17,17	0,27	101,17	0.001	1.012	0,004	0,106	0,005	0,255	0,006	0,46	0,74
REC-10	0,37	29,8	37,73	4,73	10,66	0,19	0,22	17,19	0,24	101,16	0.000	1.014	0,004	0,103	0,005	0,258	0,006	0,46	0,74

San Miguel deposit

Sample	TiO_2	Al_2O_3	Cr_2O_3	Fe_2O_3	FeO	V_2O_3	MnO	MgO	NiO	Total	Ti	Al ^{VI}	V	Fe^{3+}	Mn^{2+}	Fe^{2+}	Ni	# Cr	# Mg
I-12-D2-1	0,18	13,51	57,03	3,53	12,38	0,06	0,23	14,35	0,15	101,59	0.001	0,497	0,00	0,08	0,01	0,32	0,004	0,74	0,67
I-12-D2-2	0,20	13,30	56,85	3,53	11,97	0,08	0,28	14,60	0,10	101,01	0.002	0,492	0,00	0,08	0,01	0,31	0,003	0,74	0,68
I-12-D2-3	0,18	13,26	56,52	3,63	12,10	0,19	0,16	14,46	0,13	100,70	0.001	0,492	0,01	0,09	0,00	0,32	0,003	0,74	0,68
I-12-D2-4	0,18	13,40	57,35	3,58	12,41	0,05	0,29	14,39	0,24	101,99	0.001	0,492	0,00	0,08	0,01	0,32	0,006	0,74	0,67
I-12-D2-5	0,18	13,45	57,04	3,79	11,86	0,08	0,20	14,75	0,12	101,60	0.001	0,494	0,00	0,09	0,01	0,31	0,003	0,74	0,69
I-12-D2-6	0,20	13,46	57,13	3,66	12,01	0,13	0,24	14,77	0,07	101,74	0.001	0,493	0,00	0,09	0,01	0,31	0,002	0,74	0,69
I-12-D2-7	0,18	13,36	57,02	3,51	12,29	0,03	0,23	14,39	0,18	101,20	0.000	0,494	0,00	0,08	0,01	0,32	0,005	0,74	0,68
I-12-D2-8	0,16	13,27	56,85	3,46	12,18	0,13	0,20	14,36	0,20	100,89	0.001	0,492	0,00	0,08	0,01	0,32	0,005	0,74	0,68
I-12-D2-9	0,23	13,41	56,98	3,49	12,19	0,06	0,26	14,58	0,12	101,41	0.002	0,494	0,00	0,08	0,01	0,32	0,003	0,74	0,68
I-12-D2-10	0,15	13,32	56,84	4,07	12,02	0,11	0,24	14,61	0,10	101,62	0.001	0,49	0,00	0,10	0,01	0,31	0,003	0,74	0,68

Tetas de Camarioca deposit

Sample	TiO_2	Al_2O_3	Cr_2O_3	Fe_2O_3	FeO	V_2O_3	MnO	MgO	NiO	Total	Ti	Al ^{VI}	V	Fe^{3+}	Mn^{2+}	Fe^{2+}	Ni	# Cr	# Mg
I-3-1	0,41	16,44	50,67	4,85	13,97	0,12	0,26	13,46	0,26	100,60	0.001	0,607	0,00	0,11	0,01	0,37	0,006	0,67	0,63
I-3-2	0,40	16,47	50,60	4,46	14,03	0,06	0,13	13,33	0,34	100,00	0.001	0,611	0,00	0,11	0,00	0,37	0,009	0,67	0,63
I-3-3	0,42	16,25	50,87	5,12	14,26	0,06	0,23	13,36	0,28	100,99	0.001	0,599	0,00	0,12	0,01	0,37	0,007	0,68	0,63
I-3-4	0,42	16,47	51,08	4,89	14,31	0,14	0,22	13,51	0,29	101,39	0.002	0,603	0,00	0,11	0,01	0,37	0,007	0,68	0,63
I-3-5	0,41	16,28	50,39	5,20	13,82	0,11	0,28	13,50	0,28	100,49	0.002	0,602	0,00	0,12	0,01	0,36	0,007	0,67	0,63
I-3-6	0,44	16,41	50,75	4,59	14,01	0,07	0,25	13,39	0,30	100,36	0.001	0,607	0,00	0,11	0,01	0,37	0,008	0,67	0,63
I-3-7	0,36	16,57	50,70	4,71	13,85	0,14	0,31	13,58	0,19	100,48	0.001	0,611	0,00	0,11	0,01	0,36	0,005	0,67	0,64
I-3-8	0,41	16,28	50,17	5,12	14,34	0,07	0,27	13,16	0,27	100,15	0.001	0,605	0,00	0,12	0,01	0,38	0,007	0,67	0,62
I-3-9	0,39	16,01	50,37	5,14	14,00	0,11	0,23	13,28	0,28	99,94	0.001	0,596	0,00	0,12	0,01	0,37	0,007	0,68	0,63
I-3-10	0,42	16,10	50,14	4,59	14,48	0,12	0,32	13,26	0,28	100,09	0.011	0,598	0,00	0,11	0,01	0,38	0,007	0,68	0,62

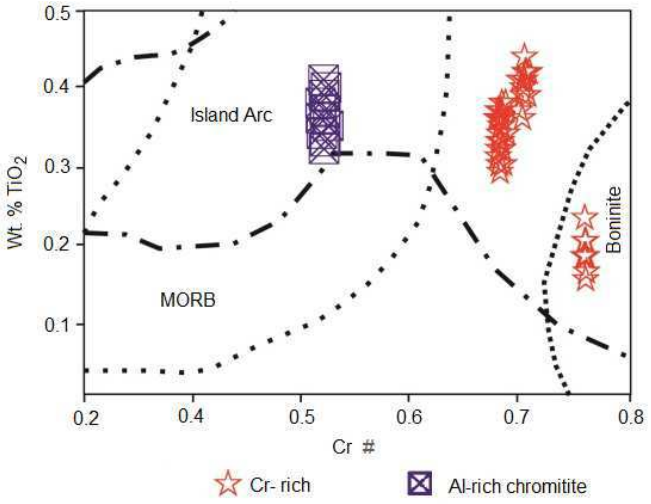

Figure 7. TiO_2 versus Cr# of chromian spinel patterns in the analyzed high-Cr and high-Al chromitites from the Havana-Matanzas Ophiolites. Fields of chromian spinel in lavas of different geochemical affinities and tectonic settings are shown for comparison (Arai, 1997).

their parental melts evolved in a suprasubduction zone (SSZ) environment encompassing forearc, incipient arc and backarc tectonic settings (Dilek and Newcomb, 2003, and references therein). This interpretation is consistent with the findings from other well-documented SSZ ophiolites and their chromitite deposits (Pearce et al., 1984; Roberts, 1988; Arai and Yurimoto, 1995; Zhou and Robinson, 1997; Melcher et al., 1997; Proenza et al., 1999; Zaccarini et al., 2011).

Conditions of PGM formation

The most common PGM documented from ophiolitic chromitites are minerals of the laurite-erlichmanite solid solution series with subordinate Os-Ir-(Ru) alloys. Most of these PGM form euhedral crystals and occur as enclosures in fresh chromite crystals. They are, therefore, considered as primary PGM (i.e. formed at a magmatic stage prior to or concomitantly with chromite crystallization. Experimental data (Brenan and Andrews, 2001; Andrews and Brenan, 2002; Bockrath et al., 2004), supported widely by a large number of natural observations (Garuti et al., 1999a, b; Zaccarini et al. 2011, and references therein), have indicated that crystallization of magmatic PGM in ophiolitic chromitites is mainly controlled by three parameters: (1) availability of PGE in the system; (2) temperatures; and (3) sulphur fugacity. Sulphur fugacity increases with decreasing temperatures (Matthews, 1994; Prouteau and Scaillet, 2013). This variation strongly influences the paragenesis of magmatic PGM. At very high temperatures (around 1300º C), laurite precipitates in equilibrium with Os-Ir-(Ru) alloys. Substitution of Os for Ru in laurite increases with decreasing temperatures and increasing sulphur fugacity. Therefore, laurite may become enriched in Os to the point of reaching the composition of erlichmanite. Compositions of the primary sulfides of the laurite-erlichmanite series can hence be used to model the conditions of PGM precipitation at high temperatures during magmatic stages. In the Havana Matanzas chromitites, all the discovered PGM can be classified as primary. Although erlichmanite is absent, and the analyzed laurite grains show limited variations in their Ru-Os ratios, the presence of magmatic osmium and iridium alloys and Ir-bearing sulfides indicate that the crystallization of PGM started at temperatures around 1300º C and at relatively high sulphur fugacities. These mineralogical observations, coupled with the fact that laurite is enriched in Ir, suggest the presence of abundant Ir in the system. Most of the PGM are spatially associated with magmatic amphiboles, indicating that they must have crystallized in the presence of fluid-rich magmas.

Conclusions

The Havana-Matanzas chromitites in western Cuba show a wide range of chemical compositions, from Cr-rich to Al-rich. Both chromitite types are spatially related to the depleted mantle tectonites near the mantle-crust transition zone, and are mainly enclosed in deformed and serpentinized dunites hosted by strongly deformed harzburgites. These chromitites are analogous in terms of their geochemistry and occurrence to those associated with SSZ ophiolites that formed as a result of the interactions of boninitic (Mg-rich andesites) and MORB-IAT melts with upper mantle peridotites.

We conclude that the main controlling factor for the bimodal compositions of the Cuban chromitites was the degree of melt/rock interaction related to the percolation of subduction-influenced melts through variably depleted peridotites in a mantle wedge. The Cr-rich chromitites in the Havana-Matanzas ophiolites are enriched in magmatic PGM, mainly laurite, which appears to have formed before or concomitantly with the host chromites.

Acknowledgements

We gratefully acknowledge our Spanish project (CGL2012-36263) that has been sponsored by the Ministerio de Economia y Competitividad. The funds through this project covered the expenses of sample preparation, and electron microprobe analyses of silicates and oxides. We thank the University Centrum for Applied Geosciences (UCAG) for providing us with access to the Eugen F. Stumpfl electron microprobe Laboratory (University of Leoben, Austria) for the PGM analysis. We express our sincere thanks to Professor Y Dilek for reviewing and editing several versions of our manuscript and for giving us the opportunity to contribute this paper to the special issue.

References

Andrews, D.R.A., Brenan, J.M. 2002. Phase-equilibrium constraints on the magmatic origin of laurite + Ru-Os-lr alloy. The Canadian Mineralogist, v. 40, pp. 1705-1716.

Arai, S, Yurimoto, H. 1995. Posible subarc origin of podiform chromitites. The Island Arc, v. 4, pp. 104–111.

Arai, S. 1997. Control of wall-rock composition on the formation of podiform chromitites as a result of magma/peridotite interaction. Resource Geology, v. 47, pp. 177–187.

Bockrath, C., Ballhaus, C., Holzheid, A. 2004. Stabilities of laurite RuS and monosulfide liquid solution at magmatic temperature. Chemical Geology, v. 208, pp. 265-271.

Brenan, J.M., Andrews, D.R.A. 2001. High-temperature stability of laurite and Ru-Os-Ir alloys and their role in PGE fractionation in mafic magmas. The Canadian Mineralogist, v. 39, pp. 341-360.

Brough, C.P., Prichard, H.M., Neary, C.r., Fisher, P.C., McDonald, I., 2015, Geochemical variations within podiform chromitite deposits in the Shetland ophiolite: Implications for petrogenesis and PGE concentration. Economic Geology, v. 110, pp. 187-208.

Butjosa, L., Proenza, J.A., Aiglsperger, T., Rebaza, A.M., Galindos, M., García-Casco, A., Iturralde-Vinent, M., Piñero-Pérez, E. 2015. Layered gabbro-hosted Al-rich chromitites at Loma Iguana area, Camagüey ophiolitic massif, Cuba: originated by crustal recycling?. SGA Meeting, Nancy 2014.

Dilek, Y. and Thy, P. 1998. Structure, petrology and seafloor spreading tectonics of the Kizildag Ophiolite, Turkey. Geological Society, London, Special Publications 1998, v. 148, pp. 43-69.

Dilek, Y. and Newcomb, S. 2003. Ophiolite concept and the evolution of geological thought. Geological Society of America Special Papers, v. 373, The Geological Society of America, Boulder, CO 80301, ISBN 0-8137-2373-6.

Dilek, Y. and Robinson, P.T., 2003. Ophiolites in Earth history: Introduction: Geological Society, London, Special Publication, v. 218, pp. 1-8, doi: 10.1144/gsl.sp.2003.218.01.01.

Dilek, Y. and Furnes, H. 2009. Structure and geochemistry of Tethyan ophiolites and their petrogenesis in subduction rollback systems. Lithos, v. 113, pp. 1-20.

Dilek, Y. and Thy, P. 2009. Island arc tholeiite to boninitic melt evolution of the Cretaceous Kizildag (Turkey) ophiolite: Model for multi-stage early arc–forearc magmatism in Tethyan subduction factories. Lithos, v. 113, pp. 68-87.

Dilek, Y. and Furnes, H. 2011, Ophiolite genesis and global tectonics: geochemical and tectonic fingerprinting of ancient oceanic lithosphere. Geological Society of America Bulletin, v. 123, pp. 387-411.

Dilek, Y. and Furnes, H. 2014, Ophiolites and their origins. Elements, v. 10, pp. 93-100.

Flint, D.E., de Albear, J.F., and Guild, P.W. 1948. Geology and chromite deposits of the Camagüey district, Camagüey province, Cuba: U.S. Geological Survey Bulletin, v. 954-B, pp. 39-63.

Fonseca, E, Zelepugin, V N, and Heredia, M. 1985. Structure of the ophiolite association of Cuba. Geotectonic, v. 1, pp. 321-329.

García-Casco, A., Iturralde-Vinent, M. A, Pindell, J. 2008. Latest Cretaceous collision/accretion between the Caribbean Plate and Caribeana: Origin of metamorphic terranes in the Greater Antilles. International Geology Review, v. 50, pp. 781- 809.

Garuti, G., Economou-Eliopoulos, M., Zaccarini, F. 1999a. Paragenesis and composition of laurite from the chromitites of Othrys (Greece): implications for Os-Ru fractionation in upper mantle of the Balkan peninsula. Mineralium Deposita, v. 34, p. 312-319.

Garuti, G., Zaccarini, F., Moloshag, V., Alimov, V. 1999b. Platinum-group minerals as indicator of sulfur fugacity in ophiolitic upper mantle: an example from chromitites of the Ray-Iz ultramafic complex, Polar Urals, Russia. The Canadian Mineralogist, v. 37, pp. 1099-1115.

González-Jiménez, J.M., Proenza, J.A., Gervilla, F., Melgarejo, J.C., Blanco-Moreno, J.A., Ruiz-Sánchez, R., Griffin, W.L. 2011. High-Cr and high-Al chromitites from the Sagua de Tánamo district, Mayarí-Cristal ophiolitic massif (eastern Cuba): Constraints on their origin from mineralogy and geochemistry of chromian spinel and platinum-group elements. Lithos, doi:10.1016/j. lithos. 2011.01.016.

González-Jiménez, J.M., Griffin W.L., Proenza, J.A., Gervilla, F., O'Reilly, S.Y., Pearson, N.J. 2014. Chromitites in ophiolites: how, where, when, why? Part II. The crystallization of chromitites. Lithos, v. 189, pp. 140–158.

Graham, I.T., Franklin, B.J., Marshall, B. 1996. Chemistry and mineralogy of podiform chromitite deposits, southern NSW, Australia: a guide to their origin and evolution. Mineralogy and Petrology, v. 37, pp. 129–150.

Henares, S., González-Jiménez, J.M., Gervilla, F., Proenza, J.A, Chang-Rodríguez, A, González-Pontón, R.B. 2010. Las cromititas del Complejo Ofiolítico de Camagüey, Cuba: un ejemplo de cromitas ricas en Al. Boletín de la Sociedad Geológica Mexicana, v. 1, pp. 173–185.

Irvine, T.N. 1967. Chromian spinel as a petrogenetic indicator. II. Petrologic applications. Canadian Journal of Earth Sciences, v. 4, pp. 71-103.

Iturralde-Vinent, M.A. 1996. Geología de las ofiolitas de Cuba. En: Iturralde-Vinent, M. (ed.), Ofiolitas y arcos volcánicos de Cuba, Miami, USA, IGCP Project 364, pp. 83-120.

Iturralde-Vinent, M.A. 1998. Sinopsis de la Constitución Geológica de Cuba. En: Melgarejo, J.C.and Proenza, J.A. (eds) Geología y Metalogénia de Cuba: Una Introducción. Acta Geologica Hispanica, v. 33, pp. 9–56.

Iturralde-Vinent, M.A., Díaz Otero, C., García-Casco, A., Van Hinsbergen, D.J.J. 2008. Paleogene Foredeep Basin Deposits of North-Central Cuba: A Record of Arc-Continent Collision between the Caribbean and North American Plates. International Geology Review, v. 50, pp. 863-884.

Kamenetsky, V.S., Crawford, A.J., Meffre, S. 2001. Factors controlling chemistry of magmatic spinel: an empirical study of associated olivine, Cr-spinel and melt inclusions from primitive rocks. Journal of Petrology, v. 42, pp. 655–671.

Kerr, A.C., Iturralde-Vinent M.A., Saunders, A.D., Babbs, T.L., Tarney, J. 1999. A new plate tectonic model of the Caribbean: Implications from a geochemical reconnaissance of Cuban Mesozoic volcanic rocks. Geological Society of America Bulletin, v. 111, pp. 1581-1599.

Lavandero, R. Strugo, M., Santa Cruz Pacheco M. Bravo, F., Melnikova, A.A., Cabrera, R. Trofimov, V.A., Romero, J., Altarriba, I. Álvarez, P., Aniatov, I. I., Badamgavin, B., Barishev, A.N., Carrillo, D. J., Casaña, X., Cuella, N., Dovnia, A.V., Formell, F., García, M., González, D. Gue, G.G., Janchivin, A., Krapiva, L.J., López, J., Lozanov, I., Montenegro, J., Pantaleón, G., Stefanov, N., Vazquez, O., Zagoskin, A.M., Zhidkov, A.Ya., 1988. Mapa de yacimientos de minerales metálicos y aguas minerales de la República de Cuba. Escala 1: 500 000, Instituto de Geología y Paleontología.

Lavandero, R., Morales, A., Padilla, I., Pantaleón, G., 1995. Perspectivas metalíferas de la región Habana-Matanzas, Centro Nacional de Información Geológica, Instituto de Geología y Paleontología, La Habana, Cuba, (unpublished).

Leblanc, M. 1995. Chromite and ultramafic rock compositional zoning through a paleotransform fault, Poum, New Caledonia. Economic Geology, v. 90, pp. 2028–2039.

Leblanc, M. and Violette, J.F. 1983. Distribution of aluminum-rich and chromium-rich chromite pods in ophiolite peridotites. Economic Geology, v. 78, pp. 293-301.

Leblanc, M. and Nicolas, A. 1992. Les chromitites ophiolitiques. Chronique de la Recherche Minière, v. 507, pp. 3-25.

Lewis, J.F., Draper, D., Proenza, J.A., Espaillat, J., Jiménez, J. 2006. Ophiolite-Related Ultramafic Rocks (Serpentinites) in the Caribbean Region: A Review of their Occurrence, Composition, Origin, Emplacement and Ni-Laterite Soil Formation. Geologica Acta Hispanica, v. 4, No. 1-2, pp. 237-263.

Llanes, A.I., Santa Cruz Pacheco, M., García, I., Morales, A., Palacio, B., Fonseca, E. 2001. Petrología y mineralización de la asociación ofiolítica de Habana-Matanza (Cuba occidental), Memorias Geomin 2001 (Published in CD, ISBN: 959-7117-10-X).

Llanes, A.I., Díaz de Villalvilla, L., Despaigne A.I., Ronneliah M., García-Jiménez, D. 2015. Geoquímica de las rocas volcánicas máficas de edad Cretácica de la región Habana-Matanzas (Cuba occidental): implicaciones paleotectónicas. Revista Ciencias de la Tierra y el Espacio, v. 16, No. 2, pp. 117-132, ISSN 1729-3790.

Malpas, J., Robinson, P.T. and Zhou, M.F. 1997. Chromitite and ultramafic rock compositional zoning through a paleotransform fault, Poum New Caledonia-a discussion. Economic Geology, v. 92, pp. 502-504.

Matthews, S.J. 1994. Buffering of melt oxygen fugacity by sulphur redox reactions in calc-alkaline magmas. Journal of the Geological Society, v. 151, pp. 815-823.

Melcher, F., Grum, W., Simon, G., Thalhammer, T.V., Stumpfl, F.E. 1997. Petrogenesis of the ophiolitic giant chromite deposits of Kimpirsai, Kazakhstan: a study of solid and fluid inclusions in chromite. Journal of Petrology, v. 38, pp. 1419-1438.

Morishita, T., Dilek, Y., Shallo, M., Tamura, A., and Arai, S. 2011. Insight into the uppermost mantle section of a maturing arc: The Eastern Mirdita ophiolite, Albania. Lithos, v. 124, pp. 215-226.

Murashko, V.I. and Lavandero, R.M. 1989. Chromite in the hyperbasite belt of Cuba. International Geology Review, v. 31, pp. 90-99.

Pearce, J.A., Lippard, S.J., and Roberts, S. 1984. Characteristics and tectonic significance of suprasubduction zone ophiolites, In: Kokelaar B.P. and Howells M.F. (eds.), Marginal Basin Geology. Geological Society of London, Special Publication, v. 16, pp.77-94.

Proenza, J., Gervilla, F., Melgarejo, J.C, and Bodinier, J.L. 1999. Al- and Cr-rich chromitites from the Mayarí–Baracoa Ophiolitic Belt, (Eastern Cuba): consequence of interaction between volatile-rich melts and peridotites in suprasubduction mantle. Economic Geology, v. 94, pp. 547-566.

Proenza, J.A., Gervilla, F. and Melgarejo, J.C. 2002. Los depósitos de cromita en complejos ofiolíticos: discusión de un modelo de formación a partir de las particularidades de las cromititas de Cuba Oriental. Boletín de la Sociedad Española de Mineralogía, v. 25, pp. 97-128.

Proenza, J.A, Melgarejo, J.C., Gervilla, F., Rodríguez-Vega, A., Díaz-Martínez, R., Ruíz-Sánchez, R., Lavaut, W. 2003. Coexistence of Cr- and Al-rich ophiolitic chromitites in a small area: the Sagua de Tánamo district, Eastern Cuba, In: Eliopoulos et al. (eds.), Mineral Exploration and Sustainable Development, Rotterdam Netherlands, Millpress, v.1, pp. 631-634.

Prouteau, G., and Scaillet, B. 2013. Experimental Constraints on Sulphur Behaviour in Subduction Zones: Implications for TTG and Adakite Production and the Global Sulphur Cycle since the Archean. Journal of Petrology, v. 54, pp. 183-213.

Pszczólkowski, A. 2002. The Margot Formation in Western Cuba, A volcanic and Sedimentary Sequence of Cenomanian–Turonianage. Bulletin of the Polish Academy of Sciences, Earth Sciences, v. 50, No.2, 13 p.

Roberts, S. 1988. Ophiolitic chromitite formation: a marginal basin phenomenon?. Economic Geology, v. 83, pp. 1034-1036.

Robinson, P.T., Zhou, M.F., Malpas, J., Bai, W.J. 1997, Podiform chromitites: Their composition, origin and environment of formation. Episodes, v. 20, No. 4, pp. 274-252.

Rollinson, H. 2008. The geochemistry of mantle chromitites from the northern part of the Oman ophiolite: inferred parental melt composition. Contributions to Mineralogy and Petrology, v. 156, pp. 273-288.

Stowe, C.W. 1994. Compositions and tectonic settings of chromite deposits through time. Economic Geology, v. 89, pp. 528-546

Thayer, T.P. 1942. Chrome resources of Cuba. U.S, Geological Survey Bulletin, v. 93-A, pp. 1-74.

Thayer, T.P. 1946, Preliminary chemical correlation of chromite with the containing rocks. Economic Geology, v. 41, pp. 202-217.

Thayer, P.T. 1964. Principal features and origin of podiform chromite deposits, and some observations on the Guleman-Soridag district, Turkey. Economic Geology, v. 59, pp. 1497-1524.

Uysal, I., Sadiklar, M.B., Tarkian, M., Karsli, O., and Aydin, F. 2005. Mineralogy and composition of the chromitites and their platinum-group minerals from Ortaca (Muðla-SW Turkey): evidence for ophiolitic chromitite genesis. Mineralogy and Petrology, v. 83, pp. 219-242.

Uysal, I., Zaccarini, F., Garuti, G., Meisel, T., Tarkian, M., Bernhardt, H.J., Sadiklar, M.B. 2007. Ophiolitic chromitites from the Kahramanmaras area, southeastern Turkey: their platinum group elements (PGE) geochemistry, mineralogy and Os-isotope signature. Ofioliti, v. 32, pp. 151-161.

Uysal, I., Ersoy, E.Y., Karsli, O., Dilek, Y., Sadiklar, M.B., Ottley, C.J., Tiepolo, M., Meisel, T., 2012. Coexistence of abyssal and ultra-depleted SSZ type mantle peridotites in a Neo-Tethyan Ophiolite in SW Turkey: constraints from mineral composition, whole-rock geochemistry (major–trace–REE–PGE), and Re–Os isotope systematics. Lithos, v. 132–133, pp. 50–69.

Yang, J.S., Robinson, P.T. and Dilek, Y. 2014. Diamonds in Ophiolites. Elements, v. 10, pp. 127-130.

Zaccarini, F., Garuti, G., Proenza, J.A., Campos, L., Thalhammer, O.A.R., Aiglsperger, T., Lewis, J.F. 2011. Chromite and platinum group elements mineralization in the Santa Elena Ultramafic Nappe (Costa Rica): geodynamic implications. Geologica Acta Hispanica, v. 9, No. 3-4, pp. 407-423.

Zhou, M.F. and Bai, W.J. 1992. Chromite deposits in China and their origin. Mineralium Deposita, v. 27, pp. 192-199.

Zhou, M.F. and Robinson, P.T. 1994. High-Cr and high-Al podiform chromitites, Western China: relationship to partial melting and melt/rock reaction in the upper mantle. International Geology Review, v. 36, pp. 678-686.

Zhou, M.F., Robinson, P.T. and Bai, W.J. 1994. Formation of podiform chromites by melt/rock interaction in the upper mantle. Mineralium Deposita, v. 29, pp. 98-101.

Zhou, M.F. and Robinson, P.T. 1997. Origin and tectonic environment of podiform chromite deposits. Economic Geology, v. 92, pp. 259-262.

by Jingsui Yang[1*], Paul T. Robinson[1] and Yildirim Dilek[2, 1]

Diamond-bearing ophiolites and their geological occurrence

[1] CARMA, State Key Laboratory of Continental Tectonics and Dynamics of China, Institute of Geology, Chinese Academy of Geological Sciences, Beijing, China. *Corresponding author E-mail: yangjsui@cags.ac.cn; yangjsui@163.com
[2] Department of Geology & Environmental Earth Science, Miami University, Oxford, OH 45056, USA

DOI: 10.18814/epiiugs/2015/v38i4/82430

We document in this study the geological occurrence of diamonds and other ultrahigh-pressure (UHP) minerals in ophiolitic mantle peridotites and podiform chromitites from different orogenic belts. These minerals exist in both high-Cr and high-Al chromitites. Most ophiolite-hosted diamonds are small (~ 200-500 µm across), and some contain distinctive inclusions (i.e., coesite, Ni-Mn-Co alloys, spessartite, tephroite). All of the analyzed diamonds have extremely light carbon isotope compositions ($\delta^{13}C$ = -28.7 to -18.3‰) and variable trace element contents that distinguish them from most kimberlitic and UHP metamorphic varieties. A wide range of highly reduced minerals, such as native elements, Ni-Mn-Co alloys, Fe-Si and Fe-C phases and moissanite (SiC) also occuras accompanying mineral separates confirming the super-reducing conditions of their environment of formation. The presence of exsolution lamellae of diopside and coesite in some chromite grains suggests chromite crystallization depths around >380 km, near the mantle transition zone. Carbon and other recycled crustal materials at these depths are likely to have been derived from previously subducted material. The peridotites encapsulating the podiform chromitites and diamonds were transported to shallow mantle by convection cells beneath oceanic spreading centers. The chromitites may have formed in the deep mantle or in shallow suprasubduction zone environments. Our observations suggest that diamonds, UHP minerals and recycled crustal material are likely to be ubiquitous in the oceanic mantle.

Introduction

In this paper we present a detailed account of the occurrence of diamonds, ultra high pressure (UHP) minerals and other recycled crustal material in the chromitites of four different ophiolites with different ages in different orogenic belts. The first-order significance of the findings of this study, as reported here is that: (1) diamonds, UHP minerals and recycled crustal material are likely to be much more widespread in the oceanic mantle than previously thought, and (2) ophiolitic peridotites and chromitites may have multi-stage development histories involving both deep and upper mantle melting events prior to their emplacement onto continental margins or into accretionary complexes. The latter inference is particularly important for the petrogenetic evolution of oceanic lithosphere (Dilek, 2015). In the first part of the paper we summarize chromitite types and their occurrence and characteristics as background information. We then document the internal structure of the four different ophiolites with a focus on their upper mantle peridotite units, and the petrography and geochemistry of chromitites and diamonds in them. In the last part of the paper, we evaluate the existing models for the formation of ophiolite-hosted diamonds, present our new model, and discuss its implications.

The new data, observations and interpretations on the occurrence of ophiolite-hosted diamonds and other unusual UHP minerals in ophiolitic chromitites, as reported here, should stimulate new discussions on the shallow mantle origin of oceanic peridotites (Dilek, 2015). The search for *in-situ* diamonds in peridotites and chromitites of ophiolites around the world with different ages and tectonic settings of formation during the next several years and their results will be highly critical for the course of these discussions.

Historical Background

Tantalizing reports of diamonds from alpine ultramafic rocks have circulated for many years. The first known report of such an occurrence is by Dresser (1913) who described a single grain of diamond from an ophiolite in Quebec, Canada. However, this mineral was only identified optically and is generally considered to have been periclase, formed during thermo-chemical decomposition of the rocks. Numerous other occurrences of diamonds associated with non-kimberlitic ultramafic rocks have been reported from sites around the world (Kaminsky, 2007), but unfortunately most of these diamonds are placer deposits whose sources are uncertain. On the other hand, many of these placer deposits contain platinum group minerals (PGM) that are typically associated with chromitites and deep mantle peridotites, suggesting their possible derivation from ophiolites.

The link between diamonds and ophiolites became clearer in 1981 with the separation of diamonds from podiform chromitites of the

Luobusa and Dongqiao ophiolites in Tibet (IGCAGS, 1981). Following the initial discovery during separation of PGM from the chromitites, diamonds were also recovered from alluvial sediments in streams draining the Dongqiao ophiolite. Details of the diamonds and their host rocks were published in Chinese by Yan et al. (1987) but attracted little further attention. Subsequent detailed studies of chromitites of the Luobusa ophiolite have produced a wide range of unexpected minerals including diamond, moissanite, PGM, metallic alloys, native elements and crustal-type minerals, particularly zircon (Bai et al., 2000: 2001; Yang et al., 2003; Robinson et al., 2004). Follow-up studies identified an intergrowth of coesite and kyanite, as well as a diamond inclusion within a PGM grain (Yang et al., 2007). Yamamoto et al. (2009) reported the occurrence of coesite and clinopyroxene exsolution lamellae within a chromite grain. However, these previous discoveries received skeptical comments because the scientific community considered it impossible to totally rule out natural or anthropogenic contamination of the samples.

The breakthrough in this research was achieved with the documentation of *in-situ* diamonds in the chromitites of both the Luobusa and Ray-Iz (Polar Urals, Russia) ophiolites, confirming that they were intrinsic components of their host rocks (Yang et al., 2014, 2015). In addition, both corundum and moissanite have been found as *in-situ* grains in the peridotites of the Luobusa ophiolite (Robinson et al., 2015). The in-situ grains were obtained by mounting small pieces of chromitite in epoxy, placing them in a Buehler Phoenix Beta Twin plate grinder/polisher and grinding the surfaces down in 100-µm increments (Yang et al., 2015). The grains were first identified with a scanning electron microscope (SEM) and then confirmed by Raman analysis. There is no possibility that the in-situ grains (100-200 µm in diameter) could have come from the diamond-coated disks, used for grinding because the disks were coated with angular diamond chips with a maximum diameter of 37 µm. All of the in-situ grains, both diamonds and other minerals, are enclosed in circular to irregular patches of amorphous carbon.

Having demonstrated the intrinsic character of the UHP and highly reduced minerals in the Luobusa and Ray-Iz ophiolites, which are characterized by high-Cr, metallurgical grade chromitites, our research then focused on the Sartohay and Hegenshan ophiolites in western and northern China, respectively, that have only high-Al, refractory ore. This most recent work has been undertaken to determine whether diamonds and the other unusual minerals are related to chromitite composition in ophiolites. We have found that diamonds and UHP minerals also exist in the refractory chromitites of these two ophiolites (Tian et al., 2015; Huang et al., 2015).

Nature of chromitites

Two basic types of chromitites have been recognized: stratiform and podiform (Thayer, 1960, 1964). Here we distinguish between chromite (individual grains) and chromitite (bodies and layers of aggregated chromite). Stratiform chromitites occur as relatively thin layers of massive chromite with a wide areal extent interlayered with mafic and ultramafic cumulates in large bodies such as the Stillwater, Muskox, and Bushveld intrusions (e.g., Irvine, 1977). Based on their textures and occurrence within layered sequences they are interpreted as cumulate layers precipitated from mafic magmas, although the processes by which such vast amounts of chromite are extracted from mafic magmas are still unclear. The large mafic intrusions hosting stratiform chromitites occur exclusively in stable cratonic areas (Fig. 1).

Podiform chromitites, in contrast, are relatively small, tabular to lenticular bodies of chromite hosted chiefly in the mantle sections of

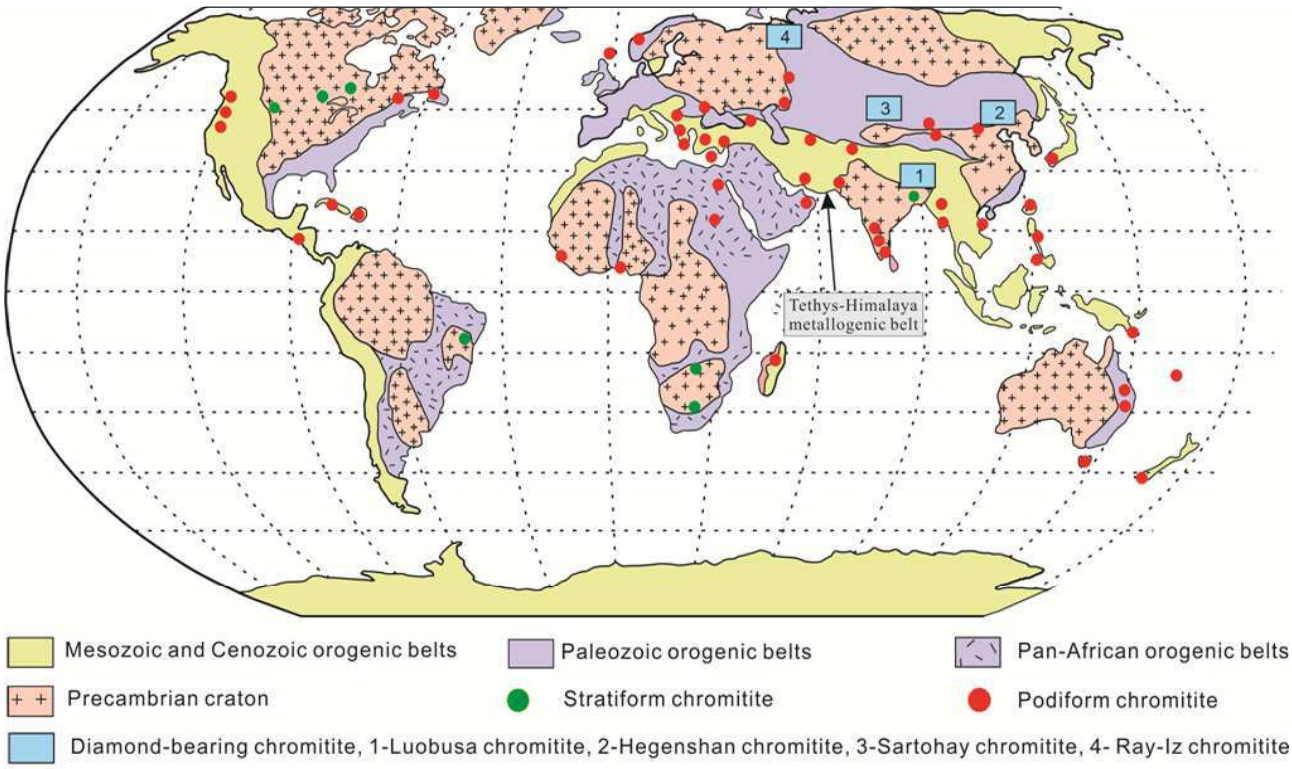

Figure 1. Generalized geological map of the world showing the major orogenic belts and the distribution of major stratiform and podiform chromitites.

ophiolites (Thayer, 1964, 1969; Dickey, 1975), although some small chromitites may also occur in the overlying cumulate sequences. Most podiform chromitites extend for less than 100 m along-strike and rarely exceed 50 min thickness. Unlike stratiform chromitites, these bodies display a wide range of textures ranging from layered, massive, and disseminated to nodular, antinodular and brecciated (Thayer, 1964). Podiform chromitites are commonly hosted in residual mantle peridotites, characterized by depleted harzburgites and minor fertile lherzolites, and are typically associated with small pods, veins and envelopes of dunite. Detailed studies of these dunites indicate that they are the products of melt–rock reaction during which pyroxene is dissolved and olivine is precipitated (Kelemen, 1990; Kelemen et al., 1992; Arai and Yurimoto, 1994; Zhou et al., 1996). The chromian content of the chromitites is generally thought to be related to the composition of the parental magma, with Cr-rich bodies having been derived from boninitic melts and more aluminous bodies from MORB-like or arc tholeiite magmas (Arai and Yurimoto, 1994; Zhou et al., 1996). However, it is clear that chromite compositions can also be modified by melt–rock reactions (e.g., Zhou et al., 1996; Castro et al., 2015). Because podiform chromitites occur only in ophiolites, they are typically found in Phanerozoic orogenic belts (Fig. 1). However, some Neoproterozoic podiform chromitites are known in the Eastern Egyptian Desert (Abd El-Rahman et al., 2012).

Chromite can crystallize as an early phase from mafic magmas as demonstrated in many layered intrusions and is also a common residual phase after partial melting of mantle peridotites during upwelling of the asthenosphere at oceanic spreading centers. Mantle sequences of many ophiolites contain podiform chromitites composed of magnesiochromite ± olivine ± other silicate phases. The orebodies vary in size from a few kilograms to a few million tons and are commonly distributed in a horizon not far below the petrological Moho. No significant podiform chromitites have been reported from *in-situ* oceanic mantle, although a few cm-size micropods of high-Al chromite have been described (Arai and Matsukage, 1998; Abe, 2011).

Both podiform chromitites and residual chromites in peridotites and dunites vary widely in major and trace element compositions. They are typically divided into high-Al, refractory varieties with Cr#s<60 [Cr#=100xCr/(Cr+Al) atomic ratio] and high-Cr, metallurgical ores with Cr#s>60). Podiform chromitites have been suggested to form mainly in suprasubduction zone (SSZ) environments, such as fore-arc and back arc basins (Arai and Yurimoto, 1995; Zhou and Robinson, 1997; Zhou et al., 2014; Rollinson and Adetunji, 2015). However, recent studies have identified many unusual minerals including UHP, highly reduced and recycled crustal minerals in such chromitites (Bai et al., 1993; Yang et al., 2003, 2007; Robinson et al., 2004; Xu, 2009, 2015; Yamamoto et al., 2013; Robinson et al., 1015).These findings raise important questions about the validity of a simple SSZ origin interpretation of podiform chromitites. It is, therefore, timely to highlight some advances in the understanding of chromitites and their host ophiolites, and to integrate all the extant data and observations into a coherent model.

Diamond-bearing ophiolites

Ophiolite studies in the Neotethyan Yarlung-Zangbo suture zone in southern Tibet and in the early Paleozoic Polar Ural orogenic belt in Russia have confirmed the presence of microdiamonds in both ophiolitic peridotites and podiform chromitites (Xu et al., 2009, 2015; Yang et al., 2014, 2015). Diamonds were also discovered recently in chromitites from the Paleozoic Sartohay ophiolite in Xinjiang and the Paleozoic Hegenshan ophiolite in Inner Mongolia, China (Tian et al., 2015; Huang et al., 2015). The salient geological characteristic features, geochemical affinities and tectonic settings of formation of these four ophiolites are summarized in Table 1.

Luobusa Ophiolite, Yarlung-Zangbo Suture Zone, Tibet

Field occurrence

The Luobusa ophiolite occurs in a fault-bounded slab, approximately 41-km long and 1-4-km wide (Fig. 2), in the eastern part of the Yarlung-Zangbo suture zone (YZSZ). It is thrust northward onto Tertiary molasse deposits of the Luobusa Formation and the Gangdese batholith (Aitchison et al., 2003), and is underlain by a mélange unit. The Luobusa ophiolite has been of great interest because it hosts the largest chromite deposit in China, containing nearly 5 million tons of high-Cr, metallurgical ore (Zhang et al., 1996). It is

Table 1. Characteristics and geological settings of diamond-bearing ophiolites covered in this study

Ophiolite Name	**Luobusa**	**Ray-Iz**	**Sartohay**	**Hegenshan**
Location	South Tibet, China	Polar Ural, Russia	Xinjiang Province, NW China	Inner Mongolia, Northern China
Geologial setting	Neo-tethys Yarlun Zangbu Suture	Early Paleozoic Ural Orogenic Belt	Late Paleozoic Central Asian Orogenic Belt	Late Paleozoic Central Asian Orogenic Belt
Crystallization ages of ophiolitic units	gabbro Sm-Nd 170±31 Ma (Zhou et al., 2002); gabbro U-Pb 148 Ma (Chan et al., 2007)	gabbro U-Pb 418±2 Ma (Schmelev and Meng, 2015); chromite, Re-Os 470±15 Ma (Ronkin et al., 2000)	gabbro Sm-Nd 395±1 Ma (Zhang et al., 1992)	ultramafics Sm-Nd 403±27 Ma (Bao et al., 1994)
Geochemical affinity and related tectonic setting	MOR + SSZ	SSZ	BAB	MOR + Fore Arc
Ore type of diamond-bearing chromite deposit	high Cr ore, Cr# 76-83	high Cr ore, Cr# 77-80	high Al ore, Cr# 50-53	high Al ore, Cr# 48
Wall rock of ore deposit	harzbugite and thin dunite envelopes	harzbugite and thin dunite envelopes	thin dunite envelopes	thin dunite envelopes

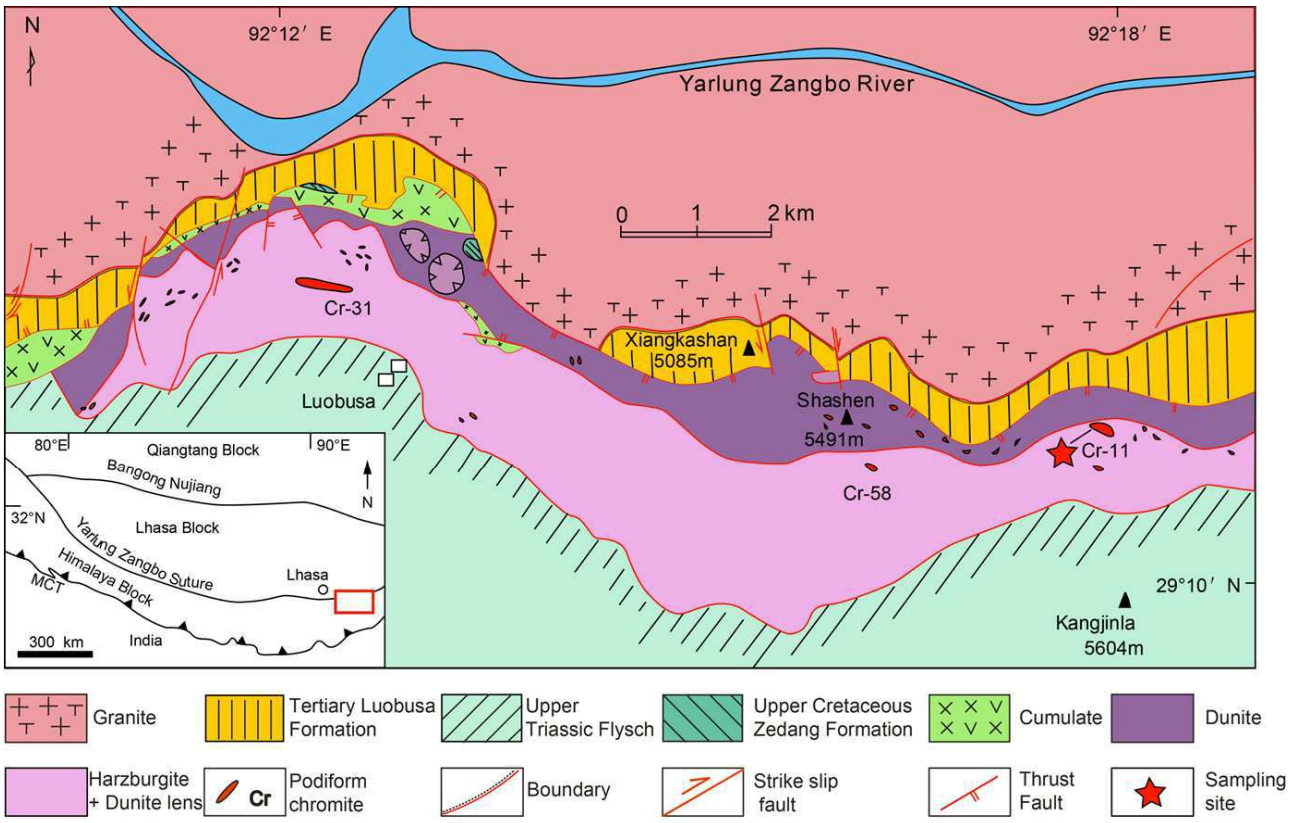

Figure 2. Geological map of the Luobusa ophiolite, Tibet, showing the distribution of the major lithologies and locations of the major chromitite orebodies (modified after Xu et al., 2009).

also the first ophiolite massif in which diamonds, highly reduced phases, and recycled crustal minerals have been documented as intrinsic parts of ophiolitic chromitites and peridotites.

The mélange beneath the ophiolite is composed of blocks of pillow lavas and cumulate rocks, including wehrlite, pyroxenite and layered and vari-textured gabbro in a serpentinite matrix (Zhou et al., 1995; Yang and Dilek, 2015). An up to 300-m-thick, transitional dunite unit overlies the mélange (Zhou et al., 2005), and is in turn overlain by clinopyroxene-bearing harzburgites that contain numerous dunite dikes, some of which are associated with stringers or bands of chromite. These cpx-bearing harzburgites are transitional upward into depleted harzburgite, containing numerous lenses, layers and pods of chromitite, most of which have well-developed dunite envelopes (Zhou et al., 1996, 2014). Zircon separates from a gabbroic dike crosscutting the serpentinized peridotite have yielded a $^{206}Pb/^{238}U$ age of 148±4.5 Ma as the minimum igneous age of the Luobusa ophiolite (Chan et al., 2007).

The majority of the upper mantle peridotites in the Luobusa ophiolite consist of harzburgite and clinopyroxene-bearing harzburgite (>75 vol%), dunite (~20 vol%), and chromitite (~3 vol%) (Fig. 2). Most of the harzburgites and clinopyroxene-bearing harzburgites are coarse-grained, massive rocks with a weakly developed foliation, and commonly show little alteration except near the podiform chromitites. The dunites are medium- to coarse-grained rocks that are moderately to strongly deformed. Podiform chromitites are mostly hosted in the harzburgites and clinopyroxene-bearing harzburgites, although some small bodies also occur in the dunites. The chromite ore bodies are grouped into three clusters, designated from west to east as the Luobusa, Xiangkashan and Kangjinla districts (Fig. 2). Most of these ore bodies are lenticular pods or bands up to 100 m long, 30-50 m wide and 1-10 m thick, and are surrounded by dunite envelopes that grade into the host harzburgite (Zhou et al., 1995).

Petrography and mineralogy

Both the harzburgite and clinopyroxene-bearing harzburgite have porphyritic textures with large (1-3 cm) subhedral grains of orthopyroxene surrounded by smaller grains of olivine and sparse magnesiochromite. The harzburgite consists mainly of forsteritic olivine (75-90 modal%), Mg-rich orthopyroxene (7-25%), and accessory minerals such as magnetite and residual magnesiochromite (1-2%). The clinopyroxene-bearing varieties are similar but also contain 2-4 modal% of small (0 5-1 mm), anhedral clinopyroxene grains. Olivine ranges in composition from about Fo 89 to 91 (Fo-forsterite component Fo [= 100xMg/(Mg+Fe) atomic ratio]) in the clinopyroxene-bearing harzburgite. Both the olivine and ortho-pyroxene crystals show deformation textures, such as deformation lamellae, slip planes, kink-bands and irregular deformation bands. Many orthopyroxene grains also have exsolution lamellae of clinopyroxene along their slip planes. In some samples, olivine and orthopyroxene have been granulated and recrystallized along micro shear zones and grain boundaries (Zhou, 1995).

Dunites associated with the ore deposits occur as envelopes and as patches and zones interspersed with the chromitite ore. Some small lenses of dunite also occur locally in the peridotites. These dunite occurrences are different from the thick, transition-zone dunite at the base of the ophiolite, and contain abundant magnesiochromite nodules (Robinson et al., 2004; 2015). Most of the dunites have

granular textures, locallyshowing plastic deformation and recrystallization features. Typical dunite samples consist of ~95 modal% olivine, ~1-2% orthopyroxene, ~2-3 % magnesiochromite, and traces of clinopyroxene.

Most of the rock-forming minerals in the peridotites, chromitites and dunites show textural evidence for at least two stages of formation; an early stage of relatively large, commonly deformed crystals, and a second stage of smaller, undeformed but recrystallized grains. Mineral compositions vary systematically from clinopyroxene-bearing harzburgite to harzburgite to dunite to chromitite, reflecting increased degrees of partial melting and/or melt-rock reaction. Olivine compositions range, for example, from Fo_{90} in the harzburgites to Fo_{90-94} in the dunites and Fo_{94-97} in the chromitites (Xu et al., 2012). The highly magnesian olivine in the chromitites is generally attributed to subsolidus Mg-Fe^{2+}reequilibration between magnesiochromite and olivine (e.g., Xu et al., 2012). Similarly, orthopyroxene compositions increase systematically from En_{89} (En [=100xMg/(Ca+Mg+Fe) atomic ratio] (in the clinopyroxene-bearing harzburgites) to En_{94} in the chromitites (Fig. 3a). The Cr_2O_3 contents in the orthopyroxene are highly variable but can reach up to nearly 1 wt.% (Fig. 3b). All of the clinopyroxenes are diopside with En values increasing from a low of 47 in the clinopyroxene-bearing harzburgites to a high of 51 in the chromitites, as CaO, Al_2O_3 and FeO decrease systematically (Fig 3c). The Cr_2O_3 contents of the clinopyroxene range up to nearly 1.5 wt.% (Fig. 3d).

Magnesiochromites in the mantle peridotites have Cr#s ranging from 30 to 77 and Mg#s ranging from 39 to 70. They mostly plot in the abyssal and island-arc fields in the Cr# vs. Mg# diagram (Fig. 4a) (Dick and Bullen, 1984), and their variable compositions probably reflect different degrees of partial melting and melt-rock reaction, rather than formation in different tectonic environments (Xu et al., 2012). In contrast, magnesiochromite in the podiform chromitites is remarkably uniform in composition. Grains from 20 different chromitites have 55-63 wt.% Cr_2O_3, 9-12 wt. % Al_2O_3 and 12-16 wt.% MgO. All of the magesiochromite grains within the chromitites have very high Cr#s (76-83) and moderately high Mg#s (56-74) (Fig. 4a) (Xu et al., 2012). The TiO_2 contents of the magnesiochromites are generally very low (<0.1 wt%) but increase slightly as the Cr# increases. We use the term magnesiochromite to describe individual grains and chromitite to designate orebodies formed by accumulations of magnesiochromite grains.

The transition-zone dunites consist chiefly of olivine with minor chromite and sparse, interstitial orthopyroxene and diopside (Zhou et al., 2005). Olivine grains are coarse- to very coarse (up to a few cm), and most are elongated, defining a crude foliation in the rock. Most of the dunites are cut by narrow shear zones filled with olivine neoblasts that are 0.05-0.1 mm across, some of which have well-developed granoblastic textures with 120° grain boundary intersections. The majority of the dunites are fresh, with only minor serpentine and talc along narrow veinlets, but more extensive alteration is locally present leading to partial or complete replacement of the primary grains by serpentine and minor talc.

Such transition-zone dunites have been interpreted in previous studies as cumulate magmatic deposits, but neither the textures nor compositions of these rocks in Luobusa are consistent with such a model. Instead, they are now considered to have formed by intense melt-rock reaction that has been carefully documented in the Luobusa peridotites (Zhou et al., 2005).

Whole-rock compositions

The Luobusa peridotites, dunites and massive chromitites have relatively uniform whole-rock compositions, whereas the disseminated and nodular chromitites vary widely depending on the relative proportions of olivine and magnesiochromite. All of the peridotites are compositionally similar with about 45 wt.% SiO_2, 42-45 wt.% MgO, 9 wt.% FeO*, 1-2 wt.% Al_2O_3 and CaO, and < 1 wt.% Cr_2O_3. The clinopyroxene-bearing varieties have slightly higher CaO and Al_2O_3 than the others. Dunites differ mainly in having slightly higher MgO (48-52 wt.%) and slightly lower SiO_2 (42-43 wt.%.). Both Al_2O_3 and CaO are < 1 wt.%, but they are consistently present because of the small amounts of diopside in these rocks. Massive chromitites have essentially the same compositions as the individual magnesiochromite grains, whereas the disseminated and nodular varieties have higher SiO_2 and MgO contents due to the increased abundance of olivine.

Although all the peridotites and dunites have very low ΣREE

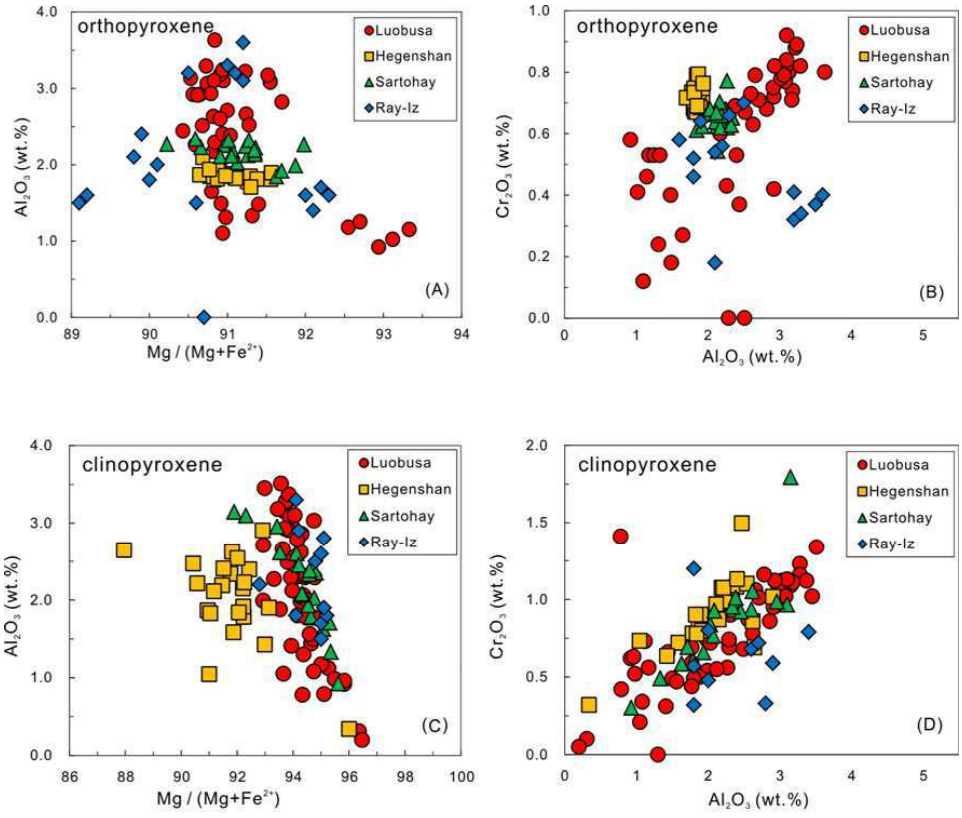

Figure 3. Plots of pyroxene compositions in the Luobusa, Ray-Iz, Sartohay and Hegenshan ophiolites (data source: this study).

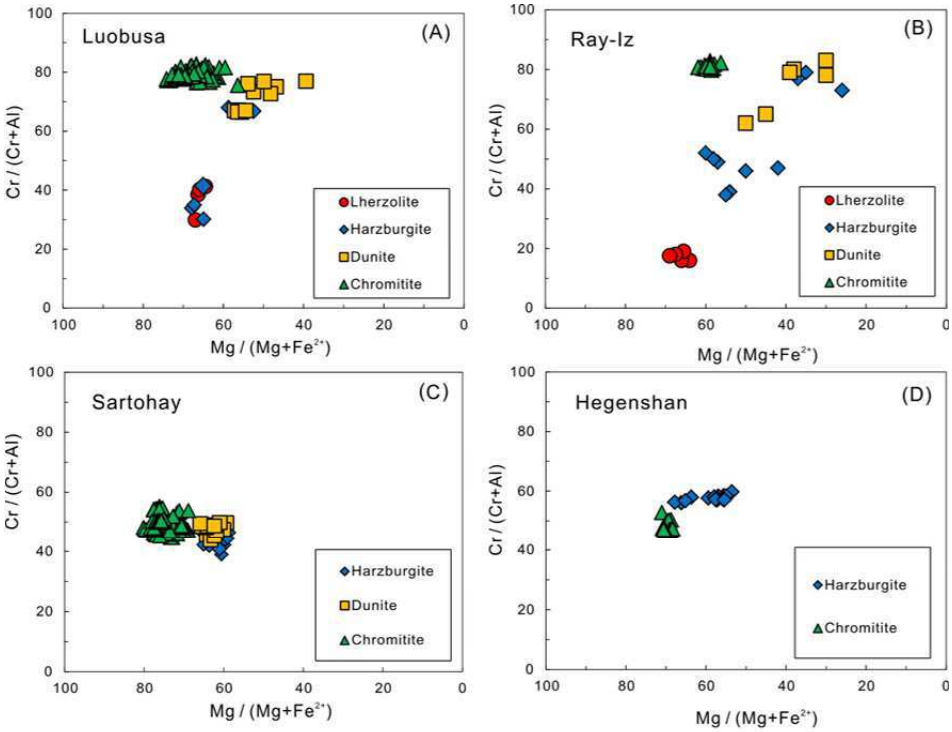

Figure 4. Plots of chromite compositions in the Luobusa, Ray-Iz, Sartohay and Hegenshan ophiolites (data source: this study).

contents, the different rock types have different chondrite-normalized REE patterns. The clinopyroxene-bearing harzburgites have 'spoon-shaped' patterns with notable enrichment in HREE (up to 0.7 times chondrite) and positive or negative anomalies in Sm and Gd (Fig. 5a). In contrast, the harzburgites have mostly 'V-shaped' patterns with both depletion and enrichment in Eu. Dunite pods and envelopes are characterized by well-developed 'U-shaped' patterns. All of these patterns likely reflect late-stage, LREE enrichment of depleted peridotites and dunites (Zhou et al., 1995). In primitive mantle-normalized, trace element 'spider' diagrams the clinopyroxene-bearing harzburgites also show irregular 'U-shaped' patterns with a steady decrease from Lu to Zr, followed by a rise in large ion lithophile elements such as Rb and Ba. Both Pb and Ta show strong positive anomalies (Fig. 6a).

Platinum group element (PGE) values are significantly low, generally between 0.01 and 0.001 times chondrite values. Chondrite-normalized patterns are relatively flat for the peridotites but show enrichment in Pd and depletion in Os, whereas the dunites show a small negative Pt anomaly. The chromitites display strong depletion in Rh, Pt and Pd and enrichment in Os, Ir and Ru (Zhou et al., 2005, 2014).

Ray-Iz Ophiolite, Uralide Orogenic Belt, Russia

We selected the early Paleozoic Ray-Iz ophiolite of the Polar Urals for comparison with the Luobusa ophiolite because: (1) it has a much older crystallization age, and (2) it occurs in a different orogenic belt far from Tibet (Fig. 7a). Both ophiolites contain abundant podiform chromitites that consist of high-Cr metallurgical varieties with Cr#s>60. We sampled the podiform chromitites and their host peridotites in the Ray-Iz massif in order to document similarities and differences between the two ophiolites and to test for the presence of UHP, highly reduced and crustal minerals.

Regional geology

The Paleozoic Uralide orogenic belt in Russia extends more than 2500 km in a roughly N-S direction, and separates Europe from Asia (Chemenda et al., 1997). It formed in the mid-Paleozoic as a result of an initial arc-continent (Magnitogosrk arc–East European Block) collision, followed by a continent-continent collision (East European block–Siberian continent) (Savelieva and Nesbitt, 1996; Brown et al., 1998). The Ray-Iz ophiolite occurs at the northeast end of this orogenic belt, lying in the Polar Urals within the Arctic Circle (Fig. 7a). In this region the orogen is about 50–100 km wide and consists of a series of west-directed thrust stacks in which volcanic arc sequences rest tectonically on continental margin sequences of the European plate.

The Paleozoic Voikar–Syninsk ophiolite belt within this part of the Polar Urals includes the Syum–Keu, Ray-Iz and Voykar–Syn'ya massifs, composed mainly of ultramafic rocks and gabbros. The ophiolites are part of a major thrust sheet sandwiched between lower–middle Paleozoic, rift–bathyal complexes on the west and Paleozoic, arc volcanic–sedimentary complexes on the east (Puchkov, 1990; Matte, 1995; Savelieva and Nesbitt, 1996; Savelieva et al., 1999). These ophiolites are accompanied by high-pressure metamorphic rocks, such as eclogite, blueschist, amphibolite and albite–lawsonite facies rocks, whose protoliths were volcanic–sedimentary country rocks and ophiolitic gabbros and dolerites (Savelieva, 1987; Dobretsov, 1991). Many of the ultramafic rocks, gabbros and mafic lavas have been metamorphosed under greenschist facies conditions and strongly deformed by late Vendian folding.

The Ray-Iz massif is an irregular body, about 20-30 km across, with an outcrop area of ~380 km^2, and is part of a south-dipping thrust sheet (Fig. 7b). Geophysical data show that the ophiolitic thrust sheet is about 1-1.5 km thick in the north and 4-7 km thick in the south (Moldavantsev and Kazak, 1977; Makeyev et al., 1985; Makeyev and Braynchaninova, 1999). A 300-m to 500-m-thick mélange zone, containing blueschist and jadeitite, crops out along the northeast margin of the massif (Kazak et al., 1976; Moldavantsev and Kazak, 1977; Makeyev et al., 1985; Perevozchikov et al., 1990a). Precambrian metamorphic rocks of the crystalline basement also crop out on both the northeast and northwest sides of the ophiolite (Makeyev et al., 1985; Puchkov, 1990). To the south, a mafic-ultramafic sheet composed of dunite, websterite, pyroxenite, metagabbro and amphibolite is thrust over the massif (GDC in Fig. 7b) (Kazak et al., 1976; Makeyev et al., 1985).

The ultramafic massif in Ray-Iz is intruded by rare jadeite-albite-bearing and ruby-bearing, metasomatic dikes. Ruby-bearing veins near the base of the massif have a Rb–Sr isochron age of 358 ± 3 Ma (Glodny et al., 2002), whereas the metasomatic veins have a Rb–Sr isochron age of 373 ± 5.4 Ma. These veins are thought to have formed by suprasubduction zone metasomatism in an oceanic setting, prior

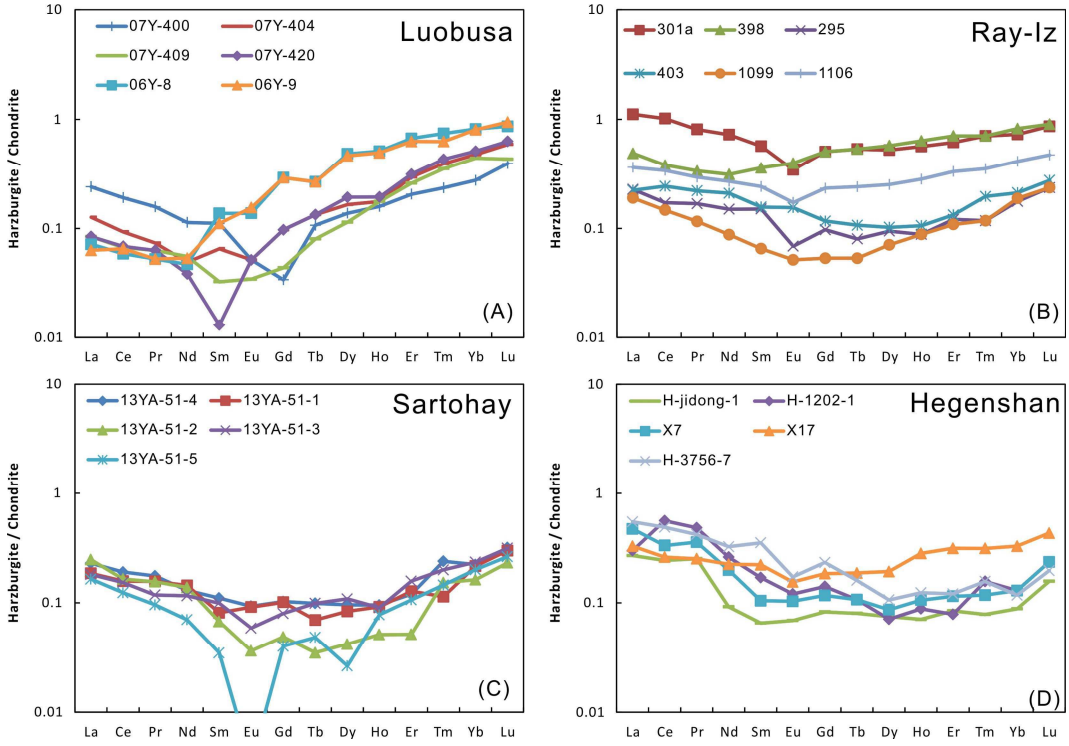

Figure 5. Chondrite-normalized REE plots of peridotites in the Luobusa, Ray-Iz, Sartohay and Hegenshan ophiolites (data source: this study).

to the subduction of the East European margin and formation of associated eclogites in the Marun–Keu complex (Glodny et al., 2003).Shmelev and Meng (2013) reported a zircon U-Pb age of 418 ± 2 Ma from a gabbro-diorite body in the Ray-Iz massif, thought to represent late Silurian island arc magmatic activity.

It has been generally postulated that the ophiolites in the Ural orogenic belt were produced during opening of the Ural paleo-ocean in the early Paleozoic. However, recently obtained isotopic data suggest that they may have formed over a relatively broad age range, from the late Proterozoic and Cambrian (Gurskaya and Smelova, 2003; Savelieva et al., 2006; Vakhrusheva, 2007) to the Devonian (Sharma et al., 1995).

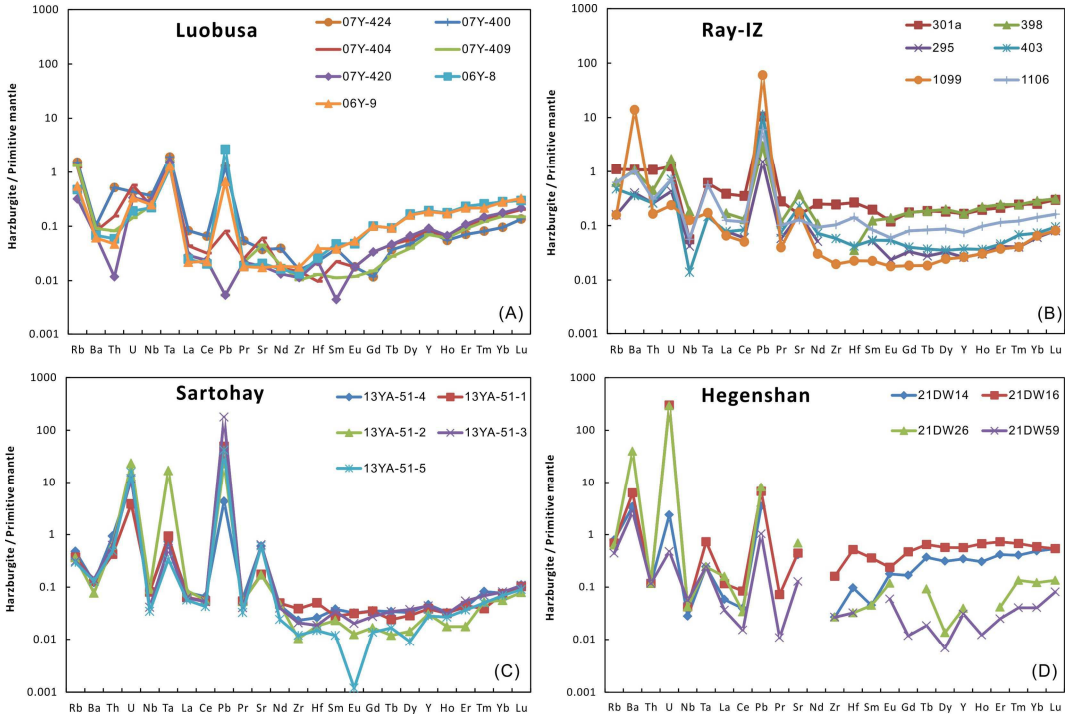

Figure 6. Primitive mantle-normalized trace element plots of peridotites in the Luobusa, Ray-Iz, Sartohay and Hegenshan ophiolites (data source: this study).

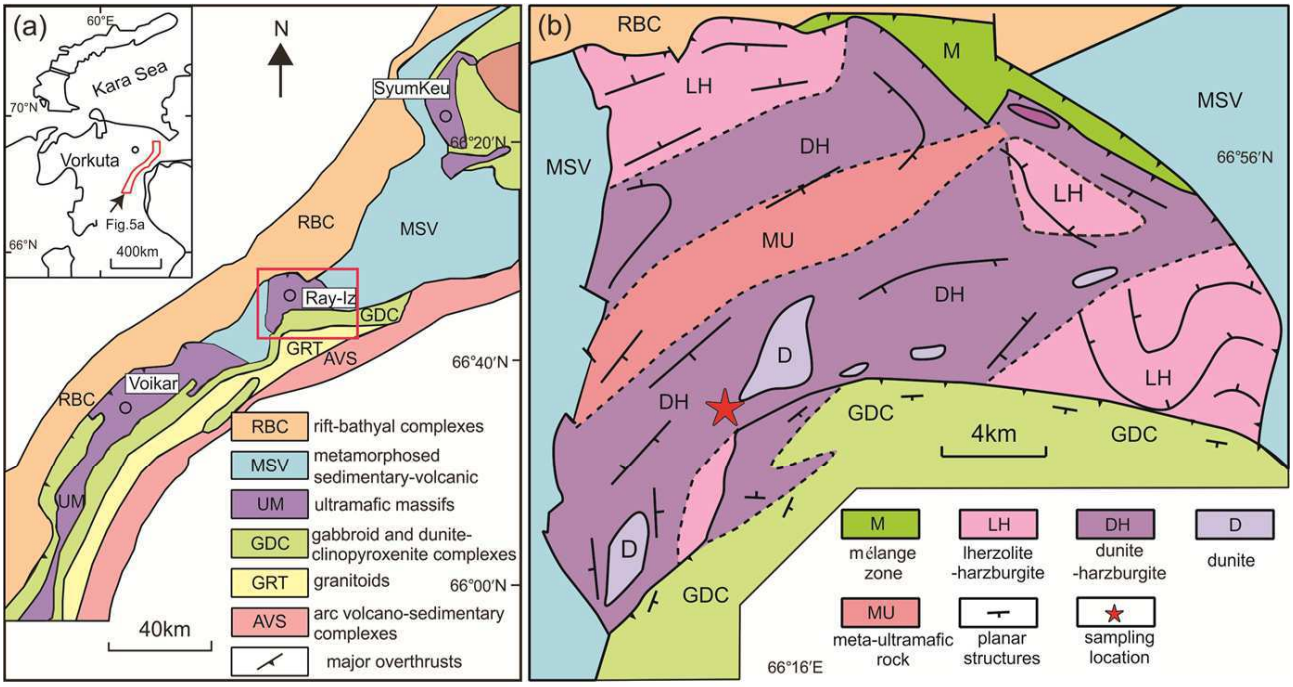

Figure 7. Geological maps of (a) the Voikar–Syninsk ophiolite belt in the Polar Urals, Russia and (b) the Ray-Iz ophiolite (Modified after Shmelev, 2011).

Field occurrence of the Ray-Iz ophiolite

The Ray-Iz ophiolite consists largely of ultramafic rocks and chromitites with minor amphibolites with a gabbroic protolith (Fig. 7b). The ultramafic complex includes a broad range of lithologies, including lherzolite, clinopyroxene-bearing harzburgite, harzburgite and dunite, locally accompanied by veins or bodies of pyroxenite and chromite segregations (Shmelev, 2011). Generally, these rocks grade into one another with changes in the proportions of olivine, pyroxene and magnesiochromite. Although the rocks are generally fresh, the massif has a complex metamorphic and deformation history, having produced various mixtures of amphibole, antigorite, clinochlore, talc and magnetite (Perevozchikov et al.,1990a, 2005; Shmelev et al., 1990; Makeyev and Braynchaninova, 1999).

The ultramafic rocks are mainly harzburgite with lesser amounts of lherzolite and about 10 vol.% dunite (Zavaritsky, 1932; Moldavantsev and Kazak, 1977; Makeyev et al., 1985). The harzburgites are concentrated in the central part of the massif, whereas the more lherzolitic rocks occur mostly on the northern and southern margins. A zone of meta-cumulates, about 1-3 km wide, crops out near the center of the massif where it appears to be in magmatic contact with the underlying harzburgite. This unit consists chiefly of layered dunite, websterite, and pyroxenite, as well as metagabbro and amphibolite.

The dunites occur as relatively thin veins and layers and as larger, irregular masses in both the lherzolites and harzburgites. As in the Luobusa ophiolite, dunites are commonly associated with the podiform chromitites. Podiform chromitites are widely distributed in the Ray-Iz massif with total estimated reserves of about 163 million tons. The largest deposits, which occur in the southern and southwestern parts of the ophiolite, include both massive and disseminated ores, many of which are associated with dunite (Makeyev, 1992; Perevozchikov et al., 2005). Some of the chromitites are enclosed within dunite envelopes, whereas others are in direct contact with the harzburgite.

The Central Chromite Deposit (CCD) is the largest of the more than 200 orebodies in the massif. It consists of several parallel bodies with both massive and disseminated ores, which extend to a depth of ~500 m. More than 40 million tons of chromite have been mined from this deposit. The chromite ore contains a variety of PGE minerals (Makeyev, 1992; Garutis et al., 1999; Walker et al., 2002; Pasava et al., 2011).

The W214 ore body is approximately 100-m-long and 5-m-wide, and extends to over 100 m depth, with a reserve of about 10 million tons of ore. The orebody is partly surrounded by a thin dunite envelope or is locally in direct contact with coarse-grained, weakly serpentinized harzburgite. In this study, chromitite samples were collected from both the CCD and W214 orebodies.

Petrography and mineralogy

Lherzolites and harzburgites make up about ~85% of the exposed ultramafic complex in Ray-Iz. The lherzolites consist of olivine (~70 modal %), orthopyroxene (15–20%), clinopyroxene (5-10 %), magnesiochromite (1–5%) and minor amounts of amphibole (calcium hornblende). They typically have porphyroclastic textures with relatively large, platy or subequant orthopyroxene grains, which commonly define a crude foliation. However, highly deformed rocks generally have been recrystallized, acquiring mosaic textures (Shmelev, 1990). Small, irregular grains of both olivine and orthopyroxene also occur as recrystallization products along grain boundaries.

With decreasing amounts of clinopyroxene, the lherzolites grade into clinopyroxene-bearing harzburgites and then into harzburgites, which are similarly characterized by protogranular to porphyroclastic textures exhibiting a weak mineral foliation. Fresh samples consist of olivine (60–70 modal%), orthopyroxene (15–25%), clinopyroxene (0-3–10%) and magnesiochromite (1–3%), commonly with coexisting minor amphibole. Olivine occurs as aggregates of large (up to 5 mm),

anhedral grains, some of which display deformation lamellae. The olivine matrix includes tabular and subequant grains of orthopyroxene and small (1–2 mm) grains of clinopyroxene and colorless pargasite. Magnesiochromite grains are evenly distributed in the rocks, mostly as very small, euhedral to anhedral grains.

Dunites occur as relatively thin veins, layers and larger bodies of variable morphology in the lherzolites and harzburgites, and have highly uniform textures and mineralogies. They consist mainly of olivine (95-100 modal %) and magnesiochromite (1-5%), but some contain very small, anhedral grains of orthopyroxene and/or clinopyroxene. These rocks typically have coarse-grained (1-5 mm) protogranular or granoblastic textures, which grade into mosaic-porphyroclastic textures in ductile shear zones. Magnesiochromite grains in the dunite are typically small and subhedral to euhedral in shape.

Both high-Al and high-Cr ores are present; the former are hosted in lherzolite and the latter in harzburgite (Shmelev et al., 2014). High-Al ores most commonly occur as schlieren or small, lenticular bodies. Massive, disseminated, nodular, banded and uneven granular textures are common. The chromitites contain more than 50 mineral species in addition to olivine and magnesiochromite, including metallic and PGE alloys, native elements and sulfides, diamonds, moissanite and crustal-type minerals (Yang et al., 2015; Robinson et al., 2015).

All of the ultramafic rocks are composed of the same major minerals (olivine, orthopyroxene, clinopyroxene, and magnesio-chromite), although the percentage and composition of the different minerals vary widely. Olivine is the most abundant and widespread mineral, and varies from extremely magnesian varieties (Fo_{95-98}) in the chromitites to relatively Fe-rich varieties (Fo_{89-92}) in the lherzolites (Shmelev, 2011; Yang et al., 2015). Olivine compositions in the harzburgites, diopside-bearing harzburgites, and dunites range between these extremes. All of the olivines are very low in CaO (<0.05 wt %), MnO and NiO (0.2-0.5 wt %), regardless of the Mg# (Yang et al., 2015).

Similar to olivine, the orthopyroxene in the mantle rocks varies in composition, although it is generally classified as enstatite. In the lherzolite-harzburgite succession, the Al_2O_3 concentration of the enstatite decreases from 2.0-3.5 wt.% in the lherzolite to 1.5-2.0 wt.% in the harzburgite with little change in the Mg# (Fig. 3a). Ortho-pyroxenes in the diopside-bearing harzburgites have compositions between these end members. The enstatite is typically low in CaO and Cr_2O_3 (0.3-0.9 wt.%) (Fig.3b).

Clinopyroxene in the lherzolites and diopside-bearing harzburgites is represented by Mg-rich diopside (Mg# =93-95) with low Al_2O_3 (1-3 wt.%) and Cr_2O_3 (0.4-1.1 wt.%) values (Fig. 3c,d). Only very small grains of clinopyroxene have been found in any of the other ultramafic rocks.

Magnesiochromite varies widely in abundance from ~1 modal% as an accessory mineral in the peridotites to nearly 100 modal% in massive chromitites. Magnesiochromite in Ray-Iz varies almost as much in composition as it does in abundance. In the lherzolites, residual grains of magnesiochromite can be highly aluminous (Al_2O_3 =48-53 wt.%), yielding Cr#s of 17-19 (Fig. 4b). These values increase to about 30-45 in the diopside-bearing harzburgites and harzburgites, as evidence of depletion. Chromitite and dunite bodies hosted in the harzburgites can have very high Cr contents (Cr_2O_3 = 54-57 wt.%, yielding Cr#s of 77-78. Cr#s as high as 84 have been reported from magnesiochromites in some of the Ray-Iz dunites (Schmelev and Meng, 2013).

The sparse amphibole in the lherzolites and diopside-bearing harzburgites is a magnesian pargasitic hornblende (Mg# = 93-99), rich in Al_2O_3 (up to 11 wt.%), Cr_2O_3, and Na_2O (1-1.5 wt.%). Amphibole in all other ultramafic rocks types is tremolite.

Two main types of chromitite are present: massive and disseminated. The massive varieties are coarse grained, fresh and red in color (with high Cr#) under the microscope, whereas some disseminated chromitites are dark (with high iron contents) under plane-polarized light. The massive varieties have very high Cr#s (80-95) and a narrow range of Mg#s (~58-63) (Fig. 4b). In contrast, magnesiochromite grains in the lherzolites, disseminated chromitites and some of the dunites have low Cr#s (~ 25-60) and high Mg#s (~60-75). The disseminated chromitites are characterized by high contents of Al_2O_3 (21-28 wt.%), intermediate Cr#s (47-50) and high Mg#s (66-71).

Whole-rock compositions

The ultramafic rocks in Ray-Iz show wide variations in their major and trace element whole-rock compositions, most of which reflect different degrees of depletion. For example, the average Mg# of lherzolite (40) increases as the rocks grade into diopside-bearing harzburgite to harzburgite to dunite, which has an average Mg# of 49. These changes are accompanied by decreases in Al_2O_3 (2.3 to 0.56 wt.%) and CaO (1.6 to 0.01 wt.%), reflecting the loss of pyroxene and increasing abundance of olivine (Shmelev, 1990). In contrast, Ni increases irregularly from 1100 ppm in the lherzolite to about 2100 ppm in both the harzburgite and dunite.

Given these trends, the ΣREE would be expected to follow a similar pattern. However, the ΣREE is 0.88–1.05 ppm in the lherzolites, 1.21–1.97 ppm in the diopside-bearing harzburgites, 0.30–1.25 ppm in the harzburgites, and 0.82–3.15 in the dunites. Chondrite-normalized REE patterns are also variable. For example, the clinopyroxene-bearing rocks have weakly developed 'spoon-shaped', chondrite-normalized REE patterns, with a gradual decrease from Lu to Nd, followed by a moderate increase in the LREE. In contrast, the harzburgites show more typical 'U-shaped' patterns, some of which are characterized by negative Eu anomalies giving them a 'V-shaped' appearance (Fig. 5b). The dunites have patterns similar to those of the harzburgites but with stronger REE enrichment, giving them a clear U-shaped appearance; two samples have La nearly 3 times chondrite values. The dunites also display pronounced negative Eu anomalies (Shmelev, 2011).

In primitive mantle-normalized trace element diagrams, the ultramafic rocks of the Ray-Iz ophiolite generally have slightly sloping patterns from Lu to Sm (without Eu anomalies) and then a general increase in Ta, U, Ba and Rb (Fig. 6b). All of the samples display a strong positive Pb anomaly and a strong negative Nb anomaly (Shmelev, 2011). The lherzolites and diopside-bearing harzburgites commonly have low negative Ti anomalies, which are absent in the harzburgites and dunites.

Sartohay Ophiolite, Central Asian Orogenic Belt, China

The middle Paleozoic Sartohay ophiolite is part of the Darbute ophiolite belt, which extends NE-SW for about 100 km along the western edge of the Junggar basin in Xinjiang province, China (Fig. 8). The Junggar basin is located in the southwestern part of the Central

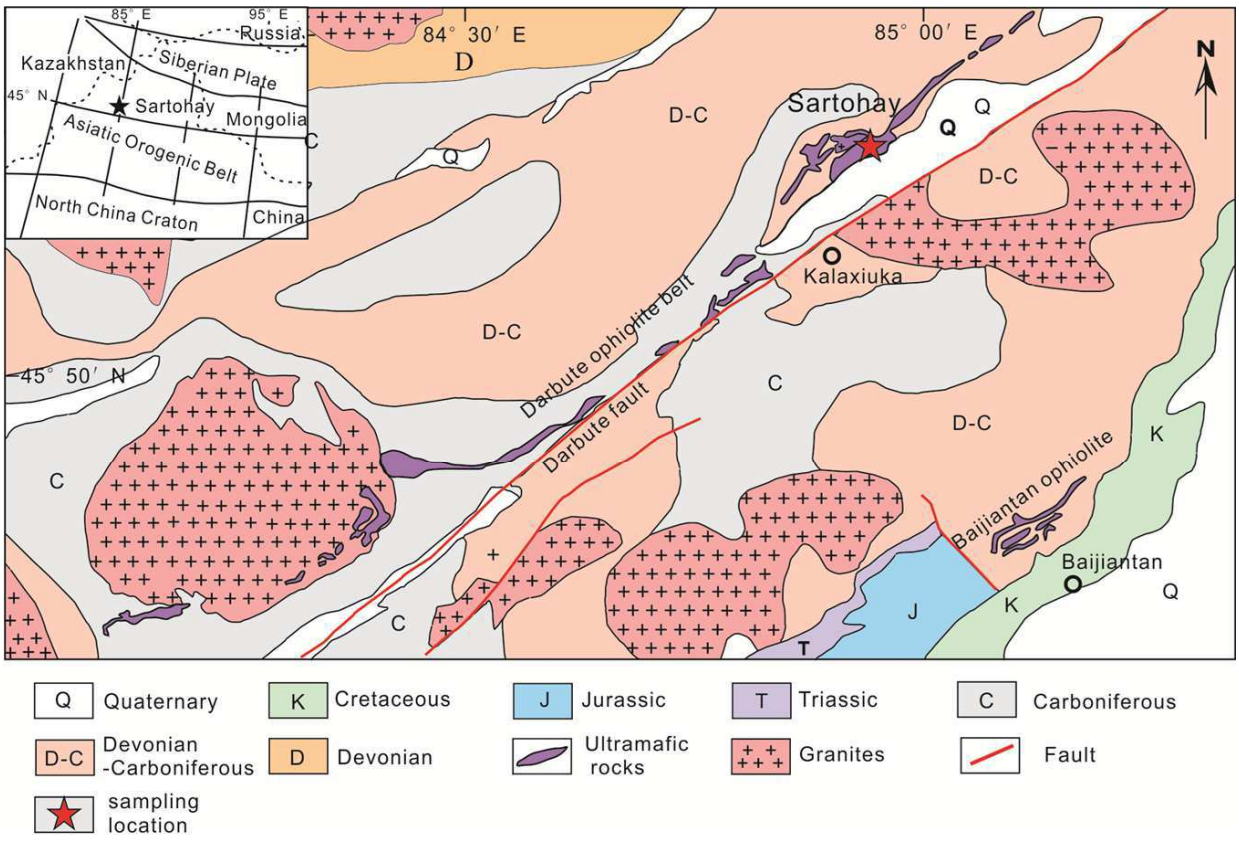

Figure 8. Geological map of the western part of the Junggar basin, Xinjiang province, China, showing the distribution of the Sartohay ophiolite along the Darbute fault (modified from Tian et al., 2015).

Asian Orogenic Belt (CAOB), which is a 2000-km-long and ~800-km-wide accretionary orogen separating the Siberian Block in the north from the North China Craton in the south. The CAOB consists of multiple suture zones, ophiolites and continental fragments (Kröner et al., 2007; Windley et al., 2007).

Regional geology

Discrete ophiolite belts in the west Junggar region include the middle Ordovician Tangbale, middle-upper Silurian Mayile, middle Ordovician Hongguleleng, middle-upper Devonian Darbute, and early Palaeozoic Baijiantan belts. Ophiolites of the Darbute belt crop out as a series of tectonic slices along the NE-SW oriented and steeply NW-dipping Darbute fault, including the Sartohay in the north and the Suluqiaoke in the south. Early-middle Devonian radiolarian and coral fossils have been reported from cherts and limestone lenses intercalated with the extrusive rocks of the Sartohay ophiolite (Wei et al., 1987; Zhang et al., 1993). This biostratigraphic Devonian age has been confirmed by zircon $^{206}Pb/^{238}U$ ages (302.5±1.7 Ma) of a gabbro from the Suluqiaoke area (Wei et al., 1987; Zhang et al., 1993) and of a leucogabbro in the Akebasitao body (Liu et al., 2009). Granitic plutons that intrude the ophiolite mélange and the country rock have been dated at ~305 Ma (Geng et al., 2009).

The Sartohay ophiolite extends for ~20 km along the Darbute fault **(**Fig. 8**)** and consists mainly of mantle peridotites, with lesser amounts of gabbro, basalt and chert. It is intruded by numerous pyroxenite, gabbro and dolerite dikes and veins. Small granitic plutons also intrude both the ophiolite and the country rocks.

The mantle peridotites consist mainly of harzburgite along with sparse dunite and lherzolite. Typically, lherzolite is restricted to the margins of the peridotite body, and dunite mainly occurs as narrow envelopes around the ubiquitous podiform chromitites. Unlike the other chromitite occurrences described in this paper, these ore bodies in Sartohay are crosscut by troctolite dikes. Most of the chromitites are lenticular or tabular in form, but they also occur as veins, fracture fillings and linear or planar segregations. The chromitite bodies vary widely in size but generally are in the range of 10-50 m long and 0.5-5 m wide. Most are concordant or semi-concordant with the foliation in the host harzburgite. Contacts with the harzburgite are typically sharp.

Peridotites are generally extensively serpentinized, and many have been hydrothermally altered to listwanite (silica-carbonate rock), particularly in the southern part of the block, along their tectonic contact with sedimentary rocks (Wei et al., 1987; Robinson et al., 2005). These metasomatic rocks consist mainly of talc, magnesite, chlorite, quartz, calcite and dolomite along with some Cr-bearing green-colored muscovite (Zhou et al., 2001; Robinson et al., 2005).

Petrography and mineralogy

The harzburgite in Sartohay is composed of 80-90 modal% olivine, 10-15%, orthopyroxene, 1-3% clinopyroxene and ~1% magnesiochromite. Most of the olivine occurs as subhedral grains, 0.5-4 mm in diameter, but a few, much smaller crystals (<0.2 mm) form inclusions in orthopyroxene. Orthopyroxene crystals are commonly short and columnar, typically less than 3 mm long, but a few larger crystals are locally present; these larger grains contain small

inclusions of both olivine and clinopyroxene. Clinopyroxene occurs as small (<0.2 mm) anhedral grains along the boundaries between the other minerals, and as exsolution lamellae in orthopyroxene crystals. Residual magnesiochromite occurs mainly as small (>1 mm), vermicular grains, commonly associated with orthopyroxene.

Small 'islands' of fresh olivine in the harzburgite have uniform compositions with an average of Fo_{91-92} (Zhou et al., 2001). Orthopyroxene grains are also relatively uniform in composition with an average of $En_{88}Fa_{3.6}Wo_{2.8}$. However, CaO contents vary from 0.35 to 5.1, corresponding to Wo values of 0.66 to 9.9, respectively. Both Al_2O_3 and Cr_2O_3 contents are relatively uniform at about 1.5-2.5 and 0.4-0.6 wt.%, respectively (Fig. 3a,b). The clinopyroxene is diopside with an average composition of $En_{48.5}Fa_{3.0}Wo_{48.5}$. All but a few grains have Al_2O_3contents of less than 2 wt.%, whereas Cr_2O_3 are mostly between 0.3 and 1 wt.% (Fig. 3c,d), with one value up to 1.5 wt.%. Residual magnesiochromite grains in the peridotites vary slightly in composition from harzburgite (Cr#=53-59) to dunite (Cr# =50-54) to lherzolite (Cr# = 41-42) (Zhou et al., 2001).

Nearly 90% of the chromitites have massive, medium-grained (1-4 mm) textures, but some very large grains or clots up to 3 cm across are also present (Zhou et al., 2001). Disseminated ores are the second most common type, and these have crystals < 1 mm in diameter. Associated with the disseminated ores are some nodular, occluded and brecciated varieties. Many of the podiform bodies have narrow rims or halos of bluish-gray chlorite that separate the ores from the surrounding dunite. Fractures in the magnesiochromites are commonly filled with a variety of secondary minerals, including uvarovite, Cr-grossular, fuchsite and magnetite. Many magnesiochromite grains also have magnetite rims due to alteration. Gangue minerals in the chromitites include olivine, orthopyroxene and diopside. Sulfide minerals are also common. Magnesiochromite grains in these bodies are uniform in composition with 41-42 wt.% Cr_2O_3, 15-17 wt.% MgO, 25-28 wt.% Al_2O_3, 12-13 wt.% FeO, and 3-4 wt.% Fe_2O_3 yielding Cr#s of 50-53 and Mg#s of 68-70 (Fig. 4c). Thus, they are all classified as refractory chromitites, characterized by low TiO_2(0.2-0.7 wt.%) and NiO (0.10-0.18 wt.%) (Zhou et al., 2001).

Troctolite and gabbro dikes commonly crosscut the podiform chromitites throughout the ophiolite. These dikes are generally oriented parallel to the tectonic fabric elements (i.e. foliation). The troctolite grades into olivine gabbro with increasing plagioclase, and into dunite with increasing olivine. The olivine-rich varieties are heavily serpentinized. The gabbros are grayish-green, medium- to coarse-grained rocks composed mainly of plagioclase and clinopyroxene with a few percent of magnetite and sparse apatite. One gabbro sample yielded a zircon $^{206}Pb/^{238}U$ age of 368 ± 11 Ma (Yang et al., 2012).

Whole-rock compositions

All of the mantle peridotites and dunites in the Sartohay ophiolite are highly serpentinized and have loss on ignition (LOI) values ranging from 9-16 wt.%. These rocks form a distinct group ranging from about 38-51 wt.% MgO and about 38-44 wt.% SiO_2 (normalized to 100% volatile free). Both CaO and Al_2O_3values increase with decreasing MgO contents, reaching maximum values of about 4 wt.% in the lherzolites (Zhou et al., 2001), whereas FeO and Cr_2O_3 contents decrease slightly. Relatively high CaO and Al_2O_3 contents in some of the dunites are due to the presence of minor plagioclase, clinopyroxene and magnesiochromite. Trace elements have very low concentrations in the ultramafic rocks and show little variation with MgO contents (Zhou et al., 2001). Primitive mantle-normalized plots of Ni, Cu and PGE in harzburgite are relatively flat, except for a small depletion in Cu, whereas the dunites have patterns weakly depleted in Rh, Pt and Pd (Zhou et al., 2001). These patterns, particularly for the harzburgites, are similar to those of MORB mantle peridotites (Edwards, 1990).

Chondrite-normalized REE patterns for the ultramafic rocks show two distinct trends (Zhou et al., 2001). Lherzolites have patterns showing ΣREE concentrations about 1 times chondrite but with distinct LREE depletion, typical of abyssal peridotites. On the other hand, both the harzburgites and dunites are significantly more depleted, but have well-developed 'U-shaped' patterns (Fig. 5c) indicating refertilization by late-stage melt impregnation. This is confirmed by the presence of small grains of plagioclase and clinopyroxene along grain boundaries in these rocks. Both the harzburgites and dunites have weak to strong, negative Eu anomalies. In primitive mantle-normalized spider diagrams, these rocks have generally sloping patterns from Lu to Tb, then flat to Zr; the remainder of the patterns are highly variable but all show strong positive anomalies in Sr, Pb, Ta and Th and negative anomalies in Nb (Fig. 6c).

Bulk-rock compositions of the podiform chromitites show wide variations depending on the abundance and character of gangue minerals. For example, massive chromitites have low SiO_2 (2-4 wt.%), but high Al_2O_3 (25-28 wt.%) and Cr_2O_3 (42-44 wt.%) with lesser amounts of FeO (7-8 wt.%) and MgO (15-16 wt.%). Mantle-normalized PGE patterns for the chromitites are strongly depleted in Pt and Pd, and their total PGE contents are much lower than those of high-Cr chromitites (Zhou et al., 2001).

Hegenshan Complex, Central Asian Orogenic Belt, Inner Mongolia

The Hegenshan complex in Inner Mongolia (Fig. 9) is another chromitite-bearing ophiolite in the CAOB. Similar to the Sartohay ophiolite, the magnesiochromites in this complex are all high-Al varieties with Cr#s<60. We thus selected this ophiolite for additional study to test whether UHP, highly reduced and crustal minerals can occur in both high-Cr and high-Al chromitites.

Regional geology

The Hegenshan ophiolite crops out in the Eren Hot-Hegenshan belt in the northern part of Inner Mongolia (Fig. 9), about 250 km north of the boundary between the CAOB and the North China Craton. It consists of four major mafic-ultramafic massifs: Chongenshan–Xiaobaliang (ca. 200 km^2), Wusnihei (ca. 80 km^2), Hegenshan (ca. 60 km^2) and Chaogenshan (ca. 100 km^2), along with about 30 much smaller blocks. Although its surface area of the Hegenshan block is only 60 km^2, regional magnetic anomalies indicate a much larger mafic-ultramafic slab at the sub-surface, beneath the sedimentary cover. Two smaller ultramafic bodies east of Hegenshan, Hebei and Baiyinshan, are likely continuations of the Hegenshan massif (Wang and Liu, 1986). All of the massifs have a core of serpentinized peridotite, but only the Chaogenshan massif contains significant amounts of gabbro and dolerite (Robinson et al., 1999; Jian et al., 2012). Previous efforts to date the peridotites and dunites were inconclusive, but Ar-Ar and zircon U/Pb dating of gabbros and dikes

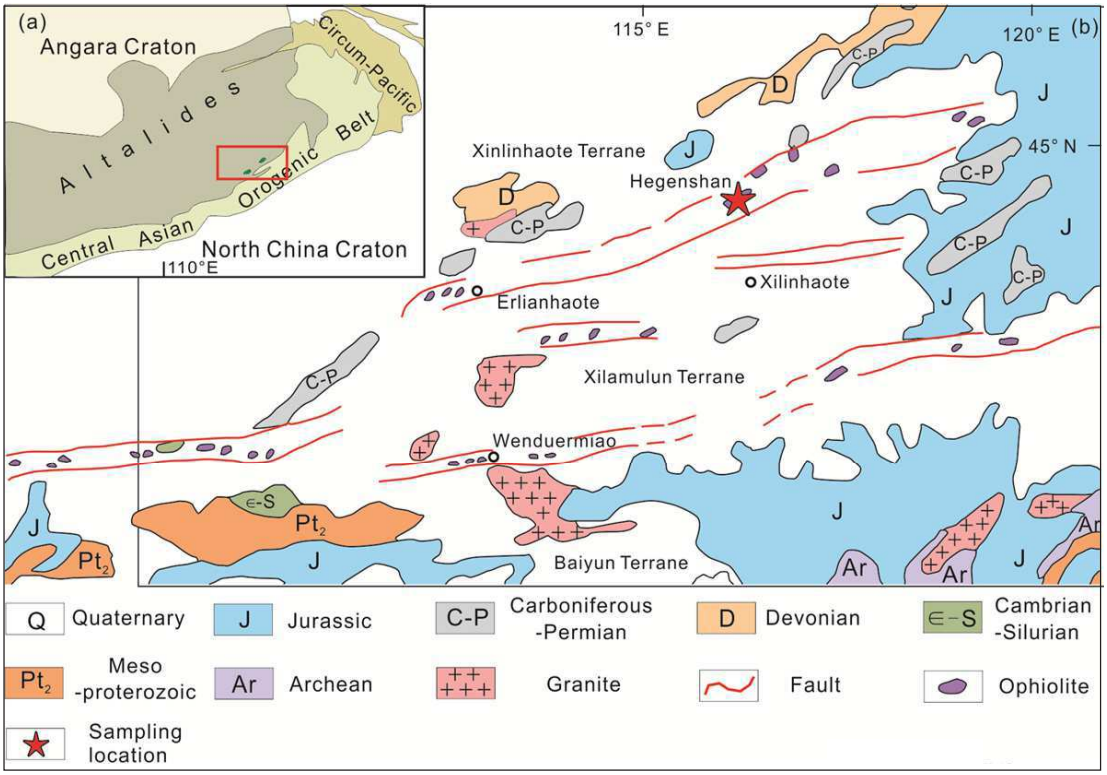

Figure 9 Geological map of part of Inner Mongolia, China, showing the major lithological units and locations of four suture zones, including the Eren Hot-Hegenshan zone in which the Hegenshan ophiolite complex is located (modified after Huang et al., 2015).

has proved more reliable. Robinson et al. (1999) obtained Ar-Ar dates of 242 Ma and 148 Ma on amphiboles from two dioritic dikes crosscutting serpentinized peridotites of the Chaogenshan massif, and Miao et al. (2008) obtained a zircon $^{206}Pb/^{238}U$ age of 289 Ma from a mafic dike in the same massif and an $^{40}Ar/^{39}Ar$ date of 293 Ma for a massive basaltic lava in the Hegenshan massif.

Field occurrence

Serpentinized harzburgite makes up the bulk of the Hegenshan massif (Fig. 9). It has a well-developed, NE-striking foliation defined by elongated orthopyroxene and magnesiochromite grains. Widespread dunite pods and lenses are associated with chromitite ores. Dunite pods, up to 400 m long and 50 m wide, generally grade into the enclosing harzburgite with increasing amounts of orthopyroxene, although locally there is a sharp contact between the dunite and harzburgite. Dunite pods are most abundant in the central part of the massif and are nearly absent along its western, northern and eastern margins. Typically, the dunite bodies are elongated parallel to the harzburgite foliation. Irregular and discontinuous pyroxenite dikes (~10 cm wide or less) crosscut both the mantle peridotites and the layered ultramafic rocks. These dikes consist entirely of light green or light brown clinopyroxene crystals, which are commonly perpendicular to the dike walls.

Significant magnesiochromite mineralization is found only in the Hegenshan massif, where chromitite occurs as podiform bodies in the harzburgite or as thin layers or bands in the cumulate sequence. Total reserves are currently estimated to be about 5 million tons of ore. Podiform bodies are typically lenticular or vein-like and are roughly concordant with the foliation in the harzburgite. The average foliation orientation is N55°E with dips ranging from 20° to 70°SE.

Petrography and mineralogy

Most of the mafic and ultramafic rocks in the Hegenshan massif have been altered extensively; dunites and peridotites are heavily serpentinized and gabbroic rocks are altered to sericite and amphibole. However, alteration is highly variable and fresh minerals are locally preserved in all lithologies.

The peridotites are chiefly harzburgite with minor lherzolite and dunite. The harzburgite consists of 60-90% olivine and 5-35% orthopyroxene with minor clinopyroxene and magnesiochromite. Trace amounts of plagioclase are present in a few samples. Clinopyroxene rarely exceeds 5% and disseminated magnesiochromite is typically less than 1%. Porphyroclastic textures are common with large (0.3-5 mm), subhedral crystals of orthopyroxene (or bastite pseudomorphs) in a matrix of smaller (0.2-3 mm), anhedral olivine grains or serpentine. Some orthopyroxene grains have exsolution lamellae of clinopyroxene and minor magnesiochromite; others have narrow reaction rims of clinopyroxene that may reflect late-stage refertilization. Olivine crystals are anhedral, typically 0.2 - 3 mm across, and have an average composition of about Fo_{91} (Huang et al. 2015). The orthopyroxenes are relatively uniform in Al_2O_3 and $Cr_2O_3$and have an average composition of $En_{89}Fs_8Wo_3$ (Fig. 3a,b). The sparse clinopyroxene forms small (0.05-1 mm), anhedral crystals along the margins of orthopyroxene grains. It has an average composition of about En_{50} but varies more widely in Al_2O_3 and Cr_2O_3 (Fig. 3c,d). Disseminated magnesiochromite forms small (0.05-1 mm), anhedral crystals, which typically occur between the silicate grains. Magnesiochromite is also commonly intergrown with orthopyroxene to form graphic, vermicular or symplectic textures. Residual magnesiochromite in the harzburgites has an average Cr# number of about 45 (Fig. 4).

Dunite is more abundant in the Hegenshan massif than in any of the other massifs, and it occurs as pods, lenses and dikes associated with chromitite in the harzburgite. Dunitic rocks contain 1-2% magnesiochromite, 0-3% orthopyroxene and traces of clinopyroxene in addition to olivine. Average olivine compositions are in the range of Fo_{91-92}. The magnesiochromite forms subhedral to euhedral crystals, commonly less than 1 mm across, and occurs as inclusions in the olivine grains or as minute crystals between them. Locally, magnesiochromite forms thin bands or layers. All of the magnesiochromites are relatively Al-rich with an average Cr# of 48.

The chromitite ores range in texture from massive or densely disseminated to thinly disseminated and nodular. Generally, the massive to densely disseminated ore occurs in the centers of the ore bodies, whereas the thinly disseminated and nodular types occur along the margins. The gangue minerals are olivine, serpentine and chlorite, rarely accompanied by minor clinopyroxene. Typically, the orebodies have rims or crusts of chlorite, ranging from 2 to 50 cm thick that separate them from the enclosing dunite. Most of the chromitites consist of relatively high-Al magnesiochromite with Cr#s of 47-53 (Fig. 4d). The associated olivine is highly magnesian due to Mg-Fe^{2+} re-equilibration with the host magnesiochromite, ranging in average composition from approximately Fo_{93} to Fo_{95}.

Whole-rock compositions

On the basis of major oxide data, we recognize three distinct geochemical and lithological groups within the ultramafic rock units of the Hegenshan massif: (1) a highly magnesian group composed mainly of dunite with MgO contents ranging from about 48 to 51 wt.%; (2) a peridotite group made of serpentinized harzburgite/lherzolite with MgO contents ranging from ~40 to 48 wt.%; and, (3) a group of ultramafic cumulates composed of troctolite and minor pyroxenite with MgO contents ranging from 18 to 40 wt.%.

The dunites represent depleted rocks with low Al_2O_3 and CaO contents, reflecting the absence of feldspar and the presence of very little clinopyroxene. In contrast, the peridotites of the second group show variations in composition, with small increases in Al_2O_3 with decreasing MgO, reflecting a transition from harzburgite to clinopyroxene-bearing harzburgite to minor lherzolite. In general, the peridotites in the Hegenshan and Chaogenshan massifs are more depleted than those in the other massifs. All of the dunites and peridotites have very high LOI (~14 wt.%), indicating extensive serpentinization of olivine and orthopyroxene.

Both chondrite-normalized REE and primitive mantle-normalized spider diagrams of the ultramafic units display irregular patterns due to the low concentrations of these elements in such depleted rocks. Some of the rocks are moderately depleted in LREE relative to HREE, although most show irregular ''U-shaped'' patterns with slight enrichment in LREE relative to MREE (Fig. 5d; Miao et al., 2008). Collectively, these features suggest refertilization by metasomatic melts/fluids (e.g. Mahe´o et al., 2004). The low concentrations of fertile elements and ΣREE are reminiscent of moderately depleted residual peridotites after variable degrees of melt extraction (Parkinson et al., 1992). Primitive mantle-normalized spider diagrams for the Hegenshan peridotites are similar to those for the Sartohay ophiolite, particularly in having strong positive anomalies in Pb, Ta, U and Ba and negative anomalies in Pr, Ce, Nb and Th (Fig. 6d).

The sparse cumulate troctolites and pyroxenites in the Hegenshan ophiolite aregenetically related, as evidenced by their systematic compositional trends with increases in Al_2O_3, FeO, CaO and TiO_2, with decreasing MgO. The troctolites, which are rich in olivine, have 24-38 wt.% MgO, whereas the pyroxenites have ~16-28 wt.% MgO. These variations are consistent with fractional crystallization of a highly mafic magma. However, the pyroxenites commonly occur as narrow dikelets that post-date the cumulate rocks.

Unusual minerals recovered from the Ophiolites

The four ophiolites discussed above have revealed a surprisingly similar collection of unusual minerals, regardless of their age, geographic location or chromitite composition (Table 2). All four ophiolites are characterized by having relatively abundant diamonds and moissanite and a variety of native elements, such as Si, Al, W, Cr, and Ti. These minerals, particularly the moissanite and the native elements, indicate crystallization in a highly reduced environment. Both Luobusa and Ray-Iz also contain a number of carbides and platinum group minerals (PGM). Metallic alloys with a vast range of composition are some of the most common materials separated from the chromitites, the most abundant varieties are FeNi, FeCr, FeSi, NiFe and CrNiFe; all of the alloys show wide variations in element proportions.

Surprisingly, the abundant reduced minerals and alloys are accompanied by a wide range of oxides, in particular Al, Si, Fe, Mg, and Ti, as well as magnesiochromite (Table 2). Because magnesiochromite is an oxide itself, it is difficult to understand how so many highly reduced minerals and alloys could have been incorporated into the chromitites without being decomposed. Finally, sulfides are also common in the chromitites; many of these sulfide minerals occur along cracks and between magnesiochromite grains, and are hence secondary. However, other sulfides, particularly the PGE variety, are hosted within magnesiochromite grains, and they are hence considered to be primary. The consistent occurrence of these unusual minerals in chromitites and peridotites of four different ophiolites clearly indicate that they are not the result of some random process, but that they rather reflect fundamental petrogenetic processes involved in ophiolite and chromitite formation.

Characteristics of ophiolite-hosted diamonds and associated minerals

Most of the diamonds are relatively uniform(ca. 0.2-0.5 mm), euhedral to subhedral, colorless or yellowish crystals (Figs. 10a; 11a; 12a;13a) with a variety of growth forms, (e.g., octahedral, cubo-octahedral and dodecahedral (Figs. 11b; 12b; 13b;14a). The diamond grains typically have sharp edges, but some are rounded with eroded or etched surfaces, indicating post-crystallization processes. *In-situ* grains can be irregular (Fig. 10b) to euhedral (Fig. 11b). All of the *in-situ* grains are hosted in small patches of amorphous carbon. Surprisingly, many diamonds, particularly those from the Ray-Iz ophiolite, are partly coated with thin metal films, mostly 0.1-1.0 μm thick (not shown). EDS analysis identified these films as consisting of Zr, ZrO, NaCl, SiO_2, Ta and FeCr. Because many zircons in the Ray-Iz massif show evidence of resorption and modification, we think that the films were produced by hydrothermal fluids. However,

Table 2. Unusual minerals recovered from chromitites of the four ophiolites covered in this study

Ophiolites	Luobusa, Tibet	Ray-Iz, Polar Urals	Sartohay, Xinjiang	Hegenshan, Inner Mongolia
Native elements	Si, Fe, Zn, Pb, Al, Cr, Sn, Ni, Os, Ir, Ru, Rh,Pd, Au, Ag, W, Cu, S, Co, Ti, Diamond, Graphite	Diamond, Cr, Ni, W, Cu, Si, Fe, Zn, Zr, Al, Ta, Pb, Co	Diamond, Fe, Si, Cr	Diamond, Mn, Ca, Graphite
Carbides	NiC, FeC, TiC, WC, (W,Co)C, SiC, CrC, NiC_4FeCrC	SiC, WC, WCoC	SiC (moissanite)	SiC (moissanite)
Nitrides	Ti_2N, Ti_2N_3, BN	0	0	0
Oxides	Al_2O_3, SnO_2, MnO, TiO_2, FeO, MgO, ZrO_2, CuO, ZnO, SiO_2	Al_2O_3, SnO_2, TiO_2, FeO, MgO, ZrO_2, CuO, ZnO, SiO_2	FeO, Fe_2O_3, TiO_2, $FeTiO_3$, SiO_2, (Ca.Mn)SiO_3	FeO, Fe_2O_3, TiO_2, SiO_2, ZnO, (Ca.Mn)SiO_3
PGE alloys	IrFe, IrOs, IrFeNiOsIr, OsRu, OsRuIr, PtFe, PtFe, PtFePd, RuOs	OsIrRu, OsIrRuCu, OsIrRuFe, OsIrRuFeCu, OsIrRuFeNi, PtFeNiCu, PtPdFeCu, PtRhFeNi, PtRhFeNiCu,	0	0
Metal alloys	AgAu, AgSn, FeSi, AlFeLa, CuZn, FeTiSiP, FeCo, FeCrNi, FeMn, FeNi, FeRu, NiFe, NiFeCr, NiFeIr, NiFeSi, NiIr, SiCa, SiCaAlFe, SiCaCu, SiCaFe, SiFeAl, SiFeAlCa, SiFeTi, SiTiFe, TiW, WCo	AgAu, CuNi, FeCrMn, FeCrNi, FeCrNiFeSi, FeAlSi, FeNiCuZn, FeCrMn, FeCrNi, FeCrNiMn, FeCrNiMnSi, FeCrNiSi, FeCrNiSiMg, FeCrNiMnTi, FeCrSi, FeP, FePAs, FeSi, NiAs, PbSn, PbZnCuFeSnAg, SnZnAg, TaCo	CrFe, CrNiFe, CrFeMn	NiMnFe, FeNiAl, NiMnCo
Oxides	Al_2O_3, CaO, (Ca, Si)O_2, CuO, FeO, Fe_2O_3, Fe_3O_4, (Fe, Mg)O, MgO, $MgAl_2O_4$, $MgAlSiO_4$, (Mg, Fe)O, PbO, SiO_2, TiO_2, (TiSi)O_2, (Zr,Si)O_2, ZnO,	FeO, (Mg,Fe)(Fe, Cr)$_2O_4$, Cr_2O_3, SiO_2, Fe_2O_3, MgO, SnO_2, Al_2O_3, NiO, TiO_2, ZrO_2, Cu_3O_2, Cu_2O, CuO, Ni_2O_3, NiO_2, ZnO, $FeTiO_3$	FeO, Fe_2O_3, Fe_3O_4, MgO, SiO_2	FeO, Fe_2O_3, Fe_3O_4, TiO_2, SiO_2, SnO_2
Sulfides	Ag_4S, FeS, IrSAs, (Pd,Fe,Cu)$_2S$, (Ni, Fe)$_3S_2$, (Os, Ru)S_2, $Ir_3S_4As_3$, FeAsS, Ni_2S, MoS_2, Ag_8S_2, Pd_6As_4, (Ni, Fe)$_4S_3$, (Fe, Ni, Co)S, Ni_3S_2, Sb_3S_5, Sb_3S_2, (Fe,Cu)$_2S_2$, PbS, RuS_2, (RuOs)$_3S_4$, MnS, Ti_7S_3	FeS_2, $CuFeS_2$, FeS, CuS, FeAsS, (FeNiCo)S, NiS, Ni_3S_2, Ni_2S, MoS_2, Sb_2S_3, (Ir, Rh)AsS, PbS, ZnS	Sulfides of Fe, Ni, Pb, Zn, As, Mo and others	FeS_2

Note: In this table we do not document the wide compositional variations within individual alloys.

similar features have also been reported on kimberlite diamonds from Russia (Makeev and Kriulina, 2012).

Cathodoluminescence (CL) analysis of the ophiolite-hosted diamonds shows that many of them have well-developed sector zoning (Figs. 14d). However, none of the grains examined thus far display the kind of growth zoning commonly found in kimberlitic diamonds (cf., Harte et al., 1999).

An early infrared (IR) study of diamond grains from orebody 31 of the Luobusa ophiolite has indicated that they are mixed IaA-IaB types with total nitrogen contents of 20-670 ppm (Bai et al., 2001; Davies et al., 1984). A later study of samples from the Kangjinla deposit has shown that those diamonds are type 1aA (Rong et al., 2013). The type IaA diamonds from the Ray-Iz peridotites have total nitrogen contents of 151-589 ppm, with nitrogen aggregation states up to 4.4%, whereas those from the chromitite have total nitrogen contents of 152-428 ppm, with nitrogen aggregation adds up to 14.6% (Fig. 16).

All of the diamonds measured thus far have markedly low C-isotopic compositions, with $\delta^{13}C$ values ranging from -18.3 to -28.7‰, yielding an average value of -24.6 ‰ (Fig. 15; Yang et al., 2013). The analyzed grains were separated from both peridotites and chromitites. Interestingly, all analysed moissanite, from whatever source, have the same range of carbon isotopes (Trumbull et al., 2009)

Mineral inclusions in diamonds provide some of the best evidence for their depth of formation and the composition of the fluids/melts from which they crystallized because of the chemical inertness of their host grains (Hunt et al., 2012). Transmission electron microscopy (TEM) has revealed a significant range of UHP and highly reduced inclusions in the ophiolite-hosted diamonds. The most common inclusions are coesite, NiMnCo alloys, and manganese-rich minerals such as spessartite (Mn garnet), tephroite (Mn olivine), as well as MnO (Fig. 17), and other solid and fluid inclusions minerals (Yang et al., 2015). These inclusions are distinctly different from most

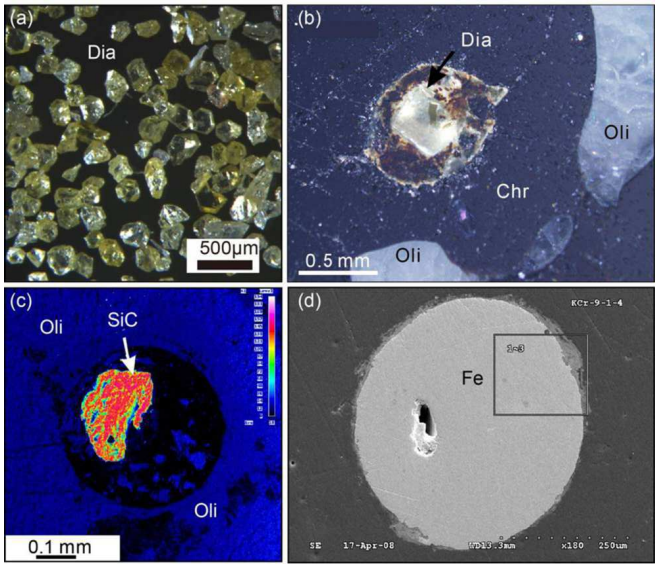

Figure 10. Examples of unusual minerals recovered from chromitites of the Luobusa ophiolite. (a) Diamonds separated from a chromitite. Typically, 100-200 μm in diameter, yellowish in color and cubo-octahedral in morphology; (b) An example of an in-situ diamond in chromitite. The diamond is about 200 μm in diameter and is set in a circular patch of amorphous carbon; (c) A carbon element map of an in-situ grain of moissanite hosted in olivine of a harzburgite. The grain, also about 200 μm across, is clearly half of a hexagonal crystal, the typical form of moissanite. Like the diamond in (b) it is set in a circular patch of amorphous carbon; (d) A SEM image of a spherical grain of native Fe about 450 μm in diameter. Such grains are abundant in all the ophiolites investigated and are commonly associated with FeO and locally with Fe_2O_3.

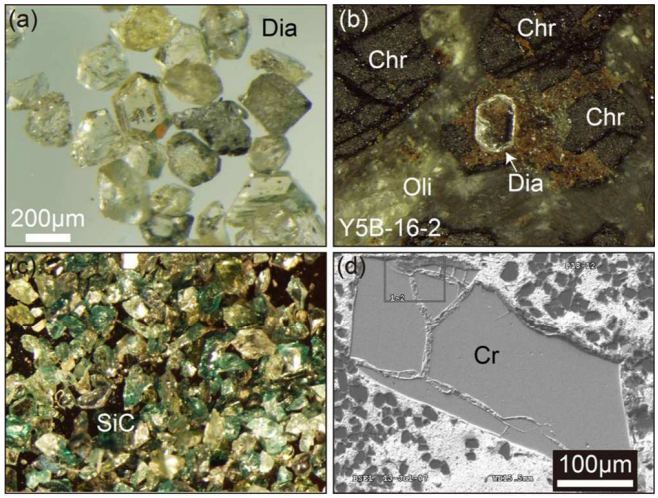

Figure 11. Examples of unusual minerals recovered from the chromitites of the Ray-Iz ophiolite. (a) Diamonds separated from chromitite. Note that they are similar in size, color and morphology to the diamonds from the Luobusa ophiolite; (b) Photomicrograph of an in-situ, euhedral diamond crystal. This grain is also hosted in a small irregular patch of brown, amorphous carbon; (c) Photomicrograph of abundant grains of moissanite separated from the chromitite. Note the angular, broken fragments and typical green to yellowish-green color of this mineral; (d) SEM image of a relatively large, blocky grain of native Cr about 700 μm long and 200 μm wide.

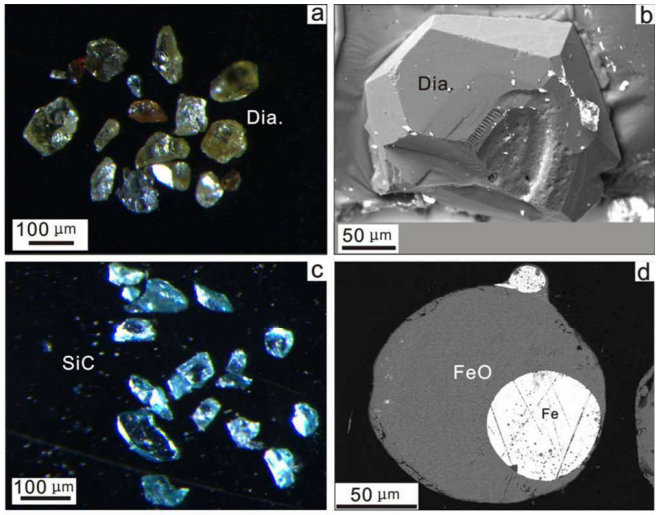

Figure 12. Examples of unusual minerals recovered from chromitites of the Sartohay ophiolite. (a) Photomicrograph of diamonds separated from chromitite. These diamonds are somewhat smaller than those from the Luobusa and Ray-Iz ophiolites (~100 μm) and have a wider range of color. However, they have the same cubo-octohedral morphology of the other examples; (b) SEM image of a nearly euhedral diamond with a cubic morphology; (c) Photomicrograph of moissanite grains from Sartohay. Note the bright blue color of these grains; (d) SEM image of a sphere of FeO, about 200 μm in diameter, containing a circular (spherical?) inclusion of native iron about 50 μm across.

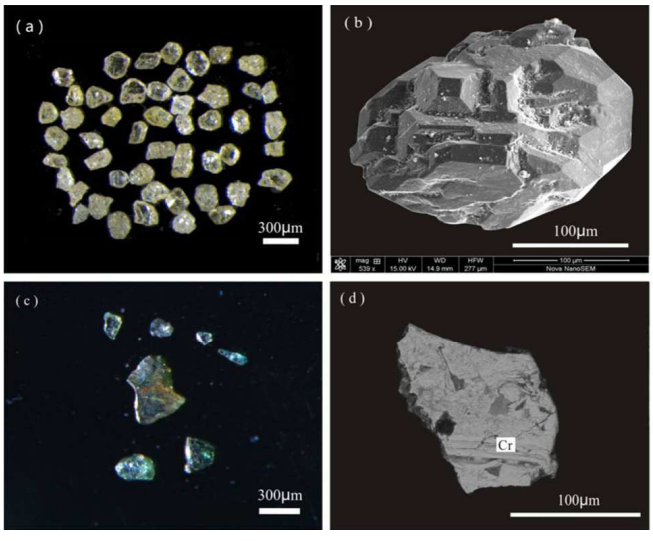

Figure 13. Examples of unusual minerals recovered from chromitites of the Hegenshan ophiolite. (a) Photomicrograph of typical ophiolite-hosted diamonds. These grains are pale yellow in color and about 200 μm in size; (b) SEM image of a diamond grain with a complex, blocky morphology; c) Photomicrograph of small, broken moissanite crystals with a characteristic bluish-green color; (d) SEM image of a small (150 μm), angular grain of native Cr.

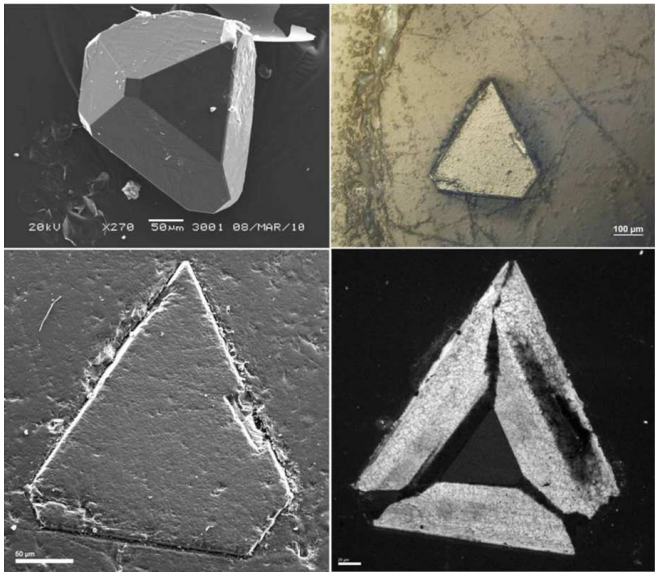

Figure 14. Various images of a euhedral diamond from the Luobusa ophiolite. (a) SEM image showing octahedral morphology; (b) Photomicrograph of an octahedral face on the diamond; (c) SEM image of the octahedral face in b; (d) Cathodoluminescence image of the octahedral face showing well-developed sector zoning in the diamond.

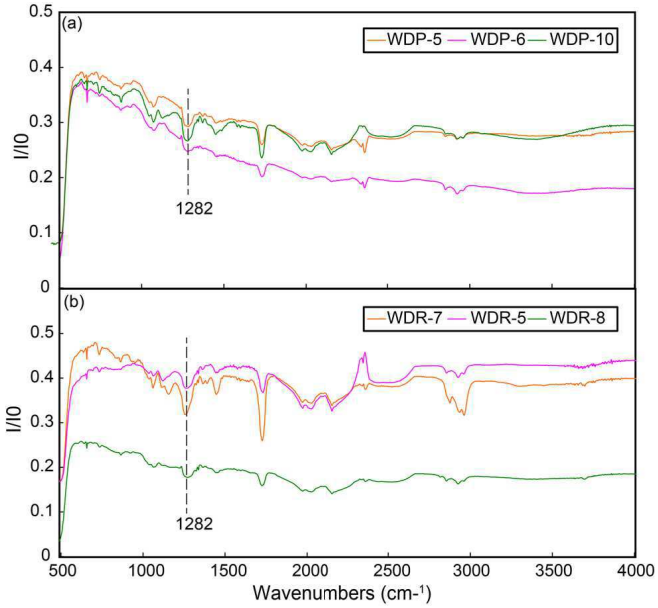

Figure 16. Representative infrared absorption spectra for diamonds from the Ray-Iz ophiolite. All of the investigated microdiamonds from this ophiolite exhibit similar absorption spectra between 4000 and 500 cm^{-1}; however, there are variations in intensity. The peak at 1282 cm^{-1} is indicative of Type IaA diamonds.

kimberlitic diamonds, which typically contain forsterite, pyrope and chromite (e.g., Spetsius and Taylor, 2008; Hunt et al., 2012).

A few of the ophiolite-hosted diamonds have been analyzed for their trace element compositions (Griffin et al., 2013). Diamonds from the Luobusa and Ray-Iz ophiolites have variable trace element contents, which are higher than those of kimberlitic diamonds. Spikes in some elements such as REE, Ni, Co, Mn, W and Ta probably reflect the presence of micro-inclusions in the grains. Although distinctly different from most kimberlitic diamonds, the ophiolite-hosted grains have chondrite-nomalized patterns highly similar to those of fibrous diamonds associated with kimberlite.

Many other minerals are associated with the ophiolite-hosted diamonds, the most abundant of which include moissanite and metallic alloys. Moissanite has been found in every chromitite and peridotite investigated thus far. It is extremely abundant in the chromitites of the Luobusa and Ray-Iz ophiolites in which it forms small, angular, colorless to yellowish-green grains (e.g. Fig. 11c). One *in-situ* grain of moissanite has been recovered from a peridotite in Luobusa. It is a small, broken fragment of a hexagonal grain lying in a circular patch of amorphous carbon like the diamonds. This grain is particularly important because it is hosted in olivine, confirming that such grains are intrinsic to the peridotites. Moissanite typically varies in color from ophiolite to ophiolite; for example grains in the Sartohay and Hegenshan ophiolites are typically bright blue (Figs. 12c and 13c), whereas as those in Luoubusa and Ray-Iz are colorless to light green.

Native elements and metallic alloys have also been found in all of the investigated ophiolites. Native iron is particularly common, and it occurs in distinctive black, shiny spheres about 100-300 µm in diameter (Fig. 10d), or as inclusions in spheres of FeO (Fig.12d). Native chromium is also quite common, typically occurring as relatively large grains (up to ~700 µm) (Fig. 11d), or as small irregular fragments (Fig. 13d). For detailed description of other native elements

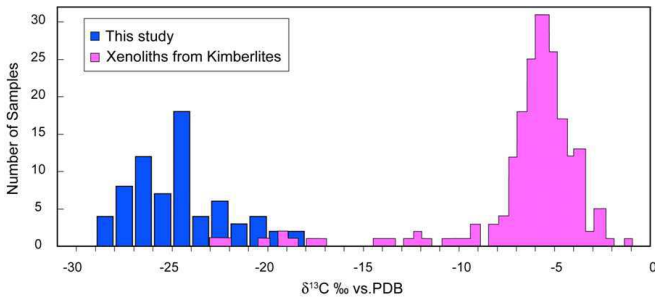

Figure 15. Histogram showing the range of carbon isotopes in ophiolite-hosted diamonds compared to kimberlite diamond. Ophiolite-hosted grains have $\delta^{13}C_{PDB}$ values ranging from -18 to -28, whereas the vast major of kimberlite diamonds have values of 0 to -8, with the lowest value being -22 (after Yang et al., 2015)

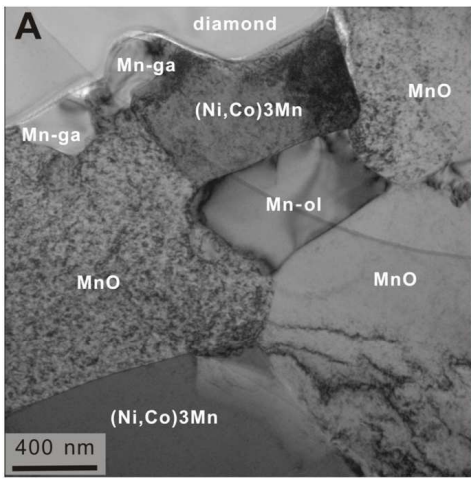

Figure 17. Inclusions of Mn-rich minerals in diamond.

and accessory minerals see Xu et al. (2015), Yang et al. (2015), and Robinson et al. (2015).

Previous models for the formation of ophiolite-hosted diamonds

Several well-documented observations should be taken into consideration when developing a coherent model for the origin of ophiolite-hosted diamonds: (1) all significant podiform chromitites occur in ophiolites that are interpreted to represent shallow mantle peridotites and oceanic crust (Dilek and Furnes, 2011, 2014); (2) diamond-bearing chromitites and peridotites contain mixtures of UHP, highly reduced minerals and crustal material (Zhou et al., 2014; Yang et al., 2015; Robinson et al., 2015), indicating a multi-stage mechanism of their formation; (3) similar UHP and highly reduced minerals occur in both high-Cr and high-Al chromitites that can coexist within the same ophiolite belt, and locally even within the same ophiolite massif; (4) UHP and highly reduced minerals spatially associated with the ophiolite-hosted diamonds appear to have formed at considerable depths in the mantle; (5) the presence of diopside and coesite exsolution lamellae in some chromite grains implies magnesiochromite crystallization at depths >380 km (Yamamoto et al., 2009); and, (5) chrome exists in very small quantities in most magmas (a few tens of ppm at most), and yet it is concentrated in ophiolites to form relatively large bodies of massive chromitite. It is highly unusual that all of the UHP, highly reduced and crustal minerals coexist far outside their normal stability fields in both ophiolitic peridotites and chromitites.

A number of different models have been proposed to explain the occurrence and formation of ophiolite-hosted diamonds and associated UHP minerals, but none of them successfully deals with the many questions posed by the presence of diamonds in this unexpected environment. One of the early models proposed by Zhou et al., (1997) calls for formation of ophiolites and their chromitites in supra-subduction zone settings. This model is focused on explaining the formation of high-Cr and high-Al chromitites in ophiolites and implicitly suggests that the UHP minerals, which already exist in the mantle peridotites, were picked up by chromitite crystallizing in SSZ mantle wedges. Taking a completely different approach, Arai (2013) has proposed that chromitites form at shallow levels in the upper mantle during convection beneath mid-ocean ridge spreading centers, and that these bodies are then recycled via subduction back into the deep mantle, where they acquire their UHP and highly reduced phases from carbon-rich fluids. However, the mechanism by which the fluids enter the chromitites is unclear in this model, and the related interpretations do not account for the abundance of high-Cr chromitites, which are found only in ophiolites (cf. Liou et al., 2014). A variation of this model by McGowan et al. (2015) proposes recycling of ophiolite slabs into the mantle transition zone where they are thought to remain for millions of years before being emplaced rapidly as coherent bodies into suture zones during slab rollback. Another recent paper by Miura et al. (2012) recognizes the occurrence of both concordant and discordant chromitites in the Oman ophiolite and postulates that the concordant bodies are high-Al chromitites that came from near the mantle transition zone, whereas the discordant bodies have slightly higher Cr contents, lack UHP minerals, and appear to have formed in SSZ settings. This model does not work in the Luobusa ophiolite of Tibet in which both concordant and discordant chromitites have high Cr#s and contain UHP and highly reduced phases.

In their revised model, Zhou et al. (2014) have proposed that an influx of asthenospheric mantle through a slab breakoff–generated window could lead to large-scale crystallization of chromitite in a SSZ environment. This model assumes that the UHP and highly reduced minerals already exist in oceanic peridotites where they were incorporated into the chromitites. One major drawback with this model is that there is no regional geological evidence for a slab breakoff event (i.e. high-K volcanism as demonstrated from other orogenic belts; Kadioglu et al., 2006; Dilek and Altunkaynak, 2007, 2009; Dilek and Sandvol, 2009) at the time of SSZ ophiolite formation, and that no explanation is provided for the causes and driving forces for such slab breakoff events.

Yang et al. (2015) have proposed that the UHP and highly reduced minerals, originated in the mantle transition zone, were mixed with subducted surface material (i.e. oceanic sediments), and that they were then encapsulated in magnesiochromite grains. This model envisions that the chromitites were crystallized near the top of the mantle transition zone, and that they were subsequently brought to shallow mantle levels by asthenospheric upwelling, either in a plume or beneath a spreading ocean ridge. In this interpretation both residual magnesiochromite grains and podiform chromitites are thought to be widely present in the oceanic mantle. If an oceanic slab of such material is trapped in the upper plate of a subduction zone, it might be uplifted and emplaced to become an ophiolite when underthrust by a partially subducted continental margin (Dilek, 2003; Dilek and Newcomb, 2003; and the papers therein).

A new model for ophiolite-hosted diamonds and global implications

We present a new, refined model here (Fig. 18), which incorporates various observations and interpretations provided in the previous models summarized above, and our most recently obtained data from all four ophiolites. In this model, previously subducted slabs of continental and oceanic crust resting in the lower part of the mantle transition zone are partially melted at high temperatures in a highly reduced environment. H_2O, CO_2 and other fluids released from these rocks become reduced to single element material, such as C and H. The melts then rise through the mantle to the top of, or above, the transition zone, where diamonds can be encapsulated in high-pressure magnesiochromite (with dissolved Si), and such minerals as stishovite and qinsongite may crystallize from the melts or fluids. With continued upwelling, coesite exsolution lamellae form in the chromite grains, and stishovite is replaced by coesite, but the diamonds are preserved as inclusions in magnesiochromite grains (Yang et al., 2007, 2014; Yamamoto et al., 2009). We infer in this model that diamonds can form in both MOR and BAB settings.

Diamonds have been recovered so far from ophiolites in five suture zones globally, indicating that they may be ubiquitous in oceanic mantle peridotites. These ophiolite-hosted diamonds have the similar characteristics regardless of whether they occur in peridotites or chromitites. Co-Mn-Ni alloys and some other unusual mineral inclusions that have been recovered from ophiolite-hosted diamonds differ significantly from the mineral inclusions in kimberlitic diamonds.

Nano-sized inclusions of TiN and BN in coesite have been

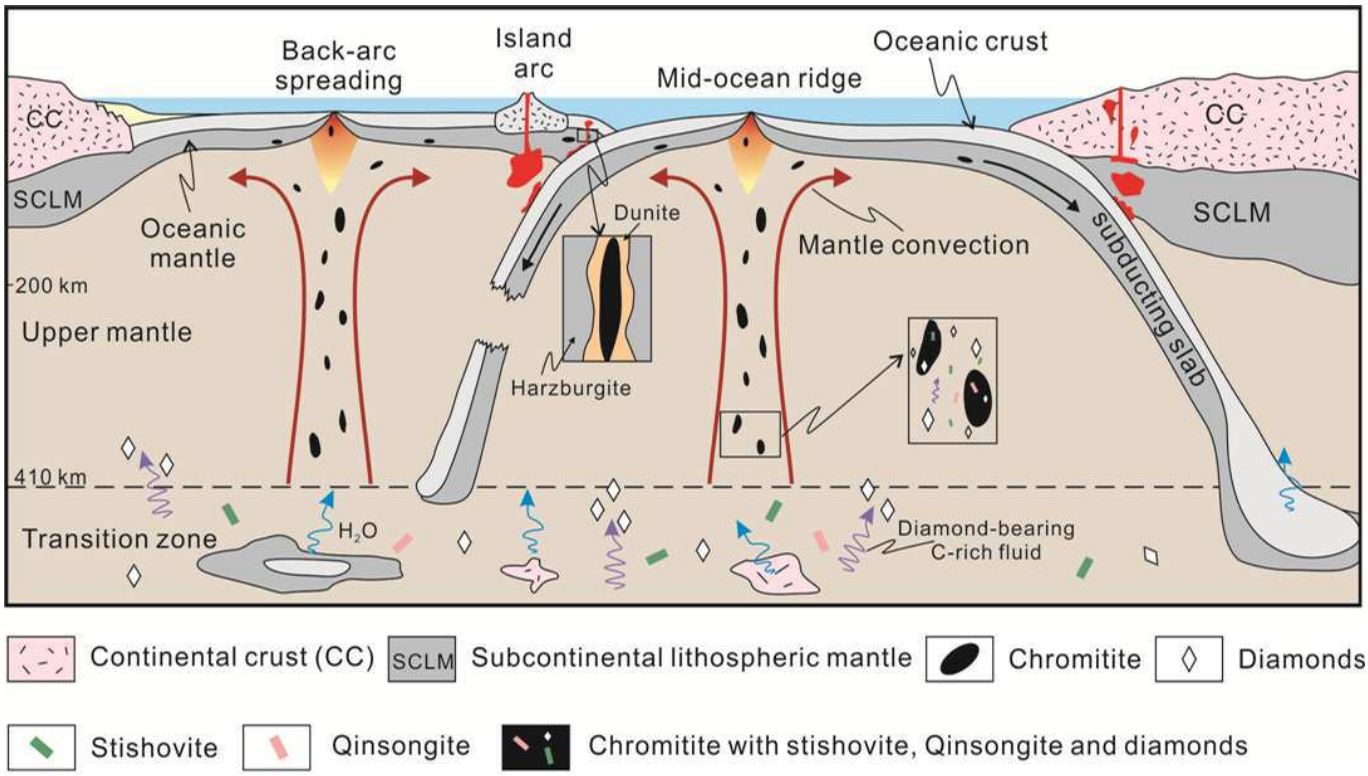

Figure 18. A new model to explain the presence of ophiolite-hosted diamonds in chromitites and mantle peridotites in MOR and BAB environments.(data and information from Yang et al., 2014; Miura et al., 2012; Liou et al., 2014).

identified using FIB and TEM techniques, and they are considered to be UHP in origin (Dobrzhinetskaya et al., 2009). Recently, the International Mineralogical Association Commission on New Minerals and Mineral Names (IMA-CNMMN) has confirmed that the BN is a new mineral, called Qingsongite (Dobrzhinetskaya et al., 2014), which occurs intergrown with kyanite and coesite. The associated mineral assemblages constrain the estimated pressures of their formation to 10-15 GPa, assuming temperatures of ~1300 °C and formation depths of > 300 km. Qingsongite is thus a typical UHP mineral, and the boron it contains is sourced from the Earth's surface via subduction. This finding demonstrates that oceanic slabs may get subducted to great depths in the mantle (>300 km and down to the Transition Zone).

The presence of UHP minerals within ophiolitic chromitites has been generally considered "forbidden" by conventional concepts of ophiolite petrogenesis under high-T, low-P conditions in mid-oceanic ridges or backarc spreading axes (Liou et al., 2012). The new data and observations on the occurrence of ophiolite-hosted diamonds and other unusual UHP minerals in ophiolitic chromitites, as reported in this study, are likely to modify these views on the shallow mantle origin of oceanic peridotites.

Acknowledgements

We thank members of the CARMA group including Liang Dongyang, Xu Xiangzheng, Chen Yanhong, Xiong Fahui, Huang Zhu, Tian Yazhaou, Wu Weiwei, and Zhang Lan for their help with this study in both the field and laboratory, and with the preparation of the figures. Our work in Tibet, Polar Urals and the Central Asian Orogenic Belt has been generously supported by the NSF-China and CGS. Y. Dilek's research in Tibet has been supported by the Chinese Academy of Geological Sciences. We express our sincere thanks to T. Tsujimori (Japan) and Ji-Feng (Gary) Xu (China) for their thorough and insightful comments of our manuscript that helped us sharpen its focus and organization.

References

Abe, N., 2011, Petrology of podiform chromitite from the ocean floor at the 15. DEG. 20'N FZ in the MAR, Site 1271, ODP Leg 209: Journal of Mineralogical and Petrological Sciences, v. 43106, no. 2, pp. 97-102.

Aitchison, J., Davis, A., 2003, Mesozoic radiolarians from the Yarlung Tsangpo and Bangong-Nujiang suture zones in western Tibet: INTERRAD X Tenth meeting of the International Association of Radiolarian Paleontologists, Lausanne, Switzerland, 7-13 September 2003, Abstracts and Programme.

Arai, S., 1997, Origin of podiform chromitites: Journal of Asian Earth Sciences, v. 15, pp. 303-310.

Arai S. 2013. Conversion flow-pressure chromitites to ultrahigh-pressure chromitites by deep recycling: a good inference. Earth and Planetary Science Letters, v.379, pp. 81–87.

Arai, S., Matsukage, K., 1998, Petrology of a chromitite micropod from Hess Deep, equatorial Pacific: a comparison between abyssal and alpine-type podiform chromitites: Lithos, v. 43, no. 1, pp. 1-14.

Arai, S. and Yurimoto, H., 1994, Podiform chromitites of the Tari-Misaka ultramafic complex, southwestern Japan, as mantle-melt interaction products. Economic Geology, v. 89, pp. 1279-1288.

Arai, S. and Yurimoto, H., 1995, Possible sub-arc origin of podiform chromitites. The Island Arc, v. 4, pp. 104-111.

Bai, W.J., Yang, J.S., Robinson, P.T., Fang, Q.S., Zhang, Z.M., Yan, B.G. and Hu, X.F., 2001, Study of Diamonds from Chromitites in the Luobusa Ophiolite, Tibet: Acta Geologica Sinica, v. 75, no. 3, pp. 404-409 (in Chinese with English abstract).

Bai, W.J., Zhou, M.F. and Robinson, P.T., 1993, Possibly diamond-bearing

mantle peridotites and podiform chromitites in the Luobusa and Donqiao ophiolites, Tibet: Canadian Journal of Earth Sciences, v.30, no. 8, pp. 1650-1659.

Bai, W.J., Zhou, M.F., Robinson, P.T., Fang, Q.S., Zhang, Z.M., Yan, B.G., Hu, X.F. and Yang J.S., 2000, Origin of podiform chromitites, diamond and associated mineral assemblage in the Luobusa ophiolite, Tibet: Seismological Press, Beijing (in Chinese).

Bao Z. W., Chen, H. S. and Zhang, Z. T., 1994. Study on REE and Sm-Nd isotopes of Hegenshan ophiolite, Inner Mongolia: Geochimica, v. 23, No. 4, pp.339-348 (in Chinese with English Abstract).

Brown, D., Alvarez-Maron, J., Juhlin, C., Perez-Estaun, A., Puchkov, V., Ayala, V., Kimbell, G. and Gorozhanina, Y., 1998, Crustal-scale structure and kinematic development of the footwall to the main Uralian Fault, Southern Ural (abstract): 6thZonenshain Conference on Plate Tectonics and Europrobe Workshop on Uralides, Moscow, pp.186.

Castro, A.I.L., Proenza, J.A., Zaccarini, F., Garuti, G., and Sarlabous, M.S.C.B., 2015, Al- and Cr-rich chromitites from the Eastern Havana-Matanzas ophiolites (Western Cuba). Episodes, v. 38, No. 4, pp. 334-343, doi: 10.18814/epiiugs/2015/v38i4/82429.

Chan, G.H.N., Crowley, Q., Searle, M., Aitchison, J.C. and Horstwood, M., 2007, U-Pb zircon ages of the Yarlung Zangbo suture zone ophiolites, south Tibet. Abstract volume 22th Himalaya-Karakoram-Tibet Workshop, Hong Kong, China, 2007, p. 12.

Chemenda, A., Matte, O. and Sokolov, V., 1997, A model of Paleozoic obduction and exhumation of high–pressure. Low-temperature in rocks in the southern Urals: Tectonophysics, v. 276, pp. 217-227.

DePaolo, D. J., 1988.Neodymium Isotope Geochemistry. An Introduction. Berlin: Springer-Verlag, 187 pp.

Dick, H.J.B., Bullen, T., 1984, Chromian spinel as a petrogenetic indicator in abyssal and alpine-type peridotites and spatially associated lavas: Contributions to Mineralogy and Petrology, v. 86, no. 1, pp. 54-76.

Dickey, J.S., 1975, Ahypothesis of origin for podiform chromite deposits: Geochimica Et Cosmochimica Acta, v. 39, no. 6, pp.1061-1074.

Dilek, Y., 2003, Ophiolite concept and its evolution: In, Geological Society of America Special Papers, v. 373, p. 1-16.

Dilek, Y., 2015, Ophiolites: Mantle sources, melt evolution and emplacement mechanisms, Preface. Episodes, v. 38, No. 4, pp. 227-229, doi: 10.18814/epiiugs/2015/v38i4/82417.

Dilek, Y. and Newcomb, S., 2003, Ophiolite concept and the evolution of geological thought. Geological Society of America Special Papers, v. 373, The Geological Society of America, Boulder, CO 80301, ISBN 0-8137-2373-6.

Dilek and Altunkaynak, S., 2007,Cenozoic crustal evolution and mantle dynamics of post-collisional magmatism in Western Anatolia: International Geology Review, v. 49, pp. 431-453.

Dilek and Altunkaynak, S., 2009, Geochemical and temporal evolution of Cenozoic magmatism in western Turkey: mantle response to collision, slab break-off, and lithospheric tearing in an orogenic belt: In, Geological Society, London, Special Publications, v. 311, pp. 213-233.

Dilek, Y. and Sandvol, E., 2009,Seismic structure, crustal architecture and tectonic evolution of the Anatolian-African Plate Boundary and the Cenozoic Orogenic Belts in the Eastern Mediterranean Region: In, Geological Society, London, Special Publications, v. 327, pp. 127-160.

Dilek, Y. and Furnes, H., 2011, Ophiolite genesis and global tectonics: geochemical and tectonic fingerprinting of ancient oceanic lithosphere: Geological Society of America Bulletin, v. 123, pp. 387-411.

Dilek, Y. and Furnes, H., 2014, Ophiolites and their origins: Elements, v. 10, pp. 93-100.

Dobrzhinetskaya, L.F., Wirth, R., Yang, J., Hutcheon, I.D., Weber, P.K., and Green, H.W. II., 2009, High-pressure highly reduced nitrides and oxides from chromitite of a Tibetan ophiolite. Proceedings of the National Academy of Sciences, v. 106, pp. 19233–19238.

Dobrzhinetskaya, L.F., Wirth, R., Yang, J.,Green, H.W. II., Hutcheon, I. D., Weber, P. K. andEdwardS. Grew, E.S., 2014.Qingsongite, natural cubic boron nitride: The first boron mineral from the Earth's mantle American Mineralogist, v. 99, pp. 764–772.

Dresser, J.A., 1913, Preliminary report on the serpentine and associated rocks of southern Quebec: Geological Survey of Canada, v.22, pp.103.

Edwards, S.J., 1990, Harzburgites and refractory melts in the Lewis Hills massif, Bay of Islands Ophiolite complex-the base-metals and precious-metals story: Canadian Mineralogist, v. 28, no. 3, pp. 537-552.

El-Rahman,Y A., Polat, A., Dilek, Y., Kusky, T.M., El-Sharkawia, M. and Said, A., 2012, Cryogenian ophiolite tectonics and metallogeny of the Central Eastern Desert of Egypt: International Geology Review, v. 1, pp. 1-15

Gavies, G., Collins, A.T. and Spear, P., 1984, Sharp Infra-res absorption lines in diamond: Solid State Communication, v. 49, no. 5, pp. 433-436.

Garutis, G., Zaccarini, F., Moloshag, V. and Alimov, V., 1999, Platinum-group minerals as indications of sulfur fugacity in ophiolitic upper mantle: an example from chromitites of the Ray-Is ultramafic complex, Polar Urals, Russia: The Canadian Mineralogist, v. 37, pp. 1099-1115.

Geng, H.Y., Sun, M., Yuan, C., Xiao, WJ., Xian, W.S., Zhao, G.C., Zhang, L.F., Wong, K.N. and Wu, F.Y., 2009, Geochemical, Sr–Nd and zircon U–Pb–Hf isotopic studies of Late Carboniferous magmatism in the West Junggar, Xinjiang: implications for ridge subduction?: Chemical Geology, v. 266, No. 3, pp.364-389.

Glodny, J., Bingen, B., Austrheim, H., Molina, J.F. and Rusin, A., 2002, Precise eclogitization ages deduced from Rb/Sr mineral systematics: the Maksyutov complex, Southern Urals, Russia: Geochimica et Cosmochimica Acta, v. 66, no. 7, pp.1221-1235.

Glodny, J., Austrheim, H. and Molina, J.F., 2003, Rb/Sr record of fluid-rock interaction in eclogites: The Marun-Keu complex, Polar Urals, Russia: Geochimica Et Cosmochimica Acta, v. 67, no. 22, pp.4353-4371.

Griffin, W.L., Yang, J.S., Robinson, P., Howell, D., Shi, R., O Reilly, S.Y. and Pearson, N.J., 2013, Going up or going down? Diamonds and super-reducing UHP assemblages in ophiolitic mantle: Goldschmidt 2013 Conference Abstracts, pp. 1215

Gurskaya, L.I. and Smelova, L.V., 2003, Formation and the structure of the Syumkeu Massif, the Polar Urals: Geol. Rudn. Mestorozhd, v. 45, no. 4, pp. 353-371.

Harte, B., Fitzsimons, I. C. W., Harris, J. W. and Otter, M. L., 1999, Carbon isotope ratios and nitrogen abundances in relation to cathodoluminescence characteristics for some diamonds from the Kaapvaal Province, S. Africa: Mineralogical Magazine, v. 63, no. 6, pp. 829-829.

Hunt, L., Stachel, T., McCandless, T. E., Armstrong, J. andMuelenbachs, K., 2012, Diamonds and their mineral inclusions from the Renard kimberlites in Quebec: Lithos, v. 142, pp. 267-284.

Huang, Z., Yang, J.S., Robinson, P. T., Zhu, Y. W., Xiong, F. H., Liu, Z., Zhang, Z. M., and Xu W., 2015, The discovery of diamond in chromitites of the Hegenshan ophiolite, Inner Mongolia, China:Acta Geologica Sinica, v. 89, pp. 341-350.

Irvine, T.N., 1977, Origin of chromitite layers in the Muskox intrusion and other stratiform intrusions: a new interpretation: Geology, v. 5, no. 5, pp. 273-2773.

Institute of Geology, Chinese Academy of Geological Sciences, 1981. The discovery of Alpine-type diamond bearing ultrabasic intrusions in Xizang (Tibet): Geological Review, v. 27, no. 5, pp. 445–447 (in Chinese with English Abstract).

Jian, P., Kröner, A., Windley, B.F., Shi, Y.R., Zhang, W., Zhang, L.Q. and Yang, W.R., 2012, Carboniferous and Cretaceous mafic–ultramafic massifs in Inner Mongolia (China): A SHRIMP zircon and geochemical study of the previously presumed integral "Hegenshan ophiolite": Lithos, v. 142, pp. 48-66.

Kadioglu, Y.K., Dilek, Y., and Foland, K.A., 2006, Slab break-off and syncollisional origin of the Late Cretaceous magmatism in the Central Anatolian crystalline complex, Turkey: Geological Society of America Special Papers, v. 409, pp. 381-415.

Kaminsky, F.V., 2007, Non-kimberlitic diamondiferous igneous rocks: 25 years on: Journal Geological Society of India, v. 69, no. 3, pp. 557.

Kazak, A.P., Dobretsov, N.L. and Moldavantsev, Y.E., 1976, Glaucophane schists, jadeitites, vesuvianites and nephrites of ultrabasiticRai-Iz massif: Geology and Geophysics, v. 2, pp. 60-66 (in Russian).

Kelemen, P.B., 1990, Reaction between ultramafic rock and fractionating basaltic magma I. Phase relations, the origin of calc-alkaline magma series, and the formation of discordant dunite: Journal of Petrology, v. 1, no. 31, pp. 51-98.

Kelemen, P.B., Dick, H.J.B. and Quick, J.E, 1992Formation of harzburgite by pervasive melt/rock reaction in the upper mantle: Nature, v. 6388, no. 358, pp. 635-641.

Kröner, A., Windley, B.F., Badarch, G., Tomurtogoo, O., Hegner, E., Jahn, B.M., Gruschka, S., Khain, E.V., Demoux, A. and Wingate, M.T.D., 2007, Accretionary growth and crust formation in the Central Asian Orogenic Belt and comparison with the Arabian-Nubian shield: Geological Society of America Memoirs, v. 200, pp. 181-209.

Liou, J.G., Zhang, R.Y., Liou, F.L., Zhang, Z.M., Ernst, W.G., 2012. Mineralogy,petrology, U-Pb geochronology, and geologic evolution of the Dabie-Sulu classicultrahigh-pressure metamorphic terrane, East-Central China. American Mineralogist, v. 97, pp. 1533–1543.

Liou, J.G.,Tsujimori, T., Yang, J.S., Zhang, R.Y.andErnst, W.G., 2014, Recycling of crustal materials through study of ultrahigh-pressure minerals in collisional orogens ophiolites, and xenoliths: A review. Journal of Asian Earth Sciences.DOI: 10.1016/j.jseaes.2014.09.011.

Liu, F., Yang, J.S.,Dilek, Y., Xu, Z.Q., Xu, X.Z., Liang, F.H., Chen, S.Y., Lian, D.Y., 2014. Geochronology and geochemistry of the basaltic lavas in the Dongbo and Purangophiolites of the Yarlung-Zangbo Suture zone: Plume-influenced continental margin-type oceanic lithosphere in southern Tibet. Gondwana Research, http://dx.doi.org/10.1016/j.gr.2014.08.002.

Liu, X.J., Xu, J.F., Wang, S.Q., Hou, Q.Y., Bai, Z.H. and Lei, M., 2009, Geochemistry and dating of E-MORB type mafics from Dalabute ophiolite in West Junggar, Xinjiang and geological implications: Acta Petrological Sinica, v. 25, no. 6, pp. 1373-1389.

Mahéo, G., Bertrand, H., Guillot, S., Villa, I. M., Keller, F. and Capiez, P., 2004, The South Ladakh ophiolites (NW Himalaya, India): an intra-oceanic tholeiitic arc origin with implication for the closure of the Neo-Tethys: Chemical Geology, v. 203 no. 3, pp. 273-303.

Makeyev, A.B., 1992, Mineralogy of alpine-type ultramafics in the Ural:Nauka, St. Petersburg, pp. 1-195. (in Russian).

Makeyev, A.B., Braynchaninova, N.I., 1999,Topomineralogy of ultramafics in the Polar Ural: Nauka, St. Petersburg, pp. 1-122 (in Russian).

Makeyev, A.B., Kriulina, G.Y., 2012, Metal films on the surfaces and within diamond crystals from Arkhangelskaya and Yakutian diamond provinces: Geology of Ore Deposits, v. 54, no. 8, pp. 663-673.

Makeyev, A.B., Perevozchikov, B.V. and Afanacyev, A.K., 1985, Chromite in the Polar Urals: Komi Branch of the Academy of Sciences of USSR, Syktyvkar, Russia, pp. 1-152. (in Russian).

McGowan, N.M., Griffin, W.L., González-Jiménez, J.M., Belousova, E., Afonso, J.C., Shi, R.D, McCammon, C.A., Pearson, N.J. and O'Reilly, S.Y., 2015, Tibetan chromitites: Excavating the slab graveyard: Geology, v. 43, no. 2, pp. 179-182.

Miao, L.C., Fan, W.M., Liu, D.Y., Zhang, F.Q., Shi, Y.R. and Guo, F., 2008, Geochronology and geochemistry of the Hegenshan ophiolitic complex: Implications for late-stage tectonic evolution of the InnerMongolia-Daxinganling Orogenic Belt, China: Journal of Asian Earth Sciences, v. 32, no.5, pp.348-370.

Miura, M., Arai, S., Ahmed, A. H., Mizukami, T., Okuno, M. and Yamamoto, S., 2012, Podiform chromitite classification revisited: A comparison of discordant and concordant chromitite pods from Wadi Hilti, northern Oman ophiolite: Journal of Asian Earth Sciences, v. 59, pp. 52-61.

Moldavantsev, Yu.E., Kazak, A.P., 1977, Rai-Iz massif. In: Sobolev,V.S., Dobretsov, N.L.,(Eds.), Petrology andmetamorphism of ancient ophiolites (Polar Urals and West Sayan as examples): Nauka, Novosibirsk, pp. 38-59 (in Russian).

Pasava, J., Knesl, I., Vymazalova, A., Vavrin, I., Gurskaya, L.I. and Kolbantsev, L.R., 2011, Geochemistry and mineralogy of platinum-group elements (PGE) in chromites from Centralnoye I, Polar Urals, Russia: Geoscience Frontiers, v. 2, pp. 81-85.

Parkinson, I.J., Pearce, J.A. and Thirlwall, M.F., 1992, Trace element geochemistry of peridotites from the Izu-Bonin-Mariana forearc, Leg 125: Proceedings of the Ocean Drilling Program Scientific Results.

Perevozchikov, B.V., Chashchukhin, I.S. and Tsritsyn E.P., 1990a. Metamorphism of ultramafic rocks massif and their primal composition. In: Puchkov, V.N., Shteinberg, D.S. (Eds.), Structure, Evolution and Minerogenesis of the Rai-Iz Ultramafic Massif:The Ural Branch of the Academy of Sciences of USSR, Sverdlovsk, Russia, pp. 29-57 (in Russian).

Perevozchikov, B.V., Kenig, V.V., Lukin, A.A. and Ovechkin, A.M., 2005, Chromites of the Rai-Iz massif in the Polar Urals (Russia): Geology of Ore Deposits v. 47, pp. 206.

Puchkov, V.N., 1990, Tectonic position and geological feature of massif. In: Puchkov, V.N., Shteinberg, D.S. (Eds.), Structure, Evolution and Minerogenesis of the Rai-Iz Ultramafic Massif: The Ural Branch of the Academy of Sciences of USSR, Sverdlovsk, Russia, pp. 4-10 (in Russian).

Robinson, P.T., Zhou, M.F., Hu, X.F., Reynolds, P., Bai, W.J. and Yang, J.S., 1999, Geochemical constraints on the origin of the Hegenshan Ophiolite, Inner Mongolia, China:Journal of Asian Earth Sciences, v. 17, no. 4, pp. 423-442.

Robinson, P.T., Bai, W.J., Malpas, J., Yang, J.S., Zhou, M.F., Fang, Q.S., Hu, X., Cameron, S. and Staudigel, H., 2004, Ultra-high pressure minerals in the Luobusa Ophiolite, Tibet, and their tectonic implications: Geological Society, London, Special Publications, v. 226, pp. 247-271.

Robinson, P.T., Malpas, J., Zhou, M.F., Ash, C., YANG, J.S. and Bai, W.J., 2005, Geochemistry and origin of Listwanites in the Sartohay and Luobusa ophiolites, China: International Geology Review, v. 47, no. 2, pp. 177-202.

Robinson, P.T., Trumbull, R.B. and Schmitt, A., 2015,The origin and significance of crustal minerals in ophiolitic chromitites and peridotites: Gondwana Research, v. 27, no. 2, pp. 486–506.

Rollinson, H., Adetunji, J., 2015, The geochemistry and oxidation state of podiform chromitites from the mantle section of the Oman ophiolite: A review: Gondwana Research, v.27, pp. 543–554.

Rong, H., Yang, J.S., Zhang, Z.M. and Xu, X.Z., 2013, A preliminary study of FT-IR on the diamonds from the Luobusa Chromitites of Tibet and the eclogite of CCSD-MH, China: Acta Petrologica Sinica, v. 29, no. 6, pp. 1861-1866 (in Chinese with English abstract).

Savelieva, G.N., Nesbitt, R.W., 1996, A synthesis of the stratigraphic and tectonic setting of the Uralian ophiolites: Journal of the Geological Society, v. 153, no. 7, pp. 525-537.

Savelieva, G.N., Suslov, P.V., Larionov, A.V. and Berezhanaya, N.G., 2006, Age of zircons from chromites in the residual ophiolitic rocks as a reflection of upper mantle magmatic events: Doklady Earth Sciences, v. 411, no. 2, pp. 1401-1406.

Sharma M., Wasserburg G.J., Pappanastassiou, D.A., Quick, J.E., Sharkov, E.V. and Lazko, E.E., 1995, High 143 Nd/144 Nd in extremely depleted mantle rocks: Earth and Planetary Science Letters, v. 135, no. 1, pp. 101-114.

Shmelev, V.R., Goncharenko, A.I., Chernyshev, A.I., Puchkov, V.N., Perevozchikov, B.V., 1990. Tectonics of ultramafic and gabbroic rocks. In: Puchkov, V.N., Shteinberg, D.S. (Eds.), Structure, Evolution and Minerogenesis of the Rai-Iz Ultramafic Massif: The Ural Branch of the Academy of Sciences of USSR, Sverdlovsk, Russia, pp. 88-148 (in Russian).

Shmelev, V.R., 2011. Mantle ultrabasites of ophiolite complexes in the Polar Urals: Petrogenesis and geodynamic environments: Petrology, v. 19, pp. 618-640.

Shmelev, V.R. and Meng, F. C., 2013, The Nature and Age of Basic Rocks of the Rai_Iz Ophiolite Massif (Polar Urals). Doklady Earth Sciences, v. 451, No. 1, pp. 758–761.

Shmelev, V.R., Perevozchikov, B. V. and Moloshag, V. P., 2014, The Rai_Iz ophiolite massif in the Polar Urals: geology and chromite deposits. Field Trip Guidebook. 12th International Platinum Symposium, Yekaterinburg, Russian, pp. 1–46.

Thayer, T.P., 1964, Principal features and origin of podiform chromite deposits, and some observations on the Guelman-Soridag District, Turkey: Economic Geology, v. 59, no.8, pp. 1497-1524.

Thayer, T.P., 1960, Some critical differences between alpine-type and stratiform peridotite-gabbro complexes: International Geological Congress 21st, v. 13, pp.247-259.

Thayer, T.P., 1969, Alpine-type sensustrictu(ophiolitic) peridotites: Refractory residues from partial melting or igneous sediments? A contribution to the discussion of the paper: "The origin of ultramafic and ultrabasic rocks" by Wyllie, P.J.: Tectonophysics, v. 7, pp. 511-516.

Tian, Y. Z., Yang, J. S., Robinson, P.T., Xiong, F.H., Li, Y., Zhang, Z.M., Liu, Z., Liu, F., Niu, X. L., 2015. Diamond discovered from chromitites in the Sartohay ophiolite, Xinjiang Province, China. Acta Geologica Sinica, v. 89, pp. 801-809.

Trumbull, R.B., Yang, J.S., Robinson, P. T., Di Pierro, S., Vennemann, T. and Wiedenbeck, M., 2009, The carbon isotope composition of natural SiC (moissanite) from the Earth's mantle: New discoveries from ophiolites: Lithos, v. 113, pp. 612-620.

Vakhrusheva, N.V., 2007, Non Serpentinized Harzburgites and Websterites of the Voikar–Syn'ya Massif: Mineralogy, Geochemistry, and Sm–Nd Age, Ul'trabazitbazitovyekompleksyskladchatykhoblastei, pp. 293-296.

Walker, R.J., Prichard, H.M., Ishiwatari, A. and Pimentel, M., 2002. The osmium isotopic composition of convecting upper mantle deduced from ophiolite chromites: Geochimica et Cosmochimica Acta, v. 66, pp. 329-345.

Wang, Q. and Liu, X.Y., 1986, Paleoplate tectonics between Cathaysia and Angaraland in Inner Mongolia of China: Tectonics, v. 5, no. 7, pp. 1073-1088.

Wei, W.Z., Dong, X.Y., Zeng, H.Q.i. and Gao, J.P., 1987, The geological characteristics and origin of ultramaficrocks and chromitites, Sartohay, Xinjiang: Northwest Geology Science, no. 2, pp. 57-58 (in Chinese).

Windley, B F., Alexeiev, D., Xiao, W J., Kröner, A. and Badarch, G., 2007, Tectonic models for accretion of the Central Asian Orogenic Belt: Journal of the Geological Society, v. 64, pp. 31-47.

Xia, B., Chen, G.W., Wang, R., Wang, Q., 2008a. Seamount volcanism associated with the Xigaze ophiolite, Southern Tibet. Journal of Asian Earth Sciences, v. 32, pp. 396-405.

Xu X.Z., Yang, J.S., Chen, S.Y.,Fang Q.S., Bai, W.J. and Ba D.Z., 2009, Unusual mantle mineral group from chromitite orebody Cr-11 in the Luobusa Ophiolite of the Yarlung-Zangbo Suture Zone, Tibet: Journal of Earth Sciences, v. 20, no. 2, pp. 284-302.

Xu, X.Z., Yang, J.S., Ba, D.Z., Guo, G.L., Robinson, P.T. and Li, J.Y., 2012, Petrogenesis of the Kangjinla peridotite in the Luobusa ophiolite, Southern Tibet: Journal of Asia Earth Sciences, v. 42, pp. 553-568

Xu. X.Z., Yang, J.S., Robinson, P.T., Xiong, F.H., Ba, D.Z. and Guo, G.L., 2015, Origin of ultrahigh pressure and highly reduced minerals in podiform chromitites and associated mantle peridotites of the Luobusa ophiolite, Tibet: Gondwana Research, v. 27, no. 2, pp. 686-700.

Yamamoto, S., Komiya, T., Hirose, K. and Maruyama, S., 2009, Coesite and clinopyroxene exsolution lamellae in chromites: In-situ ultrahigh-pressure evidence from podiform chromitites in the Luobusa ophiolite, Southern Tibet: Lithos, v. 109, no. 3, pp. 314-322.

Yamamoto, S., Komiya, T., Yamamoto, H., Kaneko, Y., Terabayashi, M., Katayama, I., Iizuka, T., Maruyama, S., Yang, J.S. and Kon, Y., 2013, Recycled crustal zircons from podiform chromitites in the Luobusa ophiolite, southern Tibet: Island Arc, v. 22, pp. 89-103.

Yan, B., Liang, R., Fang, Q., Yang, F. and Wang, F., 1987, Characteristics of diamond and associated minerals in Qiaoxi and Hongqu, Xizang:Bulletin of the Institute of Geology, Chinese Academy of Geological Sciences, v. 14, pp. 61-125 (in Chinese with English Abstract).

Yang, G.X., Li,Y.J., Gu, P.Y., Yang, B.K., Tong,.L.L and Zhang, H.W.,2012, Geochronological and geochemical study of the Darbut Ophiolitic complex in the West Junggar (NW China): implications for petrogenesis and tectonic evolution: Gondwana Research, v. 21, pp. 1037-1049.

Yang, G.X. and Dilek, Y., 2015, OIB and P-Type ophiolites along the Yarlung-Zangbo Suture Zone (YZSZ), Southern Tibet: Poly-phase melt history and mantle sources of the Neotethyan ocean lithosphere. Episodes, v. 38, No. 4, pp. 250-265, doi: 10.18814/epiiugs/2015/v38i4/82420.

Yang, J.S., Bai, W.J., Fang, Q.S., Yan, B.G., Shi, N.C., Ma, Z.S., Dai, M.Q. and Xiong, M., 2003, Silicon-rutile-an ultrahigh pressure (UHP) mineral from an ophiolite: Progress in Natural Science, v. 13, no. 7, pp. 528-531.

Yang, J.S., Dobrzhinetskaya, L., Bai, W.J., Fang, Q.S., Robinson, P.T., Zhang J.F. and Green, H.W., 2007, Diamond-and coesite-bearing chromitites from the Luobusa ophiolite, Tibet: Geology, v. 35, no. 10, p.875-878.

Yang, J.S., Robinson, P.T., and Dilek. Y., 2014. Diamonds in Ophiolites: Elements v.10, p. 127-130.

Yang, J.S., Meng, F.C., Xiang, Z.X., Robinson, P.T., Dilek, Y., Makeyev, A.B., Wirth, R., Wiedenbeck, M. and Cliff. J., 2015, Diamonds, native elements and metal alloys from chromitites of the Ray-Iz ophiolite of the Polar Urals: Gondwana Research, v. 27, p.459-485.

Yin, J.Y., Long, X.P., Yuan, C., Sun, M., Zhao, G.C. and Geng, H.Y., 2013, A Late Carboniferous–Early Permian slab window in the West Junggar of NW China: Geochronological and geochemical evidence from mafic to intermediate dikes: Lithos, v. 175, no. 1, pp. 146-162.

Zavaritsky, A.N., 1932, Peridotite massif Rai-Iz in Polar Urals: ONTI, Moscow, pp. 220 (in Russian).

Zhang, C., Zhai, M.G., Allen,, M.B., Saunders, A.D., Wang, G.R. and Huang, X., 1993, Implications of Palaeozoic ophiolites from Western Junggar, NW China, for the tectonics of central Asia: Journal of the Geological Society, v. 150, no. 3, pp. 551-561.

Zhang, C. and Huang X., 1992,The ages and tectonic settings of ophiolites in West Junggar, Xinjiang: Geological Review, v. 38, pp. 509–523 (in Chinese with English abstract).

Zhang, H.Y., Ba, D.Z., Guo, T.Y., Xue, J.Z. and Mo, X.X., 1996, Metallogenic characteristics of the Luobusa podiform chromite deposit in Tibet: Tibet Geology, v. 1, pp. 1-3 (in Chinese with English abstract).

Zhou, M.-F., Robinson, P.T., Malpas, J., Edwards, S., Qi, L., 2005. REE and PGE geochemicalconstraints on the formation of dunites in the Luobusa ophiolite, Southern Tibet: Journal of Petrology, v. 46, pp.615–639.

Zhou, M.F., Robinson, P.T., 1996, Podiform chromitites in the Luobusa ophiolite (southern Tibet): Implications for melt-rock interaction and chromite segregation in the upper mantle: Journal of Petrology, v. 37, no. 1, pp. 3-21.

Zhou, M.F., Robinson, P.T., 1997, Origin and tectonic environment of podiform chromite deposits: Economic Geology, v. 92, pp. 259-262.

Zhou, M.F., Robinson, P.T., Malpas, J., Aitchison, J., Sun, M., Bai, W.J., Hu, X.F. and Yang, J.S., 2001. Melt/mantle interaction and melt evolution in the Sartohay high-Al chromite deposits of the Dalabute ophiolite (NW China): Journal of Asian Earth Sciences, v. 19, no. 4, pp. 517-534.

Zhou, M.F., Robinson, P.T., Su, B.X., Gao, J.F., Li, J.W., Yang, J.S. and Malpas, J., 2014, Compositions of chromite, associated minerals, and parental magmas of podiform chromite deposits: The role of slab contamination of asthenospheric melts in suprasubduction zone environments: Gondwana Research, v. 26, pp. 262-283.

Zhou, M.F., Robinson, P.T., Malpas, J., Edwards, S.J. and Qi, L., 2005, REE and PGE geological constraints on the formation of dunites in the Luobusa ophiolite, Southern Tibet: Journal of Petrology, v. 46, no. 3, pp. 615-639.

Zhou, M.F., Robinson, P.T., Su, B.X., Gao, J.F., Yang, J.S. and Malpas, J., 2014, Compositions of chromite, associated minerals, and parental magmas of podiform chromite deposits: The role of slab contamination of asthenospheric melts in suprasubduction zone environments: Gondwana Research, v. 26, no. 1, pp. 262-283.

Zhou, S., Mo, X.X., Mahoney, J.J., Zhang, S.Q., Guo, T.Y., and Zhao, Z.D., 2002, Geochronology and Nd and Pb isotope characteristics of gabbro dikes in the Luobusha ophiolite: Chinese Science Bulletin, v. 47, pp. 143-146.

In memory of Anders Wikström (1937-2015)

Anders Wikström was born in 1937. He studied at Uppsala University, in Sweden, graduating in Mathematics, Chemistry and Geology in 1961 and obtaining his Doctoral degree in 1968 in Mineralogy and Petrology with a thesis dealing with retrograde reactions in eclogites. Between 1968 and 2000, when he retired, Anders was employed as state geologist and then senior state geologist at the Geological Survey of Sweden. He was very active in the study of granites and metamorphic rocks from Sweden. In 2012 he contacted the IUGS Heritage Stone Task Group with the purpose of bringing greater attention to historically important natural stones that had been used in construction for centuries in from Sweden, notably Kolmården stone and Swedish porphyries. Published information on these was largely in Swedish so he authored two papers on this subject in English to bring these to the attention of the wider scientific community and general public. This led to museums in Sweden and from Russia to seek copies of the papers and to arrange talks at Stockholm and Uppsala.

Anders Wikström presenting his poster on the Kolmården serpentine marble. EGU 2013. Photo by Lola Pereira.

Anders was passionate about music (he played tenor saxophone and enjoyed the Christmas season by playing with local bands in supermarkets), he loved animals, especially his dogs and cats, and sailing until he had to sell his boat after 45 years of use. He remained very active in writing on and discussing science until he was diagnosed with Amyotrophic Lateral Sclerosis in the Summer of 2015. On the 8th of November he passed away. He leaves wife, children and grandchildren, who receive our sincere condolences. We, in IUGS, have lost a valued colleague and a very dear friend.